Université de Montréal

Synthesis of Aza- and α,α-Disubstituted Glycinyl Peptides and Application of Their Electronic and Steric Interactions for Controlling Peptide Folding, and for Biomedical Applications

By

Ms. Fatemeh Mohammadpourmir

Département de chimie
Faculté des arts et des sciences

Thesis presented to Faculté des études supérieures et postdoctorales
to obtain Doctor of Philosophy (Ph. D.)
in Chemistry

January 2019

Université de Montréal
Faculté des études supérieures et postdoctorales

This Thesis entitled:

Synthesis of Aza- and α,α-Disubstituted Glycinyl Peptides and Application of Their Electronic and Steric Interactions for Controlling Peptide Folding, and for Biomedical Applications

Presented by:
Ms. Fatemeh Mohammadpourmir

Thesis was evaluated by a jury composed of the following persons:

Prof. Andreea Schmitzer, President of jury
Prof. Stephen Hanessian, Member of jury
Prof. William D. Lubell, Research director
Prof. Daniel Garcia Rivera, External examiner
Prof. David Morse, Representative of the Dean

Résumé

Les peptides présentent un grand potentiel thérapeutique, que ce soit en tant qu'ingrédient actif ou d'excipient pour la délivrance de médicament. Toutefois, certains désavantages comme leur faible biodisponibilité, une stabilité métabolique limitée et un manque de sélectivité limitent leur utilisation. Le développement de mimes peptidiques possédant de meilleures propriétés pharmacologiques est donc nécessaire. La présente thèse doctorale est orientée vers deux objectifs: a) le développement d'analogues azapeptides agissant comme modulateurs du récepteur prostaglandine F2α (FP) et b) le développement de méthodes de synthèse et d'analyse conformationnelle de résidus glycine $C^{\alpha,\alpha}$-di substitué stériquement encombrés.

Les azapeptides sont une classe de mimes peptidiques où le carbone α d'au moins un acide aminé est remplacé par un atome d'azote. Cette modification qui emploie un semicarbazide en tant que mime d'acide aminé réduit la flexibilité conformationnelle et peut induire des repliements β.

Les accouchements prématurés représentent un défi du point de vue médical. Malgré les efforts déployés pour retarder les accouchements prématurés, le taux de naissances prématurées ne cesse d'augmenter dans les pays industrialisés. Le récepteur prostaglandine F2α (FP) a été utilisé comme cible pour le développement d'agents tocolytiques (qui retardent l'accouchement). Les analogues aza-amino acyl proline ont démontré la capacité de moduler effectivement le récepteur FP et à inhiber les contractions utérines reliées au prostaglandines F2α par un mécanisme allostérique de signalétique biaisée d'un récepteur couplé à une protéine G. De plus, l'activité de ces analogues dépend de la nature de la chaine latérale de l'aza-acide aminé.

Pour acquérir une meilleure compréhension de la relation structure-activité des azapeptides modulant le récepteur FP, une approche orientée sur la diversité a été développée pour introduire différentes chaines latérales sur le résidu aza-amino acyl proline par alkylation de résidus aza-Gly-Pro, ainsi que par catalyse au cuivre sur des résidus aza-propargylglycine. Différents analogues furent préparés pour étudier l'influence de la taille de la chaine latérale, de l'hydrophobicité et de l'aromaticité sur l'activité. De plus, une librairie fut préparée par modification d'un résidu peptidique 4-hydroxyproline ancré sur support solide. Ces analogues furent utilisés pour étudier l'influence du pliement des cycles, de l'hydrophobicité et des substituants sur l'activité. Les

différents analogues ont été testés en fonction de leur capacité à moduler les contractions utérines liées au PGF2α. Les nouveaux analogues ont montré que l'activité envers les contractions myométriales était sensible aux changements de conformation dans la région du tour β, ainsi qu'à la nature, la taille et la lipophilicité de la chaine latérale du résidu aza-acide aminé.

La synthèse de peptides contenant des résidus acide-2-amino-2-adamantane (Adm) a été explorée pour examiner l'influence de résidus stériquement encombrés sur la conformation. Une série de *N*-formyl-Adm di- et tripeptides possédant une variété de composantes *C*- terminales a été synthétisée par une réaction multi-composante de Ugi en utilisant l'adamantan-2-one en tant que précurseur. La conformation de la chaine principale des peptides stériquement encombrés a été déterminée en utilisant l'analyse par diffraction des rayons X. Le fort encombrement causé par le résidu Adm restreint l'espace conformationnel aux régions typiques de repliements. La conformation de la chaine peptidique est influencée par la nature du groupe *C*-terminal. Les groupes *C*-terminaux encombrés, comme les groupes *tert*-butyl a favorisent les repliements γ standards alors que les groupes moins encombrés favorisent les repliements α- et β.

Des tripeptides homo-oligo-Adm possédant un groupe *C*-terminal *iso*-propyl et *tert*-butyl amide ont été préparés en utilisant des réactions de Ugi séquentielles. L'analyse des trimères cristallisés par diffraction des rayons X a démontré que les analogues comportant le groupement *iso*-propyl adoptait un repliement α avec un seul pont hydrogène formant un cycle de 13 membres. Les analogues comportant le groupement *tert*-butyl, quant à eux, formaient deux tours γ consécutifs caractéristique d'une hélice γ en formation.

Des méthodes efficaces de synthèse d'azapeptides et d'oligomères encombrés de glycine $C^{\alpha,\alpha}$-di substitué ont été développées. En utilisant ces outils, les effets de contraintes stériques et électroniques de peptides ont respectivement été explorés par l'étude de modulateurs de FP bioactifs dans le but de retarder les accouchements prématurés et par l'analyse conformationnelle d'oligomères d'Adm. Le présent ouvrage a contribué à acquérir une meilleure compréhension de la relation structure-activité d'azapeptides modulateurs du récepteur FP. De plus, les facteurs contrôlant la conformation des résidus Adm stériquement encombrés ont été élucidés par la construction de trois différents éléments de structure secondaire (repliements α, β, et γ) dépendant

de la nature du groupement *C*-terminal. Ceci offre un grand potentiel pour des applications en chimie des peptides et dans le domaine biomédical.

Mots-clefs : Peptidomimétique, prostaglandine F2α, aza-propargylglycine, tour α, tour β, tour γ, acides aminés C^{α}-di-substitués, repliement peptidique, acide-2-amino-2-adamantane, angle de torsion.

Abstract:

Peptides exhibit pharmaceutical potential as active ingredients and excipients in drug delivery systems. Their shortcomings, such as low bioavailability, poor selectivity and limited metabolic stability have however necessitated the design and synthesis of peptidomimetics to improve pharmacological properties. The body of this Ph.D. thesis has been targeted towards two objectives: a) the development of azapeptide analogs as modulators of the prostaglandin $F_{2\alpha}$ receptor (FP), and b) the development of methods for the construction, and the conformational analysis of bulky $C^{\alpha,\alpha}$-disubstituted glycine amino acids.

Azapeptides are a class of peptidomimetic in which the C^{α} unit of at least one amino acid residue is replaced by a nitrogen atom. This modification features a semicarbazide as an amino amide surrogate, which reduces conformational flexibility and can induce β-turn conformation.

Preterm birth is an unmet medical need. Despite efforts to counter the onset of preterm labor, the rate of premature birth has increased steadily in developed countries. The prostaglandin F2α receptor (FP) was pursued as target for designing tocolytic (labor delaying) agents. Aza-amino acyl proline analogs had been shown to modulate FP and to inhibit PGF2α-mediated uterine contractions by an allosteric mechanism involving biased G protein-coupled receptor signalling. Moreover, the activity of these analogs was found to be contingent on the nature of their aza-residue side chains.

To better understand of the structure-activity relationships of azapeptide modulators of FP, diversity-oriented approaches were devised to introduce different side chains onto the aza-amino acyl proline residue by alkylation of aza-Gly-Pro analogs, as well as by copper-catalyzed reactions on an aza-propargylglycine (aza-Pra) residue. Analogs were prepared to study the influences of side chain size, hydrophobicity and aromaticity on activity. In addition, a set of proline residue analogs were prepared by the modification of a 4-hydroxyproline peptide linked to a solid support. These analogs were synthesized to study the influence of ring pucker, hydrophobicity and substituents on activity. Analogs were tested for ability to modulate PGF_{2a}-mediated uterine contractions. Study of the novel modulators demonstrated that activity on myometrial contractions was sensitive to changes in the conformation at the turn region, as well as the size, nature and lipophilicity of the aza-residue side chain.

The chemistry of peptides bearing 2-amino adamantane-2-carboxylic acid (Adm) was explored to examine the influence of the bulky residue on conformation. A set of *N*-formyl-Adm di- and tripeptides possessing various *C*-terminal components was synthesized by the development of a multiple-component Ugi reaction sequence using adamantan-2-one as precursor to the bulky residue. The backbone conformation of the hindered peptides was determined using X-ray analysis. The steric bulk of the Adm residue restricted conformational space to a region typical of an intramolecular hydrogen-bonded α- and γ-turn, as well as a distorted type-II (II′) β-turn. The *C*-terminal residue influenced the backbone conformation. Bulkier *C*-terminal groups, such as *t*-butyl, favored regular γ-turns. Smaller *C*-terminal residues favored α- and β-turn geometry.

Employing an iterative Ugi sequence homo-oligo-Adm tripeptides were prepared possessing *i*-propyl and *t*-butyl *C*-terminal amides. Crystallization of the Adm trimers and X-ray analysis in the solid state demonstrated that the *i*-propyl analog adopted the conformation of a single 13-membered hydrogen-bonded α-turn. On the other hand, the *t*-butyl analog exhibited two consecutive γ-turns in an incipient γ-helix conformation.

Effective methods have thus been developed for the assembly of azapeptides and sterically bulky $C^{\alpha,\alpha}$-disubstituted glycine oligomers. With such methods in hand, the effects of electronic and steric constraint on peptide conformation have been respectively explored in studies of biologically active FP modulators to develop therapy to delay labor, and in conformational analyses of Adm oligomers. This thesis has thus contributed to a better understanding of structure-activity relationships of azapeptide modulators of FP. Moreover, the factors controlling the conformation of the bulky Adm residue have been elucidated in the construction of three different secondary elements (α-, β- and γ-turns) contingent on the *C*-terminal residues. The results offer interesting potential for biomedical and peptide chemistry.

Keywords: peptidomimetic, azapeptide, prostaglandin F2α, aza-propargylglycine, α-turn, γ-turn, C^{α}–disubstituted glycine, peptide folding, 2-amino adamantane-2-carboxylic acid, torsion angle.

Note

This thesis describes my research on the application of electronic and steric interactions to control peptide folding for biomedical applications. This thesis has been written employing submitted manuscripts. I specify herein the different contributions of the authors of each of the manuscripts in the respective chapters.

The introduction (Chapter 1), and unless specified otherwise below, the following chapters, all were written by me and edited by Professor William D. Lubell.

The manuscript in chapter 2 entitled "Paired Utility of Aza-Amino Acyl Proline and Indolizidinone Amino Acid Residues for Peptide Mimicry: Conception of Prostaglandin F2α Receptor Allosteric Modulators that Delay Preterm Birth" describes the synthesis, isolation, characterization and structure-activity relationship study of peptide mimics containing aza-amino acyl proline and indolizidinone amino acid residues to develop allosteric modulators of the prostaglandin F2α receptor. This paper is being acceopted to the *Journal of Medicinal Chemistry*. The results on the synthesis and study of the analogs described in this article were obtained in collaboration with N. D. Prasad Atmuri, another Ph.D. candidate in Professor Lubell's laboratory. I performed the synthesis, isolation and characterization of all aza-amino acyl proline analogs. All the indolizidinone peptide analogs were synthesized and characterized by N. D. Prasad Atmuri. Under my direction, Jennifer Rudon Fores, a visiting M.Sc. student from Pierre et Marie Curie University (UPMC) performed the synthesis of certain aza-Lys analogs. All analogs were tested for their activity in reducing PGF2α-induced uterine contractions and delaying labor by our collaborators Dr. Xin Hou and Professor Chemtob from the Département de pédiatrie, Université de Montréal. The sections concerning the indolizidinones and azapeptides were respectively written by N. D. Prasad Atmuri and me, and both were edited by Professor Lubell.

The manuscript in chapter 3 entitled "Crystal-State Conformational Analysis of Adm Peptides. Influence of the *C*-Terminal Substituent" describes my original syntheses, isolation and characterization of set of *N*-formyl-Adm di- and tripeptides possessing various *C*-terminal components by conception of an Ugi multiple-component reaction sequence. This manuscript is submitted to the journal *Peptide Science* for publication in a special issue devoted to the 8th Peptide

Engineering Meeting (PEM 8) h eld in Berlin, Germany (November 8-10, 2018). The conception and design of the study was defined by Professor Lubell and Professor Toniolo (Department of Chemistry, University of Padova, Italy). I performed all the experimental, characterization and crystallization steps. Dr. Crisma (Institute of Biomolecular Chemistry, University of Padova, Italy) crystallized OHC-Adm-Aib-OMe and performed its X-ray crystallographic analysis, all other crystal structures were solved at the Université de Montréal regional center. I wrote the first draft of the manuscript and contributed to its revision which was edited by Dr. Crisma and Professors Lubell and Toniolo.

The manuscript in Chapter 4 entitled "**Isolated α−Turn and Incipient γ −Helix**" presents the unique abilities of homo-oligo-adamantyl peptides to adopt α− and γ −turn conformations in the solid state and solution. Assembled by an Ugi multicomponent reaction strategy, *N*-formyl-adamantyl tripeptide *tert*-butyl and *iso*-propyl amides were respectively found to adopt an incipient γ −helix and an isolated α−turn conformation by X-ray diffraction crystallography. The manuscript has been prepared for submission to *Chem. Sci*. The conception and design of the study was defined by Professor Lubell and Professor Toniolo (Department of Chemistry, University of Padova, Italy). I performed all the experimental, characterization, crystallization and NMR studies. Dr. Crisma performed the FT-IR studies of both tripeptides at different concentrations in solution. I wrote the original draft of the manuscript which was edited by Dr. Crisma and Professors Lubell and Toniolo.

In Chapter 5, I have written the conclusion and perspectives of this thesis, which were edited by Professor Lubell.

Table of contents

List of Figures

List of Schemes

List of Tables

List of abbreviations

[α]	specific rotation
c	concentration
°C	degree Celsius
NMR	*nuclear magnetic resonance*
J	coupling constant (in NMR)
MHz	megahertz (in NMR)
ppm	parts per million (in NMR)
br	broad (in NMR)
s	singlet (in NMR)
d	doublet (in NMR)
t	triplet (in NMR)
dd	doublet of doublet (in NMR)
m	multiplet (in NMR)
COSY	correlation spectroscopy
HMBC	heteronuclear Multiple Bond Correlation
NOESY	nuclear overhauser effect spectroscopy
DEAD	diethyl azodicarboxylate
DIAD	diisopropyl azodicarbocylate
DPPA	diphenylphosphoryl azide
TFA	trifluoracetic acid
eq	equivalent
FA	formic acid
Fmoc	fluorenylmethyloxycarbonyl
Bn	benzyl
Cbz	benzyloxycarbonyl

Boc	*tert*-butoxycarbonyl
t-Bu$(Me)_2$SiCl	*tert*-butyldimethylsilyl chloride
h	hours
HPLC	high performance liquid chromatography
HRMS	high resolution mass spectrometry
IR	infrared
DIPEA	*N*,*N*-diisopropylethylamine
DIC	*N*,*N*-diisopropylcarbodiimide
NMM	*N*-methyl morpholine
TBTU	2-(1H-benzotriazole-1-yl)-1,1,3,3-tetramethylaminium tetrafluoroborate
HBTU	2-(1H-benzotriazol-1-yl)-1,1,3,3-tetramethyluronium hexafluorophosphate
HOAt	hydroxy-azabenzotriazole
HOBt	hydroxybenzotriazole
IBC	isobutyl chloroformate
L	liter
LCMS	liquid chromatography mass spectrometry
Me	methyl
Et	ethyl
i-Pr	*iso*-propyl
t-Bu	*Tert*-butyl
mp	melting point
TLC	thin layer chromatography
R_f	retention factor (in chromatography)
RT	retention time
rt	room temperature
SAR	structure−activity relationship
CuAAC	copper-catalyzed azide-alkyne cycloaddition
GPCR	G-protein-coupled receptor

FP	prostaglandin F2α receptor
PGF2α	prostaglandin F2α
SMAC	Second mitochondria-derive activator of caspase
Aib	2-Aminoisobutyric acid
Adm	Adamantane amino acid
Ac_nc	1-aminocyclalkane-1-carboxylic acid
Ac	acetyl

In memory of my parents

To my family

With love and eternal appreciation

Acknowledgement

I would like to take this opportunity to express my gratitude for my thesis supervisor, Professor William D. Lubell for welcoming me and trusting me to be part of his group. It was an honor for me to be his student during my PhD research studies. His knowledge, patient guidance and encouragement enabled this great desire of my life to become a reality. This thesis would never have been possible without his tireless efforts. No words can express my respect and gratitude for him.

I would like to thank my thesis committee, Professor Andreea-Ruxandra Schmitzer and Professor Stephen Hanessian for all their encouragement and guidance during my stay at the Université de Montréal.

I am grateful to all the past and present members of the Lubell group for sharing their knowledge, their experience, their wisdom and their friendship. I thank especially Dr. Yésica Garcia-Ramos and Dr. Mariam Traoré creating a dynamic friendly work environment, Dr. Mohamed Atfani and Azade Geranurimi for all their support, and Julien Poupart and Cynthia Crifar for their assistance with the French language.

I acknowledge the assistance of members of the Université de Montreal facilities: Dr. Alexandra Fürtös, Karine Gilbert, Marie-Christine Tang and Louiza Mahrouche for HRMS and LCMS analyses; Dr. Pedro Aguiar, Cedric Malveau, Sylvie Bilodeau and Antoine Hamel for NMR analyses; Tierry Maris and Françine Bélanger for X-ray diffraction analyses; Denis Deschenes and Kevin Delorme for FT-IR analyses.

I am indebted to our collaborators, Dr. Sylvain Chemtob and Xin Hou from Sainte-Justine Hospital, and Professor Claudio Toniolo and Dr. Marco Crisma from the Institute of Biomolecular Chemistry, University of Padova. Thank you for your interest, passion and patience in sharing your knowledge.

I would like to thank my family to whom I owe a great deal for your continuous support and encouragement. I am sincerely thankful for the roles played by my parents, who passed before the completion of my thesis. My mother and father made numerous sacrifices for me and my siblings for which we will be always grateful. Many thanks go to my brothers and sister.

Finally, I would like to thank my husband Mehdi, and my son Karan, I could not be able to finish this work without their patience, kindness and support.

Chapter 1 : Introduction

1.1 Peptides

1.1.1 Geometric Representations

Amino acids are the building blocks of peptides and proteins. There are twenty different amino acids that usually occur in protein structures. A typical amino acid has an amine ($-NH_2$) and a carboxylate functional group ($-CO_2H$). These two functional groups are attached to a central carbon atom, which is referred to as C^{α} (Figure 1.1). Furthermore, the side chain R group is usually attached to C^{α}, and gives unique character and specific properties to the amino acid. Amino acid side chains can have hydrophilic (basic, acidic and uncharged) and hydrophobic character. These features, the amino acid sequence in the polypeptide, and the environment, all may act to establish the folded structure of a protein.

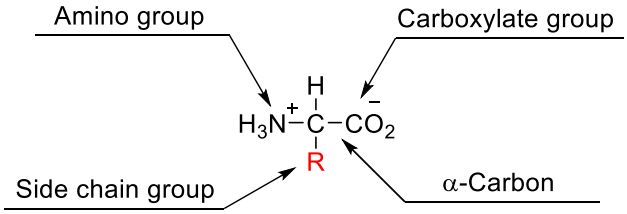

Figure 1.1. The general formula of an amino acid with amine and carboxylate groups ionized at pH 7.0.

The peptide bond is a chemical bond that forms between the amine group of one amino acid and the carboxyl group of the other amino acid. Formation of amide bonds between amino acids gives rise to longer peptide and protein chains (Figure 1.2).

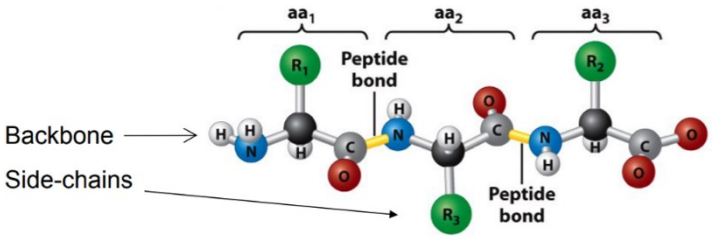

Figure 1.2. The general formula of a peptide backbone structure.[1]

Peptides adopt unique three dimensional structures to perform specific functions,[2] but their formation from the linear sequence remains unpredictable. Four types of peptide structure have been introduced by Kaj Ulrik Linderstrøm-Lang in 1952.[3] The linear sequence of amino acids is

known as *Primary structure*. This sequence is specified by genetic information.[4] *Secondary structure* forms when the peptide chain folds at localized portions of the backbone by intramolecular hydrogen bonds and repeating ϕ and ψ angles. α-Helices,[5] β-strands[6] and turns[7-8] are the major secondary structural elements.[4] The three-dimensional position of the peptide atoms in space represents its *Tertiary structure.* This structure is mostly stabilized by the formation of a hydrophobic core, as well as through hydrogen bonds, salt bridges and disulfide bonds. Association of two or more polypeptide chains (protein *subunits*) with their own tertiary structure in a larger complex, is referred to as *Quaternary structure.*

For the transformation from unfolded chains to highly ordered protein structures, different intramolecular contacts compensate to overcome the entropic and enthalpic penalties for folding and breaking interactions with solvent. For example, many amino acid residues in peptides and proteins have nonpolar side chains, which exhibit poor solubility in water and aggregate in aqueous media. The hydrophobic effect describes the insolubility and clustering of these nonpolar residues in aqueous environment, and serves as a lead contributor to protein folding and conformational stabilization contingent on the size and shape of buried side chains.[9-10] Experiments on 22 proteins with 36 to 534 residues showed that approximately 60% of the overall stability of small-to-medium sized proteins is due on average to the hydrophobic effect.[11]

The hydrogen bond is a type of non-covalent bond that is formed between electronegative acceptor atoms (N, O and to some extend S) and hydrogen bond donors (usually NH or OH). Hydrogen bonds are crucial in protein folding, secondary structure formation, and molecular recognition. Unfolded protein side chain and backbone residues make hydrogen bonds with solvent. Upon folding, these contacts will break with a loss of energy that may be compensated by intramolecular hydrogen bonding to give rise to specific conformations in the polypeptide chain. α-Helices and β-sheets are among the most stable conformations of polypeptide chains, because they maximize respectively intra- and inter-chain hydrogen-bonding potential.[10,12]

Non-covalent, pH dependent contacts between proximal positively and negatively charged residues are known as salt bridges. Electrostatic attractions in salt bridges can stabilize polypeptide folding. For example, negatively charged Asp and Glu side chains may associate with their positively charged Arg, Lys and His counterparts at local sites in peptides to stabilize folded structures. Less important than hydrophobic and hydrogen bond interactions, optimized charged interactions can significantly increase the stability of folded proteins.[13-14]

Disulfide bonds may stabilize folded peptide and protein structures by reducing conformational entropy and destabilizing the unfolded state. Disulfide bonds form upon oxidation of thiol side chains of cysteine residues. Clustering of hydrophobic residues around disulfide bonds can also entropically stabilize folded proteins.[15]

1.1.2 Backbone Conformation

The backbone conformation and consequently the secondary structures of peptides and proteins are defined by the torsion angles (dihedral angles) ϕ, ψ and ω of each residue. The angle of rotation about the amide carbonyl carbon and nitrogen atoms is called omega (ω) (Figure 1.3). Amide bond resonance rigidifies the peptide bond to planar geometry restricting ω torsion angle values to 0° and 180° when the neighboring backbone atoms are respectively in *E-cis* and *Z-trans* conformations.[16] The angles of rotation about N-C^{α} and C^{α}-C are called respectively phi (ϕ) and psi (ψ) (Figure 1.3). A clockwise rotation about either bond, as observed from the *N*- to *C*-direction is assigned as a positive value.

Each residue can adopt a defined range of ϕ and ψ angles, due to steric and stereochemical restrictions of the side chains. The dihedral angles are defined as 180° when the polypeptide is in the extended planar conformation, and the ϕ and ψ angles are define to be 0° when the amide bond and one of the two bonds on each side of C^{α} are in the same co-planar orientation.[1]

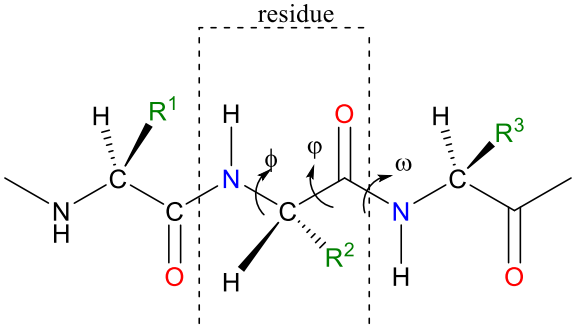

Figure 1.3. The backbone dihedral angles ϕ, ψ and ω at 180° values in an extended peptide chain.

1.1.3 The Ramachandran plot

In 1965, G. N. Ramachandran and coworkers graphed the ϕ and ψ values of amino acid residues creating the so-called Ramachandran plot (Figure 1.4).[17] Plotting of individual peptide residue ϕ and ψ values demonstrated that certain residues adopted specific energetically favorable conformations.[17-18] For example, glycine has a broad range of ϕ and ψ angle values

due to the absence of a side chain (C^{β}) and symmetry. The allowed ϕ and ψ region (57%) of glycine is significantly greater than that for alanine (20%),[19] and other side chain containing amino acids due to steric hindrance. In proline, the side chain is covalently bound to the amine nitrogen in a five-membered pyrrolidine ring that reduces significantly rotation about the N-C^{α} bond limiting the ϕ value around $-60°$. Moreover, steric interactions with the ring restrict the ψ value to two minima at $\psi = -55$ and $+145°$.[20] Incapable of serving as a hydrogen bond donor, proline is frequently found in turns and at the end of helices, and plays roles as a sheet and helix disruptor.

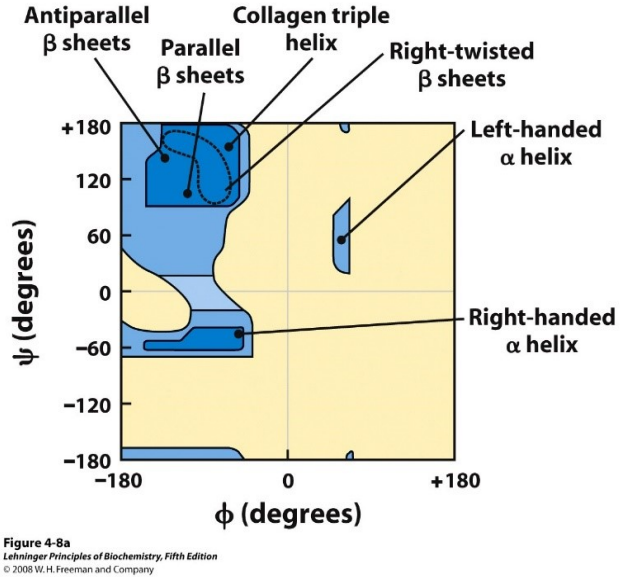

Figure 1.4. A typical Ramachandran plot with the ϕ and ψ value for various allowed secondary structures.[1]

Peptide secondary structures are contingent upon backbone dihedral angle values. The Ramachandran plot provides a means to distinguish between favorable and unfavorable conformations. Three major secondary structures correlate with allowed regions (blue color, Figure 1.4). β-Sheets, α-helix and α_L-helix are respectively distributed in the upper left, lower left and upper right quadrants. The β-sheets region is broad and contains different clusters including parallel and antiparallel β-sheets. In disallowed conformations of the yellow regions, the distance between peptide atoms becomes closer than the sum of their van der Waals radii. Glycine does not

possess any side chain, and can adopt ϕ and ψ angles in all four quadrants. Glycine is observed in peptide turn regions in which other residues would be too sterically hindered.[1]

1.1.4. Peptide secondary structure elements

Packing of nonpolar, hydrophobic side chains creates a hydrophilic core and hydrophilic outer faces. Hydrophilic backbone carbonyl and amino groups may operate as proton acceptors and donors to form hydrogen bonds with the environment, or intramolecular hydrogen bonding patterns known as secondary structures: e.g., α-helices, β-sheets and turns. Among helical secondary structures, the α-helix is characterized by a 3.6 amino acid per turn repeat with ideal ϕ and ψ dihedral angles values at −57° and −47°, and a hydrogen bond between the i to $i + 4$ residue amide carbonyl oxygen and NH groups.[5] Other helix conformations known as the 3_{10}[21] (3 residues, 10 atoms per turn) and π-helix[22] (4.1 residues per turn) feature respectively hydrogen bonds between residues i and $i + 3$, and i and $i + 5$.

The β-sheet secondary structures are pleated conformations featuring β-strands, which are chains of 3 to 10 residues with extended backbones that pair together through intermolecular hydrogen bonds.[23] Turns are secondary structures that change the peptide direction, and are important domains in molecular recognition and folding.[24] Helices may be considered as multiple conjoined turns.

Different classes of turns are categorized based on the backbone dihedral angles and the size of the cycle that forms between residue i and residue $i + n$: δ-, γ-, β-, α- and π-turns.[7] The smallest turn called the δ-turn (also called C_8-conformation) features an intramolecular hydrogen bond between the backbone NH of residue $i + 1$ and the carbonyl of residue $i + 2$,[8,25] and requires a central *cis* amide disposition.[25]

γ-Turns involve intramolecular hydrogen bonds between the backbone NH of residue i and the carbonyl of residue $i + 2$. The *trans* amide groups are situated in two planes and make an angle about 115°. Two conformers are possible with equatorial and axial projection of the side chain R at the central residue (Figure 1.5). The ideal backbone torsion angles ϕ and ψ for an L-residue are respectively $-75°$ and $+65°$ for the equatorial more stable, inverse γ-turn, and $+75°$ and $-65°$ for the axial less stable, classical γ-turn.[8, 26-27] In spite of a strongly bent hydrogen bond, the distance between H(i)···O($i + 2$) is normal and may thus contribute in the stabilization of the folded peptide.

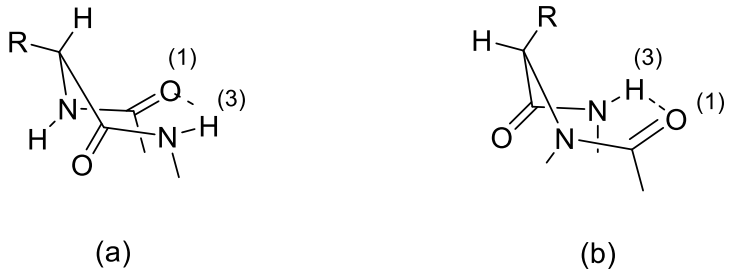

Figure 1.5. The (a) equatorial and (b) axial 3→1 intramolecular H-bond (C_7) in peptide γ-turns

The β-turn (also called the C_{10} form) involves an intramolecular hydrogen bond between the backbone NH of residue *i* and the carbonyl oxygen of residue *i* + 3 (Figure 1.6).[7,28] β-Turns are important structures for protein folding,[29] and molecular recognition.[24] First recognized in silk proteins by Geddes, three types of β-turn (I-III and their mirror images I′-III′) were stereochemically defined by Venkatachalam.[30] Later, Hutchinson and Thornton defined nine types of β-turn, namely types I, I', II, II', III, VIa1, VIa2, VIb and IV,[31] based on the criterion that the distance between C^{α} of residue *i* and the residue *i* + 3 must be less than 7 Å and the structures are not helical.[7] The dihedral angles of residues *i* + 1 and *i* + 2 are used to define the different β-turn types (Table 1.1).[31]

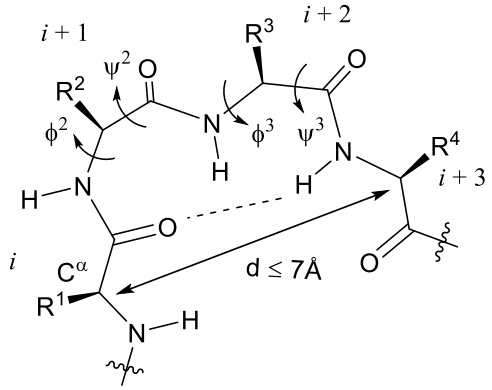

Figure 1.6. Representative β-turn conformation

Table 1.1. Dihedral angle values for different β-turn types

Type of β−turn	ϕ^1	ψ^1	ϕ^2	ψ^2
I	−60	−30	−90	0
II	−60	120	80	0
I’	60	30	90	0
II’	60	−120	−80	0
VIa1	−60	120	−90	0
VIa2	−120	120	−60	0
VIb	−135	135	−75	160
VIII	−60	−30	−120	120
IV	Other values			

The α-turn (C_{13} form) features an intramolecular hydrogen bond between the backbone NH and carbonyl oxygen of the *i* and *i* + 4 residues which lie at a C^{α}–C^{α} distance of < 7 Å.[8] Rarer and less well studied than γ- and β-turns, α-turns exist in pentapeptide chains that are not part of helical secondary structures.[32-33] In 1996, Pavone conducted a systematic search on 190 proteins, from which nine different α-turn types were classified, based on backbone dihedral angles of residues *i* + 1, *i* + 2, and *i* + 3.[32] In the right- and left-handed α-helices, the ϕ and ψ dihedral angles are respectively −57°, −47°, and +57°, +47°, and the amide bonds are in the *trans* conformation.[8,32]

The largest turns involved in intramolecular hydrogen bonds, π-turns exist between backbone NH and carbonyl oxygen of the *i* and *i* + 5 residues.[7] Rajashankar and Ramakumar

classified four types of π-turns based on the dihedral angles of the *i* +1 to *i* + 4 residues.[34] The dihedral angles of all four types have similar values with opposite signs.[34-35]

1.2 Peptide-based drug discovery and peptidomimetics

Natural and man-made peptides are often employed in drug discovery, because of their capacity to mimic and block physiological pathways.[36] Since the advent of insulin in 1922 and its application as treatment of diabetes,[37-38] diverse peptides have been explored as potential drugs. Over 60 peptide drugs have been approved by the FDA for the treatment of various indications including osteoporosis,[39] gastrointestinal problems,[40] cancers[41] and bacterial infections.[36, 42]

Despite their potential, peptides have limited utility due in part to their poor bioavailability, low stability and lack of selectivity.[43] To improve the pharmacological properties of natural peptides and retain their biological potency, synthetic molecules with alternative structures, so called peptidomimetics have emerged as tools for peptide-based medicinal chemistry. By restricting peptide flexibility using covalent, steric and electronic constraints, peptidomimetics can serve to obtain information on the biologically active conformation of the native peptide when bound to its receptor target.[44]

A wide range of peptidomimetics have been developed to replicate turn secondary structures. For example, Freidinger lactams,[45-47] azabicycloalkanone amino acids[48-50] and benzodiazepinones,[51] all have proven successful as covalent constraints to favor β−turn geometry (Figure 1.7). The use of electronic constraints in azapeptides and fluoroprolines has proven an alternative strategy to promote β-turn conformation. Moreover, steric constraints produced by C^{α}-C^{α}-disubstituted glycines and 5-*tert*-butyl proline have been used to induce peptide backbones to adopt turn topology.[52-53]

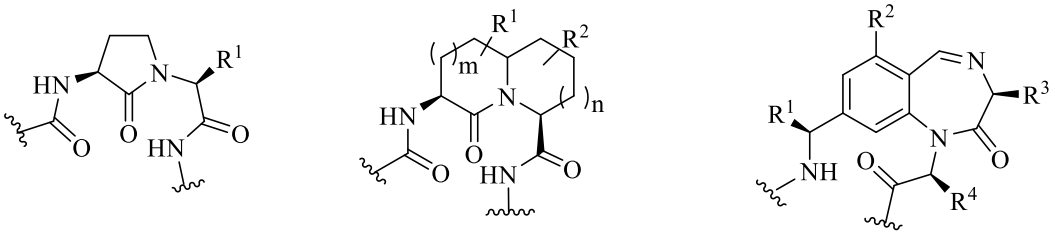

Freidinger Lactam | Azabicyclo[X.Y.0]alkanone | Benzodiazepinone (BDZ)

Figure 1.7. Examples of covalent constraints that favor β-turn conformation

1.2.1. Azapeptides

Azapeptides are a class of peptide mimic in which the C^{α} unit of at least one amino acid is substituted by a nitrogen atom introducing a semicarbazide as an amino amide surrogate.[54-55] This structural modification can increase metabolic stability and protease resistance due to the replacement of the amide bond by a urea function. Moreover, lone pair-lone pair electron repulsion between the two adjacent hydrazine nitrogen (NH-N^{α}) and urea palanarity (N^{α}-CO-NH) impose constraints on the ϕ and ψ dihedral angles. The combination of these properties accompanied with dynamic chirality at N^{α} can favour β−turn geometry as illustrated by computational analyses, CD and NMR spectroscopy, and X-ray crystallography (Figure 1.8).[54,56]

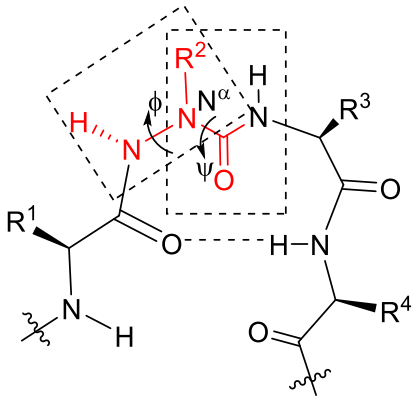

Figure 1.8. Representative azapeptide β–turn conformation

Azapeptides are attractive tools for drug design. Since the synthesis and evaluation of [azaVal[3]] angiotensin II (bovine, Asp-Arg-azaVal-Tyr-Val-His-Pro-Phe) in 1963, which exhibited longer duration of action but lower potency relative to its peptide analog in a standard blood pressure assay,[57] several aza-analogs have been tested and demonstrated varying degrees of activity.[55] Among them the luteinizing hormone-releasing hormone (LH-RH) agonist [D-Ser(*t*-Bu)[6], azaGly[10]]-LH-RH (**1**, Zoladex®, AstraZeneca) is employed for the treatment of prostate and breast cancer (Figure 1.9).[58] Atazanavir (**2**, Reyataz®, Bristol Myers) is another approved azapeptide drug that acts as an HIV protease inhibitor.

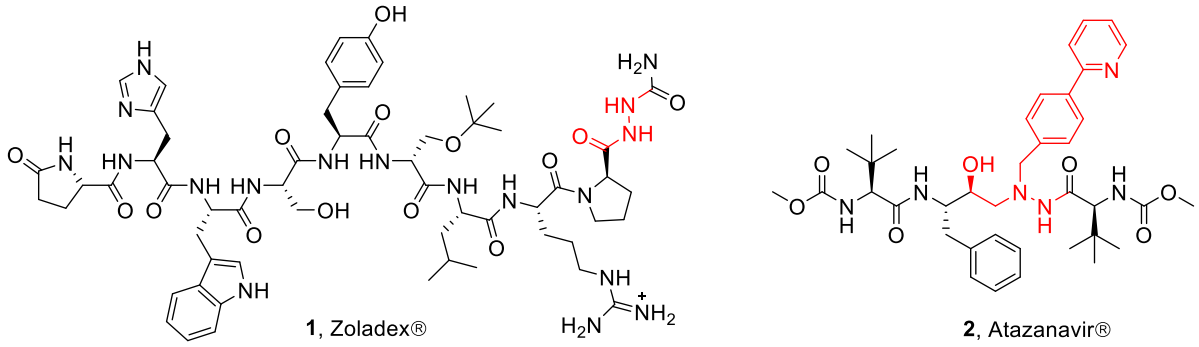

Figure 1.9. The chemical structures of Zoladex® and Reyataz®

1.2.2 C^{α}-Disubstituted glycines

C^{α}−Disubstituted glycines cause steric constraints that restrict the peptide backbone to favor specific secondary structures.[59-60] The α,α-disubstituted amino acid may also enhance metabolic stability and increase potency and receptor selectivity.[59, 61-63]

α−Aminoisobutyric acid (Aib) is a constituent of natural peptaibol antibiotics,[64] such as I.C.I. 13959,[65] alamethicin[66] and zervamicin.[67] In the Ramachandran plot, Aib occupies only 1% of the total surface, compared to 18% and 54% respectively for Ala and Gly.[68-69] The gem-dimethyl group on C^{α} imparts restriction to the right- and left-handed α-helixes ($\phi = \pm 57°$, $\psi = \pm 47$) and 3_{10}-helixes ($\phi = \pm 60°$, $\psi = \pm 30°$),[70] as characterized by X-ray analyses.[70-73]

X-ray diffraction analysis as well as FT-IR and NMR spectroscopy in solvents of low polarity (e.g., $CDCl_3$) have shown that achiral α,α-dialkylglycines with longer alkyl substituents (e.g. $C^{\alpha,\alpha}$-diethyl-,[74-75] $C^{\alpha,\alpha}$-di-*n*-propyl-,[75] $C^{\alpha,\alpha}$-di-*n*-butyl-,[71] $C^{\alpha,\alpha}$-dibenzyl-[76] and $C^{\alpha,\alpha}$diphenylglycine[77]), as well as 9-amino-9-fluorenecarboxylic acid,[78] all prefer to adopt extended C_5-conformations. Increased side-chain length forces these residues into extended conformations to diminish steric interactions along the backbone. Consequently, the energy difference between fully extended and helical conformation decreases. The stability order of 3_{10}-(and α-) helices versus the fully extended conformation is strongly contingent on the (N-C^{α}-C') τ angle. The τ value of $\leq 107°$ favors a fully extended conformation over the helical structure.[79]

The calculation of conformational energy and X-ray analysis of 1-amino-1-cyclopropane carboxylic acid (Ac_3c) analogs have demonstrated a preference for the region in which ϕ and ψ torsion angles are 90 ° and 0°, respectively. This region corresponds to the $i + 2$ position of type

I/I' and type II/II' β-turns.[70] On the other hand, the computational and experimental studies of 1-amino-1-cyclopentane carboxylic acid analogs demonstrated a preference to adopt regular type III β-bends or 3_{10}-helices with envelope or half chair conformations.[80-81] Although computation suggested the backbone torsion angles of 1-amino-1-cyclohexane carboxylic acid analogs (Ac_6c, **3a,** Figure 1.10) may adopt γ-turn and α/3_{10}-helical forms with the cyclohexane ring in chair conformation and the amino substituent in axial orientation,[82-83] the X-ray and solution state analyses have revealed Ac_6c oligomers in 3_{10}-helices.[70] Increasing bulkiness on the cyclohexane moiety by introducing a phenyl group at the *β*-position was shown by computation and experimentation to stabilize the γ-turn geometry with $\phi = 74.2°$ and $\psi = -30.5°$ and a hydrogen bond between the carbonyl group of residue *i* and the NH group of residue *i* + 2 (**4**, Figure 1.10).[84]

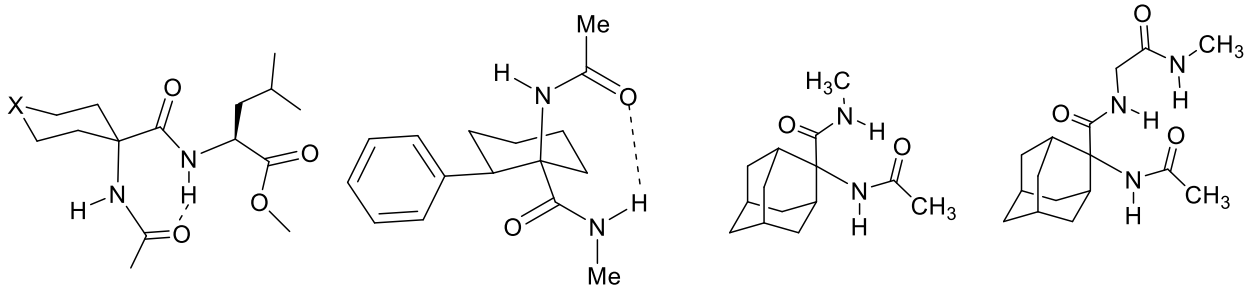

3a: X = S
3b: X = CH_2

4 **5** **6**

Figure1.10. Representative peptides that may favor γ-turn geometry due to bulky C^{β} substituents

2-Amino-adamantane-2-carboxylic acid (Adm) was also shown by spectroscopic methods to be a γ-turn inducer in model peptides **5** and **6** (Figure 1.10).[85] In Ac-Xaa-NHMe, the *C*-terminal amide is shifted further downfield in the NMR spectrum of X = Adm relative to X = Aib or Gly indicative of an intramolecular seven-membered hydrogen bond, which is less influenced by changes in solvent composition relative to the *N*-terminal NH.[26, 85]

The poor reactivity of Adm has however retarded efforts to prepare longer oligomers. In a noteworthy effort, the Toniolo laboratory synthesized a set of Adm dipeptides,[27] using the α-azido acyl chloride approach.[86] By this method, they could couple a maximum of three consecutive Adm residues to provide 'N_3'-Adm_3-OH; however, the last coupling yield dropped to 9% and prevented further elongation. Analysis of 15 analogs by X-ray crystallography demonstrated that two had torsion angles within the helical region (e.g., Z-Adm-OH: $\phi = -57°$ to $-61°$ and $\psi = -51°$ to $-66°$), and the other 13 analogs exhibited ϕ and ψ dihedral angles belonging to the γ-

turn region ($\phi = -73°$ to $-76°$ and $\psi = 83°$ to 96°). Only five analogs met the C=O···H-N C_7-intramolecular hydrogen bond distance (<2.55Å) characteristic of normal γ-turns. The other eight adopted so-called "open γ-turn" structures. The average τ angle value (104.5°) for the Adm residues showing a preference for γ-turn conformers was smaller than the standard tetrahedral value (109.5°) and values of Adm residues in helical conformation (106.9°).[27]

Solid state analysis of the analog 'N_3'-$(Adm)_3$-NH*i*Pr' showed two consecutive regular γ-turns with hydrogen bonds in an incipient of the fully developed γ-helix (C_7-helix). Three consecutive γ-turns have however yet to be observed.

1.3 Project aims and objectives

1.3.1 Study of the relationships between azapeptide and indolizidin-2-one turn mimics in labor-delaying modulators of the prostaglandin F2α receptor

Natural proline is known to adopt the $i + 2$ position of type I and type II β-turns.[24] Aza-residues (e.g., azaAsn, azaAsp and azaAla) *N*-terminal to proline have been shown by X-ray crystallography to adopt the $i + 1$ position of type I β-turns in model dipeptides,[87] in which the aza-residue exhibits *R*-chirality. Computational analyses of model azapeptide (e.g., Ac-aza-Gly-Ala-NHMe and Ac-aza-Ala-Ala-NHMe) have demonstrated that although the type I β-turn is an energy minimum, the corresponding type II β-turn is less than a kcal higher in energy.[56]

(*S*,*S*,*S*)-Methyl 3-*N*-(Boc)-amino indolizidin-2-one-9-carboxylate (Boc-I^2aa-OMe) has previously been shown by X-ray crystallography to exhibit dihedral angle geometry similar to type II' β-turn. In calcitonin gene-related peptide antagonists, replacement of the Gly-Pro dipeptide by I^2aa and azaGly-Pro residues gave analogs with 7- and 10-fold greater potency.[49] Similarly, increased caspase-9 mediated apoptotic cell death has been exhibited relative to the parent Ala-Val-Pro-Ile Smac (second mitochondria-derived activator of caspase) protein mimic by analogs in which the Val-Pro dipeptide was swapped for aza-amino acyl proline and I^2aa residues.[88-89] Finally, aza-amino acyl proline counterparts of the I^2aa analog PDC113.824 have been shown to inhibit myometrial contractions with similar efficacy by way of modulation of the prostaglandin F2α receptor (FP).[50]

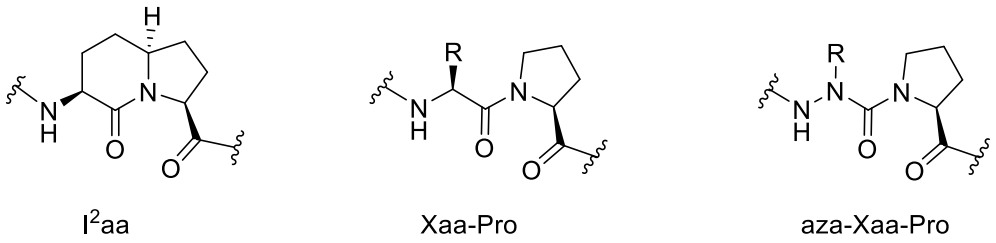

Figure 1.11. Peptide fragments containing I^2aa, X-aa-Pro, and azaXaa-Pro motifs

In light of this knowledge, the synthesis of various aza-amino acyl proline analogs was investigated to gain a better understanding of the impact of the aza-residue side chain and proline residue on allosteric modulation of FP towards inhibitors of preterm labor. Different diversity-oriented synthesis methods were explored to introduce a variety of side chains onto the aza-amino acyl proline modulators featuring alkylation of aza-glycinyl-proline analogs as well as copper catalyzed reactions on aza-propargylglycinyl residues. Moreover, a solid-phase method was developed for the preparation of modulators in which hydroxyproline was employed to synthesize fluoroproline and aminoproline analogs. The potency of the analogs in reducing myometrial contractions was tested in the laboratory of Professor S. Chemtob in the Departments of Pediatrics of the Université de Montréal. Moreover, the aza-Gly-Pro and aza-Phe-Pro analogs were shown to delay labor in a model of premature birth. The results of this study form part of a larger manuscript that is presented in Chapter 2.

1.3.2 Exploration of the factors influencing Adm residue conformation

Towards the goal to synthesize Adm oligomers that may adopt a γ-helix conformation with three consecutive γ-turns, a multiple component Ugi reaction sequence was conceived. In Chapter 3, this approach was used to synthesize a series of di- and tripeptides to explore the influence of the *C*-terminal amide on Adm residue conformation. Subsequently in Chapter 4, two Adm trimers were prepared having respectively *i*-Pr and *t*-Bu *C*-terminal amides. Information on the conformational preferences of these oligomers was obtained using a combination of X-ray crystallographic analysis, as well as NMR and FT-IR spectroscopy studies.

1.4. Conclusion

This thesis describes applications of electronic and steric interactions to control peptide folding and to study the biological activity of allosteric modulators of the prostaglandin-F2α (PGF2α) receptor (FP). Novel approaches have been developed for synthesizing libraries of

azapeptides, which were examined as modulators of FP and tested for ability to inhibit PGF2α-induced uterine contractions. The structure-activity relationships from examination of the azapeptides have provided information on the requirements for modulator activity as well as promising leads for the development of therapeutic agents to delay preterm birth. Towards the application of steric interactions to control peptide folding, novel methods for the synthesis of peptides bearing 2-amino adamantane-2-carboxylic acid (Adm) residues were conceived and used to examine the influence of *C*-terminal amides on Adm oligomer conformation. As demonstrated by X-ray crystallography, the Adm analogs can adopt a range of α-, β- and γ-turn in the solid state, contingent on the *C*-terminal amide. In sum, this thesis provides effective synthetic methods for the synthesis and use of aza- and bulky C^{α}-disubstituted amino acid analogs for studying the folding and biomedical applications of peptide structures.

References for Chapter 1

1. Nelson, D. L., Lehninger, A.L.; Cox, M. M., *Lehninger Principles of Biochemistry.* Macmillan: 2008.
2. Fersht, A., A guide to Enzyme Catalysis and Protein Folding. *Structure and Mechanism in Protein Science* **1999**, 508-539.
3. Linderstrøm-Lang, K. U., *Lane Medical Lectures: Proteins and Enzymes*. Stanford University Press: 1952; Vol. 6.
4. Nelson, D. L.; Cox, M. M., Biological membranes and transport. *Lehninger Principales of Biochemistry* **2000**, *3*, 389-436.
5. Pauling, L.; Corey, R. B.; Branson, H. R., The structure of proteins: two hydrogen-bonded helical configurations of the polypeptide chain. *Proc. Natl. Acad. Sci.* **1951**, *37*, 205-211.
6. Pauling, L.; Corey, R. B., Configurations of polypeptide chains with favored orientations around single bonds two new pleated sheets. *Proc. Natl. Acad. Sci.* **1951**, *37*, 729-740.
7. Chou, K.-C., Prediction of tight turns and their types in proteins. *Anal. Biochem.* **2000**, *286*, 1-16.
8. Toniolo, C.; Benedetti, E., Intramolecularly Hydrogen-Bonded Peptide Conformation. *Critical Reviews in Biochemistry* **1980**, *9*, 1-44.
9. Rose, G. D.; Geselowitz, A. R.; Lesser, G. J.; Lee, R. H.; Zehfus, M. H., Hydrophobicity of amino acid residues in globular proteins. *Science* **1985**, *229*, 834-838.
10. Rose, G. D.; Wolfenden, R., Hydrogen bonding, hydrophobicity, packing, and protein folding. *Annu. Rev. Biophys. Biomol. Struct.* **1993**, *22*, 381-415.
11. Pace, C. N.; Fu, H.; Fryar, K. L.; Landua, J.; Trevino, S. R.; Shirley, B. A.; Hendricks, M. M.; Iimura, S.; Gajiwala, K.; Scholtz, J. M., Contribution of hydrophobic interactions to protein stability. *J. Mol. Biol.* **2011**, *408*, 514-528.
12. Hubbard, R. E.; Kamran Haider, M., Hydrogen bonds in proteins: role and strength. *Encyclopedia of Life Science*. Wiley: New York, 2010.
13. Bosshard, H. R.; Marti, D. N.; Jelesarov, I., Protein stabilization by salt bridges: concepts, experimental approaches and clarification of some misunderstandings. *J. Mol. Recognit.* **2004**, *17*, 1-16.

14. Strickler, S. S.; Gribenko, A. V.; Gribenko, A. V.; Keiffer, T. R.; Tomlinson, J.; Reihle, T.; Loladze, V. V.; Makhatadze, G. I., Protein stability and surface electrostatics: a charged relationship. *Biochemistry* **2006**, *45*, 2761-2766.
15. Wedemeyer, W. J.; Welker, E.; Narayan, M.; Scheraga, H. A., Disulfide bonds and protein folding. *Biochemistry* **2000**, *39*, 4207-4216.
16. Ramachandran, G. N.; Ramakrishnan, C.; Sasisekharan, V., Stereochemistry of polypeptide chain configurations. *J. Mol. Biol.* **1963**, *7*, 95-99.
17. Ramakrishnan, C.; Ramachandran, G., Stereochemical criteria for polypeptide and protein chain conformations: II. Allowed conformations for a pair of peptide units. *Biophysical Journal* **1965**, *5*, 909-933.
18. Hollingsworth, S. A.; Karplus, P. A., A fresh look at the Ramachandran plot and the occurrence of standard structures in proteins. *Biomol. concepts* **2010,** *1*, 271-283.
19. Ramakrishnan, C.; Srinivasan, N., Glycyl residues in proteins and peptides: an analysis. *Current Science* **1990**, *59*, 851-862.
20. Schimmel, P. R.; Flory, P. J., Conformational energies and configurational statistics of copolypeptides containing L-proline. *J. Mol. Biol.* **1968**, *34*, 105-120.
21. Tonlolo, C.; Benedetti, E., The polypeptide 3_{10}-helix. *Trends biochem. Sci.* **1991**, *16*, 350-353.
22. Low, B. W.; Baybutt, R., The π helix—a hydrogen bonded configuration of the polypeptide chain. *J. Am. Chem. Soc.* **1952**, *74*, 5806-5807.
23. Pauling, L.; Corey, R. B., The pleated sheet, a new layer configuration of polypeptide chains *Proc. Natl. Acad. Sci.* **1951**, *37*, 251-256.
24. Rose, G. D.; Glerasch, L. M.; Smith, J. A., Turns in peptides and proteins. *Adv. in Protein Chem.* **1985**, *37*, 1-109.
25. Toniolo, C.; Crisma, M.; Moretto, A.; Peggion, C.; Formaggio, F.; Alemán, C.; Cativiela, C.; Ramakrishnan, C.; Balaram, P., Peptide δ-Turn: Literature Survey and Recent Progress. *Chem. Eur. J.* **2015**, *21*, 13866-13877.
26. Némethy, G.; Printz, M. P., The γ turn, a possible folded conformation of the polypeptide chain. Comparison with the β turn. *Macromolecules* **1972**, *5*, 755-758.

27. Mazzier, D.; Grassi, L.; Moretto, A.; Alemán, C.; Formaggio, F.; Toniolo, C.; Crisma, M., En route towards the peptide γ-helix: X-ray diffraction analyses and conformational energy calculations of Adm-rich short peptides. *J. Pept. Sci.* **2017**, *23*, 346-362.
28. Rotondi, K. S.; Gierasch, L. M., Natural polypeptide scaffolds: β-sheets, β-turns, and β-hairpins. *Biopolymers (Peptide Science)* **2006**, *84*, 13-22.
29. Marcelino, A. M. C.; Gierasch, L. M., Roles of β-turns in protein folding: from peptide models to protein engineering. *Biopolymers* **2008**, *89* , 380-391.
30. Venkatachalam, C., Stereochemical criteria for polypeptides and proteins. V. Conformation of a system of three linked peptide units. *Biopolymers* **1968**, *6*, 1425-1436.
31. Hutchinson, E. G.; Thornton, J. M., A revised set of potentials for β-turn formation in proteins. *Protein Science* **1994**, *3*, 2207-2216.
32. Pavone, V.; Gaeta, G.; Lombardi, A.; Nastri, F.; Maglio, O.; Isernia, C.; Saviano, M., Discovering protein secondary structures: Classification and description of isolated α-turns. *Biopolymers* **1996**, *38*, 705-721.
33. Chou, K. C., Prediction and classification of α-turn types. *Biopolymers* **1997**, *42*, 837-853.
34. Rajashankar, K.; Ramakumar, S., π-Turns in proteins and peptides: Classification, conformation, occurrence, hydration and sequence. *Protein science* **1996**, *5*, 932-946.
35. Dasgupta, B.; Chakrabarti, P., π-Turns: types, systematics and the context of their occurrence in protein structures. *BMC structural biology* **2008**, *8*, 39.
36. Lau, J. L.; Dunn, M. K., Therapeutic peptides: Historical perspectives, current development trends, and future directions. *Bioorg. Med. Chem.* **2018**, *26*, 2700-2707.
37. Banting, F. G.; Best, C. H.; Collip, J. B.; Campbell, W. R.; Fletcher, A. A., Pancreatic extracts in the treatment of diabetes mellitus. *Can. Med. Assoc. J.* **1922**, *12*, 141.
38. Rendell, M., Insulin: moments in history. *Drug Dev. Res.* **2008**, *69*, 95-100.
39. Camacho, P. M.; Petak, S. M.; Binkley, N.; Clarke, B. L.; Harris, S. T.; Hurley, D. L.; Kleerekoper, M.; Lewiecki, E. M.; Miller, P. D.; Narula, H. S.; Pessah-Pollack, R.; Tangpricha, V.; Wimalawansa, S. J.; Watts, N. B., American Association of Clinical Endocrinologists and American College of Endocrinology Clinical Practice guidelines for the diagnosis and treatment of postmenopausal osteoporosis—2016. *Endocrine Practice* **2016**, *22*, 1-42.

40. Clemmensen, C.; Müller, T. D.; Woods, S. C.; Berthoud, H.-R.; Seeley, R. J.; Tschöp, M. H., Gut-brain cross-talk in metabolic control. *Cell* **2017**, *168*, 758-774.
41. Chang, Y. S.; Graves, B.; Guerlavais, V.; Tovar, C.; Packman, K.; To, K.-H.; Olson, K. A.; Kesavan, K.; Gangurde, P.; Mukherjee, A., Stapled α-helical peptide drug development: A potent dual inhibitor of MDM2 and MDMX for p53-dependent cancer therapy. *Proc. Natl. Acad. Sci.* **2013**, *110*, 3445-3454.
42. Vlieghe, P.; Lisowski, V.; Martinez, J.; Khrestchatisky, M., Synthetic therapeutic peptides: science and market. *Drug discovery today* **2010**, *15*, 40-56.
43. Mason, J. M., Design and development of peptides and peptide mimetics as antagonists for therapeutic intervention. *Future Med. Chem.* **2010**, *2*, 1813-1822.
44. Grauer, A.; König, B., Peptidomimetics–a versatile route to biologically active compounds. *Eur. J. Org. Chem.* **2009**, *2009*, 5099-5111.
45. Freidinger, R. M.; Veber, D. F.; Perlow, D. S.; Saperstein, R., Bioactive conformation of luteinizing hormone-releasing hormone: evidence from a conformationally constrained analog. *Science* **1980**, *210*, 656-658.
46. Jamieson, A. G.; Boutard, N.; Beauregard, K.; Bodas, M. S.; Ong, H.; Quiniou, C.; Chemtob, S.; Lubell, W. D., Positional scanning for peptide secondary structure by systematic solid-phase synthesis of amino lactam peptides. *J. Am. Chem. Soc.* **2009**, *131*, 7917-7927.
47. Boutard, N.; Jamieson, A. G.; Ong, H.; Lubell, W. D., Structure–Activity Analysis of the Growth Hormone Secretagogue GHRP-6 by α-and β-Amino γ-Lactam Positional Scanning. *Chem Biol Drug Des* **2010**, *75*, 40-50.
48. Cluzeau, J.; Lubell, W. D., Design, synthesis, and application of azabicyclo [X.Y.0] alkanone amino acids as constrained dipeptide surrogates and peptide mimics. *Biopolymers (Peptide Science)* **2005**, *80*, 98-150.
49. Boeglin, D.; Hamdan, F. F.; Melendez, R. E.; Cluzeau, J.; Laperriere, A.; Héroux, M.; Bouvier, M.; Lubell, W. D., Calcitonin gene-related peptide analogs with aza and indolizidinone amino acid residues reveal conformational requirements for antagonist activity at the human calcitonin gene-related peptide 1 receptor. *J. Med. Chem.* **2007**, *50*, 1401-1408.

50. Bourguet, C. B.; Goupil, E.; Tassy, D.; Hou, X.; Thouin, E.; Polyak, F.; Hébert, T. E.; Claing, A.; Laporte, S. A.; Chemtob, S.; Lubell, W. D., Targeting the prostaglandin F2α receptor for preventing preterm labor with azapeptide tocolytics. *J. Med. Chem.* **2011**, *54*, 6085-6097.
51. Hata, M.; Marshall, G. R., Do benzodiazepines mimic reverse-turn structures? *J comput Aided Mol Des* **2006**, *20*, 321-331.
52. Halab, L.; Lubell, W. D., Use of steric interactions to control peptide turn geometry. Synthesis of type VI β-turn mimics with 5-tert-butylproline. *J. org. chem.* **1999**, *64*, 3312-3321.
53. Halab, L.; Lubell, W. D., Influence of *N*-terminal residue stereochemistry on the prolyl amide geometry and the conformation of 5-*tert*-butylproline type VI β-turn mimics. *J. Peptide Sci.* **2001**, *7*, 92-104.
54. Proulx, C.; Sabatino, D.; Hopewell, R.; Spiegel, J.; García Ramos, Y.; Lubell, W., Azapeptides and their therapeutic potential. *Future Med. Chem.* **2011**, *3*, 1139–1164.
55. Gante, J., Azapeptides. *Synthesis* **1989**, *21*, 405-413.
56. Thormann, M.; Hofmann, H.-J., Conformational properties of azapeptides. *Journal of Molecular Structure (theochem)* **1999**, *469*, 63-76.
57. Hess, H.-J.; Moreland, W. T.; Laubach, G. D., N-[2-Isopropyl-3-(L-aspartyl-L-arginyl)-carbazoyl]-L-tyrosyl-L-valyl-L-histidyl-L-prolyl-L-phenylalanine,[1] an Isostere of Bovine Angiotensin II. *J. Am. Chem. Soc.* **1963**, *85*, 4040-4041.
58. Bolla, M.; Collette, L.; Blank, L.; Warde, P.; Dubois, J. B.; Mirimanoff, R.-O.; Storme, G.; Bernier, J.; Kuten, A.; Sternberg, C.; Mattetaer, J.; Lopez Torecilla, J.; Pfeffer J. R.; Cutajar, C. L.; Zurlo, A.; Pierart, M., Long-term results with immediate androgen suppression and external irradiation in patients with locally advanced prostate cancer (an EORTC study): a phase III randomised trial. *The Lancet* **2002**, *360*, 103-108.
59. Tanaka, M., Design and synthesis of chiral α,α-disubstituted amino acids and conformational study of their oligopeptides. *Chem. Pharm. Bull.(Tokyo)* **2007**, *55*, 349-358.
60. Toniolo, C.; Formaggio, F.; Kaptein, B.; Broxterman, Q. B., You are sitting on a gold mine! *Synlett* **2006**, *2006*, 1295-1310.

61. Prasad, S.; Mathur, A.; Gupta, N.; Jaggi, M.; Singh, A. T.; Rajendran, P.; Sanna, V. K.; Datta, K.; Mukherjee, R., Bombesin analogs containing α-amino-isobutyric acid with potent anticancer activity. *J. Pept. Sci.* **2007**, *13*, 54-62.
62. Habashita, H.; Kokubo, M.; Hamano, S.-i.; Hamanaka, N.; Toda, M.; Shibayama, S.; Tada, H.; Sagawa, K.; Fukushima, D.; Maeda, K.; Mitsuya, H., Design, synthesis, and biological evaluation of the combinatorial library with a new spirodiketopiperazine scaffold. Discovery of novel potent and selective low-molecular-weight CCR5 antagonists. *J. Med. Chem.* **2006**, *49*, 4140-4152.
63. Humphrey, J. M.; Chamberlin, A. R., Chemical synthesis of natural product peptides: coupling methods for the incorporation of noncoded amino acids into peptides. *Chem. Rev.* **1997**, *97*, 2243-2266.
64. Benedetti, E.; Bavoso, A.; Di Blasio, B.; Pavone, V.; Pedone, C.; Toniolo, C.; Bonora, G. M., Peptaibol antibiotics: a study on the helical structure of the 2-9 sequence of emerimicins III and IV. *Proc. Natl. Acad. Sci.* **1982**, *79*, 7951-7954.
65. Kenner, G.; Sheppard, R., α-Aminoisobutyric acid, β-hydroxyleucine, and γ-methylproline from the hydrolysis of a natural product. *Nature* **1958**, *181* (4601), 48.
66. Meyer, C.; Reusser, F., A polypeptide antibacterial agent isolated from Trichoderma viride. *Experientia* **1967**, *23*, 85-86.
67. Karle, I. L.; Flippen-Anderson, J.; Sukumar, M.; Balaram, P., Conformation of a 16-residue zervamicin IIA analog peptide containing three different structural features: 3_{10}-helix, α-helix, and β-bend ribbon. *Proc. Natl. Acad. Sci.* **1987**, *84*, 5087-5091.
68. Marshall, G. R., In Intra-Science Chemistry Report. *Kharasch, N., Ed* **1971**, 305-316.
69. Burgess, A. W.; Leach, S. J., An obligatory α-helical amino acid residue. *Biopolymers* **1973**, *12*, 2599-2605.
70. Toniolo, C.; Crisma, M.; Formaggio, F.; Peggion, C., Control of peptide conformation by the Thorpe-Ingold effect (C^{α}-tetrasubstitution). *Biopolymers (Peptide Science)* **2001**, *60*, 396-419.
71. Toniolo, C.; Bonora, G. M.; Bavoso, A.; Benedetti, E.; di Blasio, B.; Pavone, V.; Pedone, C., Preferred conformations of peptides containing α,α-disubstituted α-amino acids. *Biopolymers* **1983**, *22*, 205-215.

72. Toniolo, C.; Benedetti, E., Structures of polypeptides from α-amino acids disubstituted at the α-carbon. *Macromolecules* **1991**, *24*, 4004-4009.

73. Hummel, R. P.; Toniolo, C.; Jung, G., Conformational transitions between enantiomeric 3_{10}-helices. *Angew. Chem. Int. Ed. Engl.* **1987**, *26*, 1150-1152.

74. Benedetti, E.; Barone, V.; Bavoso, A.; Di Blasio, B.; Lelj, F.; Pavone, V.; Pedone, C.; Bonora, G.; Toniolo, C.; Leplawy, M., Structural versatility of peptides from $C^{\alpha,\alpha}$-dialkylated glycines. I. A conformational energy computation and x-ray diffraction study of homo-peptides from $C^{\alpha,\alpha}$-diethylglycine. *Biopolymers* **1988**, *27*, 357-371.

75. Tanaka, M.; Imawaka, N.; Kurihara, M.; Suemune, H., Helical *versus* Planar Conformation of Homooligopeptides Prepared from Diethylglycine (= 2-Amino-2-ethylbutanoic Acid). *Helvetica Chimica Acta* **1999**, *82*, 494-510.

76. Valle, G.; Crisma, M.; Maria Bonora, G.; Toniolo, C., Structural versatility of peptides from $C^{\alpha,\alpha}$-disubstituted glycines. Preferred conformation of the $C^{\alpha,\alpha}$-dibenzylglycine residue. *J. Chem. Soc. Perkin Trans. 2* **1990**, 1481-1487.

77. Pavone, V.; Lombardi, A.; Saviano, M.; Nastri, F.; Zaccaro, L.; Maglio, O.; Pedone, C.; Omote, Y.; Yamanaka, Y.; Yamada, T., Conformational behaviour of $C^{\alpha,\alpha}$-diphenylglycine: folded *vs.* extended structures in DϕG-containing tripeptides. *J. Peptide sci.* **1998**, *4*, 21-32.

78. Lombardi, A.; De Simone, G.; Galdiero, S.; Nastri, F.; Di Costanzo, L.; Makihira, K.; Yamada, T.; Pavone, V., The crystal structure of Afc-containing peptides. *Biopolymers* **2000**, *53*, 150-160.

79. Crisma, M.; Formaggio, F.; Alemán, C.; Torras, J.; Ramakrishnan, C.; Kalmankar, N.; Balaram, P.; Toniolo, C., The fully-extended conformation in peptides and proteins. *Peptide Science* **2018**, 110, e23100.

80. Toniolo, C.; Crisma, M.; Formaggio, F.; Benedetti, E.; Santini, A.; Iacovino, R.; Saviano, M.; Di Blasio, B.; Pedone, C.; Kamphuis, J., Preferred conformation of peptides rich in alicyclic $C^{\alpha,\alpha}$-disubstituted glycines. *Peptide Science* **1996**, *40*, 519-522.

81. Crisma, M.; Toniolo, C., Helical screw-sense preferences of peptides based on chiral, C^{α}-tetrasubstituted α-amino acids. *Peptide Science* **2015**, *104*, 46-64.

82. Paradisi, M. P.; Torrini, I.; Zecchini, G. P.; Lucente, G.; Gavuzzo, E.; Mazza, F.; Pochetti, G., γ-Turn conformation induced by α,α-disubstituted amino acids with a cyclic six-membered side chain. *Tetrahedron* **1995**, *51*, 2379-2386.

83. Rao, S. N.; Chan, M. F.; Balaji, V. N., Conformational studies using molecular mechanics on model peptides with 1-aminocycloalkane 1-carboxylic acid residues. *Bull. Chem. Soc. Jpn.* **1997**, *70*, 293-299.

84. Avenoza, A.; Campos, P. J.; Cativiela, C.; Peregrina, J. M.; Rodríguez, M. A., *Ab initio* calculations for *N*-methyl-1-(*N'*-acetylamino)-*t*-2-phenylcyclohexane-*r*-1-carboxamide: a γ-turn mimetic. *Tetrahedron* **1999**, *55*, 1399-1406.

85. Kuroda, Y.; Ueda, H.; Nozawa, H.; Ogoshi, H., Adamantyl amino acid as γ-turn inducer for peptide. *Tetrahedron Lett.* **1997**, *38*, 7901-7904.

86. Meldal, M.; Juliano, M. A.; Jansson, A. M., Azido Acids in a Novel Method of Solid-Phase Peptide Synthesis. *Tetrahedron Lett.* **1997**, *38*, 2531-2534.

87. AndrÉ, F.; Boussard, G.; Bayeul, D.; Didierjean, C.; Aubry, A.; Marraud, M., Aza-peptides II. X-Ray structures of aza-alanine and aza-asparagine-containing peptides. *J. Pept res.* **1997**, *49*, 556-562.

88. Bourguet, C. B.; Boulay, P.-L.; Claing, A.; Lubell, W. D., Design and synthesis of novel azapeptide activators of apoptosis mediated by caspase-9 in cancer cells. *Bioorg. Med. Chem. Lett.* **2014**, *24*, 3361-3365.

89. Chingle, R.; Ratni, S.; Claing, A.; Lubell, W. D., Application of constrained aza-valine analogs for Smac mimicry. *Peptide Science* **2016**, *106*, 235-244.

Paired Utility of Aza-Amino Acyl Proline and Indolizidinone Amino Acid Residues for Peptide Mimicry: Conception of Prostaglandin F2α Receptor Allosteric Modulators that Delay Preterm Birth

2.1. Context

On the rise worldwide, preterm birth (<37 weeks of gestational age) is an unmet healthcare need with the highest per patient costs of any medical urgency.[1-2] Modern labor suppressing drugs (tocolytics) cause uterine quiescence, but prolong pregnancy only up to a few days, and are associated with side effects to mother and infant.[3] Towards improved tocolytics, the prostaglandin F2α (PGF2α) receptor (FP) was targeted because of its increased expression during labor and the fact that FP-knockout mice fail to deliver pups.[4] Based on the second extracellular loop of this G protein-coupled receptor (GPCR), FP modulators were conceived, such as the indolizidin-2-one amino acid (I^2aa) analog PDC113.824 (*S*-**2.1a**) and aza-amino acyl proline counterparts **2.2a-c** which were shown to inhibit myometrial contractions by way of an allosteric mechanism featuring biased signalling.[5] Considering the side chain component of the aza-amino acyl prolines appeared to influence the biased mechanism of FP modulation, diversity-oriented approaches were pursued to synthesize allosteric ligands featuring modifications of this purported turn region.

2.1.1. Modification of aza-residue side chain and influence on activity

Diversification of aza-residue side chains is inherently challenging due to the difficulty in differentiating hydrazine nitrogen for incorporation into peptide structures.[6] Solution and solid phase methods for installing regioselectively side chains onto *N*-terminal semicarbazone peptides have however overcome this challenge giving access to aza-peptide libraries.[7-8] Expanding on the approach to alkylate benzophenone semicarbazone prolyl peptides, different benzylic side chains were introduced onto the aza-residue to prepare various azaPhe-Pro FP modulators.[5] Moreover, by way of aza-amino acid chlorides, aza-propargylglycine (azaPra) prolyl peptides were synthesized. The azaPra residue was subsequently employed in copper-catalyzed azide-alkyne cycloadditions (CuAAC)[6], so-called A^3-reactions,[9] and oxidized to a carboxylic acid to further elaborate the aza-residue in the FP modulators.

Reported independently by the groups of Sharpless and Meldal in 2002,[10,11] CuAAC couples efficiently functionalized azide and terminal alkyne groups regioselectively to produce 1,2,3-triazoles.

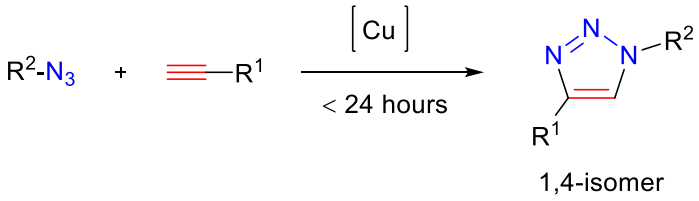

Scheme 2.1. Cu-catalyzed azide-alkyne cycloaddition reaction

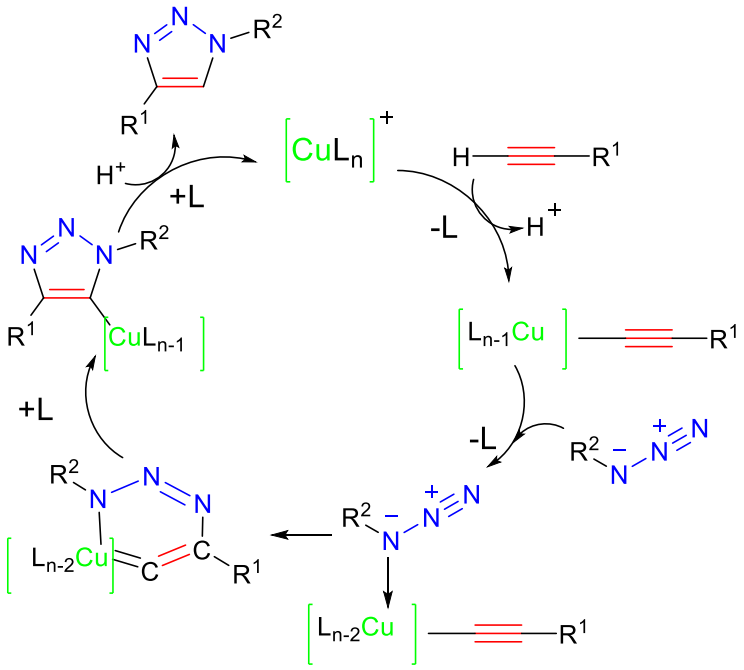

Figure 2.1. Sharpless mechanism for CuAAC[10]

The CuAAC mechanism has been suggested to involve the rapid formation of a copper(I)-acetylide (Figure 2.1), which coordinates to the azide leading to formation of a six-membered metallocycle.[10] The six-membered ring undergoes ring contraction to yield the triazolide copper which release the triazole upon protonation. Although often used as the source of copper(I), CuI alone is not an efficient catalyst for CuAAC, and in most cases employed in combination with an amine additive in non-aqueous, non-protonic solvent.

Among different literature methods, the combination of CuI, DIPEA and HOAc exhibited the highest efficiency for CuAAC reaction between azaPra peptide **2.39c** and a set of aryl azides and sodium azide, to prepare aza-1,2,3-triazole-3-alanines.[12] Both electron-rich and electron-poor aryl azides furnished aza-1,2,3-triazole-3-alanines in good conversions. Six triazoles were

synthesized to study the influence of size, aromaticity and hydrogen bonding at the aza-residue side chain for activity in reducing myometrium contractions.

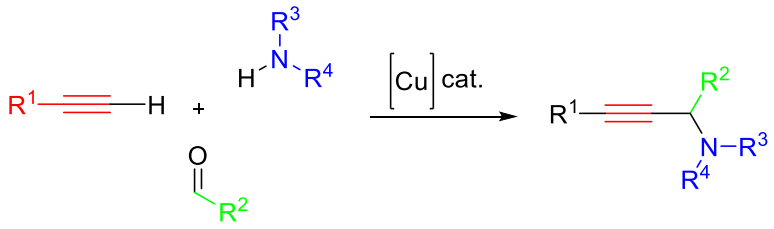

Scheme 2.2. Synthesis of propargyl amine using Cu catalyzed A^3 coupling reaction

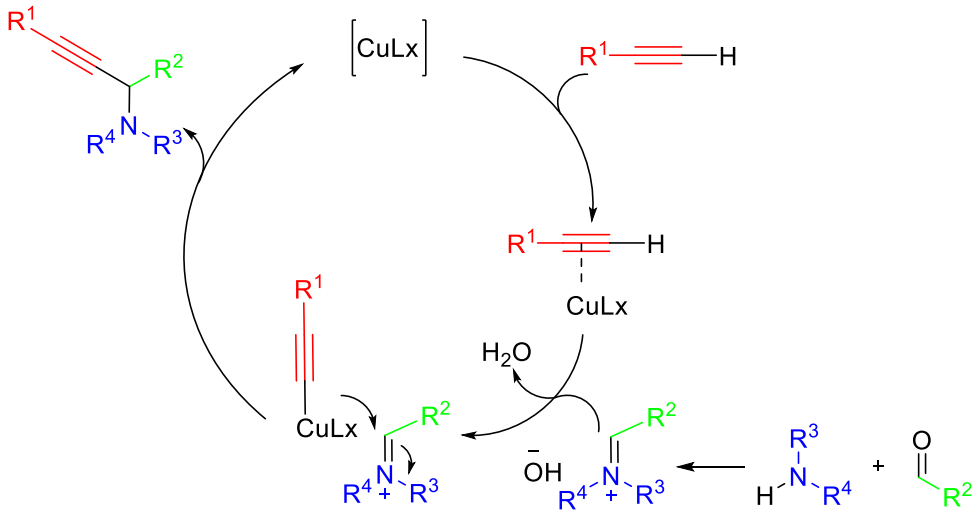

Figure 2.2. The proposed mechanism for copper catalyzed A^3 coupling reaction[13]

The A^3-reaction is a multiple component reaction that assembles together aldehyde, acetylene and secondary amine components by a copper-catalyzed reaction (Scheme 2.2).[13] The proposed mechanism for the A^3 coupling, involves the C-H activation of the alkyne by the copper catalyst to form the copper acetylide, which reacts with the imine or iminium ion to provide the propargylamine with regeneration of catalyst (Figure 2.2).[13]

The azaPra residue **2.39c** was thus used as alkyne component in reactions with secondary amines, formaldehyde and CuI in dioxane at 80 °C to provide aza-*N*,*N*-disubstituted aminobut-2-ynylglycines, that may be considered as rigid aza-lysine analogs.[9] Aza-lysine peptides **2.8m−r** were isolated by HPLC after reactions with six secondary amines: dimethylamine, pyrrolidine, piperidine, morpholine, diallylamine and methylbenzylamine. Examining the influences of size and positive charge using these ligands to reduce PGF2α-induced uterine contractions, aza-4-

piperidinobutynylglycine **2.8o** was found to exhibit the best activity in the series, but was less potent than the parent aza-Gly-Pro peptide **2.2a**.

To explore the effect of side chain orientation, alkynes **2.8m** and **2.8n** were reduced using catalytic hydrogenation with palladium-on-carbon to make saturated analogs. Both azapeptides with basic amine side chains failed to reduce PGF2α-induced myometrial contractions.

Oxidation of azaPra peptide benzyl ester **2.39c** with OsO_4, $NaIO_4$ and hexamethylenetetramine afforded aza-aspartate **2.41** in 89% yield.[14] After ester hydrolysis and purification by HPLC, aza-Asp peptide **2.7** was investigated in the myometrial contraction assay, which demonstrated that the negative charge diminished activity.

Aza-residue side chain size and hydrophobicity had significant impact, which typically lowered activity in the myometrial contraction assay.

2.1.2 Modification of proline ring and effect on peptide activity

Proline forms tertiary amides (prolyl amides), which can exist as *cis* and *trans* isomers. Moreover, the proline ring can adopt C^{γ}-*exo*- and *endo*-puckers. Previously, 4-position ring substituents have been shown to influence both the prolyl amide isomer population and ring pucker.[15] To examine the influence of 4-position substituents on activity, a solid phase approach was developed, in which 4-hydroxyproline (Hyp) was converted to its respective 4-fluoro- (Flp) and 4-aminoproline (Amp) analogs.

The Hyp-azapeptides *R*-**2.54b-d** were first synthesized on Wang resin using an Fmoc-protecting group strategy. Aza-residues were coupled to tripeptide **2.49** as *N*-Fmoc-aza-amino acid chlorides.[16] To circumvent the formation of oxadiazolone during introduction of aza-glycine, the 4-ethoxybenzyl group was employed as a temporary protecting group that was removed during the cleavage of azapeptide from resin using TFA. The *N*-Fmoc-aza-amino acid chlorides were prepared by activation of alkylated *N*-Fmoc carbazates **2.50b–d** using 15% phosgene in toluene and coupled to tripeptide on resin **2.49** in the presence of DIEPA. After Fmoc removal, the phenylacetyl group was installed using phenylacetic anhydride in dichloromethane, and the 4*R*-hydroxyl group was liberated using tetra-*n*-butylammonium fluoride (TBAF) in THF.

(4*R*)-Alcohols *R*-**2.54b-d** were first converted into their (4*S*)-isomers *S*-**2.54b-d** using the Mitsunobu reaction with 4-nitrobenzoic acid, PPh_3 and diisopropyl azodicarboxylate (DIAD) in

THF, followed by benzoate removal without Fmoc cleavage using NaN_3 in MeOH.[17] In the Mitsunobu reaction, a betaine intermediate results from the reaction of triphenylphosphine and the dialkyl azodicarboxylate (DIAD) with protonation from a pro-nucleophile such as 4-nitrobenzoic acid.[18-19] Alcohol oxygen activation occurs on reaction with the phosphonium of the betaine intermediate to form an oxyphosphonium ion, which is displaced by the carboxylate anion with inversion of configuration at carbon (Figure2.3).[18-19]

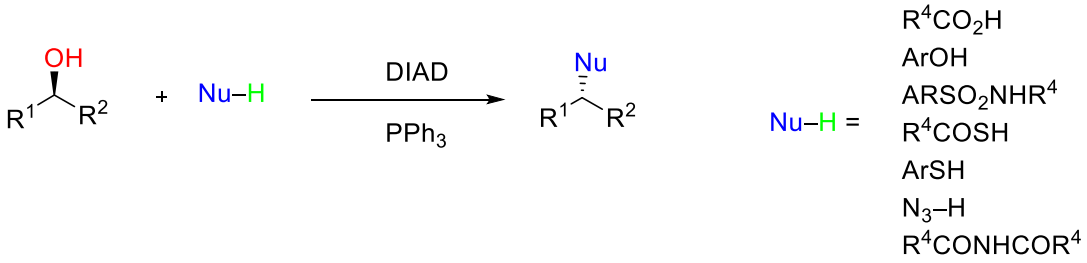

Scheme 2.3. a representative Mitsunobu reaction

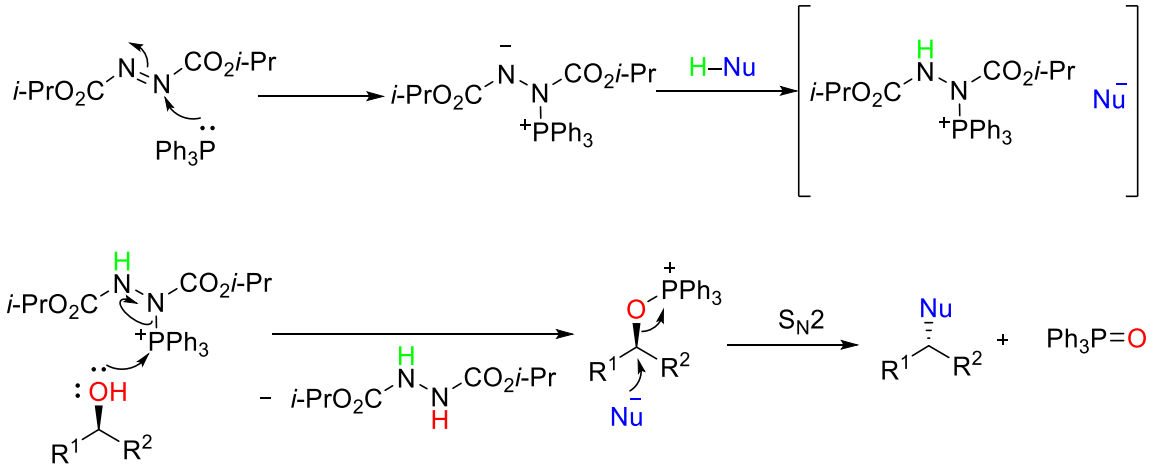

Figure 2.3. The proposed mechanism for the Mitsunobu reaction[19]

The resin-bound 4*R*- and 4*S*-Hyp-azapeptides (*R*- and *S*-**2.54b-d**) were subjected to fluorination chemistry with diethylaminosulfur trifluoride (DAST) as fluorine source to prepare 4*S*- and 4*R*-Flp-azapeptides with inversion of stereochemistry.[17] Moreover, (4*S*)- and (4*R*)-Amp-azapeptides *S*- and *R*-**2.57b-c** were also synthesized by activation of the respective 4*R*- and 4*S*-Hyp-azapeptides on resin using *p*-nitrophenylsulfonyl chloride, followed by S_N2 displacement using NaN_3,[17] azide reduction with tris(2-carboxyethyl)phosphine (TCEP), and resin cleavage. Attempts to prepare aza-*p*-ethoxyphenylalaninyl azidoprolines *S*- and *R*-**2.56d** on resin failed due

to inability to activate the hydroxyl group as a *p*-nitrophenylsulfonate;[20] instead, Fmoc-azido prolines were respectively synthesized in solution using Mitsunobu conditions with 4*R*- and 4*S*-*N*-(Fmoc)hydroxyproline *tert*-butyl esters, diphenylphosphoryl azide (DPPA) and diethyl azodicarboxylate (DEAD), and incorporated into aza-Gly-Amp peptide sequences *S*- and *R*-**2.57a**.

In addition to possible interactions with the FP receptor, the 4-substituted prolines were explored because of their influences on prolyl amide isomer geometry and ring puckering. The inductive effects of 4-Flp and 4-Hyp are contingent on their stereochemistry such that 4*R*-diastereomers exhibit C$^{\gamma}$-*exo* puckers and higher *trans*-amide populations than their 4*S*-counterparts which favor C$^{\gamma}$-*endo* puckers.[21] Ionization of the amine of 4-Amp favors the *endo* pucker.[22] In spite the reported influences of 4-position substituents on conformation, analysis of the eighteen different Hyp, Flp and Amp analogs found only four analogs that retained some inhibitory activity on myometrial contractions: aza-Pra-4*R*-Hyp *R*-**2.11c**, aza-Gly-4*S*-Flp *S*-**2.12a**, aza-Gly-4*R*-Amp *R*-**2.13a** and aza-Phe-4*S*-Amp *S*-**2.13b**. Considering the active analogs possessed different 4-position stereochemistry and aza-residue side chains, no clear correlations were observed between FP modulation, ring pucker and conformation. Notably, aza-Pra-4*R*-Hyp *R*-**2.11c** did exhibit similar activity to aza-Gly-Pro **2.2a** and represents a possible lead for further development.

2.2. Conclusion

To further study the relationships between structure and activity of FP modulators **2.2a-c** towards improved tocolytics for prevention of preterm labor, a set of diversity-oriented approaches were developed to introduce various side chains on the aza-residue and to modify the 4-position of the proline residue. The analogs were synthesized to explore the influences of size, hydrophobicity, aromaticity and hydrogen bonding properties on the activity. Analysis of the thirty-six analogs in the myometrial contraction assay revealed a limited set of active ligands and demonstrated a high sensitivity to structural modifications of the azapeptide FP modulators.

References for Chapter 2

1. Blencowe, H.; Cousens, S.; Chou, D.; Oestergaard, M.; Say, L.; Moller, A.-B.; Kinney, M.; Lawn, J., Born too soon: the global epidemiology of 15 million preterm births. *Reproductive Health* **2013**, *10*, S2.
2. Mathews, T.; MacDorman, M. F.; Thoma, M. E., Infant mortality statistics from the 2013 period linked birth/infant death data set. *National Vital Statistics Reports* **2015**, *64*, 1-30.
3. Hernandez, W. R.; Francisco, R. P.; Bittar, R. E.; Gomez, U. T.; Zugaib, M.; Brizot, M. L., Effect of vaginal progesterone in tocolytic therapy during preterm labor in twin pregnancies: Secondary analysis of a placebo-controlled randomized trial. *J. Obstet. Gynaecol. Res.* **2017**, *43*, 1536-1542.
4. Sugimoto, Y.; Yamasaki, A.; Segi, E.; Tsuboi, K.; Aze, Y.; Nishimura, T.; Oida, H.; Yoshida, N.; Tanaka, T.; Katsuyama, M.; Hasumoto, K.-y.; Murata, T.; Hirata, M.; Ushikubi, F.; Negishi, M.; Ichikawa, A.; Narumiya, S., Failure of parturition in mice lacking the prostaglandin F receptor. *Science* **1997**, *277*, 681-683.
5. Bourguet, C. B.; Goupil, E.; Tassy, D.; Hou, X.; Thouin, E.; Polyak, F.; Hébert, T. E.; Claing, A.; Laporte, S. A.; Chemtob, S.; Lubell, W. D., Targeting the prostaglandin $F_{2\alpha}$ receptor for preventing preterm labor with azapeptide tocolytics. *J. Med. Chem.* **2011**, *54*, 6085-6097.
6. Proulx, C.; Lubell, W. D., Aza-1, 2, 3-triazole-3-alanine synthesis via copper-catalyzed 1,3-dipolar cycloaddition on aza-progargylglycine. *J. Org. Chem.* **2010**, *75*, 5385-5387.
7. Bourguet, C. B.; Proulx, C.; Klocek, S.; Sabatino, D.; Lubell, W. D., Solution-phase submonomer diversification of aza-dipeptide building blocks and their application in aza-peptide and aza-DKP synthesis. *J. Pept. Sci.* **2010**, *16*, 284-296.
8. Sabatino, D.; Proulx, C.; Klocek, S.; Bourguet, C. B.; Boeglin, D.; Ong, H.; Lubell, W. D., Exploring side-chain diversity by submonomer solid-phase aza-peptide synthesis. *Org. Lett.* **2009**, *11*, 3650-3653.
9. Zhang, J.; Proulx, C.; Tomberg, A.; Lubell, W. D., Multicomponent diversity-oriented synthesis of aza-lysine-peptide mimics. *Org. Lett.* **2013**, *16*, 298-301.
10. Rostovtsev, V. V.; Green, L. G.; Fokin, V. V.; Sharpless, K. B., A stepwise huisgen cycloaddition process: copper (I)-catalyzed regioselective "ligation" of azides and terminal alkynes. *Angew. Chem.* **2002**, *114*, 2708-2711.

11. Tornøe, C. W.; Christensen, C.; Meldal, M., Peptidotriazoles on solid phase:[1,2,3]-triazoles by regiospecific copper (I)-catalyzed 1,3-dipolar cycloadditions of terminal alkynes to azides. *J. Org. Chem.* **2002**, *67*, 3057-3064.
12. Shao, C.; Wang, X.; Zhang, Q.; Luo, S.; Zhao, J.; Hu, Y., Acid–base jointly promoted copper (I)-catalyzed azide–alkyne cycloaddition. *J. Org. Chem.* **2011**, *76*, 6832-6836.
13. Peshkov, V. A.; Pereshivko, O. P.; Van der Eycken, E. V., A walk around the A^3-coupling. *Chem. Soc. Rev.* **2012**, *41*, 3790-3807.
14. Le Quement, S. T.; Nielsen, T. E.; Meldal, M., Divergent Pathway for the Solid-Phase Conversion of Aromatic Acetylenes to Carboxylic Acids, α-Ketocarboxylic Acids, and Methyl Ketones. *J. Comb. Chem.* **2008**, *10*, 546-556.
15. Bretscher, L. E.; Jenkins, C. L.; Taylor, K. M.; DeRider, M. L.; Raines, R. T., Conformational stability of collagen relies on a stereoelectronic effect. *J. Am. Chem. Soc.* **2001**, *123*, 777-778.
16. Boeglin, D.; Lubell, W. D., Aza-amino acid scanning of secondary structure suited for solid-phase peptide synthesis with Fmoc chemistry and aza-amino acids with heteroatomic side chains. *J. Comb. Chem.* **2005**, *7*, 864-878.
17. Pandey, A. K.; Naduthambi, D.; Thomas, K. M.; Zondlo, N. J., Proline editing: a general and practical approach to the synthesis of functionally and structurally diverse peptides. Analysis of steric versus stereoelectronic effects of 4-substituted prolines on conformation within peptides. *J. Am. Chem. Soc.* **2013**, *135*, 4333-4363.
18. Fletcher, S., The Mitsunobu reaction in the 21st century. *Org. Chem. Front.* **2015**, *2*, 739-752.
19. Hughes, D. L., Progress in the Mitsunobu reaction. A review. *Organic Preparations and Procedures International* **1996**, *28*, 127-164.
20. Thomas, K. M.; Naduthambi, D.; Zondlo, N. J., Electronic control of amide cis-trans isomerism via the aromatic-prolyl interaction. *J. Am. Chem. Soc.* **2006**, *128*, 2216-2217.
21. Newberry, R. W.; Raines, R. T., 4-Fluoroprolines: Conformational analysis and effects on the stability and folding of peptides and proteins. In *Peptidomimetics I*, Springer 2016; pp 1-25.

22. Sonar, M. V.; Ganesh, K. N., Water-induced switching of β-structure to polyproline II conformation in the 4*S*-aminoproline polypeptide via H-bond rearrangement. *Org. Lett.* **2010,** *12*, 5390-5393.

Article 1

Fatemeh M. Mir, N. D. Prasad Atmuri, Jennifer Rodon Fores, Xin Hou, Sylvain Chemtob, William D. Lubell. Paired Utility of Aza-Amino Acyl Proline and Indolizidinone Amino Acid Residues for Peptide Mimicry: Conception of Prostaglandin F2α Receptor Allosteric Modulators that Delay Preterm Birth. Just accepted *J. Med. Chem.*

DOI: 10.1021/acs.jmedchem.9b00056

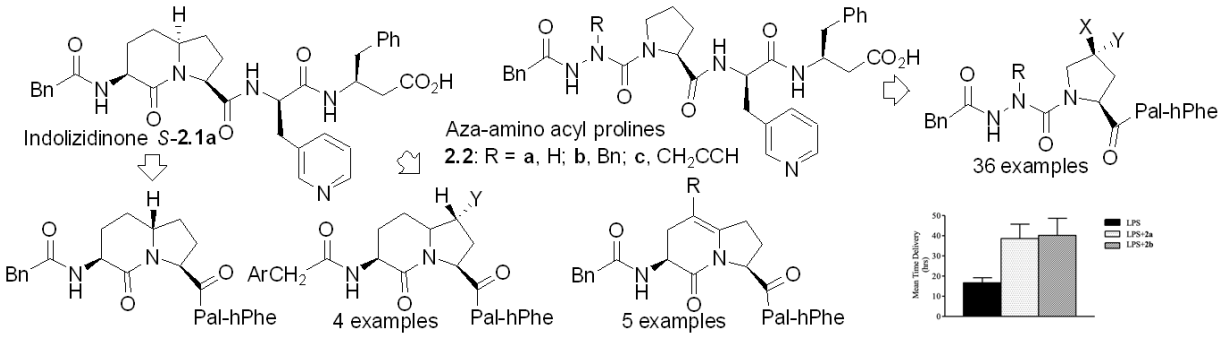

The results on the synthesis and study of the analogs described in this manuscript were obtained in collaboration with N. D. Prasad Atmuri, another Ph.D. candidate in Professor Lubell's laboratory. All the indolizidinone peptide analogs were synthesized and characterized by N. D. Prasad Atmuri and the results are not included in this thesis.

Paired Utility of Aza-Amino Acyl Proline and Indolizidinone Amino Acid Residues for Peptide Mimicry: Conception of Prostaglandin F2α Receptor Allosteric Modulators that Delay Preterm Birth

Fatemeh M. Mir [†§], N. D. Prasad Atmuri [†§], Jennifer Rodon Fores [†], Xin Hou[‡], Sylvain Chemtob[‡], William D. Lubell [†*]

†Département de Chimie, Université de Montréal, C.P. 6128 Succursale Centre-Ville, Montréal H3C 3J7 QC, Canada

‡Centre Hospitalier Universitaire Sainte-Justine Research Center, Montréal H3T 1C5, QC, Canada

ABSTRACT : Peptide mimicry employing a combination of aza-amino acyl proline and indolizidinone residues has been used to develop allosteric modulators of the prostaglandin F2α receptor. Systematic study of the *N*-terminal phenylacetyl moiety, and the conformation and side chain functions of the central turn dipeptide residue has demonstrated the sensitive relationships between modulator activity and topology. Examination of aza-Gly-Pro and aza-Phe-Pro analogs **2.2a** and **2.2b** in a murine preterm labor model featuring treatment with lipopolysaccharide demonstrated their capacity to extend significantly (>20 h) the average time of delivery offering new prototypes for delaying premature birth.

INTRODUCTION:

Complementary methods to mimic relevant secondary structures offer potential for parallel investigation of structure-activity relationships in peptide-based drug discovery. Paired utility for type II′ β-turn mimicry has specifically been exhibited by aza-amino acyl proline and indolizidin-2-one amino acid (I^2aa) scaffolds in several biologically active peptides.[1] For example, 10- and 7-fold greater potency

was observed respectively on replacement of the Gly-Pro dipeptide by azaGly-Pro and I^2aa in calcitonin gene-related peptide antagonists.[1a] Moreover, increased caspase-9 mediated apoptotic cell death has been exhibited relative to the parent Ala-Val-Pro-Ile Smac (second mitochondria-derived activator of caspase) protein mimic by analogs in which the Val-Pro dipeptide was swapped for aza-amino acyl proline and I^2aa residues.[1b, 1c] Pertinent to the present study, similar activity and efficacy in inhibiting myometrial contractions by way of modulation of the prostaglandin-F2α (PGF2α) receptor (FP) has been exhibited by the I^2aa analog PDC113.824 (*S*-**2.1a**) and its aza-amino acyl proline counterparts **2.2a**–**c** (Figure 2.4).[1d] To better seize the advantages of the paired utility of aza-amino acyl proline and I^2aa peptide derivatives, a series of diversity-oriented methods are now presented for synthesizing analogs of the related turn mimics in *S*-**2.1a** and **2.2** to conceive novel FP modulators.[2]

In a program targeted on the development of novel tocolytic (labor suppressing) agents that can delay labor and inhibit preterm birth, modulators *S*-**2.1a** and **2.2a**–**c** have been valuable prototypes and probes for mediating FP signalling and myometrial contractions. For example, I^2aa analog *S*-**2.1a** inhibited selectively PGF2α-induced myometrial contractions in a mouse model delaying labor up to 42 h.[3] Examination of the action of *S*-**2.1a** has revealed an allosteric mechanism implicating biased signalling.[3] In the absence of the endogenous agonist PGF2α, *S*-**2.1a** is inactive. Without competing for the binding site of the orthosteric ligand, *S*-**2.1a** modulated the exchange rate of PGF2α with tritium-labeled PGF2α. Downstream of the FP receptor, *S*-**2.1a** potentiated PGF2α-mediated activation of protein kinase C and mitogen-activated protein kinase (ERK1/2) signalling, but reduced $G_{\alpha 12}$-dependent activation of RhoA/ROCK signalling leading to actin remodeling and contraction of human myometrial cells.[3]

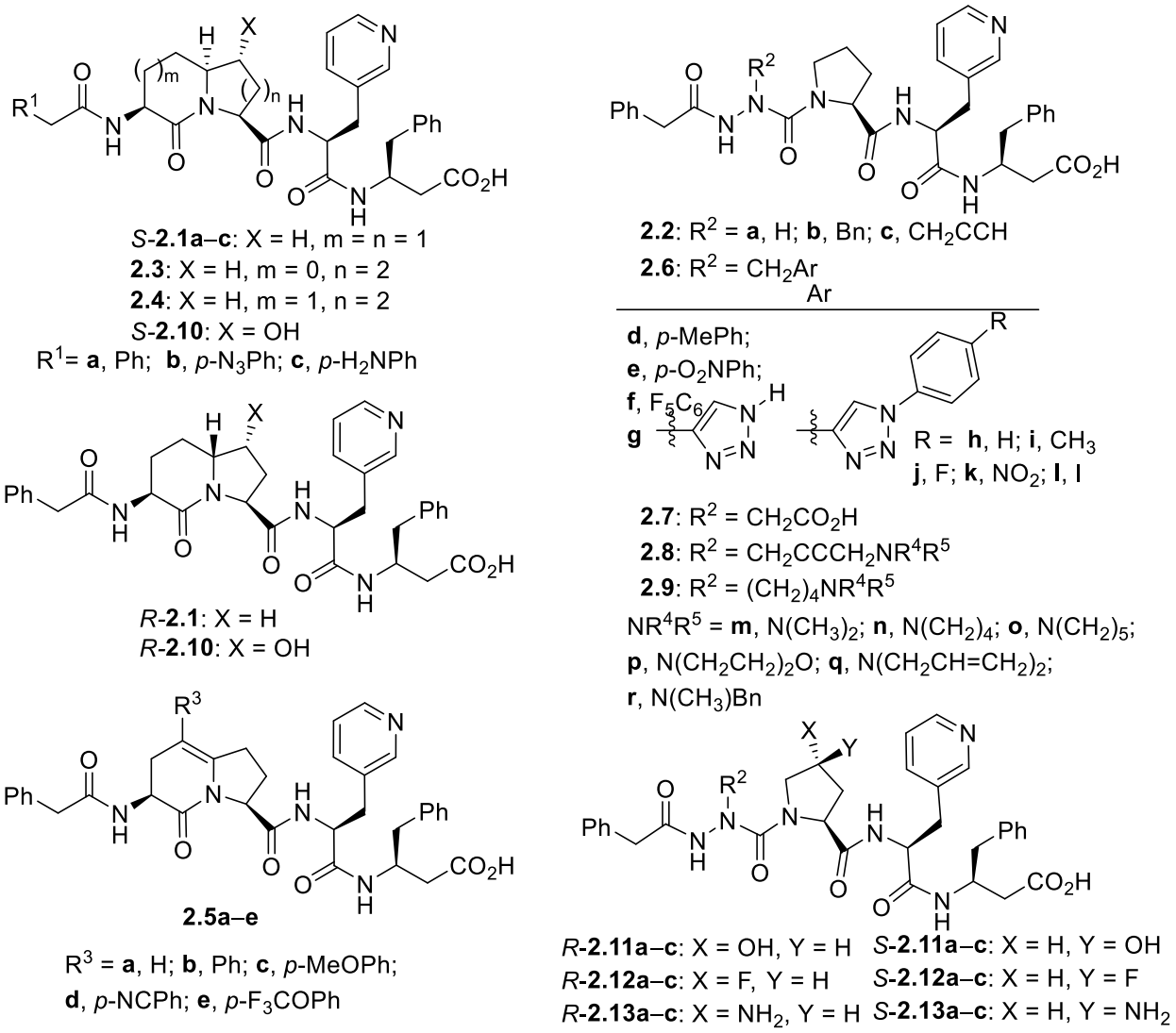

Figure 2.4. I[2]aa and aza-amino acyl proline FP modulators *S*-**2.1a** and **2.2a**–**c**, and related counterparts

Replacement of the I[2]aa scaffold with aza-amino acyl-L-proline analogs gave azapeptides **2.2a**–**c**, which exhibited similar effects on myometrial contraction and ERK1/2 signalling; however, varying influences on RhoA/ROCK signalling contingent on the aza-residue side chain.[1d] The latter result was particularly interesting for two reasons. In the first place, the complementarity of aza-amino acyl-L-proline and I[2]aa residues was highlighted because earlier attempts failed to provide active analogs from replacement of the I[2]aa scaffold with alternative indolizidin-9-one and quinolizidinone amino acid residues. Furthermore, modification of the aza-amino acid side chain offered potential to modulate biased signalling to ideally create alternative probes for studying FP receptor signalling towards the development of improved tocolytic agents.

The healthcare drivers for developing tocolytic prototypes such as *S*-**2.1a** and **2.2a**–**c** include the growing significance of preterm birth before 37 weeks of pregnancy, and the associated socioeconomic consequences. Preterm birth is correlated with 60-80% of all perinatal deaths,[4] and long-term neonatal and infant healthcare outcomes, including neurodevelopmental handicap, chronic respiratory illness, infections, and long-term impairment.[5] In spite of advances in knowledge of risk factors and medical interventions to reduce perinatal death, success has been limited in the prediction and prevention of preterm labor, the rate of which has risen globally, such that 15 million babies are estimated to be born prematurely per year.[6] Healthcare costs connected to preterm birth are significant: >$26.2 billion in 2005 in the USA alone amounting to $51,600 per premature birth.[7] Tocolytic drugs currently used in the clinical setting to block uterine contractions have marginal efficacy and at times are associated with significant adverse effects to either the mother and/or fetus.[8] Although they may extend gestation for the 48 hours needed to administer corticosteroids to the parturient for fetal surfactant maturation, for many patients, gestation needs to be prolonged for longer periods. Prevention of preterm birth remains a major health concern associated with serious short- and long-term complications to infants in industrialized and agrarian countries worldwide.

In the pursuit of improved tocolytics to inhibit preterm labor and probes to better understand the importance of FP mediated signalling pathways in labor, a set of diversity-oriented methods for making azapeptide and indolizidin-2-one amino acids have been developed and used to prepare a series of analogs of *S*-**2.1a** and **2.2a**–**c**. In the case of the I^2aa scaffold found in *S*-**2.1a**, methods have been conceived that illustrate the value of 5-iodoindolizidin-2-ones, which were prepared by transannular cyclization of unsaturated macrocycles.[9] In contrast to the corresponding 6-iodopyrroloazepinone counterpart,[9a] which served effectively in S_N1 chemistry to install a variety of side chains onto the seven membered cycle,[10] attempts to perform substitution chemistry on the 5-iodoindolizidin-2-ones **2.16** and **2.17** resulted in elimination to the corresponding unsaturated indolizidin-2-ones **18** and **19** (Scheme 2.4). The latter have however provided valuable intermediates for the synthesis of indolizidin-2-ones having different ring fusion stereochemistry (e.g., *R*- and *S*-**2.1a**) and substituents on both the five (e.g., *R*- and *S*-**2.10**) and six (e.g., **2.5b**–**e**) membered rings. In parallel, the aza-amino acyl proline dipeptide of **2.2a**–**c** has been elaborated on the aza-residue using a combination of submonomer chemistry in which side chains were introduced by alkylation of an aza-glycine residue (e.g., **2.6c**–**f**),[11] as well as diversification of the acetylene of an aza-propargylglycine (azaPra) residue in solution (e.g., **2.6g**–**l** and **2.7**–**2.9**). In addition, to explore modification of the proline ring system, a solid-phase approach has been introduced for the

assembly of modulators in which hydroxyproline has served to prepare a diverse set of analogs (e.g., **2.11**–**2.13**) using so called proline editing.[12]

The influences of analogs **2.1**–**2.13** have been studied on spontaneous and PGF2α-induced contractions of the myometrium in mouse tissue removed immediately after parturition. The limited activity of many of the analogs reflects significantly the relevance of conformation and the impact of substituents on biological activity. Moreover, the significant potency of the aza-Gly-Pro and aza-Phe-Pro derivatives **2.2a** and **2.2b** as effective counterparts of *S*-**2.1a** has been further demonstrated in a mouse model for preterm labor. In sum, the reported study has highlighted novel methods for using the dual combination of aza-amino acyl proline and I^2aa scaffolds as complementary tools for studying peptide-based drug design and further illustrates the promise of aza-Gly-Pro **2.2a** and aza-Phe-Pro **2.2b** as prototypes for delaying preterm birth.

RESULTS AND DISCUSSION:

Parallel development of methods to study the I^2aa and aza-amino acyl proline components of *S*-**2.1a** and **2.2a**–**c** has focused on both the conformation and substituents of theses dipeptide mimics. Initially, methods were developed for the modification of the I^2aa ring fusion and six-membered ring system. Considering that the I^2aa six-membered ring would occupy the same position as the aza-residue of the aza-amino acyl proline dipeptide, methods were also employed to diversify the semicarbazide side chain. Finally, approaches were used for modifying the five-membered rings of the I^2aa and Pro components.

5-Iodoindolizidine-2-ones **2.16** and **2.17** were respectively synthesized via transannular cyclizations of 9-membered unsaturated lactams **2.14** and **2.15** (Scheme 2.4).[9a,13] Phenylacetamide benzyl ester **2.14** was prepared from the corresponding *N*-(Boc)amino methyl ester[13] by a sequence featuring treatment with HCl gas in dichloromethane, acylation using phenylacetyl chloride and Hünig's base, saponification with LiOH, and carboxylate alkylation with benzyl bromide and $NaHCO_3$ (Experimental Section). In spite of changes to an *N*-terminal amide and larger ester, transannular cyclization of **2.14** with iodine in THF proceeded in the same fashion as carbamate **2.15** with regiocontrol and diastereoselectivity to afford the (3*S*,5*R*,6*R*,9*S*)-indolizidin-2-one **2.16** in 76% yield.[9a]

Attempts to add side chain diversity by displacement of iodides **2.16** and **2.17** were unsuccessful using various nucleophiles; instead, elimination of the bridge head proton occurred to form enamine. Enamines **2.18** and **2.19** were effectively prepared by iodide elimination with triethylamine at 80 °C in acetonitrile; however, concomitant loss of the Fmoc group necessitated protection with di-*tert*-butyldicarbonate. Olefin reduction provided access to different ring fusion stereochemistry. For example, hydride reduction of enamine **2.18** with sodium cyanoborohydride and catalytic acetic acid in EtOH gave a 2:1 diasteroisomeric ratio in favor of the convex over the concave isomers (e.g., *R*- and *S*-**2.21**: 57% and 21% yields). Alternatively, hydrogenation of enamine **2.19** with palladium-on-carbon in EtOH furnished selectively concave isomer *S*-**2.20** in 86% yield. Indolizidinone ring fusion stereochemistry was ascertained by NOESY NMR experiments based on the observed transfer of magnetization between the ring fusion and C3 protons in *S*-**2.21**, and confirmed by X-ray crystallography (Figure 2.5).

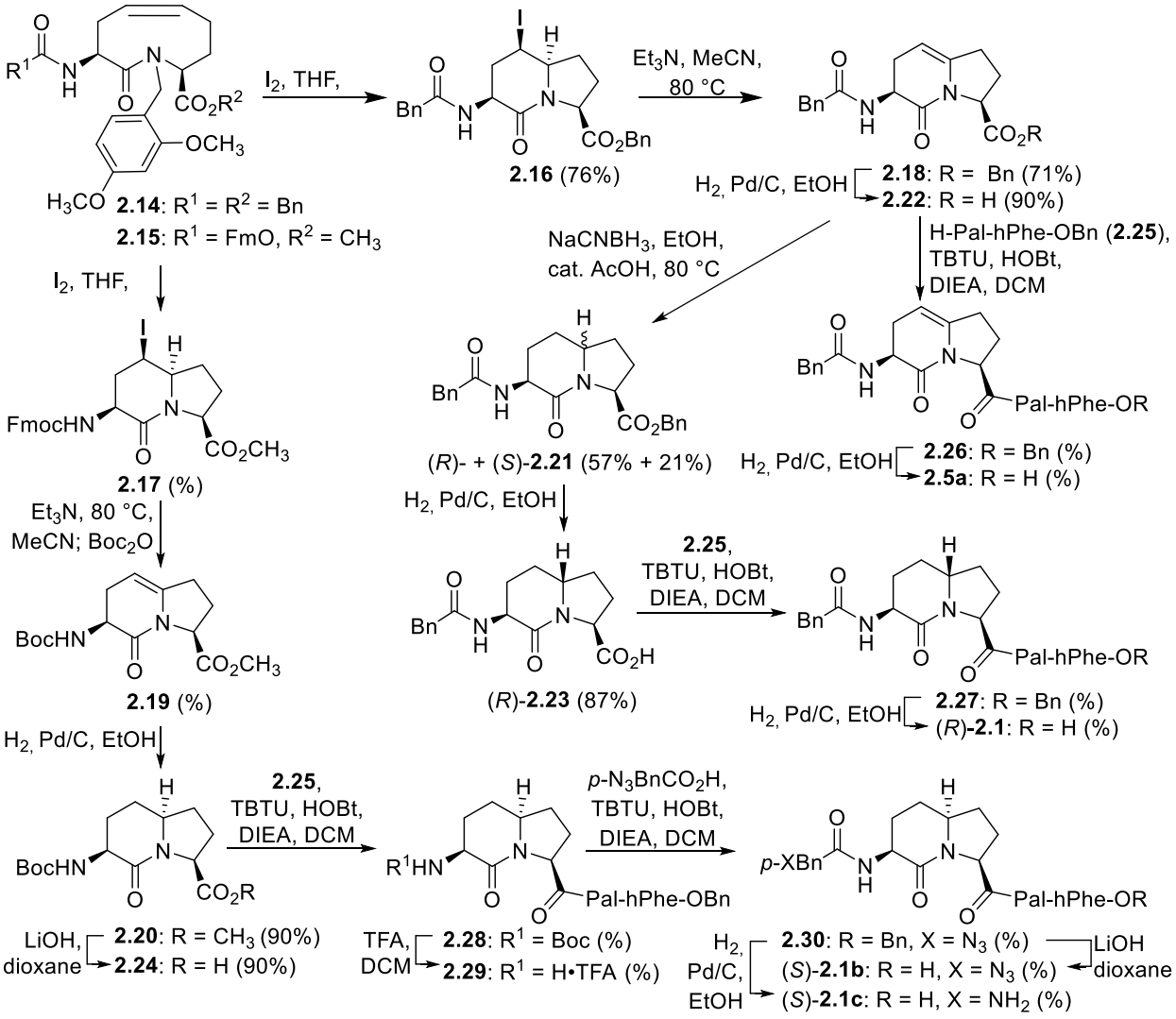

Scheme 2.4: Synthesis of indolizidin-2-one analogs *R*-**2.1a**, *S*-**2.1b**, *S*-**2.1c** and **2.5a**

Analogs of modulator *S*-**2.1a** were synthesized from unsaturated Δ^5-indolizidinone **2.18** and ring fusion stereoisomers **2.20** and **2.21**. Hydrogenolysis of benzyl ester **2.18** using palladium-on-carbon in EtOH under a balloon of hydrogen for <10 min occurred with concomitant olefin reduction to give a 1:1 mixture of acids **2.22** and *S*-**2.23**, which was used in the subsequent peptide coupling step. Benzyl ester *R*-**2.21** was converted to acid *R*-**2.23** under similar hydrogenolytic conditions. Saponification of methyl ester **2.20** with LiOH in dioxane gave carboxylic acid **2.24**. The four acids **2.22**, *S*-**2.23**, *R*-**2.23** and **2.24** were coupled to (*S*,*S*)-pyridinylalaninyl-β-homophenylalanine benzyl ester (**2.25**)[1d] using TBTU, HOBt, and DIEA to give protected peptides **2.26**–**2.28** in 26–67% yields.

In the interest of exploring diversity at the phenylacetamide component as well as preparing a potential photoaffinity labeling agent, *p*-azido- and *p*-aminophenylacetamide analogs *S*-**2.1b** and *S*-**2.1c** were prepared by routes commencing with removal of the Boc group from peptide **2.28** using HCl gas and acylation of the resulting hydrochloride salt **2.29** using 2-(4-azidophenyl)acetic acid, TBTU, HOBt, and DIEA in CH_2Cl_2 to provide 4-azidophenylacetamide **2.30**. Hydrolysis of benzyl ester **2.30** with LiOH in dioxane gave acid *S*-**2.1b**. Hydrogenolytic cleavages of benzyl esters **2.26**, **2.27** and **2.30** using palladium-on-carbon in ethanol under a balloon of hydrogen furnished respectively modulator analogs **2.5a**, *R*-**2.1a** and *S*-**2.1c**, which were purified by preparative reverse-phase HPLC (Table 2.1).

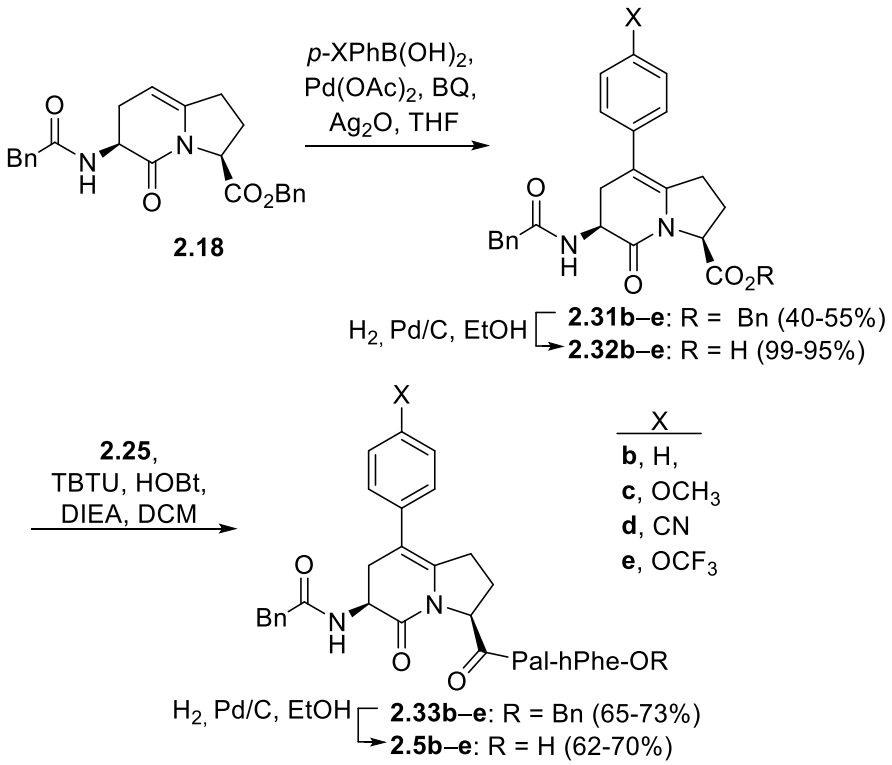

Scheme 2.5. Synthesis of 5-aryl-indolizidinone analogs **2.5b**–**e**

The modification of the six-membered ring of the I^2aa moiety was next explored by C-H bond activation and arylation at C5 using palladium-catalysis (Scheme 2.5). Four aryl boronates were coupled to enamine **2.18** using $Pd(OAc)_2$, 1,4-benzoquinone (BQ) and silver oxide in THF at 80 °C to provide **2.31b**–**e** in 40–55% yields. Hydrogenolytic cleavages of benzyl esters **2.31b**–**e**, respective couplings of the resulting acids **2.32b**–**e** to dipeptide **2.25**, and benzyl ester cleavages

as discussed for the synthesis of **2.5a** gave the 5-aryl analogs **2.5b**–**e**, which were purified by preparative reverse-phase HPLC (Table 2.1).

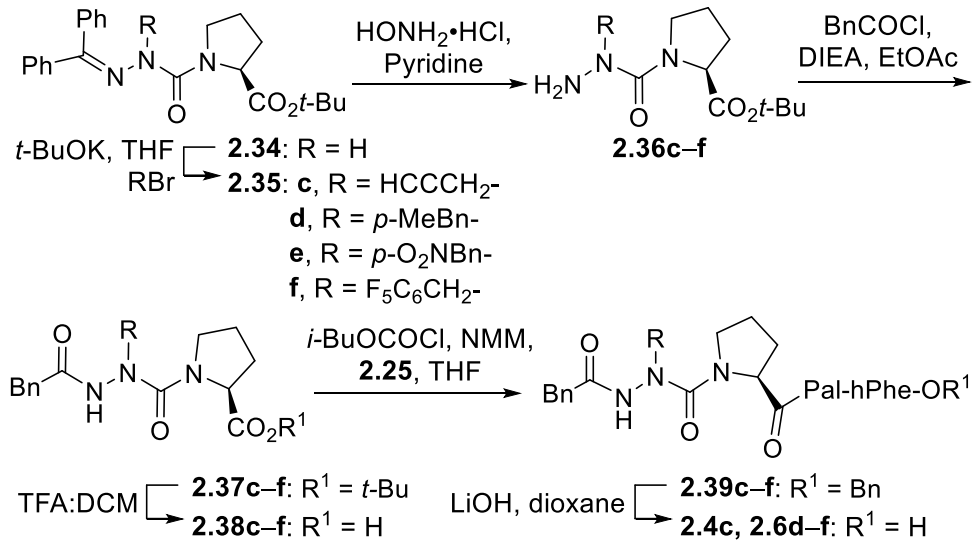

Scheme 2.6. Synthesis of aza-Pra-Pro and aza-Phe-Pro peptides **2.2c** and **2.6d**–**f**

In parallel to efforts to modify the six-membered ring of the I^2aa residue, a set of methods was employed to append a series of side chains on the aza-residue to make analogs of azapeptides **2.2a**–**c**. Modification of the aza-residue side chain was first explored by the synthesis and alkylation of aza-glycinyl proline *t*-butyl ester **2.34** using propargyl bromide, as well as *p*-methyl-, *p*-nitro- and pentafluoro benzyl bromides (Scheme 2.6).[11a] The propargyl side chain was selected for further diversification as discussed below. The three benzyl groups were chosen to contrast the influences of aromatic electron-density and hydrophobicity for activity with those of 5-arylindolizidinones **2.5b**–**e**. Aza-dipeptides **2.38c**–**f**, all were prepared from the respective azaPra and azaPhe analogs **2.35c** and **2.35d**–**f** by benzhydrylidene removal using hydroxylamine hydrochloride in pyridine, acylation of the resulting semicarbazide with phenylacetyl chloride, and *tert*-butyl ester removal in a TFA/DCM solution. They were then coupled to dipeptide **2.25** using *iso*-butyl chloroformate and *N*-methylmorpholine to furnish azapeptide benzyl esters **2.39c**–**f**, which after saponification with LiOH in dioxane and RP-HPLC purification afforded aza-amino acyl prolyl peptides **2.6d**–**f** (Table 2.1).

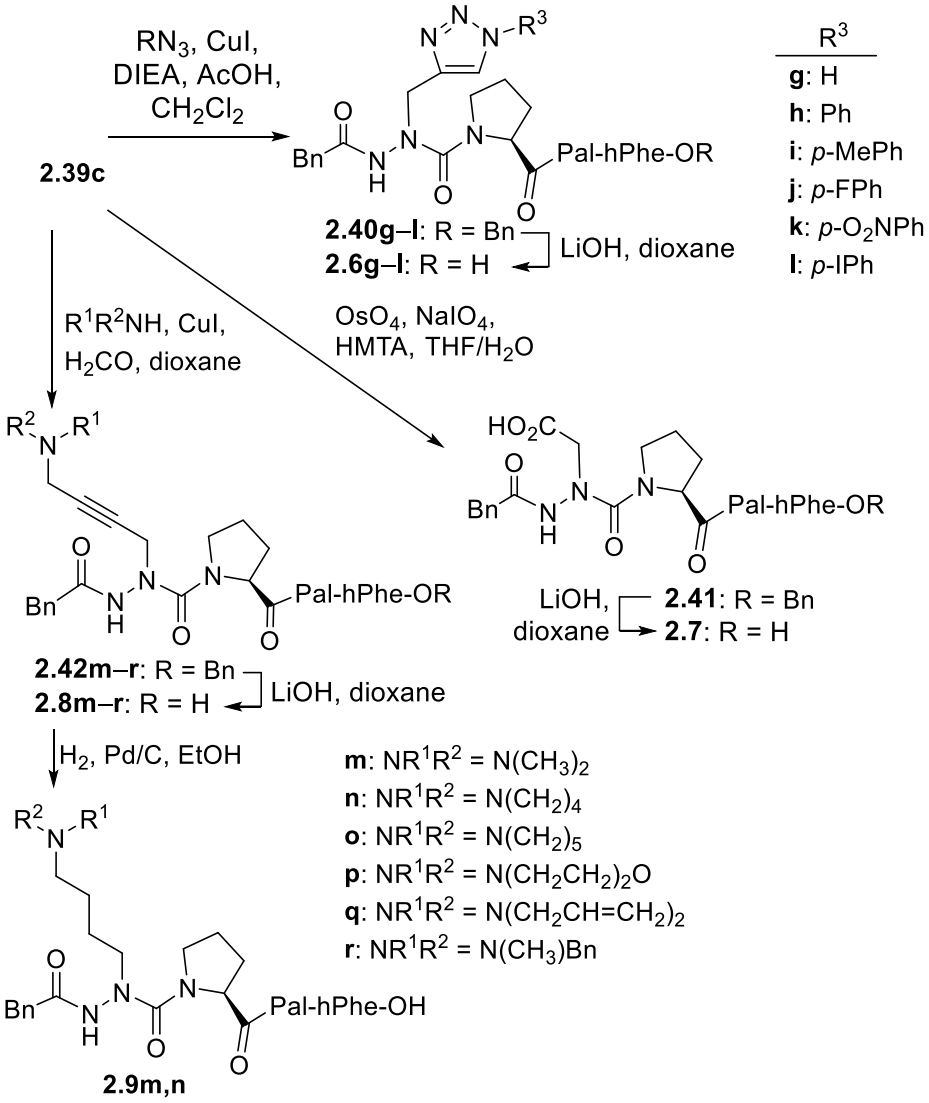

Scheme 2.7. Aza-triazole-alanine, aza-Asp and aza-Lys analog synthesis by azaPra diversification

With azaPra peptide **2.39c** in hand, diversity-oriented routes were used to prepare a broader group of side chain analogs including aza-1,2,3-triazole-3-alanine, aza-aspartate and aza-lysine analogs **2.6**–**2.9** to study the influences of charge and hydrogen-bonding at the side chain for activity (Scheme 2.7). A set of six aza-1,2,3-triazole-3-alanines **2.40g**–**l** was synthesized from azaPra peptide **2.39c** by copper-catalyzed azide-alkyne cycloadditions. Among various methods explored, 1,3-dipolar cycloadditions were best accomplished with sodium azide and aryl azides using CuI and DIPEA in AcOH.[14] After benzyl ester saponification, triazole-alanine peptides **2.6g**–**l** were purified by HPLC (Table 2.1). The azaPra peptide **2.39c** was converted to aza-

aspartate **2.41** in 89% yield using an $OsO_4/NaIO_4$/hexamethylenetetramine-mediated oxidation.[15] Hydrolysis of benzyl ester **2.41** and HPLC purification gave aza-Asp peptide **7**. Finally, in Mannich-like additions on the acetylene moiety,[16] azaPra peptide **2.39c** reacted in dioxane at 80 °C with copper iodide, formaldehyde and a set of six secondary amines: dimethylamine, pyrrolidine, piperidine, morpholine, diallylamine and methylbenzylamine. After saponification as described above, the set of aza-lysines **2.8m**–**r** was isolated by HPLC in 40 to 80% yields. Acetylenes **2.8m** and **2.8n** were reduced using catalytic hydrogenation with palladium-on-carbon to afford more flexible aza-Lys analogs **2.9m** and **2.9n**.

The five-membered ring of the I^2aa residue was modified by allylic oxidation of 5,6-dehydroindolizidin-2-one **2.18** with selenium dioxide and TBHP in dioxane to give a separable mixture of 5- and 7-hydroxy-dehydroindolizidin-2-ones **2.43** and **2.44** (Scheme 2.8). Olefin **2.43** was reduced using sodium cyanoborohydride and catalytic acetic acid in EtOH at 80 °C to give a 3:1 mixture of convex and concave diastereomers (e.g., *R*- and *S*-**2.45**, 44% and 26% yields) after chromatography. The regio- and stereochemistry of 5- and 7-hydroxyindolizidin-2-ones **2.43**–**2.45** were assigned using COSY and NOESY NMR spectroscopic experiments and X-ray crystallography of *R*-**2.45** (Figure 2.5). Employing a similar sequence of benzyl ester hydrogenolysis and couplings to dipeptide **25**, 7-hydroxindolizidinones *R*-**2.46** and *S*-**2.46** were respectively converted to acids *R*-**2.10** and *S*-**2.10**, which were purified by preparative reverse-phase HPLC (Table 2.1).

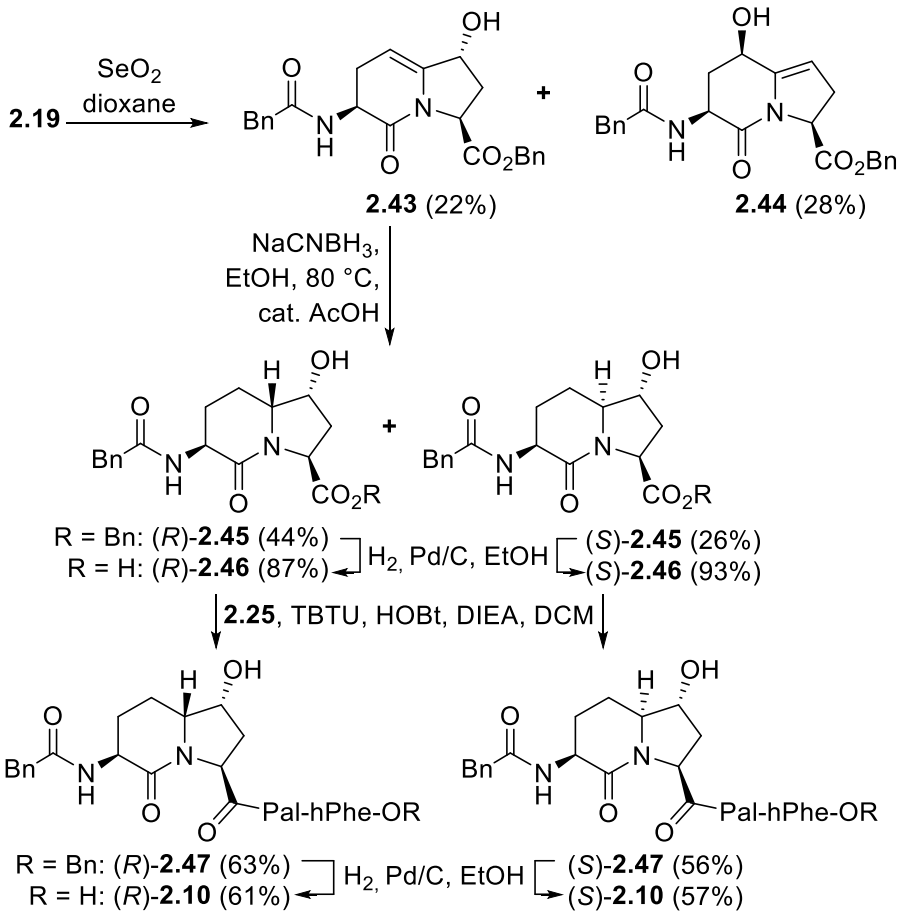

Scheme 2.8. Synthesis of 7-hydroxy-indolizidinones *R*- and *S*-**2.10**

In parallel, a set of proline residue analogs of azapeptides **2.2a**–**c** was prepared using 4-hydroxyproline. The related 4-hydroxy (Hyp), 4-fluoro- (Flp) and 4-aminoproline (Amp) analogs were generated to study influences of the ring pucker, hydrophobicity and substituents on activity.[12,17] A solid-phase route was developed featuring modification of Hyp azapeptides (*R*)-**2.54b**–**d** (Scheme 2.9).

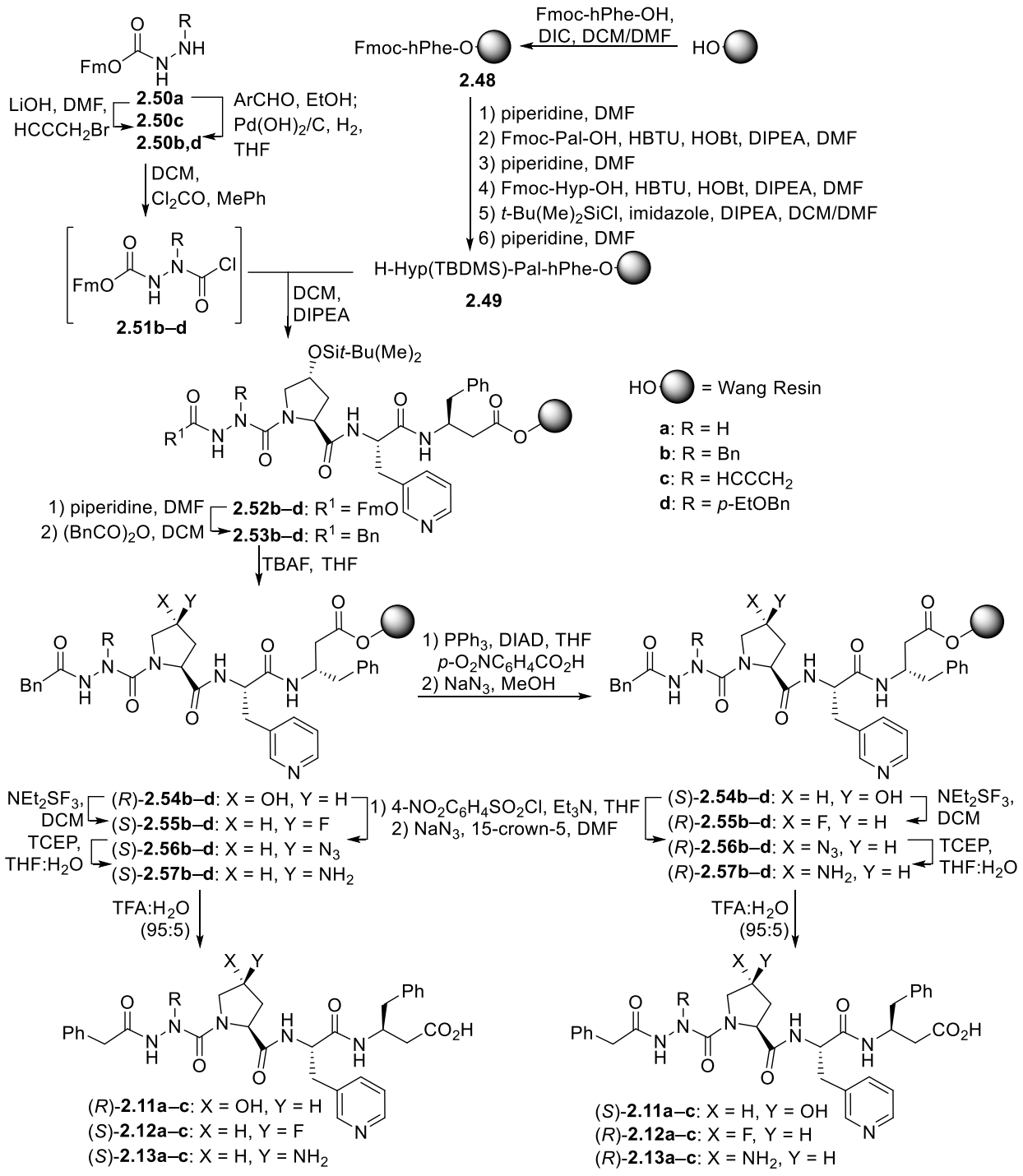

Scheme 2.9. Solid-phase synthesis of 4*R*- and 4*S*-Hyp-, Flp- and Amp-azapeptides **2.11**–**2.13**

N-Fmoc-β–Homophenylalanine (Fmoc-hPhe-OH) was coupled to Wang resin by way of its symmetrical anhydride to provide β-amino ester resin **2.48**. After capping unreactive sites with acetic anhydride, linear tripeptide resin **2.49** was synthesized by Fmoc removals, couplings of *N*-(Fmoc)pyridylalanine and (4*R*)-Fmoc-Hyp-OH, and hydroxyl group silylation. Central to the success of the solid-phase synthesis of azapeptides was the effective introduction of the aza-residue using different *N*-Fmoc-aza-amino acid chlorides.[18] To avoid formation of oxadiazolone in the synthesis of the aza-glycinyl-proline analogs,[19] the 4-ethoxybenzyl side chain was employed as a temporary protecting group, which was removed during cleavage of the azapeptide from the resin with TFA. The benzyl and 4-ethoxybenzyl side chains were added to the aza-residue by reductive aminations of semicarbazones formed from the corresponding aldehydes and fluorenylmethyl carbazate **2.50a** in EtOH, using palladium hydroxide-on-carbon in THF.[18] Propargyl carbazate **2.50b** was synthesized by alkylation of **2.50a** with propargyl bromide and lithium hydroxide in DMF.[20] Activation of carbazates **2.50b**–**d** with phosgene in toluene gave the corresponding *N*-Fmoc-aza-amino acid chlorides, which were coupled to tripeptide resin **2.49**.[18] After aza-amino acylation, the Fmoc group was removed from **2.52b**–**d** and the aza-residues were phenylacetylated using the corresponding anhydride in dichloromethane. The 4*R*-hydroxyl group was liberated from resins **2.53b**–**d** using tetra-n-butylammonium fluoride (TBAF) in THF and converted to the 4*S*-alcohol *S*-**2.54b**–**d** employing a two-step process featuring Mitsunobu reaction with 4-nitrobenzoic acid, PPh_3 and diisopropyl azodicarboxylate (DIAD) in THF, followed by nitrobenzoate removal without Fmoc cleavage using NaN_3 in MeOH.[12]

With 4*R*- and 4*S*-hyroxyproline azapeptides *R*- and *S*-**2.54b**–**d** in hand, syntheses were pursued to make the diasteromeric 4*S*- and 4*R*-Flp and Amp azapeptides *R*- and *S*-**2.55b**–**d** and **2.57b**–**d** (Scheme 2.9). Fluorination of 4*R*- and 4*S*-hydroxyprolines *R*- and *S*-**2.54b**–**d** was accomplished using diethylaminosulfur trifluoride (DAST) in dichloromethane via S_N2 chemistry with inversion of stereochemistry. Aminoprolines *S*- and *R*-**2.57b**–**c** were prepared from alcohols *R*- and *S*-**2.54b**–**c** by activation as the corresponding *p*-nitrophenylsulfonates,[12] followed by S_N2 displacement using NaN_3. Attempts to synthesize aza-*p*-ethoxyphenylalaninyl azidoprolines *S*- and *R*-**2.56d** using the same protocol were however unsuccessful, likely due to interactions between the electron rich aromatic ring of the *p*-ethoxybenzyl group and Hyp ring. Prolyl amide-π interactions are known to favor *cis*-amide bond isomers,[21] which in the case of **2.56d** may have

prevented activation of the hydroxyl group as a *p*-nitrophenylsulfonate. To circumvent this obstacle, the 4*S*- and 4*R*-*N*-Fmoc-azidoprolines were synthesized in solution, coupled onto the resin and elongated with *N*-Fmoc-aza-4-ethoxyphenylalaninyl chloride and phenyl acetic anhydride to obtain azidoproline peptides *S*- and *R*-**2.56d**. Azides *S*- and *R*-**2.56b**–**d** were reduced with tris(2-carboxyethyl)phosphine (TCEP) to provide the corresponding amines *S*- and *R*-**2.57b**–**d**. Finally, resin cleavage was performed using 95:5 TFA/H_2O to provide Hyp, Flp and Amp azapeptides *R*- and *S*-**2.11**–**2.13a**–**c** after HPLC purification (Table 2.1).

The stereochemical assignments of bicycles **2.16**, **2.21** and **2.43**–**2.45** were made using 2D NMR spectroscopy and X-ray crystallography [Supporting Information (SI)]. After the ring protons in the bicycle were assigned using COSY experiments to ascertain through-bond correlations, configuration assignments at the amino acid derived α-carbons were correlated to the newly generated ring fusion, iodide and alcohol bearing carbons using NOESY experiments to determine through-space nuclear Overhauser effects (Figure 2.5).

Table 2.1. Purity, retention times and mass spectrometric analyses of I^2aa and aza-Xaa-Pro analogs

entry	*Compounds*	*RT (min) in*		*Purity at 214/254 nm (%)*	*MS [M+1]/[M+Na]*	
		CH_3OH	CH_3CN		m/z (calc.)	m/z (obs.)
1	Phenylacetyl-(3*S*,6*R*,9*S*)-I^2aa-Pal-hPhe (*R*-**1**)	8.1 [h]	4.7[d]	≥ 96	626.2973	626.2981
2	4-Azidophenylacetyl-(3*S*,6*S*,9*S*)-I^2aa-Pal-hPhe (*S*-**1b**)	5.7 [c]	5.3[d]	≥ 96	689.2807	689.2817
3	4-Aminophenylacetyl-(3*S*,6*S*,9*S*)-I^2aa-Pal-hPhe (*S*-**1c**)	6.4 [d]	-	≥ 96	663.2902	663.2903
4	Phenylacetyl-(3*S*,9*S*)-5-Δ^5-I^2aa-Pal-hPhe (**5a**)	6.1 [b]	5.0[d]	≥ 96	646.2636	646.2641
5	Phenylacetyl-(3*S*,9*S*)-5-Ph-Δ^5-I^2aa-Pal-hPhe (**5b**)	6.7 [c]	6.0[d]	≥ 96	722.2949	722.2951
6	Phenylacetyl-(3*S*,9*S*)-5-(4-methoxyphenyl)-Δ^5-I^2aa-Pal-hPhe (**5c**)	5.9[f]	8.1[d]	≥ 96	730.3235	730.3262
7	Phenylacetyl-(3*S*,9*S*)-5-(4-cyanophenyl)-Δ^5-I^2aa-Pal-hPhe (**5d**)	6.0 [h]	6.7[d]	≥ 96	725.3082	725.3104
8	Phenylacetyl-(3*S*,9*S*)-5-(4-trifloromethylphenyl)-Δ^5-I^2aa-Pal-hPhe (**5e**)	10.7 [c]	8.9[d]	≥ 96	784.2952	784.2964
9	Phenylacetyl-aza-(4-Me)Phe-Pro-Pal-hPhe (**6d**)	9.5[g]	5.1[b]	≥ 96	705.3395	705.3394
10	Phenylacetyl-aza-(4-O_2N)Phe-Pro-Pal-hPhe (**6e**)	7.3[c]	6.3[d]	≥ 99	736.3086	736.3091
11	Phenylacetyl-aza-(pentafluoro)Phe-Pro-Pal-hPhe (**6f**)	10.3 [a]	5.4 [b]	≥ 99	787.2768	787.2780
12	Phenylacetyl-aza-(triazole)Ala-Pro-Pal-hPhe (**6g**)	5.8[e]	5.0 [d]	≥ 99	682.3096	682.3111
13	Phenylacetyl-aza-(1-phenyltriazole)Ala-Pro-Pal-hPhe (**6h**)	4.4[f]	6.0 [d]	≥ 99	758.3409	758.3408
14	Phenylacetyl-aza-(1-toluyltriazole)Ala-Pro-Pal-hPhe (**6i**)	6.7[g]	6.3 [d]	≥ 97	772.3566	772.3581
15	Phenylacetyl-aza-[1-(4-fluorophenyl)triazole]Ala-Pro-Pal-hPhe (**6j**)	8.9 [b]	4.7 [d]	≥ 97	776.3315	776.3331
16	Phenylacetyl-aza-[1-(4-nitrophenyl)triazole]Ala-Pro-Pal-hPhe (**6k**)	7.7[g]	6.1 [d]	≥98	803.3259	803.3276
17	Phenylacetyl-aza-[1-(4-iodophenyl)]triazole-Ala-Pro-Pal-hPhe (**6l**)	6.5[h]	5.9[h]	≥ 99	884.2376	884.2383
18	Phenylacetyl-aza-Asp-Pro-Pal-hPhe (**7**)	7.6 [b]	5.0[d]	≥ 99	659.2824	659.2836
19	Phenylacetyl-aza-[(*N*,*N*-dimethylamino)but-2-ynyl]Gly-Pro-Pal-hPhe (**8m**)	5.4[b]	4.2[d]	≥ 98	696.3504	696.3509
20	Phenylacetyl-aza-[(pyrrolidinyl)but-2-ynyl]Gly -Pro-Pal-hPhe (**8n**)	6.3[d]	4.4[d]	≥ 99	722.3661	722,3652
21	Phenylacetyl-aza-[(piperidinyl)but-2-ynyl]Gly-Pro-Pal-hPhe (**8o**)	5.8[b]	4.4[i]	≥ 99	736.3817	736.3822
22	Phenylacetyl-aza-[(morpholino)but-2-ynyl]Gly-Pro-Pal-hPhe (**8p**)	7.1[j]	4.4[i]	≥ 99	738.3610	738.3620
23	Phenylacetyl-aza-[(*N*,*N*-diallylamino)but-2-ynyl]Gly-Pro-Pal-hPhe (**8q**)	2.2[e]	4.6[i]	≥ 99	748.3817	748.3821
24	Phenylacetyl-aza-[(*N*-methyl,*N*-benzyl)but-2-ynyl]Gly-Pro-Pal-hPhe (**8r**)	6.6 [b]	4.9 [d]	≥ 99	772.3817	772.3840
25	Phenylacetyl-aza-(*N*,*N*-dimethyl)Lys-Pro-Pal-hPhe (**9m**)	5.7[b]	4.4[d]	≥ 99	700.3817	700.3814

26	Phenylacetyl-aza-[(pyrrolidinyl)butyl]Gly-Pro-Pal-hPhe (**9n**)	5.7[b]	6.6[d]	> 99	726.3974	726.3980
27	Phenylacetyl-(3S,6S,7R,9S)-7-hydroxy-I^{2}aa-Pal-hPhe (*R*-**10**)	5.6[b]	4.5[d]	≥ 96	664.2742	664.2714
28	Phenylacetyl-(3S,6S,7S,9S)-7-hydroxy-I^{2}aa-Pal-hPhe (*S*-**10**)	5.2[b]	4.4[d]	≥ 96	664.2742	664.2748
29	Phenylacetyl-aza-Gly-(4*R*)-Hyp-Pal-hPhe (*R*-**11a**)	6.7[d]	4.4[d]	> 99	617.2718	617.2698
30	Phenylacetyl-aza-Phe-(4*R*)-Hyp-Pal-hPhe (*R*-**11b**)	6.5[e]	5.8[d]	≥ 96	707.3188	707.3208
31	Phenylacetyl-aza-Pra-(4*R*)-Hyp-Pal-hPhe (*R*-**11c**)	5.6[k]	5.2[d]	≥ 99	655.2875	655.2892
32	Phenylacetyl-aza-Gly-(4*S*)-Hyp-Pal-hPhe (*S*-**11a**)	6.9[d]	4.5[d]	≥ 99	617.2718	617.2728
33	Phenylacetyl-aza-Phe-(4*S*)-Hyp-Pal-hPhe (*S*-**11b**)	6.7[e]	5.8[d]	≥ 99	707.3188	707.3217
34	Phenylacetyl-aza-Pra-(4*S*)-Hyp-Pal-hPhe (*S*-**11c**)	8.1[d]	5.2[d]	≥ 99	655.2875	655.2878
35	Phenylacetyl-aza-Gly-(4*S*)-Flp-Pal-hPhe (*S*-**12a**)	7.6[d]	6.2[d]	~82	619.2675	619.2697
36	Phenylacetyl-aza-Phe-(4*S*)-Flp-Pal-hPhe (*S*-**12b**)	7.6[d]	6.0[d]	≥ 99	709.3144	709.3162
37	Phenylacetyl-aza-Pra-(4*S*)-Flp-Pal-hPhe (S-**12c**)	5.4[d]	5.3[d]	≥ 99	657.2831	657.2857
38	Phenylacetyl-aza-Gly-(4*R*)-Flp-Pal-hPhe (*R*-**12a**)	6.8[d]	4.6[d]	≥ 95	619.2675	619.2678
39	Phenylacetyl-aza-Phe-(4*R*)-Flp-Pal-hPhe (*R*-**12b**)	9.5[d]	6.2[d]	≥ 97	709.3144	709.3146
40	Phenylacetyl-aza-Pra-(4*R*)-Flp-Pal-hPhe (*R*-**12c**)	8.3[d]	5.5[d]	≥ 95	657.2831	657.2834
41	Phenylacetyl-aza-Gly-(4*S*)-Amp-Pal-hPhe (*S*-**13a**)	5.2[d]	4.9[d]	≥ 99	616.2878	616.285
42	Phenylacetyl-aza-Phe-(4*S*)-Amp-Pal-hPhe (*S*-**13b**)	8.4[d]	5.2[d]	≥ 95	706.3348	706.3349
43	Phenylacetyl-aza-Pra-(4*S*)-Amp-Pal-hPhe (*S*-**13c**)	7.7[d]	6.1[l]	~91	654.3035	654.3038
44	Phenylacetyl-aza-Gly-(4*R*)-Amp-Pal-hPhe (*R*-**13a**)	5.6[d]	5.0[d]	≥ 95	616.2878	616.2852
45	Phenylacetyl-aza-Phe-(4*R*)-Amp-Pal-hPhe (*R*-**13b**)	8.4[d]	5.2[d]	≥ 99	706.3348	706.3356
46	Phenylacetyl-aza-Pra-(4*R*)-Amp-Pal-hPhe (*R*-**13c**)	7.2[d]	4.6[d]	≥ 99	654.3035	654.3039

Isolated purity determined by LC-MS analysis using gradients of X-Y% A [MeOH (0.1% FA)/H_2O (0.1% FA)] or B [MeCN (0.1% FA)/H_2O (0.1% FA)] over Z min: [a]70-90% A or B /20; [b]20-80% A or B/14; [c]30-95% A or B /14; [d]10-90% A or B/14; [e]40-90% A or B /12; [f]50-90% A or B /14; [g]50-80% A or B /14, [h]30-90% A or B /14; [i]5-80% A or B /14; [j]30-80% A or B /12; [k]40-70% A or B/15; [l]5-90% A or B/15.

Previously, 3-*N*-(Fmoc)amino-5-iodo-indolizidinone-9-carboxylate **2.17** (Scheme 2.4) was assigned based on observation of magnetization transfer between the C3, C5 and C6 protons.[9a] 3-Phenylacetamide **2.16** exhibited similar long range nuclear Overhauser effects indicating that such modification at the 3-position nitrogen had no effect on the regio- and diastereoselectivity of the transannular cyclization. Similarly, magnetization transfer between the C3 and C6 protons was observed in the NOSEY spectrum of indolizidinone (6*S*)- **2.21**, the stereochemical assignment of which was confirmed by X-ray crystallography.

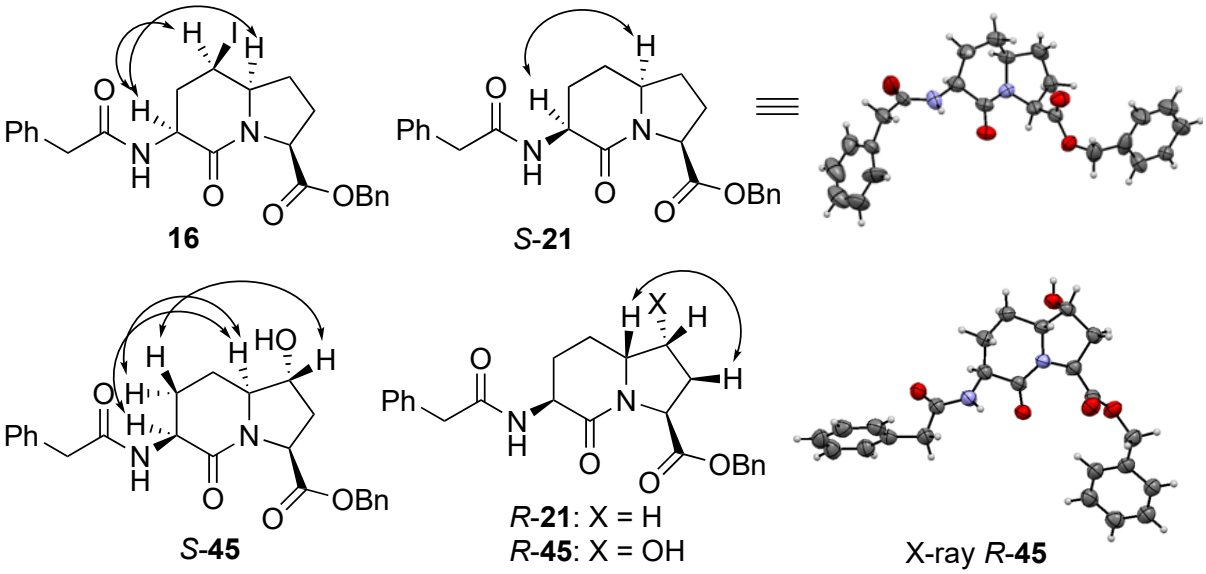

Figure 2.5. Assignment of relative stereochemistry by NOSEY correlations and X-ray structures.

The protons on carbons bearing hydroxyl groups were consistently up-field of those on nitrogen bearing carbons. Similar to the C3-protons of proline analogs,[22] the β–C8 proton appeared consistently up-field of the α–C8 proton due to an anisotropic effect caused by the C9 carboxylate. The *R*-configuration of the ring fusion C6-protons in (6*R*)- **2.21** and (6*R*)- **2.45** were assigned based on the observed transfer of magnetisation with the β–C8 proton. The assignment of alcohol (6*R*)- **2.45** was consistent with allylic oxidation from the less sterically hindered face of olefin **2.18** and confirmed by X-ray crystallography; the alcohol stereochemistry of (5*S*)- **2.44** is based similarly on the facial selectivity of the oxidation. In their X-ray crystal structures, the dihedral angle values of the backbone within bicycles *S*-**2.21** and *R*-**2.45**, both resembled those of the central residues of an ideal type II′ β-turn (Table 2.2).

Table 2.2. Comparison of dihedral angles from X-ray analysis and ideal type I and II′ β-turns

Type β-turn	ϕ^{i+1}, °	ψ^{i+1}, °	ϕ^{i+2}, °	ψ^{i+2}, °
Boc-(3*S*,6*S*,9*S*)-I^{2}aa-OMe[23]	−158	−176	−78	179
PhAc-(3S,6S,9S)-I^{2}aa-OBn (*S*-**21**)	−139	−175	−71	144
	−120	−173	−75	148
PhAc-7-OH-(3*S*,6*R*,7*S*,9*S*)-I^{2}aa-OBn (*R*-**45**)	−134	−142	−64	157
Boc-aza-Ala-Pro-NH*i*-Pr[24]	−68	−18	−58	−25
Pivaloyl-D-Ala-Pro-NH*i*-Pr[25]	60	−140	−89	9
Ideal type I β-turn[26]	−60	−30	−90	0
Ideal type II′ β-turn [26]	60	−120	−80	0

STRUCTURE ACTIVITY RELATIONSHIP STUDIES

Previously, the indolizidinone peptide mimic *S*-**2.1a** (PDC113.824) exhibited high efficacy (98% inhibition) and potency (IC_{50} = 1.1 nmol/L) in a porcine ocular micro-vessel assay, and delayed labor significantly in murine models induced respectively with lipopolysaccharide and PGF2α.[1d,27b] Modifications of *S*-**2.1a** by replacement of the (3*S*,6*S*,9*S*)-I^{2}aa residue by its D-enantiomer [(3*R*,6*R*,9*R*)-I^{2}aa], and related indolizidin-9-one, quinolizidinone, and pyrroloazepinone, 5,6-, 6,6- and 7,5-fused bicycles (e.g., **2.3a** and **2.4a**),[1d,27] and a ten-membered macrocycle system,[27a] as well as examination of the enantiomer of *S*-**1a**,[1d,27b] all gave analogs that exhibited no inhibition of myometrial contractions. On the other hand, aza-amino acyl proline

analogs **2.2a**–**c** displayed activity contingent on the nature of the aza-amino acid side chain, and reduced the tension and duration of PGF2α-induced myometrial contractions with similar efficacy as *S*-**2.1a**.[1d,27b] Moreover, modulators possessing Gly-Pro and D-Ala-Pro residues were previously shown to have lower activity than aza-Gly-Pro **2.2a**.[27a] Further investigation of the turn regions of *S*-**2.1a** and **2.2** was thus pursued in parallel to provide more detailed structure activity relationships for guiding development of novel modulators of FP as potential tocolytic agents for inhibiting preterm labor.

The activity of *S*-**2.1a** in the myometrial contraction assay proved to be very sensitive to structural modifications (Figure 2.6). For example, replacement of the phenyl acetyl moiety by *p*-azido and *p*-amino counterparts (e.g., *S*-**2.1b** and *S*-**2.1c**) diminished activity, respectively. Changing the ring fusion stereochemistry from the (3*S*,6*S*,9*S*)-I^2aa residue in *S*-**2.1a** to the (3*S*,6*R*,9*S*)-I^2aa isomer in *R*-**2.1a** reduced significantly the activity, which was one third that of *S*-**2.1a** at 10 μM (Figure S2.2). Flattening the ring in Δ^5-I^2aa analog **2.5a** improved activity relative to *R*-**2.1a,** but gave only half the activity of *S*-**2.1a** at 1 μM. A concave I^2aa residue was thus shown to be a prerequisite for high activity.

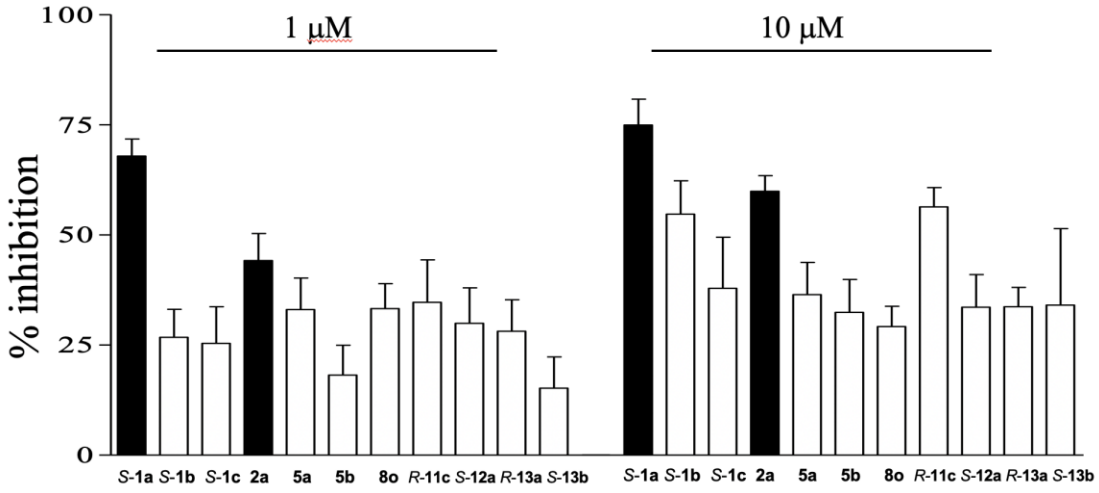

Figure 2.6. Effects of *S*-**2.1a**, **2.2a** and analogs on mean tension induced by PGF2α. Results are expressed as % inhibition, calculated as (A-B)/A, where A is the increase in mean tension induced by PGF2α in the absence of a 20-min pre-treatment with FP inhibitor and B is the increase in mean tension induced by PGF2α in the presence of a 20-min pre-treatment with FP inhibitor.

The addition of aromatic rings to the 5-position of Δ^5-I^2aa analog **2.5a** demonstrated tolerance for the phenyl group in **2.5b**, but not for larger substituents (e.g., 4-methoxy, 4-cyano

and 4-trifluoromethoxyphenyl analogs **2.5c**–**2.5e**), which caused a complete loss of activity. In contrast to our previously reported FP modulators, which do not typically exhibit effect in the absence of exogenous PGF2α, 5-(4-trifluoromethoxyphenyl)-Δ^5-I^{2}aa **2.5e** exhibited activity in the presence of the endogenous orthosteric ligand (Figure S2.3).

The influence of substitution on the 6-membered lactam of **2.5a** may be compared with the effects of different side chains on azapeptide **2.2a**, on which benzyl and propargyl residues were tolerated.[1d] Attempts to introduce larger and less electron rich aromatic side chains onto azapeptide **2.2a** (e.g., **2.6d**-**l**) resulted in loss of activity correlating with the inactivity of **2.5c**-**e**. In the cases of **2.6f** and **2.6k**, the analogs were insoluble as the zwitterion and examined as the sodium salts, which exhibited half the activity of **2.2a** at 10 μM (Figure S2.2). Examination of the activity of azapeptides **2.7**-**2.9** featuring carboxylate and basic amine side chains yielded aza-4-piperidinobutynylglycine **2.8o**, which exhibited similar activity as **2.5a**, and aza-4-(*N*,*N*-dimethylamino)butynylglycine **2.8m**, which was inactive at 1 mM but showed about half the activity of **2.2a** at 10 μM (Figure S2.2), demonstrating further the restrictive size requirement and need for a lyophilic moiety at this residue.

The conformational preferences of aza-amino acyl proline residues have been examined to a limited extent in dipeptide models by X-ray crystallographic and spectroscopic methods.[24, 28] For example, X-ray crystallographic analyses of *N*-Cbz-azaAsn(Me)-Pro-NH*i*-Pr, *N*-Cbz-azaAsp(Et)-Pro-NH*i*-Pr, *N*-Boc-azaAla-Pro-NH*i*-Pr (Table 2.2), and *N*-*i*-Pr-azaAla-Pro-O*t*-Bu, all indicated that in the solid state, the aza-residue exhibited *R*-like chirality and the aza-amino acyl proline dipeptide adopted respectively ϕ and ψ dihedral angle values indicative of the $i + 1$ and $i + 2$ residues of an ideal type I β-turn.[24,28] Although the type I β-turn has been described as an energy minimum adopted by model azapeptides (e.g., Ac-aza-Gly-Ala-NHMe and Ac-aza-Ala-Ala-NHMe) in computational analyses, the corresponding type II β-turn was less than one kcal higher in energy.[29] Examination of *N*-*i*-Pr-azaAla-Pro-O*t*-Bu in solution at low temperature (–90°C in CD_2Cl_2) by NMR spectroscopy indicated four methyl singlets corresponding to two pairs of prolyl amide *cis* and *trans* isomers with one major *trans* amide conformer representing two-thirds of the total population.[28] At ambient temperature, *N*-*i*-Pr-azaAla-Pro-O*t*-Bu exhibited infrared spectra in hexane and CH_2Cl_2 exhibiting strong concentration independent absorptions at 3260 cm^{-1} corresponding to an intramolecular hydrogen bond involving the azaAla NH and semicarbazide carbonyl oxygen indicating a more extended conformation.[28] Potential for conformational liberty

and adoptive chirality may both account for the activity of **2.2a-c** and related aza-amino acyl proline analogs, which may assume backbone geometry similar to the I^2aa residue in *S*-**2.1a**.

The influence of a ring substituent on the proline residue in *S*-**2.1a** and **2.2** was next explored typically with limited success. For example, neither (6*R*,7*R*)- nor (6*S*,7*R*)-7-hydroxyl-I^2aa analogs *R*- and *S*-**2.10a** exhibited activity in the myometrial contraction assay. Similarly, among the (2*S*,4*R*)- and (2*S*,4*R*)-4-hydroxyproline analogs *R*- and *S*-**2.11a**–**c**, only aza-Pra-4*R*-Hyp *R*-**2.11c** exhibited activity, which was comparable to azapeptide **2.2a**. Among the (2*S*,4*R*)- and (2*S*,4*R*)-4-fluoroproline analogs *R*- and *S*-**2.12a**–**c**, only aza-Gly-4*S*-Flp *S*-**2.12a** exhibited activity. Moreover, aza-Gly-4*R*-Amp *R*-**2.13a** and aza-Phe-4*S*-Amp *S*-**2.13b** retained activity among the 4-aminoproline analogs.

4-Position substituents on proline have been shown to influence both the ring pucker and prolyl amide isomer equilibrium.[30,31] (2*S*,4*R*)-Hydroxy- and fluoroprolines exhibit C^{γ}-*exo* puckers and higher *trans*-amide populations than their (2*S*,4*S*)-counterparts which favor a C^{γ}-*endo* pucker.[30] (4*S*)-Aminoproline has been shown to fluctuate between ring puckers contingent on pH with amine protonation favoring the C^{γ}-*endo* pucker.[31] Considering that active analogs were observed with both (2*S*,4*R*)- and (2*S*,4*S*)-stereochemistry contingent on the aza-residue side chain, the 4-position substituent may influence factors other than receptor engagement, such as cell permeability, which may influence performance in the *ex vivo* myometrial contraction assay.

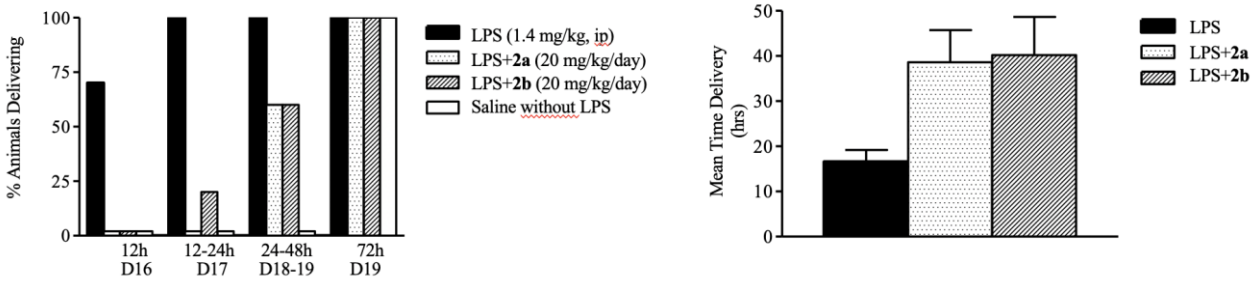

Figure 2.7. Tocolytic action of azapeptides **2.2a** and **2.2b** in LPS-induced preterm labor in mice. Left) Percentage of animals delivered following injection of LPS (B, 1.4 mg/kg by intraperitoneal injection) in the presence or absence of azapeptides **2.2a** and **2.2b** (20 mg/kg/day). Pregnant mice were treated with azapeptides **2.2a** and **2.2b** (20 mg/kg/day) starting on day 16 of gestation. Control mice were injected with saline. Bars are presented at 12, 15–24, 24–48 h, and 72 h. The time in hours refers to time of delivery following LPS treatment. Right) Average delivery time after LPS treatment.

Finally, the tocolytic effects of azapeptides **2.2a** and **2.2b** were examined in a preterm labor model in which mice near term were treated with azapeptide and lipopolysaccharide (LPS) *Escherichia coli* endotoxin, which is known to promote a general inflammatory state resulting in prostaglandin synthesis, and induced premature delivery.[32] Following LPS injection into mice at gestational day 16, all the animals tested delivered within 12–24 h (Figure 2.7). Pretreatment with azapeptide prior to LPS injection significantly delayed delivery, such that by gestational day 17, <20% of treated animals delivered. Azapeptide-treated mice did not deliver until day 19 even after treatment with LPS. Azapeptides **2.2a** and **2.2b** extended significantly (>20 h) the average time of delivery following LPS treatment compared with untreated animals (Figure 2.7b). Considering the results with azapeptides **2.2a** and **2.2b** in the *ex vivo* myometrial contraction assay and *in vivo* preterm LPS model, their ability to delay preterm labor is due in part through the inhibition of uterine contraction.

CONCLUSION

The relationships between structure and function of novel modulators of FP has been studied towards the development of potential tocolytics for delaying premature birth. Commencing from the understanding that indolizidin-2-one amino acids and aza-amino acyl proline derivatives share a common preference for mimicry of the central residues of type II' β-turns,[1] diversity-oriented methods were developed in parallel for the synthesis of analogs of lead indolizidin-2-one *S*-**2.1a** and azapeptides **2.2**. Peptides *S*-**2.1a** and azapeptides **2.2** had previously exhibited similar activity and efficacy in inhibiting myometrial contractions by way of modulation of the prostaglandin-F2α receptor; moreover, *S*-**2.1a** delayed labor for up to 42 h in mice. Parallel study on structural modifications of *S*-**2.1a** and **2.2** demonstrated that activity in the myometrial contraction assay was sensitive to the conformation, size, nature and lipophilicity of the modified analogs. The significance of the conformation of the I^2aa was demonstrated by the significant loss of activity of the convex bridge-head isomer *R*-**2.1a** and the regaining of activity in its flatter counterpart Δ^5-I^2aa **2.5a**. Substitution on the six-membered lactam of the I^2aa residue and the aza-amino acid side chain indicated a limited tolerance for aromatic and lipophilic residues, with a limited set of analogs retaining activity including 5-phenyl Δ^5-I^2aa **2.5b**, aza-Phe-Pro **2.2b** and aza-4-piperidinobutynylglycine **2.8o**. Although hydroxylation of the proline moiety of the I^2aa residue in **2.10a** abolished inhibitory activity on uterine contractions, certain replacements of the proline residue in the more flexible azapeptide **2.2** by Hyp, Flp and Amp analogs retained activity,

contingent on aza-residue side chain: e.g. *R*-**2.11c**, *S*-**2.12a**, *R*-**2.13a** and *S*-**2.13b**. Although the structure-activity profile indicated high sensitivity to changes of the ligand at the turn region, the potential for the azapeptides to serve as alternative prototypes for developing tocolytic agents was further evidenced by the ability of aza-Gly-Pro **2.2a** and aza-Phe-Pro **2.2b** to delay labor from 12-24 h in a LPS-induced mouse model of preterm birth. Effective synthetic methods for employing the parallel utility of I^2aa and azapeptide residues have thus revealed a sensitive structure-activity relationship profile from which active ligands have emerged exhibiting promise for delaying preterm labor.

EXPERIMENTAL

Ex Vivo Myometrial Contraction Assay

Ex vivo myometrial contraction was measured as previously described.[32] Briefly, uteri from mice were obtained from animals immediately following term delivery. Myometrial strips (2–3 mm wide and 1–2 cm long) from both were suspended in organ baths containing Krebs buffer equilibrated with 95% oxygen at 37 °C with an initial tension at 2 g. After 1 h of equilibration, changes in mean basal tension, as well as peak, duration, and frequency of spontaneous contraction in the absence or presence of PGF2α and azapeptide or I^2aa analog were recorded with a Biopac digital polygraph system.

Murine Preterm Labor Model

Timed-pregnant CD-1 mice at 16 days gestational (normal term is 19.2 days) were anesthetized with isoflurane (2%). Primed osmotic pumps (Alzet pump, Alzet, Cupertino, CA) containing either saline or azapeptide **2.2a** and **2.2b** (20 mg/day/animal) were subcutaneously implanted on the backs of the animals; infusion of azapeptide was immediately preceded by bolus injection of azapeptide (0.1 mg/animal intraperitoneally). Within 15 min after placement of the pumps, animals were injected with lipopolysaccharide (LPS) *Escherichia coli* endotoxin (35 μg/animal intraperitoneally) to mimic the inflammatory/infectious component of human preterm labor. Animals were inspected every hour for the first 18 h and every 2 h thereafter to document the timing of birth. All experiments were approved by the Animal Care Committee of Centre Hospitalier Universitaire Sainte-Justine (Montreal, Quebec, Canada).

Materials and Methods

Anhydrous solvents (THF, DMF, CH_2Cl_2, and CH_3OH) were obtained by passage through solvent filtration systems (GlassContour, Irvine, CA). All reagents from commercial sources were used

as received. Wang resin (1.1 mmol/g, 75-100 mesh) was purchased from Advanced Chemtech™; benzophenone hydrazone, benzyl bromide, 4-nitrobenzyl bromide, 80% propargyl bromide in toluene, 4-ethoxybenzaldehyde, hydroxylamine hydrochloride, pyridine, piperidine, formic acid (FA), *N,N*-diisopropylethylamine and 15% phosgene in toluene, all were purchased from Aldrich; amino acids and coupling reagents such as HBTU and diisopropylcarbodiimide (DIC) were purchased from GL Biochem™; solvents were obtained from VWR international. (2*S*)-(3-Pyridyl)alaninyl-(3S)-β-homophenylalanine benzyl ester hydrochloride (**2.25**) was prepared according to the literature procedure and exhibited ^{1}H NMR spectral data and R_f value identical to the reported literature.[1d] Purification by silica gel chromatography was performed on 230-400 mesh silica gel; analytical thin-layer chromatography (TLC) was performed on Silica gel 60 F254 (Aluminium Sheet) and visualised by UV absorbance or staining with iodine. Melting points are uncorrected and were obtained on sample that was placed in a capillary tube using a Mel-Temp melting point apparatus equipped with a thermometer and reported in degree Celsius (°C). ^{1}H and ^{13}C NMR spectra were recorded at room temperature (298 K) in $CDCl_3$ (7.26 ppm/77.16 ppm), DMSO (d6) (2.50 ppm/39.52 ppm) or CD_3OD (3.31 ppm/ 49.0 ppm) on Brucker AV (300/75, 500/125 and 700/175 MHz) instruments and referenced to internal solvent. Chemicals shifts are reported in parts per million (ppm); coupling constant (*J*) values in Hertz; abbreviations for peak multiplicities are s (singlet), d (doublet), t (triplet), q (quadruplet), qu (quintuplet), m (multiplet) and br (broad). Certain ^{13}C NMR chemical shifts values were extracted from HSQC spectra. High Resolution Mass Spectrometry (HRMS) data were obtained by the Centre Régional de Spectrométrie de Masse de l'Université de Montréal. Either protonated molecular ions $[M + H]^+$, $[M + 2H]/2^+$ or sodium adducts $[M + Na]^+$ were used for empirical formula confirmation. X-ray structures were solved on a Brucker Venture Metaljet diffractometer by the Laboratoire de diffraction des rayons X de Université de Montréal. Specific rotations, $[\alpha]_D$ were measured at 25°C at the specified concentrations (*c* in g/100 mL) using a 0.5 dm cell on a Perkin Elmer Polarimeter 589 and expressed using the general formula: $[\alpha]_D^{25} = (100 \times \alpha)/(d \times c)$.

Aza and I^{2}aa peptides purifications and analysis. All final peptides were purified on a preparative column (C18 Gemini column™) using a gradient from pure water (0.1% FA) to mixtures with MeOH (0.1% FA) at a flow rate of 10 mL/min. Specific compounds were analyzed and purified on a reverse-phase XTerra ™ C18 column (150 × 4.6 mm, 5 μm) using a binary solvent system [10-90% methanol (0.1% FA) in water (0.1% FA) over 15 min] at a flow rate of

0.8 mL/min with UV detection at 214 nm. Purity of azapeptides (>95%) was evaluated using analytical LC-MS on a 5 μM, 50 mm x 4.6 mm C18 Phenomenex Gemini column™ in two different solvent systems: water (0.1% FA) with CH_3CN (0.1% FA) and water (0.1% FA) with MeOH (0.1% FA) at a flow rate of 0.5 mL/min using the appropriate linear gradient.

Solid-phase azapeptide synthesis: Fmoc deprotection, peptide elongation, and resin aliquot analysis. Peptide synthesis was performed in syringe tubes equipped with Teflon™ filters, stopcock and stopper with agitation on an automated shaker. Wang resin (1.1 mmol/g 75-100 mesh) was employed and yields were based on initial resin loadings. Fmoc group removal was performed by treating the resin with 20% piperidine in DMF for 30 min. The resin was washed sequentially with DMF (3 x 10 mL), DCM (3 x 10 mL), DMF (3 x 10mL) and Et_2O (2 x 10 mL). To ascertain coupling efficiency, 1 to 2 mg of resin was treated with TFA : H2O (95:5) for 10 min, and filtered. The filtrate was evaporated under vacuum. The residue was treated with Et_2O, centrifuged for 2 min, decanted, and the remaining solid was dissolved in MeOH and analysed by LC-MS.[33]

Phenylacetyl-aza-(4-methyl)phenylalaninyl-(2*S*)-prolyl-(2*S*)-(3-pyridyl)alaninyl-(3*S*)-*β*-homophenylalanine (2.6d).

Benzyl ester **2.39d** (20 mg, 25.2 μmol) was dissolved in 0.5 mL of dioxane, treated with 1 N LiOH (0.5 mL) and stirred for 1 h. The volatiles were evaporated under reduced pressure. The remaining aqueous phase was acidified with 1N HCl to pH 3 and extracted twice with ethyl acetate (2×10 mL). The organic layers were combined, dried with Na_2SO_4, filtered and concentrated under vacuum. The residue was purified by preparative HPLC on a C18 reverse phase column using a gradient of 70% to 90% MeOH containing 0.1% FA in water containing 0.1% FA over 40 min at a flow rate of 10 mL/min. The collected fraction were freeze-dried to afford acid **2.6d** (10.6 mg, 60%) as white solid: $[\alpha]^{20}_D = -168$ (*c* 0.19, CH_3OH); ^{1}HNMR (700 MHz, CH_3OD) δ1.18 (m, 1H), 1.78 (m, 2H), 2.12-2.16 (m, 2H), 2.33 (s, 3H), 2.47 (m, 2H), 2.73 (dd, *J* = 9.3, 13.4 Hz, 1H), 2.81-2.85 (m, 1H), 3.04-3.07 (m, 2H), 3.14-3.18 (m, 1H), 3.43 (m, 2H), 3.56 (s, 2H), 3.89 (br, 1H), 4.27 (dd, *J* = 7.0, 10.3 Hz, 1H), 4.38 (m, 2H), 7.07 (d, *J* = 8.0 Hz, 2H), 7.11-7.15 (m, 5 H), 7.26-7.29 (m, 5H), 7.31-7.33 (m, 3H), 7.58 (d, *J* = 7.8 Hz, 1H), 8.29 (s, 1H), 8.37 (d, *J* = 4.8 Hz, 1H); ^{13}C NMR (125 MHz, CH_3OD) δ 21.2, 26.5, 30.9, 35.1, 41.2, 41.3, 43.5, 50.7, 51.3, 54.8, 56.0, 64.2, 125.2, 127.1, 128.4, 129.2, 129.8, 130.3, 130.4, 130.5, 131.0, 134.2, 135.8, 136.0, 138.7, 138.8,

140.0, 148.2, 150.6, 162.2, 171.9, 172.1, 174.8, 179.0; HRMS Calcd*m/z* for $C_{40}H_{45}N_6O_6$ $[M+H]^+$ 705.3395, found 705.3394.

Phenylacetyl-aza-(4-nitro)phenylalaninyl-(2*S*)-prolyl-(2*S*)-3-pyridylalaninyl-(3*S*)-*β*-homophenylalanine (2.6e).

Employing the procedure described for the synthesis of acid **2.6d** using ester **2.39e** (25 mg, 0.03 mmol), acid **2.6e** was purified using a gradient for elution from 30% to 95% MeOH containing 0.1% FA in water containing 0.1% FA over 40 min at a flow rate of 10 mL/min and isolated as white solid (12 mg, 55 %): $[\alpha]^{20}_D = -105.6$ (*c* 0.5, CH_3OH); ^{1}H NMR (700 MHz, CD_3OD) δ 1.22 (m, 1H), 1.80 (m, 2H), 2.17 (m, 1H), 2.56 (m, 2H), 2.81 (dd, *J* = 8.3, 13.7 Hz, 1H), 2.87 (t, *J* = 12.7 Hz, 1H), 2.99 (dd, *J* = 3.6, 13.2 Hz, 1H), 3.13 (dd, *J* = 3.7, 14.3 Hz, 1H), 3.2 (m, 1H), 3.4 (m, 1H), 3.60 (s, 2H), 4.08 (br, 1H), 4.26 (dd, *J* = 7.6, 9.7 Hz, 1H), 4.43 (dd, *J* = 4.1, 11.1 Hz, 1H), 4.48 (m, 1H), 5.09 (br, 1H), 7.15-7.19 (m, 3H), 7.25-7.33 (m, 9H), 7.43 (d, *J* = 6.9 Hz, 2H), 7.58 (s, 1H), 8.15 (m, 2H), 8.30 (m, 1H), 8.38 (1H); ^{13}C NMR (125MHz, CD_3OD) δ 26.5, 30.9, 35.1, 39.8, 41.2, 41.3, 49.6, 51.3, 55.0, 55.9, 64.2, 124.6, 125.3, 127.5, 128.5, 129.4, 129.9, 130.4, 130.8, 131.1, 135.7, 135.9, 138.8, 139.4, 145.2, 148.3, 148.9, 150.6, 162.0, 172.2, 172.3, 174.6, 174.8; HRMS Calcd*m/z* for $C_{39}H_{42}N_7O_8$ $[M+H]^+$ 736.3086, found 736.3091.

Phenylacetyl-aza-pentafluorophenylalaninyl-(2*S*)-prolyl-(2*S*)-3-pyridylalaninyl-(3*S*)-*β*-homophenylalanine (2.6f).

Employing the procedure described for the synthesis of acid **2.6d** using **2.39f** (26 mg, 0.03 mmol), Acid **2.6f** was isolated as white solid (13.6 mg, 58 %): $[\alpha]^{20}_D = -87$ (*c* 0.1, CH_3OH); ^{1}HNMR (700 MHz, CD_3OD) δ 1.26 (m, 1H), 1.82 (m, 2H), 2.20 (m, 1H), 2.60 (d, *J* = 6.4 Hz, 2H), 2.80 (dd, *J* = 9.1, 13.4 Hz, 1H), 2.81 (m, 1H), 2.99 (d, *J* = 10.6, 1H), 3.07 (dd, *J* = 3.6, 14.2 Hz, 1H), 3.13-3.17 (m, 1H), 3.39 (m, 1H), 3.63 (s, 2H), 4.28 (dd, *J* = 7.07, 10.3 Hz, 1H), 4.38 (m, 2H), 4.47-4.51 (m, 1H), 5.16 (m, 1H), 7.15-7.21 (m, 3H), 7.23-7.30 (m, 5H), 7.43 (s, 1H), 7.51 (s, 1H), 7.59 (s, 1H), 7.76 (s, 1H), 8.23 (s, 1H), 8.43 (d, *J* = 4.2 Hz, 1H); ^{13}C NMR (175 MHz, CD_3OD) δ 26.5, 30.9, 35.0, 39.8, 41.1, 41.5, 43.0, 49.6, 51.3, 55.9, 64.2, 125.8, 127.5, 128.5, 129.4, 129.8, 130.4, 130.8, 135.3, 136.7, 138.1, 139.5, 141.8, 143.3, 146.7, 148.1, 149.0, 161.9, 164.8, 171.8, 172.7, 174.3, 174.4; HRMS Calcd *m/z* for $C_{39}H_{38}F_5N_6O_6$ $[M+H]^+$ 787.2768, found 787.2780.

Phenylacetyl-aza-1,2,3-triazole-3-alaninyl-(2*S*)-prolyl-(2*S*)-3-pyridylalaninyl-(3*S*)-*β*-homophenylalanine (2.6g).

In a 20 mL vial, a mixture of CuI (4.2 mg, 0.022 mmol) and DIPEA (7.7 μL, 0.044 mmol) in anhydrous CH_2Cl_2 (2 mL) was stirred for 3 min, treated with phenylacetyl-aza-propargylglycinyl-(2*S*)-prolyl-(2*S*)-3-pyridylalaninyl-(3*S*)-*β*-homophenylalanine benzyl ester (**2.39c**, 80 mg, 0.11 mmol), followed by $TMSN_3$ (45 μL, 0.33), stirred for 5 min, treated with AcOH (2.5 μL, 0.044 mmol), and stirred for 5h at room temperature. The reaction mixture was treated with 10 mL of NH_4OH. The phases were separated. The aqueous phase was extracted three times with CH_2Cl_2. The organic layers were combined, dried with Na_2SO_4, filtered and concentrated under vacuum. The residue was then passed through column containing silicagel (2.6 cm diameter x 5 cm high) using 100% EtOAc as eluent. Ester **2.40g** (30 mg, 36%) was isolated as white foam: $R_f = 0.35$ (8% MeOH/CH_2Cl_2); $[\alpha]^{20}_D = 7.7$ (*c* 1, $CHCl_3$); HRMS Calcd*m/z* for $C_{42}H_{46}N_9O_6$ $[M+H]^+$ 772.3566, found 772.3586. Ester **2.40g** (20 mg, 0.026 mmol) was dissolved in dioxane (1 mL), and treated with a solution of 1N LiOH (1 mL) for 1h. The volatiles were evaporated under reduce pressure. The remaining aqueous volume was acidified to pH = 3 using 1N HCl and extracted with ethyl acetate. The organic layers were combined, dried over Na_2SO_4, filtered and evaporated to a residue, that was purified by preparative HPLC on a C18 reverse-phase column using a gradient for elution from 40% to 90% MeOH (0.1% FA) in water (0.1% FA) over 40 min at a flow rate of 10 mL/min. Freeze-drying of the collected fractions gave acid **2.6g** (7 mg, 40%) as white solid: $[\alpha]^{20}_D = -10.5$ (*c* 0.2, MeOH); ^{1}H NMR (700 MHz, CD_3OD) δ 1.19 (m, 1H), 1.77 (m, 2H), 2.16 (m, 1H), 2.58 (d, *J* = 6.6 Hz, 2H), 2.78 (m, 2H), 2.97 (dd, *J* = 5.0, 13.3 Hz, 1H), 3.07 (dd, *J* = 3.9, 14.5 Hz, 1H), 3.11 (m, 1H), 3.40 (m, 1H), 3.61 (d, *J* = 14.8 Hz, 1H), 3.65 (d, *J* = 14.8 Hz, 1H), 4.22 (m, 1H), 4.26 (dd, *J* = 7.1, 10.5 Hz, 1H), 4.39 (m, 1H), 4.48 (m, 1H), 5.07 (m, 1H), 7.14-7.17 (m, 3H), 7.25-7.24 (m, 3H), 7.29-7.32 (m, 4H), 7.52 (d, *J* = 6.9 Hz, 1H), 7.59 (br, 1H), 7.67 (br, 1H), 7.87 9br, 1H), 8.19 (s, 1H), 8.23 (s, 1H), 8.37 (d, *J* = 4.8 Hz, 1H); ^{13}C NMR (175 MHz, CD_3OD) δ 26.5, 30.9, 35.1, 39.6, 41.2, 41.4, 49.5, 49.6, 51.2, 55.9, 64.2, 125.2, 127.5, 128.5, 129.4, 129.9 (2C), 130.5 (2C), 130.8, 135.7, 135.9, 138.8, 139.4, 148.3, 150.6, 162.0, 165.8, 172.2, 172.4, 174.6. HRMS m/z calcdfor $C_{35}H_{40}N_9O_6$ $[M + H]^+$ 682.3096, found 682.3111.

Phenylacetyl-aza-1-phenyl-1,2,3-triazole-3-alaninyl-(2*S*)-prolyl-(2*S*)-3-pyridylalaninyl-(3*S*)-*β*-homophenylalanine (2.6h).

Employing the protocol for the synthesis of triazole **2.6g** using azidobenzene (39 mg, 0.33 mmol), ester **2.40h** (65 mg, 70%) was isolated as a white foam: R_f 0.21 (7% MeOH in CH_2Cl_2); $[\alpha]^{20}_D =$ 8.7 (*c* 1.16, $CHCl_3$); HRMS Calcd*m/z* for $C_{48}H_{50}N_9O_6$ $[M+H]^+$ 848.3879, found 848.3895.

Hydrolysis of ester **2.40h** (38 mg, 0.048 mmol) and HPLC purification using a gradient of 50% to 90% MeOH (0.1% FA) in water (0.1% FA) over 40 min at a flow rate of 10 mL/min provided acid **2.6h** (20 mg, 55 %) as white powder: $[\alpha]^{20}_{D}$ = 14 (*c* 0.5, CH_3OH); ^{1}HNMR (700 MHz, CD_3OD) δ 1.21 (m, 1H), 1.76 (m, 2H), 2.15 (m, 1H), 2.56 (d, *J* = 6.8 Hz, 2H), 2.79 (dd, *J* = 8.2, 13.5 Hz, 1H), 2.83 (dd, *J* = 11.3, 11.8 Hz, 1H), 2.96 (dd, *J* = 5.1, 13.6 Hz, 1H), 3.08 (dd, *J* = 4.2, 14.5 Hz, 1H), 3.12 (m, 1H), 3.44 (m, 1H), 3.62 (d, *J* = 14.6 Hz, 1H), 3.67 (d, *J* = 14.6 Hz, 1H), 4.28 (dd, *J* = 7.2, 10.06 Hz, 1H), 4.39 (m, 1H), 4.42 (dd, *J* = 4.3, 11.0 Hz, 1H), 4.45-4.49 (m, 1H), 5.03 (m, 1H), 7.14-7.20 (m, 4H), 7.23-7.26 (m, 4H), 7.29-7.31 (m, 3H), 7.49 (t, *J* = 7.5 Hz, 1H), 7.52 (d, *J* = 7.9 Hz, 1H), 7.58 (m, 2H), 7.82 (d, *J* = 7.8 Hz, 2H), 8.24 (s, 1H), 8.36 (m, 2H); ^{13}C NMR (175 MHz, CD_3OD) δ 26.5, 30.9, 35.2, 39.9, 41.2, 41.3, 46.6, 49.7, 51.2, 55.9, 64.1, 121.6, 124.2, 125.2, 127.5, 128.4, 129.4, 129.8, 130.1, 130.4, 130.8, 131.0, 135.7, 135.9, 138.3, 138.7, 139.4, 144.8, 148.3, 150.6, 161.7, 172.1, 172.4, 174.6, 175.0. HRMS m/z calcdfor $C_{41}H_{44}N_9O_6$ $[M + H]^+$ 758.3409, found 758.3408.

Phenylacetyl-aza-1-toluyl-1,2,3-triazole-3-alaninnyl-(2*S*)-prolyl-(2*S*)-3-pyridylalaninyl-(3*S*)-*β*-homophenylalanine (2.6i).

Employing the protocols for the synthesis of triazole **2.6g** using 4-azidotoluene (43 mg, 0.33 mmol), ester **2.40i** (78 mg, 82%) was isolated as off-white solid: R_f 0.29 (5% MeOH in CH_2Cl_2); $[\alpha]^{20}_{D}$ =10 (*c* 1, $CHCl_3$); HRMS Calcd*m/z* for $C_{49}H_{51}N_9O_6Na$ $[M+Na]^+$ 884.3855, found 884.3850. Hydrolysis of ester **2.40i** (30 mg, 0.035 mmol) and HPLC purification using a gradient of 50% to 80% MeOH (0.1% FA) in water (0.1% FA) over 40 min at a flow rate of 10 mL/min provided acid **2.6i** (10 mg, 37 %): $[\alpha]^{20}_{D}$ = 24.8 (*c* 0.5, CH_3OH); ^{1}HNMR (700 MHz, CD_3OD) δ 1.24 (m, 1H), 1.77 (m, 2H), 2.16 (m, 1H), 2.43 (s, 3H), 2.57 (d, *J* = 6.9 Hz, 2H), 2.79 (dd, *J* = 8.1, 13.5 Hz, 1H), 2.85 (dd, *J* = 11.2, 14.0 Hz, 1H), 2.95 (dd, *J* = 5.0, 13.6 Hz, 1H), 3.10 (dd, *J* = 4.5, 14.2 Hz, 1H), 3.12 (m, 1H), 3.44 (m, 1H), 3.63 (d, *J* = 14.6 Hz, 1H), 3.67 (d, *J* = 14.6 Hz, 1H), 4.28 (dd, *J* = 7.2, 10.1 Hz, 1H), 4.39 (m, 1H), 4.42 (dd, *J* = 4.3, 10.6 Hz, 1H), 4.44-4.48 (m, 1H), 5.02 (m, 1H), 7.16-7.21(m, 4H), 7.23-7.26 (m, 4H), 7.31 (d, 7.3 Hz, 2H), 7.36-7.37 (m, 1H), 7.39 (d, *J* = 8.4 Hz, 2H), 7.59 (br, 1H), 7.68 (d, *J* = 8.40 Hz, 2H), 8.26 (s, 1H), 8.31 (s, 1H), 8.40 (d, 1H); ^{13}C NMR (175 MHz, CD_3OD) δ 21.1, 26.5, 30.9, 35.2, 39.4, 41.2, 41.3, 46.6, 49.5, 51.2, 55.8, 64.1, 121.6, 124.1, 125.5, 127.5, 128.4, 129.4, 129.8, 130.4, 130.8, 131.4, 135.7, 136.0, 136.3, 139.3, 139.9, 140.6, 144.6, 147.4, 149.7, 161.7, 172.0, 172.4, 174.4, 174.6. HRMS m/z calcdfor $C_{41}H_{42}FN_9O_6$ $[M + H]^+$ 772.3566, found 772.3581.

Phenylacetyl-aza-1-(4-flourophenyl)-1,2,3-triazole-3-alaninyl-(2*S*)-prolyl-(2*S*)-3-pyridylalaninyl-(3*S*)-*β*-homophenylalanine (2.6j).

Employing the protocols for the synthesis of of triazole **2.6g** using 1-azido-4-fluorobenzene (45 mg, 0.33 mmol), ester **2.40j** (79.5 mg, 83%) was isolated as white foam: R_f 0.18 (5% MeOH in CH_2Cl_2); $[\alpha]^{20}_D$ = 5 (*c* 1, $CHCl_3$); HRMS Calcd for $C_{48}H_{49}FN_9O_6$ $[M+H]^+$ 866.3784, found 866.3811. Hydrolysis of ester **2.40j** (30 mg, 0.035 mmol) and HPLC purification using a gradient of 20% to 80% MeOH (0.1% FA) in water (0.1% FA) over 40 min at a flow rate of 10 mL/min, provided acid **2.6j** (11.3 mg, 42 %): $[\alpha]^{20}_D$ = 15.4 (*c* 0.6, CH_3OH); ^{1}H NMR (700 MHz, CD_3OD) δ 1.19 (m, 1H), 1.75 (m, 2H), 2.17 (m, 1H), 2.55 (d, *J* = 6.0 Hz, 2H), 2.78 (dd, *J* = 7.9, 13.6 Hz, 1H), 2.82 (dd, *J* = 11.4, 14.2 Hz, 1H), 2.94 (dd, *J* = 4.9, 13.6 Hz, 1H), 3.07 (dd, *J* = 4.2, 14.4 Hz, 1H), 3.12 (dd, , *J* = 8.6, 17.5 Hz, 1H), 3.44 (m, 1H), 3.62 (d, *J* = 14.7 Hz, 1H), 3.69 (d, *J* = 14.7 Hz, 1H), 4.27 (dd, *J* = 7.30, 10.1 Hz, 1H), 4.41-4.43 (m, 2H), 4.45-4.48 (m, 1H), 4.99 (m, 1H), 7.14-7.20 (m, 4H), 7.22-7.26 (m, 4H), 7.29-7.34 (m, 5H), 7.52 (d, *J* = 7.8 Hz, 1H), 7.83 (dd, *J* = 4.6, 8.9 Hz, 2H), 8.23 (s, 1H), 8.35-8.38 (m, 2H); ^{13}C NMR (175 MHz, CD_3OD) δ 26.5, 30.9, 35.2, 39.7, 41.2, 41.3, 46.7, 49.6, 51.2, 55.8, 64.1, 117.6 (d), 123.8 (d), 124.4, 125.2, 127.5, 128.4, 129.4, 129.8, 130.4, 130.8, 134.7, 135.8 (d), 138.8, 139.3, 144.8, 148.2, 150.6, 161.6, 163.3, 164.7, 172.1, 172.3, 174.6, 174.8. HRMS m/z calcd. for $C_{41}H_{42}FN_9O_6$ $[M + H]^+$ 776.3315, found 776.3331.

Phenylacetyl-aza-1-(4-nitrophenyl)-1,2,3-triazole-3-alaninyl-(2*S*)-prolyl-(2*S*)-3 pyridylalaninyl-(3*S*)-*β*-homophenylalanine (2.6k).

Employing the protocol described for the preparation of triazole **2.6g** using 1-azido-4-nitrobenzene (54 mg, 0.33 mmol), ester **2.40k** (70 mg, 71%) was obtained as white foam: R_f 0.24 (8% MeOH in CH_2Cl_2); $[\alpha]^{20}_D$ = 29.6 (*c* 0.75, $CHCl_3$); HRMS Calcd *m/z* for $C_{48}H_{49}N_{10}O_8$ $[M+H]^+$ 893.3729, found 893.3772. Hydrolysis of ester **2.40k** (30 mg, 0.034 mmol) and HPLC purification using the protocol described for **2.6i** provided acid **2.6k** (10 mg, 37 %) as solid; $[\alpha]^{20}_D$ = 20 (*c* 0.45, CH_3OH); ^{1}HNMR (700 MHz, CD_3OD) δ 1.19 (m, 1H), 1.76 (m, 2H), 2.15 (m, 1H), 2.55 (t, *J* = 7.4 , 2H), 2.79 (dd, *J* = 7.7, 13.6 Hz, 1H), 2.83 (dd, *J* = 11.5, 14.1 Hz, 1H), 2.92 (dd, *J* = 5.3, 13.4 Hz, 1H), 3.08 (dd, *J* = 4.1, 14.3 Hz, 1H), 3.11 (dd, *J* = 8.6, 17.3 Hz, 1H), 3.45 (m, 1H), 3.62 (d, *J* = 14.5 Hz, 1H), 3.66 (d, *J* = 14.5 Hz, 1H), 4.28 (dd, *J* = 7.2, 9.9 Hz, 1H), 4.43-4.47 (m, 2H), 4.53 (m, 1H), 4.95 (m, 1H), 7.13-7.21 (m, 6H), 7.22-7.24 (m, 2H), 7.28-7.31 (m, 3H), 7.53 (d, , *J* = 7.6 Hz, 1H), 8.13 (d, *J* = 9.0 Hz, 2H), 8.23 (s, 1H), 8.36 (d, *J* = 4.1 Hz, 1H), 8.44 (d, *J* = 9.0 Hz, 2H), 8.62 (s, 1H); ^{13}C NMR (175 MHz, CD_3OD) δ 26.5, 30.9, 35.2, 39.3, 41.2, 41.3, 46.8, 49.5, 51.2, 55.7,

64.1, 122.0, 124.5 125.2, 126.5, 127.5, 128.4, 129.4, 129.8, 130.4, 130.8, 135.7, 135.8, 138.8, 139.2, 142.5, 145.5, 148.2, 148.8, 150.6, 161.4, 166.4, 172.1, 172.3, 174.6; HRMS m/z calcdfor $C_{41}H_{42}N_{10}O_8$ $[M + H]^+$ 803.3259, found 803.3276.

Phenylacetyl-aza-1-(4-iodophenyl)-1,2,3-triazole-3-alaninyl-(2*S*)-prolyl-(2*S*)-3-pyridylalaninyl-(3*S*)-*β*-homophenylalanine (2.6l).

Employing the protocol to make triazole **2.6g** using 1-azido-4-iodobenzene (81 mg, 0.33 mmol), ester **2.40l** (102 mg, 95%) was isolated as white foam: R_f 0.27 (5% MeOH in CH_2Cl_2); $[\alpha]^{20}_D$ = 11.8 (c 0.5, $CHCl_3$); HRMS Calcd *m/z* for $C_{48}H_{49}IO_6$ $[M+H]^+$ 974.2845, found 974.2858. Hydrolysis of **2.40l** (30 mg, 0.031 mmol) and HPLC purification using a gradient of 30% to 90% MeCN (0.1% FA) in water (0.1% FA) over 40 min at a flow rate of 10 mL/min provided acid **2.6l** (8.2 mg, 30 %): $[\alpha]^{20}_D$ = 128 (*c* 0.08, CH_3OH); ^{1}H NMR (700 MHz, CD_3OD) δ 1.20 (m, 1H), 1.76 (m, 2H), 2.15 (m, 1H), 2.55 (d, *J* = 4.8, 2H), 2.78 (dd, *J* = 7.8, 13.5 Hz, 1H), 2.83 (t, *J* = 12.5 Hz, 1H), 2.92 (dd, *J* = 5.09, 13.30 Hz, 1H), 3.08 (dd, *J* = 4.20, 14.5 Hz, 1H), 3.12 (dd, , *J* = 9.5, 18 Hz, 1H), 3.44 (m, 1H), 3.62 (d, *J* = 14.5 Hz, 1H), 3.66 (d, *J* = 14.5 Hz, 1H), 4.28 (dd, *J* = 7.2, 10.1 Hz, 1H), 4.41-4.46 (m, 4H), 7.15-7.20 (m, 4H), 7.21 (d, *J* = 7.2 Hz, 2H), 7.25 (t, *J* = 7.5 Hz, 2H), 7.30 (d, *J* = 7.4 Hz, 2H), 7.35 (dd, *J* = 5.2, 7.6 Hz, 1H), 7.55 (d, *J* = 6 Hz, 1H), 7.62 (d, *J* = 8.7 Hz, 2H), 7.93 (d, *J* = 8.7 Hz, 2H), 8.20 (s, 1H), 8.38 (d, *J* = 4.6 Hz, 1H), 8.40 (s, 1H); ^{13}C NMR (175 MHz, CD_3OD) δ 26.5, 30.9, 35.2, 39.3, 41.2, 41.3, 46.7, 49.6, 51.2, 55.8, 64.1, 94.6, 123.3, 124.1, 125.3, 127.5, 128.4, 129.4, 129.8, 130.4, 130.8, 135.7, 136.0, 138.0, 139.2, 140.2, 145.0, 147.9, 150.2, 161.6, 164.8, 172.1, 172.3, 174.5, 174.6; HRMS m/z calcdfor $C_{41}H_{42}IN_9O_6$ $[M + H]^+$ 884.2376, found 884.2383.

Phenylacetyl-aza-aspartyl-(2*S*)-prolyl-(2*S*)-3-pyridylalaninyl-(3*S*)-*β*-homophenylalanine (2.7).

Phenylacetyl-aza-propargylglycinyl-(2*S*)-prolyl-(2*S*)-3-pyridylalaninyl-(3*S*)-*β*-homophenyl alanine benzyl ester (**2.39c**, 20 mg, 0.03 mmol) was dissolved in 4 mL of 1:1 THF/H_2O and treated sequentially with OsO_4 (0.15 mg, 0.6 μmol), hexamethylenetetramine (HMTA, 8.4 mg, 0.06 mmol) and $NaIO_4$ (26 mg, 0.12 mmol). The mixture was stirred at room temperature for 16 h. The volatiles were removed on a rotary evaporator. The aqueous volume was extracted with CH_2Cl_2. The organic layers were combined, washed with brine, dried over Na_2SO_4, and evaporated to a residue, that was passed through a column of silica gel (2.6 cm diameter x 5 cm high) with 20% *iso*-propylalcohol in $CHCl_3$ as eluent to afford benzyl ester **2.41** as brown foam (20 mg, 89%): R_f

0.42 (10% MeOH:$CHCl_3$); HRMS Calcd *m/z* for $C_{41}H_{45}N_6O_8$ $[M+H]^+$ 749.3293, found 749.3314. Hydrolysis of ester **2.41** (20 mg, 0.03 mmol) and HPLC purification using a gradient for elution from 20% to 80% MeOH (0.1% FA) in water (0.1% FA) over 40 min at a flow rate of 10 mL/min afforded acid **7** (12 mg, 70 %): $[\alpha]^{20}_D$ = 5.6 (*c* 0.14, CH_3OH); ^{1}H NMR (700 MHz, CD_3OD) δ 1.18 (m, 1H), 1.76 (m, 2H), 2.13 (m, 1H), 2.57 (d, *J* = 5.0 Hz, 2H), 2.73-2.78 (m, 2H), 2.94 (dd, *J* = 4.8, 13.3 Hz, 1H), 3.04 (d, *J* = 12.4 Hz, 1H), 3.14 (m, 1H), 3.56 (m, 1H), 3.65-3.73 (m, 3H), 4.23 (dd, *J* = 7.4, 9.4 Hz, 1H), 4.36 (d, *J* = 9.0 Hz, 1H), 4.46 (m, 1H), 4.69 (m, 1H), 7.11-7.16 (m, 3H), 7.21-7.25 (m, 2H), 7.28-7.31 (m, 2H), 7.36 (d, *J* = 7.3 Hz, 2H), 7.49 (d, *J* = 6.0 Hz, 1H), 8.23 (s, 1H), 8.37 (d, *J* = 4.1 Hz, 1H), 8.41 (s, 2H); ^{13}C NMR (175 MHz, CD_3OD) δ 26.3, 31.0, 35.0, 40.1, 41.1, 41.8, 49.8, 51.2, 55.1, 55.9, 64.2, 125.2, 127.3, 128.4, 129.3, 129.8, 130.5, 130.8, 135.9, 136.0, 138.7, 139.5, 148.2, 150.6, 161.6, 168.5, 172.1, 172.3, 174.9, 175.1; HRMS Calcd*m/z* for $C_{34}H_{39}N_6O_8$ $[M+H]^+$ 659.2824, found 659.2836.

Phenylacetyl-aza-4-(*N*,*N*-dimethylamino)but-2-ynylglycinyl-(2*S*)-prolyl-(2*S*)-3 pyridylalaninyl-(3*S*)-*β*-homophenylalanine (2.8m).

Propargylglycine **2.39c** (80 mg, 0.11 mmol) was dissolved in 1.3 mL of distilled dioxane, and treated sequentially with dimethylamine 40% wt in H_2O (15 µL, 0.13 mmol), CuI (2.1 mg ,0.01 mmol) and paraformaldehyde (6.7 mg, 0.22 mmol). The mixture was heated at 80 °C for 1 h, when complete consumption of starting material was observed by TLC. The volatiles were removed on rotary evaporator. The residue was passed through column of silica gel (2.6 cm diameter x 5 cm high) with 20% *iso*-propanol in $CHCl_3$ as eluent. Evaporation of the collected fractions gave benzyl ester **2.42m** (64 mg, 74%) as white foam: R_f 0.22 (5% MeOH in $CHCl_3$); HRMS Calcd *m/z* for $C_{45}H_{52}N_7O_6$ $[M+H]^+$ 786.3974, found 786.3986. Hydrolysis of ester **2.42m** (30 mg, 0.04 mmol) as described for the synthesis of **2.6d** and purification by preparative HPLC using a gradient for elution from 20% to 80% MeOH (0.1% FA) in water (0.1% FA) over 35 min at a flow rate of 10 mL/min gave acid **2.8m** (19 mg, 75 %) as white powder: $[\alpha]^{20}_D$ = 4.6 (c 0.92, CH_3OH); ^{1}HNMR (700 MHz, CD_3OD) δ 1.20 (m, 1H), 1.76 (m, 2H), 2.14 (m, 1H), 2.51 (m, 8H), 2.78 (dd, *J* = 7.8, 13.6 Hz, 1H), 2.88 (t, *J* = 12.7 Hz, 1H), 2.98 (dd, *J* = 5.1, 13.6 Hz, 1H), 3.11-3.17 (m, 2H), 3.45 (m, 1H), 3.48-3.55 (m, 2H), 3.66-3.72 (m, 2H), 3.94 (d, *J* = 16.9 Hz, 1H), 4.20 (dd, *J* = 7.2, 9.9 Hz, 1H), 4.27 (d, *J* = 16.9 Hz, 1H), 4.41-4.43 (m, 2H), 7.10-7.15 (m, 3H), 7.20 (m, 2H), 7.26 (t, *J* = 7.4 Hz, 1H), 7.34 (m, 3H), 7.38 (d, *J* = 7.2 Hz, 2H), 7.58 (d, *J* = 7.5 Hz, 1H), 8.30 (s, 1H), 8.39 (s, 1H); ^{13}C NMR (175 MHz, CD_3OD) δ 26.4, 31.0, 35.1, 40.4, 41.0, 41.3, 41.8, 43.7, 48.2, 49.9,

51.1, 55.9, 64.2, 77.8, 83.3, 125.2, 127.4, 128.5, 129.4, 129.9, 130.5, 130.9, 135.8, 135.9, 138.7, 139.3, 148.3, 150.6, 161.0, 172.2, 172.3, 174.5, 175.9. HRMS m/z calcdfor $C_{38}H_{46}N_7O_6$ $[M + H]^+$ 696.3504, found 696.3509.

Phenylacetyl-aza-4-(pyrrolidino)but-2-ynylglycinyl-(2*S*)-prolyl-(2*S*)-3-pyridylalaninyl-(3*S*)-*β*-homophenylalanine (2.8n).

Employing the protocol to acid **2.8m** using pyrrolidine (9.2 μL, 0.13 mmol), ester **2.42n** (70 mg, 88%) was isolated as pale green foam: R_f 0.55 (5% MeOH in $CHCl_3$); HRMS Calcd *m/z* for $C_{47}H_{54}N_7O_6$ $[M+H]^+$ 812.4130, found 812.4151. Hydrolysis of **2.42n** (30 mg, 0.025 mmol) and HPLC purification using a gradient for elution from 10% to 90% MeOH (0.1% FA) in water (0.1% FA) over 40 min at a flow rate of 10 mL/min afforded azapeptide **2.8n** (14 mg, 80 %) as white powder: $[\alpha]^{20}_D$ = 3.9 (*c* 1.08, CH_3OH); ^{1}HNMR (700 MHz, CD_3OD) δ 1.19 (m, 1H), 1.75 (m, 2H), 1.96 (m, 4H), 2.13 (m, 1H), 2.51 (m, 2H), 2.77 (m, 1H), 2.85 (m, 1H), 2.98 (dd, *J* = 4.8, 13.3 Hz, 1H), 3.10-3.17 (m, 6H), 3.34 (m, 1H), 3.69 (m, 2H), 3.77 (m, 2H), 3.93 (d , *J* = 16.0, 1H), 4.20 (dd , *J* = 7.4, 9.6 Hz, 2H), 4.41 (m, 2H), 7.10-7.14 (m, 3H), 7.20 (d, *J* = 6.8 Hz , 2H), 7.27 (t, *J* = 7.2 Hz, 1H), 7.33 (t, *J* = 7.2 Hz, 3H), 7.38 (d, *J* = 7.4 Hz, 2H), 7.58 (s, 1H), 8.31 (s, 1H), 8.40 (s, 1H); ^{13}C NMR (175 MHz, CD_3OD) δ 24.4, 26.3, 31.0, 35.1, 40.8, 40.9, 41.3, 41.9, 44.3, 50.2, 51.0, 54.3, 56.0, 64.2, 77.1, 83.3, 125.3, 127.4, 128.5, 129.4, 129.9, 130.5, 131.0, 135.8, 135.9, 138.7, 139.4, 148.4, 150.7, 160.9, 172.2, 172.3, 174.6, 176.6. HRMS m/z calcdfor $C_{40}H_{48}N_7O_6$ $[M + H]^+$ 722.3661, found 722.3652.

Phenylacetyl-aza-4-(piperidinyl)but-2-ynylglycinyl-(2*S*)-prolyl-(2*S*)-3-pyridylalaninyl-(3*S*)-*β*-homophenylalanine (2.8o).

Employing the protocol described for the synthesis of acid **2.8m** using piperidine (13 μL, 0.13 mmol), ester **2.42o** (84 mg, 92%) was isolated as light green foam: R_f 0.53 (5% MeOH in $CHCl_3$); $[\alpha]^{20}_D$ = 25.2 (c 0.83, $CHCl_3$); HRMS Calcd *m/z* for $C_{48}H_{55}N_7O_6Na$ $[M+Na]^+$ 848.4106, found 848.4117. Hydrolysis of **2.42o** (30 mg, 0.04 mmol) and HPLC purification as described for the preparation of acid **2.8m** afforded azapeptide **2.8o** (19.3 mg, 73%) as white solid: $[\alpha]^{20}_D$ = –81.3 (c 0.1, CH_3OH); ^{1}H NMR (700 MHz, CD_3OD) δ 1.20 (m, 1H), 1.55 (m, 2H), 1.73-1.76 (m, 6H), 2.14 (m, 1H), 2.53 (s, 2H), 2.76 (dd, *J* = 7.8, 13.4 Hz, 1H), 2.84 (m, 1H), 2.92 (m, 3H), 2.99 (dd, *J* = 3.7, 13.4 Hz, 2H), 3.10-3.17 (m, 2H), 3.45 (m, 1H), 3.61 (s, 2H), 3.71 (m, 2H), 3.92 (d, *J* = 16.4 Hz, 1H), 4.20 (dd, *J* = 7.1, 9.7 Hz, 1H), 4.32 (d, *J* = 16.9 Hz, 1H), 4.39-4.43 (m, 2H), 7.12-7.13 (m, 3H), 7.20-7.21 (m, 2H), 7.26 (t, *J* = 7.4 Hz, 1H), 7.33 (m, 3H), 7.39 (d, *J* = 7.3 Hz, 2H),

7.56 (m, 1H), 8.29 (s, 1H), 8.39 (s, 1H), 8.44 (s, 1H); ^{13}C NMR (175 MHz, CD_3OD) δ 23.4, 25.1, 26.4, 30.9, 35.1, 40.6, 41.1, 41.2, 41.8, 47.5, 49.9, 51.1, 53.9, 55,9, 64.2, 77.1, 83.8, 125.2, 127.4, 128.5, 129.4, 129.9, 130.5, 130.9, 135.8, 135.9, 138.7, 139.4, 148.3, 150.6, 161.1, 172.1, 172.3, 174.4, 174.5; HRMS Calcd*m/z* for $C_{41}H_{49}N_7O_6$ $[M+2H]^{+2}$ 368.6945, found 368.6945.

Phenylacetyl-aza-4-(morpholino)but-2-ynylglycinyl-(2*S*)-prolyl-(2*S*)-3-pyridylalaninyl-(3*S*)-*β*-homophenylalanine (2.8p).

Employing the protocol described for the synthesis of amine **2.8m** using morpholine (11 μL, 0.13 mmol), ester **2.42p** (72 mg, 80%) was isolated as pale green foam: R_f 0.35 (12% *i*-PrOH in $CHCl_3$); $[\alpha]^{20}_D$ = 32.2 (*c* 1, $CHCl_3$); HRMS Calcd *m/z* for $C_{47}H_{53}N_7O_7Na$ $[M+Na]^+$ 850.3899, found 850.3913. Hydrolysis of ester **2.42p** (30 mg, 0.036 mmol) and HPLC purification using a gradient for elution from 40% to 90% MeOH (0.1% FA) in water (0.1% FA) over 40 min at a flow rate of 10 mL/min gave azapeptide **2.8p** (14 mg, 53%) as white powder: $[\alpha]^{20}_D$ = 30.4 (*c* 0.18, CH_3OH); ^{1}H NMR (700 MHz, CD_3OD) δ 1.38 (m, 1H), 1.78 (m, 1H), 1.81 (m, 1H), 2.17 (m, 1H), 2.49 (dd, *J* = 6.9, 16.1 Hz, 1H), 2.54 (dd, *J* = 6.8, 16.4, 1H), 2.77 (dd, *J* = 8.0, 13.7 Hz, 1H), 2.93 (dd, *J* = 5.5, 13.7 Hz, 1H), 2.97 (m, 1H), 3.16 (m, 1H), 3.20-3.23 (m, 1H), 3.31 (m, 4H), 3.45 (m, 1H), 3.73 (s, 2H), 3.90 (s, 4H), 4.01 (m, 2H), 4.08 (d, *J* = 16.5, 1H), 4.26 (t, *J* = 8.2 Hz, 1H), 4.40-4.43 (m, 2H), 4.46 (m, 1H), 7.18-7.21 (m, 1H), 7.23-2.24 (m, 4H), 7.26 (t, *J* = 7.4 Hz, 1H), 7.34 (t, *J* = 7.7 Hz, 2H), 7.40 (d, *J* = 7.71 Hz, 2H), 7.69 (s, 1H), 7.88 (s, 1H), 8.40 (s, 1H), 8.58 (s, 1H); ^{13}C NMR (175 MHz, CD_3OD) δ 26.5, 30.9, 35.2, 39.3, 41.2, 41.3, 41.4, 47.3, 49.4, 51.1, 52.6, 55.3, 63.9, 65.2, 73.8, 86.9, 127.0, 127.6, 128.5, 129.5, 129.9, 130.5, 130.8, 135.9, 138.2, 139.3, 144.0, 146.1, 158.0, 160.9, 171.4, 172.6, 174.4, 174.5; HRMS Calcd*m/z* for $C_{40}H_{48}N_7O_7$ $[M+H]^+$ 738.3610, found 738.3620.

Phenylacetyl-aza-4-(*N*,*N*-diallylamino)but-2-ynylglycinyl-(2*S*)-prolyl-(2*S*)-3-pyridylalaninyl-(3*S*)-*β*-homophenylalanine (2.8q).

Employing the protocol described for the preparation amine **2.8m** using diallylamine (16 μL, 0.13 mmol), ester **2.42q** (80 mg, 87%) was isolated as yellow foam: R_f 0.43 (12% *i*-PrOH in $CHCl_3$); $[\alpha]^{20}_D$ = 18.4 (*c* 1, $CHCl_3$); HRMS Calcd *m/z* for $C_{49}H_{55}N_7O_6$ $[M+H]^+$ 838.4287, found 838.4292. Hydrolysis of ester **2.42q** (30 mg, 0.036 mmol) and purification by HPLC a gradient for elution from 30% to 80% MeOH (0.1% FA) in water (0.1% FA) over 40 min at a flow rate of 10 mL/min gave azapeptide **2.8q** (17 mg, 63%) as white powder: $[\alpha]^{20}_D$ = 22.6 (*c* 0.38, CH_3OH); ^{1}H NMR (700 MHz, CD_3OD) δ 1.51 (m, 1H), 1.82 (m, 1H), 1.90 (m, 1H), 2.21 (m, 1H), 2.52 (dd, *J* = 7.3,

16.3 Hz, 1H), 2.58 (dd, , *J* = 6.5, 16.2, 1H), 2.78 (dd, *J* = 8.1, 13.4 Hz, 1H), 2.95 (dd, *J* = 5.4, 13.5 Hz, 1H), 3.03 (m, 1H), 3.21-3.23 (m, 1H), 3.29-3.31 (m, 1H), 3.49 (m, 1H), 3.76 (s, 2H), 3.87 (d, *J* = 7.1, 4H), 4.01 (s, 2H), 4.10 (d, *J* = 17.4, 1H), 4.29 (t, *J* = 8.1 Hz, 1H), 4.42 (m, 1H), 4.47 (m, 1H), 4.53 (m, 1H), 5.64 (s, 1H), 5.66 (s, 2H), (d, *J* = 1.2 Hz, 1H), 5.95-6.01 (m, 2H), 7.21-7.24 (m, 1H), 7.26-7.28 (m, 5H), 7.35 (t, *J* = 7.7 Hz, 2H), 7.43 (d, *J* = 7.9 Hz, 2H), 7.92-7.94 (m, 1H), 8.12 (s, 1H), 8.48 (s, 1H), 8.71 (d, *J* = 5.5 Hz, 1H)); ^{13}C NMR (175 MHz, CD_3OD) δ 26.5, 30.9, 35.2, 39.2, 41.2, 41.3, 41.8, 42.6, 49.4, 51.1, 55.2, 56.1, 63.9, 73.5, 87.2, 127.2, 127.6 (2C), 128.0, 128.5, 129.5, 129.9, 130.6, 130.9, 135.9, 139.4, 139.7, 141.3, 143.2, 148.4, 161.0, 171.0, 172.7, 174.4, 174.6; HRMS Calcd*m/z* for $C_{42}H_{50}N_7O_6$ $[M+H]^+$ 748.3817, found 748.3821.

Phenylacetyl-aza-4-(*N*-methyl-*N*-benzylamino)but-2-ynylglycinyl-(2*S*)-prolyl-(2*S*)-3-pyridylalaninyl-(3*S*)-*β*-homophenylalanine (2.8r).

Employing the protocol described for the preparation of amine **2.8m** using *N*-methyl-*N*-benzylamine (17 μL, 0.13 mmol), ester **2.42r** (74 mg, 78%) was isolated as a foam: R_f 0.74 (5% MeOH in $CHCl_3$); HRMS Calcd*m/z* for $C_{51}H_{56}N_7O_6$ $[M+H]^+$ 862.4287, found 862.4305. Hydrolysis of ester **2.42r** (29 mg, 0.035 mmol) and HPLC purification using the protocol for the synthesis of acid **2.8m** gave azapeptide **2.8r** (19 mg, 70 %) as white powder: $[\alpha]^{20}_D$ = 5.6 (c 0.14, CH_3OH); ^{1}H NMR (700 MHz, CD_3OD) δ 1.19 (m, 1H), 1.78 (m, 2H), 2.15 (m, 1H), 2.32 (s, 3H), 2.52 (d, *J* = 5.3 Hz, 2H), 2.74 (dd, *J* = 8.2, 13.7 Hz, 1H), 2.82 (dd, *J* = 11.7, 14.2 Hz, 1H), 2.98 (dd, *J* = 4.6, 13.5 Hz, 1H), 3.08 (dd, *J* = 3.9, 14.4 Hz, 1H), 3.14-3.18 (m, 1H), 3.21 (d, *J* = 16.7 Hz, 1H), 3.25 (d, *J* = 16.7 Hz, 1H), 3.47 (m, 1H), 3.61 (dd, *J* = 12.7, 18.9 Hz, 2H), 3.69 (d, *J* = 13.4 Hz, 1H), 3.73 (d, *J* = 13.4 Hz, 1H), 4.0 (d, *J* = 16.7 Hz, 1H), 4.22 (dd, *J* = 7.1, 10.1 Hz, 1H), 4.38 (dd, *J* = 3.6, 11.3 Hz, 1H), 4.42-4.47 (m, 2H), 7.10-7-12 (m, 3H), 7.20-7.23 (m, 3H), 7.27-7.30 (m, 3H), 7.32-7.33 (m, 4H), 7.37 (d, J = 7.4 Hz, 2H), 7.54 (d, *J* = 7.6 Hz, 1H), 8.27 (s, 1H), 8.37 (d, J = 4.2 Hz, 1H), 8.50 (s, 1H); ^{13}C NMR (700 MHz, CD_3OD) δ 26.4, 31.0, 35.0, 40.7, 41.2, 41.3, 41.4, 42.0, 45.9, 49.9, 51.2, 56.0, 61.2, 64.2, 80.4, 81.2, 125.2, 127.3, 128.4, 128.8, 129.3, 129.5, 130.0, 130.5, 130.8, 130.9, 135.7, 136.0, 138.1, 138.7, 139.5, 148.3, 150.6, 161.2, 172.0, 172.3, 174.6, 176.0; HRMS Calcd*m/z* for $C_{44}H_{50}N_7O_6$ $[M+H]^+$ 772.3817, found 772.3840.

Phenylacetyl-aza-(*N*,*N*-dimethyl)lysinyl-(2*S*)-prolyl-(2*S*)-3-pyridylalaninyl-(3*S*)-*β*-homophenylalanine (2.9m).

Ester **2.42m** (16 mg, 0.02 mmol) was dissolved in EtOH, treated with $Pd(OH)_2$ on carbon (10 mol% of 20 wt%), placed under H_2 gas (70 psi), and stirred at room temperature for 16 h. The

black reaction mixture was filtered over a pad of Celite™. The pad was washed with EtOAc, and the filtrate and washings were evaporated to a residue, that was purified by HPLC using the protocols described for the preparation of acid **2.8m** to afford acid **2.9m** (10 mg, 70%) as white powder: $[\alpha]^{20}_{D}$ = 108 (*c* 0.05, CH_3OH); ^{1}HNMR (700 MHz, CD_3OD) δ 1.12 (m, 1H), 1.52-1.62 (m, 2H), 1.71 (m, 2H), 1.76-1.80 (m, 2H), 2.11 (m, 1H), 2.43 (s, 2H), 2.77 (m, 5H), 2.85-2.91 (m, 2H), 2.94-2.99 (m, 2H), 3.02-3.06 (m, 1H), 3.08-3.13 (m, 2H), 3.38-3.42 (m, 2H), 3.54 (m, 1H), 3.67-3.72 (m, 3H), 4.22 (t, *J* = 8.4 Hz, 1H), 4.39 (m, 1H), 4.45 (dd, *J* = 3.5, 10.8 Hz, 1H), 7.12-7.14 9 (m, 1H), 7.18 (t, *J* = 7.4 Hz, 2H), 7.22-7.26 (m, 2H), 7.30-7.33 (m, 2H), 7.38 (d, *J* = 7.6 Hz, 2H), 7.58 (m, 1H), 8.30 (s, 1H), 8.39 (s, 1H), 8.53 (s, 2H); ^{13}C NMR (700 MHz, CD_3OD) δ 23.1, 24.3, 24.8, 25.0, 31.1, 33.7, 35.5, 41.3, 41.5, 50.1, 50.6, 50.8, 51.3, 55.7, 58.9, 63.9, 125.2, 127.4, 128.5, 129.4, 129.9, 130.5, 130.8, 135.8, 135.9, 138.8, 139.8, 148.3, 150.7, 161.2, 170.1, 172.2, 174.9, 177.9; HRMS Calcd*m/z* for $C_{38}H_{50}N_7O_6$ $[M+H]^+$ 700.3817, found 700.3814.

Phenylacetyl-aza-4-(pyrrolidono)butylglycinyl-(2*S*)-prolyl-(2*S*)-3-pyridylalaninyl-(3*S*)-*β*-homophenylalanine (2.9n).

Employing the protocol for the preparation of aza-lysine **2.9m** using ester **2.42n** (16 mg, 0.02 mmol), acid **2.9n** (10 mg, 70%) was isolated after purification by HPLC using the protocols described for the preparation of acid **2.8m** as a solid: $[\alpha]^{20}_{D}$ = 108 (*c* 0.05, CH_3OH); HRMS Calcd *m/z* for $C_{40}H_{53}N_7O_6$ $[M+2H]^{+2}$ 363.4023, found 363.7040.

Phenylacetyl-azaPra-(2*S*,4*R*)-Hyp-(2*S*)-3-Pal-(3*S*)-*β*-hPhe [(*R*)- 2.11c].

In a plastic syringe tube equipped with Teflon™ filter, stopper and stopcock, azapeptide resin **2.54c**, (200 mg, 0.14 mmol) was treated with a freshly made solution of TFA/H_2O (95:5, v/v, 5 mL). The syringe was flushed with argon, sealed, and shaken for 2 h at room temperature. The resin was filtered and washed with TFA and DCM. The filtrate was concentrated, dissolved in Et_2O, centrifuged (1200 rpm) for 5 min, and decanted. The residue was dissolved in minimum amount of acetonitrile diluted with water and freeze-dried. The azapeptide was dissolved in a 10% methanol in H_2O solution and analyzed by LC-MS on a C18 Phenomenex Gemini column™ (50 × 4.6 mm, 5 μm) using a flow rate of 0.5 mL/min and a gradient of 40-70% MeOH (0.1% FA) in water (0.1% FA). Azapeptide (*R*)- **2.11c** (60 mg) was shown to be of 61% purity by analytical LCMS, and purified on a preparative column (C18 Gemini column™) using a gradient of 40-70% MeOH (0.1% FA) in water (0.1% FA) at a flow rate of 10 mL/min to afford (*R*)- **2.11c** (14.4 mg, 39%): $[\alpha]^{20}_{D}$ = 158 (*c* 0.1, CH_3OH); ^{1}HNMR (700 MHz, CD_3OD) δ 1.26 (m, 1H), 2.11 (m, 1H),

2.32 (d, *J* = 6.7 Hz, 2H), 2.72-2.75 (m, 2H), 2.78 (dd, *J* = 11.9, 14.1 Hz, 1H), 2.97 (dd, *J* = 4.9, 13.6 Hz, 1H), 3.05 (dd, *J* = 4.2, 14.4 Hz, 1H), 3.24 (dd, *J* = 3.5, 11.3 Hz, 2H), 3.69 (d, *J* = 14.5 Hz, 1H), 3.75 (d, *J* = 14.5 Hz, 1H), 3.87 (d, *J* = 16Hz, 1H), 4.19 (m, 1H), 4.37 (dd, *J* = 4.2, 11.2 Hz, 1H), 4.40-4.43 (m, 1H), 4.44-4.48 (m, 2H), 7.12 (m, 3H), 7.19-7.21 (m, 2H), 7.22-7.25 (m, 1H), 7.29-7.33 (m, 3H), 7.38 (d, *J* = 7.2 Hz, 2H), 7.51 (d, *J* = 7.6 Hz, 1H), 8.2 (s, 1H), 8.37 (dd, *J* = 1.4, 4.9 Hz, 1H); ^{13}C NMR (175 MHz, CD_3OD) δ 35.0, 38.8, 39.5, 41.1, 41.2, 49.5, 54.8, 55.9, 59.4, 62.3, 70.6, 75.2, 78.6, 125.3, 127.5, 128.5, 129.4, 129.9, 130.5, 130.9, 135.7, 135.9, 138.8, 139.2, 148.2, 150.5, 161.9, 172.1, 172.5, 174.4, 174.5; HRMS m/z calcdfor $C_{35}H_{39}N_6O_7$ $[M + H]^+$ 655.2875, found 655.2892.

Phenylacetyl-azaGly-(2*S*,4*R*)-Hyp-(2*S*)-3-Pal-(3*S*)-*β*-hPhe [(*R*)- 2.11a].

Employing a similar procedure as described for the preparation of azapeptide (*R*)- **2.11c**, *N*'-4-ethoxybenzyl carbazate **2.50d** (0.42 mmol) was converted to aza-glycine peptide (*R*)- **2.11a** (45 mg of purity 36%) which was analyzed and purified on a reverse-phase XTerra ™ C18 column (150 × 4.6 mm, 5 μm) using a binary solvent system consisting of 10-90% methanol (0.1% FA) in water (0.1% FA) over 15 min at a flow rate of 0.8 mL/min with UV detection at 214 nm. Freeze-drying of the collected fractions gave azapeptide (*R*)- **2.11a** [2.7 mg, 17 %, shown to be of 99% purity (Table 2.1) by LC-MS on a GeminiTM C18 reverse-phase column (50 × 4.6 mm, 5 μm), using a flow rate of 0.5 mL/min and gradient of 10-90% MeOH (0.1% FA) or 10-90% CH_3CN (0.1% FA) in water (0.1% FA)]: $[\alpha]^{20}_D$ = 56.6 (*c* 0.08, CH_3OH); ^{1}H NMR (700 MHz, CD_3OD) δ 1.70 (m, 1H), 2.06-2.09 (m, 1H), 2.42 (s, 2H), 2.72 (dd, *J* = 7.8, 13.6 Hz, 1H), 2.79 (dd, *J* = 6.2, 13.4 Hz, 1H), 2.88 (dd, *J* = 10.4, 14.1 Hz, 1H), 3.11 (dd, *J* = 4.8, 14.1 Hz, 1H), 3.38 (d, *J* = 10.1 Hz, 1H), 3.54-3.62 (m, 3H), 4.29 (m, 1H), 4.37-4.39 (m, 2H), 4.46 (dd, *J* = 5.1, 9.9 Hz, 1H), 7.17-7.22 (m, 2H), 7.23-7.28 (m, 6H), 7.31-7.33 (m, 3H), 7.65 (d, *J* = 7.4 Hz, 1H), 8.34 (s, 1H), 8.37 (s, 1H), 8.46 (s, 1H, formic acid); ^{13}C NMR (175 MHz, CD_3OD) δ 35.3, 39.2, 39.9, 41.3, 41.6, 49.9, 55.4, 55.8, 61.3, 70.6, 125.2, 127.4, 128.0, 129.3, 129.6, 130.4, 130.7, 135.7, 136.1, 139.0, 139.8, 148.3, 150.6, 159.0, 169.2 (formic acid), 171.9, 174.0, 175.0, 175.8; HRMS m/z calcdfor $C_{32}H_{37}N_6O_7$ $[M + H]^+$ 617.2718, found 617.2698.

Phenylacetyl-azaPhe-(4*R*)-Hyp-(2*S*)-3-Pal-(3*S*)-*β*-hPhe [(*R*)- 2.11b].

Employing a similar procedure as described for the preparation and purification of azapeptide (*R*)- **2.11c**, *N*'-benzyl carbazate **2.50b** (0.42 mmol, prepared according to reference[18]) was converted to 65 mg of product of 39% purity, and purified as described for (*R*)- **2.11c** to afford aza-

phenylalanine peptide (*R*)- **2.11b** (17 mg, 68 % yield): $[\alpha]^{20}_D$ = 79 (c 0.3, CH_3OH); ^{1}HNMR (700 MHz, CD_3OD) δ 1.38 (m, 1H), 2.16 (dd, *J* = 6.6, 13.1 Hz, 1H), 2.60 (d, *J* = 6.6 Hz , 2H), 2.80 (dd, , *J* = 8.9, 13.6 Hz, 1H), 2.91 (m, 1H), 3.00 (dd, *J* = 4.3, 13.4 Hz, 1H), 3.13 (dd, *J* = 4.7, 14.4 Hz, 1H), 3.33 (m, 1H), 3.58 (m, 1H), 3.93 (m, 1H), 4.23 (s, 1H), 4.41 (m, 1H), 4.48 (m, 1H), 4.55 (dd, *J* = 4.7, 11.6 Hz, 1H), 5.12 (m, 1H), 7.17-7.22 (m, 5H), 7.26-7.34 (m, 11H), 7.51 (m, 1H), 7.60 (br, 1H), 7.71 (br, 1H), 8.0 (br, 1H), 8.30 (s, 1H), 8.47 (d, *J* = 4.2 Hz, 1H, formic acid); ^{13}C NMR (175 MHz, CD_3OD) δ 35.0, 38.7, 39.7, 41.2, 41.4, 49.6, 55.4, 55.8, 59.5, 62.3, 70.7, 126.2, 127.5, 128.5, 128.9, 129.4, 129.7, 129.9, 130.4, 130.5, 130.8, 135.8, 137.2, 137.3, 139.5, 142.0, 145.9, 148.1, 163.0, 171.8, 172.4, 174.4, 174.7; HRMS m/z calcdfor $C_{39}H_{43}N_6O_7$ $[M + H]^+$ 707.3188, found 707.3208.

Phenylacetyl-azaGly-(2*S*,4*S*)-Hyp-(2*S*)-3-Pal-(3*S*)-*β*-hPhe [(*S*)- 2.11a].

At 0 °C, a solution of triphenylphosphine (260 mg, 1.0 mmol) in THF (6 mL) was treated with diisopropylazodicarboxylate (DIAD, 0.2 mL, 1.0 mmol), and the resulting orange solution was added to (2*S*,4*R*)-hydroxyproline resin (*R*)- **2.54d** (300 mg, 0.21 mmol) at the same temperature. The resin mixture was treated 4-nitrobenzoic acid (170 mg, 1 mmol), removed from ice bath, agitated on an automated shaker at room temperature for 16 h, and washed with THF (3 x 10 mL), DMF (3 x 10mL), DCM (3 x 10 mL), DMF (3 x 10mL) and Et_2O (2 x 10 mL) to furnish the benzoate resin, which was treated with a solution of sodium azide (NaN_3) (65.0 mg, 1.0 mmol) in CH_3OH (4.0 mL) and heated with sonication at 50 ºC for 12 h. (2*S*,4*R*)-Hydroxyproline resin (*S*)- **2.54d** was obtained after filtration and washing with DMF (3 x 10mL), DCM (3 x 10 mL), DMF (3 x 10mL) and Et_2O (2 x 10 mL). Resin cleavage and purification of 30 mg of material of 32% purity as described for (*R*)- **2.11a** afforded (*S*)- **2.11a** (5 mg, 52 %): $[\alpha]^{20}_D$ = 91.6 (*c* 0.12, CH_3OH); ^{1}H NMR (700 MHz, CD_3OD) δ 1.98 (m, 1H), 2.27-2.31 (m, 1H), 2.39 (s, 2H), 2.69 (dd, *J* = 7.6, 13.2 Hz, 1H), 2.76 (dd, *J* = 5.8, 13.1 Hz, 1H), 2.95 (m, 1H), 3.04 (d, *J* = 10.7 Hz, 1H), 3.47 (d, *J* = 10.4 Hz, 1H), 3.55 (d, *J* = 3.7 Hz, 1H), 3.56 (d, *J* = 4.9 Hz, 1H), 3.60 (d, *J* = 14.5 Hz, 1H), 4.36-4.38 (m, 2H), 4.40 (m, 2H), 7.17-7.23 (m, 4H), 7.25-7.3 (m, 5H), 7.34 (d, *J* = 7.4 Hz, 2H), 7.67 (d, *J* = 5.4 Hz, 1H), 8.34 (m, 2H), 8.48 (s, 1H, formic acid); ^{13}C NMR (175 MHz, CD_3OD) δ 35.1, 38.6, 40.2, 41.4, 41.6, 50.0, 55.9, 56.4, 61.8, 71.2, 125.2, 127.4, 128.0, 129.3, 129.6, 130.4, 130.7, 135.7, 136.1, 139.2, 139.8, 148.1, 150.6, 158.9, 169.4 (formic acid), 172.1, 174.2, 175.6, 176.3; HRMS m/z calcd for $C_{32}H_{37}N_6O_7$ $[M + H]^+$ 617.2718, found 617.2728.

Phenylacetyl-azaPhe-(2*S*,4*S*)-Hyp-(2*S*)-3-Pal-(3*S*)-*β*-hPhe [(*S*)- 2.11b].

The protocol for the preparation of azapeptide (*S*)- **2.11a** was employed starting with (2*S*,4*R*)-hydroxyproline resin (*R*)- **2.54b** (200 mg, 0.14 mmol). Purification was performed using 30 mg of the resulting material of 57% purity and the protocol described for azapeptide (*R*)- **2.11c** to afford aza-Phe peptide (*S*)- **2.11b** (4 mg, 23 %): $[\alpha]^{20}_{D}$ = 61 (*c* 0.42, CH_3OH); ^{1}H NMR (700 MHz, CD_3OD) δ 1.29 (m, 1H), 1.60 (m, 1H), 2.32 (m, 1H), 2.52-2.34 (m, 2H), 2.81 (dd, *J* = 8.4, 13.8 Hz, 1H), 2.93-2.99 (m, 2H), 3.16 (dd, , *J* = 5.3, 14.2 Hz, 1H), 3.58 (s, 2H), 3.59-3.60 (m, 1H), 4.06 (m, 1H), 4.32 (t, *J* = 5.6 Hz, 1H), 4.36 (m, 1H), 4.44-4.48 (m, 2H), 4.99 (m, 1H), 7.19-7.23 (m, 6H), 7.26-7.34 (m, 9H), 7.75 (dd, *J* = 5.7, 7.8 Hz, 1H), 7.99 (br, 1H), 8.40 (s, 1H), 8.59 (d, *J* = 5.1 Hz, 1H); ^{13}C NMR (175 MHz, CD_3OD) δ 24.2, 34.9, 37.8, 39.5, 41.0, 41.5, 55.4, 55.7, 57.7, 62.3, 70.6, 127.4, 127.6, 128.4, 128.9, 129.5, 129.7, 129.8, 130.4, 130.6, 130.8, 135.7, 137.2, 139.1, 139.5, 142.6, 144.8, 146.4, 162.2, 171.4, 172.6, 174.4, 174.9; HRMS m/z calcd for $C_{39}H_{43}N_6O_7$ $[M + H]^+$ 707.3188, found 707.3217.

Phenylacetyl-azaPra-(*2S*,4*S*)-Hyp-(2*S*)-3-Pal-(3*S*)-*β*-hPhe [(*S*)- 2.11c].

The protocol for the preparation and purification of azapeptide (*S*)- **2.11a** was employed starting with (2*S*,4*R*)-hydroxyproline resin (*R*)- **2.54c** (200 mg, 0.14 mmol), and purifying 30 mg of material with 48% purity to afford (*R*)- **2.11c** (4.45 mg, 31 %): $[\alpha]^{20}_{D}$ = 26 (*c* 0.7, CH_3OH); ^{1}H NMR (700 MHz, CD_3OD) δ 1.35 (m, 1H), 2.30 (m, 1H), 2.50 (m, 2H), 2.69 (dd, *J* = 8.3, 13.6 Hz, 1H), 2.73 (t, *J* = 2.5 Hz, 1H), 2.77 (m, 1H), 2.97 (m, 2H), 3.18 (dd, *J* = 6.6, 10.3 Hz, 1H), 3.62 (m, 1H), 3.69 (d, *J* = 14.7 Hz, 1H), 3.26 (d, *J* = 14.7 Hz, 1H), 3.84 (m, 1H), 4.26 (m, 1H), 4.29-4.35 (m, 2H), 4.39 (m, 1H), 4.44 (m, 1H), 7.09-7.10 (m, 3H), 7.18-7.19 (m, 2H), 7.24 (t, *J* = 7.5 Hz, 1H), 7.29-7.34 (m, 3H), 7.4 (d, *J* = 7.4 Hz, 2H), 7.50 (d, *J* = 7.6 Hz, 1H), 8.26 (s, 1H), 8.36 (d, *J* = 3.9 Hz, 1H), 8.50 (s, 1H, formic acid); ^{13}C NMR (175 MHz, CD_3OD) δ 35.0, 38.0, 40.8, 41.0, 41.2, 49.5, 49.9, 56.3, 57.3, 62.1, 70.1, 75.1, 78.7, 125.2, 127.3, 128.4, 129.3, 129.8, 130.6, 130.9, 135.6, 135.9, 138.9, 139.4, 148.2, 150.6, 161.3, 169.8 (formic acid), 172.0, 172.5, 174.3; HRMS m/z calcd for $C_{35}H_{39}N_6O_7$ $[M + H]^+$ 655.2875, found 655.2878.

Phenylacetyl-azaGly-(2*S*,4*S*)-Flp-(2*S*)-3-Pal-(3*S*)-*β*-hPhe [(*S*)- 2.12a].

Hydroxyproline resin (*R*)- **2.54d** (300 mg, 0.21 mmol) swollen in anhydrous DCM (6.0 mL) at 0 ºC was treated with DAST, agitated on an automated shaker for 4h, filtered and washed with DMF (3 x 10mL), DCM (3 x 10 mL), DMF (3 x 10mL) and Et_2O (2 x 10 mL) to provide resin (*S*)- **2.55d**, which was subjected to 95:5 TFA:H_2O (5 mL). Filtration of the resin and washing with TFA and DCM, followed by evaporation of the filtrate and washings gave 90 mg of material of 20% purity,

which was purified by preparative HPLC as described for azapeptide (*R*)- **2.11a** to obtain (*S*)- **2.12a** (1.8 mg, 15 %): $[\alpha]^{20}_D = 98$ (*c* 0.15, CH_3OH); HRMS m/z calcdfor $C_{35}H_{36}FN_6O_6$ $[M + H]^+$ 619.2675, found 619.2697.

Phenylacetyl-azaPhe-(2*S*,4*S*)-Flp-(2*S*)-3-Pal-(3*S*)-*β*-hPhe [(*S*)- 2.12b].

Hydroxyproline resin (*R*)- **2.54b** (200 mg, 0.14 mmol) was reacted using the protocol described for the synthesis of fluoroproline (*S*)- **2.12a** to provide 61 mg of material of 65% purity. Purification was performed as described for the preparation of azapeptide (*R*)- **2.11c** to afford (*S*)- **2.12b** (16.7 mg, 42 %): $[\alpha]^{20}_D = 30$ (*c* 0.6, CH_3OH); ^{1}H NMR (700 MHz, CD_3OD) δ 1.29 (m, 1H), 1.99 (m, 1H), 2.34-2.43 (m, 1H), 2.55 (d, *J* = 6.4 Hz, 2H), 2.79 (dd, *J* = 9.4, 14.0 Hz, 1H), 2.96 (dd, *J* = 4.9, 13.7 Hz, 1H), 3.00 (dd, *J* = 4.2, 14.5 Hz, 1H), 3.53 (d, *J* = 14.5 Hz, 1H), 3.57 (d, *J* = 14.5 Hz, 1H), 3.59-3.67 (m, 1H), 3.75 (dd,, 1H , 4.02 (m, 1H), 4.41 (dd, *J* = 4.3, 10.6 Hz, 1H), 4.45-4.49 (m, 1H), 4.62 (dd, *J* = 3.8, 10.2 Hz, 1H), 5.02 (m, 1H), 5.12 (m, 1H), 5.20 (m, 1H), 7.15-7.18 (m, 3H), 7.20-7.22 (m, 2H), 7.24-7.25 (m, 3H), 7.27-7.34 (m, 8H), 7.50 (d, *J* = 8.0 Hz, 1H), 8.28 (s, 1H), 8.34 (d, *J* = 3.8 Hz, 1H), 8.39 (s, 1H, formic acid); ^{13}C NMR (175 MHz, CD_3OD) δ 35.3, 37.5 (d), 39.1, 41.3, 41.6, 42.3, 49.6, 54.3 (d), 55.9, 61.0, 93.0 (d), 125.3, 127.5, 128.1, 129.4, 129.5, 129.6, 129.8, 130.3, 130.4, 130.5, 130.7, 135.7, 136.1, 139.3, 139.6, 148.1, 150.5, 161.9, 168.3 (formic acid), 171.9, 173.9, 174.3, 174.7; HRMS m/z calcdfor $C_{39}H_{42}FN_6O_6$ $[M + H]^+$ 709.3144, found 709.3162.

Phenylacetyl-azaPra-(2*S*,4*S*)-Flp-(2*S*)-3-Pal-(3*S*)-*β*-hPhe [(*S*)- 2.12c].

Hydroxyproline resin (*R*)- **2.54c** (200 mg, 0.14 mmol) was reacted according to the protocol described for the synthesis of fluoroproline (*S*)- **2.12a** to provide 83 mg of material of 40% purity. Purification was performed as described for the preparation of azapeptide (*R*)- **2.11c** to afford (*S*)- **2.12c** (17.2 mg, 53 %): $[\alpha]^{20}_D = 66$ (*c* 0.23, CH_3OH); ^{1}H NMR (700 MHz, CD_3OD) δ 1.97-2.02 (m, 1H), 2.31-2.40 (m, 1H), 2.49 (s, 2H), 2.73-2.74 (m, 2H), 2.93-2.98 (m, 2H), 3.56-3.66 (m, 2H), 3.72-3.78 (m, 2H), 3.93 (d, *J* = 16.9 Hz, 1H), 3.38 (dd, *J* = 3.9, 11.0 Hz, 1H), 4.41-4.46 (m, 2H), 4.56 (dd, *J* = 2.7, 10.6 Hz, 1H), 4.59 (m, 1H), 5.10 (s, 1H), 5.17 (s, 1H), 7.12-7.13 (m, 2H), 7.19-7.23 (m, 3H), 7.26-7.27 (m, 1H), 7.30 (t, *J* = 7.6 Hz, 2H), 7.38 (d, *J* = 7.3 Hz, 2H), 7.47 (d, *J* = 7.3 Hz, 1H), 8.25 (s, 1H), 8.34 (d, *J* = 1.8 Hz, 1H), 8.5 (s, 1H); ^{13}C NMR (175 MHz, CD_3OD) δ 35.2, 35.9, 40.7, 41.2, 41.3, 41.4, 49.9, 56.0 (d), 56.2, 62.1, 75.1, 78.7, 92.7 (d), 125.1, 127.3, 128.4, 129.3, 129.8, 130.6, 130.8, 135.5, 135.6, 138.9, 139.4, 148.1, 150.6, 160.9, 168.6 172.1, 172.9, 174.2; HRMS m/z calcdfor $C_{35}H_{38}FN_6O_6$ $[M + H]^+$ 657.2831, found 657.2857.

Phenylacetyl-azaGly-(2*S*,4*R*)-Flp-(2*S*)-3-Pal-(3*S*)-*β*-hPhe [(*R*)- 2.12a].

Hydroxyproline resin (*S*)- **2.54d** (200 mg, 0.14 mmol) was reacted according to the protocol described for the synthesis of fluoroproline (*S*)- **2.12a** to provide 78 mg of material of 30% purity. Purification was performed as described for the preparation of azapeptide (*R*)- **2.11a** to afford (*R*)- **2.12a** (6.2 mg, 27 %): $[\alpha]^{20}_{D} = 78$ (*c* 0.2, CH_3OH); HRMS m/z calcdfor $C_{35}H_{36}FN_6O_6$ $[M + H]^+$ 619.2675, found 619.2687.

Phenylacetyl-azaPhe-(2*S*,4*R*)-Flp-(2*S*)-3-Pal-(3*S*)-*β*-hPhe [(*R*)- 2.12b].

Hydroxyproline resin (*S*)- **2.54b** (200 mg, 0.14 mmol) was reacted according to the protocol described for the synthesis of fluoroproline (*S*)- **2.12a** to provide 74 mg of material of 40% purity. Purification was performed as described for the preparation of azapeptide (*R*)- **2.11c** to afford (*R*)- **2.12b** (22 mg, 75 %): $[\alpha]^{20}_{D} = 52$ (*c* 0.78, CH_3OH); ^{1}H NMR (700 MHz, CD_3OD) δ 1.63-1.68 (m, 1H), 2.48 (m, 1H), 2.59 (m, 2H), 2.81 (dd, *J* = 8.7, 13.6 Hz, 1H), 2.96-3.01 (m, 2H), 3.18 (dd, *J* = 5.0, 13.7 Hz, 1H), 3.41-3.49 (m, 2H), 3.57 (s, 2H), 4.00 (br, 1H), 4.44 (m, 2H), 4.55 (dd, *J* = 6.9, 11.5 Hz, 1H), 5.08 (s, 1H), 5.15 (s, 1H), 7.20-7.34 (m, 13 H), 7.66 (br, 1H), 7.71 (m, 1H), 7.92 (br, 2H), 8.38 (br, 1H), 8.56 (m, 1H); ^{13}C NMR (175 MHz, CD_3OD) δ 35.2, 36.6 (d), 39.5, 41.2, 41.4, 49.3, 49.5 (d), 55.7, 57.6, 61.9, 93.0 (d), 127.1, 127.6, 128.5, 129.0, 129.5, 129.8, 129.9, 130.4 (2C), 130.8, 135.7, 137.1, 138.4, 139.5, 143.5, 145.6, 162.5, 162.7, 171.4, 172.5, 173.9, 174.5; HRMS m/z calcdfor $C_{39}H_{42}FN_6O_6$ $[M + H]^+$ 709.3144, found 709.3146.

Phenylacetyl-azaPra-(2*S*,4*R*)-Flp-(2*S*)-3-Pal-(3*S*)-*β*-hPhe [(*R*)- 2.12c].

Hydroxyproline resin (*S*)- **2.54c** (200 mg, 0.14 mmol) was reacted according to the protocol described for the synthesis of fluoroproline (*S*)- **2.12a** to provide 85 mg of material of 43% purity. Purification was performed as described for the preparation of azapeptide (*R*)- **2.11c** to afford (*R*)- **2.12c** (13 mg, 36 %): $[\alpha]^{20}_{D} = 90$ (*c* 0.19, CH_3OH); ^{1}H NMR (700 MHz, CD_3OD) δ 2.42 (m, 1 H), 2.51 (m, 2H), 2.71-2.76 (m, 2H), 2.79 (m, 1H), 2.98 (dd, *J* = 4.2, 14.1 Hz, 1H), 3.04 (dd, *J* = 4.4, 14.5 Hz, 1H), 3.33 (m, 1H), 3.38 (m, 1H), 3.57 (m, 2H), 3.69 (d, *J* = 14.5 Hz, 1H), 3.75 (d, *J* = 14.5 Hz, 1H), 3.89 (br, 1H), 4.37 (dd, *J* = 4.0, 10.5 Hz, 1H), 4.46 (dd, *J* = 6.8, 11.7 Hz, 2H), 4.60 (br, 2H), 5.03 (s, 1H), 5.10 (s, 1H), 7.13 (m, 3H), 7.20-7.22 (m, 2H), 7.24-7.26 (m, 1H), 7.29-7.32 (m, 3H), 7.37 (d, *J* = 7.5 Hz, 2H), 7.52 (br, 1H), 8.21 (s, 1H), 8.36 (d, *J* = 4.2 Hz, 1H), 8.49 (s, 1H); ^{13}C NMR (175 MHz, CD_3OD) δ 35.1, 36.6 (d), 40.5, 41.1, 41.2, 49.8, 56.0, 57.3 (d), 61.9, 75.3, 78.5, 92.4, 93.4, 125.3, 127.4, 128.5, 129.3, 129.9, 130.5, 130.9, 135.6, 135.7, 138.7, 139.4,

148.3, 150.6, 161.5, 169.5, 171.9, 172.5, 173.6; HRMS m/z calcdfor $C_{35}H_{38}FN_6O_6$ $[M + H]^+$ 657.2831, found 657.2834.

Phenylacetyl-azaGly-(2*S*,4*S*)-Amp-(2*S*)-3-Pal-(3*S*)-*β*-hPhe [(*S*)- 2.13a].

Diethyl azodicarboxylate (DEAD, 0.15 mL, 0.98 mmol) and diphenylphosphoryl azide (0.21 mL, 0.98 mmol) were added slowly to a solution of (2*S*,4*R*)-*N*-Fmoc-4-hydroxyproline *tert*-butyl ester (200 mg, 0.49 mmol, prepared according to references[34]) and triphenylphosphine (256 mg, 0.98 mmol) in anhydrous THF (8 mL). The reaction mixture was purged with argon and left to react at room temperature for 16h. The volatiles were evaporated and the residue was dissolved in EtOAc (15 mL) and washed with $NaHCO_3$ (15 mL) and water, dried over Na_2SO_4, filtered and evaporated to a residue, which was purified by column chromatography using 25% EtOAc in hexane to give (2*S*,4*S*)-*N*-Fmoc-4-azidoproline *tert*-butyl ester as white foam (140 mg, 66%): R_f = 0.29 (25% EtOAc in hexane); ^{1}H NMR (DMSO-*d6*, 100^{o}C, 500MHz) δ 1.41 (9H, s), 2.02–2.05 (1H, m), 2.52-2.57 (1H, m), 3.47–3.58 (1H, dd, *J* = 3.3, 11.8 Hz), 3.66-3.71 (1H, m), 4.38–4.42 (2H, dd, *J* = 3.1, 9.3 Hz), 4.31-4.34 (1H, m), 4.36-4.41 (2H, m), 7.33 (2H, t, *J* = 7.5 Hz), 7.42 (2H, t, *J* = 7.5 Hz), 7.64 (2H, d, *J* = 7.5 Hz), 7.86 (2H, d, *J* = 7.5 Hz); ^{13}C NMR (DMSO-*d6*, 100 ℃, 125 MHz) δ 27.1, 46.5, 50.6, 51.2, 57.8, 58.3, 66.4, 80.5, 119.5, 124.5, 126.5, 127.1, 140.3, 143.4, 153.3, 169.4. HRMS Calcd*m/z* for $C_{24}H_{26}N_4O_4Na$ $[M+Na]^+$ 457.1846, found 457.1854.

(2*S*,4*S*)-*N*-Fmoc-4-Azidoproline *tert*-butyl ester (190 mg, 0.44 mmol) was treated with a 90% TFA in DCM solution (3 mL), stirred for 1 h at room temperature, evaporated, dissolved and co-evaporated from DCM 3 times. The residue was dissolved in EtOAc and extracted with $NaHCO_3$. The aqueous phase was acidified with HCl (1N) to pH 3 and extracted with EtOAc (3×10 mL). The combined organic phase was washed with brine, dried over Na_2SO_4 and evaporated to (2*S*,4*S*)-*N*-Fmoc-4-azidoproline (159 mg, 96%), which was used in the next step without further purification.

(4*S*)-Azidoprolyl-Pal-hPhe-O-Wang resin was synthesized from (2*S*,4*S*)-*N*-Fmoc-4-azidoproline (159 mg, 0.42 mmol, 3eq) using the protocol described for the synthesis of (4*R*)-H-Hyp(TBDMS)-Pal-hPhe-O-Wang resin **2.49**, reacted with *N*-Fmoc-aza-4-ethoxyphenylalaninyl chloride, which was prepared from *N*'-4-ethoxybenzyl fluorenylmethyl carbazate, and elongated according to the protocol for the synthesis of phenylacetyl-azaPra-(4*R*)-Hyp(TBDMS)-Pal-hPhe-O-Wang resin **2.53c** to obtain phenylacetyl-aza(4-EtO)Phe-(4*S*)-azidoprolyl-Pal-hPhe-O-Wang resin (*R*)- **2.56d**. Azide reduction with tris-(2-carboxy)ethylphosphine (TCEP, 120 mg, 0.42 mmol) in 9 : 1 THF :

H_2O for 4 h, and resin cleavage using 95:5 TFA:H_2O (5 mL) provided 69 mg of material of 36% purity, which was purified as described for azapeptide (*R*)- **2.11a** to afford (*S*)- **2.13a** (14.7 mg, 59 %): $[\alpha]^{20}_D = 21$ (*c* 0.32, CH_3OH); ^1H NMR (700 MHz, CD_3OD) δ 2.25 (m, 1H), 2.36 (d, *J* = 6.2 Hz, 2H), 2.53 (m, 1H), 2.78 (dd, *J* = 7.5, 13.6 Hz, 1H), 2.87 (dd, *J* = 6.9, 13.5 Hz, 1H), 2.99 (dd, *J* = 8.6, 14.5 Hz, 1H), 3.08 (dd, *J* = 5.9, 14.5 Hz, 1H), 3.58 (s, 2H), 3.67 (d, *J* = 11.4 Hz, 1H), 3.76 (dd, *J* = 5.6, 11.5 Hz, 1H), 3.99 (m, 1H), 4.29 (m, 1H), 4.42 (dd, *J* = 6.0, 8.5 Hz, 1H), 4.49 (dd, *J* = 1.8, 9.6 Hz, 1H), 7.19-7.24 (m, 4H), 7.25-7.30 (m, 5H), 7.34 (d, *J* = 7.4 Hz, 2H), 7.71 (d, *J* = 7.6 Hz, 1H), 8.35 (d, *J* = 4.9 Hz, 1H), 8.40 (s, 1H), 8.4.2 (s, 2H, formic acid); ^{13}C NMR (175 MHz, CD_3OD) δ 33.8, 35.2, 40.1, 41.2, 41.6, 50.4, 51.4, 52.2, 56.7, 60.5, 125.3, 127.5, 128.0, 129.4, 129.5, 130.3, 130.5, 135.1, 136.2, 139.2, 139.8, 148.3, 150.7, 157.7, 168.7 (formic acid), 171.7, 173.9, 175.7, 177.5; HRMS m/z calcdfor $C_{32}H_{38}N_7O_6$ $[M + H]^+$ 616.2878, found 616.285.

Phenylacetyl-azaPhe-(2*S*,4*S*)-aminoprolyl-(2*S*)-3-Pal-(3*S*)-*β*-hPhe [(*S*)- 2.13b].

4-Nitrobenzenesulfonyl chloride (93 mg, 0.42 mmol) and Et_3N (0.12 mL, 0.84 mmol) were added sequentially to resin (*R*)- **2.54b** (200 mg, 0.14 mmol) swollen in anhydrous THF (3.0 mL). The reaction mixture was agitated on an automated shaker for 6h, washed, transferred to microwave vial, and treated with NaN_3 (27 mg, 0.42 mmol) and 15-crown-5 (83 μL, 0.42 mmol) in DMF (3.0 mL). The vial was sealed, heated with sonication at 60 ºC for 8 h, washed, reacted with tris-(2-carboxy)ethylphosphine (TCEP, 120 mg, 0.42 mmol) in 9 : 1 THF : H_2O for 4 h, and washed. The resin was subjected to 95:5 TFA:H_2O (5 mL) to provide material of 50% purity, 30 mg of which was purified as described for the synthesis of azapeptide (*R*)- **2.11a** to afford (*S*)- **2.13b** (6.8 mg, 44 %): $[\alpha]^{20}_D = 82$ (*c* 0.2, CH_3OH); HRMS m/z calcdfor $C_{39}H_{44}N_7O_6$ $[M + H]^+$ 706.3348, found 706.3349.

Phenylacetyl-azaPra-(2*S*,4*S*)-4-aminoprolyl-(2*S*)-3-Pal-(3*S*)-*β*-hPhe [(*S*)- 2.13c].

Hydroxyproline resin (*R*)- **2.54c** (200 mg, 0.14 mmol) was reacted according to the protocol described for the synthesis of aminoproline (*S*)- **2.13b** to provide 89 mg of material of 33% purity. Purification was performed as described for the preparation of azapeptide (*R*)- **2.11a** to afford (*S*)- **2.13c** (3.9 mg, 13 %): $[\alpha]^{20}_D = 139$ (*c* 0.1, CH_3OH); HRMS m/z calcdfor $C_{35}H_{40}N_7O_6$ $[M + H]^+$ 654.3035, found 654.3038.

Phenylacetyl-azaGly-(2*S*,4*R*)-aminoprolyl-(2*S*)-3-Pal-(3*S*)-*β*-hPhe [(*R*)- 2.13a].

Employing the protocol above for the synthesis of (2*S*,4*S*)-*N*-Fmoc-4-azidoproline *tert*-butyl ester, (2*S*,4*S*)-*N*-Fmoc-4-hydroxyproline *tert*-butyl ester (500 mg, 1.2 mmol, prepared according to

references[12, 34]) was converted to (2*S*,4*R*)-*N*-Fmoc-4-azidoproline *tert*-butyl ester, which was purified by column chromatography using 20% EtOAc in hexane to give a white foam (257 mg, 50%): R_f = 0.29 (20% EtOAc in hexane); ^{1}H NMR (DMSO *d6*, 100 ℃, 500 MHz) δ 1.40 (9H, s), 2.15–2.20 (1H, m), 2.32-2.36 (1H, m), 3.45–3.47 (1H, m), 3.60 (1H, dd, *J* = 3.3, 11.5 Hz), 4.21 (1H, t, *J* = 7.4 Hz), 4.24 (1H, m), 4.32-4.36 (2H, m), 4.37-4.41 (1H, m), 7.33 (2H, t, *J* = 7.3 Hz), 7.42 (2H, t, *J* = 7.5 Hz), 7.64 (2H, m), 7.87 (2H, d, *J* = 7.6 Hz); ^{13}C NMR (DMSO *d6*, 100 ℃, 125 MHz) δ 27.2, 46.4, 50.7, 50.9, 57.7, 58.0, 66.4, 80.7, 119.5, 124.4, 126.5, 127.1, 140.3, 143.3, 153.3, 170.0; HRMS Calcd*m/z* for $C_{24}H_{26}N_4O_4Na$ $[M+Na]^+$ 457.1846, found 457.1854.

(2*S*,4*R*)-*N*-Fmoc-4-Azidoproline (163 mg, 0.43 mmol) was reacted according to the protocol described for the synthesis of aminoproline (*S*)- **2.13a**, which provided 50 mg of material of 37% purity. Purification as described for the synthesis of azapeptide (*R*)- **2.11a** afforded (*R*)- **2.13a** (6.5 mg, 35 %): $[\alpha]^{20}_D$ = 40 (*c* 0.3, CH_3OH); ^{1}H NMR (700 MHz, CD_3OD) δ 2.24 (t, *J* = 6.6 Hz, 2H), 2.36 (m, 2H), 2.79 (d, *J* = 7.6 Hz, 2H), 2.90 (dd, *J* = 9.2, 14.4 Hz, 1H), 3.09 (dd, *J* = 5.4, 14.3 Hz, 1H), 3.54 (dd, *J* = 5.0, 10.8 Hz, 1H), 3.58 (d, *J* = 14.5 Hz, 1H), 3.60 (d, *J* = 14.5 Hz, 1H), 3.76 (dd, *J* = 6.5, 10.6 Hz, 1H), 3.8 (m, 1H), 4.33 (m, 1H), 4.47 (dd, *J* = 5.5, 9.2 Hz, 1H), 4.51 (t, *J* = 6.7 Hz, 1H), 7.18 (t, *J* = 7.22 Hz, 1H), 7.21-7.23 (m, 3H), 7.25-7.29 (m, 4H), 7.32-7.35 (m, 3H), 7.68 (d, *J* = 7.9 Hz, 1H), 8.37 (s, 2H), 8.44 (s, 1H, formic acid); ^{13}C NMR (175 MHz, CD_3OD) δ 34.9, 35.7, 40.0, 41.3, 41.5, 50.0, 50.7, 50.9, 56.1, 60.2, 125.2, 127.4, 128.0, 129.4, 129.6, 130.3, 130.6, 135.3, 136.2, 139.2, 139.7, 148.3, 150.7, 157.9, 169.1 (formic acid), 171.8, 173.6, 174.2, 176.8; HRMS m/z calcdfor $C_{32}H_{38}N_7O_6$ $[M + H]^+$ 616.2878, found 616.2852.

Phenylacetyl-azaPhe-(2*S*,4*R*)-aminoprolyl-(2*S*)-3-Pal-(3*S*)-*β*-hPhe [(*R*)- 2.13b].

Hydroxyproline resin (*S*)- **2.54b** (200 mg, 0.14 mmol) was reacted according to the protocol described for the synthesis of aminoproline (*S*)- **2.13b** to provide 73 mg of material of 38% purity. Purification as described for the preparation of azapeptide (*R*)- **2.11a** afforded (*R*)- **2.13b** (8.0 mg, 29 %): $[\alpha]^{20}_D$ = 154 (*c* 0.14, CH_3OH); ^{1}H NMR (700 MHz, CD_3OD) δ 1.70 (m, 1H), 2.32 (m, 1H), 2.54 (s, 2H), 2.80 (dd, *J* = 8.3, 13.5 Hz, 1H), 2.85-2.88 (m, 1H), 2.95-2.97 (m, 1H), 3.09 (dd, *J* = 4.2, 14.5 Hz, 1H), 3.55-3.58 (m, 4H), 3.79 (s, 1H), 3.99 (m, 1H), 4.42 (dd, *J* = 3.9, 10.2 Hz, 1H), 4.47 (m, 1H), 4.59 (t, *J* = 8.6 Hz, 1H), 5.04 (m, 1H), 7.15-7.20 (m, 6H), 7.24-7.32 (m, 11 H), 7.58 (s, 1H), 8.27 (s, 1H), 8.37 (s, 1H, formic acid); ^{13}C NMR (175 MHz, CD_3OD) δ 34.6, 35.1, 40.4, 41.2, 41.5, 49.9, 51.6, 54.9, 55.4, 56.1, 61.7, 125.3, 127.5, 128.5, 129.0, 129.4, 129.7, 129.9, 130.4,

130.5, 130.8, 135.6, 135.7, 136.9, 138.9, 139.5, 148.3, 150.6, 161.8, 168.2 (formic acid), 172.0, 172.6, 173.4, 175.7; HRMS m/z calcdfor $C_{39}H_{44}N_7O_6$ $[M + H]^+$ 706.3348, found 706.3356.

Phenylacetyl-azaPra-(2*S*,4*R*)-aminoprolyl-(2*S*)-3-Pal-(3*S*)-*β*-hPhe [(*R*)- 2.13c].

Hydroxyproline resin (*S*)- **2.54c** (200 mg, 0.14 mmol) was reacted according to the protocol described for the synthesis of aminoproline (*S*)- **2.13b** to provide 40 mg of material of 40% purity. Purification as described for the preparation of azapeptide (*R*)- **2.11a** afforded (*S*)- **2.13c** (2.1 mg, 13 %): $[\alpha]^{20}_D = 143$ (*c* 0.1, CH_3OH); HRMS m/z calcdfor $C_{35}H_{40}N_7O_6$ $[M + H]^+$ 654.3035, found 654.3038.

Benzhydrylidene aza-(4-methyl)phenylalaninyl-proline *tert*-butyl ester (2.35d).

A 0˚C solution of benzhydrylidene aza-glycinyl-proline *tert*-butyl ester (**2.34**, 200 mg, 0.51 mmol, 1eq, prepared according to reference[11a], in 3 mL of anhydrous THF was treated with potassium *tert*-butoxide (63 mg, 1.1 eq), stirred for 10 min, and treated with 4-methylbenzyl bromide (100 mg, 1.1 eq). The ice bath was removed. The reaction mixture was stirred overnight warming to room temperature. The volatiles were removed by rotary evaporation to give a residue, which was dissolved in 10 mL of ethyl acetate. The organic solution was washed with 10 mL of 1N NaH_2PO_4 and brine, dried over $MgSO_4$, filtered and evaporated to a residue, which was purified by chromatography on silica gel using 20% EtOAc in hexane as eluent to give aza-(4-methyl)phenylalanine **2.35d** (0.21 g, 84%) as pale yellow foam: R_f 0.26, (20% EtOAc:hexane); $[\alpha]^{20}_D = 24.5$ (*c* 1.1, $CHCl_3$); ^{1}H NMR ($CDCl_3$, 300MHz) δ 1.46 (9H, s), 1.70–1.72 (1H, m), 1.83–1.91 (2H, m), 2.09–2.13 (1H, m), 2.29 (3H, s), 3.47–3.58 (1H, m), 3.60-3.68 (1H, m), 4.38–4.42 (1H, m), 4.49 (1H, d, *J* = 15.7 Hz), 4.57 (1H, d, *J* = 15.7 Hz), 6.98-7.04 (4H, dd, *J* = 8.6, 2.3 Hz), 7.22–7.35 (5H, m), 7.39–7.42 (5H, m); ^{13}C NMR ($CDCl_3$, 75 MHz) δ 21.4, 24.8, 28.3, 29.9, 49.7, 52.9, 61.8, 81.1, 128.2, 128.3, 128.6, 128.8, 128.9, 129.2, 129.4, 129.9, 134.7, 136.4, 136.7, 139.0, 159.7, 160.3, 172.6. HRMS Calcd*m/z* for $C_{31}H_{36}N_3O_3$ $[M+H]^+$ 498.2751, found 498.2769.

Benzhydrylidene aza-(4-nitro)phenylalaninyl-proline *tert*-butyl ester (2.35e).

Employing the procedure described for the synthesis of aza-phenylalanine **2.35d** using 4-nitrobenzyl bromide (180 mg, 1.1 eq), ester **2.35e** (99 mg, 89%) was isolated after purification by chromatography on silica gel (20% EtOAc:hexane) as pale yellow foam: R_f 0.26, (20% EtOAc:hexane); $[\alpha]^{20}_D = 2.73$ (*c* 1.1, $CHCl_3$); ^{1}H NMR ($CDCl_3$, 300 MHz) δ 1.45 (9H, s), 1.77–1.83 (1H, m), 1.85–1.98 (2H, m), 2.13–2.21 (1H, m), 3.59–3.76 (2H, m), 4.45–4.50 (1H, m), 4.59 (1H, d, *J* = 16.7 Hz), 4.66 (1H, d, *J* = 16.7 Hz), 7.17-7.22 (4H, m), 7.27–7.31 (2H, m), 7.36–7.40

(6H, m), 8.06 (2H, d, J = 8.8 Hz); ^{13}C NMR ($CDCl_3$, 75 MHz) δ 24.8, 28.3, 29.9, 49.9, 52.7, 62.1, 81.4, 123.5, 128.5, 128.7 (2 C), 128.9, 129.1, 129.9, 130.4, 136.3, 138.5, 145.8, 147.1, 159.3, 160.2, 172.5. HRMS Calcd*m/z* for $C_{30}H_{33}N_4O_5$ $[M+H]^+$ 529.2446, found 529.2447.

Benzhydrylidene aza-pentafluorophenylalaninyl-proline *tert*-butyl ester (2.35f).

Employing the procedure described for the synthesis of aza-phenylalanine **2.35d** using pentafluorobenzyl bromide (146 mg, 1.1 eq), ester **2.35f** (275 mg, 94%) was isolated after purification by chromatography on silica gel (25% EtOAc:hexane) as pale yellow foam: R_f 0.43, (25% EtOAc:hexane); $[\alpha]^{20}_D$ = 12.96 (*c* 1, $CHCl_3$); ^{1}H NMR ($CDCl_3$, 300 MHz) δ 1.42 (9H, s), 1.61–1.70 (1H, m), 1.76–1.93 (2H, m), 2.00–2.09 (1H, m), 3.48–3.59 (2H, m), 4.27-4.31 (1H, m), 4.56 (1H, d, J = 14.8), 4.69 (1H, d, J = 14.8), 7.24-7.34 (4H, m), 7.37–7.42 (4H, m), 7.49-7.52 (2H, m); ^{13}C NMR ($CDCl_3$, 75 MHz) 24.1, 27.9, 29.8, 43.1, 48.8, 61.0, 81.0, 128.1, 128.3, 128.5, 128.8, 129.1, 130.1, 135.6, 137.9, 158.7, 162.6, 171.9; HRMS Calculated *m/z* for $C_{30}H_{29}F_5N_3O_3$ $[M+H]^+$ 574.2123, found 574.2144.

Aza-(4-methyl)phenylalaninyl-proline *tert*-Butyl Ester (2.36d).

Benzhydrylidene aza-(4-methyl)phenylalaninyl-proline *tert*-butyl ester (**2.35d**, 200mg, 0.4 mmol), was treated with hydroxylamine hydrochloride (56 mg, 2 eq) in 8 mL of pyridine, heated to 60°C and stirred overnight. The volatiles were evaporated. The residue was dissolved and evaporated from dichloromethane and from ethyl acetate to provide a solid, which was purified by chromatography on silica gel using EtOAc as eluent. Evaporation of the collected fractions, afforded semicarbazide **2.36d** (60 mg, 45%) as pale yellow foam: R_f 0.32 (hexane/EtOAc 1:1); $[\alpha]^{20}_D$ = –30 (*c* 1, $CHCl_3$); ^{1}H NMR ($CDCl_3$, 500 MHz) δ 1.40 (s, 9H), 1.76-1.95 (m, 3H), 2.08-2.13 (m, 1H), 2.30 (s, 3H), 3.39 (br, 2H), 3.61-3.63 (m, 2H), 4.41-4.43 (m, 1H), 4.49 (d, J = 14.8 Hz, 1H), 4.54 (d, J = 14.8 Hz, 1H), 7.11 (d, J = 7.8, 2H), 7.19 (d, J = 7.8, 2 H)); ^{13}C NMR ($CDCl_3$, 125 MHz) δ 21.2, 23.8, 28.1, 30.6, 49.5, 56.1, 62.1, 80.4, 128.6, 129.4, 133.8, 137.2, 161.0, 173.2. HRMS Calculated *m/z* for $C_{18}H_{28}N_3O_3$ $[M+H]^+$ 334.2125, found 334.2139.

Aza-(4-nitro)phenylalaninyl proline *t*-Butyl Ester (**2.36e**).

Employing the procedure described for the synthesis of semicarbazide **2.36c** using benzhydrylidene aza-(4-nitro)phenylalaninyl-proline *t*-butyl ester (**2.35e**, 120mg, 0.23 mmol), semicarbazide **2.36e** (45 mg, 54%) was isolated after purification by chromatography on silica gel

using EtOAc as eluent as a pale yellow foam: R_f 0.25 in 60% EtOAc in hexane; $[\alpha]^{20}_D$ = –22.5 (*c* 1, $CHCl_3$); ^{1}H NMR ($CDCl_3$, 300 MHz) δ: 1.44 (s, 9H), 1.81-1.97 (m, 3H), 2.12- 2.22 (m, 1H), 3.62 (m, 2H), 4.45-4.49 (m, 1H), 4.67 (s, 2H), 7.52 (d, 2H, *J* = 8.7 Hz), 8.21 (d, , 2H, *J* =8.7 Hz); ^{13}C NMR ($CDCl_3$, 75 MHz*)* δ: 24.3, 28.2, 30.6, 49.8, 56.7, 62.1, 81.1, 124.1, 129.2, 145.1, 147.7, 161.3, 173.0. HRMS Calcd*m/z* for $C_{17}H_{25}N_4O_5$ [M+H]+ 365.1819, found 365.1818. HRMS Calcd*m/z* for $C_{17}H_{24}N_4NaO_5$ [M+Na]+ 387.1639, found 387.1636.

Aza-(pentafluoro)phenylalaninyl-proline *tert*-Butyl Ester (2.36f).

Employing a modification of the procedure described for the synthesis of semicarbazide **2.36c**, using benzhydrylidene aza-(pentafluoro)phenylalaninyl-proline *tert*-butyl ester (**2.35f**, 200 mg, 0.35 mmol), after the volatiles were evaporated, the residue was partitioned between H_2O and EtOAc. The aqueous phase was extracted with EtOAc. The combined organic phases were dried over Na_2SO_4, filtered and concentrated under vacuum to provide semicarbazide **2.36f** (85 mg, 0.21 mmol, 60%), which was used in next step without further purification.

Phenylacetyl-aza-(4-methyl)phenylalaninyl-proline *tert*-butyl ester (2.37d).

Aza-(4-methyl)phenylalaninyl-proline *t*-butyl ester (**2.36d**, 60 mg, 0.18 mmol) was dissolved in 10 mL of EtOAc, treated with phenyl acetyl chloride (25 μL, 1.05 eq) and DIPEA (63 μL, 2 eq), and stirred for 16h. The volatiles were evaporated, and the residue was dissolved in ethyl acetate. The organic phase was washed with 10 mL of 1 N NaH_2PO_4 and with 10 mL of brine, dried over Mg_2SO_4, filtered and evaporated to a residue, which was purified by chromatography on silica gel using 50% ethyl acetate in hexane as eluent to afford ester **2.37d** (42 mg, 52%) as pale yellow foam: R_f = 0.45 (40% EtOAc in hexane); $[\alpha]^{20}_D$ = 7.9 (*c* 1, $CHCl_3$); ^{1}H NMR (400 MHz, $CDCl_3$) δ 1.45 (s, 9H), 1.74-1.81 (m, 2H), 1.85-1.91 (m, 1H), 2.12-2.17 (m, 1H), 2.33 (s, 3H), 3.32-3.38 (m, 1H), 3.44 (m, 3H), 4.34 (t, *J* = 7.1 Hz, 1H), 4.39 (d, *J* = 13.6 Hz, 1H), 4.67 (d, *J* = 13.6 Hz, 1H), 7.05 (dd, *J* = 8.3, 3.2 Hz, 4H), 7.11-7.13 (m, 2H), 7.27-7.28 (m, 3H), 7.33 (s, 1H); ^{13}C NMR (75 MHz, $CDCl_3$) δ 21.3, 25.3, 28.1, 29.7, 41.9, 49.0, 53.0, 61.6, 81.9, 127.5, 129.0, 129.2, 129.3, 129.4, 132.9, 133.9, 137.4, 159.5, 169.4, 172.5. HRMS Calculated *m/z* for $C_{26}H_{34}N_3O_4$ $[M+H]^+$ 452.2544, found 452.2575.

Phenylacetyl-aza-(4-nitro)phenylalaninyl-proline *tert*-butyl ester (2.37e).

Employing the procedure described for the synthesis of ester **2.37d** using aza-(4-nitro)phenylalaninyl proline *tert*-butyl ester (**2.36e**, 40 mg, 0.12 mmol), ester **2.37e** (18 mg, 37%) was isolated after purification by chromatography on silica gel (50% EtOAc:hexane) as pale

yellow foam: R_f = 0.45 (60% EtOAc in hexane); $[\alpha]^{20}_D$ = 39.2 (*c* 1, $CHCl_3$); ^1H NMR ($CDCl_3$, 300 MHz) δ 1.38 (s, 9H), 1.68-1.85 (m, 3H), 2.04-2.14 (m, 1H), 3.22-3.30 (m, 1H), 3.40 (m, 3H), 4.26 (t, *J* =7.3 Hz, 1H), 4.42 (d, *J* = 15 Hz, 1H), 4.64 (d, *J* = 15 Hz, 1H), 7.06-7.09 (m, 1H), 7.19-7.22 (m, 4 H), 7.29 (m, 1H), 7.51 (br s, 1H), 7.96 (d, *J* = 8.6 Hz, 2H); ^{13}C NMR (75 MHz, $CDCl_3$) δ 25.6, 28.3, 30.0, 42.3, 49.2, 53.4, 61.7, 82.1, 123.9, 128.0, 129.3, 19.4, 130.2, 134.0, 144.0, 147.7, 159.4, 169.5, 172.8. HRMS Calcd*m/z* for $C_{25}H_{30}N_4NaO_6$ $[M+Na]^+$ 505.2058, found 505.2066.

Phenylacetyl-aza-pentaflourophenylalaninyl-proline *tert*-butyl ester (2.37f).

Employing the procedure described for the synthesis of ester **2.37d** using aza-pentaflourophenylalaninyl-proline *tert*-butyl ester (**2.36f**, 85 mg, 0.21 mmol), ester **2.37e** (71 mg, 64%) was isolated after purification by chromatography on silica gel (30% EtOAc:hexane) as pale yellow foam: R_f = 0.34 (40% EtOAc in hexane); $[\alpha]^{20}_D$ = 14 (*c* 1, $CHCl_3$); ^1H NMR ($CDCl_3$, 400 MHz) δ 1.44 (s, 9H), 1.75-1.93 (m, 3H), 2.12-2.19 (m, 1H), 3.30-3.43 (m, 1H), 3.37-3.44 (m, 1H), 3.51 (s, 2H), 4.28 (t, *J* = 6.8, 1H), 4.66 (d, *J* = 14.3 Hz, 1H), 4.77 (d, *J* = 14.3 Hz, 1H), 7.21-7.23 (m, 2 H), 7.30-7.35 (m, 3H), 7.81 (br, 1H); ^{13}C NMR (75 MHz, $CDCl_3$) δ 25.4, 28.2, 29.9, 30.0, 42.1, 49.1, 61.8, 82.0, 127.5, 128.0, 128.9, 129.3 (2C), 129.4, 129.7, 133.8, 159.1, 169.6, 172.5. HRMS Calcd*m/z* for $C_{25}H_{26}F_5N_3NaO_4$ $[M+Na]^+$ 550.1744, found 550.1736.

Phenylacetyl-aza-(4-methyl)phenylalaninyl-(2*S*)-prolyl-(2*S*)-3-pyridylalaninyl-(3*S*)-*β*-homophenylalanine benzyl ester (2.39d).

Phenylacetyl-aza-(4-methyl)phenylalaninyl-(2*S*)-proline *tert*-butyl ester (**2.38d**, 40 mg, 0.09 mmol) was dissolved in a solution of 1:1 TFA:DCM (2 mL), and stirred for 2h at room temperature, when complete consumption of starting material was confirmed by TLC and mass spectrometry. The volatiles were evaporated. The residue was dissolved and co-evaporated three times from DCM. The residue was dissolved in EtOAc and extracted with saturated $NaHCO_3$. The aqueous layers were combined, acidified with 1N HCl to pH = 3 and extracted with EtOAc. The organic layers were combined, and evaporated to acid **2.37d** (34.5 mg, 0.088 mmol, 99%), which was dissolved in THF (4 mL), cooled to –15°C, treated with isobutyl chloroformate (13 μL, 0.096 mmol) and *N*-methylmorpholine (15 μL, 0.13 mmol), stirred for 5-10 min, treated with a solution of dipeptide benzyl ester **2.25** (36.7 mg, 0.088 mmol) in EtOAc (2 mL), and stirred at –15°C for 2h. The volatiles were evaporated. The residue was purified by chromatography on silica gel using 5% MeOH in DCM as eluent to afford benzyl ester **2.39d** (40 mg, 57%) as pale yellow foam: R_f = 0.42 (10% MeOH: CH_2Cl_2); $[\alpha]^{20}_D$ = –12.2 (*c* 1, $CHCl_3$); ^1H NMR (400 MHz, $CDCl_3$) δ 1.24-1.28

(m, 1H), 1.67-1.73 (m, 2H), 2.19 (m, 1H), 2.33 (s, 3H), 2.60-2.72 (m, 2H), 2.86- 2.97 (m, 3H), 3.01-3.06 (m, 1H), 3.27-3.36 (m, 2H), 3.60 (s, 2H), 3.87 (d, *J* = 13.7 Hz, 1H), 4.32 (dd, *J* = 6.9, 10.9 Hz, 1H), 4.54-4.60 (m, 2H), 4.99 (d, *J*= 13.7 Hz, 1H), 5.08 (d, *J*= 12.3 Hz, 1H), 5.13 (d, *J*= 12.3, 1H), 6.99 (d, *J* = 7.9 Hz, 2H), 7.07 (d, *J*= 7.9 Hz, 2H), 7.15-7.22 (m, 8H), 7.27-7.29 (m, 2H), 7.31-7.38 (m, 5H), 7.51 (d, *J* = 7.8 Hz, 1H), 7.56 (d, *J* = 8.7 Hz, 1H), 8.29 (br, 1H), 8.34 (s, 1H), 8.37 (d, *J* = 4.6 Hz, 1H); ^{13}C NMR (175 MHz, $CDCl_3$) δ 21.4, 25.9, 29.9, 34.1, 38.8, 40.6, 41.6, 48.2, 50.3, 53.8, 54.5, 63.2, 66.6, 123.9, 126.6, 128.1, 128.3, 128.5, 128.6, 128.7, 129.3, 129.4, 129.5, 129.6, 129.8, 129.9, 132.3, 133.1, 136.3, 137.0, 138.2, 138.3, 147.5, 150.2, 160.7, 170.1, 170.4, 171.1, 171.7; HRMS m/z calcdfor $C_{47}H_{50}N_6O_6Na$ $[M + Na]^+$ 817.3684, found 817.3681.

Phenylacetyl-aza-(4-nitro)phenylalaninyl-(2*S*)-prolyl-(2*S*)-3-pyridylalaninyl-(3*S*)-*β*-homophenylalanine benzyl ester (2.39e).

Employing the procedure described for the synthesis of ester **2.39d** using phenylacetyl-aza-(4-nitro)phenylalaninyl-(2*S*)-proline (**2.38e**, 0.80 mg, 0.19 mmol), ester **2.39e** (100 mg, 64%) was isolated after purification by chromatography on silica gel (6% MeOH in CH_2Cl_2) as pale yellow foam: R_f 0.33 (10% MeOH in CH_2Cl_2); $[\alpha]^{20}_D = -9.8$ (*c* 1, $CHCl_3$); ^{1}H NMR (300 MHz, $CDCl_3$) δ 1.73 (m, 2H), 1.85 (m, 1H), 2.12 (m, 1H), 2.60 (d, *J* = 6.0 Hz, 2H), 2.78-2.96 (m, 3H), 2.99-3.08 (m, 1H), 3.28 (dd, *J* = 3.5, 14.5 Hz, 1H), 3.39 (m, 1H), 3.60 (s, 2H), 4.10 (m, 1H), 4.37 (m, 1H), 4.49-4.59 (m, 2H), 4.89 (m, 1H), 5.10 (d, *J*= 3.3 Hz, 2H), 7.11-7.23 (m, 10H), 7.29-7.31 (m, 4H) 7.32-7.35 (m, 4H), 7.44 (d, *J* = 7.6 Hz, 2H), 7.97 (d, *J* = 8.6 Hz, 2H), 8.23 (br, 1H); ^{13}C NMR (125 MHz, $CDCl_3$) δ 25.8, 29.8, 34.1, 38.2, 40.1, 41.5, 48.1, 50.1, 53.6, 54.2, 62.6, 66.6, 123.7, 123.8, 126.7, 128.0, 128.4, 128.5, 128.6, 128.7, 129.1, 129.3, 129.7, 130.0, 130.3, 133.6, 135.9, 136.7, 137.8, 143.7, 147.5, 147.6, 150.1, 160.7, 170.0, 170.3, 171.1, 17.5; HRMS Calcd*m/z* for $C_{46}H_{47}N_7O_8$ $[M+H]^+$ 826.3559, found 826.3570.

Phenylacetyl-aza-pentafluorophenylalaninyl-(2*S*)-prolyl-(2*S*)-3-pyridylalaninyl-(3*S*)-*β*-homophenylalanine benzyl ester (2.39f).

Employing the procedure described for the synthesis of ester **2.39d** using phenylacetyl-aza-pentafluorophenylalaninyl-(2*S*)-proline (**2.38f**, 0.80 mg, 0.17 mmol), ester **2.39f** (101 mg, 75%) was isolated after purification by chromatography on silica gel (5% MeOH in CH_2Cl_2) as pale yellow foam: R_f 0.31 (5% MeOH in CH_2Cl_2); $[\alpha]^{20}_D = -3.2$ (*c* 1, $CHCl_3$); ^{1}H NMR (500 MHz, $CDCl_3$) δ 1.40 (m, 1H), 1.71 (m, 3H), 2.18 (m, 1H), 2.58-2.68 (m, 2H), 2.85-2.92 (m, 2H), 2.94-2.98 (m, 2H), 3.20-3.27 (m, 1H), 3.32 (dd, *J* = 3.5, 14.8 Hz, 1H), 3.66 (s, 2H), 4.17 (d, *J* = 13.9

Hz, 1H), 4.31-4.36 (m, 1H), 4.53-4.62 (m, 2H), 5.04-5.14 (m, 2H), 7.20-7.22 (m, 8H), 7.30-7.37 (m, 8H), 7.54 (d, *J* = 8.0 Hz, 1H), 8.34 (s, 1H), 8.41 (d, *J* = 5.3 Hz, 1H); ^{13}C NMR (125 MHz, $CDCl_3$) δ 25.7, 34.1, 38.3, 40.2, 41.6, 42.2, 45.2, 48.1, 50.1, 54.2, 63.0, 66.5, 123.8, 126.6, 128.3, 128.5, 128.6, 128.7, 129.2, 129.5, 129.7, 132.8, 134.0, 136.1, 136.6, 137.3, 137.9, 146.9, 147.1, 147.9, 150.4, 160.3, 170.2, 170.3, 171.1, 171.2; HRMS Calcd*m/z* for $C_{46}H_{44}F_5N_6O_6$ $[M+H]^+$ 871.3237, found 871.3241.

_N_-Fmoc-_β_-Homophenylalanine Wang resin 2.48

Fmoc-*β*-homophenylalanine (2.3 g, 5.72 mmol) in dry DCM (40 mL) and DMF (1.5 mL) was cooled to 0 °C, treated with DIC (0.44 mL, 2.86 mmol), stirred for 20 min, and evaporated under vacuum to a residue. The symmetrical anhydride residue was dissolved in dry DMF (12 mL) and transferred to a plastic syringe containing Wang resin (75-100 mesh, 1.3 g, 1.1 mmol/g, 1.43 mmol), which was prewashed with DMF (3 x 10 mL), DCM (3 x 10 mL) and DMF (3 x 10 mL), and swollen in DMF (12 mL) for 30 min. The mixture was agitated on an automated shaker for 12 h. The resin was filtered and washed with DMF (3 x 10 mL), DCM (3 x 10 mL), DMF (3 x 10 mL) and Et_2O (2 x 10mL). The resin loading of *N*-Fmoc-*β*-homophenylalanine (typically 0.7 mmol/g) was assessed by measurement of the resulting dibenzofulvene-piperidine adduct at λ = 301 nm upon treatment of a measured resin aliquot with the Fmoc removal conditions. The resin was swollen in a 1:9 acetic anhydride/pyridine (v/v) mixture, shaken for 5 min, and washed with DMF (10 x 3 mL), DCM (10 x 3 mL), and DMF (10 x 3 mL).[33]

(4_R_)-H-Hyp(TBDMS)-Pal-hPhe-O-Wang resin 2.49.

N-Fmoc-Pyridylalanine (2.2 g, 5.72 mmol) was coupled to *β*-homoPhe-O-Wang resin **2.48** using HBTU (2.18g, 5.72 mmol), HOBt (0.773 g, 5.72 mmol) and DIPEA (1.99 mL, 11.44 mmol) for 2 h. The resin was washed, subjected to the Fmoc removal conditions, washed and coupled to *N*-Fmoc-hydroxyproline (2.02 g, 5.72 mmol) using the coupling conditions described above. The hydroxyl group was protected by treating the resin twice with solutions of *t*-Bu$(Me)_2$SiCl (2.2 g, 14.3 mmol) and imidazole (0.97g, 14.3 mmol) in dry DCM (10mL), and 8% DIPEA in DMF.[12] Cleavage of a 1-2 mg of resin and LC-MS analysis [40-90% MeOH (0.1% FA) in water (0.1 FA)] as described above indicated the peptide was of 79% purity. Peptide resin **2.49** was obtained after resin washing, Fmoc removal and resin washing.

_N_'-Propargyl fluorenylmethyl carbazate (2.50c).

A suspension of LiOH (0.39 g, 16 mmol) in 50 mL of DMF was cooled to 0 °C for 20 min, treated with 9-*H*-fluoren-9-ylmethyl carbazate (**2.50a**, 2 g, 8 mmol), stirred for 45 min, and treated with a solution of propargyl bromide (15 mol% in toluene, 1.2 mL, 8 mmol). The ice bath was removed. The reaction mixture was stirred at room temperature for 12h. The volatiles were evaporated. The residue was dissolved in ethyl acetate. The organic phase was washed with 1N NaH_2PO_4 (3 x 10 mL) and brine (3 x 10 mL), dried over Na_2SO_4, filtered and evaporated to a residue, which was purified by flash chromatography on silica gel using 20% ethyl acetate in hexane as eluent to afford carbazate **2.50c** as white solid (1.05 g, 45 %); mp 147-148 °C; ^{1}H NMR (500 MHz, DMSO-d6) δ 3.10 (s, 1H), 3.49 (s, 2H), 4.23 (t, *J* = 6.8 Hz, 1H), 4.30 (d, *J* = 7.1 Hz, 2H), 4.90 (m, 1H), 7.34 (t, *J* = 7.1 Hz, 2H), 7.41 (t, *J* = 7.5 Hz, 2H), 7.71 (d, *J* = 7.4 Hz, 2H), 7.90 (d, *J* = 7.5 Hz, 2H), 8.83 (br s, 1H); ^{13}C NMR (125 MHz, DMSO-d6) δ 39.4, 46.6, 65.6, 74.2, 81.2, 120.1, 125.3, 127.1, 127.7, 140.7, 143.8, 156.7.

***N'*-4-Ethoxybenzyl Fluorenylmethyl Carbazate (2.50d).**

A suspension of fluorenylmethyl carbazate **2.50a** (1.7 g, 6.66 mmol) and 4-ethoxybenzaldehyde (1.0 g, 6.66 mmol) in EtOH (0.2 M) was heated at reflux for 2h, and concentrated in vacuo. The hydrazone residue was dissolved in THF (0.2 M), added to a suspension of $Pd(OH)_2$ on carbon (147 mg, 10 mol %, 20 wt %) in THF (0.2 M), placed under H_2 gas (70 psi), and stirred at room temperature for 16 h. The mixture was filtered over Celite™ and washed with THF. The filtrate and washings were concentrated in vacuo. Purification of the residue by chromatography on silica gel using 30% ethyl acetate in hexane afforded *N*'-4-ethoxybenzyl fluorenylmethyl carbazate (**2.50d**, 2.40 g, 93%) as white solid: mp 105-108 °C; R_f 0.3 (30% EtOAc in hexane); ^{1}H NMR (400 MHz, DMSO-d6) δ 1.30 (t, *J* = 7.0 Hz, 3H), 3.80 (s, 2H), 3.98 (q, *J* = 6.9 Hz, 2H), 4.20 (t, *J* = 7.0 Hz, 1H), 4.30 (d, *J* = 6.9 Hz, 2H), 4.80 (br, 1H), 6.84 (d, *J* = 8.4 Hz, 2H), 7.19 (d, *J* = 7.5 Hz, 2H), 7.32 (t, *J* = 7.6 Hz, 2H), 7.41 (t, *J* = 7.5 Hz, 2H), 7.67 (d, *J* = 7.3 Hz, 2H), 7.88 (d, *J* = 7.5 Hz, 2H), 8.66 (br, 1H); ^{13}C NMR (75 MHz, DMSO-d6) δ 14.7, 46.7, 53.7, 62.9, 65.4, 114.0, 120.1, 125.2, 127.0, 127.6, 129.7, 140.7, 143.8, 154.5, 156.8, 157.5. HRMS Calcd*m/z* for $C_{24}H_{24}N_2O_3$ $[M+Na]^+$ 411.1679, found 411.1682.

Phenylacetyl-azaPra-(4*R*)-H-Hyp-Pal-hPhe-O-Wang resin 2.54c.

A solution of *N*'-propargyl carbazate **2.50c** (1.2 g, 4.2 mmol) in DCM (30 mL) was treated with a 15% phosgene solution in toluene (8.3 mL, 8.4 mmol) at 0° C for 20 min, when TLC indicated complete consumption of starting material. The excess phosgene and other volatiles were removed

under reduced pressure to furnish Fmoc-propargylglycinyl chloride residue **2.51c**, which was dissolved in DCM (15 mL) and transferred to a syringe containing peptide resin **2.49** (2.0 g, 1.4 mmol). The resin mixture was treated with DIPEA (1.5 mL, 8.4 mmol), agitated for 12 h on an automated shaker, and washed to afford resin **2.52c**. Removal of the Fmoc group from resin **2.52c**, washing, followed by treatment of the resin with phenyl acetic anhydride (1.1 g ,4.2 mmol) and triethylamine (1.2 mL ,8.4 mmol) in DCM (15 mL), and washing afforded resin **2.53c**. The TBDMS group was removed from resin **2.53c** by treatment with a 1 M TBAF solution in THF (2 mL) at room temperature for 6 h. Azapeptide resin **2.54c** was obtained after filtration and washing with DCM (3 x 10 mL), DMF (3 x 10mL) and Et_2O (2 x 10 mL).

ASSOCIATED CONTENT

Supporting Information. The Supporting Information is available free of charge on the ACS Publications. NMR spectra (^1H, ^{13}C and 2D) of all new compounds, purity and analytical HPLC chromatograms for all of that I^2aa and aza-amino acyl proline FP modulators of biologically tested. X-ray data for compounds *S*-**21** and *R*-**45** (PDF and CIF).

AUTHOR INFORMATION

Corresponding Author

For W.D.L.: phone, 514-343-7339; fax, 202-513-8788;

E-mail: lubell@chimie.umontreal.ca

Author Contributions

§ These authors contributed equally to this paper and are listed alphabetically.

Notes

The authors declare no competing financial interest**.**

ACKNOWLEDEGMENT

We thank the Canadian Institutes of Health Research (CIHR) and the Natural Sciences and Engineering Research Council of Canada (NSERC) for funding for a Discovery Research Project, and for the Collaborative Health Research Project "Treatment of Preterm Birth with

ProstaglandinF2alpha Receptor Modulators" No. 337381. We acknowledge the assistance of members of the Université de Montreal facilities: Dr. A. Fürtös, K. Gilbert, M.-C. Tang and L. Mahrouche (mass spectroscopy), C. Malveau, Dr. P. Aguiar and S. Bilodeau (NMR spectroscopy) and Mr. T. Maris (X-ray). F. M. Mir, individually would like to thank A. Geranurimi for her kind supports. Shastri Indo-Canadian Institute, India is thanked for a Quebec Tuition Fee Exemption grant to N.D.P.A.

ABBREVIATIONS

Boc, *tert*-butyloxycarbonyl; Fmoc, Fluorenylmethyloxycarbonyl; DMF, dimethylformamide; FA, formic acid; IC_{50}, inhibitor concentration; TFA, trifluoroacetic acid; FP, prostaglandin F2α receptor; PGF2α, prostaglandin F2α; LPS, Lipopolysaccharides; SI, Supporting Information; TLC, thin layer chromatography; Smac, second mitochondria-derived activator of caspase; I^2aa, indolizidin-2-one amino acid.

REFERENCES

1. (a) Boeglin, D.; Hamdan, F. F.; Melendez, R. E.; Cluzeau, J.; Laperriere, A.; Héroux, M.; Bouvier, M.; Lubell, W. D., Calcitonin gene-related peptide analogs with aza and indolizidinone amino acid residues reveal conformational requirements for antagonist activity at the human calcitonin gene-related peptide 1 receptor. *J. Med. Chem.* **2007**, *50*, 1401-1408; (b) Bourguet, C. B.; Boulay, P.-L.; Claing, A.; Lubell, W. D., Design and synthesis of novel azapeptide activators of apoptosis mediated by caspase-9 in cancer cells. *Bioorg. Med. Chem. Lett.* **2014**, *24*, 3361-3355; (c) Chingle, R.; Ratni, S.; Claing, A.; Lubell, W. D., Application of constrained aza-valine analogs for Smac mimicry. *Peptide Science* **2016**, *106*, 235-244; (d) Bourguet, C. B.; Goupil, E.; Tassy, D.; Hou, X.; Thouin, E.; Polyak, F.; Hébert, T. E.; Claing, A.; Laporte, S. A.; Chemtob, S.; Lubell, W. D., Targeting the prostaglandin F2α receptor for preventing preterm labor with azapeptide tocolytics. *J. Med. Chem.* **2011**, *54*, 6085-6097.

2. (a) Proulx, C.; Sabatino, D.; Hopewell, R.; Spiegel, J.; Garcıa-Ramos, Y.; Lubell, W., Azapeptides and their therapeutic potential. *Future Med. Chem.*, **2011**, 3, 1139–1164;(b) Vagner, J.; Qu, H.; Hruby, V. J., Peptidomimetics, a synthetic tool of drug discovery. *Curr. Opin. Chem. Biol.* **2008**, *12*, 292-296; (c) Khashper, A.; Lubell, W. D., Design, synthesis, conformational analysis and application of indolizidin-2-one dipeptide mimics. *Org. Biomol. Chem.* **2014**, *12*, 5052-5070.

3. Goupil, E.; Tassy, D.; Bourguet, C.; Quiniou, C.; Wisehart, V.; Pétrin, D.; Le Gouill, C.; Devost, D.; Zingg, H. H.; Bouvier, M.; Saragovi H. U.; Chemtob, S.; Lubell, W. D.; Claing, A.; Hébert, T. E.; Laporte S. A., A novel biased allosteric compound inhibitor of parturition, selectively impedes the PGF2α-mediated Rho/ROCK signalling pathway. *Journal of Biological Chemistry* **2010**, *285*, 25624-25636.

4. (a) Sebayang, S. K.; Dibley, M. J.; Kelly, P. J.; Shankar, A. V.; Shankar, A. H.; Group, S. S., Determinants of low birthweight, small-for-gestational-age and preterm birth in Lombok, Indonesia: analyses of the birthweight cohort of the SUMMIT trial. *Tropical Medicine & International Health* **2012**, *17*, 938-950; (b) Petrini, J. R.; Callaghan, W. M.; Klebanoff, M.; Green, N. S.; Lackritz, E. M.; Howse, J. L.; Schwarz, R. H.; Damus, K., Estimated effect of 17 alpha-hydroxyprogesterone caproate on preterm birth in the United States. *Obstetrics & Gynecology* **2005**, *105*, 267-272.

5. Berkowitz, G. S.; Papiernik, E., Epidemiology of preterm birth. *Epidemiologic reviews* **1993,** *15*, 414-443.

6. (a) Organization, W. H., http://www. who. int/mediacentre/factsheets/fs340/en. *url>* http://www. *who. int/mediacentre/factsheets/fs241/en/</url* **2014**; (b) Purisch, S. E.; Gyamfi-Bannerman, C., Epidemiology of preterm birth. *Seminars in perinatology* **2017**, *41*, 387-391.

7. Behrman, R. E.; Butler, A. S., *Preterm birth: causes, consequences, and prevention*. The obstetrician and gynaecologist. **2008**, *10*, 280.

8. (a) Haas, D. M.; Caldwell, D. M.; Kirkpatrick, P.; McIntosh, J. J.; Welton, N. J., Tocolytic therapy for preterm delivery: systematic review and network meta-analysis. *BMJ* **2012,** *345*, e6226; (b) Olson, D. M.; Christiaens, I.; Gracie, S.; Yamamoto, Y.; Mitchell, B. F., Emerging tocolytics: challenges in designing and testing drugs to delay preterm delivery and prolong pregnancy. *Expert Opinion on Emerging Drugs* **2008**, *13*, 695-707; (c) Hernandez, W. R.; Francisco, R. P.; Bittar, R. E.; Gomez, U. T.; Zugaib, M.; Brizot, M. L., Effect of vaginal progesterone in tocolytic therapy during preterm labor in twin pregnancies: Secondary analysis of a placebo-controlled randomized trial. *J. Obstet. Gynaecol. Res.* **2017,** *43*, 1536-1542.

9. (a) Surprenant, S.; Lubell, W. D., From Macrocycle Dipeptide Lactams To Azabicyclo [X.Y.0] alkanone Amino Acids: A Transannular Cyclization Route for Peptide Mimic Synthesis. *Org. Lett.*

2006, *8*, 2851-2854; (b) Atmuri, N. P.; Lubell, W. D., Insight into Transannular Cyclization Reactions To Synthesize Azabicyclo [X.Y.Z] alkanone Amino Acid Derivatives from 8-, 9-, and 10-Membered Macrocyclic Dipeptide Lactams. *J. Org. Chem.* **2015**, *80*, 4904-4918.

10. Godina, T. A.; Lubell, W. D., Mimics of peptide turn backbone and side-chain geometry by a general approach for modifying azabicyclo [5.3.0] alkanone amino acids. *J. Org. Chem.* **2011**, *76*, 5846-5849.

11. (a) Bourguet, C. B.; Proulx, C.; Klocek, S.; Sabatino, D.; Lubell, W. D., Solution-phase submonomer diversification of aza-dipeptide building blocks and their application in aza-peptide and aza-DKP synthesis. *J. Pept. Sci.* **2010**, *16*, 284-296; (b) Garcia-Ramos, Y.; Proulx, C.; Lubell, W. D., Synthesis of hydrazine and azapeptide derivatives by alkylation of carbazates and semicarbazones. *Can. J. Chem.* **2012**, *90*, 985-993.

12. Pandey, A. K.; Naduthambi, D.; Thomas, K. M.; Zondlo, N. J., Proline editing: a general and practical approach to the synthesis of functionally and structurally diverse peptides. Analysis of steric versus stereoelectronic effects of 4-substituted prolines on conformation within peptides. *J. Am. Chem. Soc.* **2013**, *135*, 4333-4363.

13. Kaul, R.; Surprenant, S.; Lubell, W. D., Systematic study of the synthesis of macrocyclic dipeptide β-turn mimics possessing 8-, 9-, and 10-membered rings by ring-closing metathesis. *J. Org. Chem.* **2005**, *70*, 3838-3844.

14. Shao, C.; Wang, X.; Zhang, Q.; Luo, S.; Zhao, J.; Hu, Y., Acid–base jointly promoted copper (I)-catalyzed azide–alkyne cycloaddition. *J. Org. Chem.* **2011,** *76*, 6832-6836.

15. Le Quement, S. T.; Nielsen, T. E.; Meldal, M., Divergent Pathway for the Solid-Phase Conversion of Aromatic Acetylenes to Carboxylic Acids, α-Ketocarboxylic Acids, and Methyl Ketones. *J. Comb. Chem.* **2008,** *10*, 546-556.

16. Zhang, J.; Proulx, C.; Tomberg, A.; Lubell, W. D., Multicomponent diversity-oriented synthesis of aza-lysine-peptide mimics. *Org. Lett.* **2013**, *16*, 298-301.

17. Kang, Y. K.; Choi, H. Y., Cis–trans isomerization and puckering of proline residue. *Biophysical Chemistry* **2004**, *111*, 135-142.

18. Boeglin, D.; Lubell, W. D., Aza-amino acid scanning of secondary structure suited for solid-phase peptide synthesis with Fmoc chemistry and aza-amino acids with heteroatomic side chains. *J. Comb. Chem.* **2005**, *7*, 864-878.

19. Gibson, C.; Goodman, S. L.; Hahn, D.; Hölzemann, G.; Kessler, H., Novel solid-phase synthesis of azapeptides and azapeptoides via Fmoc-strategy and its application in the synthesis of RGD-mimetics. *J. Org. Chem.* **1999**, *64*, 7388-7394.

20. Ahsanullah; Chingle, R.; Ohm, R. G.; Chauhan, P. S.; Lubell, W. D., Aza-propargylglycine installation by aza-amino acylation: Synthesis and Ala-scan of an azacyclopeptide CD36 modulator. *Peptide Science*, **2019**, *111*, e24102.

21. Thomas, K. M.; Naduthambi, D.; Zondlo, N. J., Electronic control of amide cis-trans isomerism via the aromatic-prolyl interaction. *J. Am. Chem. Soc.* **2006**, *128*, 2216-2217.

22. Mauger, A.; Irreverre, F.; Witkop, B., The stereochemistry of 3-methylproline. *J. Am. Chem. Soc.* **1966**, *88*, 2019-2024.

23. Lombart, H.-G.; Lubell, W. D., Rigid dipeptide mimetics: efficient synthesis of enantiopure indolizidinone amino acids. *J. Org. Chem.* **1996**, *61*, 9437-9446.

24. AndrÉ, F.; Boussard, G.; Bayeul, D.; Didierjean, C.; Aubry, A.; Marraud, M., Aza-peptides II. X-Ray structures of aza-alanine and aza-asparagine-containing peptides. *J. Pept. Res.* **1997**, *49*, 556-562.

25. Nair, C.; Vijayan, M., Structural characteristics of prolyl residues-A Review. *Journal of the Indian Institute of Science* **2013**, *63*, 81.

26. Venkatachalam, C., Stereochemical criteria for polypeptides and proteins. V. Conformation of a system of three linked peptide units. *Biopolymers* **1968**, *6*, 1425-1436.

27. (a) Boukanoun, M. K.; Hou, X.; Nikolajev, L.; Ratni, S.; Olson, D.; Claing, A.; Laporte, S. A.; Chemtob, S.; Lubell, W. D., Investigation of the active turn geometry for the labor delaying activity of indolizidinone and azapeptide modulators of the prostaglandin F2α receptor. *Org. Biomol. Chem.* **2015**, *13*, 7750-7761; (b) Bourguet, C. B.; Claing, A.; Laporte, S. A.; Hébert, T. E.; Chemtob, S.; Lubell, W. D., Synthesis of azabicycloalkanone amino acid and azapeptide

mimics and their application as modulators of the prostaglandin F2α receptor for delaying preterm birth. *Can. J. Chem.* **2014**, *92*, 1031-1040.

28. Greenlee, W.; Thorsett, E.; Springer, J.; Patchett, A.; Ulm, E.; Vassil, T., Azapeptides: a new class of angiotensin-converting enzyme inhibitors. *Biochem. Biophys. Res. Commun.* **1984**, *122*, 791-797.

29. Thormann, M.; Hofmann, H.-J., Conformational properties of azapeptides. *Journal of Molecular Structure: Theochem* **1999**, *469*, 63-76.

30. Newberry, R. W.; Raines, R. T., 4-Fluoroprolines: Conformational analysis and effects on the stability and folding of peptides and proteins. In *Peptidomimetics I*, Springer: 2016; pp 1-25.

31. Siebler, C.; Trapp, N.; Wennemers, H., Crystal structure of (4S)-aminoproline: conformational insight into a pH-responsive proline derivative. *J. Pept. Sci.* **2015**, *21*, 208-211.

32. Peri, K. G.; Quiniou, C.; Hou, X.; Abran, D.; Varma, D. R.; Lubell, W. D.; Chemtob, S. In *THG113: a novel selective FP antagonist that delays preterm labor*, Seminars in perinatology 2002 Elsevier; pp 389-397.

33. Conroy, T.; Jolliffe, K. A.; Payne, R. J., Efficient use of the Dmab protecting group: applications for the solid-phase synthesis of N-linked glycopeptides. *Org. Biomol. Chem.* **2009**, *7*, 2255-2258.

34. (a) Tietze, L. F.; Brasche, G.; Grube, A.; Böhnke, N.; Stadler, C., Synthesis of Novel Spinosyn A Analogs by Pd-Mediated Transformations. *Chem. Eur. J.* **2007**, *13*, 8543-8563; (b) Williams, M. A.; Rapoport, H., Synthesis of conformationally constrained DTPA analogs. Incorporation of the ethylenediamine units as aminopyrrolidines. *J. Org. Chem.* **1994**, *59*, 3616-3625.

Crystal-State Conformational Analysis of Adm Peptides. Influence of the C-Terminal Substituent

3.1. Context

As mentioned in the introduction, α,α-disubstituted glycines can rigidify the peptide backbone through steric interactions to induce helix, extended and turn structures. In pursuit of a fully developed γ-helix with three consecutive γ-turns, 2-amino-adamantane-2-carboxylic acid (Adm) was examined because of earlier reports demonstrating its potential as a γ-turn inducer.[1-2] A series of di- and tripeptides were pursued to develop a more effective means for Adm oligomer synthesis and to further study the relevance of the *C*-terminal amide on the conformation of Adm residues.

The Ugi multiple component reaction had previously been used to assemble simple Adm analogs,[3] as well as Aib-Aib peptide analogs.[4] Discovered in 1960's,[5-6] the Ugi reaction combines carbonyl, amine, carboxylic acid and isocyanide components to form an *N*-(acyl)amino amide. The isocyanide serves as a reactive nucleophile and subsequently an electrophile to facilitate an intramolecular amino acylation. In the Ugi reaction mechanism, the amine and carbonyl components condense in the presence of the acid to form an iminium ion salt with loss of water. Nucleophilic addition of isocyanide to the iminium ion creates a nitrilium ion that reacts with the carboxylate to form an *O*-acyl imidate. Acyl group transfer via a Mumm type of rearrangement from the imidate oxygen to the *N*-terminal amine delivers the *N*-(acyl)amino amide (Figure 3.1).[7] Considering the literature precedent and mechanism, Adm di- and tripeptides were targeted using adamant-2-one in the Ugi reaction.

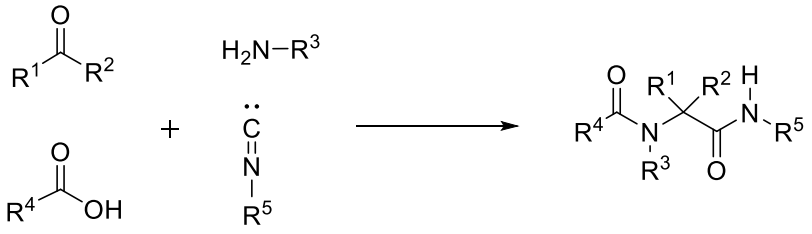

Scheme 3.1. Ugi 4C-MCR reaction

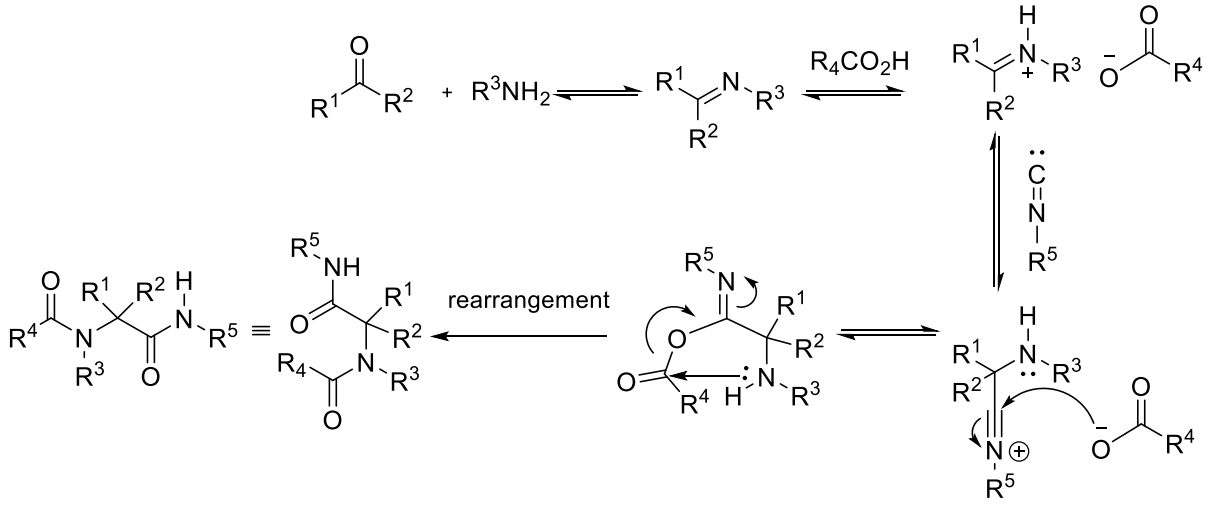

Figure 3.1 Mechanism of Ugi reaction

In Chapter 3, a set of *N*-formyl-Adm di- and tripeptides were synthesized possessing various *C*-terminal components using the Ugi reaction. The influence of the *C*-terminal amide on the Adm backbone conformation was then studied by crystallization and X-ray analysis. Although, the conformational space of Adm peptide is restricted due to the steric bulk of the Adm residue, contingent on the size of their *C*-terminal residues, the Adm peptides adopted a set of conformations including γ- and β-turn types.

References for Chapter 3

1. Kuroda, Y.; Ueda, H.; Nozawa, H.; Ogoshi, H., Adamantyl amino acid as γ-turn inducer for peptide. *Tetrahedron Lett.* **1997**, *38*, 7901-7904.
2. Mazzier, D.; Grassi, L.; Moretto, A.; Alemán, C.; Formaggio, F.; Toniolo, C.; Crisma, M., En route towards the peptide γ-helix: X-ray diffraction analyses and conformational energy calculations of Adm-rich short peptides. *J. Pept. Sci.* **2017**, *23*, 346-362.
3. Samsoniya, S.; Zurabishvili, D.; Bukia, T.; Buzaladze, G.; Lomidze, M.; Elizbarashvili, E.; Kazmaier, U., Synthesis of some Derivatives of N-(1-Adamantyl)Carbonyl-N'-Benzyliden-o-Phenylendiamine. *Bull. Georg. Natl. Acad. Sci.* **2014**, *8*, 78-84.
4. Pirali, T.; Tron, G. C.; Masson, G.; Zhu, J., Ammonium chloride promoted three-component synthesis of 5-iminooxazoline and its subsequent transformation to macrocyclodepsipeptide. *Org. lett.* **2007**, *9*, 5275-5278.
5. Ugi, I.; Steinbrückner, C., Über ein neues Kondensations-Prinzip. *Angew. Chem.* **1960,** *72*, 267-268.
6. Ugi, I., The α-addition of immonium ions and anions to isonitriles accompanied by secondary reactions. *Angew. Chem. Int. Ed. Engl.* **1962,** *1*, 8-21.
7. Dömling, A.; Ugi, I., Multicomponent reactions with isonitriles. *Angew. Chem. Int. Ed.* **2000,** *39*, 3168-3210.

Manuscript 2

Crystal-State Conformational Analysis of Adm Peptides. Influence of the C-Terminal Substituent

Fatemeh M. Mir,[1] Marco Crisma,[2] Claudio Toniolo,[2,3] William D. Lubell[1]

[1] Département de Chimie, Université de Montréal, C. P. 6128, Succursale Centre-Ville, Montréal, Québec, Canada H3C 3J7

[2] Institute of Biomolecular Chemistry, Padova Unit, CNR, 35131 Padova, Italy

[3] Department of Chemistry, University of Padova, 35131 Padova, Italy

*Submitted to Peptide Science, special issue devoted to the 8th Peptide Engineering Meeting (PEM8)

Crystal-State Conformational Analysis of Adm Peptides. Influence of the C-Terminal Substituent

Fatemeh M. Mir,[1] Marco Crisma,[2] Claudio Toniolo,[2,3] William D. Lubell[1]

[1] Département de Chimie, Université de Montréal, C. P. 6128, Succursale Centre-Ville, Montréal, Québec, Canada H3C 3J7

[2] Institute of Biomolecular Chemistry, Padova Unit, CNR, 35131 Padova, Italy

[3] Department of Chemistry, University of Padova, 35131 Padova, Italy

---

**Correspondence to:*

Prof. Claudio Toniolo, Department of Chemistry, University of Padova, via Marzolo 1, 35131 Padova, Italy. E-mail: claudio.toniolo@unipd.it

Prof. William D. Lubell, Département de Chimie, Université de Montréal, C. P. 6128, Succursale Centre-Ville, Montréal, Québec, Canada H3C 3J7. E-mail: william.lubell@umontreal.ca

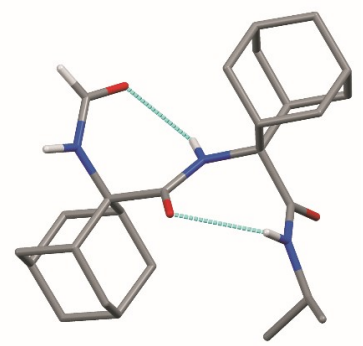

Abstract

The functionalized diamondoid α-amino acid, 2-aminoadamantane-2-carboxylic acid (Adm) has been introduced into four N^{α}-formyl homo-dipeptide alkyl amides using a solution-phase Ugi multi-component reaction approach. The conformers of the Adm peptides were determined in the crystalline state by X-ray diffraction to distinguish the influences of the *C*-terminal amide. The Adm peptides folded into open and hydrogen-bonded γ-turn geometry. Moreover, 3D-structures were observed featuring two consecutive γ-turns in an incipient γ-helical structure, a significantly distorted non-helical β-turn, as well as an S-shaped conformation with opposite helical screw sense. A significant topological variety was thus exhibited by the Adm peptides contingent on their *C*-terminal residues illustrating both the broad potential and the need for further characterization of the sterically bulky Adm residue in explorations of peptide conformational space.

Keywords: Adm peptides; γ-helix; X-ray diffraction; β-turn; γ-turn

Running title: Conformation of Adm peptides

1 INTRODUCTION

$C^{\alpha,\alpha}$-Dialkylglycines have the potential for restricting backbone conformation within peptide chains. For example, a variety of 3D-structural analyses of α-aminoisobutyric acid (Aib) residues[1-6] in different peptides in solution and in the crystal state have demonstrated the strong tendency for this achiral amino acid to induce type-III (III′) β-turns[7-12] and helical conformations.[1-4,13,14] Although $C^{\alpha,\alpha}$-cycloalkyl α-amino acid residues (*e.g.*, 1-aminocyclopentane-1-carboxylic acid, Ac_5c, and 1-aminocyclohexane-1-carboxylic acid, Ac_6c),[15] exhibited similar propensity, as the bulkiness of both $C^{\alpha,\alpha}$-substituents increases in acyclic α-amino acids of this class (*e.g.*, $C^{\alpha,\alpha}$-diethylglycine, Deg), fully-extended conformation become more stable.[16-18]

The diamondoid,[19] 2-aminoadamantane-2-carboxylic acid (Adm) residue has demonstrated intriguing potential for adopting the relatively uncommon γ-turn conformation[20-26] in X-ray diffraction studies of short Adm-rich peptides and homo-peptides.[27,28] In solution,[29] Adm derivatives, such as Ac-Adm-NHMe and Ac-Adm-Gly-NHMe were suggested to fold in γ-turn conformations based on NMR and IR absorption spectroscopic studies. Moreover, certain Adm homo-peptides[27,28] have been observed by X-ray diffraction to exhibit two consecutive, regular γ-turns, indicating the possibility to form the still uncharacterized γ-helix.[30]

The influences of the *C*-terminal substituent on the tendency of the -Adm-Adm- dipeptide sequence to adopt the γ-turn conformation have now been investigated by the synthesis and X-ray diffraction analysis of a series of di- and tripeptides *N*-terminating in a common formyl group. The sequences featured different C-terminal residues to examine the influences of size and hydrogen-bond donor and acceptor units on the peptide conformation: HCO-$(Adm)_2$-Gly-OEt (**3.4a**), HCO-$(Adm)_2$-NH*i*Pr (**3.4b**), HCO-$(Adm)_2$-NH*t*Bu (**3.4c**), and HCO-$(Adm)_2$-Aib-OMe (**3.4d**). In addition, the X-ray diffraction structure of a strictly related dipeptide, HCO-Adm-Aib-OMe (**3.2d**) was also solved and studied.

2 EXPERIMENTAL

2.1 Synthesis and characterization

Dichloromethane (DCM) and methanol (MeOH) were used after drying by passage through solvent filtration systems (GlassContour, Irvine, CA). Reagents from commercial sources were used as received. Purification by silica gel chromatography was performed on 230-400 mesh silica gel. Analytical thin-layer chromatography (TLC) was carried out on silica gel 60 F254 (Aluminum Sheet) and visualized by UV absorbance or by staining with iodine. Melting points are uncorrected and were obtained on sample in capillary tubes using a Mel-Temp melting point apparatus equipped with a

thermometer and reported in degree Celsius (°C). Infrared absorption spectra were recorded on a Bruker Alpha P spectrometer, and the frequency of absorption is reported in reciprocal centimeters (cm^{-1}). ^{1}H and ^{13}C NMR spectra were recorded at room temperature (rt) in $CDCl_3$ (7.26 ppm / 77.16 ppm) or in deuterated dimethylsulfoxide (DMSO, d_6) (2.50 ppm / 39.52 ppm) on Bruker AV (300/75 and 500/125 MHz) instruments and referenced to internal solvent. Chemicals shifts are reported in parts per million (ppm); coupling constants (*J* values) in Hertz; abbreviations for peak multiplicities are s (singlet), d (doublet), t (triplet), q (quadruplet), m (multiplet) and br (broad). High-resolution mass spectrometry (HRMS) was performed by the Centre Régional de Spectroscopie de Masse de l'Université de Montréal, using protonated molecular ions $[M + H]^+$, $[M + 2H]/2^+$ or sodium adducts $[M + Na]^+$ for empirical formula confirmation.

Peptides **3.2b-c**, **3.3b-c**, **3.4b-c** were prepared as previously described in ref 28.

HCO-Gly-OEt. A mixture of HCl · H-Gly-OEt (10 g, 70 mmol) and ammonium formate (9.20 g, 146 mmol) in CH_3CN (75 mL) was heated at reflux and stirred for 16h. The volatiles were removed under reduced pressure. The residue was partitioned between water (30 mL) and DCM (30 mL). The layers were separated. The aqueous phase was extracted with DCM (2 x 30 mL). The combined organic layer was dried over Na_2SO_4 and filtered. The filtrate was concentrated to provide HCO-Gly-OEt as a pale-yellow liquid (6.98 g, 76%) that was used without further purification. R_f 0.33 (2:8 hexane : ethyl acetate, EtOAc). ^{1}H NMR (500 MHz, $CDCl_3$): δ 1.21 (t, *J* = 7.0 Hz, 3H); 3.98 (d, *J* = 6.0, 2H), 4.14 (q, *J* = 7.2, 2H), 6.85 (br, 1H), 8.17 (s, 1H); ^{13}C NMR (500 MHz, $CDCl_3$): δ 14,0, 39.9, 61.6, 161.6, 169.6; HRMS (ESI): *m/z* calcd for $C_5H_{10}NO_3$ 132.0655; found $[M + H]^+$ 132.0657.

HCO-Aib-OMe.[31-33] A solution of H-Aib-OH (5g, 48.5 mmol) in MeOH (25 mL) was cooled to 0 °C, treated with $SOCl_2$ (7.0 mL, 97mmol) and left to stir for 16h with warming to rt. The volatiles were removed under reduced pressure to give HCl · H-Aib-OMe as a white solid in quantitative yield. The salt was dissolved in formic acid (15 mL), treated with a solution of sodium formate (3.21 g, 50.9 mmol) in a minimum amount of formic acid, and left to stir at 40 °C. After 2h, the mixture was filtered, and the filtrate was treated with 1:1 formic acid: acetic anhydride (4 mL/15 mL), heated to 80 °C and stirred for 20h. The mixture was filtered and the filtrate was concentrated under vacuum to give HCO-Aib-OMe as a pale-yellow oil, which exhibited the same characteristics as previously reported. ^{1}H NMR (300 MHz, $CDCl_3$): δ 1.58 (s, 6H), 3.74 (s, 3H), 6.68 (s, 1H), 8.10 (s, 1H).

Ethyl isocyanoacetate (**3.1a**). HCO-Gly-OEt (5.7 g, 43.5 mmol) in DCM (43 mL) was treated with triethylamine (TEA) (13.2 g, 130.5 mmol), cooled to –5 °C and treated dropwise with $POCl_3$ (8 g, 52.2 mmol). After stirring at –5 °C for 1h, the resulting reddish mixture was treated with a solution

of sat. $NaHCO_3$ (30 mL) and agitated thoroughly. The organic phase was separated, washed with brine, dried over Na_2SO_4, filtered, and evaporated under reduced pressure to afford a reddish liquid, which was purified by column chromatography using an eluent of hexane:EtOAc (7:3). Evaporation of the collected fractions gave isocyanide **3.1a** as pale-yellow oil (3.6 g, 73%). R_f 0.48 (7:3 hexane:EtOAc). ^{1}H NMR (500 MHz, $CDCl_3$): δ 1.28 (t, *J* = 7.0, 3H), 4.20 (s, 2H), 4.24 (q, *J* = 7.0, 2H); ^{13}C NMR (500 MHz, $CDCl_3$): δ 14.0, 43.5, 62.7, 161.0, 164.0; IR absorption (neat): ν 2162, 1750; HRMS (ESI): *m*/*z* calcd for $C_5H_8NO_2$ 114.0555; found $[M + H]^+$ 114.0551.

Methyl 2,2-dimethyl-isocyanoacetate (**3.1d**).[32] This compound was synthesized according to the procedure described above for **3.1a** using HCO-Aib-OMe (7.5g, 49.2 mmol), TEA (24.3 mL, 246 mmol and $POCl_3$ (6.9 mL, 73.8 mmol) at 20 °C. Evaporation of the volatiles gave an orange liquid which was purified by column chromatography using hexane:EtOAc (7:3) as eluent to furnish isocyanide **3.1d** (3.75 g, 60%) as a pale-yellow liquid which exhibited the same characteristics as previously reported. R_f 0.72 (3:7 hexane:EtOAc); ^{1}H NMR (300 MHz, $CDCl_3$): δ 1.64 (s, 6H), 3.80 (s, 3H); ^{13}C NMR (300 MHz, $CDCl_3$): δ 27.5, 53.6, 59.5, 157.9, 170.1.

HCO-Adm-Gly-OEt (**3.2a**)**.** A solution of isocyanoacetate **3.1a** (3 g, 26.5 mmol) in MeOH (2M) was treated with adamantan-2-one (3.98 g, 26.5 mmol) followed by a solution of ammonium formate ((2.0 g, 31.8 mmol) in the minimum amount of water, and stirred for 24h. The volatiles were evaporated. The residue was dissolved in $CHCl_3$, washed with water and brine, dried over Na_2SO_4, and evaporated to a residue that was purified on column chromatography using hexanes:EtOAc (1:1) as eluent to provide dipeptide **3.2a** (1.52g, 56%) as a powder: R_f 0.34 (1:1 hexanes:EtOAc); m.p. 165.2-167.2 °C; ^{1}H NMR (300 MHz, $CDCl_3$): δ 1.26 (t, *J* = 7.2, 3H); 1.67 (m, 1H), 1.71 (m, 3H), 1.76 (m, 2H), 1.83-1.84 (m, 2H), 1.94-2.04 (m, 4H), 2.68 (m, 2H), 3.99 (d, *J* = 5.8, 2H), 4.17 (q, *J* = 7.1, 2H), 5.82 (s, 1H), 7.59 (t, *J* = 5.7, 1H), 8.13 (d, *J* = 2.0, 1H); ^{13}C NMR (300 MHz, $CDCl_3$): δ 14.3, 26.5, 26.6, 32.2, 32.5, 33.9, 37.4, 41.5, 61.4, 64.9, 161.9, 169.9, 172.8; IR absorption (neat): ν 3254, 1746, 1682, 1641, 1531; HRMS (ESI): *m*/*z* calcd for $C_{16}H_{25}N_2O_4$ 309.1809; found $[M + H]^+$ 309.1818.

HCO-Adm-Aib-OMe (**3.2d**). This compound was synthesized according to the procedure described above for the synthesis of dipeptide **3.2a** using methyl 2,2-dimethyl-isocyanoacetate **3.1d** (1.27 g, 10 mmol), adamantan-2-one (1.5 g, 10 mmol), and ammonium formate (0.95 g, 15 mmol). The residue was purified on column chromatography using hexanes:EtOAc (7:3) as eluent to give dipeptide **3.2d** as a powder (1.98 g, 62%): R_f 0.50 (1:9 MeOH:EtOAc); m.p. 185.8-189.5 °C; ^{1}H NMR (300 MHz, $CDCl_3$): δ 1.48 (s, 6H), 1.66 (m, 1H), 1.70 (m, 4H), 1.75 (m, 1H), 1.82 (m 2H), 1.92-2.01 (m, 4H), 2.65 (m, 2H), 3.68 (s, 3H), 5.70 (s, 1H), 7.57 (s, 1H), 8.15 (d, *J* = 2, 1H); ^{13}C NMR (300 MHz,

$CDCl_3$): δ 25.0, 26.5, 26.7, 32.1, 32.5, 33.9, 37.3, 25.4, 56.0, 64.9, 161.9, 171.2, 174.9; HRMS (ESI): *m*/*z* calcd for $C_{17}H_{27}N_2O_4$ 323.1965, found $[M + H]^+$ 323.1976.

"CN-Adm"-Gly-OEt (**3.3a**) was synthesized from dipeptide **3.2a** (1.51g, 4.68mmol) according to procedure described above for the synthesis of isocyanoacetate **3.1a**. The volatiles were removed and the orange residue was purified by column chromatography using hexanes:EtOAc (7:3) as eluent to afford isocyanide **3.3a** as a white powder (1.03g, 72%). R_f 0.35 (7:3 hexanes:EtOAc); m.p. 87.6-90.8 °C; ^{1}H NMR (500 MHz, $CDCl_3$): δ 1.28 (t, *J* = 7.2 Hz, 3H), 1.72 (m, 2H), 1.77-1.82 (m, 5H), 1.90-1.91 (m, 1H), 1.98-2.01 (m, 2H), 2.23-2.26 (m, 2H), 2.38 (m, 2H), 4.06 (d, *J* = 5.3 Hz, 2H), 4.22 (q, *J* = 7.2, 2H), 6.56 (br, 1H); ^{13}C NMR (500 MHz, $CDCl_3$): δ 14.2, 26.1, 26.3, 33.2 (2C), 34.9, 37.2, 41.7, 61.8, 68.5, 158.7, 167.8, 169.5; IR absorption (neat): ν 3377, 2120, 1744, 1659, 1525; HRMS (ESI): *m*/*z* calcd for $C_{16}H_{23}N_2O_3$ 291.1703; found $[M + H]^+$ 291.1709.

"CN-Adm"-Aib-OMe (**3.3d**) was synthesized from dipeptide **3.2d** (1.51g, 4.68mmol) according the procedure described above for the synthesis of isocyanoacetate **3.1a** and purified by column chromatography using hexanes:EtOAc (7:3) as eluent to afford isocyanide **3.3d** as a powder (1.31g, 92%): R_f 0.56 (7:3 hexanes:EtOAc); m.p. 115.9-117.4 °C; ^{1}H NMR (300 MHz, $CDCl_3$): δ 1.58 (s, 6H), 1.72 (m, 2H), 1.75-1.81 (m, 5H), 1.89-1.90 (m, 1H), 1.94-1.97 (m, 2H), 2.22-2.25 (m, 2H), 2.33 (m, 2H), 3.74 (s, 3H), 6.55 (s, 1H); ^{13}C NMR (300 MHz, $CDCl_3$): δ 24.4, 26.2, 26.3, 33.1, 33.2, 34.9, 37.2, 52.9, 56.9, 68.6, 158.4, 166.6, 174.8; IR absorption (neat): ν 3372, 2126, 1726, 1675, 1529; HRMS (ESI): *m*/*z* calcd for $C_{17}H_{25}N_2O_3$ 305.1860; found $[M + H]^+$ 305.1869.

HCO-(Adm)$_2$-Gly-OEt (**3.4a**) was synthesized from isocyanide **3.3a** (1g, 3.43mmol) according to the procedure described above for the synthesis of dipeptide **3.2a** and purified by column chromatography using hexanes:EtOAc (3:7) as eluent to give tripeptide **3.4a** as a powder (1.1g, 67%): R_f 0.35 (3:7 hexanes:EtOAc); ^{1}H NMR (500 MHz, DMSO): δ 1.17 (t, *J* = 7.1, 3H), 1.52-1.54 (m, 4H), 1.57-1.64 (m, 8H), 1.72-1.83 (m, 5H), 1.88-1.95 (m, 6H), 2.01-2.08 (m, 2H), 2.56-2.58 (m, 3H), 3.75 (d, *J* = 2.5, 2H), 4.06 (q, *J* = 7.1, 2H), 7.25 (s, 1H), 7.77 (t, *J* = 5.7 Hz, 1H), 7.97 (d, *J* = 2.1, 1H), 8.08 (d, *J* = 1.8, 1H); ^{13}C NMR (500 MHz, DMSO): δ 14.0, 25.9, 26.0, 26.2, 26.4, 31.3, 31.7, 32.2, 32.3, 33.3 (2C), 37.1, 37.3, 41.0, 60.2, 62.8, 64.1, 161.5, 170.0, 171.4, 172.1; IR absorption (neat): ν 3275, 1761, 1650, 1513; M.p. 197-200 °C; HRMS (ESI): *m*/*z* calcd for $C_{27}H_{39}N_3O_5Na$ 508.2782; found $[M + Na]^+$ 508.2774.

HCO-(Adm)$_2$-Aib-OMe (**3.4d**) was synthesized from isocyanide **3.3d** (1g, 3.3mmol) according to the procedure described above for the synthesis of dipeptide **3.2a** and purified by column chromatography using hexanes:EtOAc (7:3) as eluent to give tripeptide **3.4d** as a powder (1.03g, 62%): R_f 0.34 (1:9 MeOH:EtOAc); m.p. 198-203 °C; ^{1}H NMR (500 MHz, $CDCl_3$): δ 1.44 (s, 6H), 1.61-1.64 (m, 2H), 1.68-1.70 (m, 8H), 1.74-1.83 (m, 6H), 1.93-1.98 (m, 6H), 2.02-2.05 (m, 2H), 2.64

(m, 2H), 2.68 (m, 2H), 3.66 (s, 3H), 5.66 (s, 1H), 6.94 (s, 1H), 7.55 (s, 1H), 8.12 (d, J = 1.9, 1H); ^{13}C NMR (500 MHz, $CDCl_3$): δ 25.1, 26.3, 26.5, 26.6, 26.9, 32.3, 32.5, 32.6, 32.7, 34.0 (2C), 37.3, 37.6, 52.3, 55.7, 64.6, 65.5, 161.6, 171.2, 172.4, 175.0; IR absorption (neat): ν 3285, 1739, 1677, 1650, 1524; HRMS (ESI): *m/z* calcd for $C_{28}H_{42}N_3O_5$ 500.3119; found $[M + H]^+$ 500.3133.

2.2 X-Ray diffraction

Single crystals, suitable for X-ray diffraction analysis, of di- and tripeptides **3.2d** and **3.4a-d** were obtained from ethyl acetate (**3.2d**), acetone (**3.4a** and **3.4c**), DCM (**3.4b**), and DCM / hexane (**3.4d**).

X-Ray diffraction data for peptide **3.2d** were collected with a Gemini E four-circle kappa diffractometer (Agilent Technologies) equipped with a 92-mm EOS CCD detector, using graphite monochromated Cu Kα radiation (λ = 1.54178 Å). Data collection and reduction were performed with the CrysAlisPro software (Agilent Technologies). A semi-empirical absorption correction based on the multi-scan technique using spherical harmonics was implemented in the SCALE3 ABSPACK scaling algorithm.

X-Ray diffraction data collection for the remaining four structures (**3.4a-d**) was performed at the Laboratoire de Diffraction des Rayons X de l'Université de Montréal with a Bruker Venture Metaljet diffractometer, equipped with a Gallium Liquid Metal Jet Source (Ga Kα radiation, λ = 1.34139 Å), Helios MX Mirror Optics, a kappa goniometer, and a Photon 100 CMOS detector. Data collection, data reduction, and absorption correction were achieved by use of the APEX 2, SAINT, and SADABS (or TWINABS where appropriate) software packages (Bruker AXS).

The structures were solved by *ab initio* procedures of the SIR 2014[34] or SHELXT[35] programs, and refined by full-matrix least-squares procedures on F^2, using all data, by application of the SHELXL-2014[36] or OLEX2[37] programs, with anisotropic displacement parameters for all of the non-hydrogen atoms. Hydrogen atoms were calculated at idealized positions and refined using a riding model.

Relevant crystal data and structure refinement parameters are reported in the *Supporting Information* (Tables S3.1-S3.5). CCDC 1880257 - 1880261 contain the supplementary crystallographic data for this paper. The data can be obtained free of charge from The Cambridge Crystallographic Data Centre via www.ccdc.cam.ac.uk/structures.

3 RESULTS

3.1 Peptide synthesis

$C^{\alpha,\alpha}$-Disubstituted glycines are generally recalcitrant to peptide bond formation because of their remarkable steric hindrance. This phenomenon becomes particularly significant in coupling

reactions to the α-amino functionality.[38,39] These unfavorable properties are magnified in couplings to Adm residues due to the increased bulkiness of the diamondoid residue.[19]

Among the different methods examined for coupling $C^{\alpha,\alpha}$-disubstituted glycines, the Ugi multi-component reaction [32,40] employing the commercially available 2-adamantone, ammonium formate, and different isocyanides (CN-R) was found to furnish Adm derivatives and peptides in relatively high yields (Scheme 3.2). Four isocyanides **3.1a-d** were investigated to begin the synthesis of a series of Adm dipeptides possessing various *C*-terminal residues: *iso*-propyl and *tert*-butyl isocyanides **3.1b** and **3.1c** were obtained from commercial sources; α-amino ester derived isocyanides **3.1a** and **3.1d** were respectively synthesized by formylation using ammonium formate and acetic anhydride, followed by isocyanide formation using $POCl_3$ and TEA. Adamantan-2-one was respectively reacted with isocyanides **3.1a**–**d** and ammonium formate in MeOH to afford N^{α}-formyl Adm-containing *C*-alkylamides and dipeptides **3.2a**–**d**. Formamides **3.2a**–**d** were converted into the corresponding isocyanides **3.3a**–**d** in excellent yields using $POCl_3$ and TEA, and elongated by the Ugi procedure to the corresponding N^{α}-formyl Adm di- and tripeptides **3.4a**–**d**.

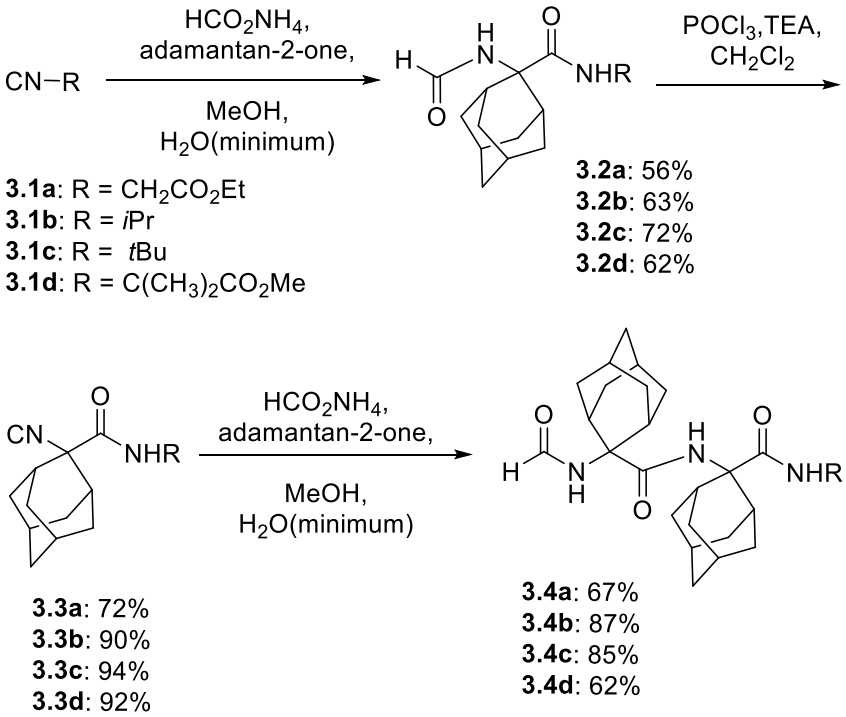

Scheme 3.2 Solution-phase syntheses of the N^{α}-formyl Adm-containing di- and tripeptides.

3.2 Crystal-state conformational analysis

The 3D-structures of the Adm-containing di- and tripeptides **3.2d** and **3.4a-d** were solved by X-ray diffraction (Figures 3.2-3.6). The *C*-terminal substituent effects on peptide conformation with

specific attention to γ-turn formation were assessed by evaluation of ϕ and ψ backbone torsion angles (Table 3.1) and intramolecular hydrogen-bond distances between amide (peptide) carbonyl and N-H groups (Table 3.2). Composed of achiral Adm, Gly and Aib residues, the five peptides were expected to crystalize in racemic conformers. For example, peptides **3.2d**, **3.4a** and **3.4b** crystallized in centrosymmetric space groups. On the other hand, peptides **3.4c** and **3.4d** crystallized in one of the Sohncke space groups in which molecules of only one handedness occur,[41] due to the rather uncommon phenomenon termed *spontaneous resolution*.[42] Crystals of peptides **3.4c** and **3.4d** were affected by twinning through inversion.

In the five structures, all of the amide, peptide and ester bonds adopt the usual *trans* isomer ($\omega = 180°$) without significant deviation ($|\Delta\omega| \leq 7.9°$) from the ideal planarity.

In the molecule arbitrarily selected as the asymmetric unit in the centrosymmetric structure of the dipeptide composed of two achiral, C^{α}-tetrasubstituted α-amino acids HCO-Adm-Aib-OMe (**3.2d**; Figure 3.2), the Adm residue adopts a left-handed, highly distorted helical conformation [ϕ^1, ψ^1 = 72.41 (16)°, 75.06 (13)°] (Table 3.1). The *C*-terminal Aib residue is also helical, but of opposite screw sense with respect to the preceding residue [ϕ^1, ψ^1 = –48.05 (16)°, –47.20 (15)°]. The overall backbone of **3.2d** can be described as S-shaped. [43,44] Without intramolecular hydrogen bonds, the amide N-H of the Adm and Aib residues form respectively intermolecular hydrogen bonds with the carbonyl oxygens of the Adm and formyl groups in a (–*x* + 1/2, *y* + 1/2, –*z* + 1/2) symmetry-related molecular packing mode featuring rows of molecules, related through a twofold axis, along the *b* direction (Table 3.2). Packing is favoured by van der Waals interactions.

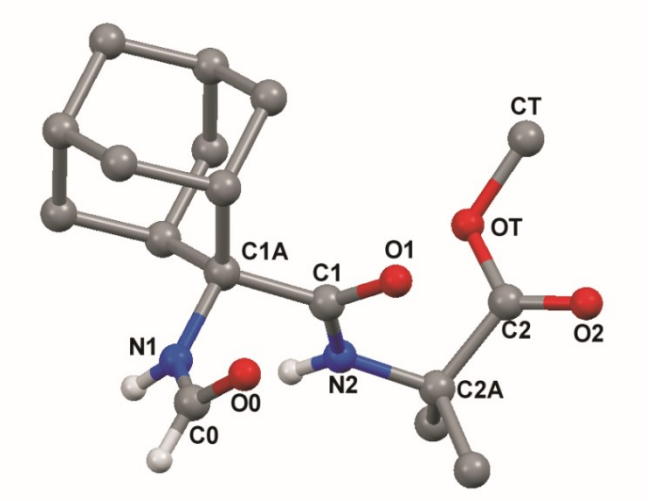

Figure 3.2. The X-ray diffraction structure of HCO-Adm-Aib-OMe (**3.2d**)

Table 3.1. Backbone ϕ and ψ torsion angles (°) observed for the X-ray diffraction structures N^{α}-formyl Adm-containing di- and tripeptides

Entry	Peptide sequence	ϕ_1	ψ_1	ϕ_2	ψ_2	ϕ_3	ψ_3	Type of turn
3.2d	HCO-Adm-Aib-OMe[a]	72.41(16)	75.06(13)	-48.05(16)	-47.20(15)			—
3.4a	HCO-$(Adm)_2$-Gly-OEt	-75.9(3)	79.2(3)	-69.2(3)	96.8(3)	84.5(3)	-158.4(2)	one γ-turn, one "open" γ-turn
3.4b	HCO-$(Adm)_2$-NH*i*Pr	76.49(12)	-79.37(10)	69.79(11)	-88.12(10)			two consecutive γ-turns
3.4c	HCO-$(Adm)_2$-NH*t*Bu	-77.5(5)	84.8(4)	-74.3(4)	70.5(4)			two consecutive γ-turns
3.4d	HCO-$(Adm)_2$-Aib-OMe	63.1(5)	-96.9(4)	-51.4(5)	-49.6(5)	56.2(5)	43.9(5)	distorted type-II′ β-turn

[a] *Abbreviations*: Aib, α-aminoisobutyric acid; OMe, methoxy; OEt, ethoxy; NH*i*Pr, *iso*-propylamino; NH*t*Bu, *tert*-butylamino.

Table 3.2. Intra- and intermolecular hydrogen-bond parameters for the X-ray diffraction structures of N^{α}-formyl Adm-containing di- and tripeptides.

Entry	Peptide sequence	Type	Donor D-H	Acceptor A	Distance (Å) D…A	Distance (Å) H…A	Angle (°) D-H…A	Symmetry equivalence of A
3.2d	HCO-Adm-Aib-OMe[a]	Intermolecular	N1-H1	O1	2.8448(14)	2.02	159.9	-*x*+1/2, *y*+1/2, -*z*+1/2
		Intermolecular	N2-H2	O0	3.0822(16)	2.23	168.4	-*x*+1/2, *y*+1/2, -*z*+1/2*z*
3.4a	HCO-$(Adm)_2$-Gly-OEt	Intramolecular	N2-H2	O0	2.935(3)	2.31	128.1	*x*, *y*, z
		Intermolecular	N1-H1	O2	2.851(3)	1.98	172.9	*x*-1, *y*, z
		Intermolecular	N3-H3	O3	3.163(3)	2.39	147.1	1-*x*, 1-*y*, 1-z
3.4b	HCO-$(Adm)_2$-NH*i*Pr	Intramolecular	N2-H2	O0	2.9167(11)	2.22	137.4	*x*, *y*, z
		Intramolecular	NT-HT	O1	2.9214(11)	2.40	120.0	*x*, *y*, z
		Intermolecular	N1-H1	O2	2.9026(12)	2.03	163.0	*x*-1, *y*, z

(ctd)

3.4c	HCO-$(Adm)_2$-NH*t*Bu	Intramolecular	N2-H2	O0	3.118(5)	2.56	122.3	*x*, *y*, *z*
		Intramolecular	NT-HT	O1	2.756(5)	2.10	131.0	*x*, *y*, *z*
		Intermolecular	N1-H1	O2	2.833(5)	2.02	153.0	*y*-*x*, 1-*x*, -1/3+*z*
3.4d	HCO-$(Adm)_2$-Aib-OMe	Intramolecular	N3-H3	O0	3.038(5)	2.20	163	*x*, *y*, *z*
		Intermolecular	N1-H1	O2	2.859(5)	2.05	156	-x, 1/2+y, 1/2-*z*

The X-ray diffraction structure of the less bulky of the two tripeptides studied, HCO-(Adm)$_2$-Gly-OEt (**3.4a**, Figure 3.3) is stabilized by a single *i* to *i*+2 intramolecular hydrogen bond between the formyl carbonyl oxygen and the central Adm(2) amide N-H in a 7-membered γ-turn conformation possessing characteristic backbone ϕ^1, ψ^1 torsion angles [–75.9 (3)°, 79.2 (3)°] for the *N*-terminal Adm(1) residue (Tables 3.1 and 3.2).[20,21,26] Moreover, the values for the central Adm(2) backbone torsion angles are close to those expected for a γ-turn. Specifically, the ϕ^2 value [–69.2 (3)°] is appropriate for a γ-turn conformation, but the ψ^2 value [96.8 (3)°] is slightly too large, suggesting formation of an "open" γ-turn. In corroboration, the intramolecular distance (2.60 Å) between the *N*-terminal Adm(1) carbonyl oxygen and the Gly(3) N-H exceeds slightly the commonly accepted limit for the onset of a hydrogen bond (≤ 2.50 Å).[45-47] The *C*-terminal Gly(3) residue is *semi*-extended [ϕ^3, ψ^3 = 84.5 (3)°, –158.4 (2)°, respectively]. Two intermolecular hydrogen bonds between the *N*-terminal Adm(1) amide N-H and central Adm(2) carbonyl of translationally equivalent molecules (*x*-1, *y*, *z*) generate molecular rows along the *a* direction. Another intermolecular hydrogen bond between opposing Gly(3) amide N-H and Gly(3) ester C=O groups form a (1-*x*, 1-*y*, 1-*z*) centrosymmetric counterpart (Table 3.2).

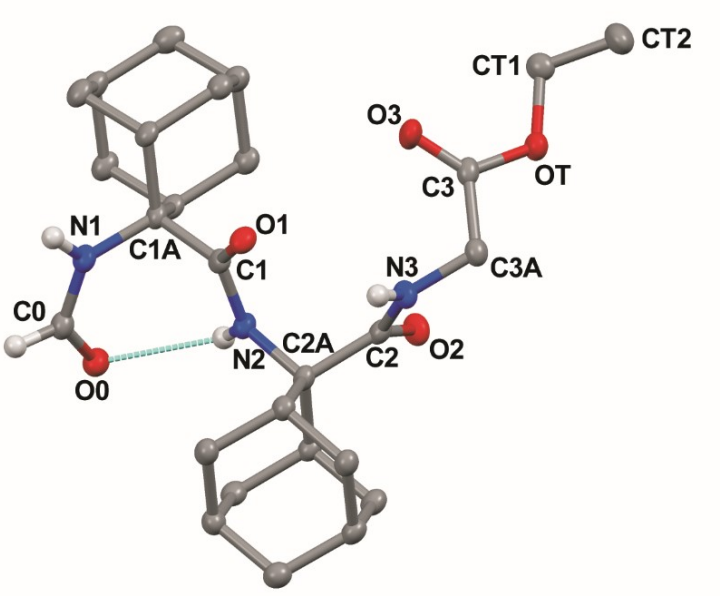

Figure 3.3. The X-ray diffraction structure of HCO-(Adm)$_2$-Gly-OEt (**3.4a**)

Peptides exhibiting two consecutive γ-turns are characteristic of incipient γ-helices and relatively rare.[26] The crystal-state conformers of dipeptide alkyl amides HCO-(Adm)$_2$-NHR **3.4b** and **3.4c** (R = *i*Pr and *t*-Bu, Figures 3.4 and 3.5) illustrated the potential for the Adm residue to favour such geometry. Both **3.4b** and **3.4c** featured a classical 7-membered ring γ-turn structure with an *i* to *i*+2 intramolecular hydrogen bond between the formyl C=O and the central Adm(2) peptide N-H groups (Table 3.2). In both **3.4b** and **3.4c**, the *N*-terminal Adm(1) residue adopted characteristic ϕ^1 and ψ^1 dihedral angles [76.49 (12)°, –79.37 (10)° for **3.4b**, and –77.5 (5)°, 84.8 (4)° for **3.4c** (Table 3.1)]. Moreover, the *C*-terminal Adm(2) adopted γ-turn geometry residue in both dipeptides, which exhibited *i* to *i*+2 intramolecular hydrogen bond distances between the *N*-terminal Adm(1) carbonyl oxygen and the alkyl amide N-H (2.40 Å and 2.10 Å, respectively, for **3.4b** and **3.4c**, Table 3.2). Although the ϕ^2, torsion angle matched ideal γ-turn geometry in both dipeptides, and the ψ^2 dihedral angle was regular for **3.4c** [70.5 (4)°], ψ^2 deviated significantly [–88.12 (10)°] from the ideal in **3.4b** (Table 3.1). In both structures, an intermolecular hydrogen bond was observed between the Adm(1) amide N-H and Adm(2) C=O in symmetry-related molecules (Table 3.2), which packed respectively along the *a* direction and around the 3_{10} screw axis in the crystals of **3.4b** and **3.4c**.

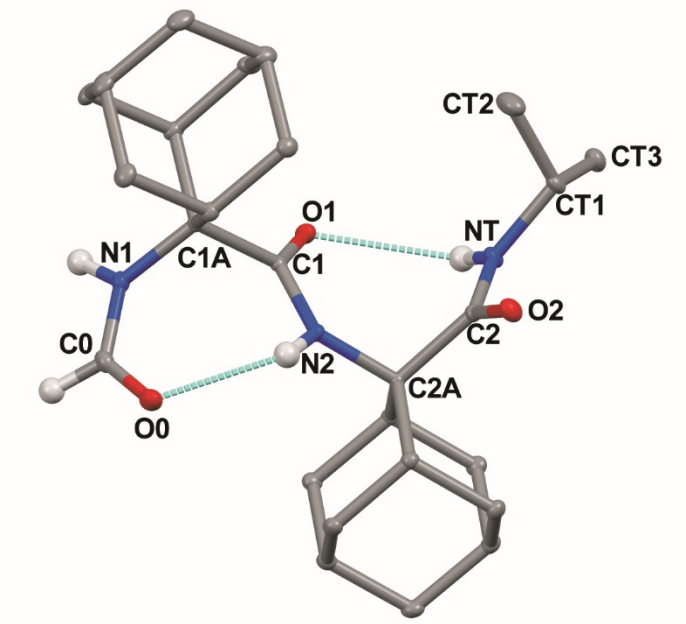

Figure 3.4. The X-ray diffraction structure of HCO-(Adm)$_2$-NH*i*Pr (**3.4b**)

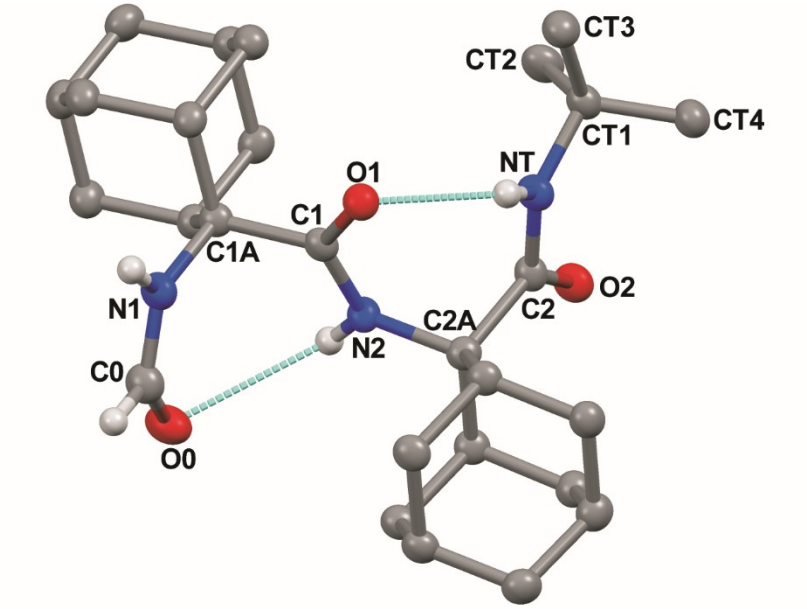

Figure 3.5. The X-ray diffraction structure of HCO-(Adm)$_2$-NH*t*Bu (**3.4c**)

In the crystal structure of the bulkier tripeptide HCO-(Adm)$_2$-Aib-OMe **3.4d** (Figure 3.6), the Adm-Adm dipeptide adopted ϕ ψ torsion angles [63.1 (5)°, –96.9 (4)°; –51.4 (5)°, –49.6 (5)° (Table 3.1)] which were reminiscent of the central residues of an ideal 10-membered ring type-II′ β-turn structure (60°, –120°; –90°, 0°).[7-12] In spite of significant distortion, an *i* to *i*+3 intramolecular hydrogen bond (2.20 Å) was observed between the formyl C=O and the Aib(3) peptide N-H groups (Table 3.2). The conformation adopted by the C-terminal Aib(3) residue was helical [ϕ^3, ψ^3 = 56.2 (5)°, 43.9 (5)°] with a screw-sense reversal with respect to the preceding Adm(2) residue. The S-shaped folding of the C-terminal -Adm(2)-Aib(3)- sequence in this structure was similar to that in dipeptide **3.2d** with more regular helical torsion angle values. Tripeptide **3.4d** packed with an intermolecular hydrogen bond between the *N*-terminal Adm(1) N-H and central Adm(2) C=O oxygen groups of (–x, ½ + y, ½ –*z*) symmetry-related molecules (Table 3.2).

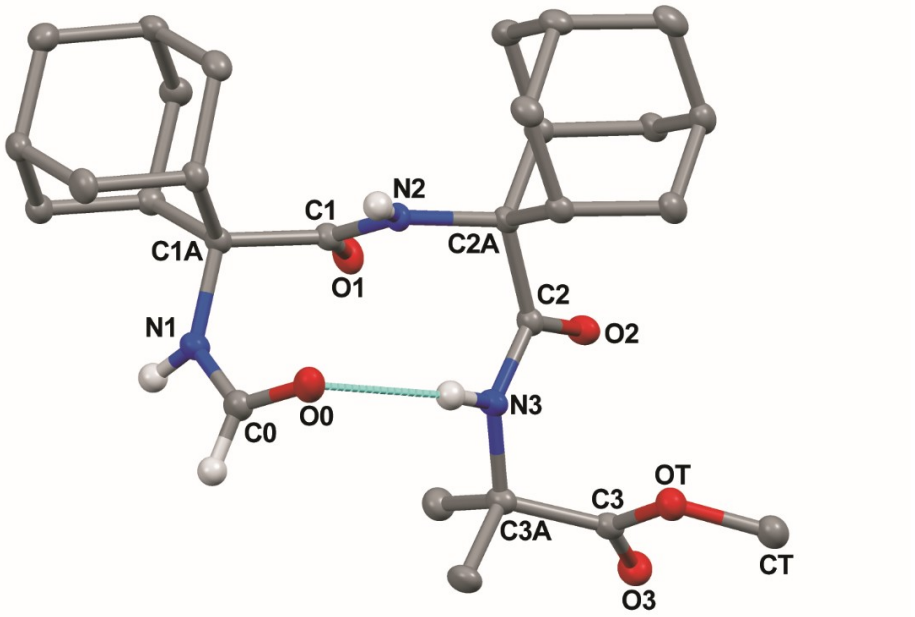

Figure 3.6. The X-ray diffraction structure of HCO-(Adm)$_2$-Aib-OMe (**3.4d**)

Previously, conformational energy calculations using density functional theory had predicted that after a consecutive γ-turn conformer, Ac-(Adm)$_2$-NHMe could adopt a distorted type-II (II′) β-turn with backbone torsion angles differing less than 10° from those found for tripeptide **3.4d** as the second most stable conformation.[27] This non-helical type of turn had however not been previously reported experimentally for *N*-acyl Adm dipeptide amide sequences. The crytal structure of **3.4d** illustrates that the double γ-turn and type-II (II′) β-turn conformations are energetically similar for Adm dipeptide sequences. Although the ϕ and ψ torsion angles of the *N*-terminal Adm(1) residue in **3.4d** are close to that of a regular γ-turn, the distance (2.67 Å) between the formyl C=O oxygen and the central Adm(2) peptide N-H is too long for an intramolecular hydrogen bond.

4 DISCUSSION

The backbone conformations of four N^{α}-formyl Adm homo-dipeptide sequences possessing various *C*-terminal secondary amide components have been determined in the crystal state using X-ray diffraction. Moreover, the corresponding -Adm-Aib- hetero-dipeptide sequence with a C-terminal ester group was also investigated. Although the results of the present study are

limited to similar sequences that may largely depend on the crystallization solvent and crystal packing forces, certain trends do emerge from examination of the influences exerted by the nature of the *C*-terminal groups.

Two ϕ and ψ regions of the Ramachandran map were predominantly found to be explored by the Adm residues. In the most extensively populated region, the two backbone torsion angles occur with comparable magnitude ($\pm 60° < \phi/\psi < \pm 80°$) and opposite sign. This region is typical of the central residue of an intramolecular hydrogen-bonded γ-turn, and the related distorted (open) γ-turn, but may be tolerated at position *i*+1 of a type-II (II′) β-turn. Such a conformer was also observed in consecutive γ-turns of incipient γ-helices. The second region was characterized by ϕ and ψ torsion angles with the *same* sign and $\psi > \pm 50°$ and accommodated at the *i*+2 position of a distorted type-II (II′) β-turn. The steric bulk of the Adm residue apparently restricts the ϕ and ψ values from adopting conformers characteristic of homo-peptides based on $C^{\alpha,\alpha}$-disubstituted glycines with smaller substituents, including the 3_{10}-helix, both corner positions of type-III (III′) / I (I′) β-turns, and all types of extended structures, including the *semi*-extended poly-$(Pro)_n$ II structure and the fully-extended structure.[16-18]

The observed backbone topologies concur with those previously reported in X-ray analyses of Adm peptides, including Adm homo-tripeptides, [27,28] in which incipient γ-helices as well as a rare isolated α-turn with average ϕ and ψ torsion angle values of the *same* sign [57.1°, 51.7°] were observed.[48-52] The two achiral amino acid components in the -CO-Adm-Aib-OR sequences analyzed in the present study, peptides **3.2d** and **3.4d**, both exhibited S-shaped helical conformations with *opposite* screw sense. The bias for this conformation may in part be due to the extremely strong propensity for the Aib residue to adopt helical geometry.[1-6] Whether this 3D-structural disposition is restricted to isolated N^{α}-acyl dipeptide esters or may be propagated to longer sequences (e.g., -$(Adm\text{-}Aib)_n$-, $n > 1$) remains to be investigated.

The steric bulk of the *C*-terminal amino substituent (-NHR) appears to influence the conformation of the -Adm-Adm- dipeptide sequence. In contrast to the influences of Aib residues observed in dipeptide **3.2d** and tripeptide **3.4d** discussed above, those of an additional Adm residue (in homo-tripeptides)[28] and *t*-Bu in dipeptide **3.4c** appear to favor a regular γ-turn conformation. On the other hand, less bulky di- and tri-substituted carbons (e.g., Cbz-Adm-Gly-OEt,[27] and Gly in tripeptide **3.4a**; *i*-Pr in dipeptide **3.4b**, HCO-$(Adm)_3$-NH*i*-Pr,[28] and 'N_3'-$(Adm)_3$-NH*i*-Pr,[27] and

Ala in Cbz-Adm-L-Ala-OMe,[27]) distorted the ideal γ-turn torsion angle values (100° < ψ < 88°) by rotating the Adm *C*-terminal amide away from serving as a correctly positioned N-H hydrogen-bond donor generating an open γ-turn and even α-helical conformations. In addition to steric bulk, the dipole interaction of ester moieties may likely dictate rotation about the Adm *C*-terminal amide to influence potential for adopting ideal γ-turn backbone torsion angles. In this context, this study offers light on design elements for favoring specific peptide secondary structures using Adm as a novel $C^{\alpha,\alpha}$-dialkylglycine residue.

ACKNOWLEDGMENTS

We would like to thank the Natural Sciences and Engineering Research Council of Canada for support. We thank Mr. T. Maris (X-ray), Dr. P. Aguiar, C. Malveau, and S. Bilodeau (NMR spectroscopy), Dr. A. Fürtös, K. Gilbert, M.-C. Tang and L. Mahrouche (mass spectroscopy) from U. de Montreal Laboratories for their assistance in analyses.

References

1. Shamala, N.; Nagaraj, R.; Balaram, P., The 3_{10} helical conformation of a pentapeptide nontaining a-aminoisobutyricAcid (Aib) : X-ray crystal structure of Tos-(Aib)5-OMe. *Chem. Commun*. **1978**, 996-997.
2. Benedetti, E.; Bavoso, A.; Di Blasio, B.; Pavone, V.; Pedone, C.; Crisma, M.; Bonora, G. M.; Toniolo, C., Linear oligopeptides. 81. Solid-state and solution conformation of homooligo(α-aminoisobutyric acids) from tripeptide to pentapeptide: Evidence for a 3_{10} helix. *J. Am. Chem. Soc.* **1982**, *104*, 2437-2444.
3. Toniolo, C.; Benedetti, E.; Structures of polypeptides from α-amino acids disubstituted at the α-carbon. *Macromolecules* **1991**, *24*, 4004-4009.
4. Karle, I. L., Controls exerted by the Aib residue: helix formation and helix reversal. *Biopolymers* **2001**, *60*, 351-365.
5. Gessmann, R.; Brückner, H.; Petratos, K., The crystal structure of Z-$(Aib)_{10}$-OH at 0.65 Å resolution: three complete turns of 3_{10}-helix. *J. Pept. Sci.* **2016**, *22*, 76-81.
6. Solá, J.; Helliwell, M.; Clayden, J., Interruption of a 3_{10}-helix by a single Gly residue in a poly-Aib motif: A crystallographic study. *Biopolymers* **2011**, *95*, 62-69.

7. Venkatachalam, C. M., Stereochemical criteria for polypeptides and proteins. V. Conformation of a system of three linked peptide units. *Biopolymers* **1968**, *6*, 1425-1436.
8. Geddes, J. A.; Parker, K. B.; Atkins, E. D. T.; Beighton, E., "Cross-β" conformation in proteins. *J. Mol. Biol.* **1968**, *32*, 343-358.
9. Lewis, P. N.; Momany, F. A.; Scheraga, H. A., Chain reversals in proteins. *Biochim. Biophys. Acta* **1973**, 303, 211-229.
10. Toniolo, C., Intramolecularly hydrogen-bonded peptide conformation. *CRC Crit. Rev. Biochem.* **1980**, *9*, 1-44.
11. Smith, J. A.; Pease, L. G., Reverse turns in peptides and protein. *CRC Crit. Rev. Biochem.* **1980**, *8*, 315-399.
12. Rose, G. D.; Glerasch, L. M.; Smith, J. A., Turns in peptides and proteins. *Adv. in protein chem.* **1985**, *37*, 1-109.
13. Pauling, R. B. Corey, H. R. Branson, The structure of proteins: two hydrogen-bonded helical configurations of the polypeptide chain. *Proc. Natl. Acad. Sci. USA* **1951**, *37*, 205-211.
14. Tonlolo, C.; Benedetti, E., The polypeptide 3_{10}-helix. *Trends Biochem. Sci.* **1991**, *16*, 350-353.
15. Toniolo, C.; Crisma, M.; Formaggio, F.; Peggion, C., Control of peptide conformation by the Thorpe-Ingold effect (C^{α}-tetrasubstitution). *Biopolymers (Peptide Science)* **2001**, *60*, 396-419.
16. Benedetti, E.; Barone, V.; Bavoso, A.; Di Blasio, B.; Lelj, F.; Pavone, V.; Pedone, C.; Bonora, G.; Toniolo, C.; Leplawy, M., Structural versatility of peptides from $C^{\alpha,\alpha}$-dialkylated glycines. I. A conformational energy computation and x-ray diffraction study of homo-peptides from $C^{\alpha,\alpha}$-diethylglycine. *Biopolymers* **1988**, *27*, 357-371.
17. Tanaka, M., Design and synthesis of chiral α,α-disubstituted amino acids and conformational study of their oligopeptides. *Chem. Pharm. Bull.(Tokyo)* **2007**, *55*, 349-358.
18. Peggion, C.; Moretto, A. Formaggio, F.; Crisma, M.; Toniolo, C., Multiple, consecutive, fully-extended 2.0_5-helix peptide conformation. *Biopolymers* **2013**, *100*, 621-636.

19. Marchand, A. P., Diamondoid hydrocarbons-delving into nature's bounty. *Science* **2003**, *299*, 52-53.
20. Némethy, G.; Printz, M. P., The γ turn, a possible folded conformation of the polypeptide chain. Comparison with the β turn. *Macromolecules* **1972**, *5*, 755-758.
21. Matthews, B. W., The γ-turn. evidence for a new folded conformation in proteins. *Macromolecules* **1972**, *5*, 818-819.
22. Flippen-Anderson, J. L.; Karle, I. L., Conformation of the cyclic tetrapeptide dihydrochlamydocin. Iabu-L-Phe-D-Pro-LX, and experimental values for 3→1 intramolecular hydrogen bonds by X-ray diffraction. *Biopolymers* **1976**, *15*, 1081-1092.
23. Milner-White, E. J.; Ross, B. M.; Ismail, R.; Belhadj-Mostefa, K.; Poet, R., One type of γ-turn, rather than the other gives rise to chain-reversal in proteins. *J. Mol. Biol.* **1988**, *204*, 777-782.
24. Jiménez, A. I.; Ballano, G.; Cativiela, C., First observation of two consecutive γ turns in a crystalline linear dipeptide. *Angew. Chem. Int. Ed.* **2005**, *44*, 400-403.
25. Kishore, R.; Balaram, P., Stabilization of γ-turn conformations in peptides by disulfide bridging. *Biopolymers* **1985**, *24*, 2041-2043.
26. Crisma, M.; De Zotti, M.; Moretto, A.; Peggion, C.; Drouillat, B.; Wright, K.; Couty, F.; Toniolo, C.; Formaggio, F., Single and multiple peptide γ-turns: literature survey and recent progress. *New J. Chem.* **2015**, *39*, 3208-3216.
27. Mazzier, D.; Grassi, L.; Moretto, A.; Alemán, C.; Formaggio, F.; Toniolo, C.; Crisma, M., En route towards the peptide γ-helix: X-ray diffraction analyses and conformational energy calculations of Adm-rich short peptides. *J. Pept. Sci.* **2017**, *23*, 346-362.
28. Mir, F. M.; Crisma, M.; Toniolo, C.; Lubell, W. D., unpublished.
29. Kuroda, Y.; Ueda, H.; Nozawa, H.; Ogoshi, H., Adamantyl amino acid as γ-turn inducer for peptide. *Tetrahedron Lett.* **1997**, *38*, 7901-7904.
30. Donohue, J., Hydrogen bonded helical configurations of the polypeptide chain. *Proc. Natl. Acad. Sci. USA* **1953**, *39*, 470-478.
31. Yamada, T.; Omote, Y.; Yamanaka, Y.; Miyadawa, T.; Kuwata, S. *Synthesis* **1998**, 991.
32. Pirali, T.; Tron, G. C.; Masson, G.; Zhu, J. Ammonium chloride promoted three-component synthesis of 5-iminooxazoline and its subsequent transformation to macrocyclodepsipeptide. *Org. Lett.* **2007**, *9*, 5275-5278.

33. Kotha, S.; Behera, M.; Khedkar, P., Environmentally benign process for the synthesis of *N*-formyl amino acid esters. *Tetrahedron Lett.* **2004**, *45*, 7589-7590.
34. Burla, M. C. ; Caliandro, R. ; Carrozzini, B.; Cascarano, G. L.; Cuocci, C. ; Giacovazzo, C. ; Mallamo, M.; Mazzone, A.; Polidori, G., Crystal structure determination and refinement via SIR2014. *J. Appl. Crystallogr.* **2015**, *48*, 306-309.
35. Sheldrick, G. M., *SHELXT*-Integrated space-group and crystal-structure determination *Acta Crystallogr. A,* **2015**, *71*, 3-8.
36. Sheldrick, G. M., Crystal structure refinement with *SHELXL Acta Crystallogr. C*, **2015**, *71*, 3-8.
37. Bourhis, L. J.; Dolomanov, O. V.; Gildea, R. J.; Howard, J. A. K.; Puschmann, H., The anatomy of a comprehensive constrained, restrained refinement program for the modern computing environment - *Olex2* dissected. *Acta Crystallogr. A,* **2015**, *71*, 59-75.
38. Formaggio, F.; Broxterman, Q. B.; Toniolo, C., in *Houben-Weyl, Methods of Organic Chemistry*, Vol. E22c, *Synthesis of Peptides and Peptidomimetics* (Eds.: M. Goodman, A. Felix, L. Moroder, C. Toniolo) Thieme, Stuttgart, Germany, **2003**, pp. 292-310.
39. Brückner, H.; Currle, M., in *Second Forum on Peptides* (Eds.: A. Aubry, M. Marraud, B. Vitoux), Libbey Eurotext, Paris, **1989**, *174*, pp. 251-255.
40. Samsoniya, S.; Zurabishvili, D.; Bukia, T.; Buzaladze, G.; Lomidze, M.; Elizbarashvili, E.; Kazmaier, U. Synthesis of some derivatives of *N*-(1-adamantyl)carbonyl-*N'*-benzyliden-*o*-phenylendiamine. *Bull. Georgian Natl. Acad. Sci.* **2014**, *8*, 85-93.
41. Nespolo, M.; Aroyo, M. I.; Souvignier, B., Crystallographic shelves: space-group hierarchy explained. *J. Appl. Crystallogr.* **2018**, *51*, 1481-1491.
42. Pérez-Garcia, L.; Amabilino, D. B., Spontaneous resolution under supramolecular control. *Chem. Soc. Rev.* **2002**, *31*, 342-356.
43. Goel, V. K.; Guha, M.; Baxia, A. P.; Dey, S.; Singh, T. P., Design of peptides with α,β-dehydro-residues: synthesis, crystal structure and molecular conformation of a peptide *N*-tertiary-butyloxycarbonyl-L-Leu-ΔPhe-L-Ile-OCH_3. *J. Mol. Struct.* **2003**, *658*, 135-141.
44. Vijayaraghavan, E.; Goel, V. K.; Dey, S.; Singh, T. P., Design of peptides with α,β-dehydro residues: synthesis, crystal structure and molecular conformation of a peptide *N*-Boc-Phe-ΔPhe-Ile-OCH_3. *Struct. Chem.* **2005**, *16*, 445-452.

45. Taylor, R.; Kennard, O.; Versichel, W. The geometry of the N–H···O=C hydrogen bond. 3. Hydrogen-bond distances and angles. *Acta Crystallogr. B* **1984**, *40*, 280-288.
46. Görbitz, C.-H., Hydrogen-bond distances and angles in the structures of amino acids and peptides. *Acta Crystallogr. B* **1989**, *45*, 390-395.
47. Torshin, I. Y.; Weber, I. T.; Harrosin, R. W. Geometric criteria of hydrogen bonds in proteins and identification of 'bifurcated' hydrogen bonds. *Protein Eng.* **2002**, *15*, 359-363.
48. Pavone, V.; Gaeta, G.; Lombardi, A.; Nastri, F.; Maglio, O.; Isernia, C.; Saviano, M., Discovering protein secondary structures: Classification and description of isolated α-turns. *Biopolymers* **1996**, *38*, 705-721.
49. Chou, K.-C., Prediction and classification of α-turn types. *Biopolymers* **1997**, *42*, 837-853.
50. Ramakrishnan, C. ; Nataraj, D. V., Energy minimization studies on α-turns. *J. Pept. Sci.* **1998**, *4*, 239-252.
51. Narita, M.; Sode, K.; Ohuchi, S., Single amino acid preferences for specific locations at type-I α-Turns in globular proteins. *Bull. Chem. Soc. Jpn* **1999**, *72*, 1807-1813.
52. Dasgupta, B.; Pal, L.; Basu, G.; Chakrabarti, P., Expanded turn conformations: Characterization and sequence-structure correspondence in α-turns with implications in helix folding. *Proteins: Struct. Funct. Bioinform.* **2004**, *55*, 305-315.

Chapter 4: Isolated α−Turn and Incipient γ −Helix

4.1. Context

Helices exhibit a shape featuring periodic folding with intramolecular hydrogen bonds. The α-helix is the most common helical shape in natural peptides. Repetition of 13-membered hydrogen bonds is characteristic in the α-helix; however, the single 13-membered hydrogen bonded turn conformation is usually disfavored due to the entropic costs of folding. Similarly, γ-turns which feature 7-membered hydrogen bonds are relatively rare. Moreover, the γ-turn helix in which a repetition of three or more 7-membered hydrogen bonds has never been observed. Fundamental information is thus still needed on the factors for controlling folding and intramolecular hydrogen bonding of peptide structures into single turns and repetitive helical structures.

As discussed in the introductory chapter, the incorporation of restricted amino acids into peptide chains is a powerful tactic for constructing peptide analogs with defined conformation. For example, oligomers of Aib residues have been extensively studied to prepare 3_{10}- and α-helical conformations.[1] The Thorpe-Ingold effect from the gem-dimethyl groups may be considered a key factor favoring such geometry.[2-3] As described in the previous chapter, 2-aminoadamantane-2-carboxylic acid (Adm) is a less well studied C^{α}-disubstituted glycine. In model peptides, Adm was shown to adopt dihedral angle orientations corresponding to the central residues of ideal α-, β- and γ-turns.

Adamantane derivatives have previously been investigated in potential therapeutics for various disease states: e.g., neurological conditions,[4] cancer,[5] hypertension,[6] malaria,[7] and tuberculosis.[8] The bulky dimensions of the adamantane can fit inside cavities of various host molecules, such as cyclodextrines,[9-10] and can block certain ion channels.[11] Adamantane analogs have lipophilicity to enter membrane lipid bilayers and have been used to transfer drugs into cells.[12]

In the interest to expand applications of Adm in peptide science and medicinal chemistry, the Ugi reaction approach that was described in the last chapter for the synthesis of di- and tri-peptides possessing one and two Adm residues has now been employed to prepare Adm-tripeptides. In this chapter, the synthesis, spectroscopic and X-ray crystallographic structural characterization of Adm-tripeptides with two different *C*-terminal amides (*i*-Pr and *t*-Bu) is disclosed. The subtle difference of the *C*-terminal amide has had a significant influence on the

conformation of the Adm-tripeptides in the solid state. A single turn of an α-helix and two turns of a γ-helix were observed by X-ray crystallography of the two different amides, which appeared to exhibit IR and NMR spectroscopic properties in solution which were characteristic of a γ-helix. Pushing the Ugi method toward the synthesis of Adm-tripeptides in this chapter, new frontiers have been explored for using Adm residues in the stabilization of rare peptide turns and helices. The effectiveness of the synthetic method and the consistent formation of the solid-state structures independent of crystallization solvent, both bear well for future applications of Adm in peptide and biomedical science.

References for Chapter 4

1. Pengo, B.; Formaggio, F.; Crisma, M.; Toniolo, C.; Bonora, G. M.; Broxterman, Q. B.; Kamphuis, J.; Saviano, M.; Iacovino, R.; Rossi, F., Linear oligopeptides. Part 406.[1] Helical screw sense of peptide molecules: the pentapeptide system $(Aib)_4$/L-Val [L-(αMe)Val] in solution. *J. Chem. Soc., Perkin Trans. 2,* **1998**, 1651-1658.
2. Sola, J.; Morris, G. A.; Clayden, J., Measuring screw-sense preference in a helical oligomer by comparison of ^{13}C NMR signal separation at slow and fast exchange. *J. Am. Chem. Soc.* **2011,** *133*, 3712-3715.
3. Toniolo, C.; Crisma, M.; Formaggio, F.; Peggion, C., Control of peptide conformation by the Thorpe-Ingold effect (C^{α}-tetrasubstitution). *Biopolymers (Peptide Science)* **2001**, *60*, 396-419.
4. Malo, M.; Brive, L.; Luthman, K.; Svensson, P., Selective pharmacophore models of dopamine D_1 and D_2 full agonists based on extended pharmacophore features. *ChemMedChem* **2010**, *5*, 232-246.
5. Zefirova, O. N.; Nurieva, E. V.; Lemcke, H.; Ivanov, A. A.; Shishov, D. V.; Weiss, D. G.; Kuznetsov, S. A.; Zefirov, N. S., Design, synthesis, and bioactivity of putative tubulin ligands with adamantane core. *Bioorg. Med. Chem. Lett.* **2008**, *18*, 5091-5094.
6. Liu, J. Y.; Tsai, H. J.; Hwang, S. H.; Jones, P. D.; Morisseau, C.; Hammock, B. D., Pharmacokinetic optimization of four soluble epoxide hydrolase inhibitors for use in a murine model of inflammation. *British journal of pharmacology* **2009**, *156*, 284-296.
7. Dong, Y.; Wittlin, S.; Sriraghavan, K.; Chollet, J.; Charman, S. A.; Charman, W. N.; Scheurer, C.; Urwyler, H.; Santo Tomas, J.; Snyder, C.; Creek, D. J.; Morizzi, J.; Koltun, M.; Matile, H.; Wang, X.; Padmanilayam, M.; Tang, Y.; Dorn, A.; Brun, R.; Vennerstrom, J. L., The structure-activity relationship of the antimalarial ozonide Arterolane (OZ277). *J. Med. Chem.* **2009**, *53*, 481-491.
8. Lee, R. E.; Protopopova, M.; Crooks, E.; Slayden, R. A.; Terrot, M.; Barry, C. E., Combinatorial lead optimization of [1,2]-diamines based on ethambutol as potential antituberculosis preclinical candidates. *J. Comb. Chem.* **2003**, *5*, 172-187.

9. Liu, B.-w.; Zhou, H.; Zhou, S.-t.; Yuan, J.-y., Macromolecules based on recognition between cyclodextrin and guest molecules: Synthesis, properties and functions. *European Polymer Journal* **2015,** *65*, 63-81.
10. Harries, D.; Rau, D. C.; Parsegian, V. A., Solutes probe hydration in specific association of cyclodextrin and adamantane. *J. Am. Chem. Soc.* **2005,** *127*, 2184-2190.
11. Cady, S. D.; Luo, W.; Hu, F.; Hong, M., Structure and function of the influenza A M2 proton channel. *Biochemistry* **2009,** *48*, 7356-7364.
12. Chew, C. F.; Guy, A.; Biggin, P. C., Distribution and dynamics of adamantanes in a lipid bilayer. *Biophysical journal* **2008,** *95*, 5627-5636.

Manuscript 3

Isolated α−Turn and Incipient γ −Helix

Fatemeh M. Mir, Marco Crisma, Claudio Toniolo, William D. Lubell

Manuscript is Prepared for Chem.Sci.

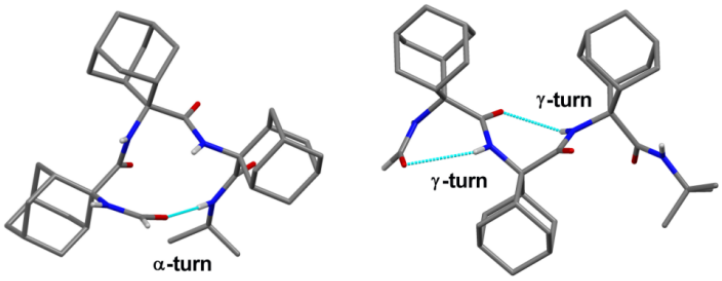

Isolated α−Turn and Incipient γ −Helix

*Fatemeh M. Mir,[†] Marco Crisma,[‡] Claudio Toniolo,[‡] William D. Lubell[†]**

[†] Département de Chimie, Université de Montréal, C. P. 6128, Succursale Centre-Ville, Montréal, Québec, Canada H3C 3J7

[‡] Department of Chemistry, University of Padova and Institute of Biomolecular Chemistry, Padova Unit, CNR, 35131 Padova, Italy

KEYWORDS: α-turn conformation, γ-turn conformation, homo-oligoadamantyl peptides, Ugi multicomponent reaction.

ABSTRACT: The unique abilities of homo-oligo-adamantyl peptides to adopt α- and γ-turn conformations are demonstrated by X-ray diffraction, and NMR and FT-IR absorption spectroscopies. Assembled by an Ugi multicomponent reaction strategy, N^{α}-formyl-adamantyl tripeptide *iso*-propyl and *tert*-butyl amides are respectively found to adopt an isolated α-turn and an incipient γ-helix conformation by X-ray diffraction crystallography. The shortest example of a single α-turn with ideal geometry is observed in the crystalline state. In solution both peptides predominantly assume γ-helical structures.

INTRODUCTION

Helices constitute the most abundant peptide and protein secondary structures in nature and play vital roles in protein-protein recognition.[1] Composed of repeating turn motifs, helices are stabilized to a large extent by backbone intramolecular C=O···H-N hydrogen bonds and minimization of side-chain steric interactions.[2] The most common natural helical structure is the α-helix,[2a] which features 13-membered intramolecular hydrogen bonds between the C=O and NH groups, respectively, of residues *i* and *i*+4 (α-turn[3] or C_{13}). On the other hand, a single α-turn in short linear peptides (≤ 5 amino acid residues), unambiguously authenticated by X-ray diffraction analysis, is rare,[4] due likely to the entropic penalty of forming such an intramolecular hydrogen bond. Conversely, single 7-membered intramolecular hydrogen-bonded (*i*+2 → *i* or C_7) γ-turn

structures[5a] have been identified in natural peptides, but the fully developed γ-helix, featuring repeating γ-turns, has yet to be observed.[5b]

$C^{\alpha,\alpha}$-Disubstituted glycines are known to be able to constrain peptides to adopt distinct secondary structures.[6,7] The backbone ϕ and ψ torsion angles adopted by these residues are typically contingent on the substituent size and nature. Specifically, $C^{\alpha,\alpha}$-dimethylglycine (α-aminoiso-butyric acid, Aib) and C^{α}-methylated analogs of proteinogenic amino acids favor folded backbone conformations in the 3_{10}-/α-helical region ($\phi = \pm 60 \pm 20°$, $\psi = \pm 30 \pm 20°$),[6,8,9] which are similarly adopted by peptides composed of 1-aminocycloalkane-1-carboxylic acid residues with four or more carbon atoms in the ring moiety.[6b,7,9] Homo-peptides from the aforementioned residues almost invariably give rise to 3_{10}-helices,[6b] and only exceptionally to α-helices.[10] These conclusions have been corroborated by a crystal-state investigation on a peptide featuring a single guest Gly residue placed in the middle of a host $(Aib)_{16}$ homo-oligomer.[11] On the other hand, a few highly sterically hindered residues, including 2-aminoadamantane-2-carboxylic acid (Adm) have been shown by X-ray diffraction analyses on model peptides to exhibit propensity for γ-turn conformations.[5b,12,13] Finally, residues with two ethyl, *n*-propyl, phenyl or benzyl substituents adopt predominantly fully-extended (C_5) conformations ($\phi \cong 180°$, $\psi \cong 180°$).[6b,7,14]

Although homo-oligomers of Aib have been commonly prepared and studied,[6,8] few examples of long oligopeptides composed of multiple residues with larger side chains have been reported due to the challenge of coupling sterically bulky α-amino acids, particularly at their α-amino functionality.[15] In this connection, it is worth pointing out that the sterically hindered Adm residue has been shown to react with protein amino acids (Gly, Leu, Phe) in acceptable yields (45-75%) by classical *C*-activating methods [*i.e.*, N^{α}-unprotected *N*-carboxyanhydride, N^{α}-acetyl/trifluoroacetyl 5(4*H*)oxazolones and EDC, *N*-ethyl-*N*′-3-(dimethylaminopropyl)carbodiimide / HOAt (7-aza-1-hydroxy-1,2,3-benzotriazole)] to provide simple dipeptides with *N*-terminal Adm residues.[12,16] The synthesis of dipeptides with *C*-terminal Adm residues is however more challenging and has been achieved (65-90% yield) using reactive acyl chloride derivatives, combined usually with an azide ($-N_3$) precursor of the α-amino group,[12] according to the procedure of Meldal,[17] but coupling yields drop precipitously (<10%) upon homo-peptide assembly to the tripeptide level, preventing further main-chain elongation.[12]

Among the potentially useful, alternative methods for synthesizing $C^{\alpha,\alpha}$-disubstituted glycines with very bulky side chains, the Ugi reactions of adamantan-2-one has previously delivered -Adm-Gly- dipeptides, albeit in modest yields.[18a] Furthermore, HCO-Aib-Aib-OMe has been assembled in 57% yield by the reaction of methyl 2-isocyano-2-methylpropanoate, acetone and ammonium formate.[18b] To the best of our knowledge, the construction of longer main chains of severely sterically bulky amino acids by the Ugi reaction has yet to be reported. Exploring the Ugi conditions, we present here access to the HCO-$(Adm)_3$-NHR tripeptides **4.1** and **4.2** (R = *i*Pr and *t*Bu, respectively). A concomitant combination of X-ray diffraction crystallography and spectroscopic methods has demonstrated that the Adm residue can favor the elusive single 13-membered intramolecularly hydrogen-bonded α-turn, as well as the almost completely developed γ-helix conformations.

RESULTS AND DISCUSSION

Synthesis

The synthesis of N^{α}-formyl-Adm homo-tripeptides **4.1** and **4.2** began respectively by reacting adamantan-2-one with *iso*-propyl and *tert*-butyl isocyanides **4.3** in methanol (MeOH) with ammonium formate dissolved in the minimum amount of water (Ugi conditions, Scheme 4.1). After heating at 70 °C for 20 hours, evaporation of the volatiles and chromatography on silica gel afforded the formamides **4.4**. Isocyanides **4.5** were prepared on treatment of **4.4** with $POCl_3$ and triethylamine in dichloromethane (DCM) between –5 to –10 °C for 1-2 hours. After aqueous workup and column chromatography, isocyanides **4.5** were isolated as solids in ≥90% yields. Exposure of isocyanides **4.5** to similar Ugi conditions as those described above gave homo-dipeptides **4.6** as solids in ≥85% yields. Subsequently, formamide to isocyanide conversion went smoothly using the $POCl_3$ conditions to afford isocyanides **4.7**. Finally, the desired homo-tripeptides **4.1** and **4.2** were synthesized using the Ugi approach. However, the reaction was relatively sluggish, and required heating for 2 days in the presence of excess ammonium formate to provide solid products after chromatography in about 60% yields.

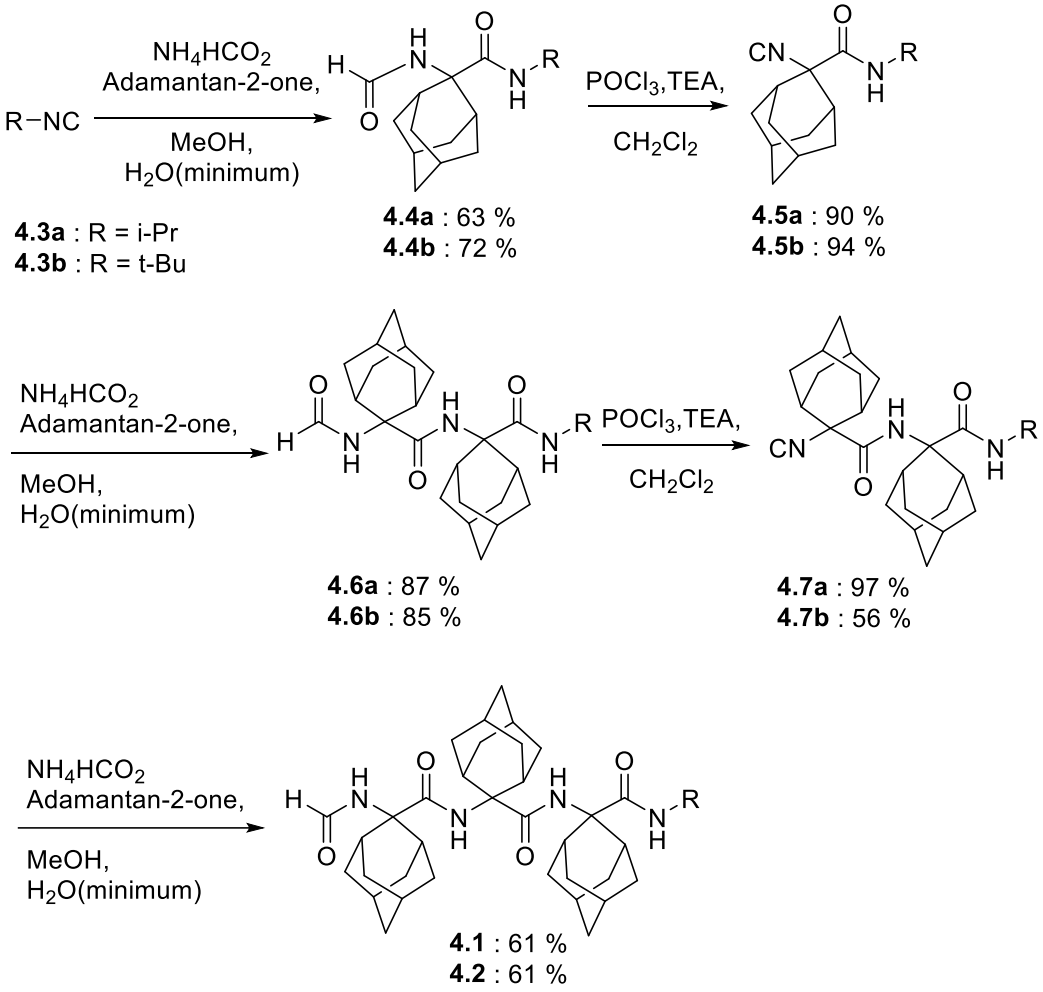

Scheme 4.1. Syntheses of the HCO-(Adm)$_3$-NHR peptides **4.1** and **4.2**.

Conformational Analysis of Tripeptides 4.1 and 4.2

X-Ray diffraction analysis. The three-dimensional structures of the Adm homo-tripeptides **4.1** and **4.2** were determined by single crystal X-ray diffraction (Fig. 4.1) and their backbone torsion angles were compared with those of ideal secondary structures (Table 4.1). A single 13-membered intramolecular hydrogen-bonded α-turn is observed in the asymmetric unit of **4.1** (R = *i*Pr). This intramolecular hydrogen bond takes place between the formamide carbonyl oxygen and the *C*-terminal amide NH group [N···O and H···O separations 3.095(3) Å and 2.22 Å, respectively; N-H···O angle 177.6°].

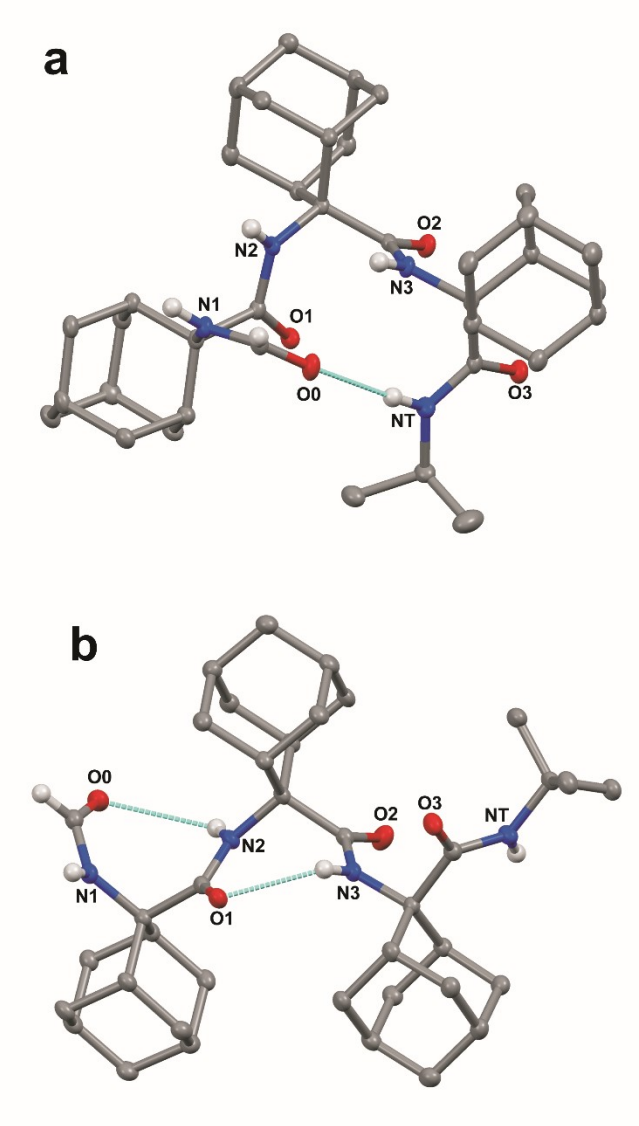

Figure 4.1. X-ray diffraction crystal structures of the HCO-(Adm)$_3$-NHR peptides **4.1** (a) and **4.2** (b). Most of the H-atoms are omitted for clarity. Intramolecular hydrogen bonds are indicated by dashed lines.

In addition, the formamide carbonyl oxygen is at a distance of 3.117(3) Å from the nitrogen atom of Adm(3), suitable for forming a 10-membered intramolecular hydrogen bond (β-turn),[19] but the H···O separation (2.61 Å) and N-H···O angle (117.4°) would be slightly outside the commonly accepted limits ($\leq$ 2.50 Å and $\geq$ 120°) for the occurrence of a hydrogen bond.[20] In the quest for possible polymorphs, peptide **4.1** was also crystallized from solvents of varying polarity

(EtOAc, acetone, $CHCl_3$) within the limits imposed by solubility. Crystals suitable for X-ray diffraction analysis were obtained from three different systems; however, all gave the identical α-turn structure, within experimental error (Table 4.1).

Table 4.1. Backbone Torsion Angles (°) of the HCO-$(Adm)_3$-NHR Peptides **4.1** (R = *i*Pr) and **4.2** (R = *t*Bu) from X-ray Diffraction Analyses

entry	ϕ^1	ψ^1	ϕ^2	ψ^2	ϕ^3	ψ^3
4.1 in acetone	–52.4	–49.0	–59.3	–46.5	–59.7	–59.6
4.1 in acetone/ $CHCl_3$	–52.8	–48.6	–59.6	–46.0	–59.5	–60.3
4.1 in acetone/EtOAc/ $CHCl_3$	–52.8	–48.8	–59.5	–46.0	–59.6	–60.2
4.2	82.1	–84.1	74.3	–82.3	80.3	–113.2

As stated above, crystallography of single α-turns is very unusual.[4] In most of examples, the backbone torsion angles are significantly distorted in comparison with those observed in regular α-helices. Conversely, in the crystal structure of **4.1**, the average ϕ and ψ torsion angles over the three Adm residues (–57°, –52°) differ only by 6° and 10°, respectively, from the canonical values (–63°, –42°) based on statistical analysis of α-helices in crystalline peptides.[2c] To the best of our knowledge, the structure of **4.1** represents the shortest peptide sequence giving rise to an *isolated* α-turn of *regular* geometry.

In the X-ray diffraction structure of tripeptide **4.2**, the backbone torsion angles (Table 4.1) and distances between hydrogen-bond donor and acceptor atoms demonstrate the presence of two consecutive γ-turns[5b] at the level of the Adm(1) and Adm(2) residues (Fig. 4.1b and *Supporting Information*). Two intramolecular hydrogen bonds are observed, namely between the formamide carbonyl oxygen and the NH group of Adm(2), and between the carbonyl oxygen of Adm(1) and the NH group of Adm(3). The former hydrogen bond is significantly elongated [N···O 3.167(15) Å, H···O 2.572(18) Å, N-H···O angle 129.4(15)°] in comparison to the latter [N···O 2.880 (14) Å, H···O 2.31(2) Å, N-H···O angle 124.5(16)°]. Indeed, the backbone torsion angles of Adm(1) deviate more markedly than those of Adm(2) from the ideal values of a γ-turn structure (ϕ, ψ = 75°,–75°).[5] The torsion angles of Adm(3) fall also in the lower-right quadrant of the Ramachandran map as

those of the two preceding residues, but formation of a third γ-turn is not observed. Conversely, the carbonyl oxygen of Adm(2), which could be the potential acceptor of the γ-turn hydrogen bond, is involved in an intermolecular hydrogen bond with the N1-H group of a symmetry-related molecule (*Supporting Information*), and the *C*-terminal amide NH group is not engaged in any hydrogen bond. To avoid intermolecular steric clashes in the crystal, the ψ torsion angle of Adm(3) is forced to adopt a value (–113.2°) which prevents the *C*-terminal amide NH group from approaching the carbonyl oxygen of Adm(2) at a suitable hydrogen-bond distance.

NMR and FT-IR Absorption Spectroscopy: To study the conformation of peptides **4.1** and **4.2** in solution, NMR and FT-IR absorption spectroscopy were performed. Sequence assignments of the NH proton resonances in the NMR spectra of peptides **4.1** and **4.2** in $CDCl_3$ were achieved by a combination of COSY and HMBC experiments, the latter optimized to identify long-range, through-bond *J* couplings (*Supporting Information*).

Solvent shielded and exposed NH protons were examined by studying influences of changes in environment on the chemical shifts of their signals (Table 4.2). Amide protons involved in hydrogen bonds display typically little variation in their chemical shifts upon changes in solvent composition and temperature.[21] As for peptides **4.1** and **4.2**, switching NMR solvent from $CDCl_3$ to dimethylsufoxide (DMSO, d_6) caused significant (2.37 and 2.58 ppm, respectively) downfield shifts for only the formamide NH proton signal, suggesting that this group is exposed to solvent in contrast to the other NH proton signals which exhibited limited variations in chemical shifts (0.02 to 0.22 ppm). This different behavior of the formamide NH proton is already evident at the very beginning (2% DMSO in $CDCl_3$) of the solvent titration curves (Figure 4.2). Similarly, for both peptides **4.1** and **4.2**, changes in temperature in the two solvents influenced significantly ($\Delta\delta/\Delta K$ = –19.1 to –26 ppb/K) the formamide NH signal relative to those of the other amide protons. The NH chemical shifts of the other amide protons varied less with temperature in the solvent of lower polarity $CDCl_3$ ($\Delta\delta/\Delta K$ = –1.4 to –7.6 ppb) than in DMSO ($\Delta\delta/\Delta K$ = –5.4 to –16.3 ppb/K).

Notably, an X-ray diffraction analysis of crystals of peptide **4.2** grown from DMSO (*bis*-DMSO solvate) highlighted the presence of only one γ-turn in each of the two independent but similar peptide conformers in the crystal matrix (Fig. 4.3 and *Supporting Information*). The surviving intramolecular hydrogen bond occurred between the formamide carbonyl oxygen and the NH group of Adm(2). The sets of ϕ and ψ torsion angles of Adm(1) in the two peptide conformers were –75.4° and 74.8°, and 76.6°, –69.9°. Three intermolecular hydrogen bonds were

observed between each peptide and two co-crystallized DMSO solvent molecules: one between the Adm(1) NH group and the oxygen atom of one molecule of DMSO, and the other two between the Adm(3) and *tert*-butyl amide NH groups together with the oxygen atom of a second DMSO molecule. In each peptide conformer, Adm(2) and Adm(3) were helical but of opposite screw sense: ϕ^2, ψ^2, ϕ^3, ψ^3 = 59.8°. 64.1°, –59.0°, –55.5°; –60.0°, –66.9°, 61.1°, 58.5°.

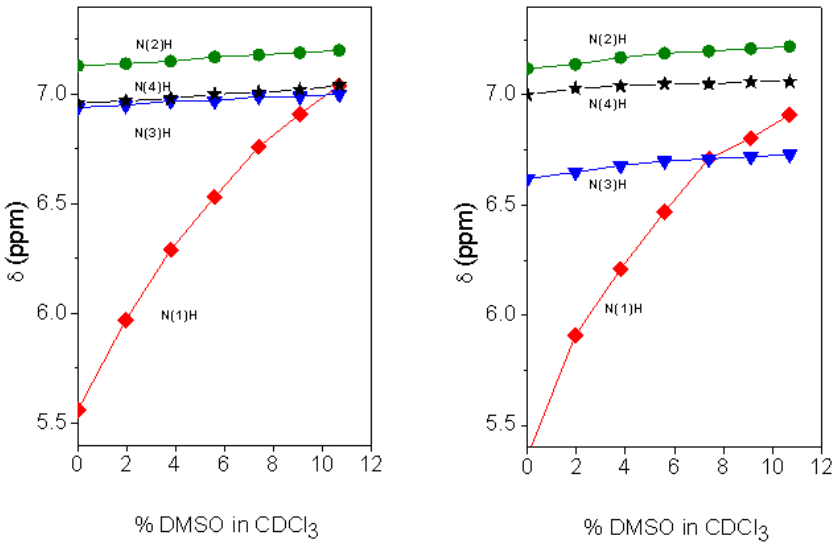

Figure 4.2. Plot of the chemical shifts of the NH signals in the NMR spectra of HCO-(Adm)$_3$-NH*i*Pr **4.1** (left) and HCO-(Adm)$_3$-NH*t*Bu **4.2** (right) as a function of the addition of increasing percentages (*v*/*v*) of DMSO to the $CDCl_3$ solution. Peptide concentration: 1.0 mM.

Table 4.2. Influence of Solvent and Temperature on the Chemical Shifts of the NH Signals of HCO-(Adm)$_3$NHR Peptides **4.1** and **4.2** in $CDCl_3$ and DMSO

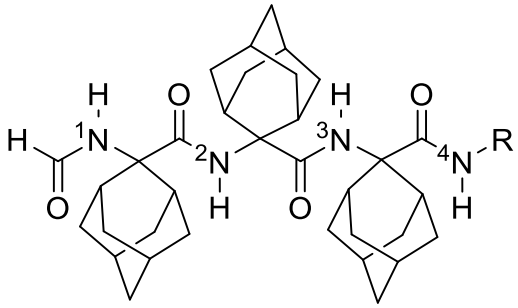

entry	δ $CDCl_3$	δ DMSO	Δδ/Δsol	Δδ/ΔK $CDCl_3$	Δδ/ΔK DMSO
1: R = *i*Pr					
^{1}NH	5.67	8.04	2.37	–21.4	–20.9
^{2}NH	7.17	7.37	0.20	–1.4	–6.0
^{3}NH	7.00	7.02	0.02	–7.1	–16.3
^{4}NH	7.02	7.18	0.16	–6.3	–7.4
2: R = *t*Bu					
^{1}NH	5.46	8.04	2.58	–26.0	–19.1
^{2}NH	7.16	7.38	0.22	–1.4	–5.4
^{3}NH	6.69	6.91	0.22	–2.3	–12.3
^{4}NH	7.07	7.05	0.02	–7.6	–4.9

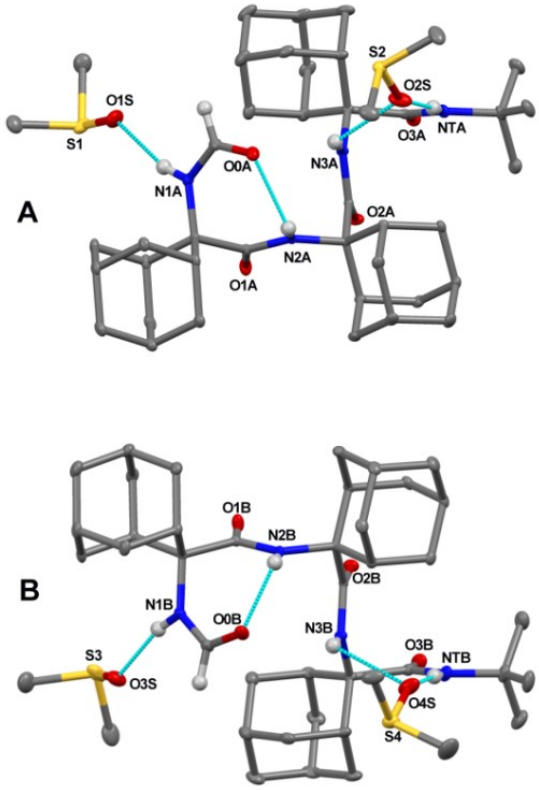

FIGURE 4.3. The two independent molecules (**A** and **B**) in the X-ray diffraction crystal structure of peptide **4.2** *bis*-DMSO solvate. Most of the H-atoms are omitted for clarity. Intramolecular and peptide-solvent hydrogen bonds are indicated by dashed lines.

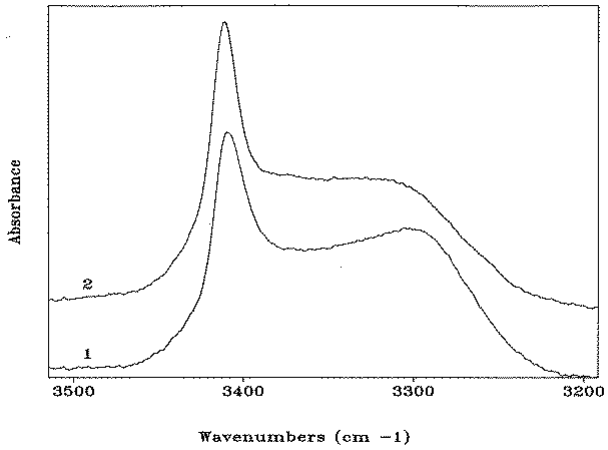

Figure 4.4. FT-IR absorption spectra (N-H stretching region) of HCO-(Adm)$_3$-NH*i*Pr (**4.1**) and HCO-(Adm)$_3$-NH*t*Bu (**4.2**) in $CDCl_3$ solution. Peptide concentration: 1.0 mM.

In the N-H stretching region (3500-3200 cm^{-1}) the FT-IR absorption spectra of peptides **4.1** and **4.2** in $CDCl_3$ solution (Figure 4.4) are very similar, being characterized by a band at 3412-3414 cm^{-1} (free, solvated NH groups) accompanied by a much more intense and broad band with maximum near 3300 cm^{-1} (hydrogen-bonded NH groups). The latter band is significantly skewed toward higher wavenumbers. For both compounds, no significant differences in spectral shape and in the relative intensity of the hydrogen-bonded *versus* free N-H stretching bands were found over the concentration range 10.0 mM – 0.1 mM (*Supporting Information*, Figures S4.3 and S4.4), strongly suggesting that the observed hydrogen bonding is essentially intramolecular. In addition, these curves do not provide any evidence for concentration-dependent conformational transitions. Overall, the spectra of both peptides are compatible with the occurrence of multiple more-or-less strongly hydrogen-bonded γ-turns. Conversely, a prevailing population of a single α-turn or combinations of two β-turns or a β-turn encompassed within an α-turn, all were unlikely, because such conformers would exhibit stretches for three or two free NH groups, respectively. Moreover, the maximum of the band associated with hydrogen-bonded N-H groups in α- or β-turns would be located at wavenumbers significantly higher than 3300 cm^{-1}.[22] Taken together, the observed NMR and FTIR absorption data indicate that both peptides assume predominantly γ-helical structures in solution.

CONCLUSIONS

To summarize, a novel method for assembling sterically congested peptides from $C^{\alpha,\alpha}$-disubstituted glycines bearing bulky side chains using the Ugi multicomponent reaction has been achieved and applied in the synthesis of N^{α}-formyl adamantyl tripeptide amides **4.1** and **4.2**. Conformational analysis has revealed the potential for the Adm residue to favor the unprecedented *single* α-turn with ideal ϕ and ψ torsion angles and an incipient γ-helical structure. Notably, the overwhelming majority of C^{α}-tetrasubstituted α-amino acids prefer 3_{10}-helices, which are generated by consecutive type-III (III′) β-turns, and subsequently α-helix conformers.[2c,6b] Conversely, access to the 3_{10}-helix appears to be unavailable to the Adm residue. In the ϕ and ψ space, the most significant difference between the two conformations is the value of the ψ torsion angle. For the Adm residue, typical ψ values for right- and left-handed 3_{10}-helices (–35° to –25° and 35° to 25°, respectively) have never been observed, likely due to a destabilizing aliphatic C-H···O interaction between the *pro-R* or *pro-S* γ-CH_2 groups with the carbonyl oxygen atom, which

would require an energetically disfavored H···O separation of the order of 2.10 Å.[23] This sterically unfavorable situation is relieved in part by increasing the ψ values to those observed in the α-helical turn of peptide **4.1** (in the range -46.5° to –59.6°) which resulted in H···O separations between 2.23 and 2.33 Å, and to a larger extent in a γ-turn conformation (peptide **4.2**), in which the observed H···O separations are >2.40 Å.

Considering the power of the Ugi multiple component method reported in this work for synthesizing sterically hindered peptides, potential now exists to harness bulky residues for various studies in peptide science. The unique γ-helical folding pattern which was observed both in solution and in the crystal state, as well as the fascinating diamondoid hydrocarbon side chains may similarly lend themselves for novel applications. In this connection, adamantane-functionalized compounds have already found important applications in medicinal chemistry as drugs to treat parkinsonism and related syndromes, and as antiviral agents to combat type-A influenza virus in humans.[24] Moreover, growing interest for these cage structures is currently being observed in other areas, including nanotechnology (as organic microelectronic components and coating agents), polymers, molecular recognition, and supramolecular chemistry.[25]

ASSOCIATED CONTENT

Supporting Information

The Supporting Information is available free of charge on the ACS Publications website at DOI: …...

X-Ray data for peptide 4.**1** (CIF)

X-Ray data for peptide 4.**2** (CIF)

X-Ray data for peptide 4.**2** *bis*-DMSO solvate(CIF)

Experimental procedures, NMR spectra, crystallographic details (PDF)

AUTHOR INFORMATION

Corresponding Author

* william.lubell@umontreal.ca

Author Contributions

The manuscript was written through contributions of all authors. The syntheses were all performed by FMMir.

Funding Sources

Any funds used to support the research of the manuscript should be placed here (per journal style).

Notes

The authors declare no competing financial interests.

ACKNOWLEDGEMENTS

We would like to thank the Natural Sciences and Engineering Research Council of Canada for support. We thank Mr. T. Maris (X-ray), C. Malveau, Dr. P. Aguiar and S. Bilodeau (NMR spectroscopy), Dr. A. Fürtös, K. Gilbert, M.-C. Tang and Louiza Mahrouche (mass spectroscopy) from U. de Montréal Laboratories for their assistance in analyses.

REFERENCES

1. Speltz, T. E.; Danes, J. M.; Stender, J. D.; Frasor, J.; Moore, T. W. A cell-permeable stapled peptide inhibitor of the estrogen receptor/coactivator interaction. *ACS Chem. Biol.* **2018**, *13*, 676-684.

2. (a) Pauling, L.; Corey, R. B. Two hydrogen-bonded spiral configurations of the polypeptide chain. *J. Am. Chem. Soc.* **1950**, *72*, 5349-5350. (b) Donohue, J. hydrogen bonded helical configurations of the polypeptide chain. *Proc. Natl. Acad. Sci. USA* **1953**, *39*, 470-478. (c) Toniolo, C.; Benedetti, E. The polypeptide 3_{10}-helix. *Trends Biochem. Sci*. **1991**, *16*, 350-353.

3. Pavone, V.; Gaeta, G.; Lombardi, A.; Nastri, F.; Maglio, O.; Isernia, C.; Saviano, M. Discovering protein secondary structures: Classification and description of isolated α-turns. *Biopolymers* **1996**, *38*, 705-721.

4. (a) Toniolo, C.; Valle, G.; Crisma, M.; Kaltenbronn, J. S.; Repine, J. T.; Van Binst, G.; Elseviers, M.; Tourwé, D. Psi [CH_2NH] backbone-modified peptides: first unequivocal observation of a C_7 structure in a linear peptide. *Pept. Res*. **1989**, *2*, 332-337. (b) Crisma, M.; Valle, G.; Monaco, V.; Formaggio, F.; Toniolo, C. N^{α}-Benzyloxycarbonyl-α-aminoisobutyrylglycyl-L-isoleucyl-L-

leucine methyl ester monohydrate. *Acta Crystallogr. C* **1994**, *50*, 563-565. (c) Flippen-Anderson, J. L.; Deschamps, J. R.; George, C.; Reddy, P. A.; Lewin, A. H.; Brine, G. A.; Sheldrick, G.; Nikiforovich, G. X-ray structure of Tyr-D-Tic-Phe-Phe-NH_2(D-TIPP-NH_2), a highly potent μ-receptor selective opioid agonist. Comparisons with proposed model structures. *J. Pept. Res.* **1997**, *49*, 384-393. (d) Karle, I. L.; Das, C.; Balaram, P. De novo protein design: crystallographic characterization of a synthetic peptide containing independent helical and hairpin domains. *Proc. Natl. Acad. Sci. USA* **2000**, *97*, 3034-3037. (e) Scalabrino, G. A.; Hogan, N.; O'Boyle, K. M.; Slator, G. R.; Gregg, D. J.; Fitchett, C. M.; Draper, S. M.; Bennett, G. W.; Hinkle, P. M.; Bauer, K.; Williams, C. H.; Tipton, K. F.; Kelly, J. A. Discovery of a dual action first-in-class peptide that mimics and enhances CNS-mediated actions of thyrotropin-releasing hormone. *Neuropharmacol.* **2007***, 52*, 1472-1481. (f) Moretto, A.; De Zotti, M.; Crisma, M.; Formaggio, F.; Toniolo, C. *N*-methylation of N^{α}-acetylated, fully C^{α}-ethylated, linear peptides. *Int. J. Pept. Res. Ther.* **2008**, *14*, 307-314. (g) Chatterjee, B.; Saha, I.; Raghothama, S.; Aravinda, S.; Rai, R.; Shamala, N.; Balaram, P. Designed peptides with homochiral and heterochiral diproline templates as conformational constraints. *Chem. Eur. J.* **2008**, *14*, 6192-6204.

5. (a) Némethy, G.; Printz, M. P. The γ-turn, a possible folded conformation of the polypeptide chain. Comparison with the β-turn. *Macromolecules* **1972**, *5*, 755-758. (b) For a recent review article, see: Crisma, M.; De Zotti, M.; Moretto, A.; Peggion, C.; Drouillat, B.; Wright, K.; Couty, F.; Toniolo, C.; Formaggio, F. Single and multiple peptide γ-turns: literature survey and recent progress. *New J. Chem.* **2015**, *39*, 3208-3216.

6. (a) Karle, I. L.; Balaram, P. Structural characteristics of α-helical peptide molecules containing Aib residues. *Biochemistry* **1990**, *29*, 6747-6756. (b) Toniolo, C.; Crisma, M.; Formaggio, F.; Peggion, C. Control of peptide conformation by the Thorpe-Ingold effect (C^{α}-tetrasubstitution). *Biopolymers* **2001,** *60*, 396-419.

7. Tanaka, M. Design and synthesis of chiral α,α-disubstituted amino acids and conformational study of their oligopeptides. *Chem. Pharm. Bull. (Tokyo)* **2007**, *55*, 349-358.

8. (a) Shamala, N.; Nagaraj, R.; Balaram, P. The 3_{10} helical conformation of a pentapeptide containing α-aminoisobutyric acid (Aib): X-ray crystal structure of Tos–$(Aib)_5$–OMe. *J. Chem. Soc., Chem. Commun.* **1978**, 996-997. (b) Benedetti, E.; Bavoso, A.; Di Blasio, B.; Pavone, V.;

Pedone, C.; Crisma, M.; Bonora, G. M.; Toniolo, C. Solid-state and solution conformation of homooligo (α-aminoisobutyric acids) from tripeptide to pentapeptide: evidence for a 3_{10} helix. *J. Am. Chem. Soc.* **1982**, *104*, 2437-2444. (c) Gessmann, R.; Brückner, H.; Petratos, K. The crystal structure of Z-$(Aib)_{10}$-OH at 0.65 Å resolution: three complete turns of 3_{10}-helix. *J. Pept. Sci.* **2016**, *22*, 76-81.

9. Toniolo, C.; Crisma, M.; Formaggio, F.; Benedetti, E.; Santini, A.; Iacovino, R.; Saviano, M.; Di Blasio, B.; Pedone, C.; Kamphuis, J. Preferred conformation of peptides rich in alicyclic $C^{\alpha,\alpha}$-disubstituted glycines. *Biopolymers* **1996**, *40*, 519-522.

10. (a) Tanaka, M.; Demizu, Y.; Doi, M.; Kurihara, M.; Suemune, H. Chiral centers in the side chains of α-amino acids control the helical screw sense of peptides. *Angew. Chem. Int. Edit*. **2004**, *43*, 5360-5363. (b) Crisma, M.; Saviano, M.; Moretto, A.; Broxterman, Q. B.; Kaptein, B.; Toniolo, C. Peptide α/3_{10}-helix dimorphism in the crystal state. *J. Am. Chem. Soc.* **2007**, *129*, 15471-15473. (c) Demizu, Y.; Doi, M.; Kurihara, M.; Maruyama, T.; Suemune, H.; Tanaka, M. One-handed helical screw direction of homopeptide foldamer exclusively induced by cyclic α-amino acid side-chain chiral centers. *Chem. Eur. J.* **2012**, *18*, 2430-2439. (d) Hirata, T.; Ueda, A.; Oba, L.; Doi, M.; Demizu, Y.; Kurihara, M.; Nagano, M.; Suemune, H.; Tanaka, M. Amino equatorial effect of a six-membered ring amino acid on its peptide 3_{10}- and α-helices. *Tetrahedron* **2015**, *71*, 2409-2420.

11. Solà, J.; Helliwell, M.; Clayden, J. Interruption of a 3_{10}-helix by a single Gly residue in a poly-Aib motif: A crystallographic study. *Biopolymers* **2011**, *95*, 62-69.

12. Mazzier, D.; Grassi, L.; Moretto, A.; Alemán, C.; Formaggio, F.; Toniolo, C.; Crisma, M. En route towards the peptide γ-helix: X-ray diffraction analyses and conformational energy calculations of Adm-rich short peptides. *J. Pept. Sci.* **2017**, *23*, 346-362.

13. Jimenez, A. I.; Ballano, G.; Cativiela, C. First observation of two consecutive γ-turns in a crystalline linear dipeptide. *Angew. Chem. Int. Edit.* **2005**, *44*, 396-399.

14. (a) Benedetti, E.; Barone, V.; Bavoso, A.; Di Blasio, B.; Lelj, F.; Pavone, V.; Pedone, C.; Bonora, G. M.; Toniolo, C.; Leplawy, M. T; Kaczmarek, K.; Redlinski, A. Structural versatility of peptides from $C^{\alpha,\alpha}$-dialkylated glycines. I. A conformational energy computation and X-ray

diffraction study of homo-peptides from $C^{\alpha,\alpha}$-diethylglycine. *Biopolymers* **1988**, *27*, 357-372. (b) Crisma, M.; Valle, G.; Bonora, G. M.; Toniolo, C.; Lelj, F.; Barone, V.; Fraternali, F.; Hardy, P.; Maia, H. Preferred conformation of peptides from $C^{\alpha,\alpha}$-symmetrically disubstituted glycines: Aromatic residues. *Biopolymers* **1991**, *31*, 637-641. (c) Peggion, C.; Moretto, A.; Formaggio, F.; Crisma, M.; Toniolo, C. Multiple, consecutive, fully-extended 2.0_5-helix peptide conformation. *Biopolymers* **2013**, *100*, 621-636.

15. Formaggio, F.; Broxterman, Q. B.; Toniolo, C. in *Houben-Weyl, Methods of Organic Chemistry*, Vol. E22c, *Synthesis of Peptides and Peptidomimetics* (Goodman, M.; Felix, A.; Moroder, L.; Toniolo, C., Eds.) Thieme: Stuttgart, Germany, **2003**, pp. 292-310.

16. (a) Nagasawa, H. T.; Elberling, J. A.; Shirota, F. N. Potential latentiation forms of biologically active compounds based on action of leucine aminopeptidase. Dipeptide derivatives of the tricycloaliphatic α-amino acid, adamantanine. *J. Med. Chem.* **1975**, *18*, 826-830. (b) Kuroda, Y.; Ueda, H.; Nozawa, H.; Ogoshi, H. Adamantyl amino acid as γ-turn inducer for peptide. *Tetrahedron Lett.* **1997**, *38*, 7901-7904.

17. Meldal, M.; Juliano, M. A.; Jansson, A. M. Azido acids in a novel method of solid-phase peptide synthesis. *Tetrahedron Lett.* **1997**, *38*, 2531-2534.

18. (a) Samsoniya, S.; Zurabishvili, D.; Bukia, T.; Buzaladze, G.; Lomidze, M.; Elizbarashvili, E.; Kazmaier, U. Synthesis of some derivatives of *N*-(1-adamantyl)carbonyl-*N'*-benzyliden-*o*-phenylendiamine. *Bull. Georgian Natl. Acad. Sci.* **2014**, *8*, 85-93. (b) Pirali, T.; Tron, G. C.; Masson, G.; Zhu, J. Ammonium chloride promoted three-component synthesis of 5-iminooxazoline and its subsequent transformation to macrocyclodepsipeptide. *Org. Lett.* **2007**, *9*, 5275-5278.

19. (a) Venkatachalam, C. M. Stereochemical criteria for polypeptides and proteins. V. Conformation of a system of three linked peptide units. *Biopolymers* **1968**, *6*, 1425-1436. (b) Geddes, J. A.; Parker, K. B.; Atkins, E. D. T.; Brighton, E. "Cross-β" conformation in proteins. *J. Mol. Biol.* **1968**, *32*, 343-358. (c) Rose, G. D.; Gierasch, L. M.; Smith, J. A. Turns in peptides and protein. *Adv. Protein Chem.* **1985**, *37*, 1-109.

20. (a) Taylor, R.; Kennard, O.; Versichel, W. The geometry of the N–H···O=C hydrogen bond. 3. Hydrogen-bond distances and angles. *Acta Crystallogr. B* **1984**, *40*, 280-288. (b) Görbitz, C. H. Hydrogen-bond distances and angles in the structures of amino acids and peptides. *Acta Crystallogr. B* **1989**, *45*, 390-395. (c) Torshin, I. Y.; Weber, I. T.; Harrosin, R. W. Geometric criteria of hydrogen bonds in proteins and identification of 'bifurcated' hydrogen bonds. *Protein Eng.* **2002**, *15*, 359-363.

21. (a) Pysh, E. S.; Toniolo, C. Conformational analysis of protected norvaline oligopeptides by high resolution proton magnetic resonance. *J. Am. Chem. Soc.* **1977**, *99*, 6211-6219. (b) Kessler, H. Conformation and biological activity of cyclic peptides. *Angew. Chem. Int. Edit.* **1982**, *21*, 512-523. (c) Dietrich, E.; Lubell, W. D. Efficient synthesis of enantiopure pyrrolizidinone amino acid. *J. Org Chem*. **2003**, *68*, 6988-6996.

22. (a) Toniolo, C.; Bonora, G. M.; Barone, V.; Bavoso, A.; Benedetti, E.; Di Blasio, B.; Grimaldi, P.; Lelj, F.; Pavone, V.; Pedone C. Conformation of pleionomers of α-aminoisobutyric acid. *Macromolecules* **1985**, *18*, 895-902. (b) Kennedy, D. F.; Crisma, M.; Toniolo, C.; Chapman, D. Studies of peptides forming 3_{10}- and α-helices and β-bend ribbon structures in organic solution and in model biomembranes by Fourier transform infrared spectroscopy. *Biochemistry* **1991**, *30*, 6541-6548.

23. Desiraju, G. R.; Steiner, T. *The weak hydrogen bond in structural chemistry and biology*; Oxford Univ. Press: Oxford, 1999; pp 108-113.

24. (a) Wanka, L.; Iqbal, K.; Schreiner, P. R. The lipophilic bullet hits the target: medicinal chemistry of adamantane derivatives. *Chem. Rev.* **2013**, *113*, 3516-3604. (b) Thomaston, J. L.; Polizzi, N. F.; Konstantinidi, A.; Wang, J.; Kologouris, A.; DeGrado, W. F. Inhibitors of the M2 proton channel engage and disrupt transmembrane networks of hydrogen-bonded waters. *J. Am. Chem. Soc.* **2018**, *140*, 15219-15226.

25. (a) Zaworodko, M. L. Crystal engineering of diamondoid networks. *Chem. Soc. Rev.* **1994**, *23*, 283-288. (b) Marchand, A.P. Diamondoid hydrocarbons. Delving into Nature's bounty. *Science* **2003**, *299*, 52-53. (c) Dahl, J. E.; Liu, S. G.; Carlson, R. M. K. Isolation and structure of higher diamondoids, nanometer-sized diamond molecules. *Science* **2003**, *299*, 96-99. (d) Gunawan, M.A.; Hierso, J. C.; Poinsot, D.; Fokin, A. A.; Fokina, N. A.; Tkachenko, B. A.; Schreiner, P. R.

Diamondoids: functionalization and subsequent applications of perfectly defined molecular cage hydrocarbons. *New J. Chem.* **2014**, *38*, 28-41. (e) Kawahata, M.; Matsui, K.; Hyodo, T.; Tominaga, M.; Yamaguchi, K. Inclusion and selectivity of amides by *p*-terphenyl derivative bearing adamantanecarboxylic acid. *Tetrahedron* **2018**, *74*, 7089-7094.

Conclusion and Perspectives

The applications of electronic and steric interactions have been investigated in peptide analogs to control folding and enhance biomedical utility. Electronic interactions in peptide mimics were examined in FP modulators to develop improved tocolytic agents for delaying labor and prolonging pregnancy. Previously, the indolizidin-2-one mimic PDC113.824 inhibited uterine contractions and delayed labor in mouse models. The activity of azapeptide counterparts of PDC113.824 were also shown to similarly diminish myometrial contractions contingent on their aza-residue side chain. By diversification of aza-phenylalanine and aza-propargylglycine (azaPra) residues, the effects of hydrophobicity, hydrogen bonding, and positively and negatively charged substituents on the aza-amino acid side chain were explored on myometrial contractions. On the other hand, the proline residues of the lead azapeptides were modified to examine influences of ring pucker and C^4 substituents on activity. Only a handful of the thirty-six azapeptide ligands that were synthesized exhibited significant potency in the myometrial contraction assay and demonstrated the sensitive relationship between modulator structure and activity. Relatively small aromatic and hydrophobic side chains on the aza-residue appeared to be tolerated. Moreover, aza-Pra-4*R*-Hyp *R*-**2.11c** exhibited similar activity as aza-Gly-Pro **2.2a** and represents a possible lead for further development.

A solution phase approach was used for the synthesis of aza-Phe-Pro and azaPra-Pro analogs featuring *N*-alkylation of an aza-Gly residue with different alkyl bromides. The azaPra-Pro peptide was then employed in diversity-oriented syntheses by a "libraries from libraries" approach that permitted synthesis of six triazole analogs using CuAAC chemistry. Employing the azaPra-Pro peptide in A^3-reactions with different amines afforded constrained aza-Lys analogs to study the effect of a positive charge and potential salt bridge on the activity. Reduction of the triple to a single bond also afforded more flexible side chains. In addition, an aza-aspartate peptide was synthesized by oxidation of aza-Pra to study the effect of a negative charge on activity. Among the newly synthesized aza-residue analogs that were tested, the (piperidinyl)but-2-ynylglycine derivative exhibited the best ability to reduce the intensity of myometrium contractions in the presence of PGF2α, but was about half as potent as the previously synthesized azaGly counterpart.

Substitution at the 4-position of the proline residue was also examined to study effects on activity of azapeptides with azaGly, azaPhe and azaPra residues. A solid-phase approach was developed featuring modification of hydroxyproline (Hyp) peptides and the use of aza-4-

ethoxyphenylalanine as an azaGly precursor. After completion of sequences on resin, the hydroxyl group of the Hyp residue underwent inversions of configuration using Mitsunobu, fluorination and amination chemistry to prepare eighteen analogs with 4*R*- and 4*S*-Hyp, Flp and Amp residues. Four of these analogs showed promising activity: phenylacetyl-azaGly-(4*R*)-Flp-PyAla-*β*-hPhe, phenylacetyl-azaGly-(4*S*)-Amp-PyAla-*β*-hPhe, phenylacetyl-azaPhe-(4*R*)-Amp-PyAla-*β*-hPhe and phenylacetyl-azaPra-(4*R*)-Hyp-PyAla-*β*-hPhe. Notably, phenylacetyl-azaPra-(4*R*)-Hyp-PyAla-*β*-hPhe exhibited similar activity compared to the azaGly-Pro lead peptide in the myometrial contraction assay.

Although few of the synthesized analogs exhibited promising activity for development as tocolytic agents, the diversity-oriented methods should have general utility for studying a variety of peptides possessing β-turn conformation, which may be induced using aza-amino acyl proline at the central residues. X-ray diffraction analysis of the active analogs may also be informative for studying their conformation in the solid state; however, limited success has been achieved in crystalizing azapeptides. The methods advanced in this study have proven to be useful for synthesizing a photo-reactive analog and may yield radio-labeled modulators to facilitate tagging of the receptor target in living cells to identify the modulator binding site. For example, probe **5.1** (Figure 5.1) has been synthesized and given to the laboratory of Professor S. Laporte (McGill University) to examine its reactivity on cells containing the FP receptor. Probe **5.1** (FAT6) was shown to potentiate mitogen-activated protein kinase (ERK1/2) phosphorylation in the presence of prostaglandin F2α with similar efficacy at the same concentrations (2μM) as observed for azapeptides **2.2a** (CAR10.0, azaGly-Pro) and **2.2c** (CAR10.1, AzaPra-Pro) in serum starved HA-FP cells.[1]

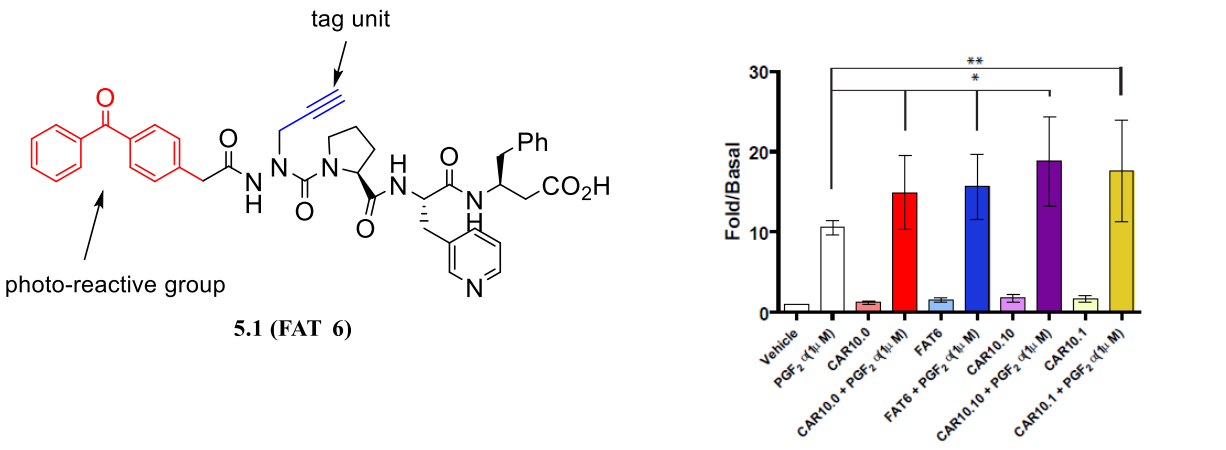

Figure 5.1. Photo-affinity labeled probe **5.1** designed for tagging the FP receptor (left), PGF2α-induced cellular contraction and ERK1/2 activation in the presence of probe **5.1** (right).

Probe **5.1** has two functional groups. The benzophenone moiety is designed as a photo-reactive group, that may covalently react with the protein receptor at the binding site region.[2] Photo-irradiation may activate the benzophenone group. The radical photo-labeling process for Tthe benzophenone moiety entails three steps: photochemical triplet state excitation, H-absorption and radical recombination to give the covalent crosslink.[3-4] Promotion of one electron from the non-bonding (n) to the antibonding (π*) orbital of the carbonyl group on irradiation at ~350 nm creates an electrophilic di-radical triplet state, which may abstract a proton radical from a nearby alkyl group. Final recombination of the generated ketyl and alkyl radicals leads to a new C−C bond.[4]

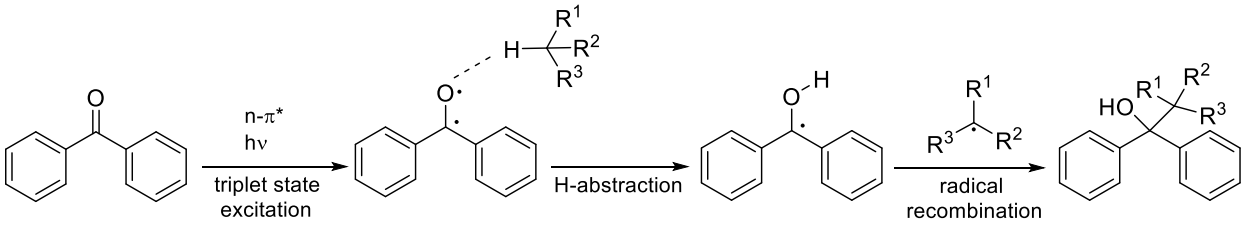

Figure 5.2. Formation of a covalent crosslink from photo-excitation of benzophenone.[5]

The propargyl group may be subsequently used to make derivatives of ligand tagged-receptor complexes using groups such as biotin to facilitate isolation for mass spectrometric characterization. Azide-biotin and azide-fluorescent probes are available for CuAAC chemistry on the azaPra residue. After covalent cross linking between the receptor protein and the benzophenone moiety at 350 nm light irradiation, cell lysis would be performed along with protein digestion to produce receptor peptide fragments.[6] The appropriate tag (such as an azido-biotin) may be added to the protein-derived fragments using CuAAC chemistry. Subsequently, the biotinylated probe-labeled peptide may be separated from unlabeled peptides using streptavidin-based affinity chromatography.[7] The enriched peptide would be analyzed using mass spectroscopy to identify the binding site of the protein receptor.[7]

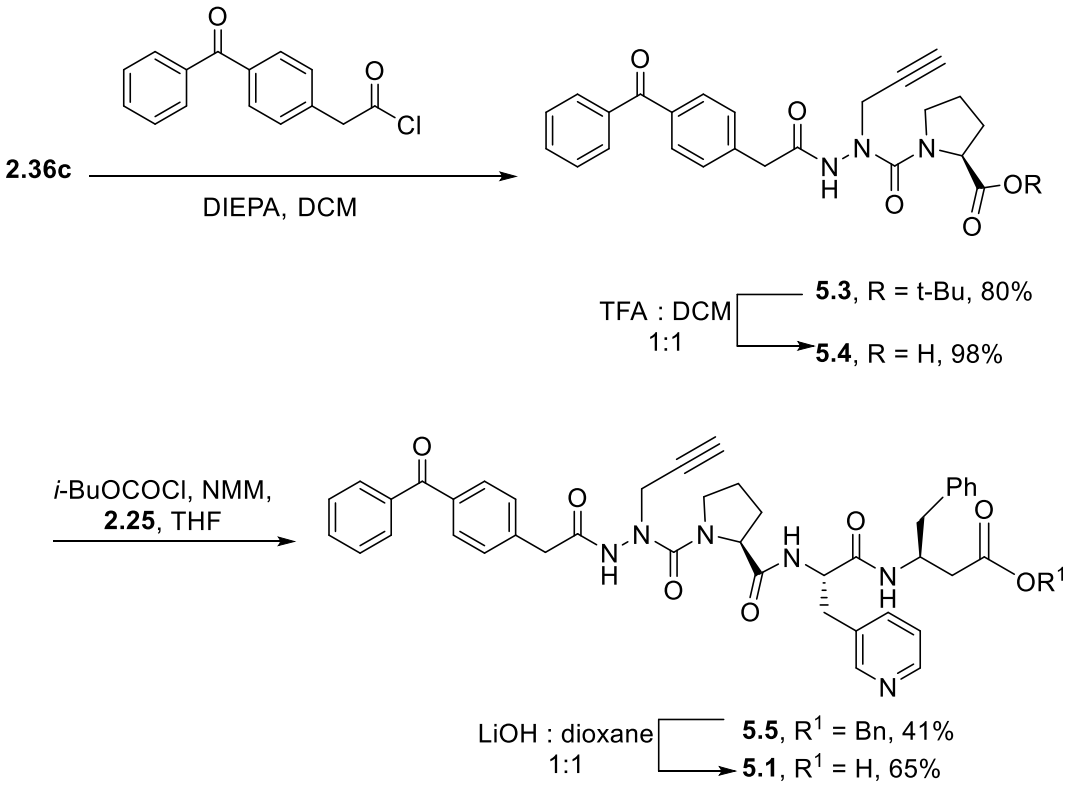

Scheme 5.1. Synthesis of azapeptide **5.1**

Employing the methods described in Chapter 2, probe **5.1** was synthesized (Scheme 5.1). Azapeptide **5.4** was prepared from azaPra analog **2.36** by acylation of the semicarbazide with *p*-(benzoyl)phenyl acetyl chloride. The *tert*-butyl ester was removed in a TFA/DCM solution. Azapeptide **5.4** was coupled to dipeptide **2.25** using *iso*-butyl chloroformate and *N*-

methylmorpholine to furnish azapeptide benzyl ester **5.5**. *p*-(Benzoyl)phenylacetyl-aza-propargylglycinyl-(2*S*)-prolyl-(2*S*)-3-pyridylalaninyl-(3*S*)-*β*-homophenylalanine **5.1** was prepared by benzyl ester saponification with LiOH in dioxane and isolated by RP-HPLC.

In the second part of this thesis, a series of 2-aminoadamantane-2-carboxylic acid (Adm) peptides were synthesized to study the influence of steric interactions on peptide backbone conformation. A solution-phase Ugi multiple-component reaction was conceived to introduce Adm into different N^{α}-formyl homo-di- and tripeptide alkyl amides. The conformers of the Adm peptides were studied by X-ray diffraction to distinguish the influences of the *C*-terminal amide. Four different residues were introduced at the *C*-terminal of N^{α}-formyl mono, di- and tri-Adm peptides: Aib-OMe, Gly-OEt, NH*i*Pr and NH*t*Bu. The *C*-terminal of the Adm peptides induced different turn conformations. For example, *C*-terminal *iso*-propyl and *tert*-butyl groups on the *N*-formyl Adm tripeptides gave respectively a single α-turn and an incipient γ-helix with two fully formed hydrogen-bonded γ-turns as observed in the solid state. Other *C*-terminal residues such as Aib-OMe, induced a β-turn geometry in the Adm dipeptide. Insight has thus been gained for controlling Adm peptide conformation using different *C*-terminal residues.

Towards the goal of preparing a fully developed γ-helix with three consecutive γ-turns, the tripeptide OHC-$(Adm)_3$-NH*t*-Bu exhibited an incipient γ-turn with two consecutive γ-turns. Extension of the tripeptide to an Adm tetrapeptide was thus pursued and has culminated in the synthesis of OHC-$(Adm)_4$-NH*t*-Bu (**5.2**, Scheme 5.2). *tert*-Butyl isocyanide **5.6** was prepared on treatment of OHC-$(Adm)_3$-NH*t*-Bu (**4.1**) with $POCl_3$ and triethylamine in dichloromethane between –5 to –10 °C for 1-2 hours. Tetrapeptide **5.2** was constructed from **5.6** using the Ugi strategy described in Chapter 3, by reacting adamantan-2-one with *tert*-butyl isocyanide **5.6** in MeOH with ammonium formate dissolved in the minimum amount of water. After heating at 70 °C for 10 days, evaporation of the volatiles and chromatography on silica gel afforded the formamide **5.2**. At the time of this writing, tetrapeptide **5.2** has eluded crystallization.

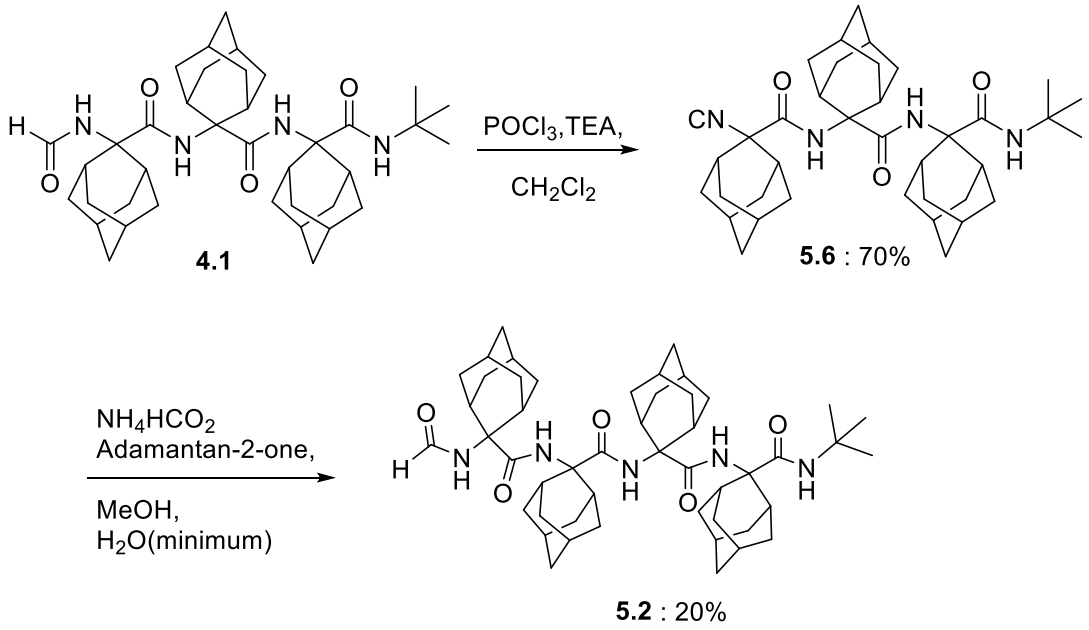

Scheme 5.2. Synthesis of HCO-(Adm)$_4$-NH*t*-Bu

Electronic and steric constraints have thus been explored to study biomedical chemistry and peptide science. Employing electronic constraints in the form of azapeptides, knowledge has been gained into the structural requirements for modulator activity of allosteric FP ligands. Insight is at hand for designing future modulators with ideally improved therapeutic utility as treatments of preterm labor. Moreover, the methods described herein offer effective access to azapeptide libraries.

Towards the study of sterically hindered amino acid residues in peptides, the Ugi multiple component method utilized in this thesis offers an effective synthetic strategy, as demonstrated by the preparation of Adm oligomers. Adamantane derivatives have found important applications in medicinal chemistry as drugs to treat Parkinsonism and related syndromes, and as antiviral agents to combat type-A influenza virus in humans. Insight gained in the synthesis and study of Adm peptides using X-ray crystallography offers potential for the design of rigid peptide turn and helical conformers. Future study of sterically hindered amino acid oligomers has thus been enabled by the methods described herein and may offer new opportunity for applications in biomedical and peptide science.

Experimental

p-(Benzoyl)phenylacetyl-aza-propargylglycinyl-proline *tert*-butyl ester (5.3)

A solution of *p*-(benzoyl)phenyl acetic acid (450 mg, 1.89 mmol, prepared according to reference 7)[8] in DCM (10 mL) was treated with thionyl chloride (150 µL, 2.09 mmol) at 0 ℃, heated to reflux and stirred for 2h. The volatiles were evaporated, and the residue was dissolved in a minimum amount of DCM and added dropwise to a solution of amine **2.36c** (280 mg, 1.1 mmol) in DCM, followed by DIEA (380 µL, 2.2 mmol). The reaction mixture was purged with argon and stirred for 20 h. The volatiles were evaporated, and the residue was purified by chromatography on a silica gel column to afford ester **5.3** (430 mg, 80%) as white foam: R_f 0.27 (60% EtOAc in hexanes); 98% purity at λ = 214 nm by analytical LC-MS on a 5 µM, 50 mm x 4.6 mm C18 Phenomenex Gemini column™ using a gradient of 60% to 90% MeOH containing 0.1% FA in water (0.1% FA) over 14 min at a flow rate of 0.4 mL/min, RT, 7.8 min.

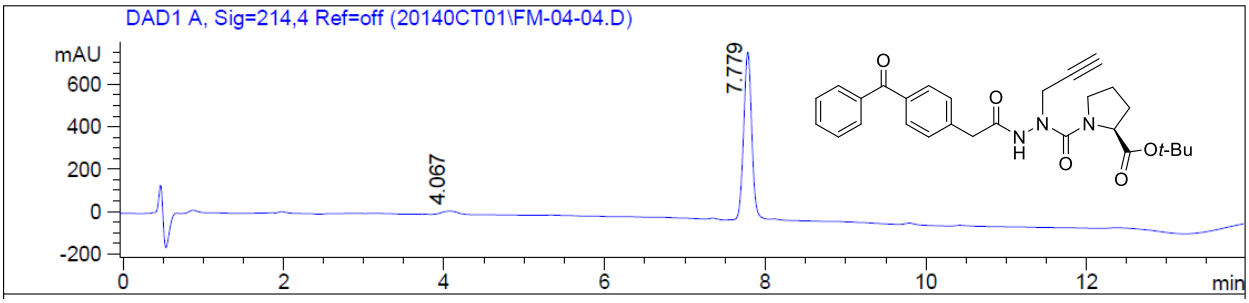

Figure 5.3. LCMS chromatogram of **5.3** [60-90% MeOH (0.1% FA)/water (0.1% FA), 14 min]; RT = 7.8 on C18 Phenomenex Gemini column™ (5 µm, 4.6 mm X 50 mm), purity >98%

p-(Benzoyl)phenylacetyl-aza-propargylglycinyl-(2*S*)-prolyl-(2*S*)-3-pyridylalaninyl-(3*S*)-*β*-homophenylalanine benzyl ester (5.5)

tert-Butyl ester **5.3** (200 mg, 0.41 mmol) was dissolved in a solution of 1:1 TFA:DCM (4 mL), and stirred for 2h at room temperature, when complete consumption of starting material was confirmed by TLC and mass spectrometry. The volatiles were evaporated. The residue was dissolved and co-evaporated three times from DCM. The residue was dissolved in EtOAc and extracted with saturated $NaHCO_3$. The aqueous layers were combined, acidified with 1N HCl to pH = 3 and extracted with EtOAc. The organic layers were combined, dried over Na_2SO_4 and evaporated to acid **5.4** (174 mg, 0.4 mmol, 98%), which was dissolved in THF (10 mL), cooled to –15°C, treated with isobutyl chloroformate (56 µL, 0.44 mmol) and *N*-methylmorpholine (66 µL,

0.6 mmol), stirred for 5-10 min, and treated with a solution of dipeptide benzyl ester **2.25** (167 mg, 0.4 mmol) in EtOAc (2 mL), and stirred at –15°C for 2h. The volatiles were evaporated, and the residue was purified by chromatography on silica gel using 10% MeOH in DCM as eluent to afford benzyl ester **5.5** (150 mg, 41%) as pale yellow foam: R_f 0.35; ^{1}H NMR (700 MHz, $CDCl_3$) δ 1.32 (m, 1H), 1.64 (m, 1H), 1.72 (m, 1H), 2.15 (m, 1H), 2.28 (t, *J* = 2.3 Hz, 1H), 2.58-2.65 (m, 2H), 2.81-2.85 (m, 2H), 2.91 (dd, *J* = 6.4, 13.6 Hz, 1H), 3.03-3.07 (m, 1H), 3.26 (dd, *J* = 3.3, 14.5 Hz, 1H), 3.26 (t, *J* = 8.8 Hz, 1H), 3.79 (d, *J* = 15.0 Hz, 1H), 3.82 (d, *J* = 15.0 Hz, 1H), 3.88 (m, 1H), 4.29 (t, *J* = 8.4 Hz, 1H), 4.36 (d, *J* = 16.5 Hz, 1H), 4.53-4.57 (m, 2H), 5.06 (d, *J* = 12.3 Hz, 1H), 5.10 (d, *J* = 12.3 Hz, 1H), 7.15-7.18 (m, 6H), 7.23 (br, 1H), 7.27-7.30 (m, 1H), 7.31-7.35 (m, 4H), 7.44-7.48 (m, 6H), 7.57-7.59 (m, 1H), 7.71 (d, *J* = 7.1 Hz, 2H), 7.76 (d, *J* = 8.2 Hz, 2H), 8.34 (s, 1H), 8.39 (d, *J* = 4.2 Hz, 1H); ^{13}C NMR (700 MHz, $CDCl_3$) δ 25.7, 29.5, 34.2, 38.4, 40.3, 40.4, 40.8, 48.1, 50.1, 54.4, 62.9, 66.6, 74.2, 78.0, 123.8, 126.6, 128.3, 128.4, 128.5 (2C), 128.6, 129.4, 129.8, 130.0, 130.8, 132.8, 134.1, 135.9, 136.6, 137.0, 137.4, 137.7, 138.4, 147.8, 150.3, 159.9, 169.9, 170.5, 171.0, 171.7, 196.2.

p-(Benzoyl)phenylacetyl-aza-propargylglycinyl-(2*S*)-prolyl-(2*S*)-3-pyridylalaninyl-(3*S*)-*β*-homophenylalanine (5.1)

Benzyl ester **5.5** (50 mg, 60 μmol) was dissolved in 1 mL of dioxane, treated with 1 N LiOH (1 mL) and stirred for 1 h. The volatiles were evaporated under reduced pressure. The remaining aqueous phase was acidified with 1N HCl to pH 3 and extracted twice with ethyl acetate (2×10 mL). The organic layers were combined, dried with Na_2SO_4, filtered and concentrated under vacuum. The residue was purified by preparative HPLC on a C18 reverse phase column using a gradient of 50% to 80% MeOH (0.1% FA) in water (0.1% FA) at a flow rate of 10 mL/min over 40 min. The collected fraction were freeze-dried to afford acid **5.1** (29 mg, 65 %) as white powder: $[\alpha]^{20}_D$ = –158 (*c* 0.26, CH_3OH); ^{1}H NMR (700 MHz, CH_3OD) δ 1.21 (m, 1H), 1.79-1.85 (m, 2H), 2.15-2.19 (m, 1H), 2.55 (d, *J* = 7.1 Hz, 2H), 2.72-2.77 (m, 2H), 2.79 (t, *J* = 2.5 Hz, 1H), 2.96 (dd, *J* = 5.3, 13.7 Hz, 1H), 3.05 (dd, *J* = 4.1, 14.3 Hz, 1H), 3.23-3.36 (m, 1H), 3.53 (t, *J* = 8.8 Hz, 1H), 3.84 (d, *J* = 14.7 Hz, 1H), 3.89 (d, *J* = 14.7 Hz, 1H), 3.93 (m, 1H), 4.24 (dd, *J* = 7.0, 10.9 Hz, 1H), 4.34 (dd, *J* = 4.0, 11.3 Hz, 1H), 4.42-4.47 (m, 2H), 7.11-7.16 (m, 3H), 7.20-7.22 (m, 2H), 7.29 (dd, *J* = 5.0, 7.9 Hz, 1H), 7.46 (t, *J* = 7.8 Hz, 2H), 7.50 (d, *J* = 7.5 Hz, 1H), 7.58 (d, *J* = 8.2 Hz, 2H), 7.61-7.62 9m, 3H), 7.73 (d, *J* = 8.2 Hz, 2H), 8.16 (s, 1H), 8.34 (d, *J* = 4.7 Hz, 1H); ^{13}C NMR

(700 MHz, $CDCl_3$) δ 26.5, 31.0, 35.0, 39.5, 40.9, 41.2, 41.3, 49.5, 51.3, 55.9, 64.2, 75.3, 78.8, 125.3, 127.5, 129.3, 129.5, 130.8 (3C), 131.5, 133.8, 135.9, 137.8, 138.6, 138.7, 139.3, 140.8, 148.3, 150.5, 161.3, 171.8, 172.1, 174.4, 174.5, 197.8; HRMS Calculated *m/z* for $C_{42}H_{43}N_6O_7$ $[M+H]^+$ 743.3188, found 743.3210.

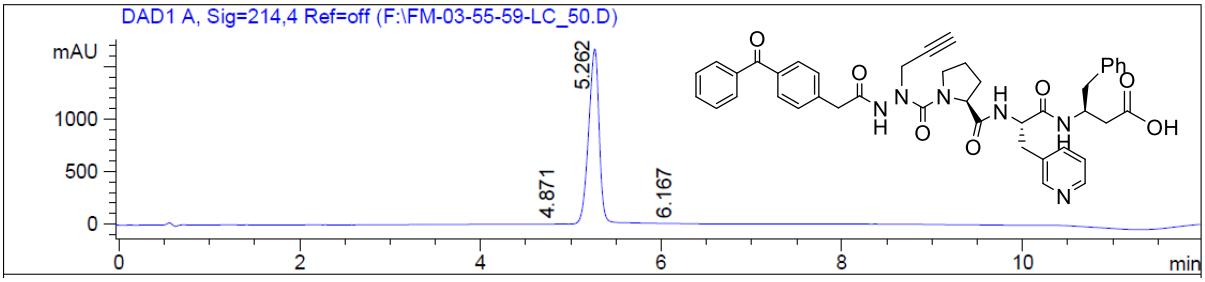

Figure 5.4.A. LCMS chromatogram of azapeptide **5.1** [50-80% MeOH (0.1% FA)/water (0.1% FA), 12 min]; RT = 5.3 on a Sunfire C18 analytical column (100Å, 3.5 µm, 4.6 mm X 100 mm), purity >99%

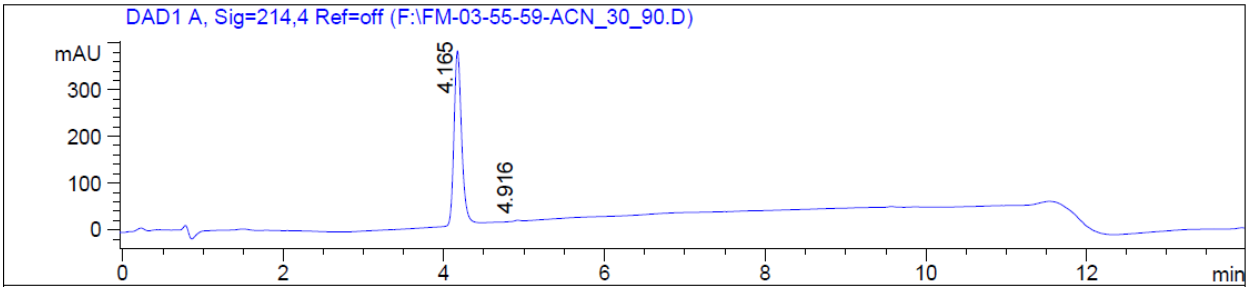

Figure 5.4.B. LCMS chromatogram of azapeptide **5.1** [30-90% MeCN (0.1% FA)/water (0.1% FA), 14 min]; RT = 4.2 on a Sunfire C18 analytical column (100Å, 3.5 µm, 4.6 mm X 100 mm), purity >99%

'Isocyano'-Adm-Adm-Adm-NH*t*-Bu (5.6)

'Isocyano'-$(Adm)_3$-NH*t*-Bu (**5.6**) was synthesized from formamide **4.2** (500 mg, 0.80 mmol) using the procedure described for the synthesis of isocyanide **3.1** that is described in Chapter 3. The residue was purified by column chromatography using 20% EtOAc in hexanes as eluent. Evaporation of the collected fractions gave isocyanide **5.6** (345 g, 70%) as white powder: R_f 0.41 (8:2 hexanes:EtOAc); ^{1}H NMR (500 MHz, $CDCl_3$) δ 1.31 (s, 9H), 1.60-1.63 (m, 3H), 1.67 (m, 2H), 1.70-1.81 (m, 18H), 1.86-2.00 (m, 11H), 2.22-2.25 (m, 2H), 2.30 (m, 2H), 2.66 (m, 2H), 2.72 (m, 2H), 5.81 (s, 1H), 6.78 (s, 1H), 7.00 (s, 1H); ^{13}C NMR (500 MHz, $CDCl_3$): δ 26.2 (2C), 26.3 (1C), 26.4 (1C), 26.5 (1C), 26.9 (1C), 28.8 (3C), 32.5 (2C), 32.6 (2C), 32.7 (2C), 32.8 (2C), 33.2 (2C), 33.3 (2C), 34.1 (2C), 34.3 (2C), 35.2 (2C), 37.2 (1C), 37.3 (1C), 37.5 (1C), 50.8 (1C), 64.9

(1C), 65.5 (1C), 69.3 (1C), 159.4 (1C), 167.0 (1C), 170.6 (1C), 171.7 (1C); HRMS Calculated *m/z* for $C_{38}H_{55}N_4O_3$ $[M+H]^+$ 615.4269, found 615.4282.

Formyl-Adm-Adm-Adm-Adm-NH*t*-Bu (5.2)

Peptide **5.2** was synthesized from isocyanide **5.6** (150 mg, 0.24 mmol) according to the procedure described for the synthesis of formamide **3.2a** that was described in Chapter 3. The reaction mixture was stirred for 10 days, and treated each day with a freshly made saturated solution of ammonium formate (1 eq). When no further improvement in reaction progress was observed by TLC and mass spectrometric analysis, the volatiles were evaporated. The resulting white solid was dissolved in water and extracted with CH_2Cl_2. The organic layers were combined, washed with brine, dried over Na_2SO_4, and evaporated to a white solid, which was purified by column chromatography using 30% EtOAc in hexanes as eluent. Evaporation of the collected fractions gave peptide **5.2** (39 mg, 20% yield) as white powder: R_f 0.27 (7:3 hexanes:EtOAc); ^{1}H NMR (700 MHz, $CDCl_3$) δ 1.32 (s, 9H), 1.54-1.60 (m, 11H), 1.65-1.71 (m, 17H), 1.75-1.84 (m, 7H), 1.94-2.01 (m, 7H), 2.10 (m, 7H), 2.60 (m, 2H), 2.65-2.69 (m, 5H), 5.88 (s, 1H), 6.86 (s, 1H), 6.90 (s, 1H), 7.04 (s, 1H), 7.37 9s, 1H), 8.11 (d, J = 1.9 Hz, 1H); ^{13}C NMR (Quantitative, 700 MHz, $CDCl_3$): δ 26.4 (1C), 26.5 (2C), 26.6 (1C), 26.7 (2C), 26.8 (1C), 28.9 (1C), 28.8 (3C), 32.4 (2C), 32.6 (2C), 32.7 (6C), 32.8 (4C), 33.0 (2C), 34.0 (4C), 34.1 (2C), 34.3 (2C), 37.4 (1C), 37.6 (1C), 37.7 (1C), 37.8 (1C), 50.8 (1C), 64.9 (1C), 65.1 (1C), 65.3 (1C), 66.0 (1C), 126.2 (1C), 171.0 (1C), 172.2 (1C), 172.4 (1C), 172.9 (1C); HRMS Calculated *m/z* for $C_{49}H_{71}N_5O_5Na$ $[M+Na]^+$ 832.5347, found 832.5356.

References for Chapter 5

1. Bourguet, C. B.; Goupil, E.; Tassy, D.; Hou, X.; Thouin, E.; Polyak, F.; Hébert, T. E.; Claing, A.; Laporte, S. A.; Chemtob, S.; Lubell, W. D., Targeting the prostaglandin F2α receptor for preventing preterm labor with azapeptide tocolytics. *J. Med. Chem.* **2011**, *54*, 6085-6097.
2. Shi, H.; Zhang, C.-J.; Chen, G. Y.; Yao, S. Q., Cell-based proteome profiling of potential dasatinib targets by use of affinity-based probes. *J. Am. Chem. Soc.* **2012**, *134*, 3001-3014.
3. Murale, D. P.; Hong, S. C.; Haque, M. M.; Lee, J.-S., Photo-affinity labeling (PAL) in chemical proteomics: a handy tool to investigate protein-protein interactions (PPIs). *Proteome science* **2016**, *15*, 14.
4. Dorman, G.; Prestwich, G. D., Benzophenone photophores in biochemistry. *Biochemistry* **1994**, *33*, 5661-5673.
5. Prestwich, G. D.; Dormán, G.; Elliott, J. T.; Marecak, D. M.; Chaudhary, A., Benzophenone photoprobes for phosphoinositides, peptides and drugs. *Photochemistry and photobiology* **1997**, *65*, 222-234.
6. Brown, R. B.; Audet, J., Current techniques for single-cell lysis. *J. R. Soc. Interface* **2008,** *5*, S131-S138.
7. Rowland, M. M.; Bostic, H. E.; Gong, D.; Speers, A. E.; Lucas, N.; Cho, W.; Cravatt, B. F.; Best, M. D., Phosphatidylinositol 3, 4, 5-trisphosphate activity probes for the labeling and proteomic characterization of protein binding partners. *Biochemistry* **2011**, *50*, 11143-11161.
8. Cisneros, J. A.; Björklund, E.; González-Gil, I. s.; Hu, Y.; Canales, A. n.; Medrano, F. J.; Romero, A.; Ortega-Gutiérrez, S.; Fowler, C. J.; López-Rodríguez, M. L., Structure–activity relationship of a new Series of reversible dual monoacylglycerol lipase/fatty acid amide hydrolase inhibitors. *J. Med. Chem.* **2012**, *55*, 824-836.

Appendix

Supporting information Manuscript 1

Fatemeh M. Mir, N. D. Prasad Atmuri, Jennifer Rodon Fores, Xin Hou, Sylvain Chemtob, William D. Lubell. Paired Utility of Aza-Amino Acyl Proline and Indolizidinone Amino Acid Residues for Peptide Mimicry: Conception of Prostaglandin F2α Receptor Allosteric Modulators that Delay Preterm Birth. Submitted for *J. Med. Chem.*

The results on the synthesis and study of the analogs described in this manuscript were obtained in collaboration with N. D. Prasad Atmuri, another Ph.D. candidate in Professor Lubell's laboratory. All the indolizidinone peptide analogs were synthesized and characterized by N. D. Prasad Atmuri and the results are not included in this thesis.

SUPPORTING INFORMATION

Paired Utility of Aza-Amino Acyl Proline and Indolizidinone Amino Acid Residues for Peptide Mimicry: Conception of Prostaglandin $F_{2\alpha}$ Receptor Allosteric Modulators that Delay Preterm Birth

Fatemeh M. Mir [†§], N. D. Prasad Atmuri [†§], Jennifer Rodon Fores [†], Xin Hou[‡], Sylvain Chemtob[‡], William D. Lubell [†]*

†Département de Chimie, Université de Montréal, C.P. 6128 Succursale Centre-Ville, Montréal H3C 3J7 QC, Canada

‡Centre Hospitalier Universitaire Sainte-Justine Research Center, Montréal H3T 1C5, Quebec, Canada

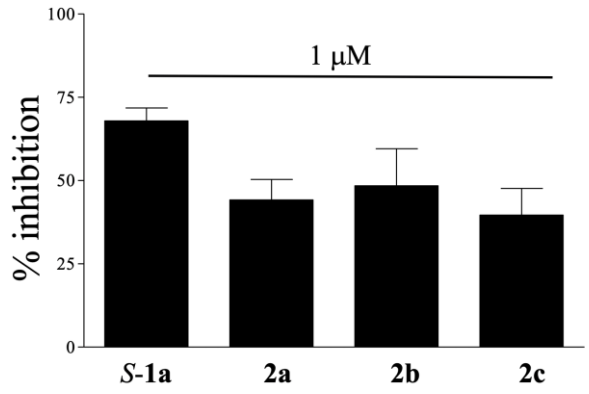

Figure S2.1. Effects of indolizidinone and azapeptide modulators on mean tension induced by PGF2α. At the beginning of each experiment, mean tension of spontaneous myometrial contractions was considered as the basal response.

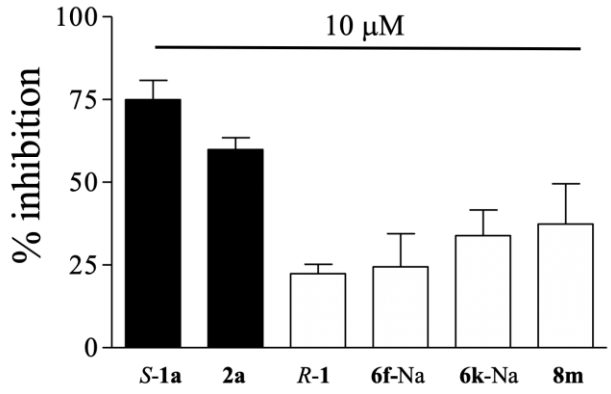

Figure S2.2. Effects of indolizidinone and azapeptide modulators on mean tension induced by PGF2α. At the beginning of each experiment, mean tension of spontaneous myometrial contractions was considered as the basal response.

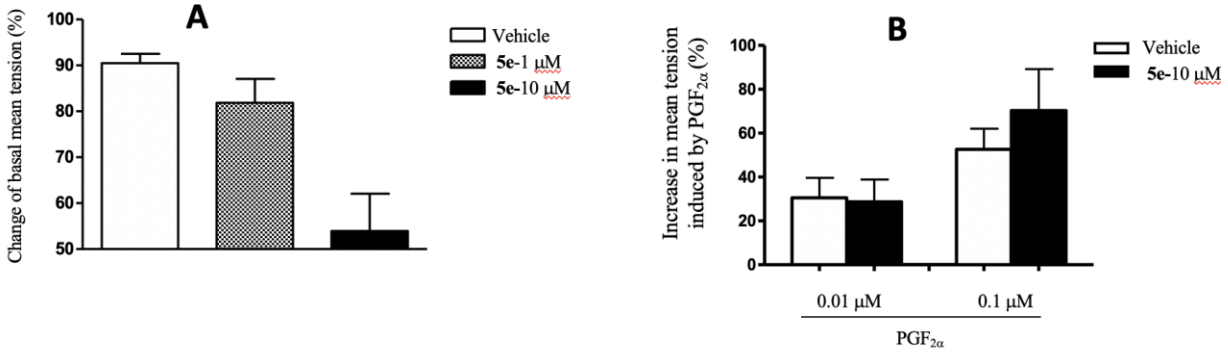

Figure S2.3. 2.5e at 10 µM caused a significant decrease in mean tension of spontaneous myometrial contraction (A), but PGF2α-induced increased mean tension of contractions was not inhibited by **2.5e** (B)

Table S2.1. Effects of indolizidinone and azapeptide modulator candidates (1 μM and 10μM) on mean tension induced by PGF2α. At the beginning of each experiment, mean tension of spontaneous myometrial contractions was considered as the basal response.

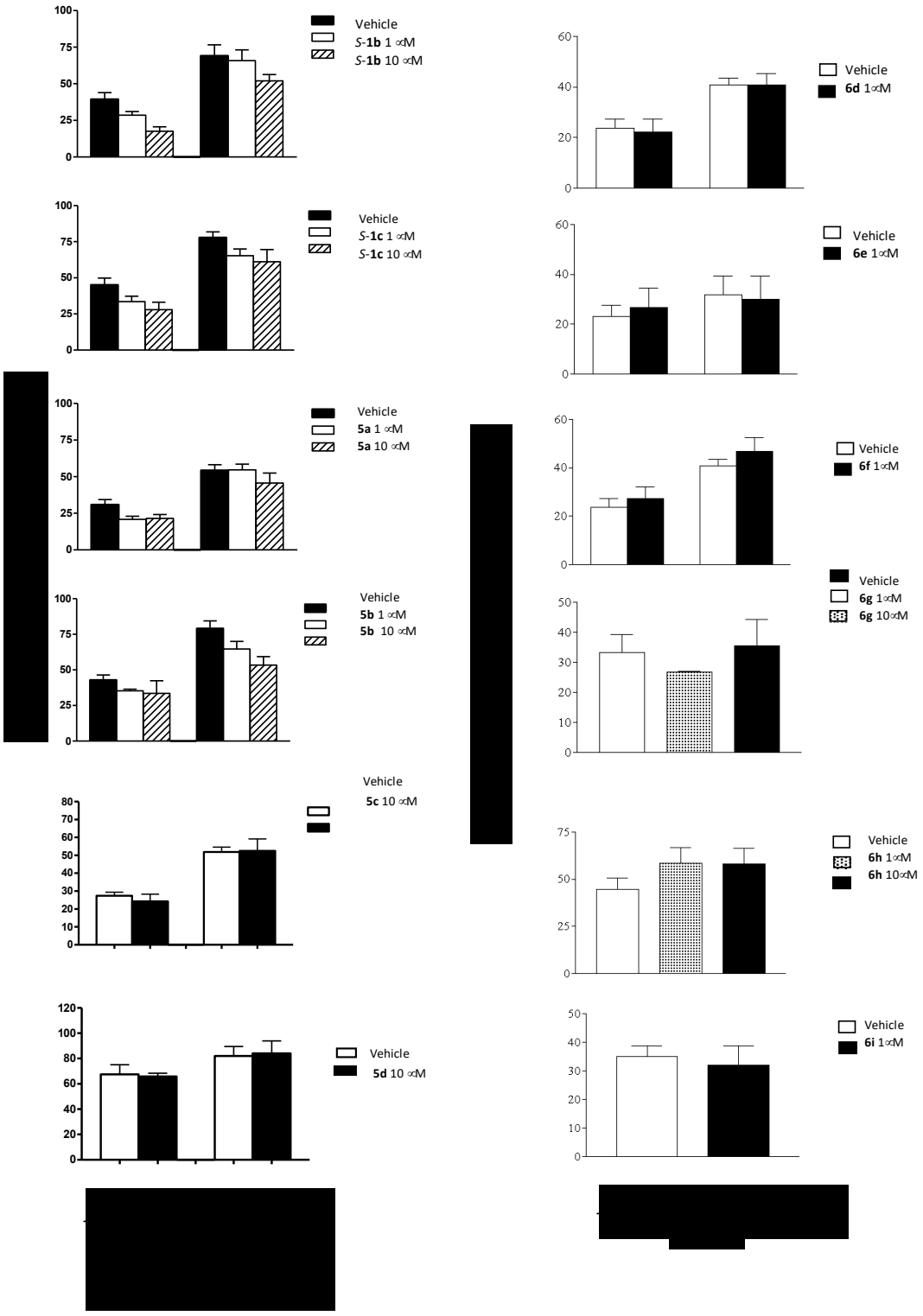

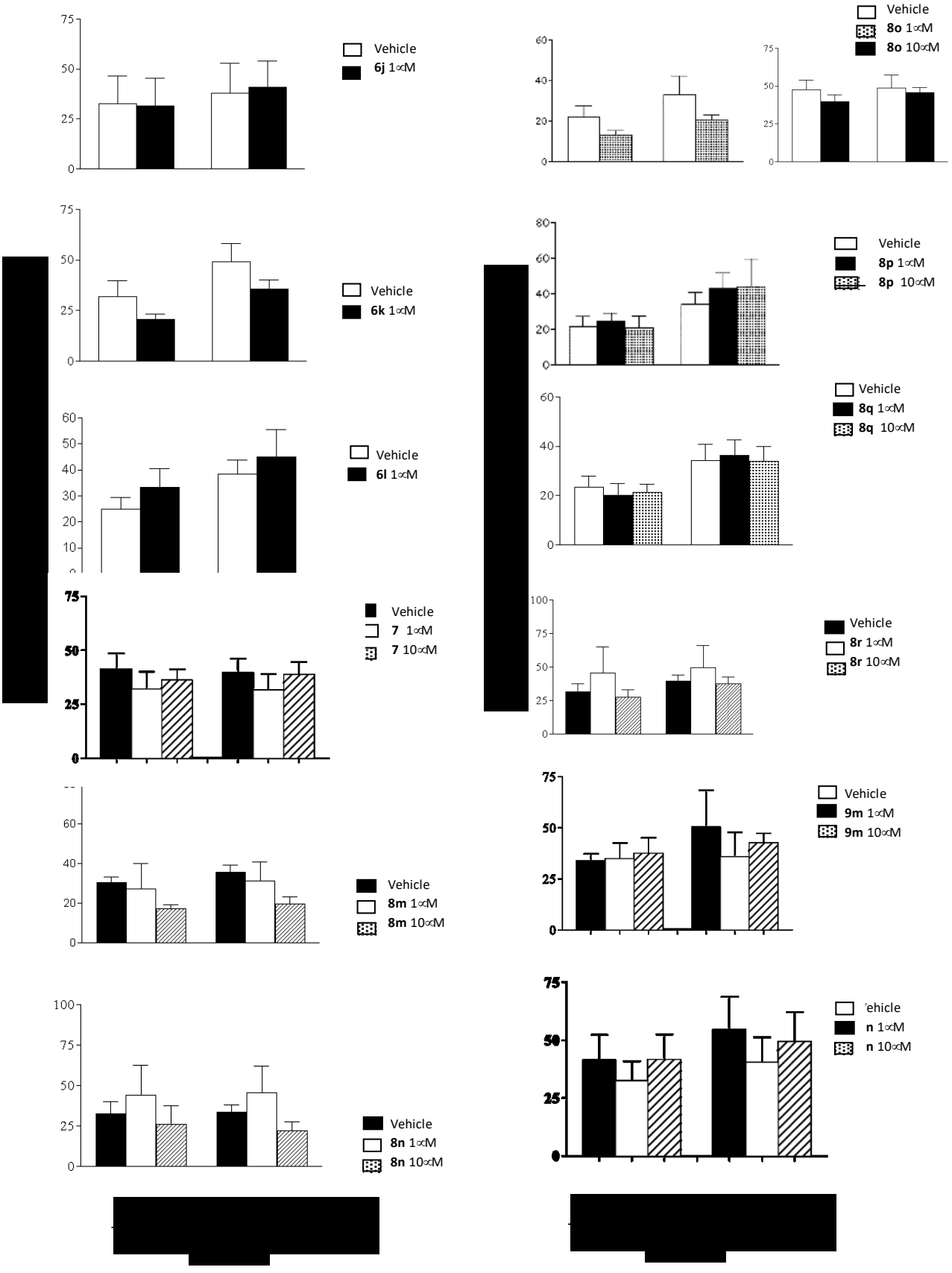

Supporting information Manuscript 1

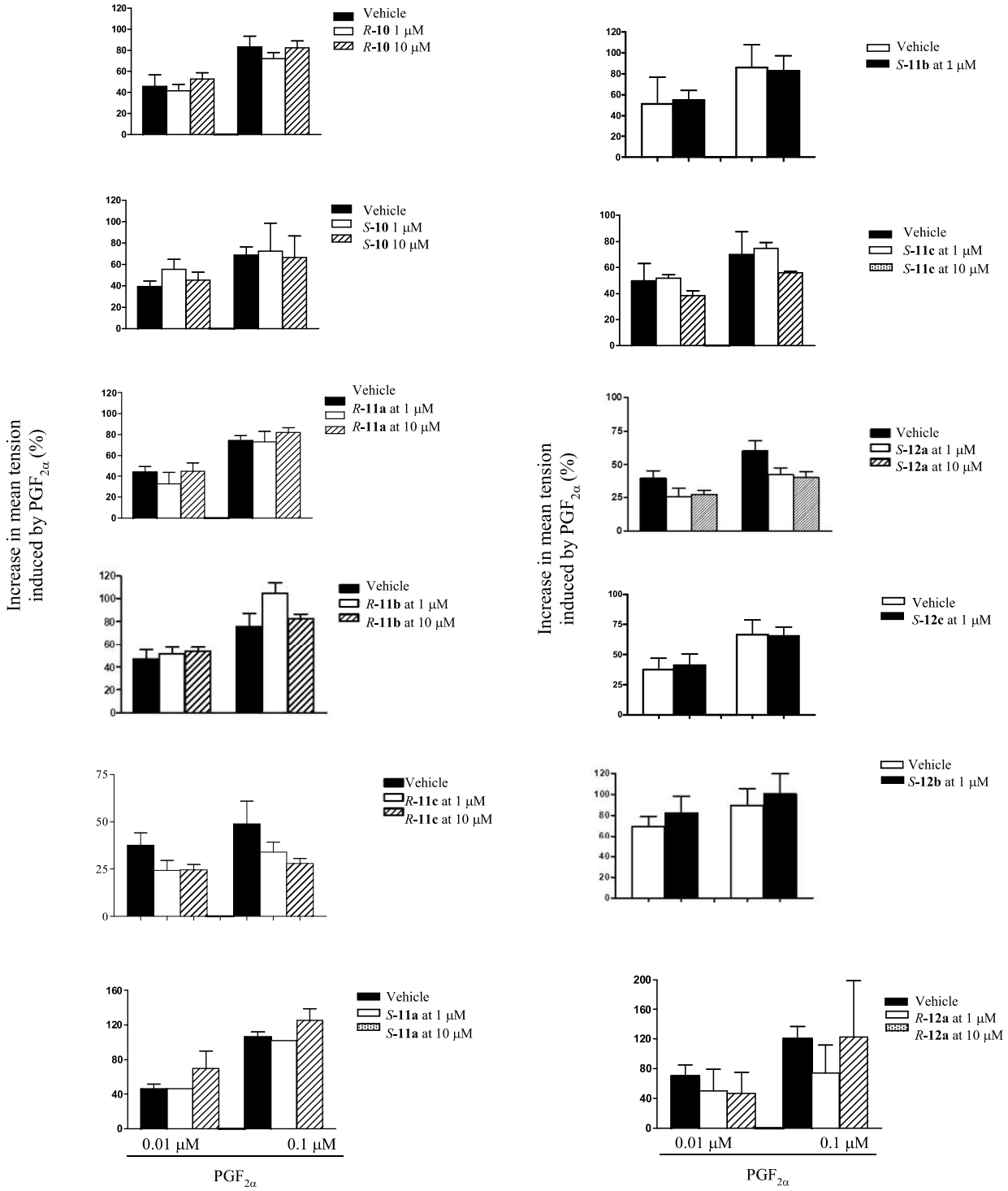
Increase in mean tension induced by $PGF_{2\alpha}$ (%)
Vehicle
R-10 1 μM
R-10 10 μM
Vehicle
S-10 1 μM
S-10 10 μM
Vehicle
R-11a at 1 μM
R-11a at 10 μM
Vehicle
R-11b at 1 μM
R-11b at 10 μM
Vehicle
R-11c at 1 μM
R-11c at 10 μM
Vehicle
S-11a at 1 μM
S-11a at 10 μM
0.01 μM
0.1 μM
$PGF_{2\alpha}$
Increase in mean tension induced by $PGF_{2\alpha}$ (%)
Vehicle
S-11b at 1 μM
Vehicle
S-11c at 1 μM
S-11c at 10 μM
Vehicle
S-12a at 1 μM
S-12a at 10 μM
Vehicle
S-12c at 1 μM
Vehicle
S-12b at 1 μM
Vehicle
R-12a at 1 μM
R-12a at 10 μM
0.01 μM
0.1 μM
$PGF_{2\alpha}$

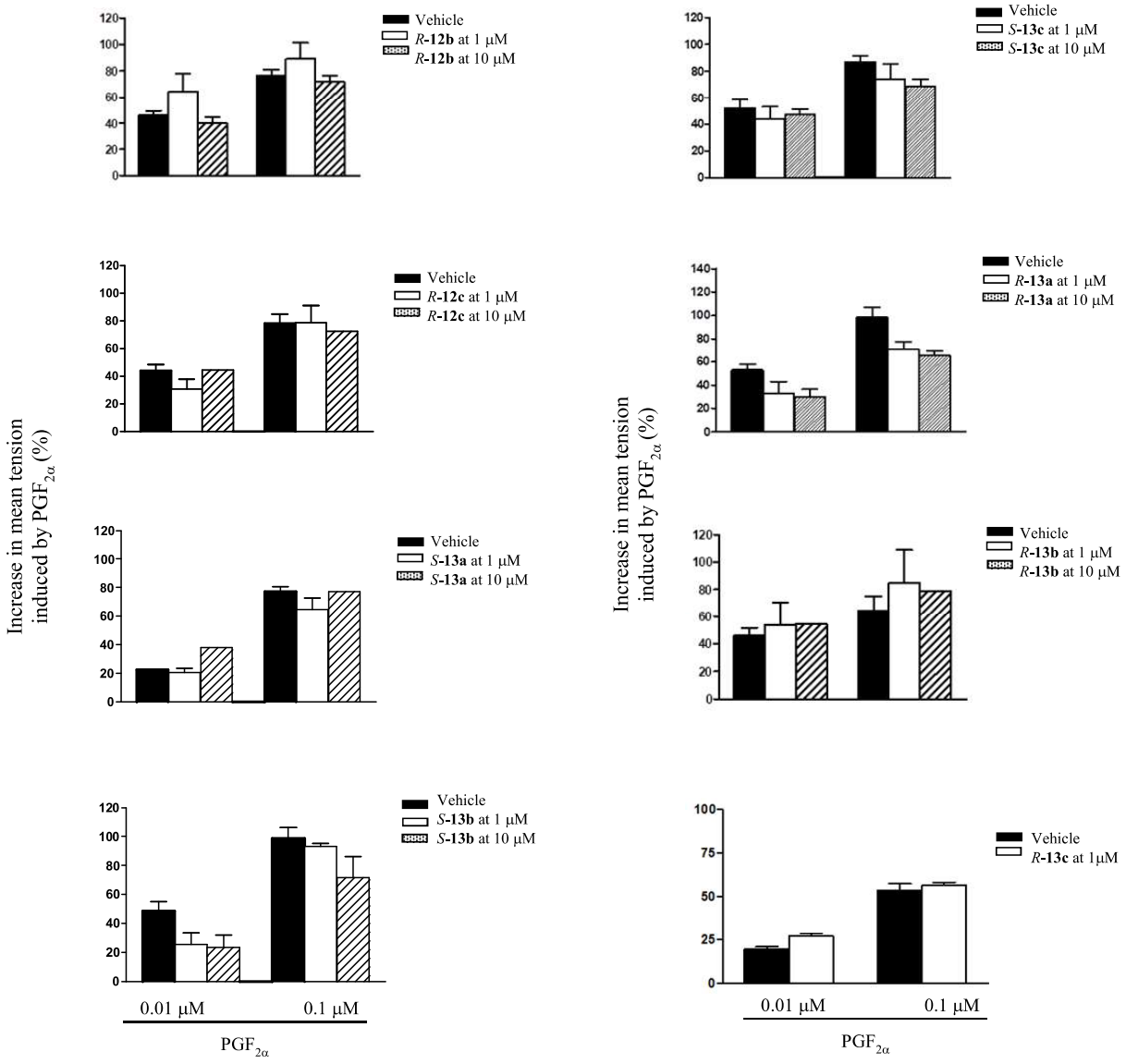
Increase in mean tension induced by $PGF_{2\alpha}$ (%)
Vehicle
R-**12b** at 1 μM
R-**12b** at 10 μM
Vehicle
S-**13c** at 1 μM
S-**13c** at 10 μM
Vehicle
R-**12c** at 1 μM
R-**12c** at 10 μM
Vehicle
R-**13a** at 1 μM
R-**13a** at 10 μM
Vehicle
S-**13a** at 1 μM
S-**13a** at 10 μM
Vehicle
R-**13b** at 1 μM
R-**13b** at 10 μM
Vehicle
S-**13b** at 1 μM
S-**13b** at 10 μM
Vehicle
R-**13c** at 1μM
0.01 μM
0.1 μM
$PGF_{2\alpha}$

^{1}H NMR 700MHz
Solvent: CD_3OD

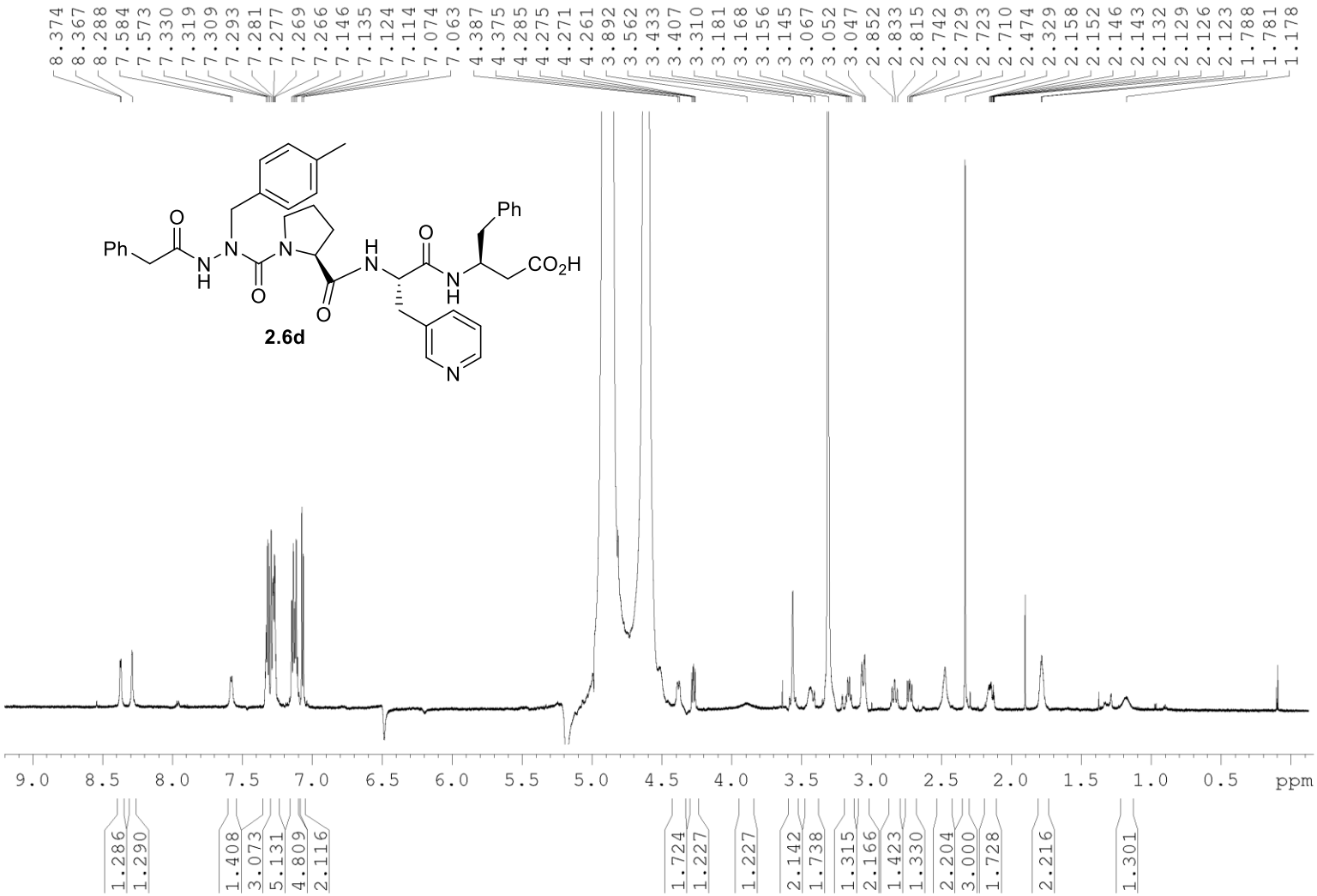

^{13}C NMR 175 MHz
Solvent: CD_3OD

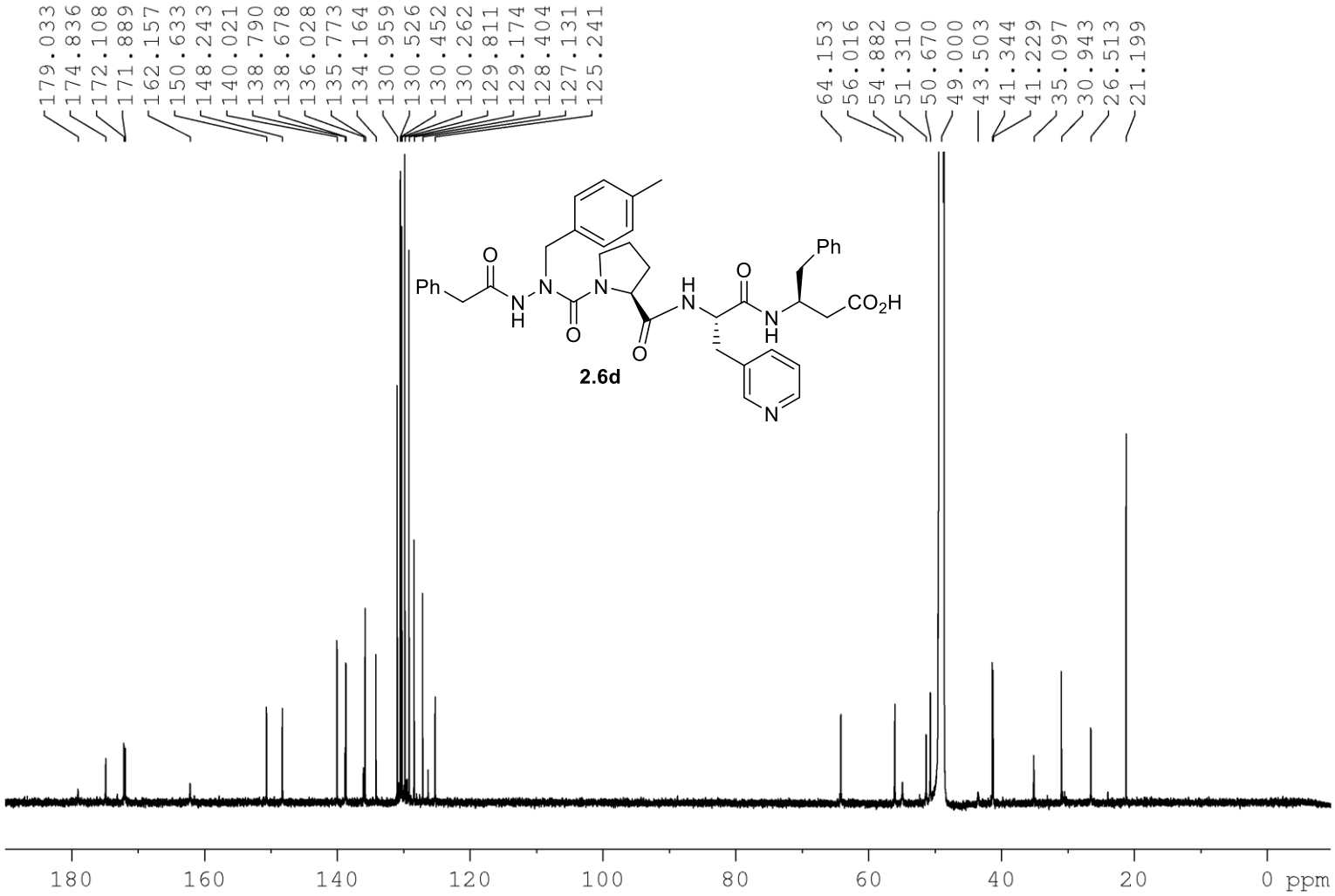

^{1}H NMR 700MHz
Solvent: CD_3OD

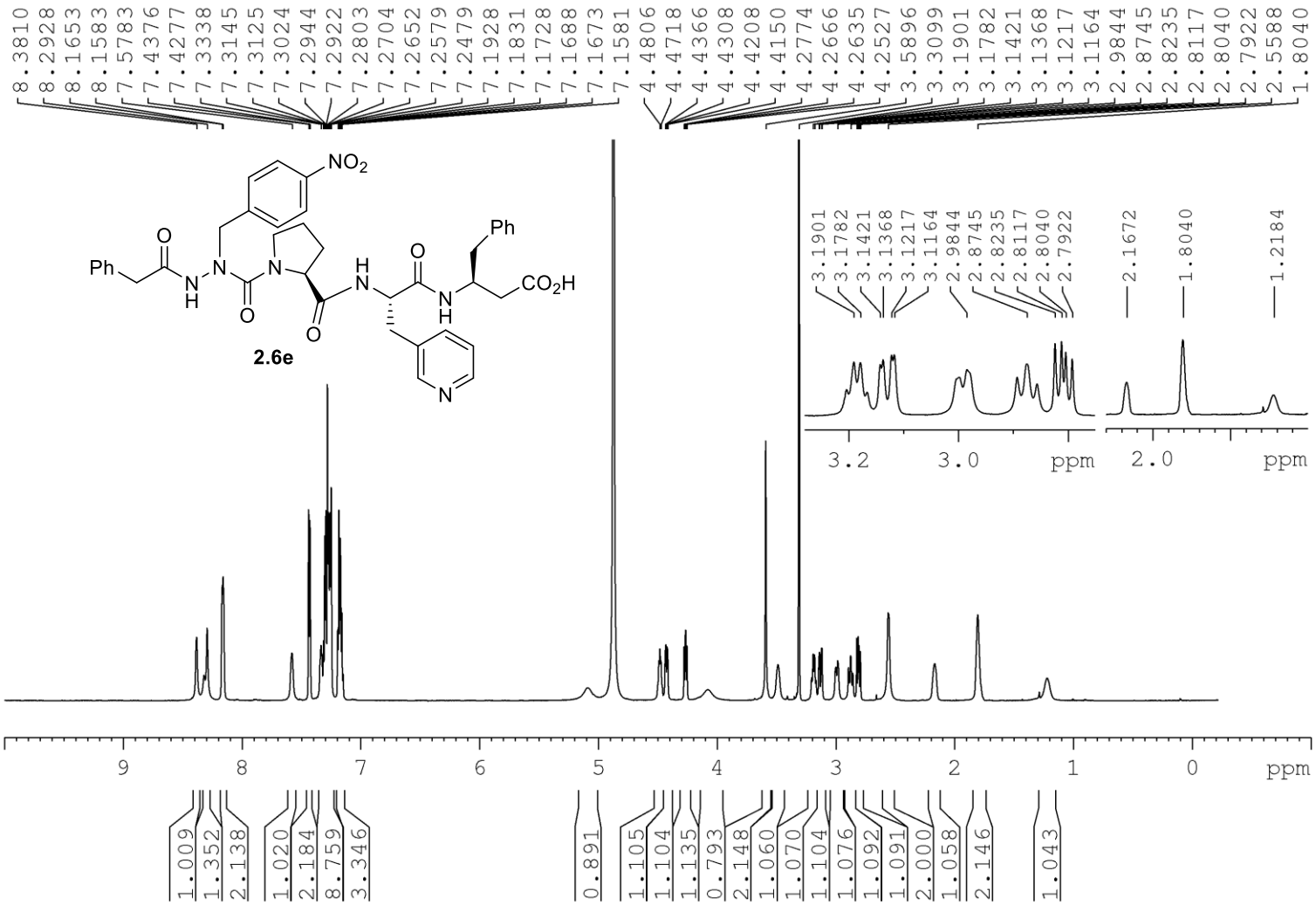

^{13}C NMR 175 MHz

Solvent: CD_3OD

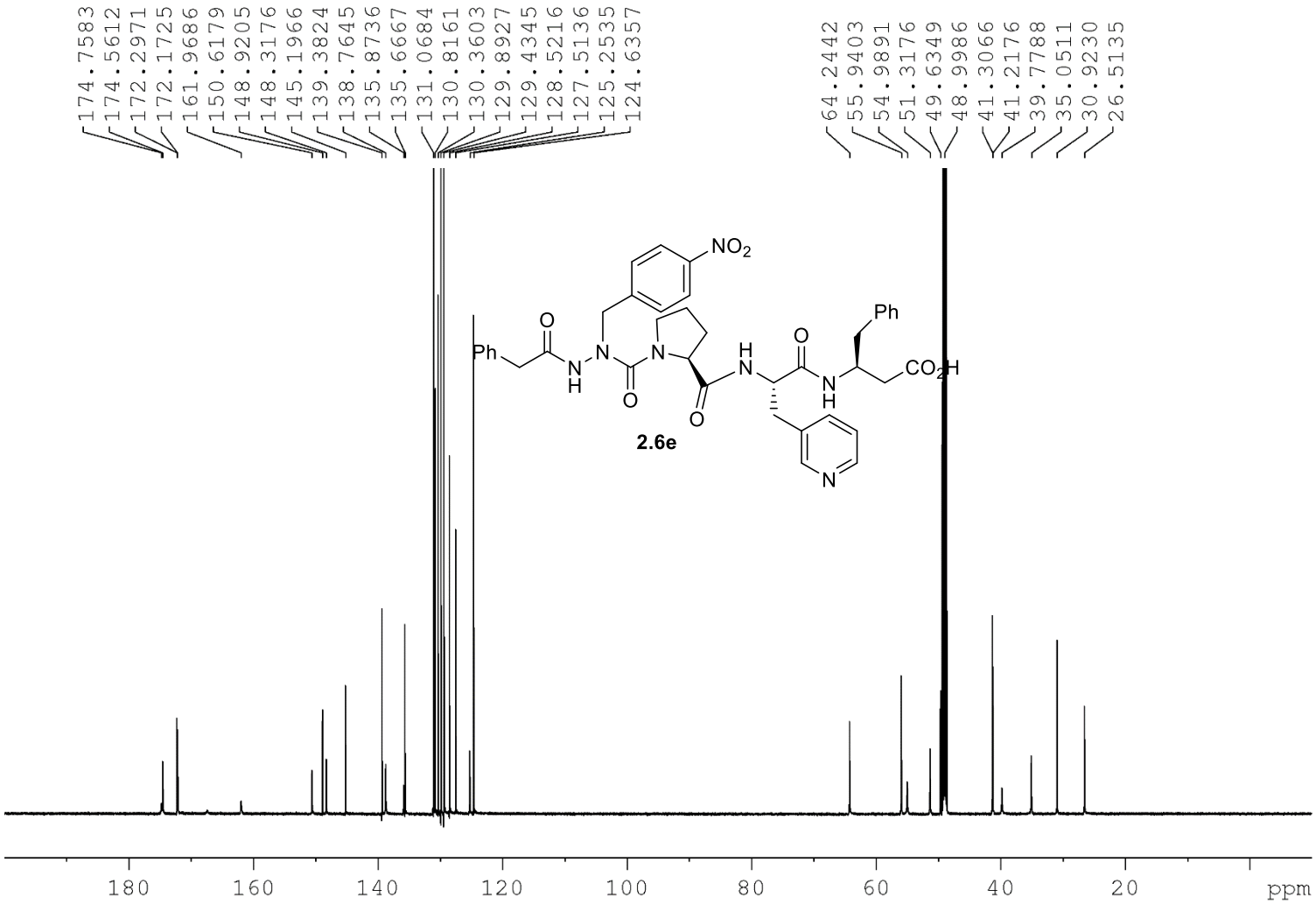

^{1}H NMR 700MHz
Solvent: CD_3OD

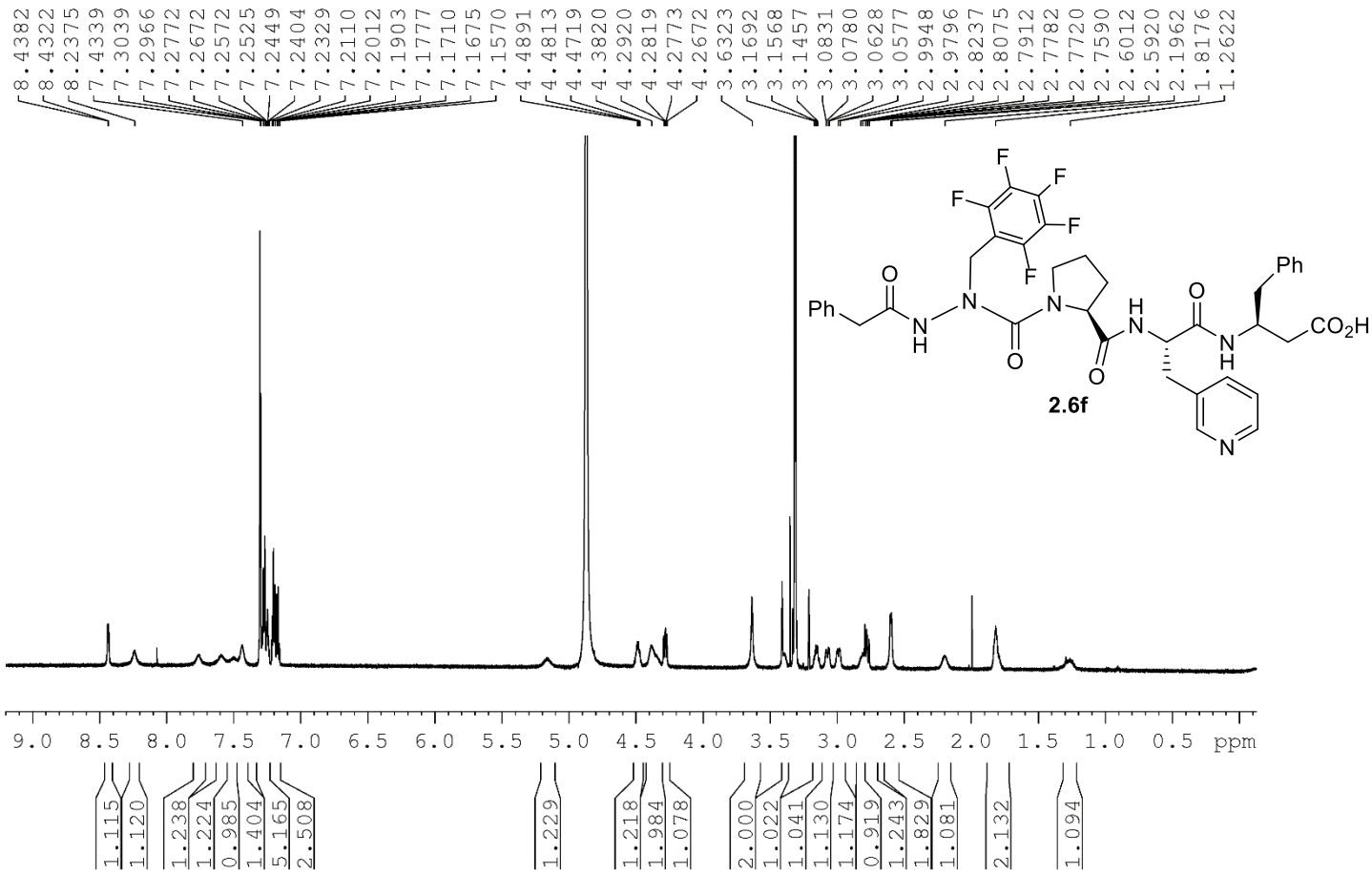

2.6f

^{13}C NMR 175 MHz

Solvent: CD_3OD

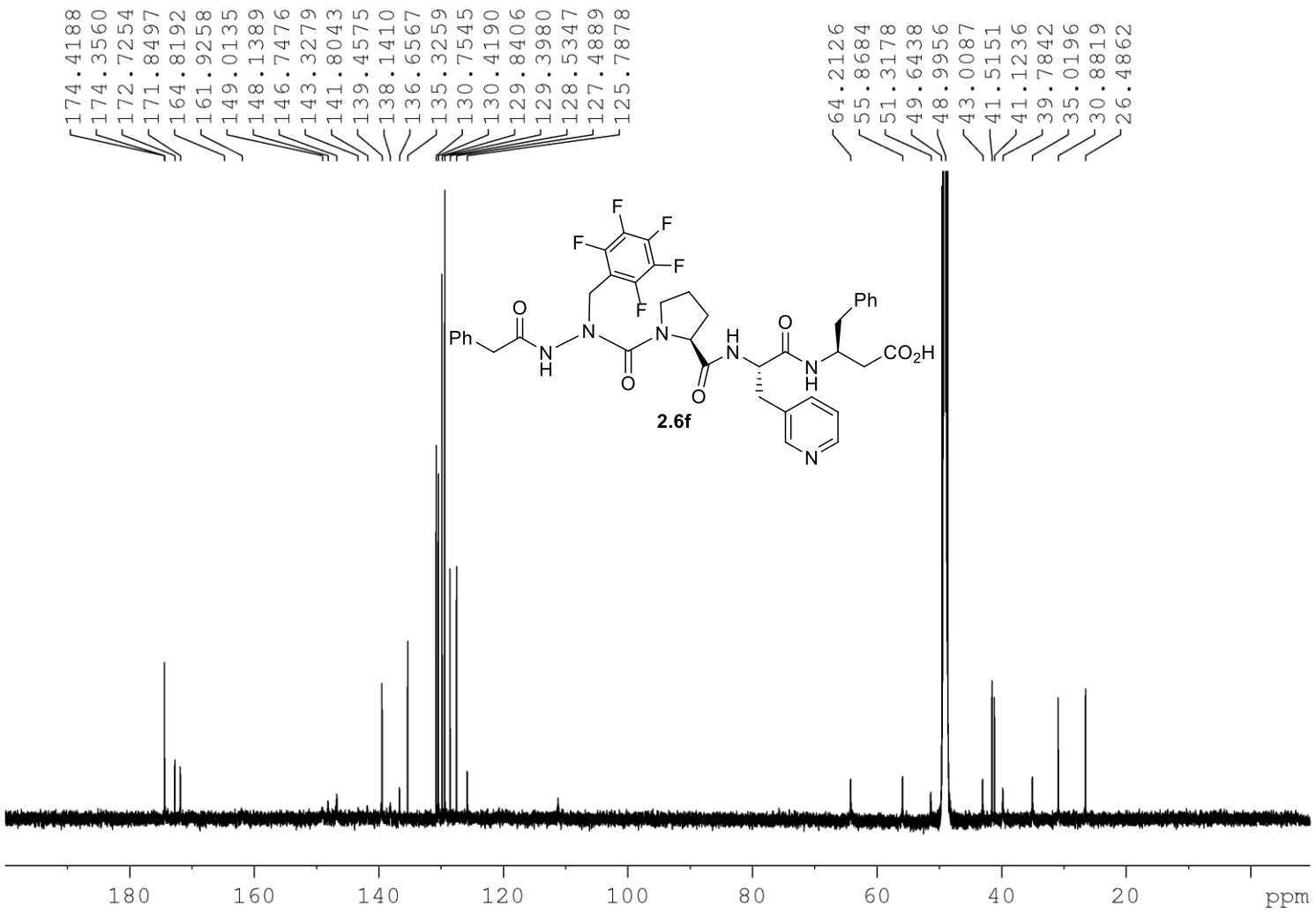

^{1}H NMR 700MHz
Solvent: CD_3OD

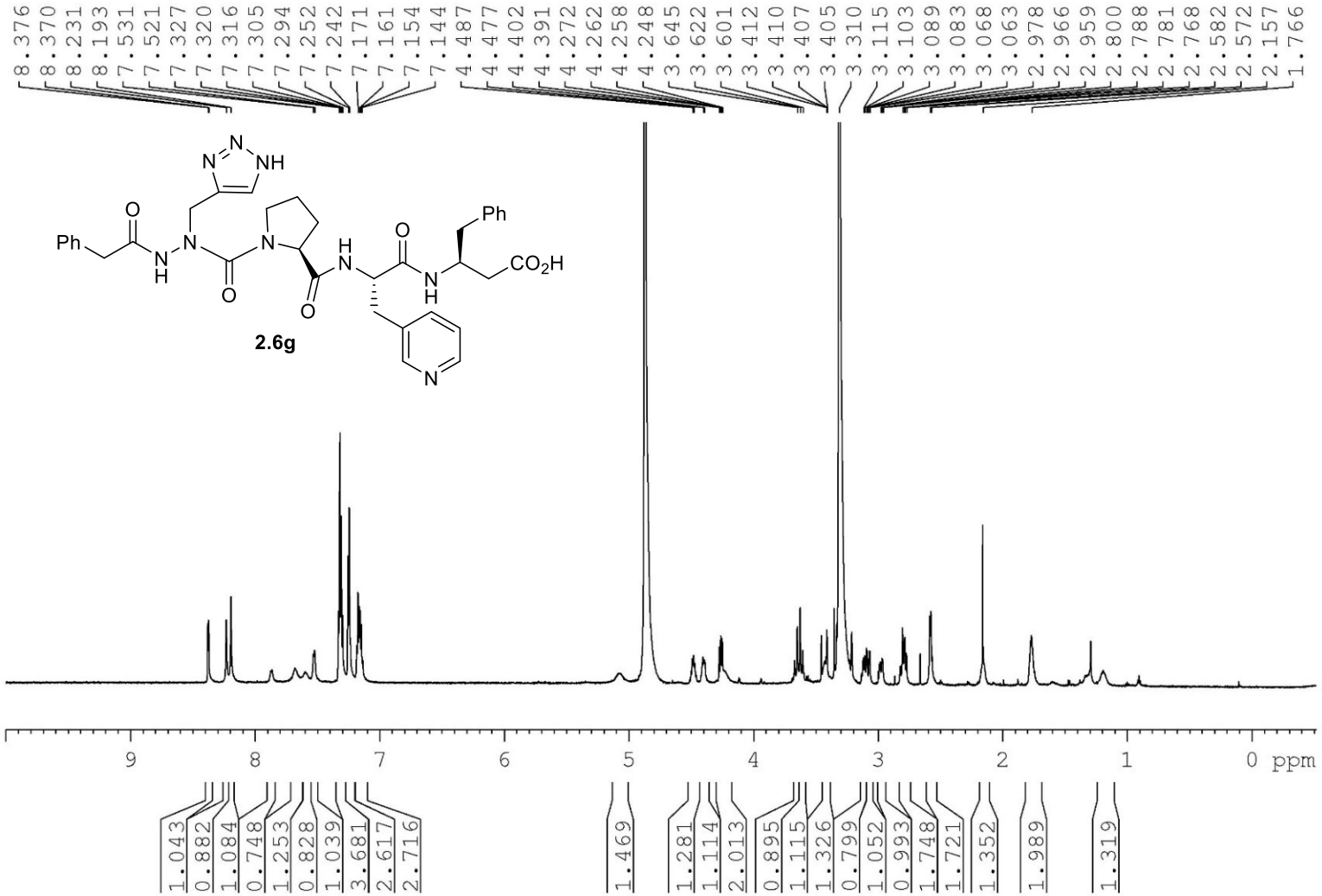

^{13}C NMR 175MHz

Solvent: CD_3OD

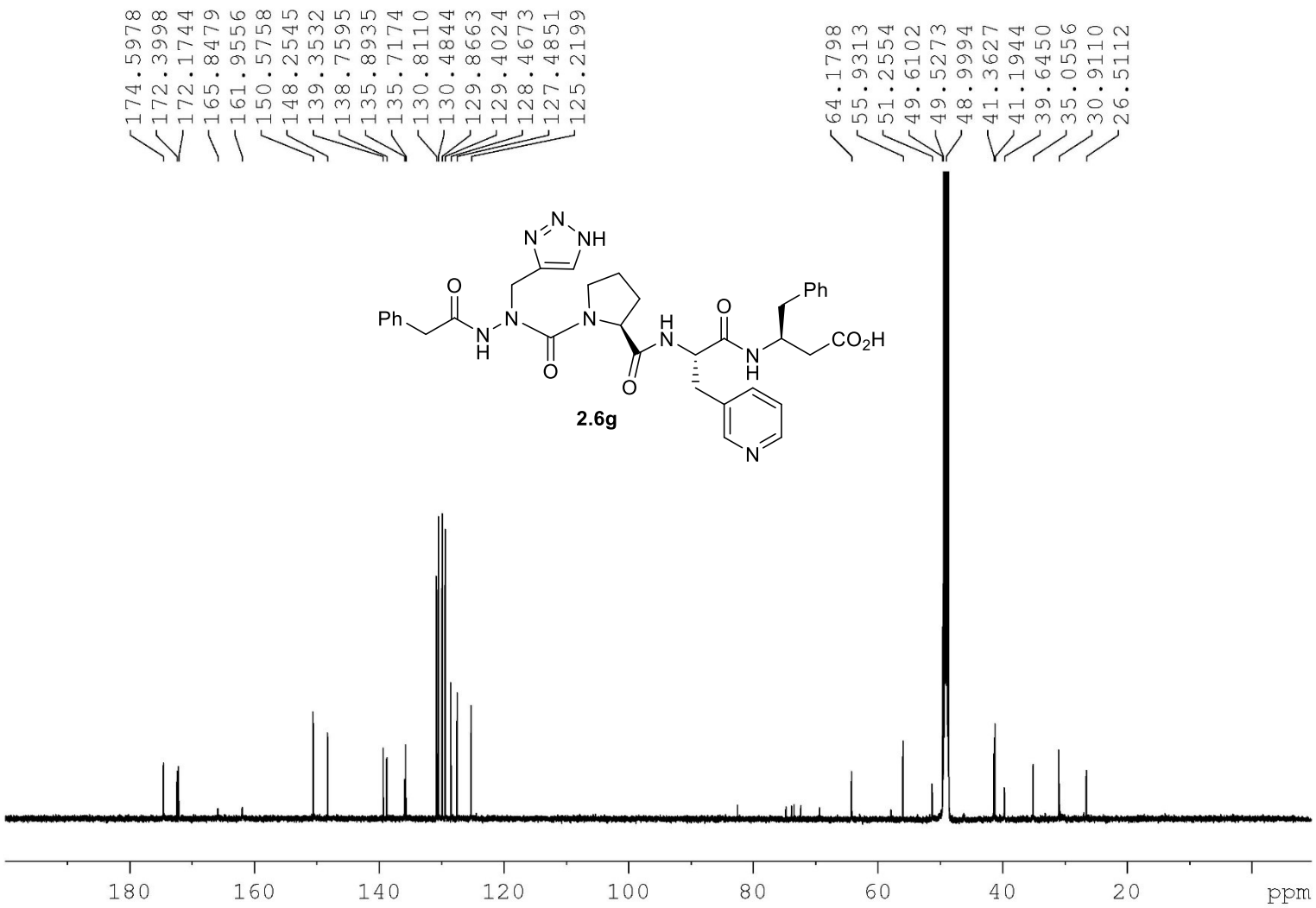

^{1}H NMR 700MHz
Solvent: CD_3OD

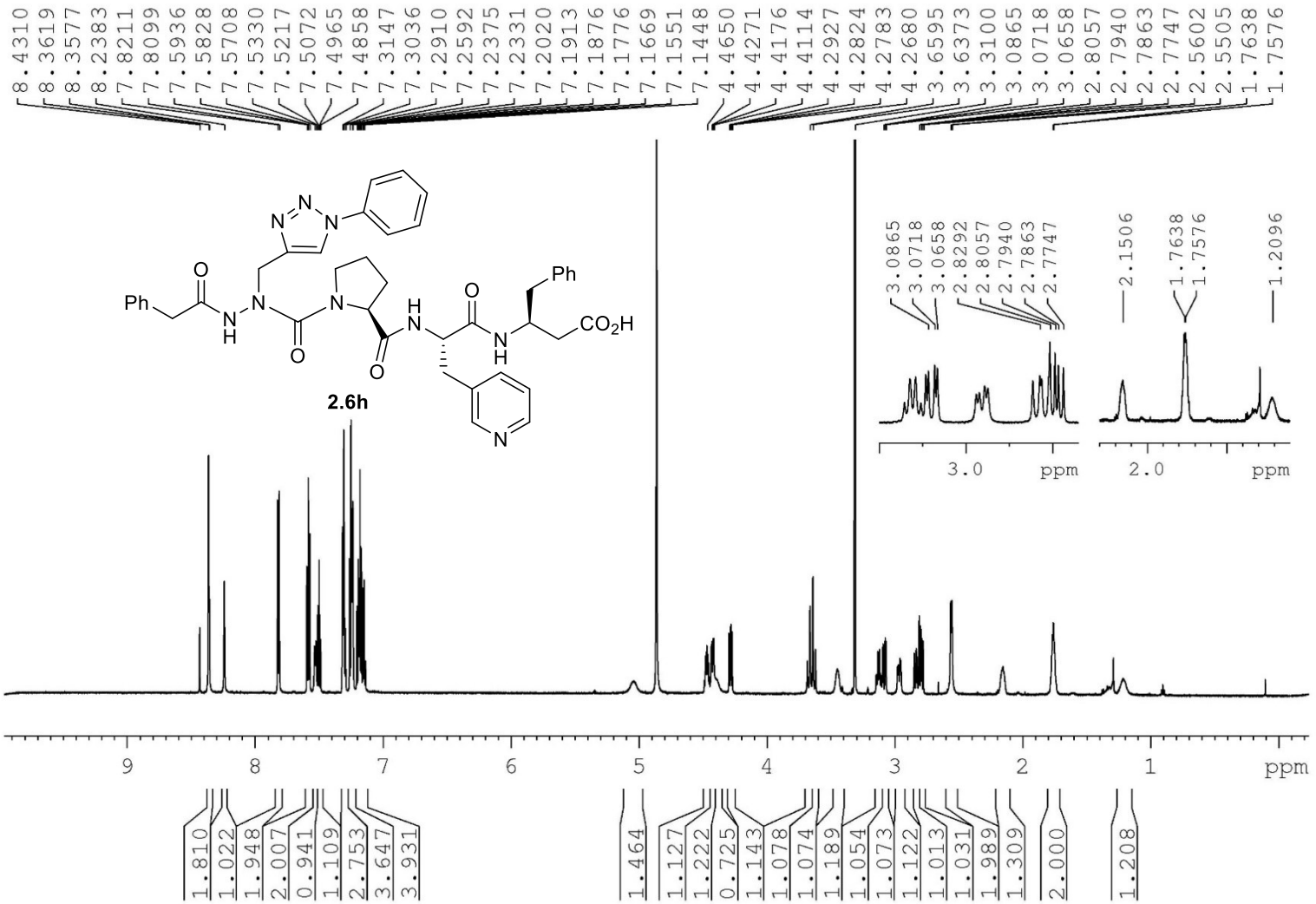

[1]H NMR 175MHz
Solvent: CD_3OD

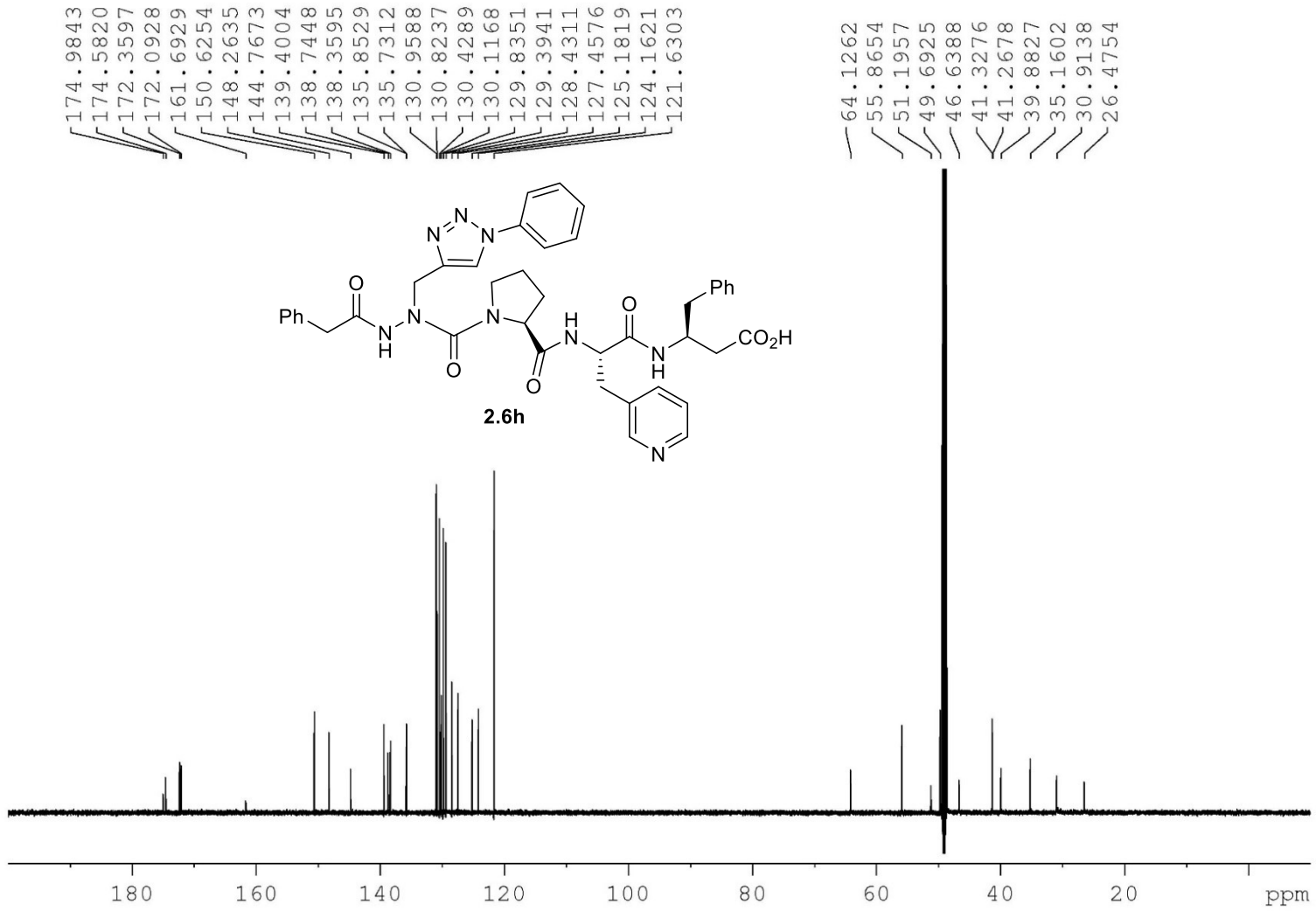

^{1}H NMR 700MHz

Solvent: CD_3OD

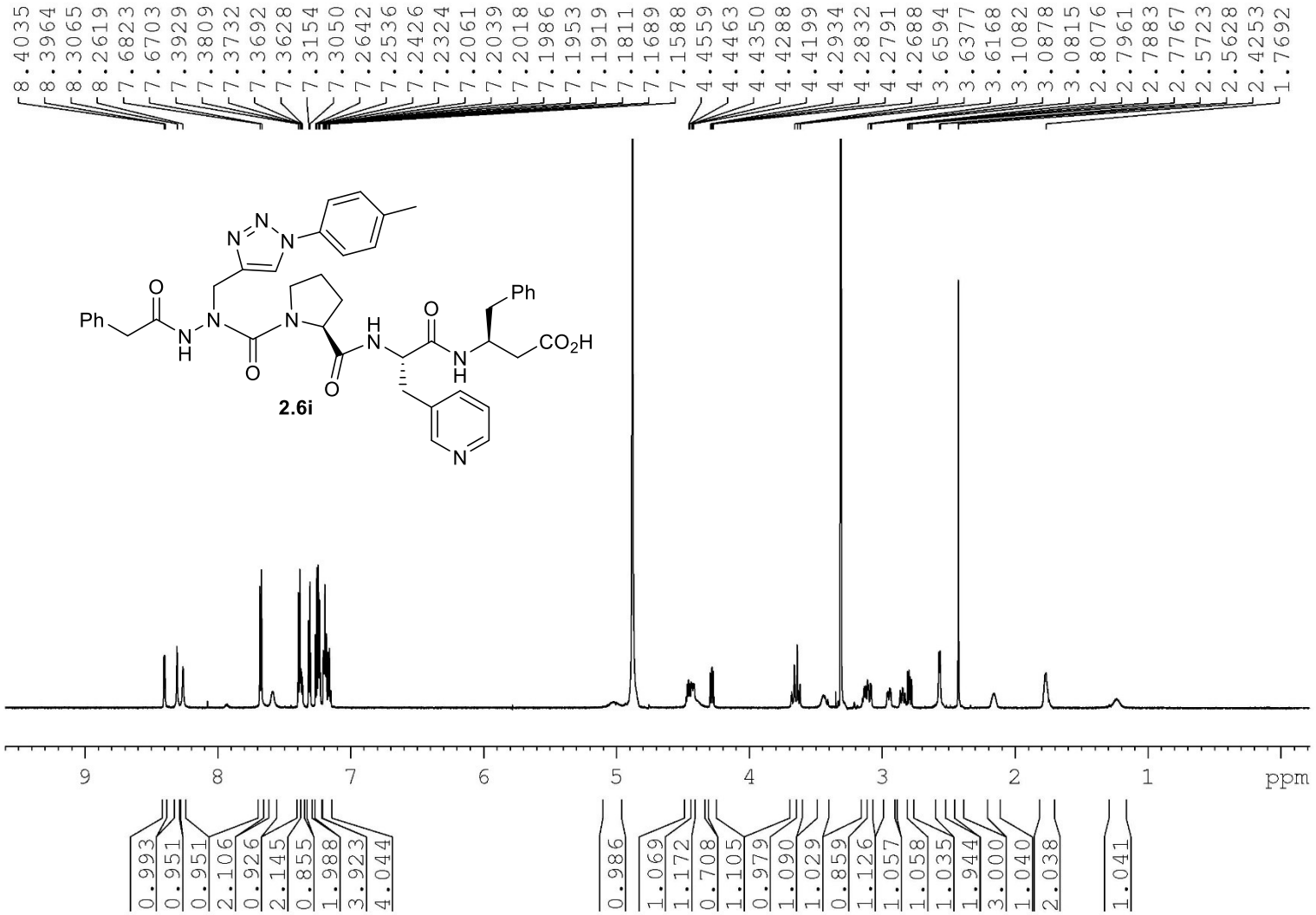

^{1}H NMR 175MHz
Solvent: CD_3OD

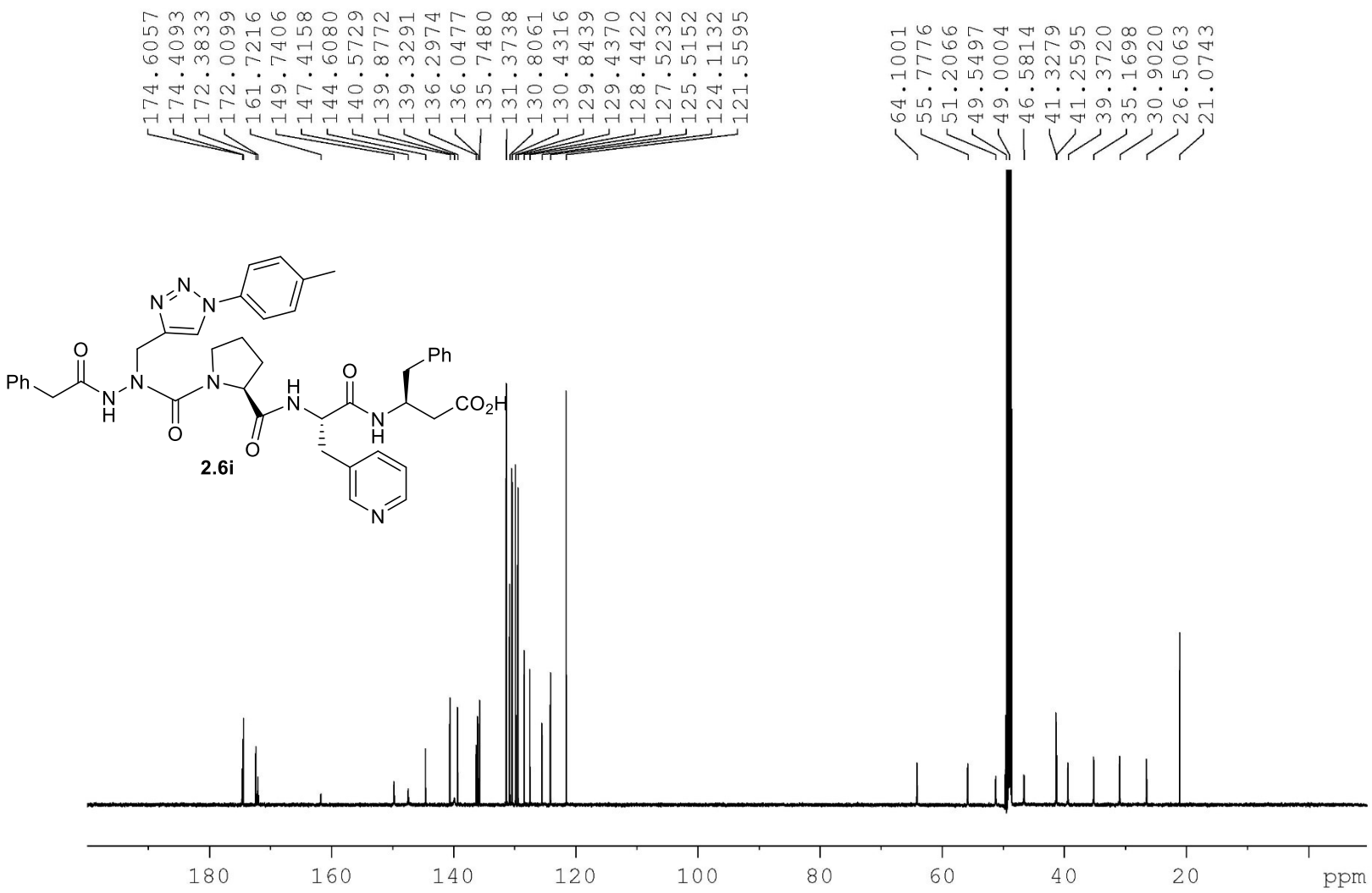

^{1}H NMR 700MHz

Solvent: CD_3OD

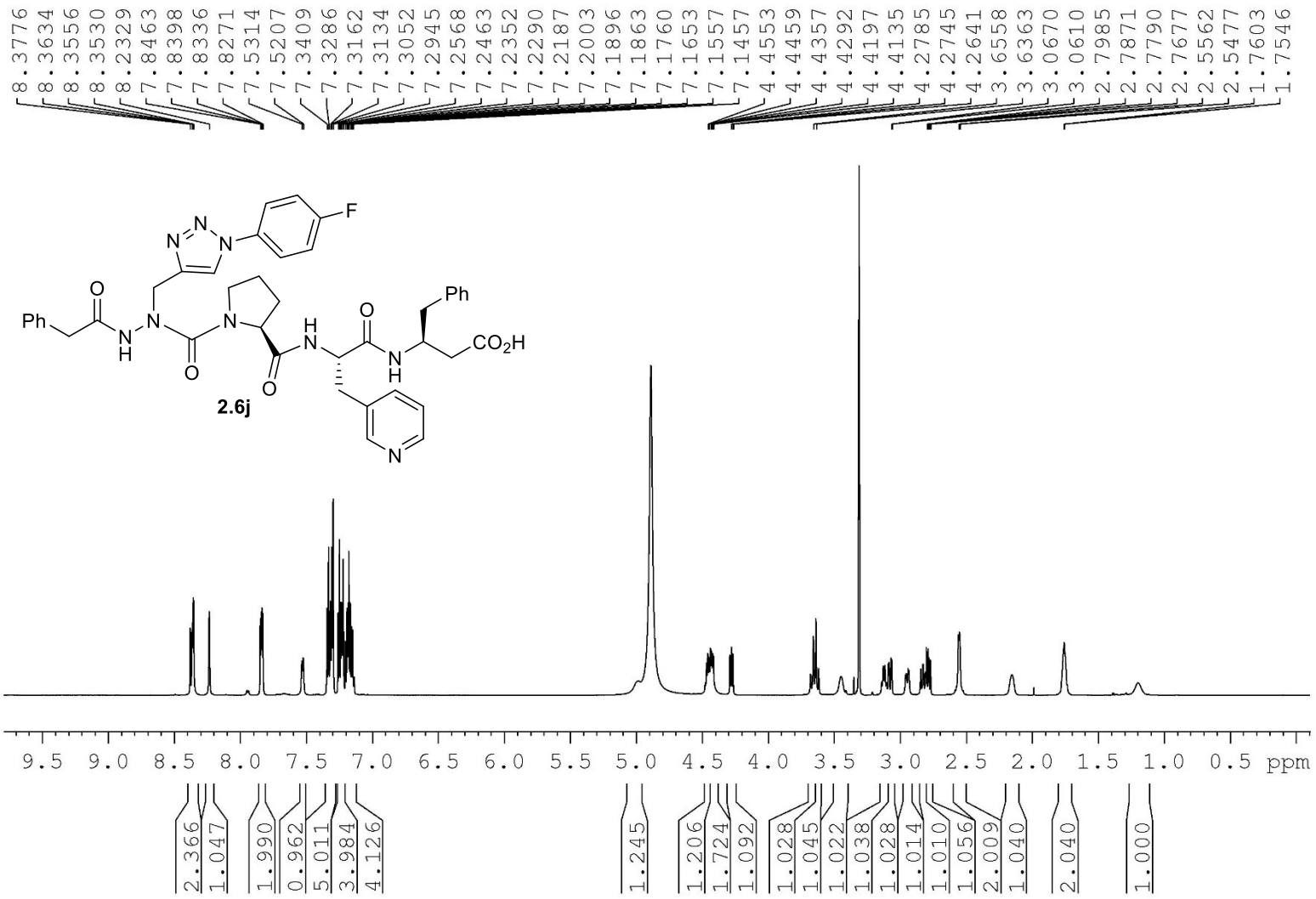

^{1}H NMR 175 MHz
Solvent: CD_3OD

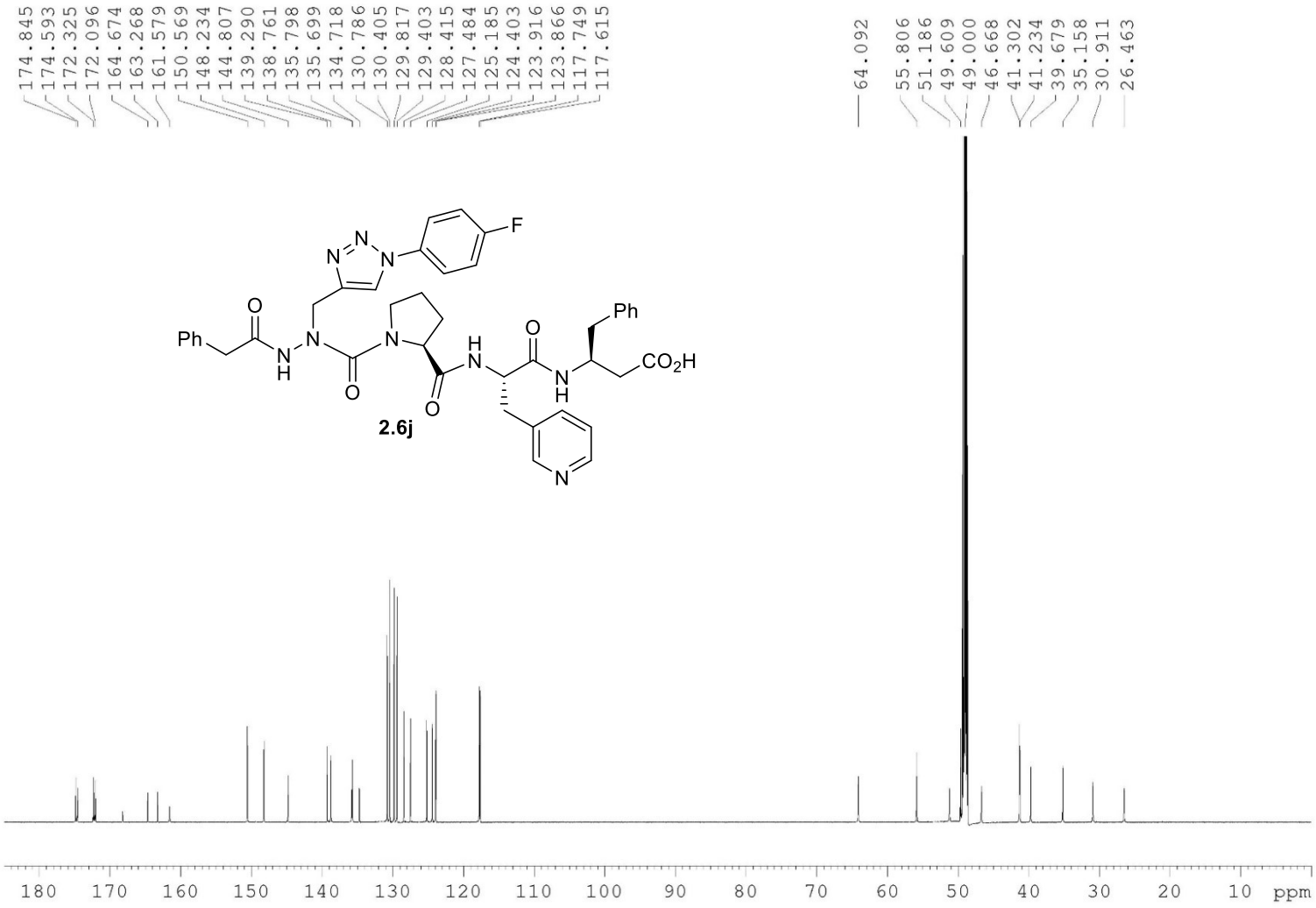

^{1}H NMR 700MHz
Solvent: CD_3OD

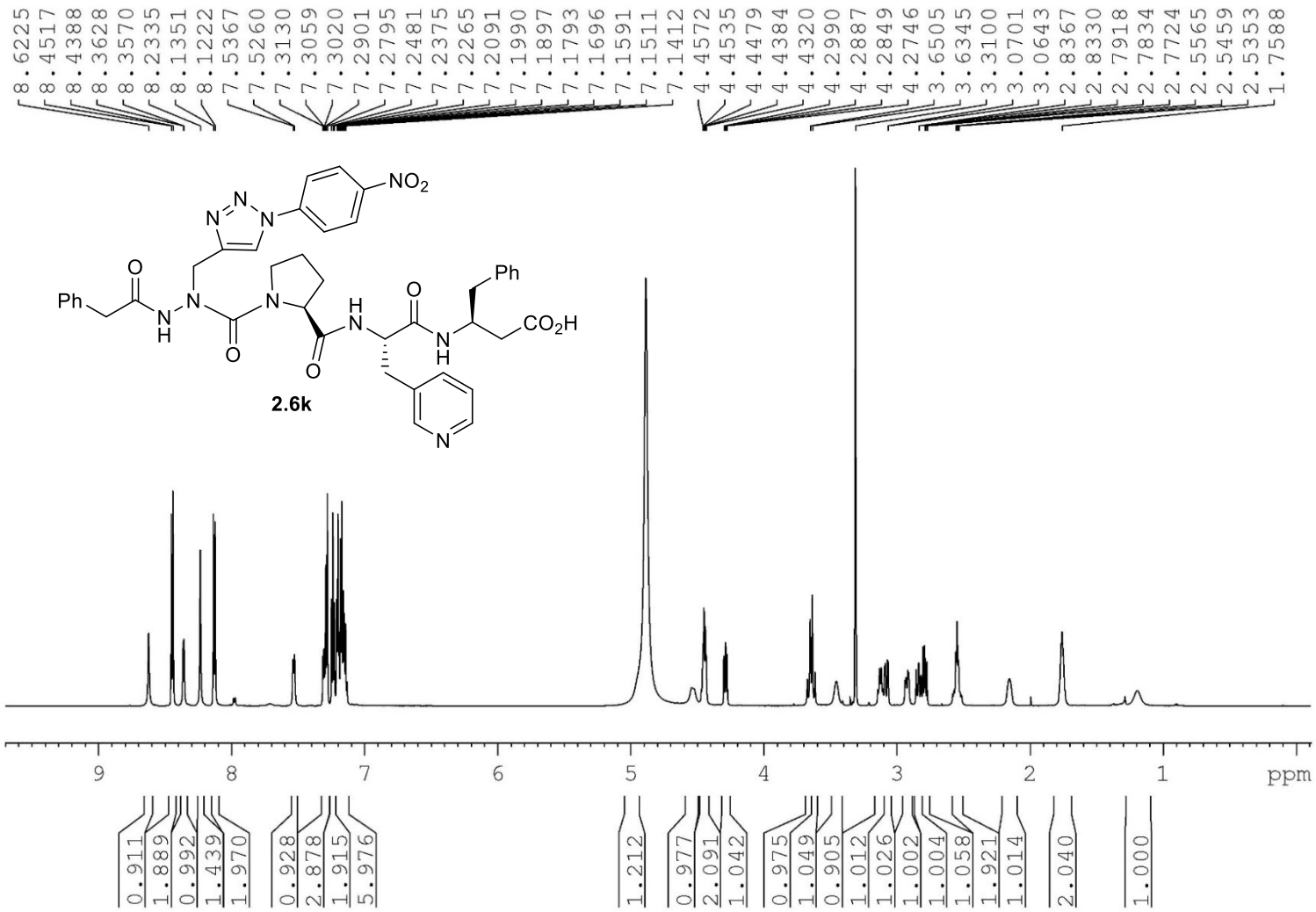

[1]H NMR 175MHz
Solvent: CD_3OD

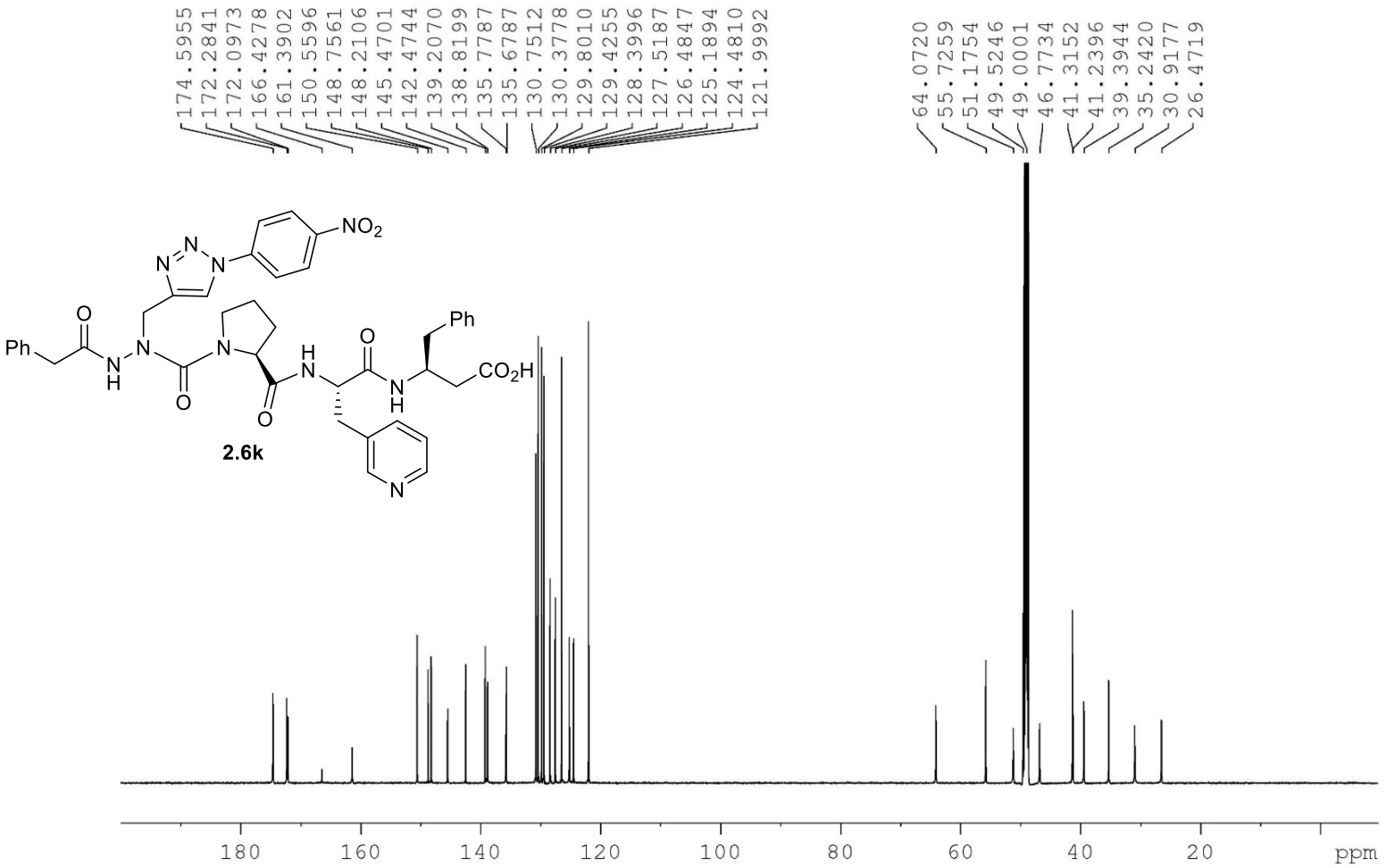

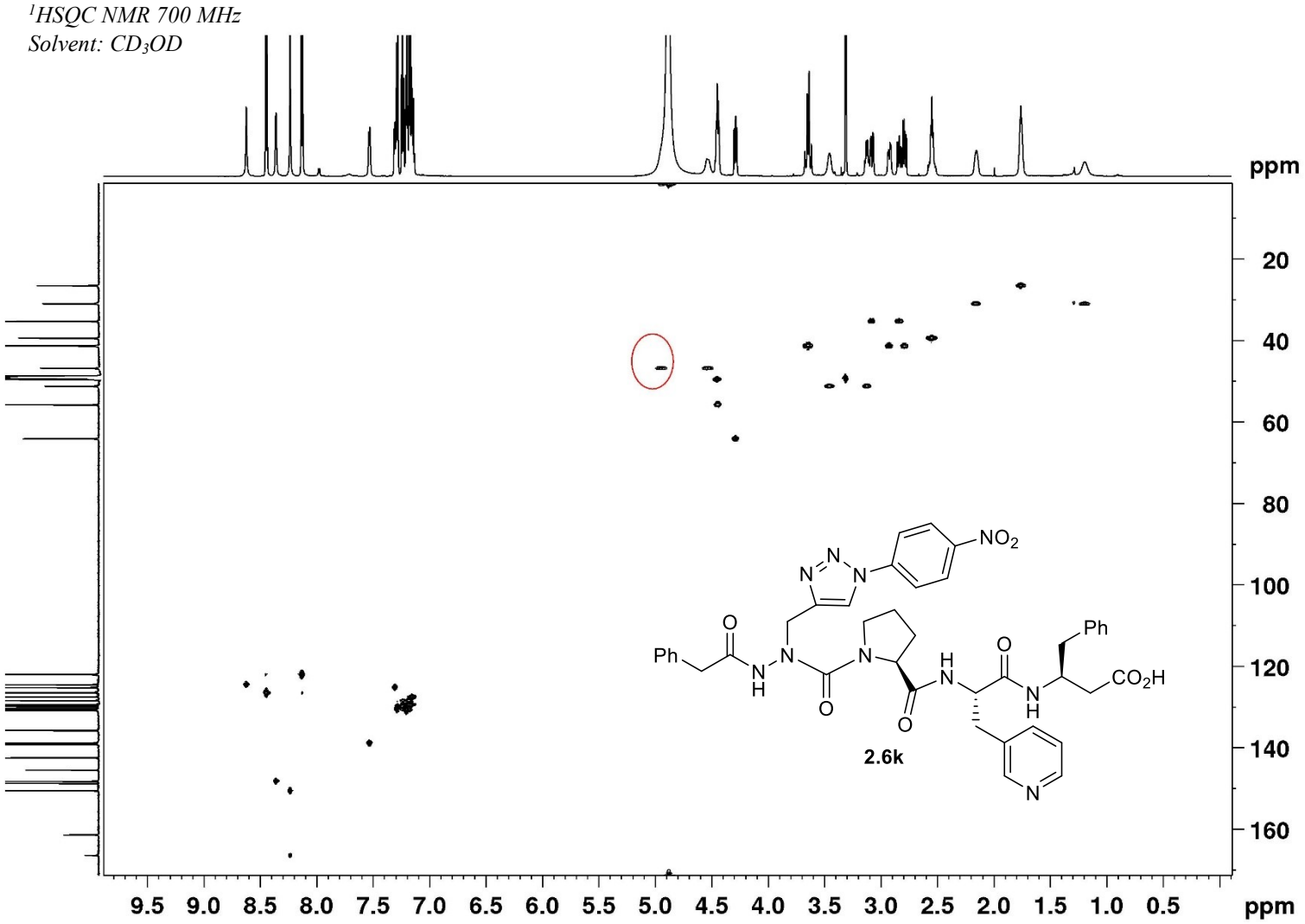
[1]HSQC NMR 700 MHz
Solvent: CD3OD
ppm
20
40
60
80
100
120
140
160
9.5 9.0 8.5 8.0 7.5 7.0 6.5 6.0 5.5 5.0 4.5 4.0 3.5 3.0 2.5 2.0 1.5 1.0 0.5
ppm
NO2
Ph
CO2H
2.6k

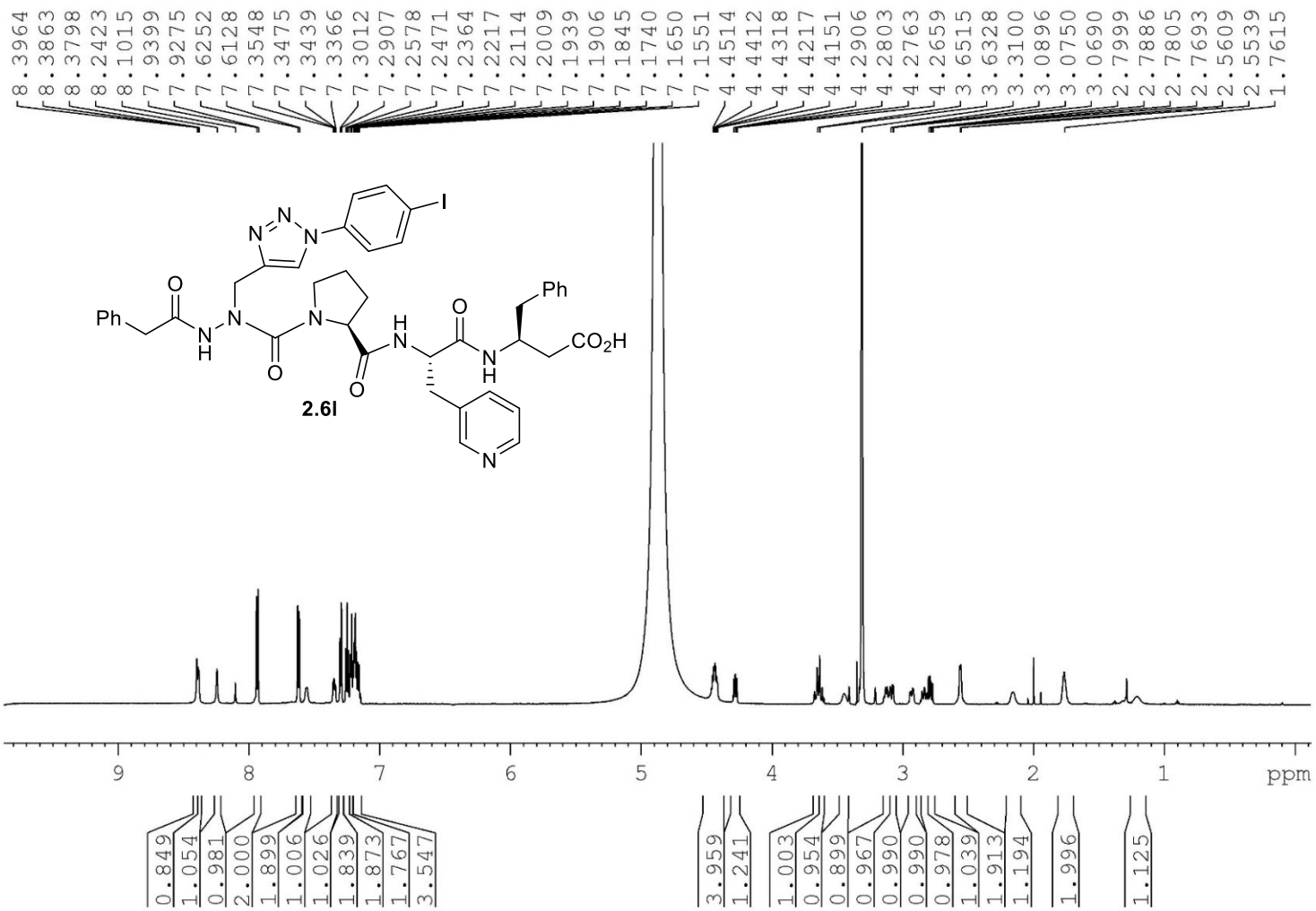
8.3964
8.3863
8.3798
8.2423
8.1015
7.9399
7.9275
7.6252
7.6128
7.3548
7.3475
7.3439
7.3366
7.3012
7.2907
7.2578
7.2471
7.2364
7.2217
7.2114
7.2009
7.1939
7.1906
7.1845
7.1740
7.1650
7.1551
4.4514
4.4412
4.4318
4.4217
4.4151
4.2906
4.2803
4.2763
4.2659
3.6515
3.6328
3.3100
3.0896
3.0750
3.0690
2.7999
2.7886
2.7805
2.7693
2.5609
2.5539
1.7615
2.6l
ppm
0.849
1.054
0.981
2.000
1.899
1.006
1.026
1.839
1.873
1.767
3.547
3.959
1.241
1.003
0.954
0.899
0.967
0.990
0.990
0.978
1.039
1.913
1.194
1.996
1.125

^{13}C NMR 175MHz
Solvent: CD_3OD

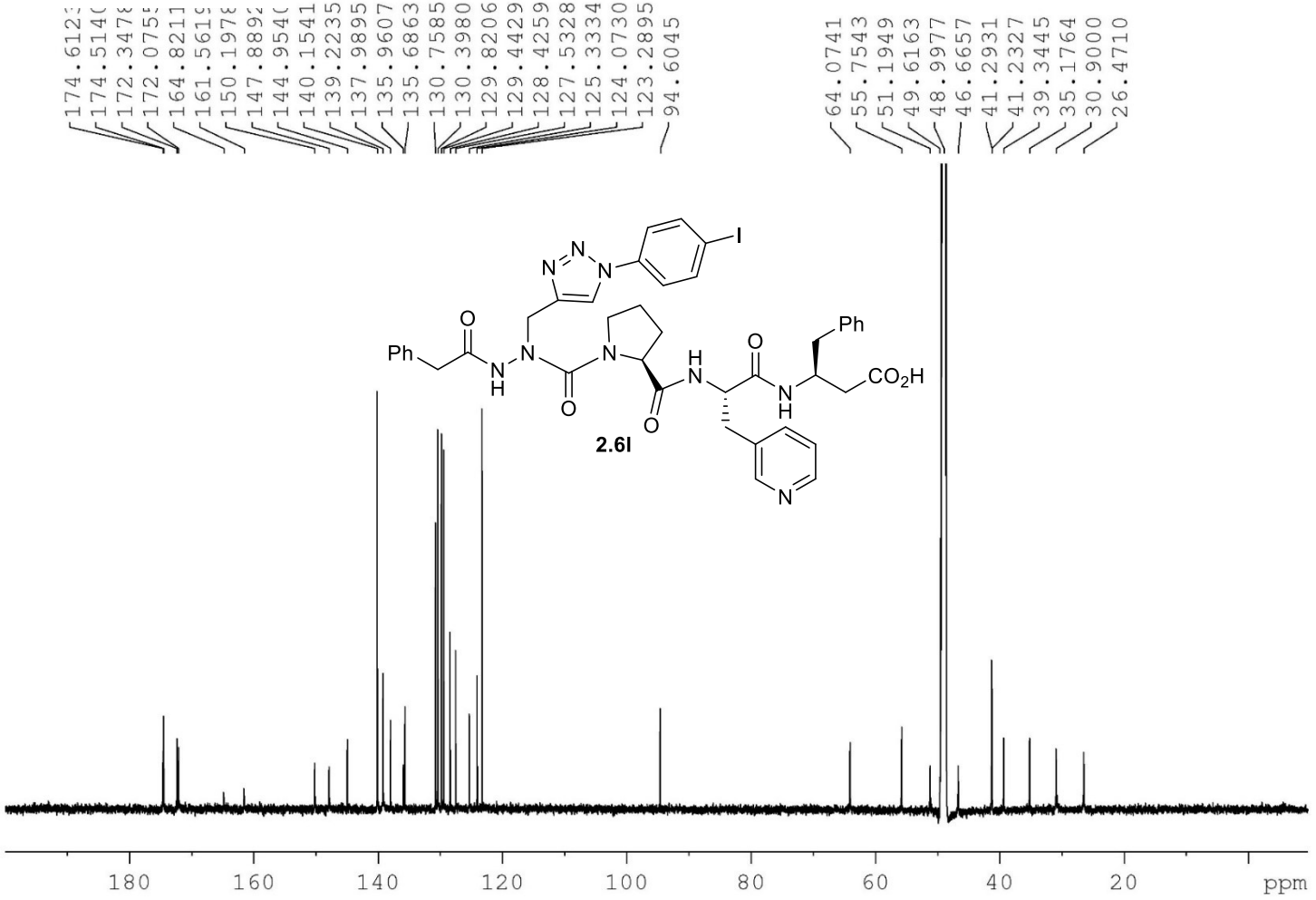

^{1}H NMR 700MHz
Solvent: CD_3OD

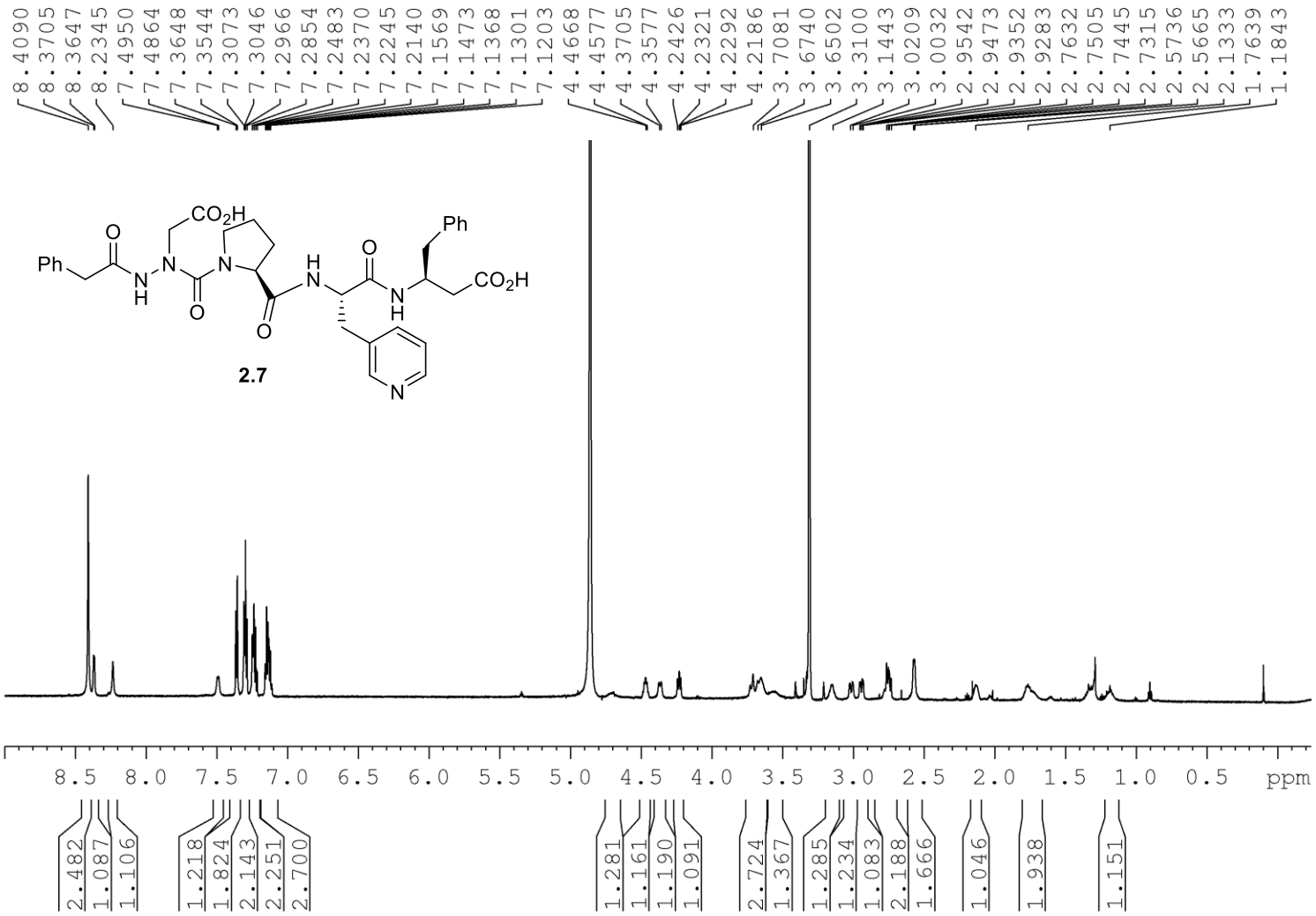

^{1}H NMR 175 MHz
Solvent: CD_3OD

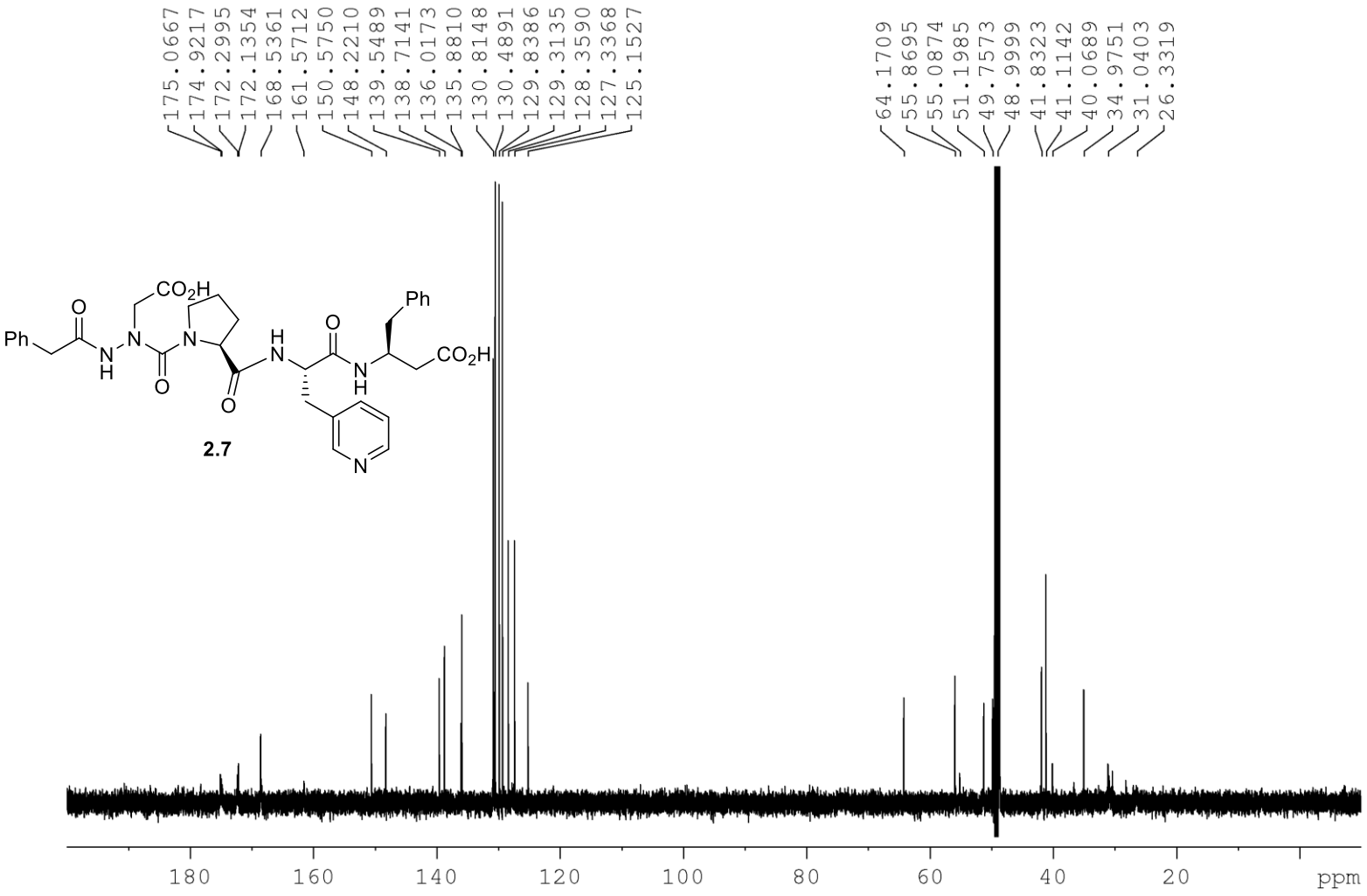

^{1}H NMR 175 MHz
Solvent: CD_3OD

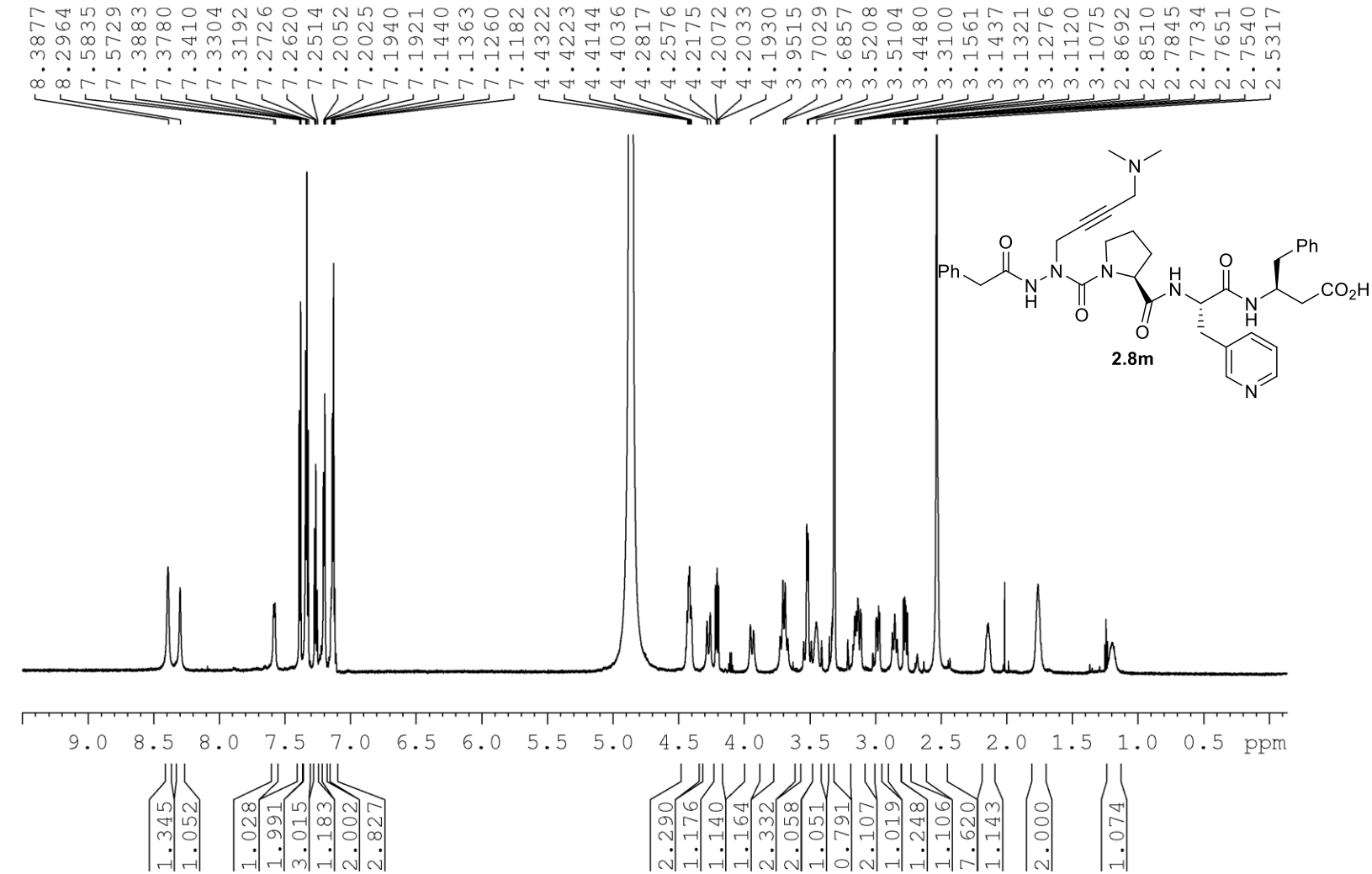

^{13}C NMR 175 MHz

Solvent: CD_3OD

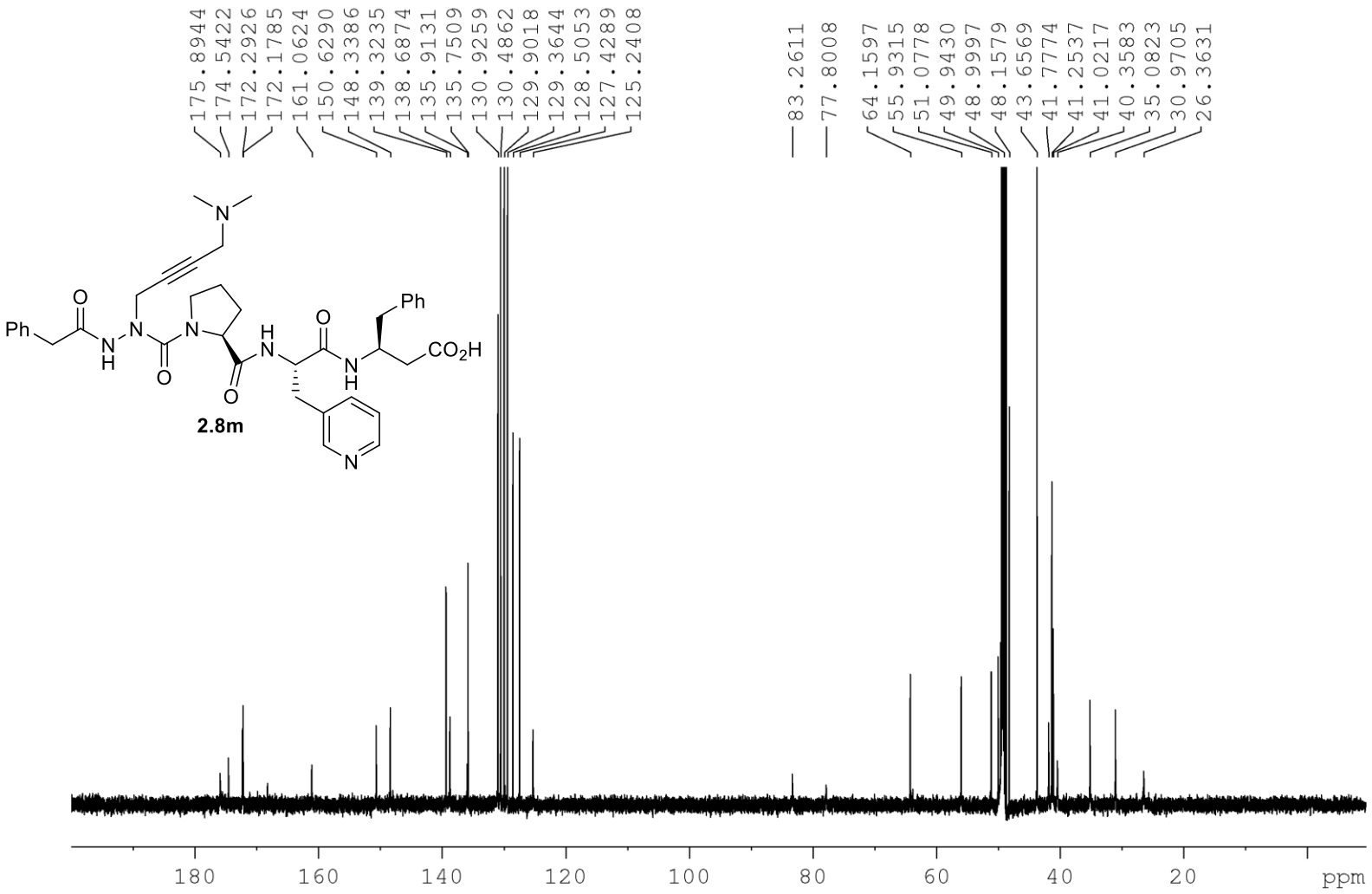

^{1}H NMR 700MHz
Solvent: CD_3OD

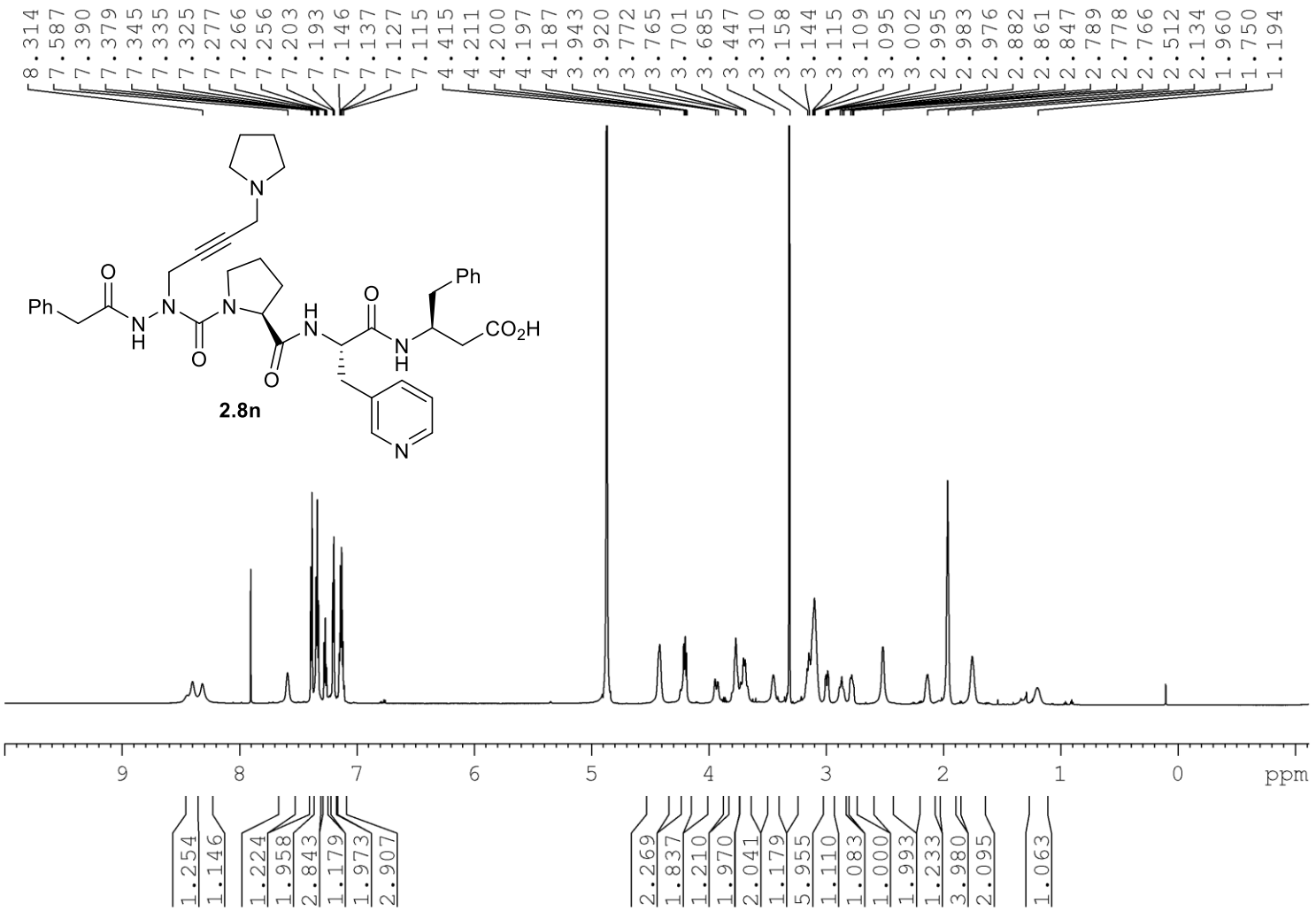

^{13}C NMR 175 MHz

Solvent: CD_3OD

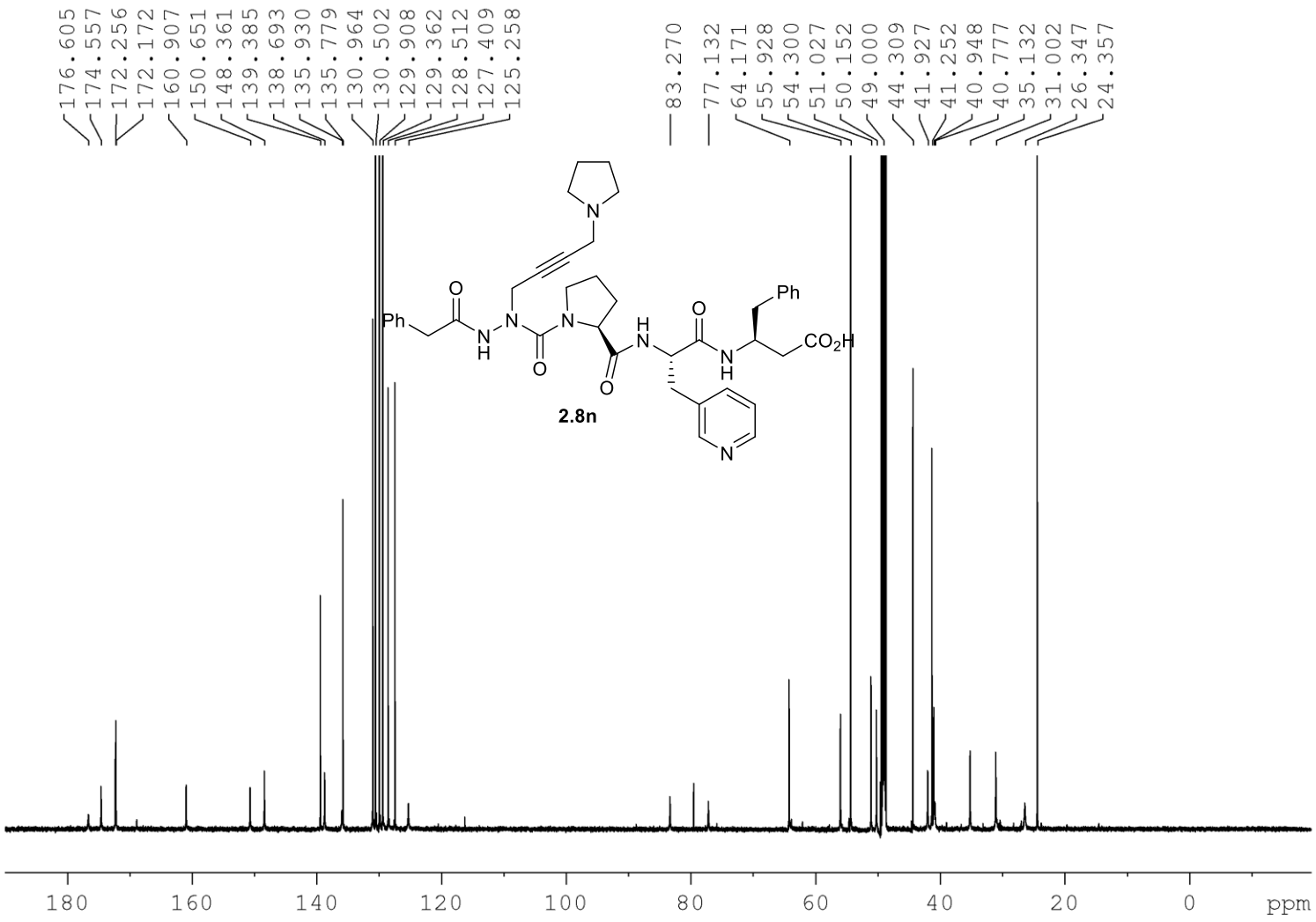

^{1}H NMR 700MHz
Solvent: CD_3OD

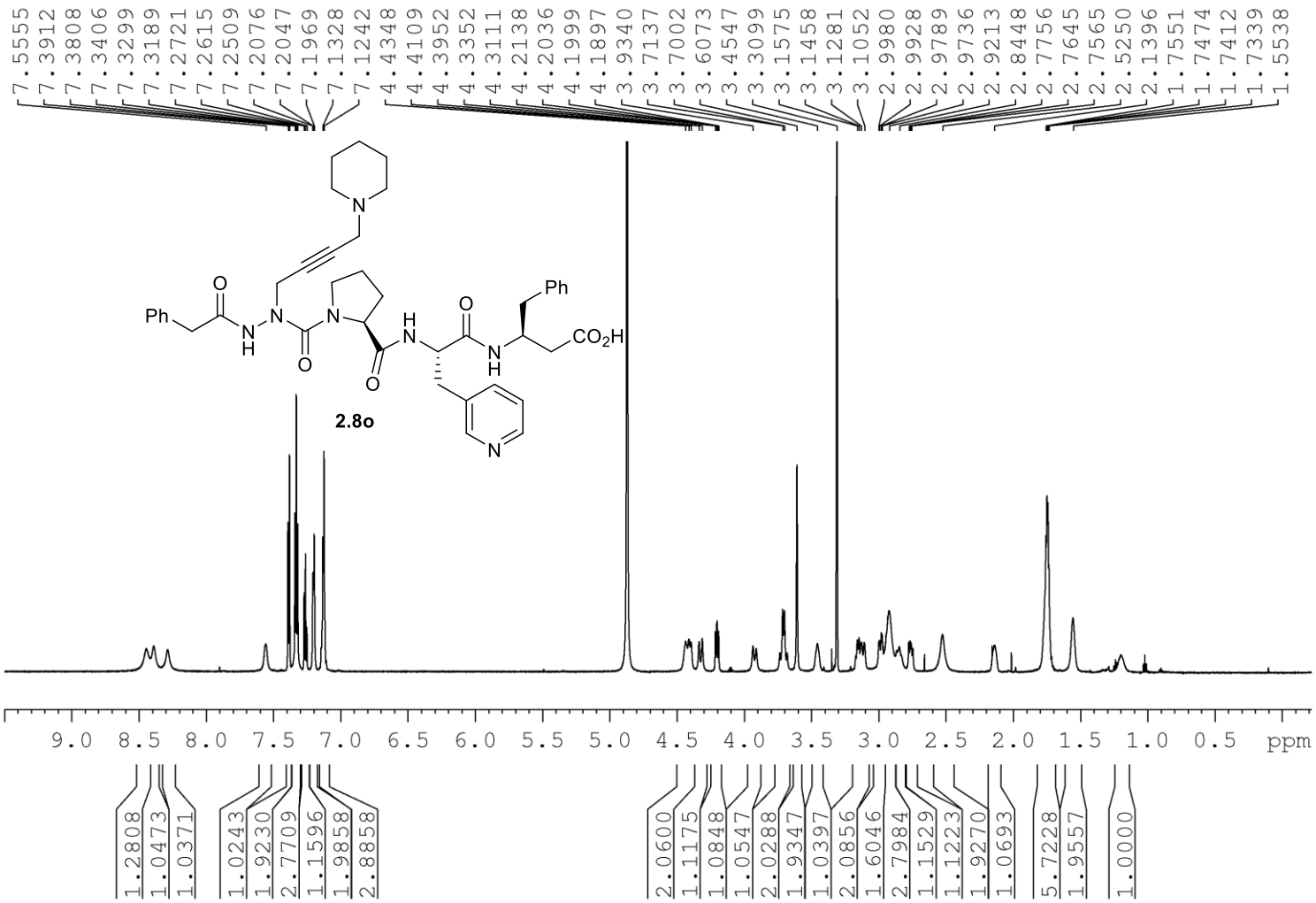

^{13}C NMR 175MHz

Solvent: CD_3OD

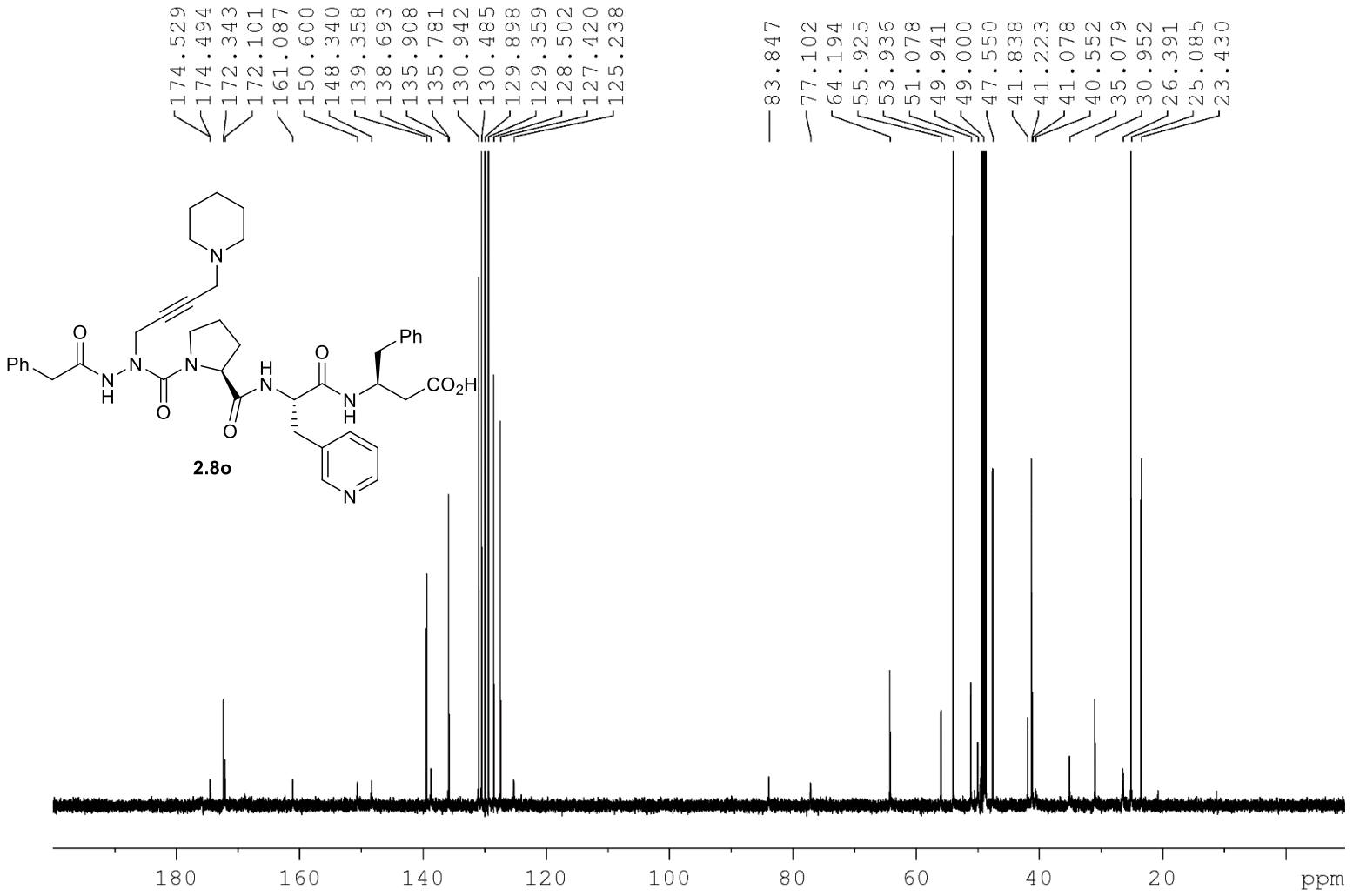

^{1}H NMR 700MHz
Solvent: CD_3OD

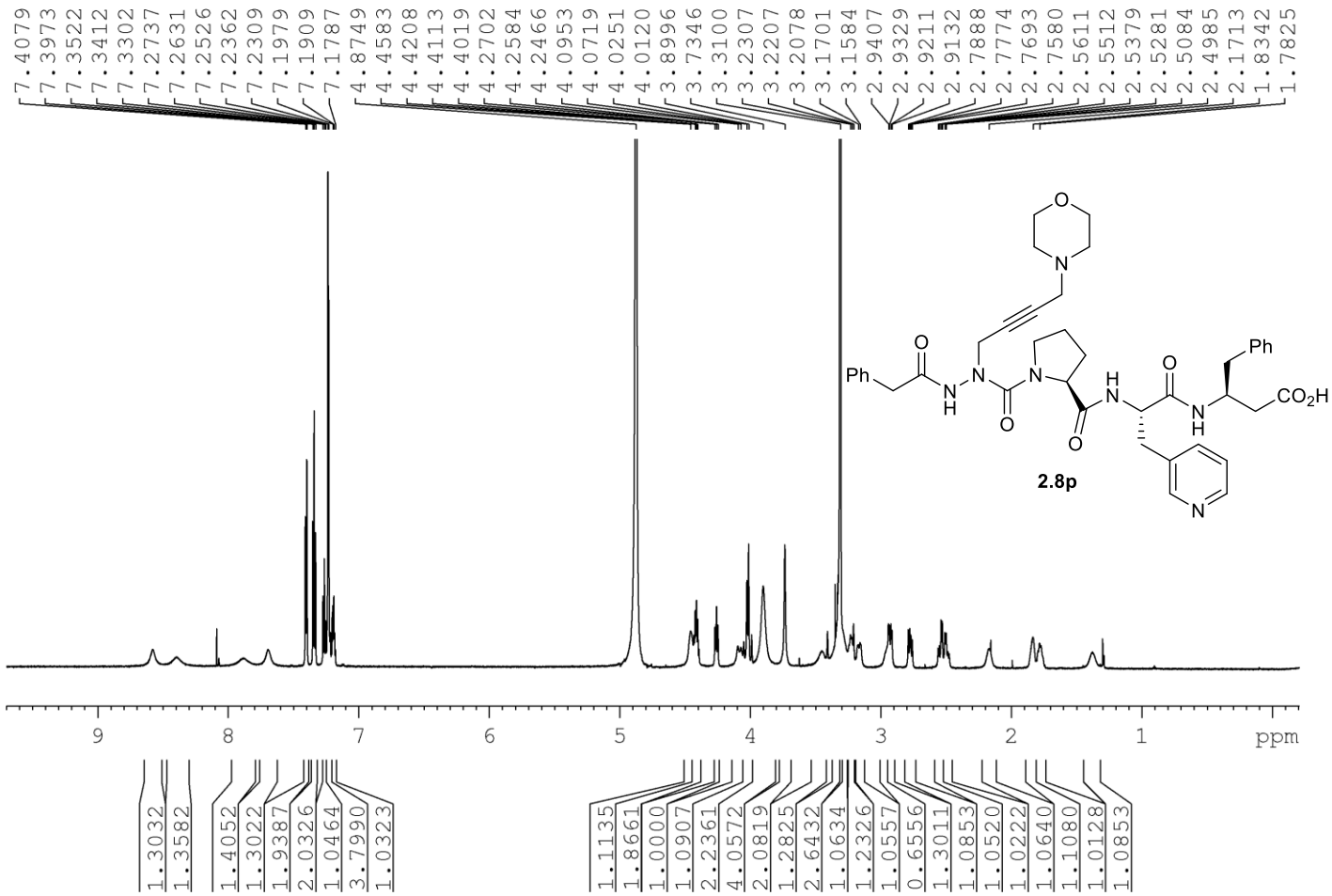

^{13}C NMR 175MHz

Solvent: CD_3OD

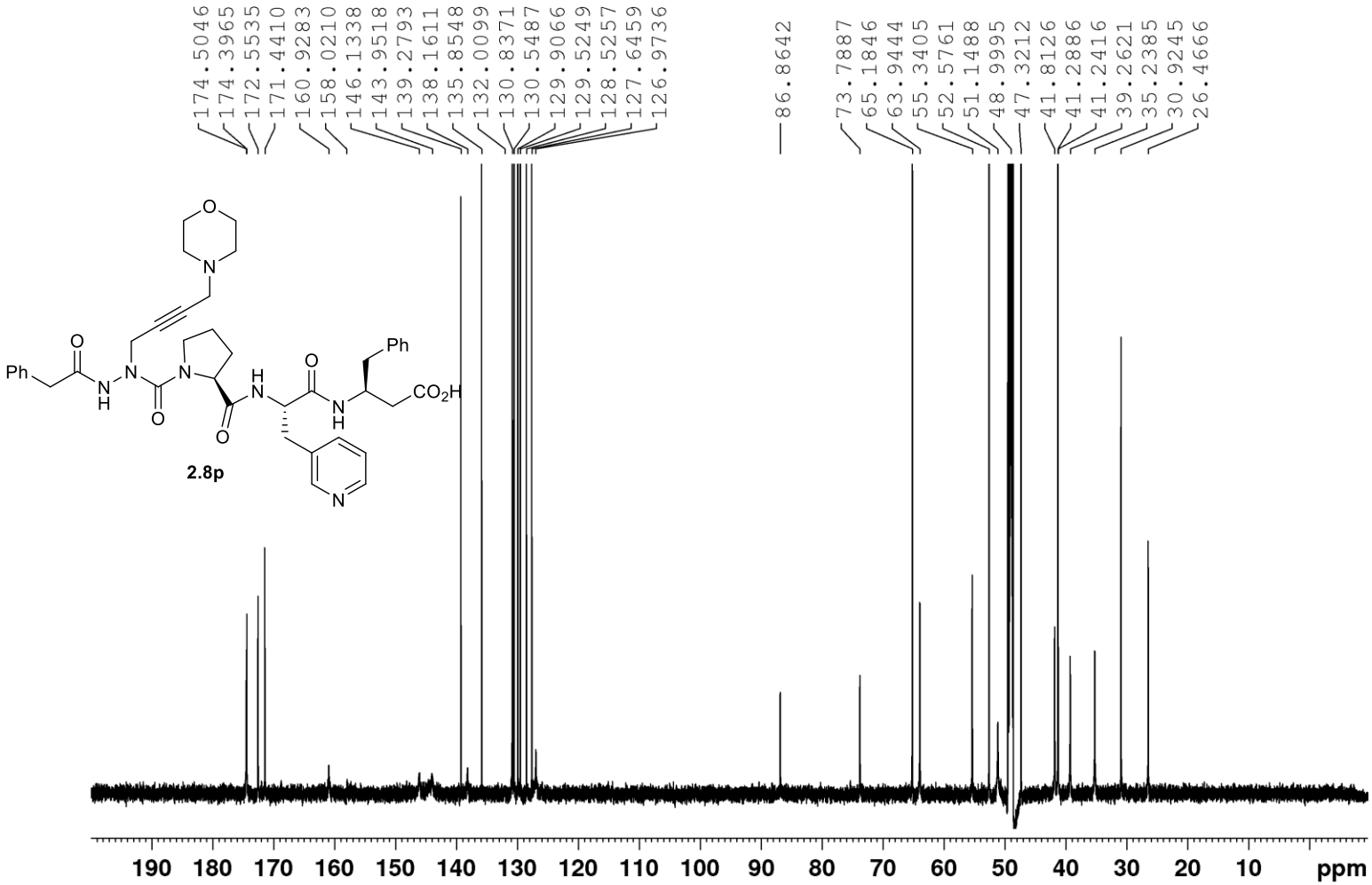

^{1}H NMR 700MHz
Solvent: CD_3OD

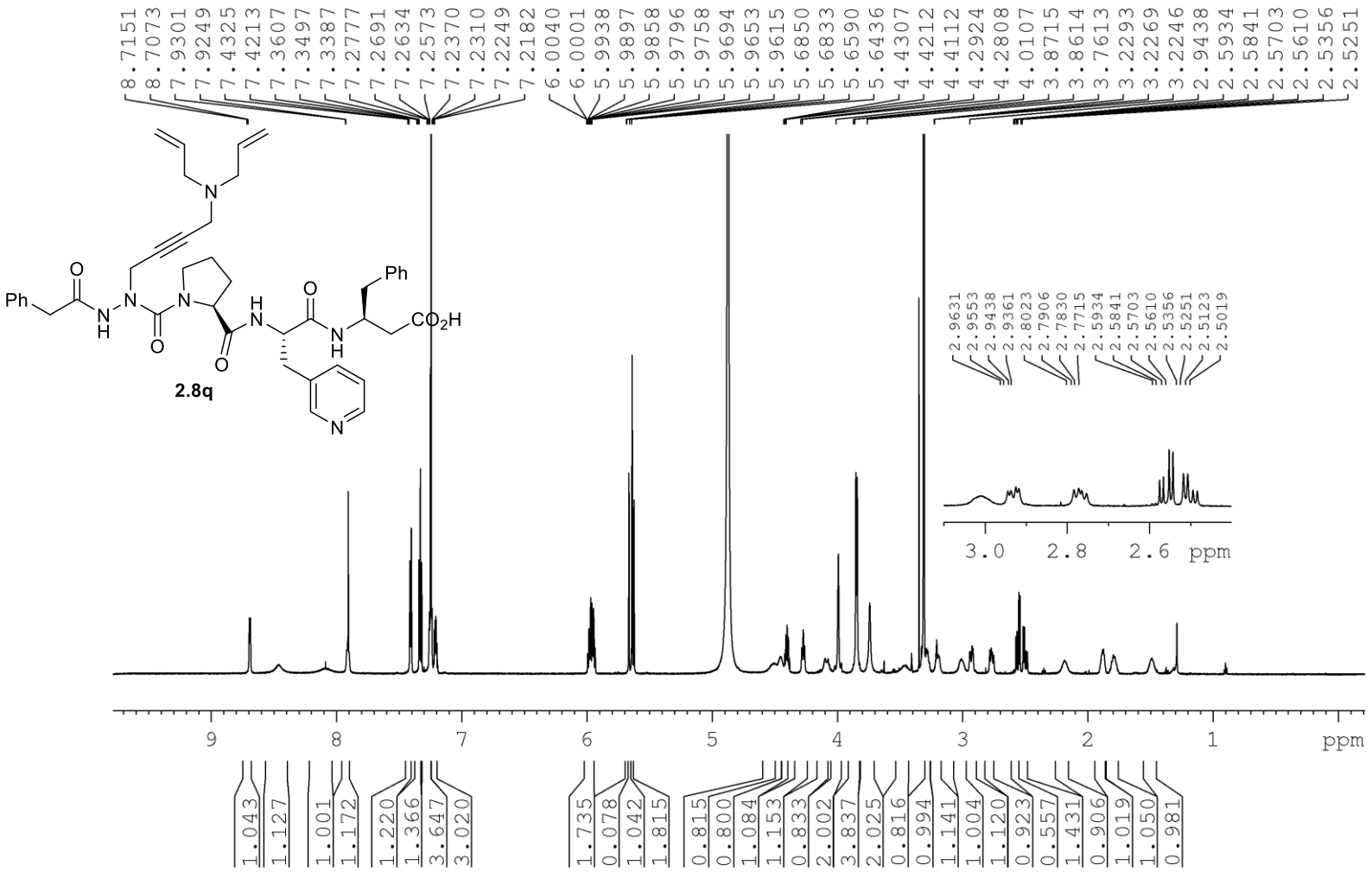

^{13}C NMR 175MHz

Solvent: CD_3OD

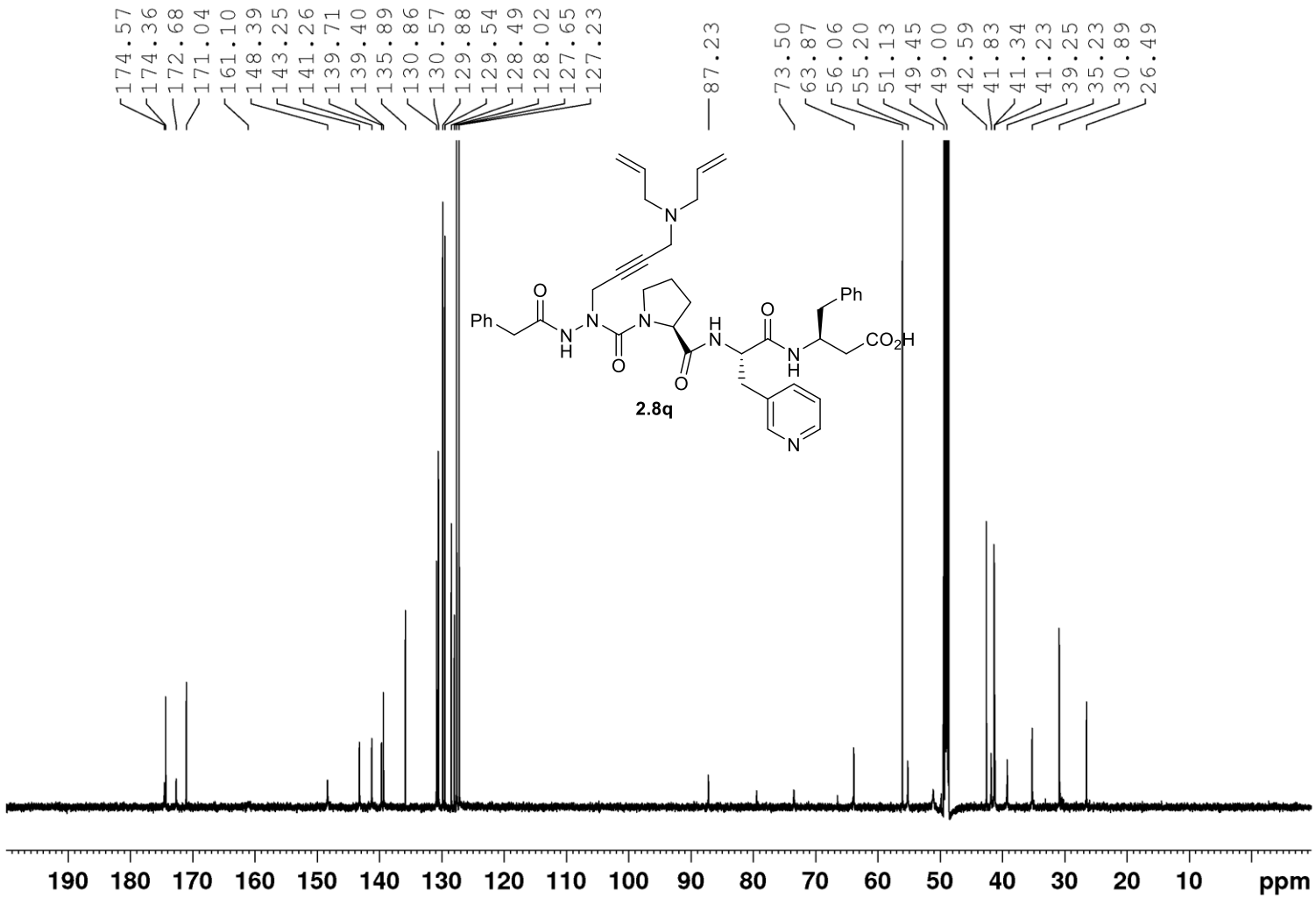

^{1}H NMR 700MHz
Solvent: CD_3OD

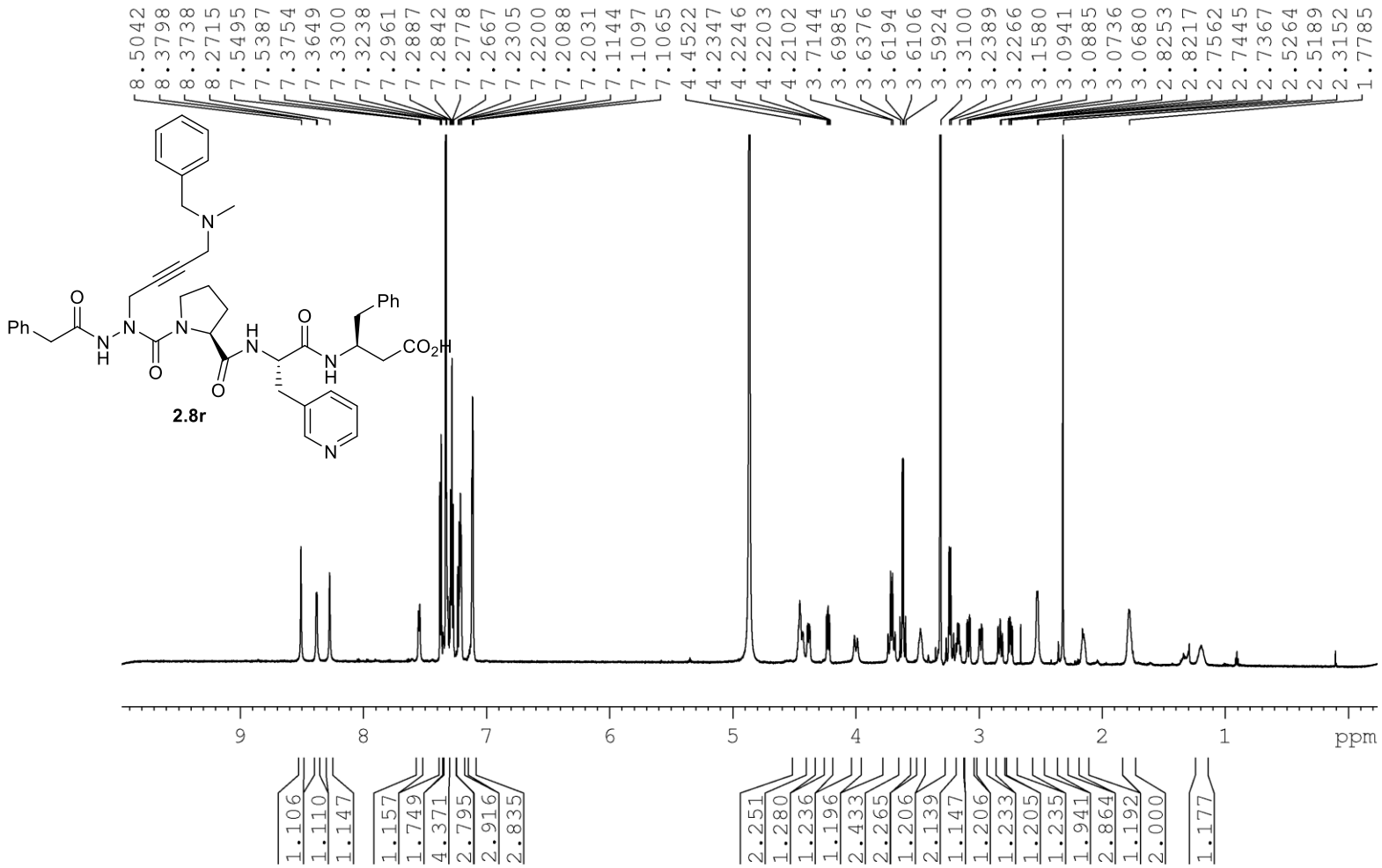

^{13}C NMR 175MHz

Solvent: CD_3OD

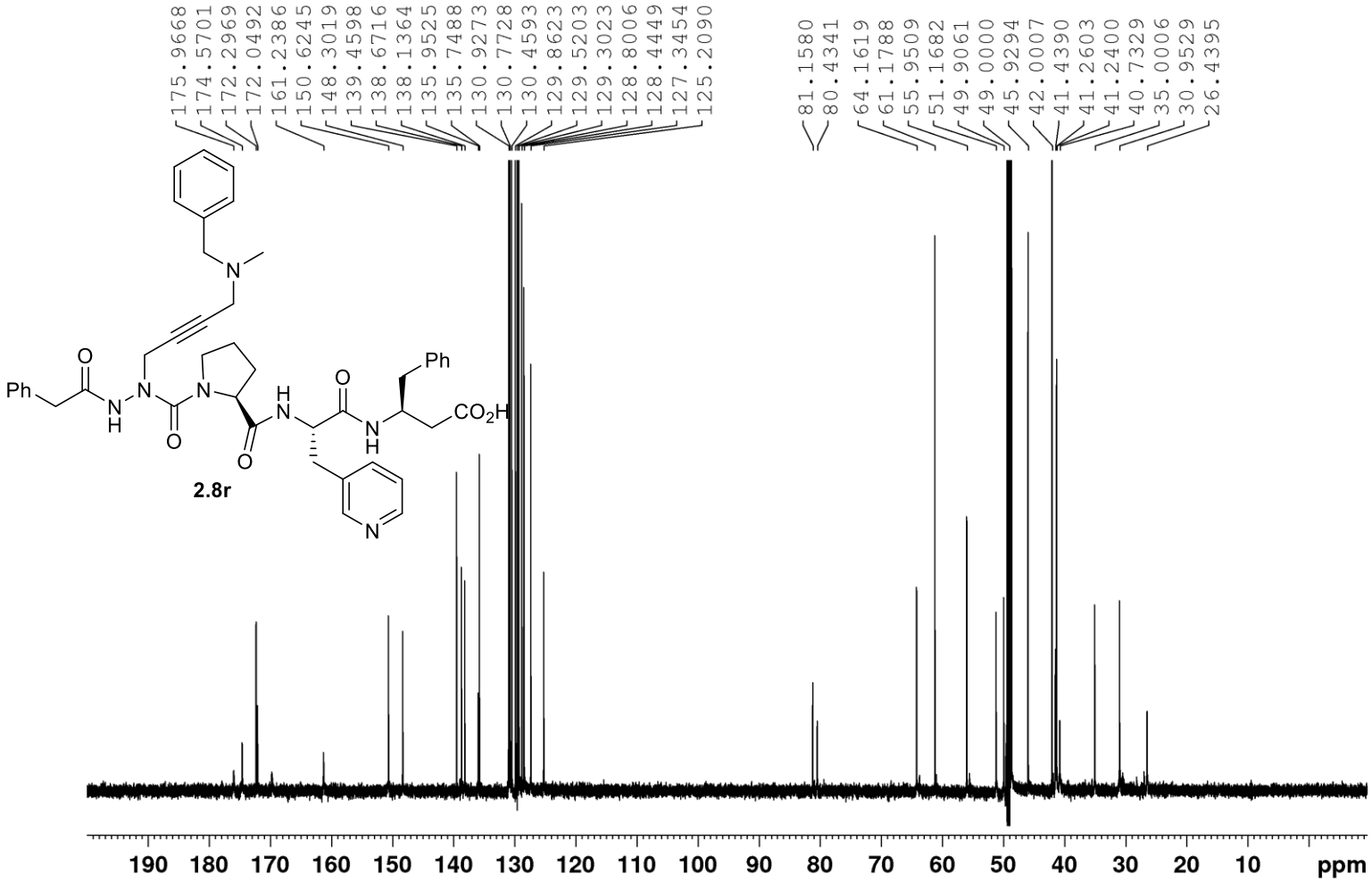

^{1}H NMR 700MHz
Solvent: CD_3OD

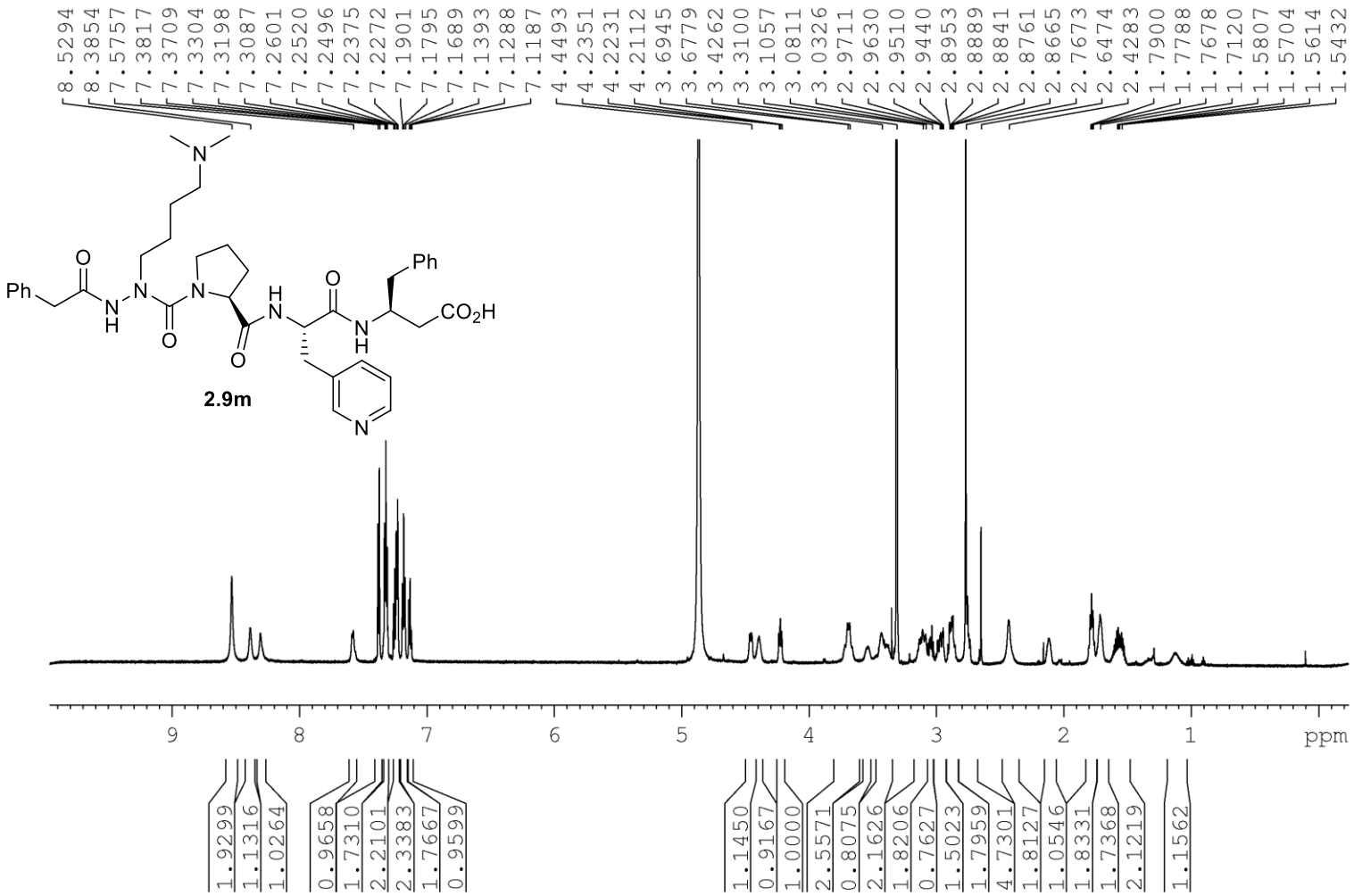

^{13}C NMR 175MHz

Solvent: CD_3OD

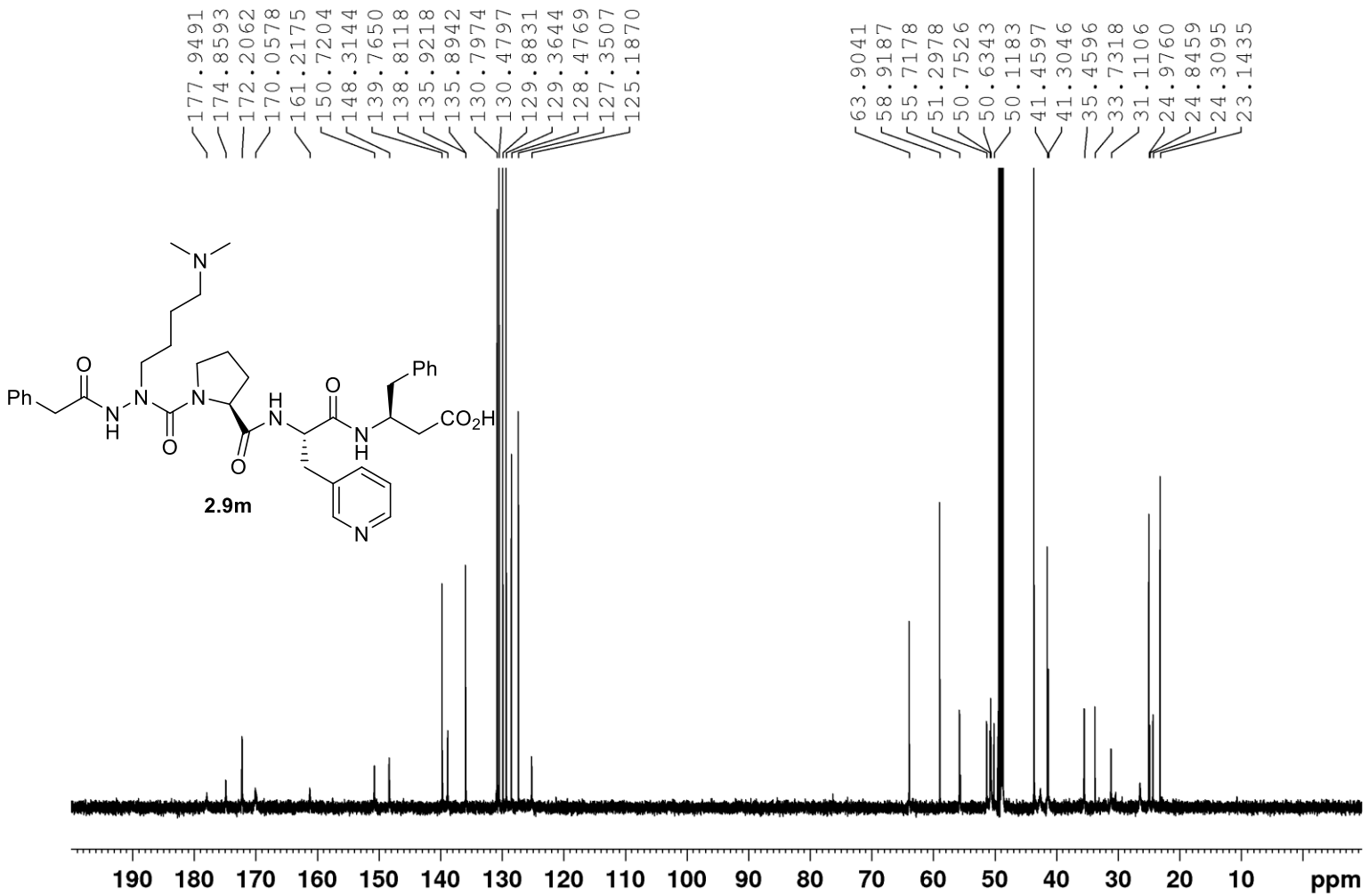

^{1}H NMR 700MHz
Solvent: CD_3OD

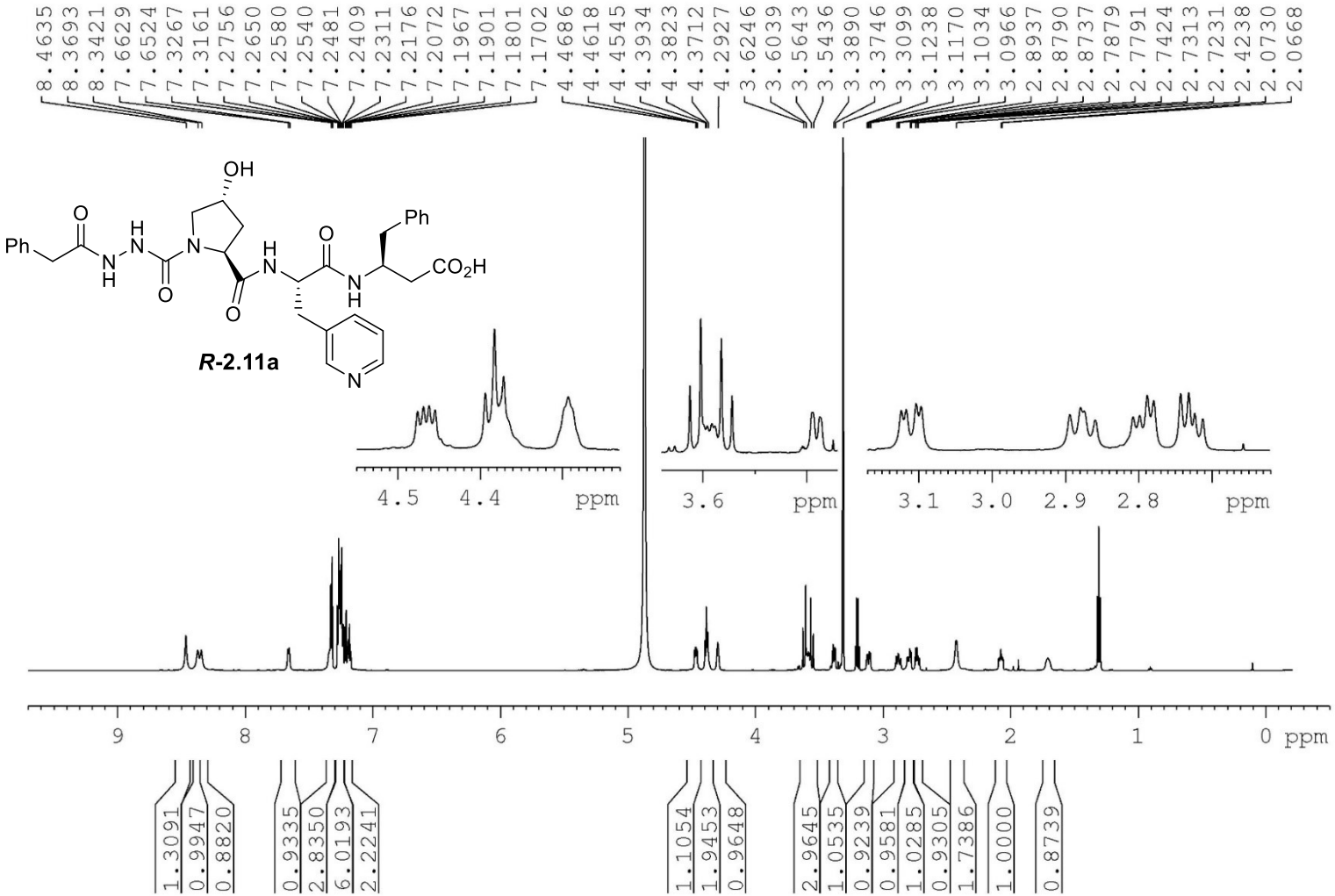

^{13}C NMR 175 MHz

Solvent: CD_3OD

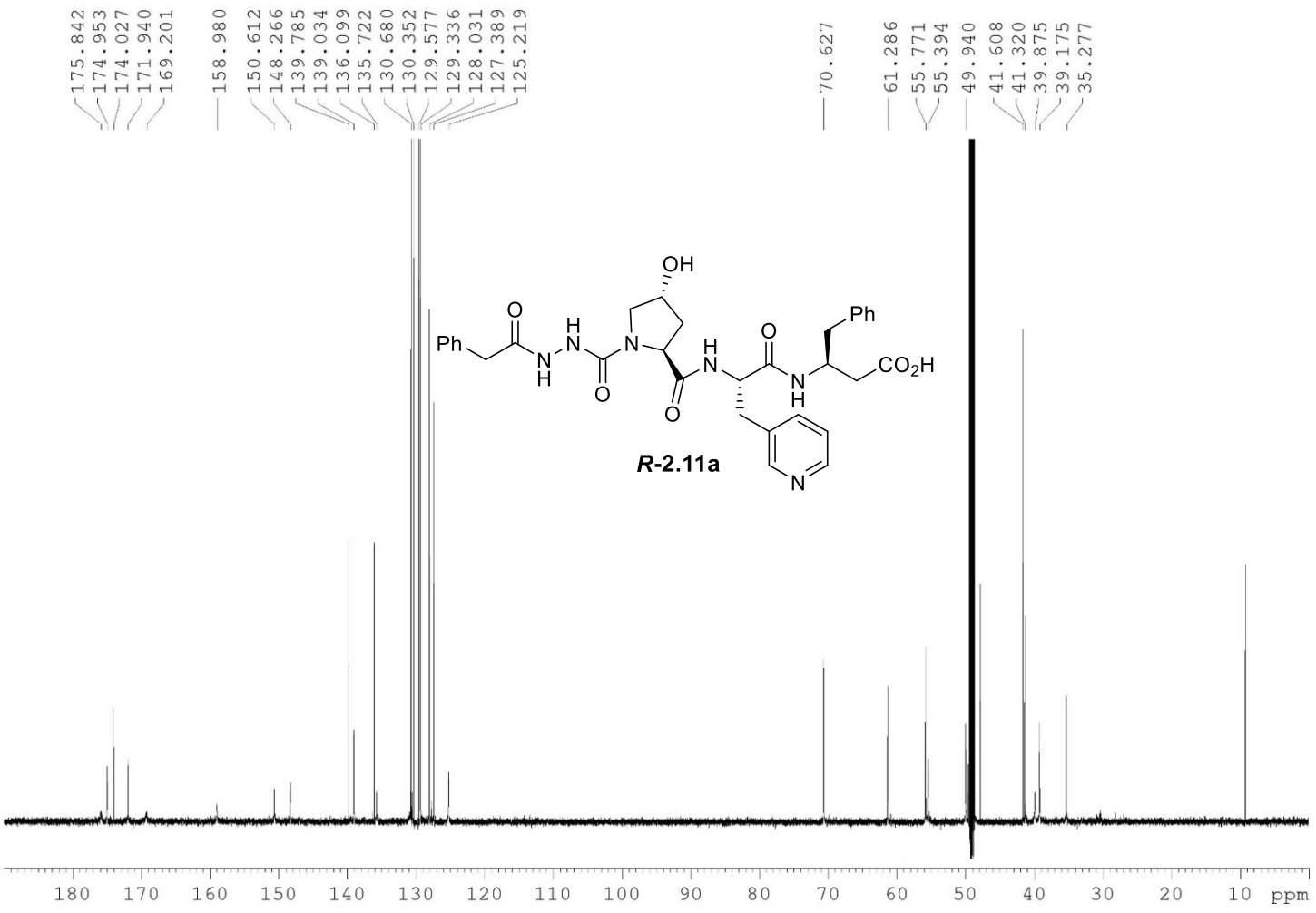

^{1}H NMR 700MHz
Solvent: CD_3OD

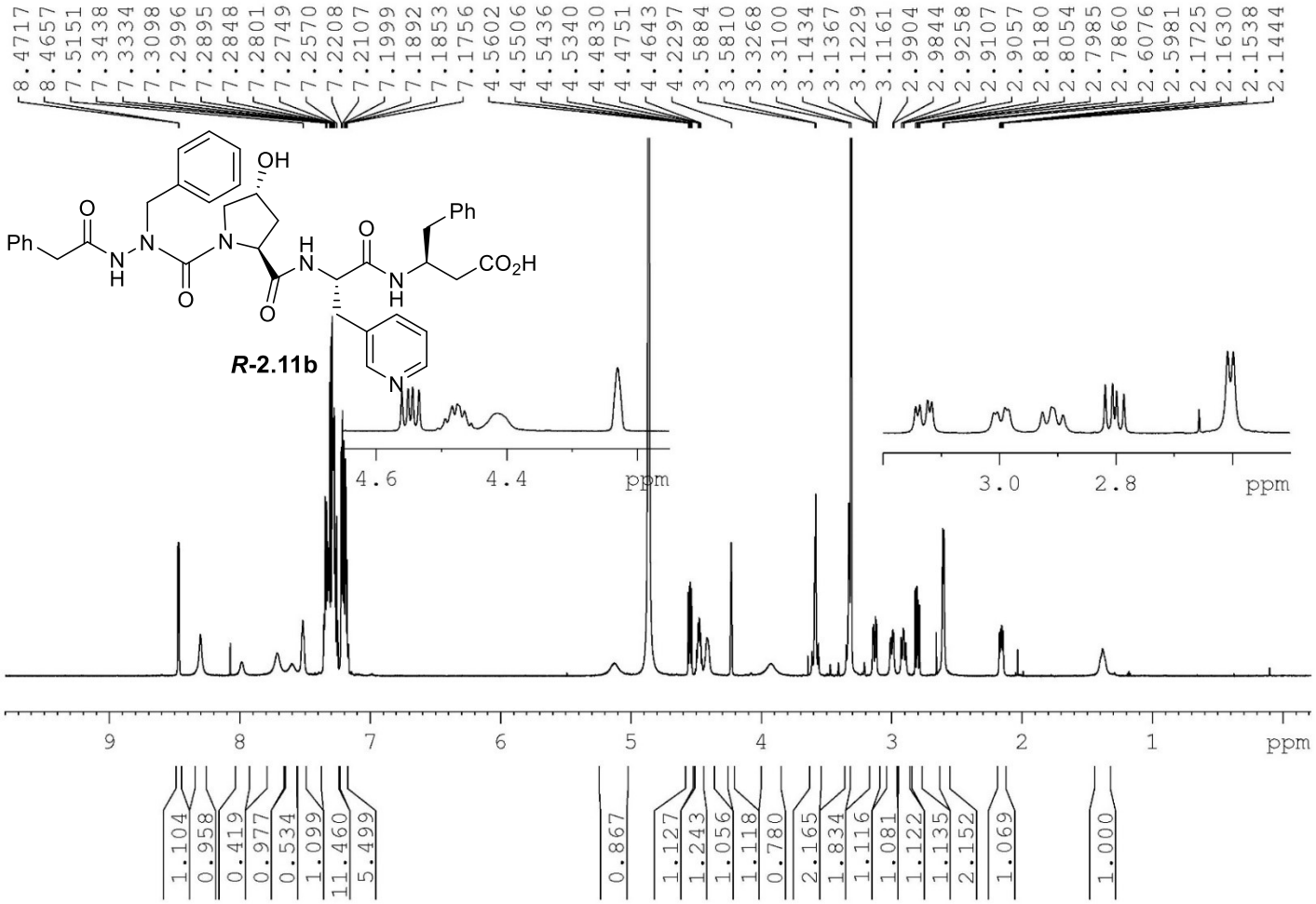

^{13}C NMR 175 MHz

Solvent: CD_3OD

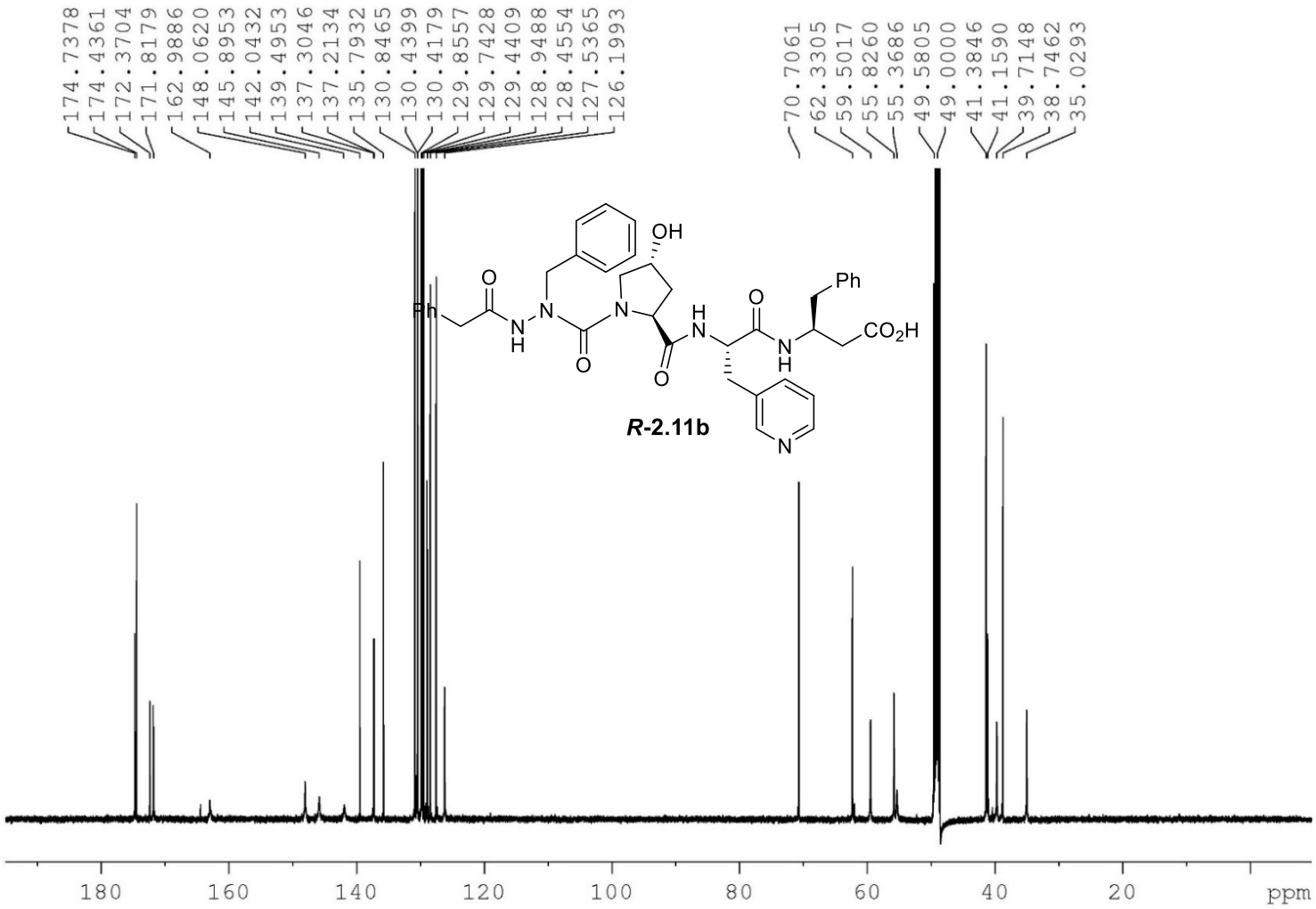

^{1}H NMR 700MHz
Solvent: CD_3OD

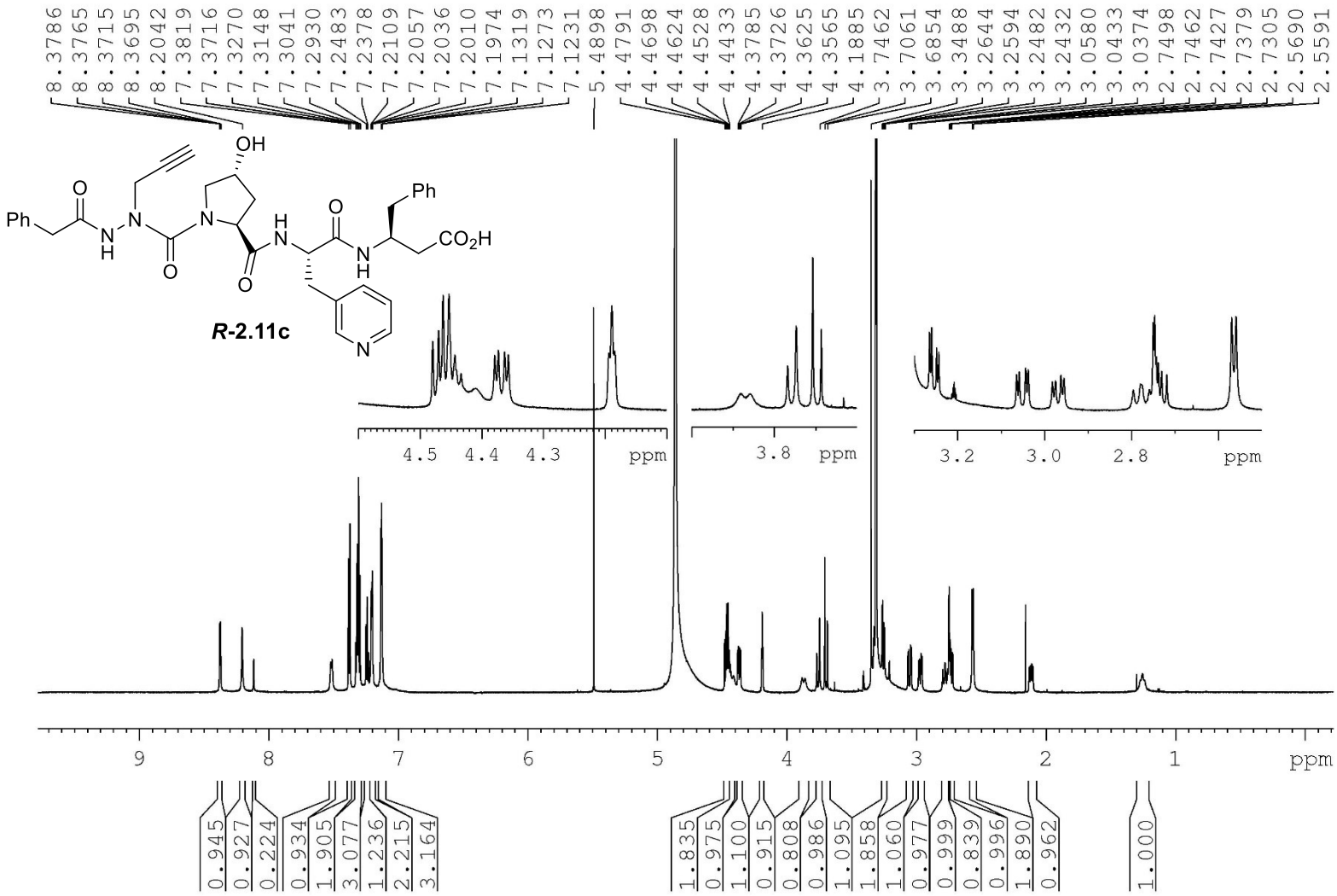

^{13}C NMR 175 MHz

Solvent: CD_3OD

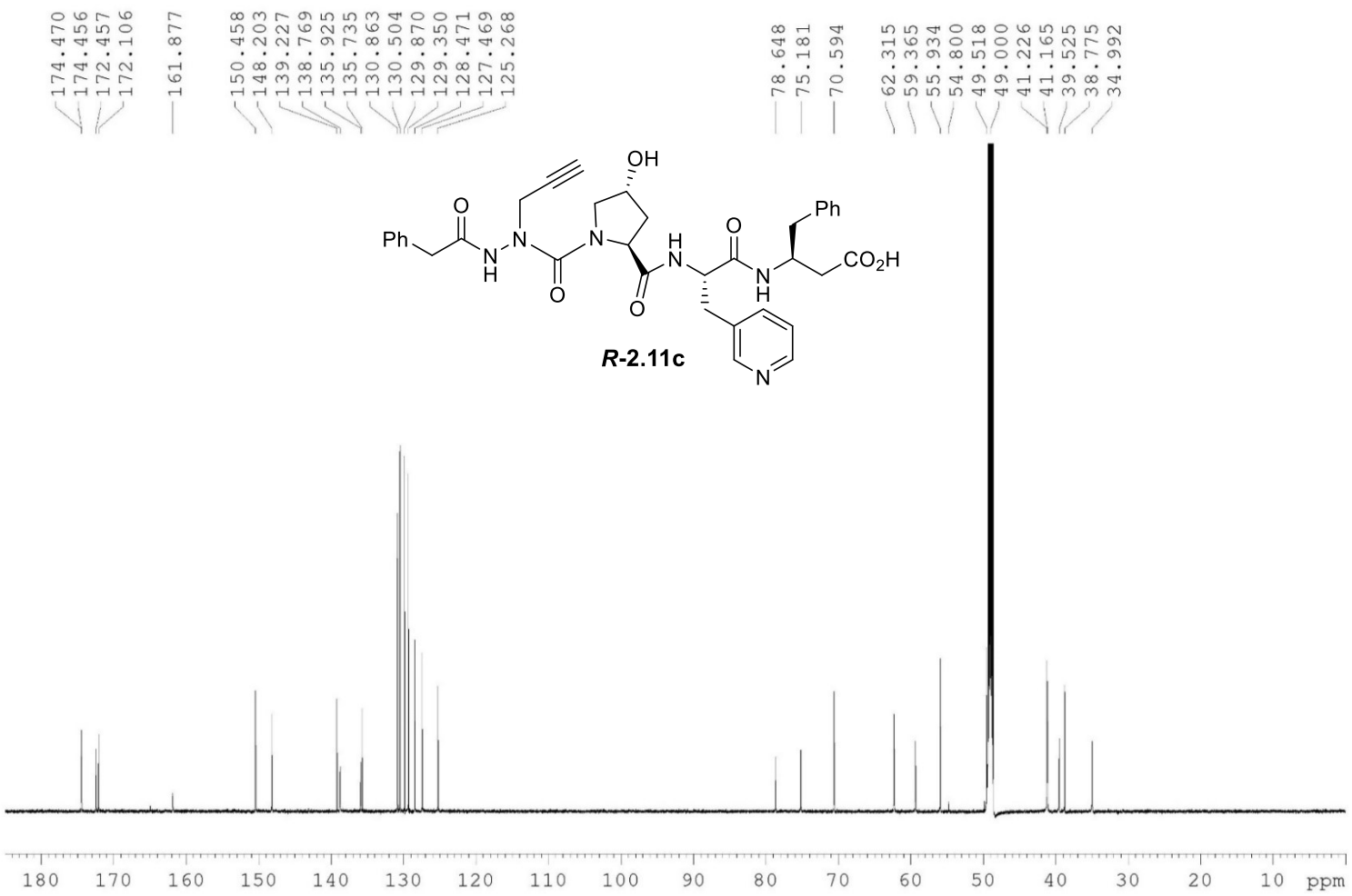

^{1}H NMR 700MHz
Solvent: CD_3OD

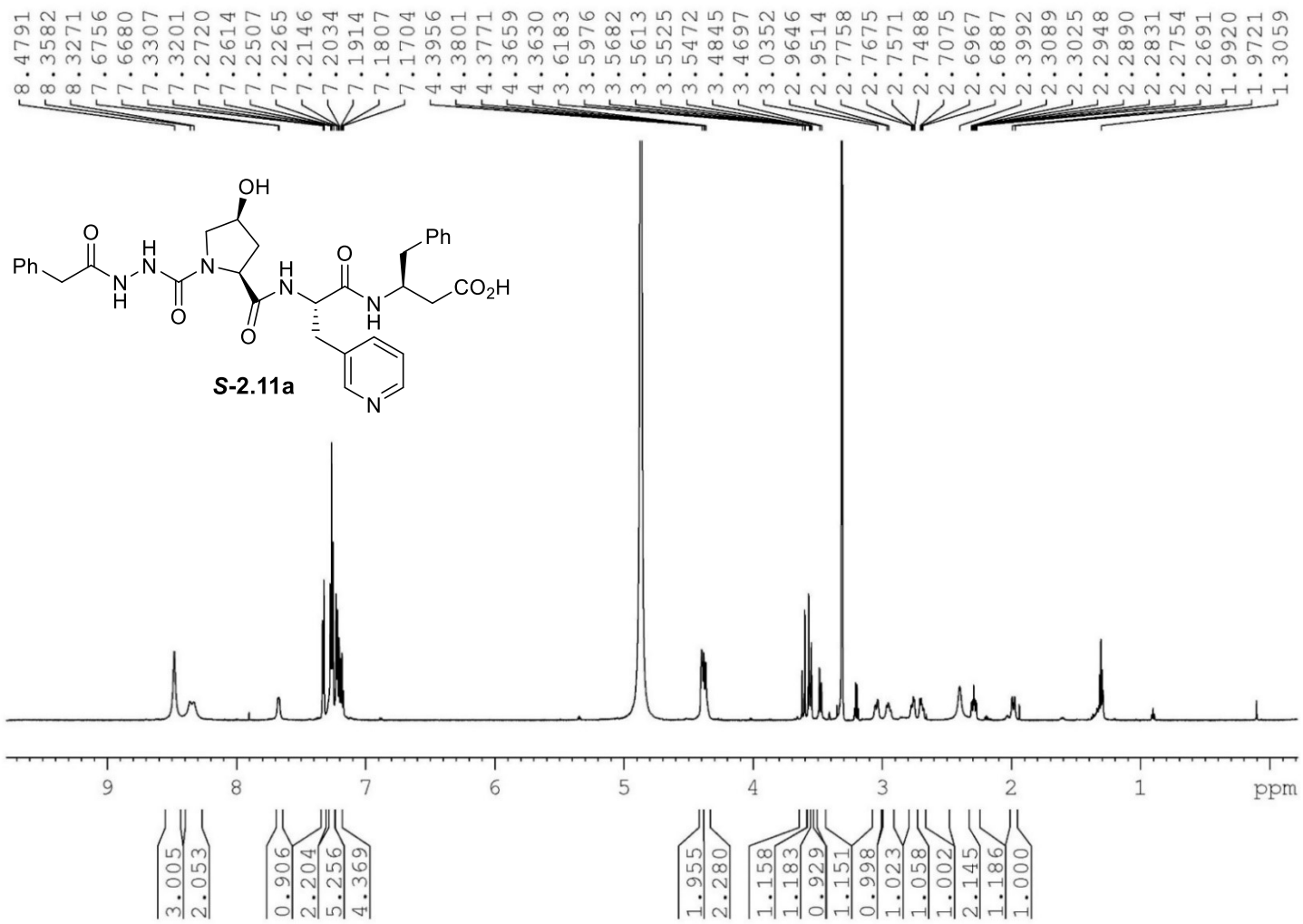

^{13}C NMR 175 MHz

Solvent: CD_3OD

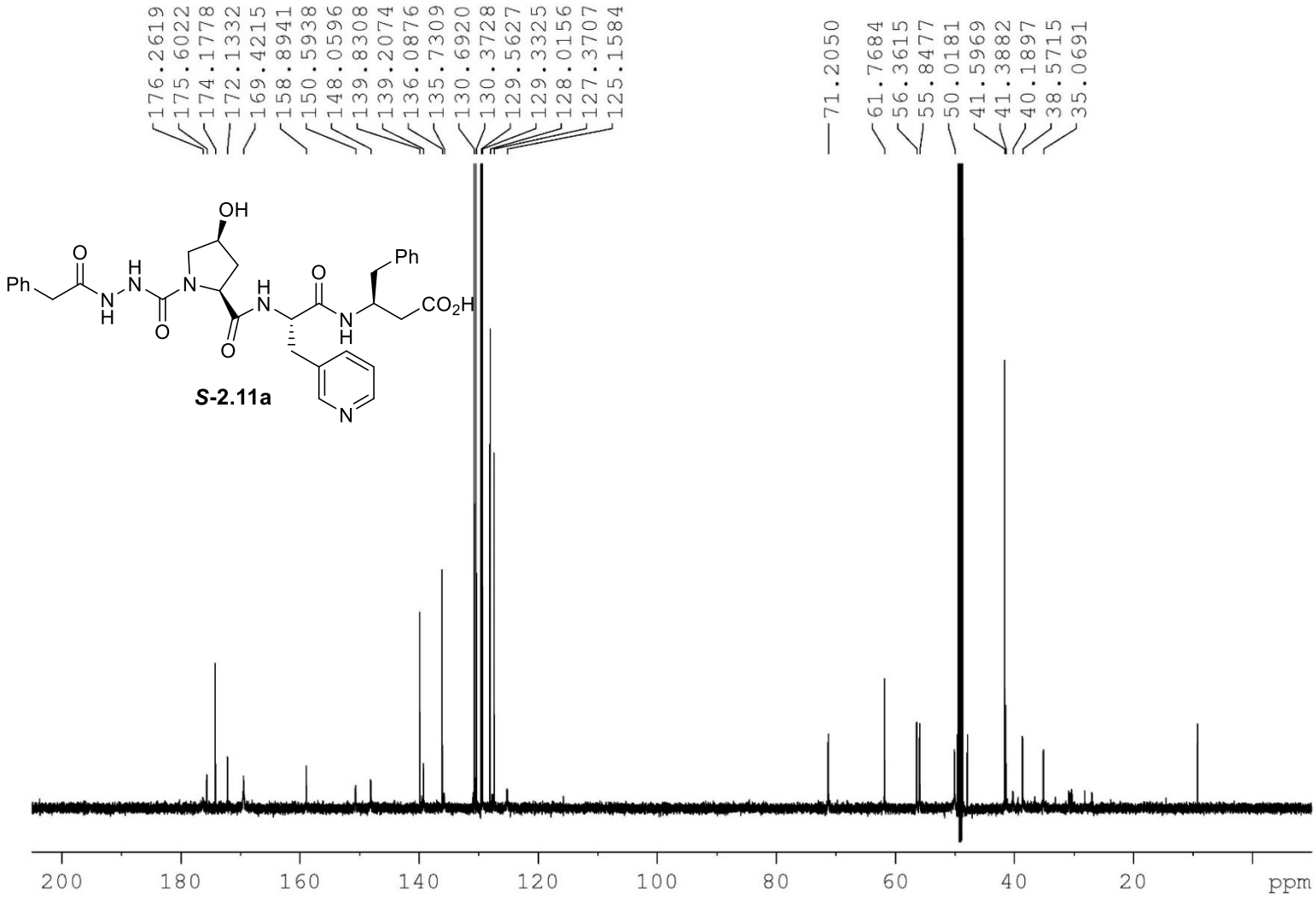

^{1}H NMR 700MHz
Solvent: CD_3OD

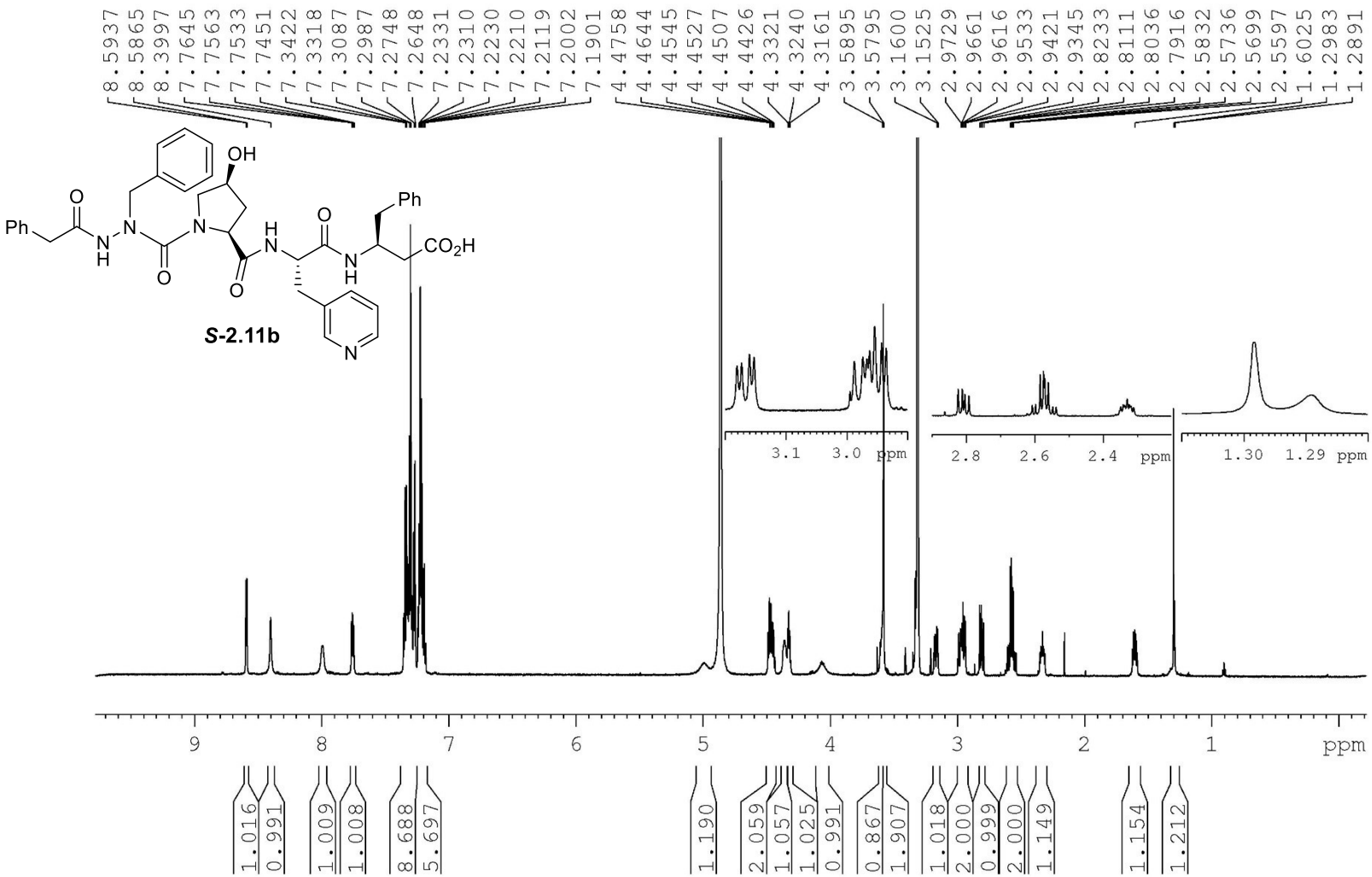

^{13}C NMR 175 MHz

Solvent: CD_3OD

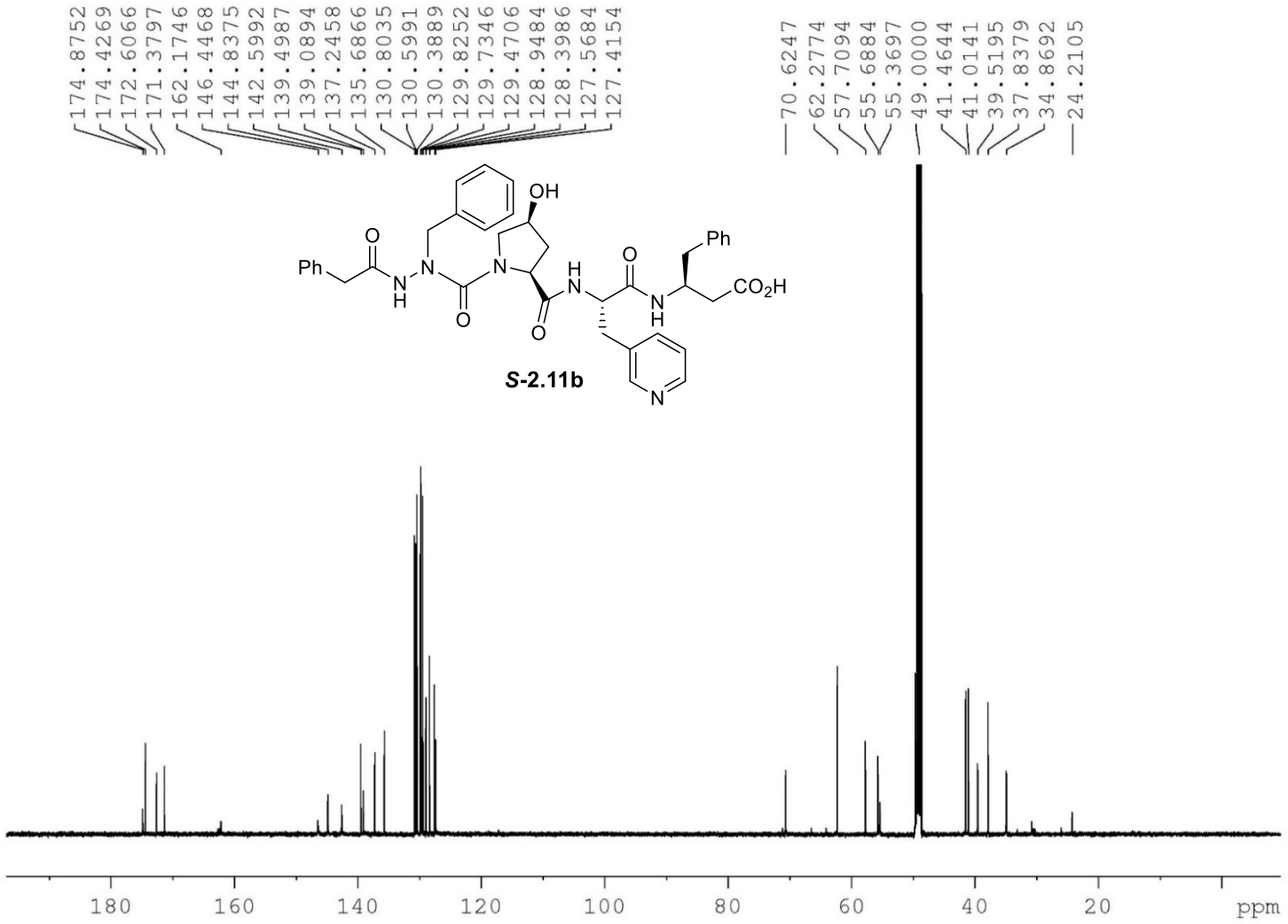

^{1}H NMR 700MHz
Solvent: CD_3OD

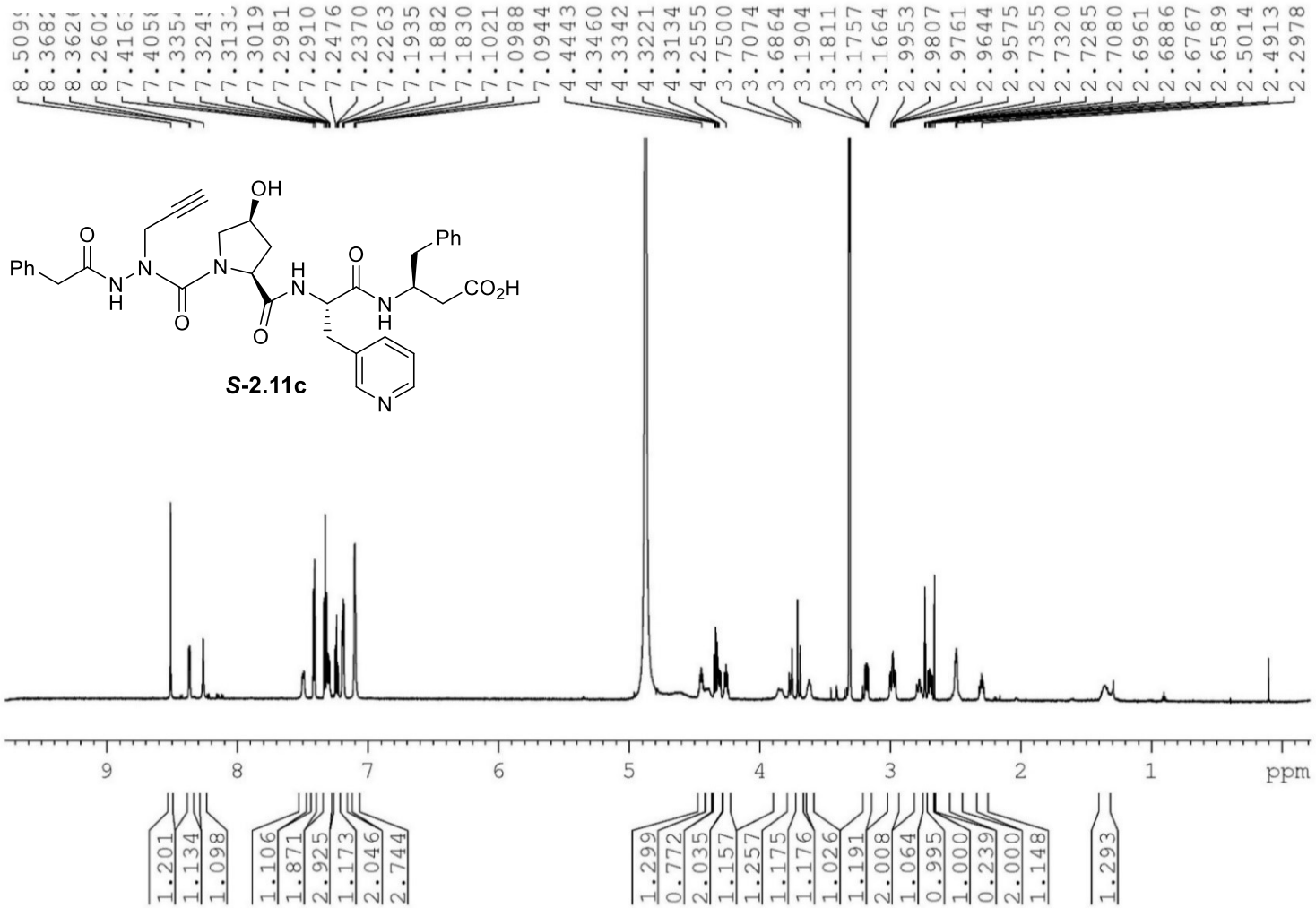

^{13}C NMR 175 MHz

Solvent: CD_3OD

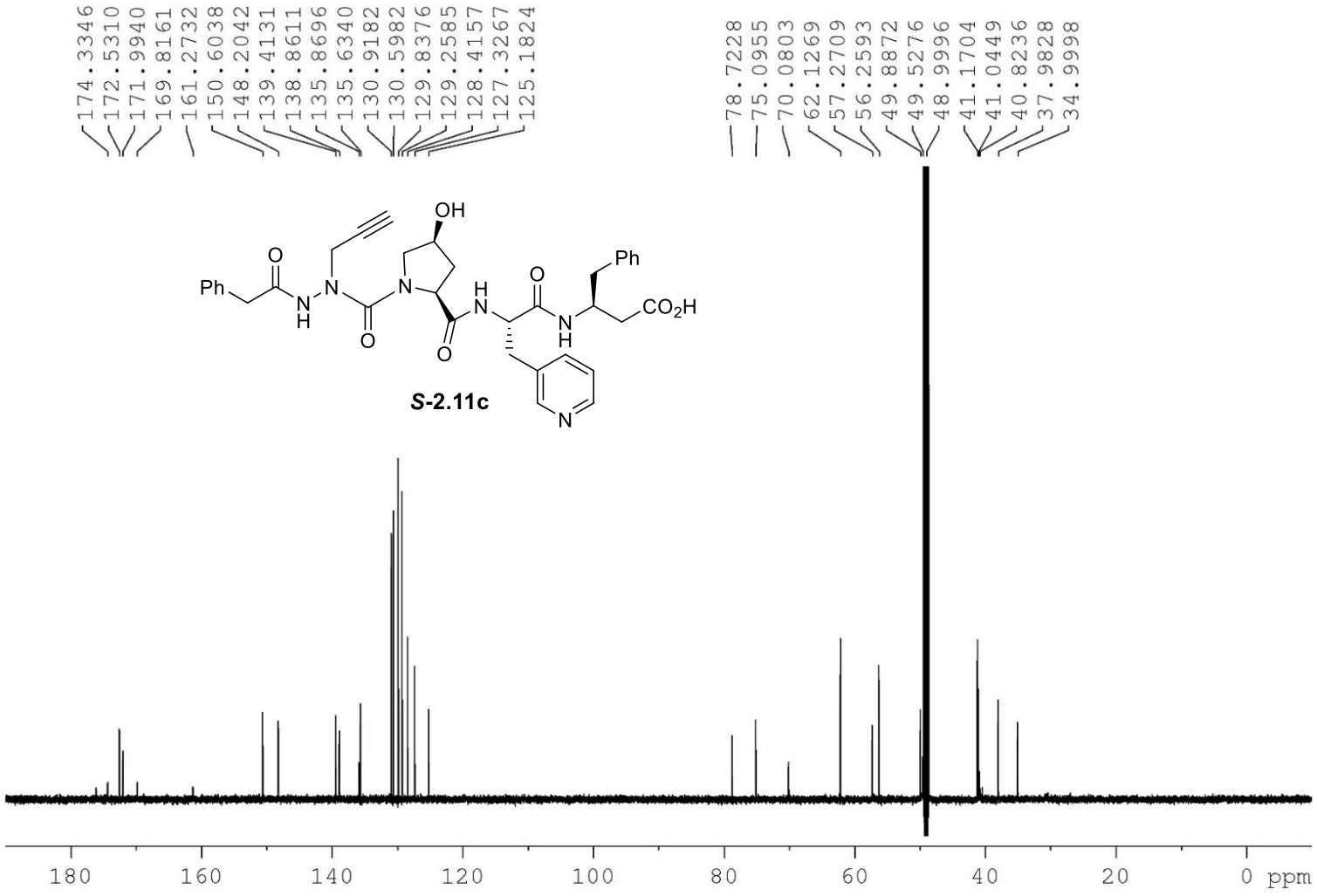

^{1}H NMR 700MHz
Solvent: CD_3OD

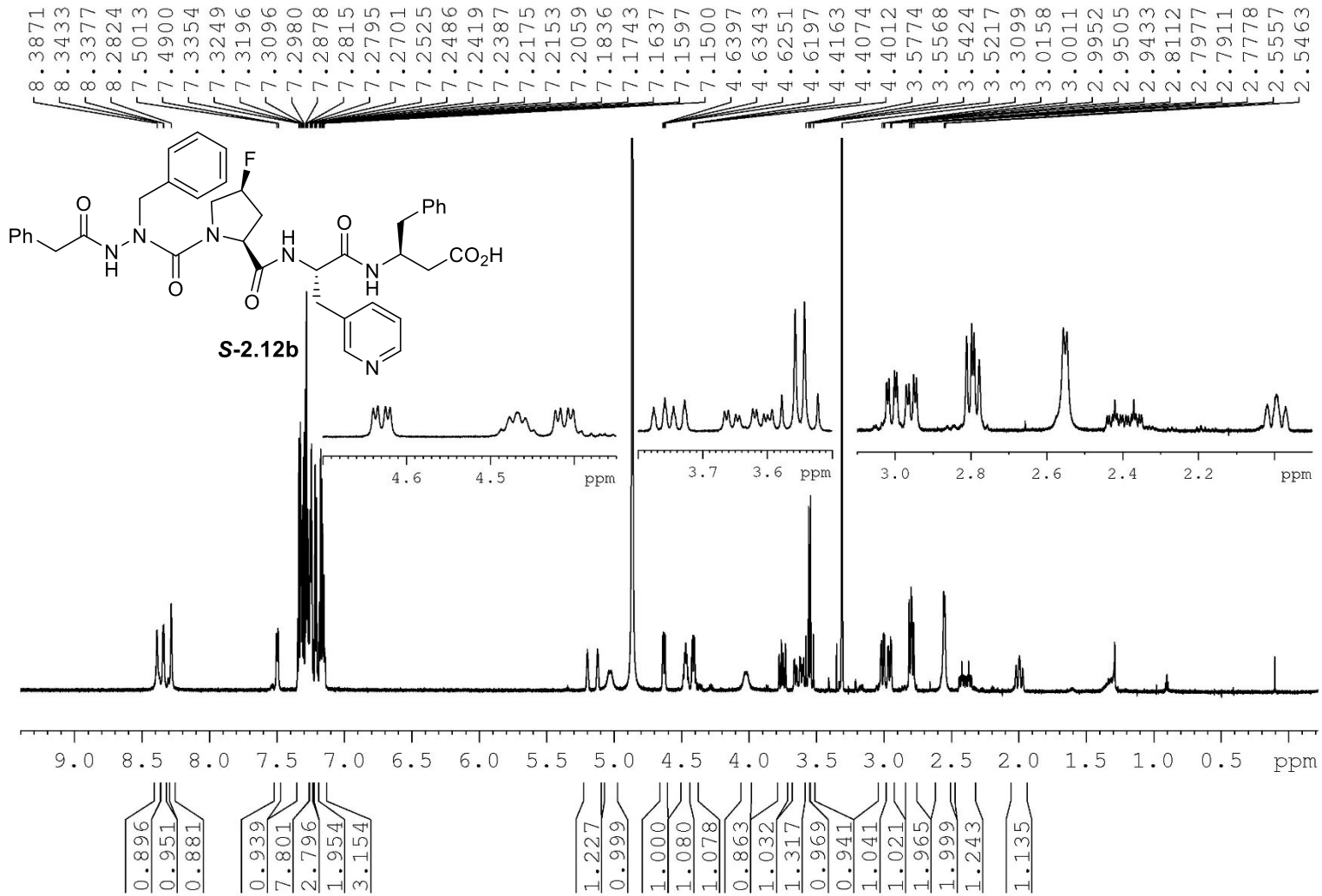

^{13}C NMR 175 MHz

Solvent: CD_3OD

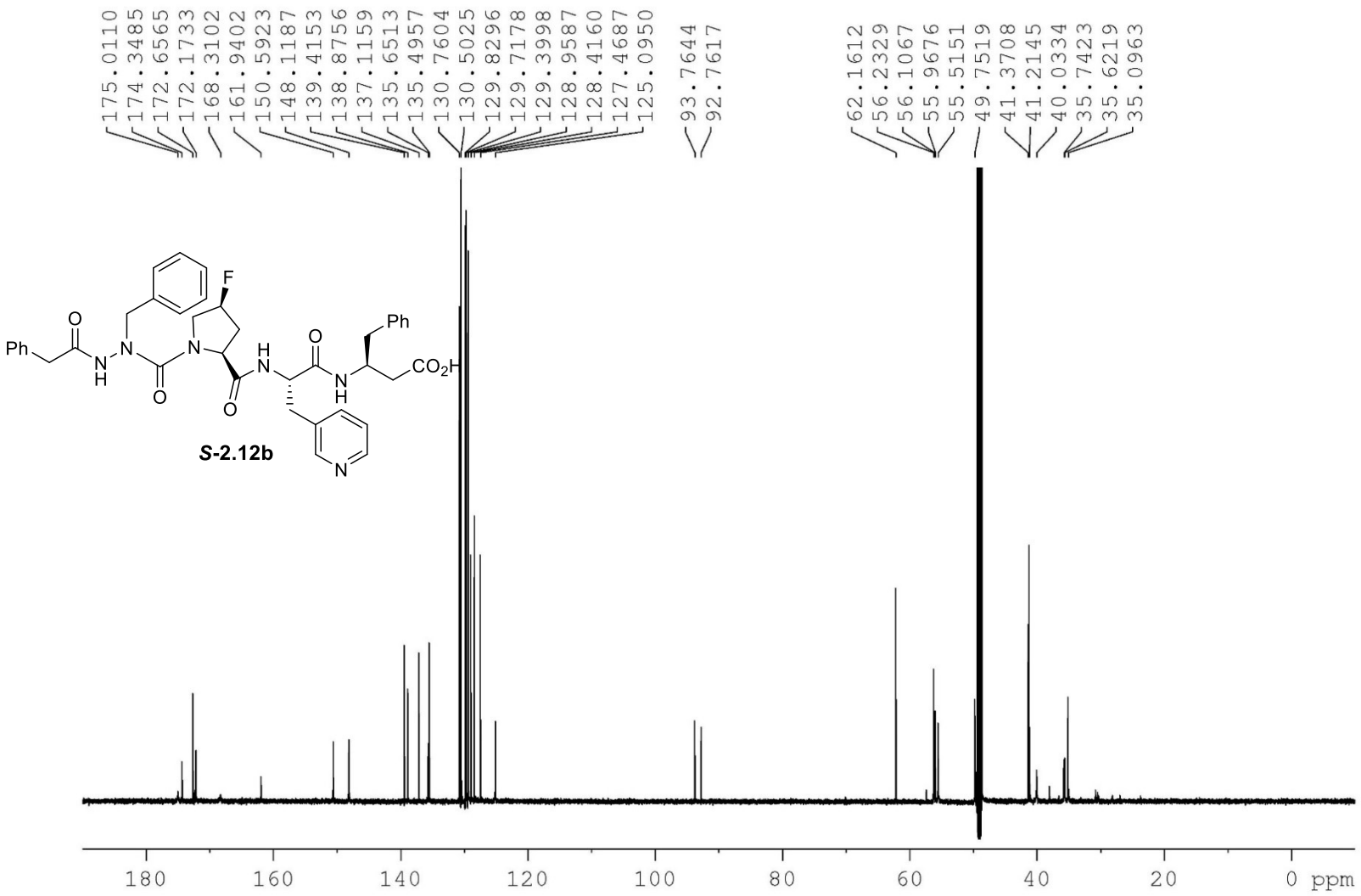

^{1}H NMR 700MHz
Solvent: CD_3OD

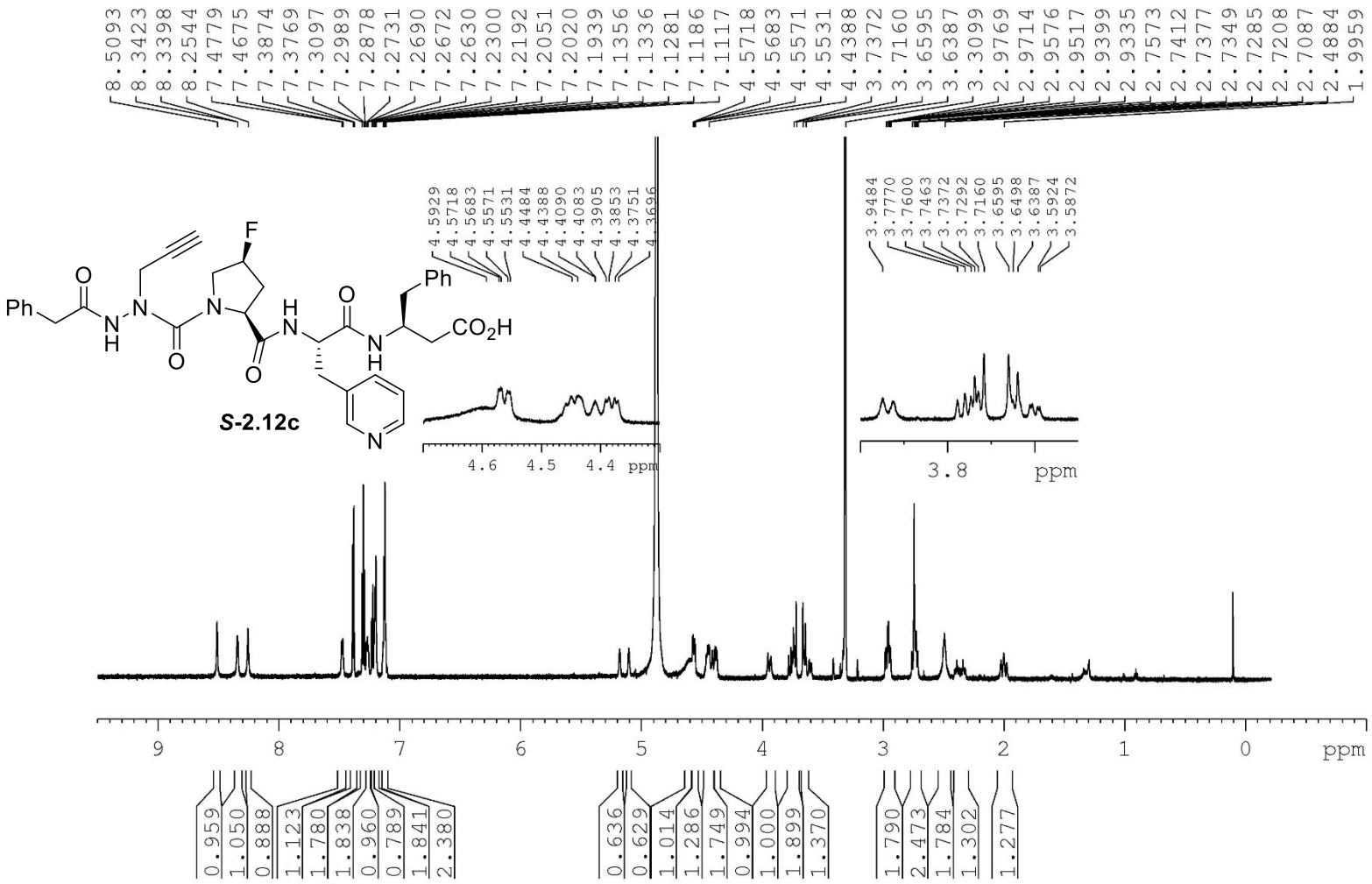

^{13}C NMR 175 MHz

Solvent: CD_3OD

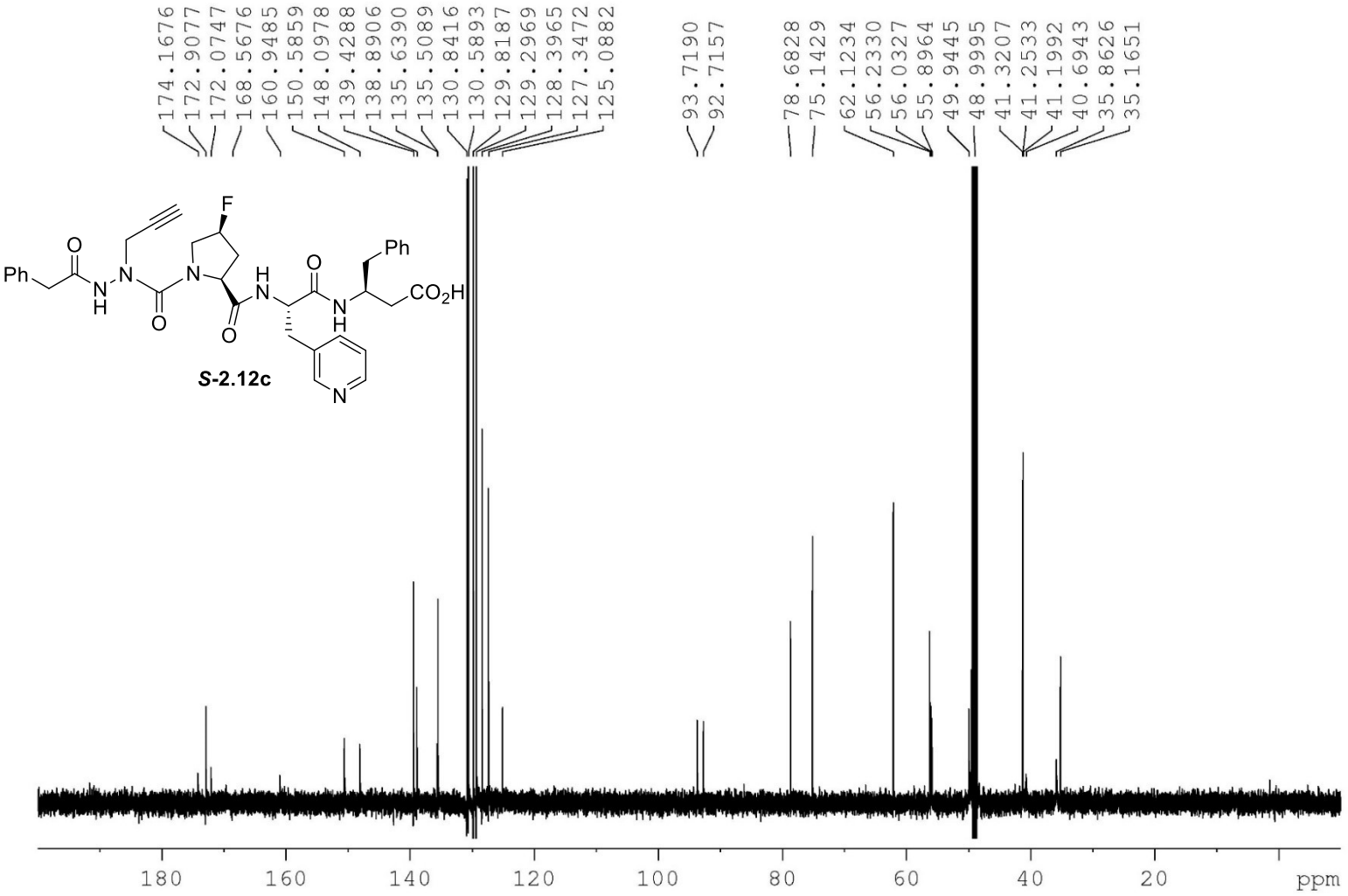

^{1}H NMR 700MHz
Solvent: CD_3OD

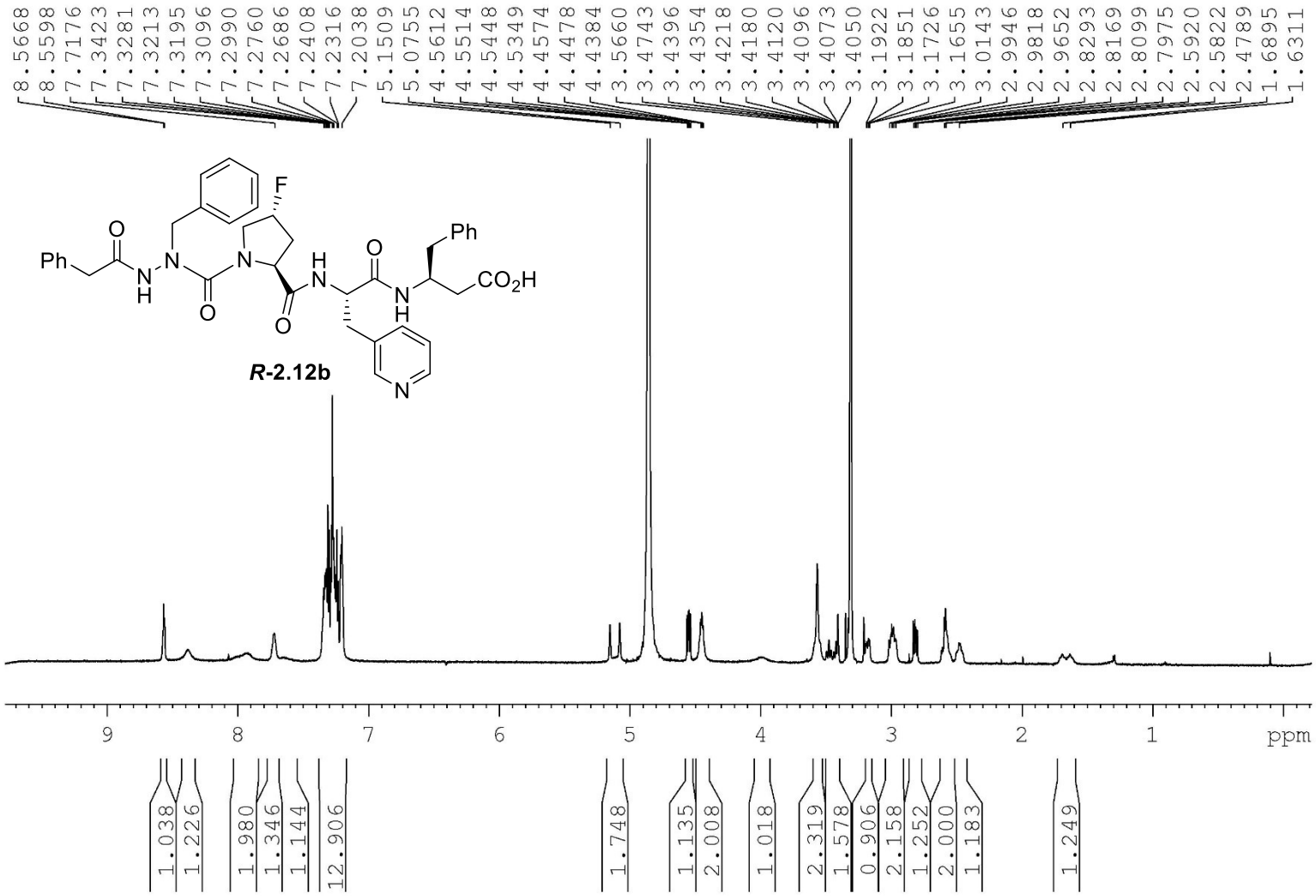

^{13}C NMR 175 MHz

Solvent: CD_3OD

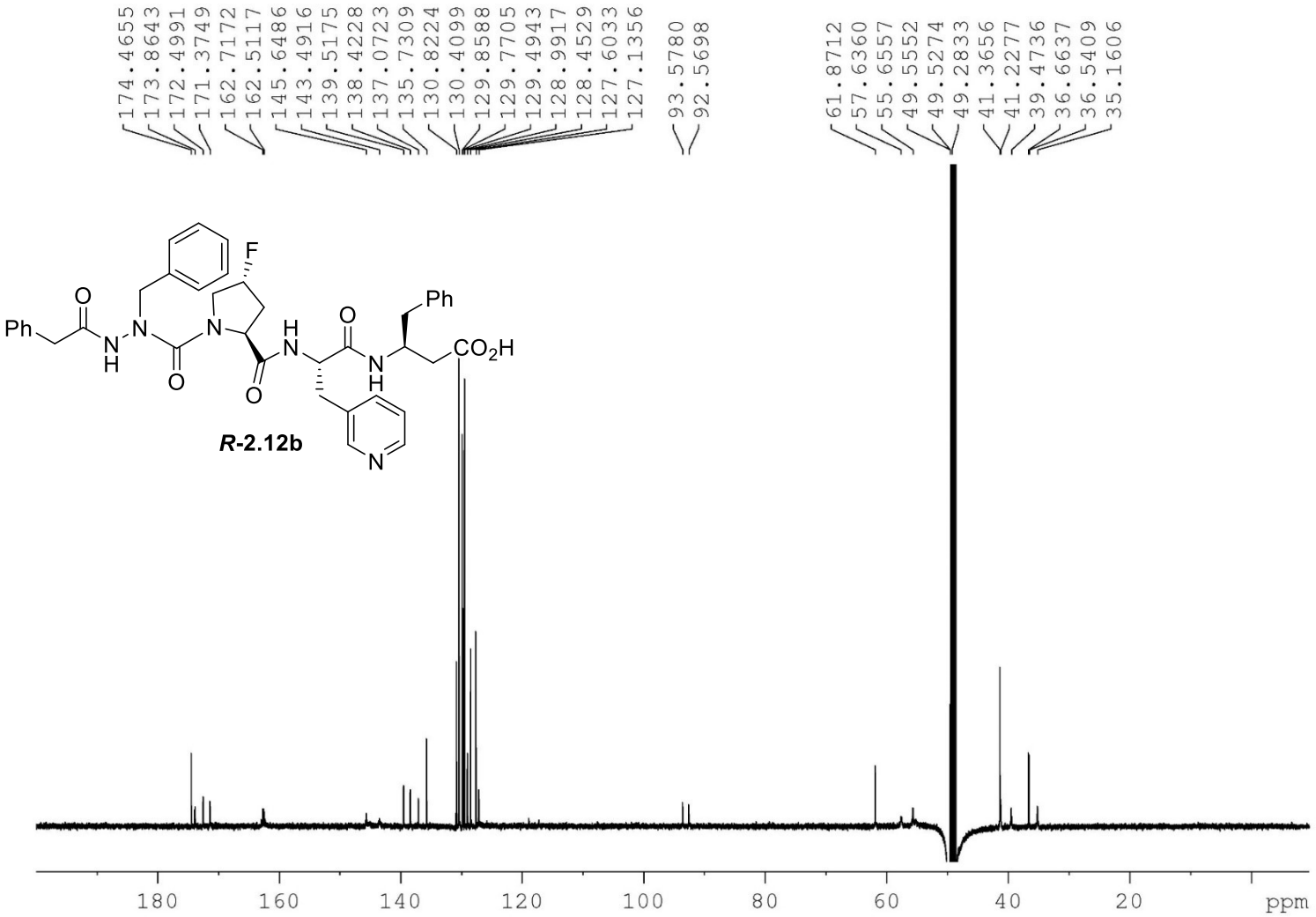

^{1}H NMR 700MHz
Solvent: CD_3OD

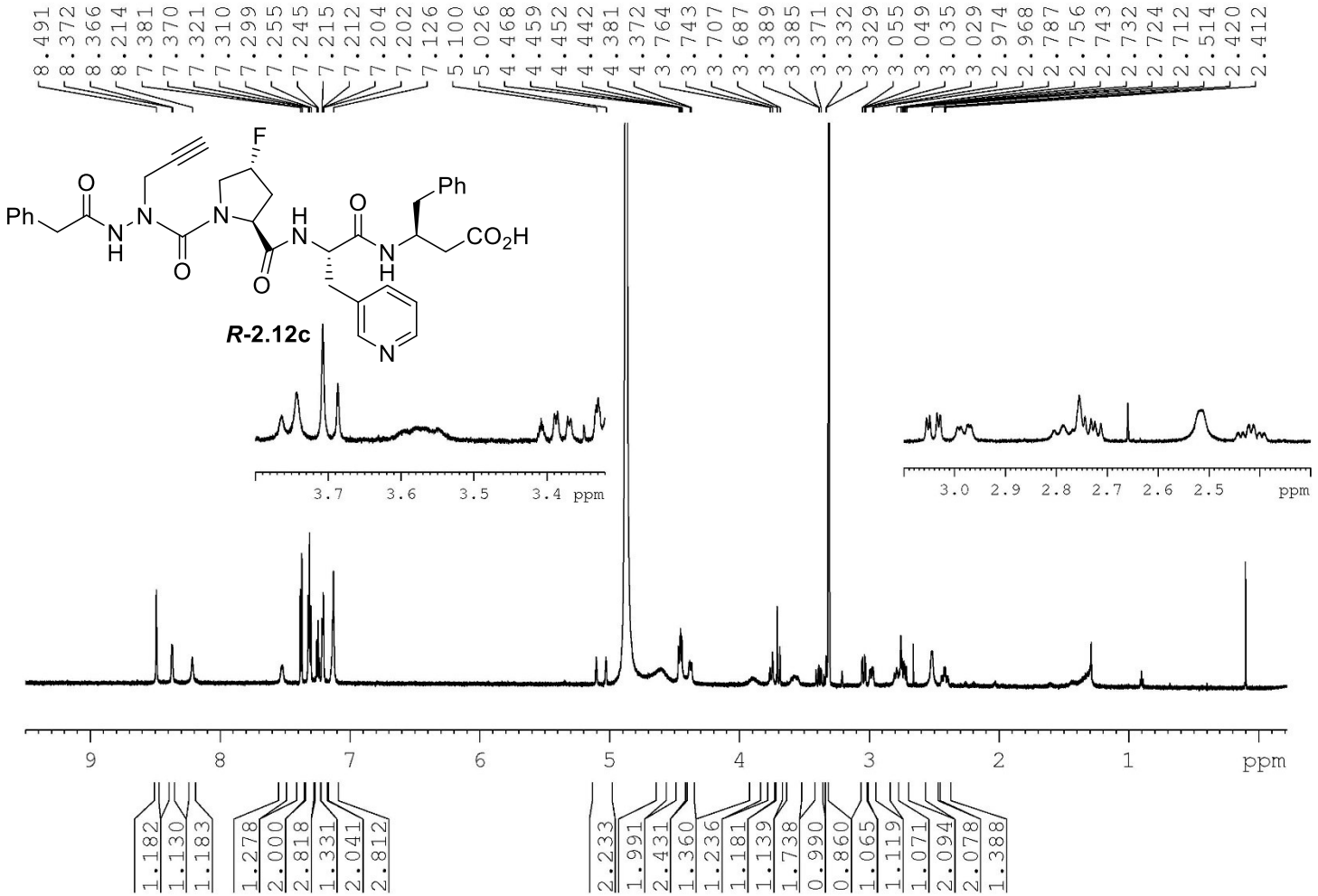

^{13}C NMR 700MHz

Solvent: CD_3OD

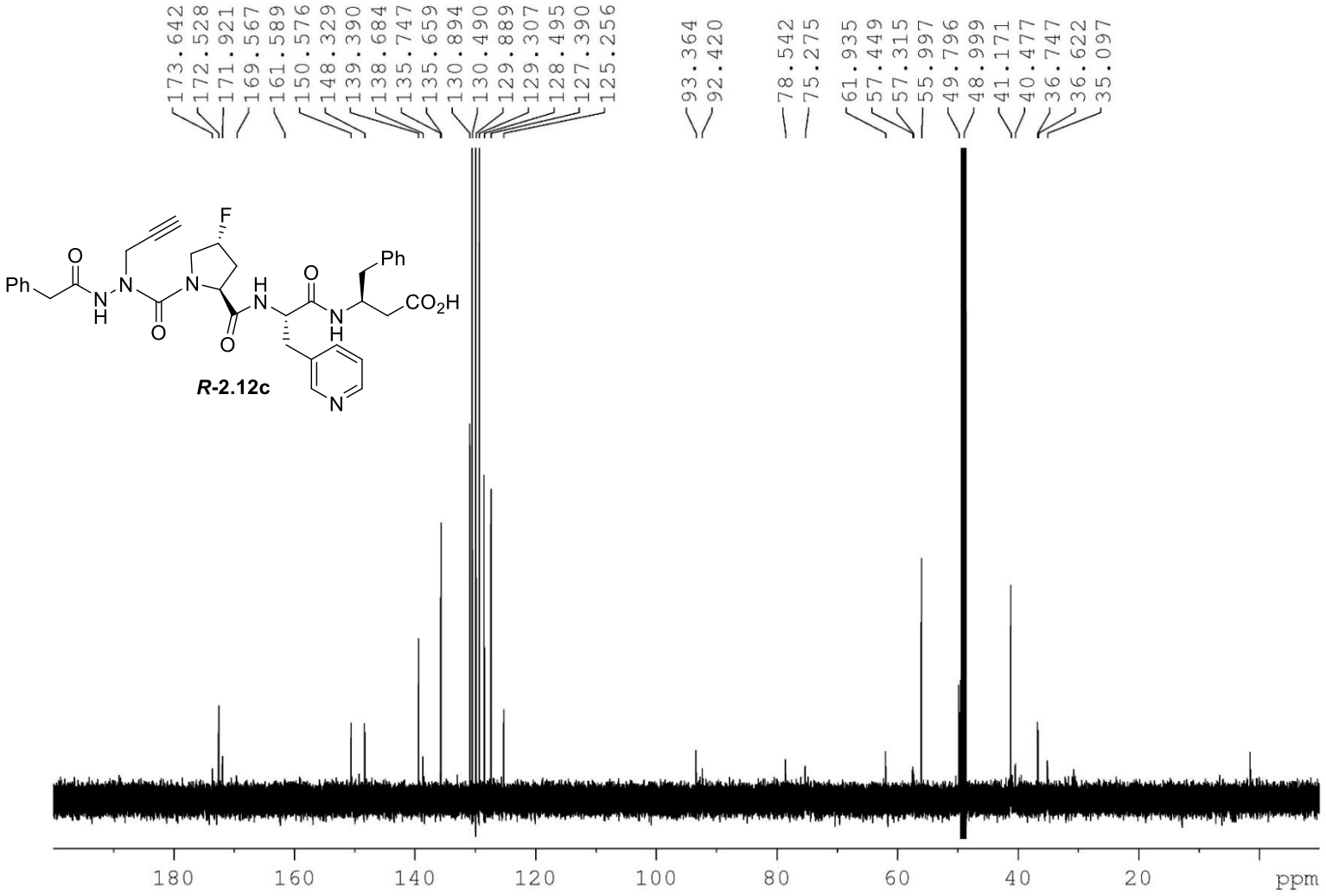

^{1}H NMR 700MHz
Solvent: CD_3OD

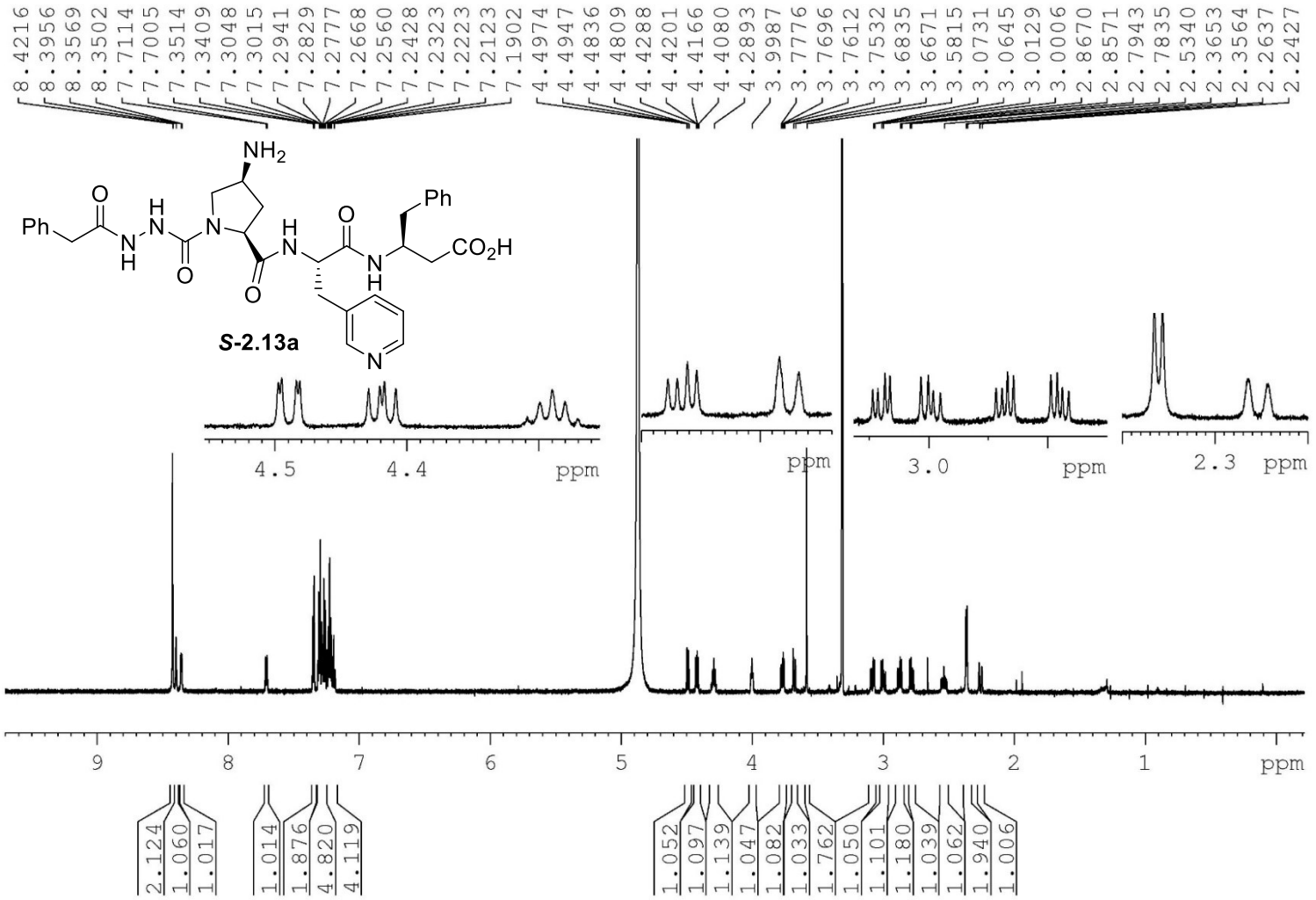

^{13}C NMR 175 MHz

Solvent: CD_3OD

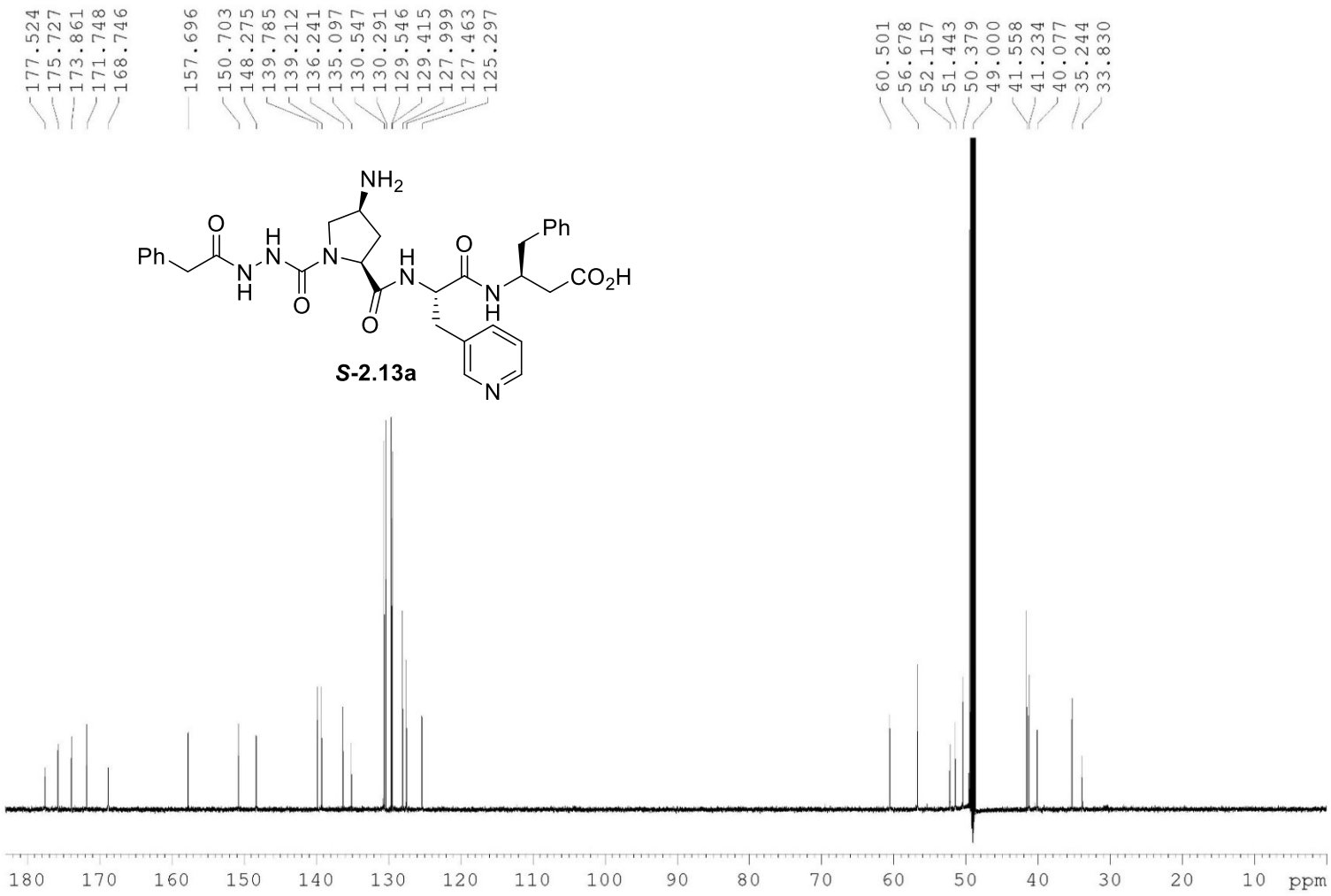

^{1}H NMR 700MHz
Solvent: CD_3OD

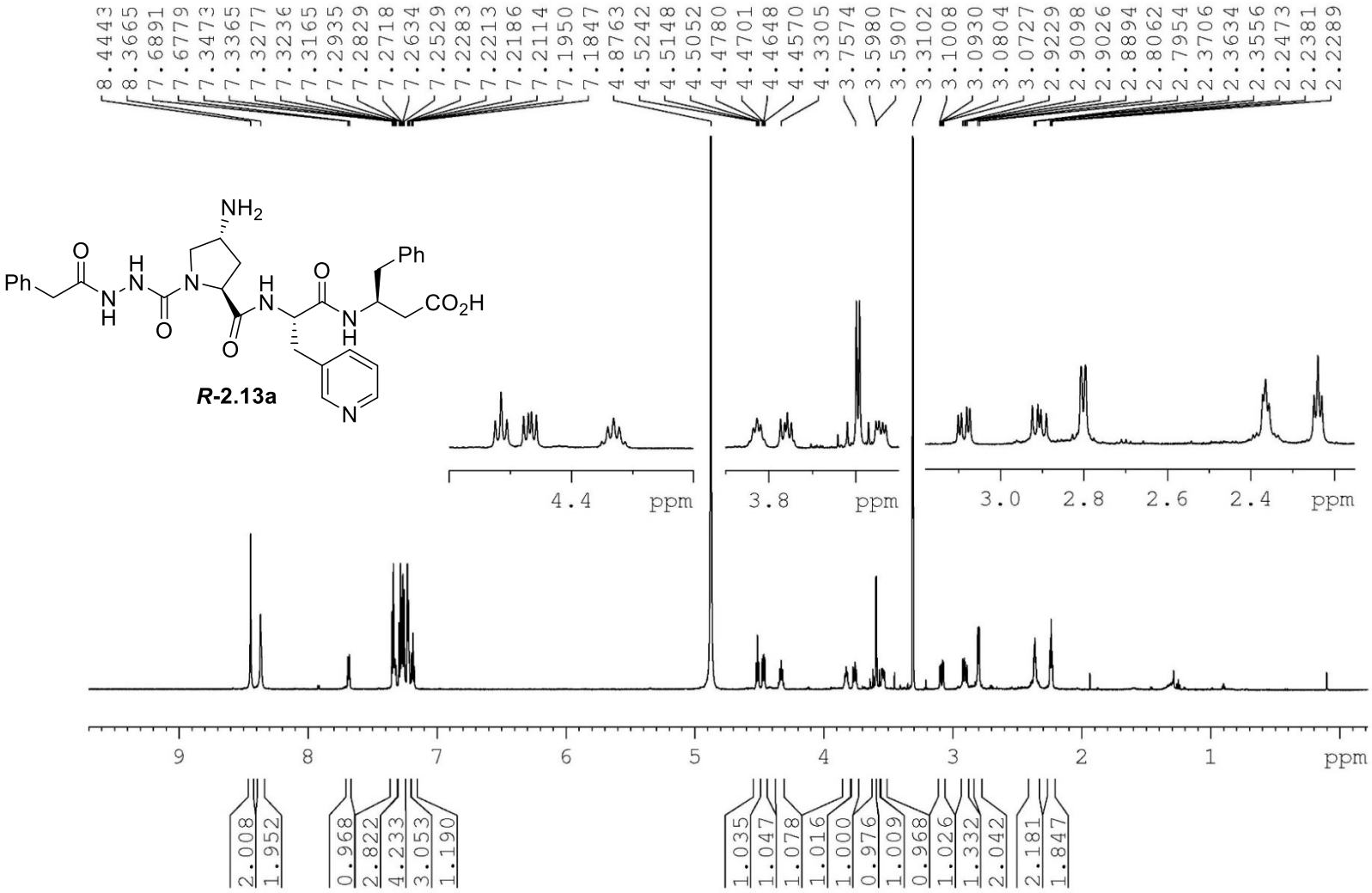

^{13}C NMR 175 MHz

Solvent: CD_3OD

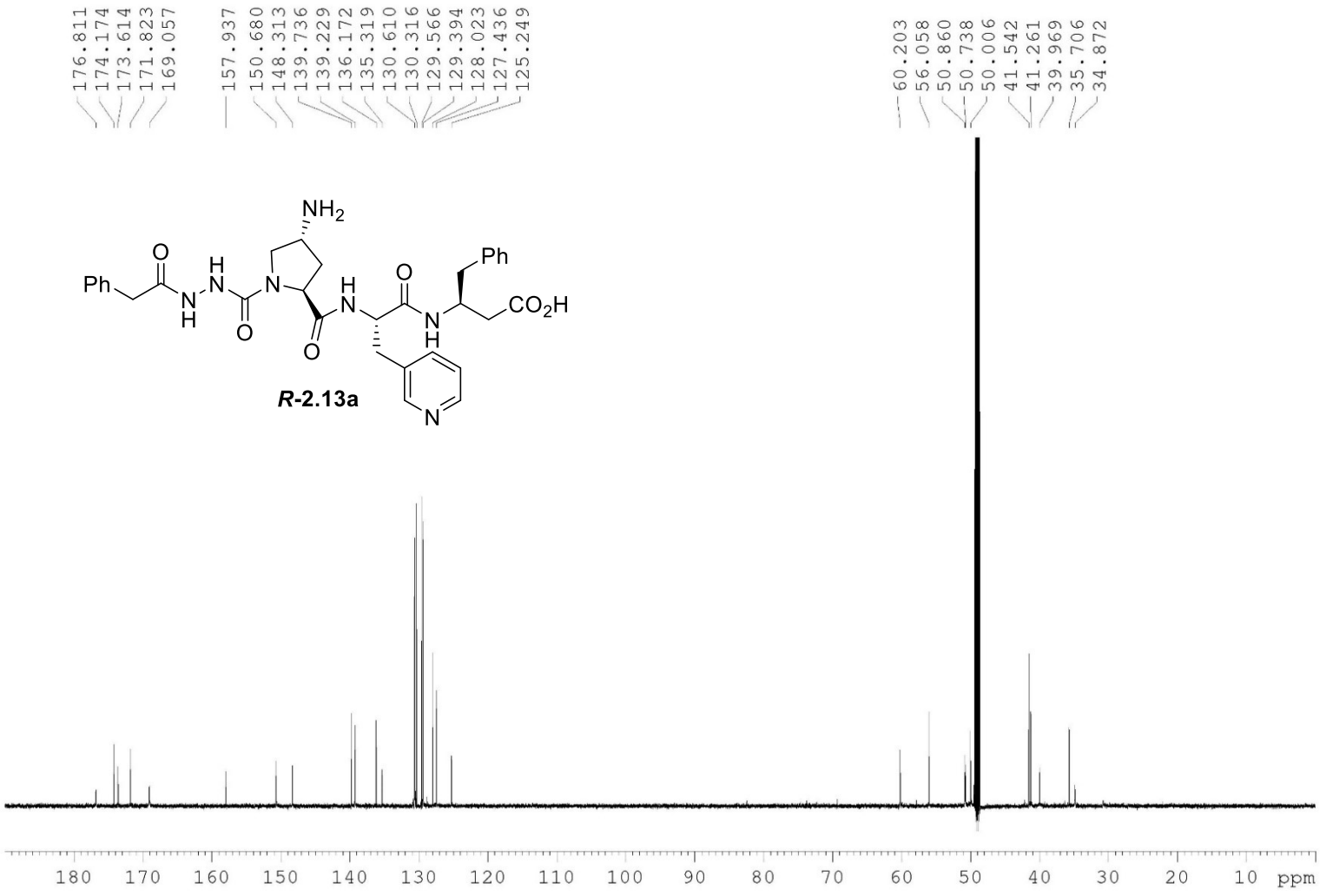

[1]H NMR 700MHz
Solvent: CD_3OD

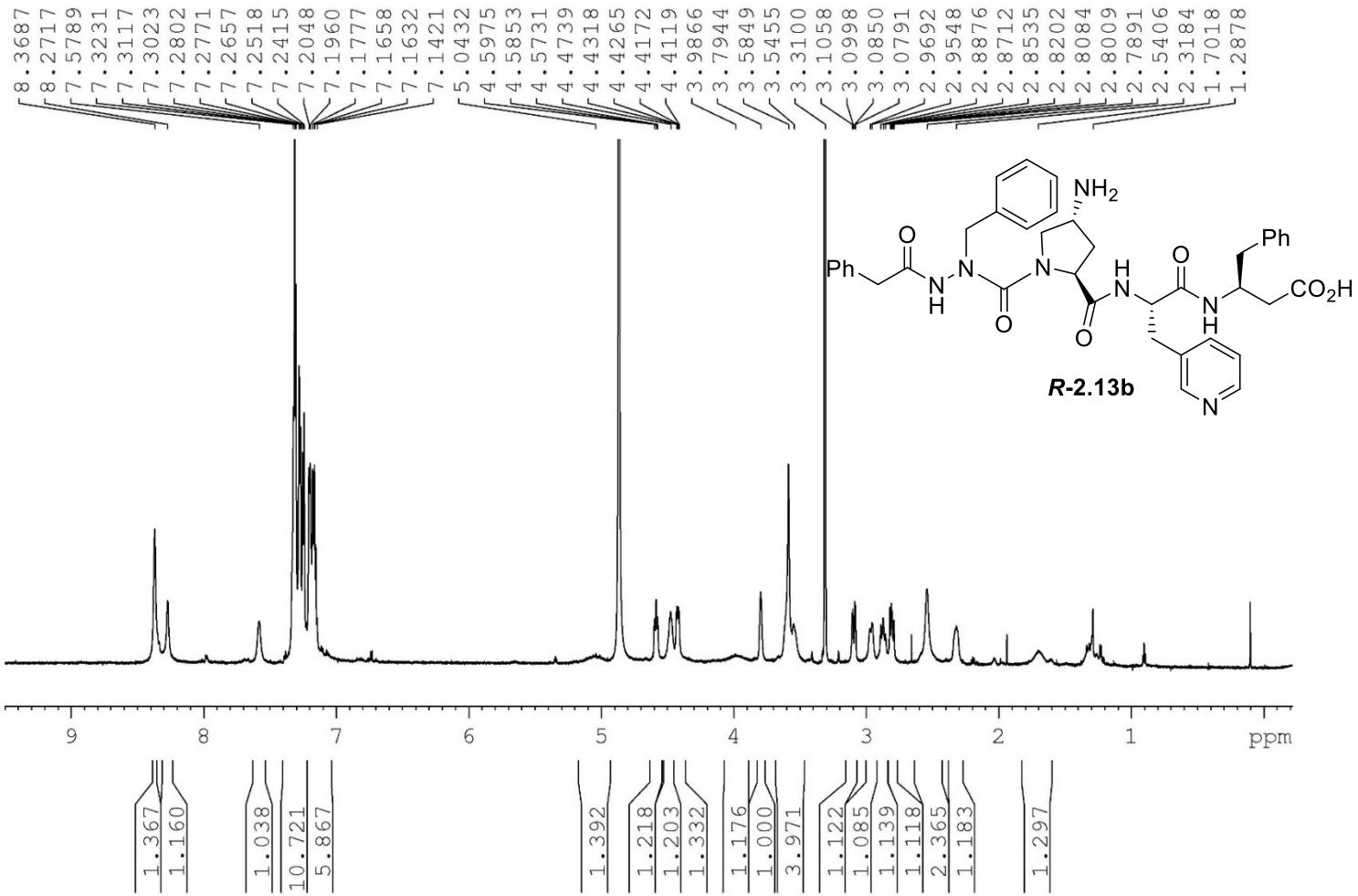

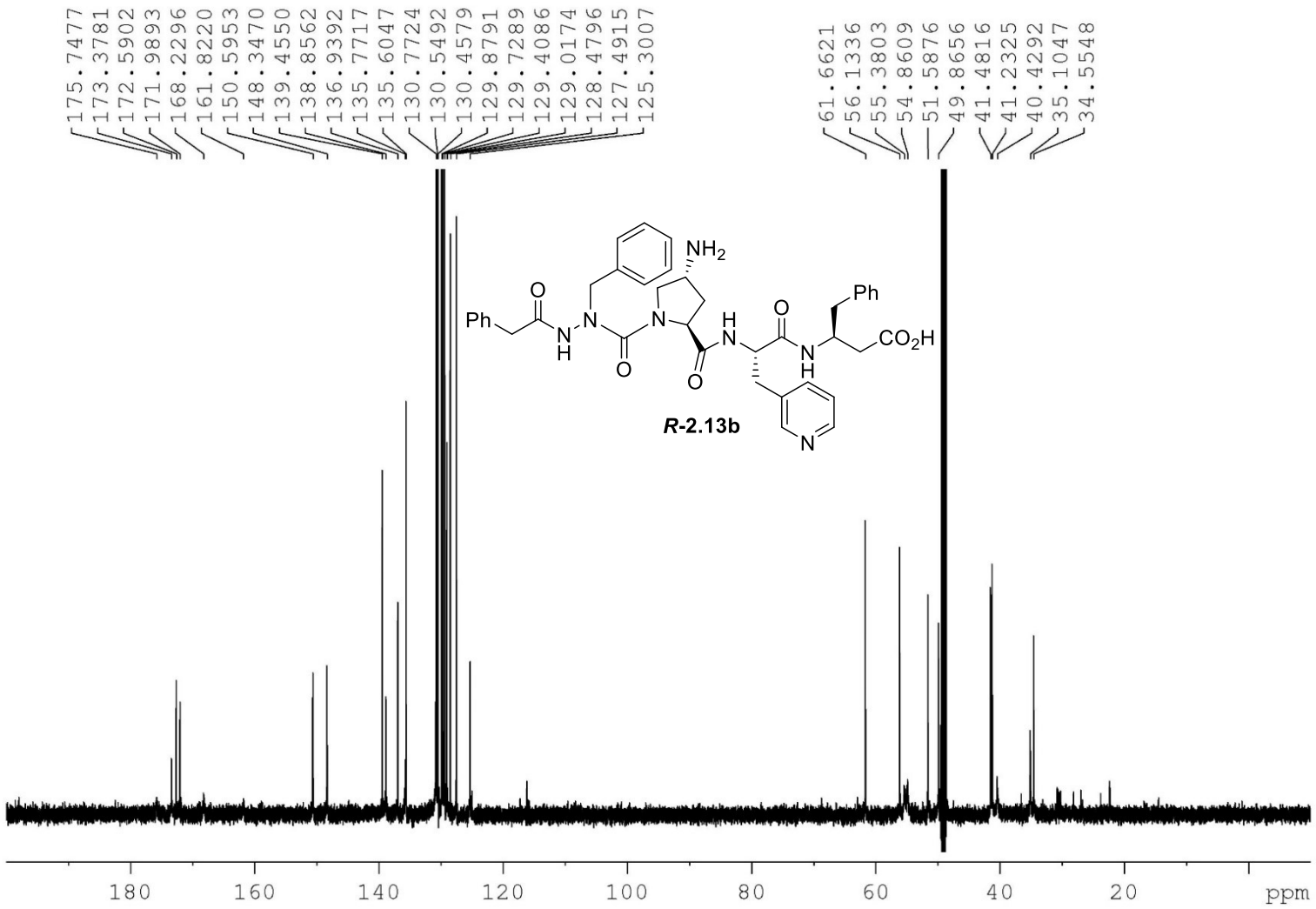
175.7477
173.3781
172.5902
171.9893
168.2296
161.8220
150.5953
148.3470
139.4550
138.8562
136.9392
135.7717
135.6047
130.7724
130.5492
130.4579
129.8791
129.7289
129.4086
129.0174
128.4796
127.4915
125.3007
61.6621
56.1336
55.3803
54.8609
51.5876
49.8656
41.4816
41.2325
40.4292
35.1047
34.5548
NH2
Ph
CO2H
R-2.13b
180
160
140
120
100
80
60
40
20
ppm

^{1}H NMR 300MHz
Solvent: $CDCl_3$

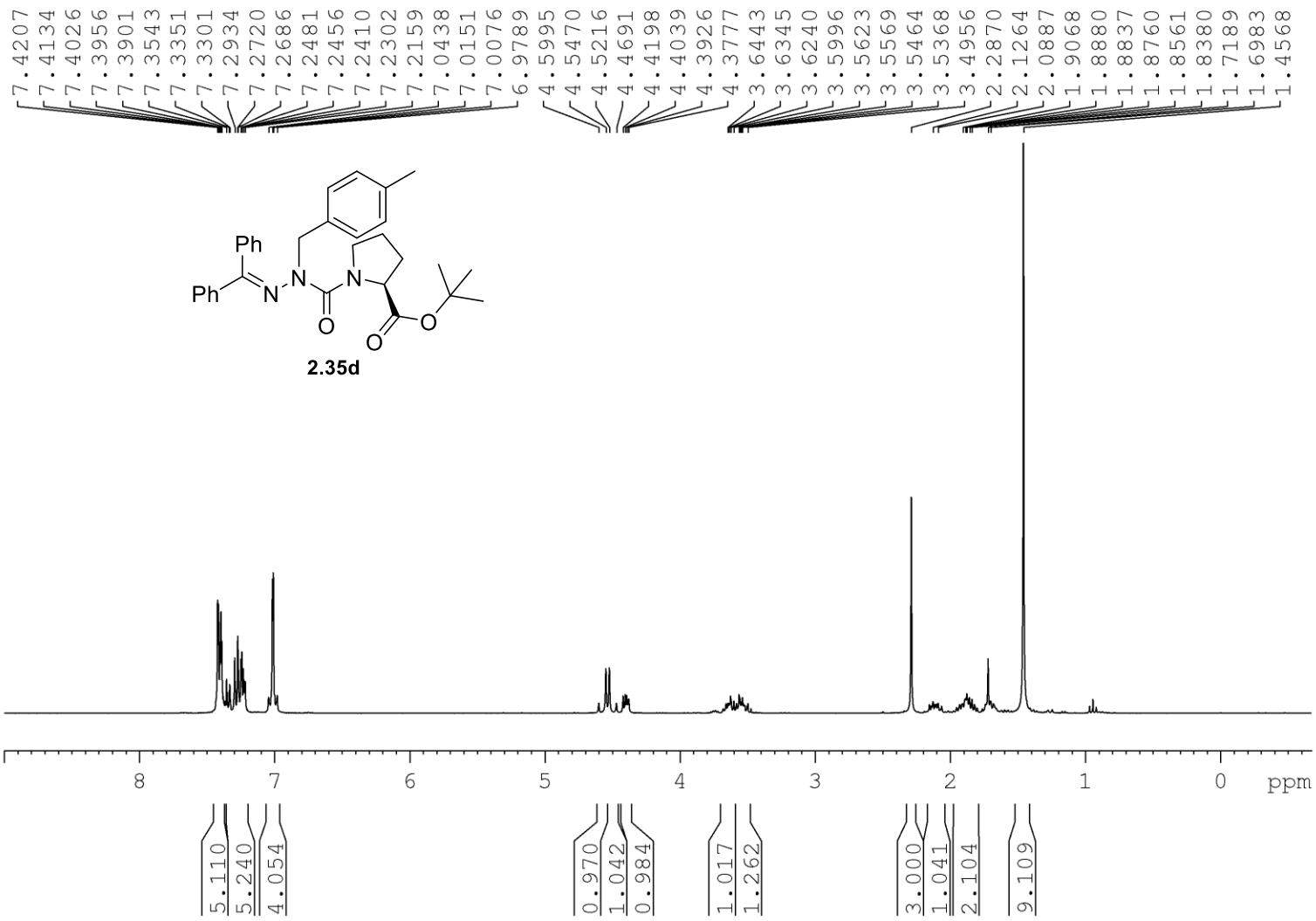

^{13}C NMR 75MHz

Solvent: $CDCl_3$

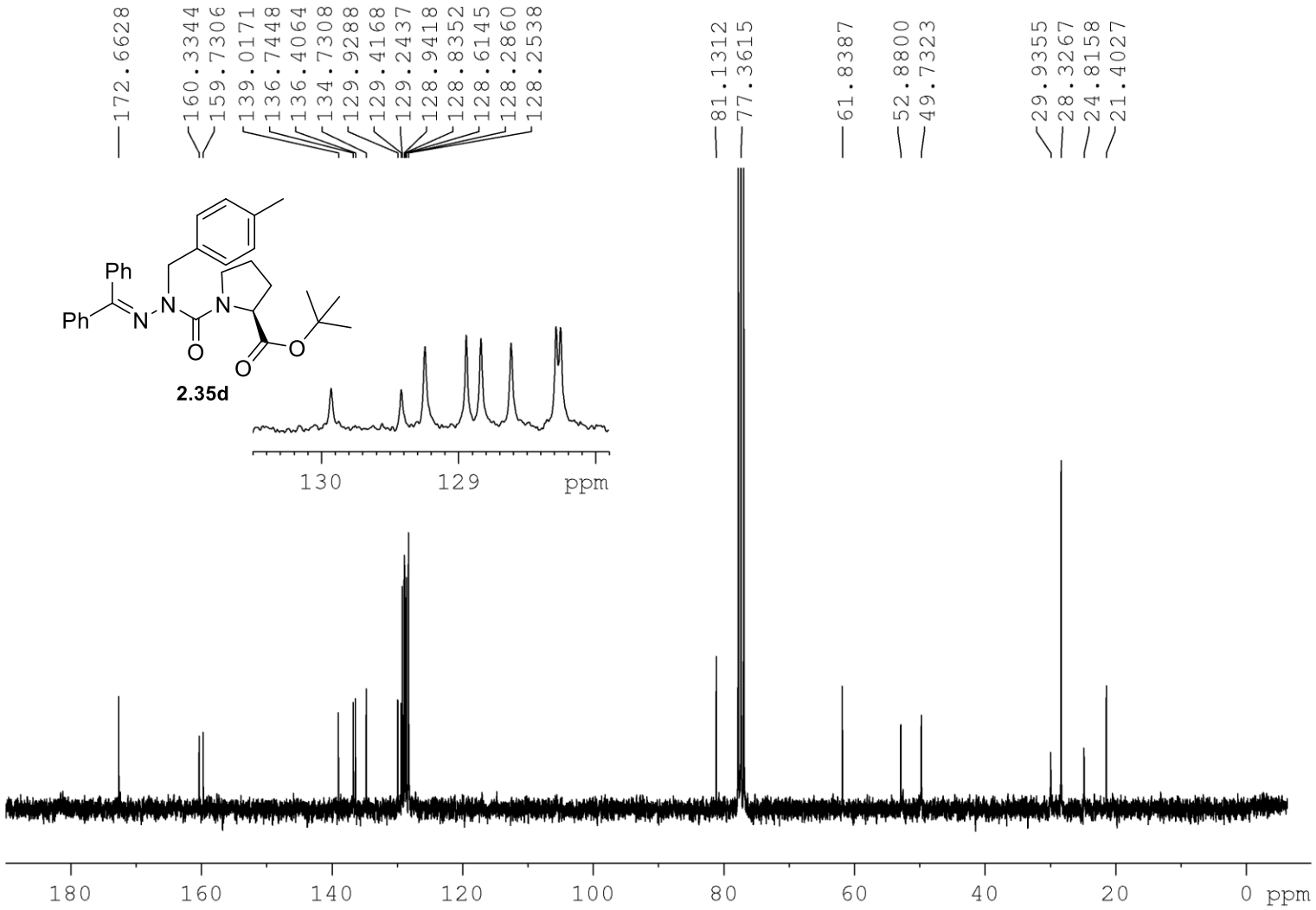

^{1}H NMR 300MHz
Solvent: $CDCl_3$

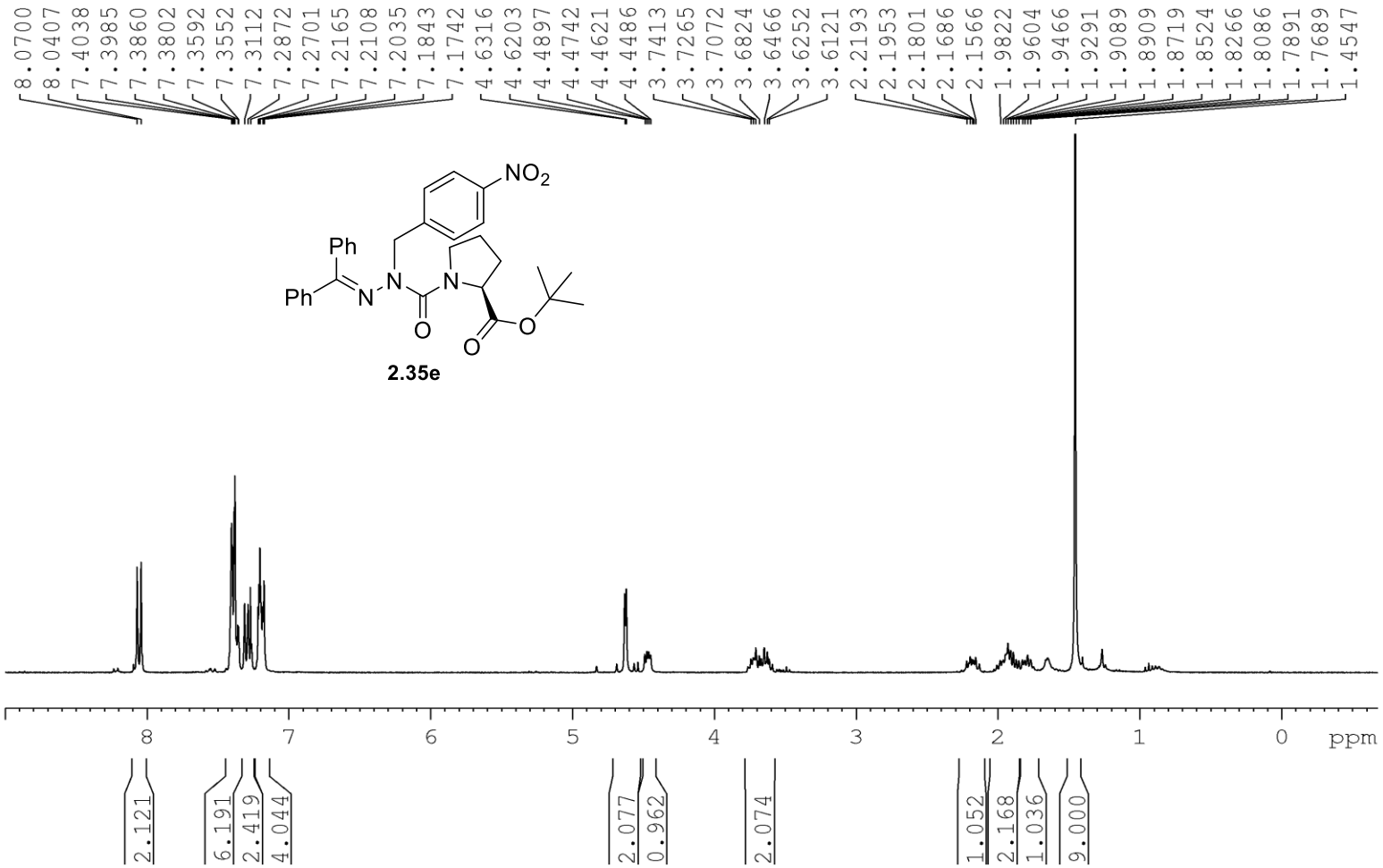

^{13}C NMR 75 MHz

Solvent: $CDCl_3$

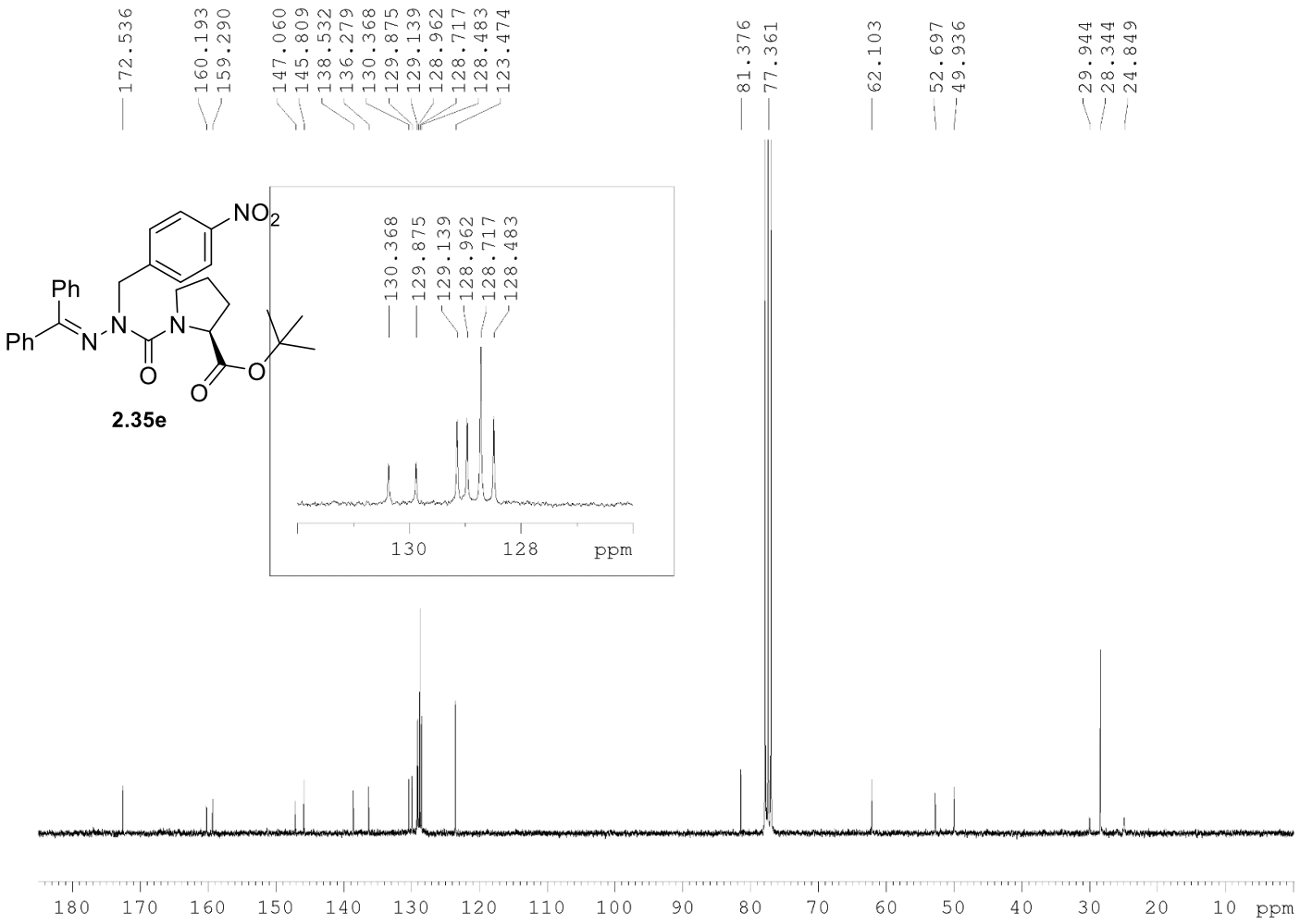

^{1}H NMR 300MHz

Solvent: $CDCl_3$

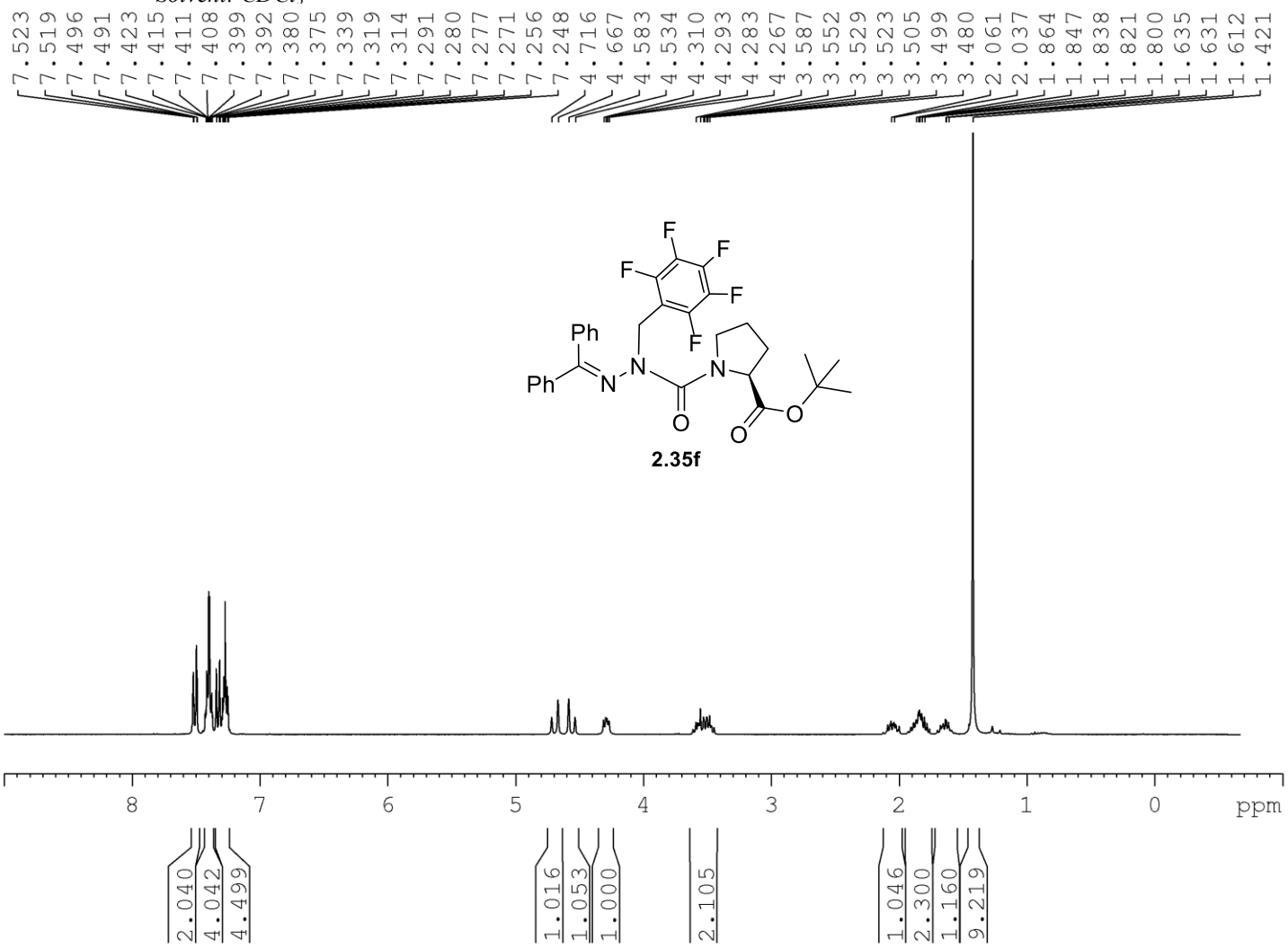

^{13}C NMR 75 MHz

Solvent: $CDCl_3$

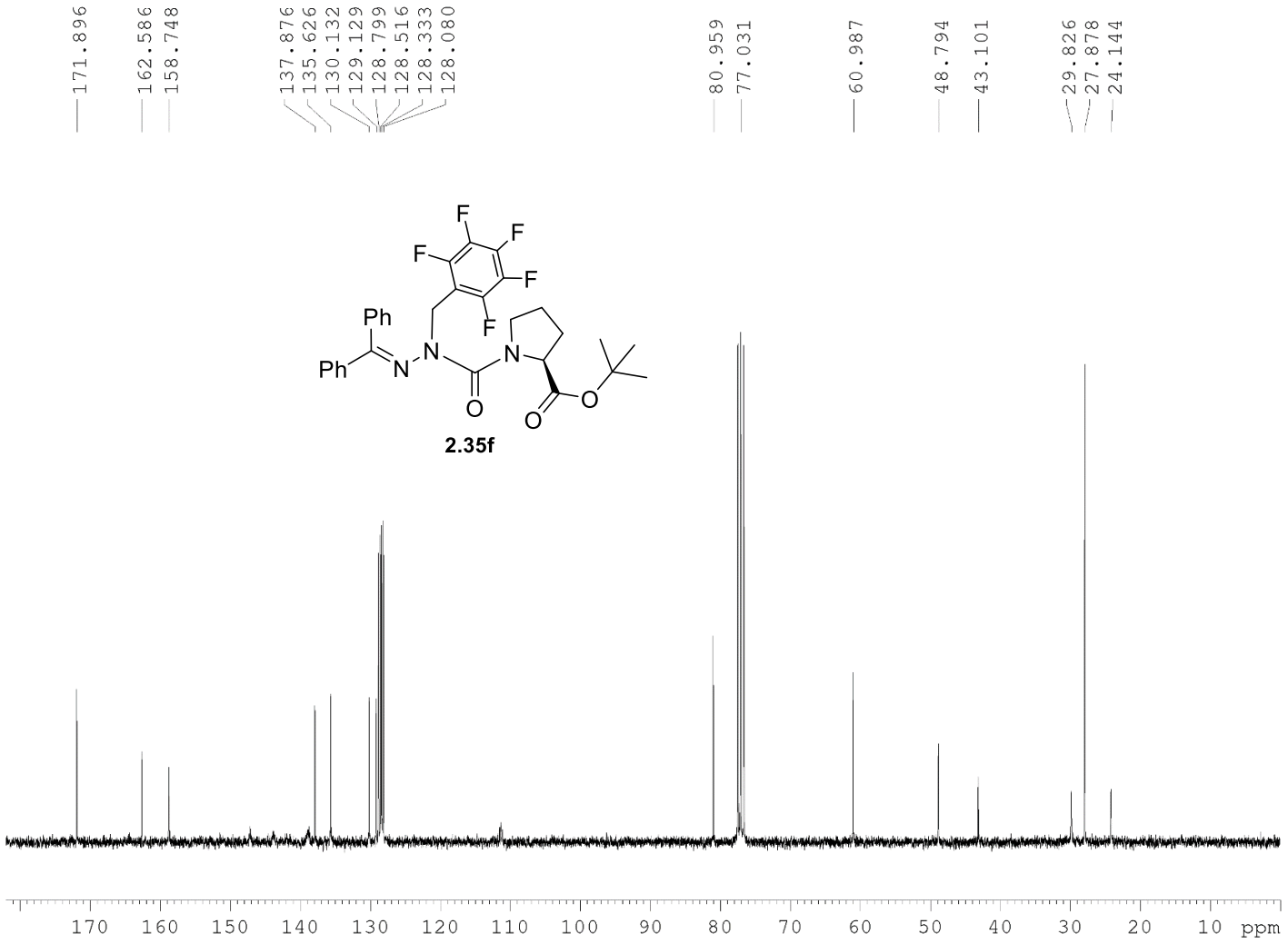

^{1}H NMR 500MHz

Solvent: $CDCl_3$

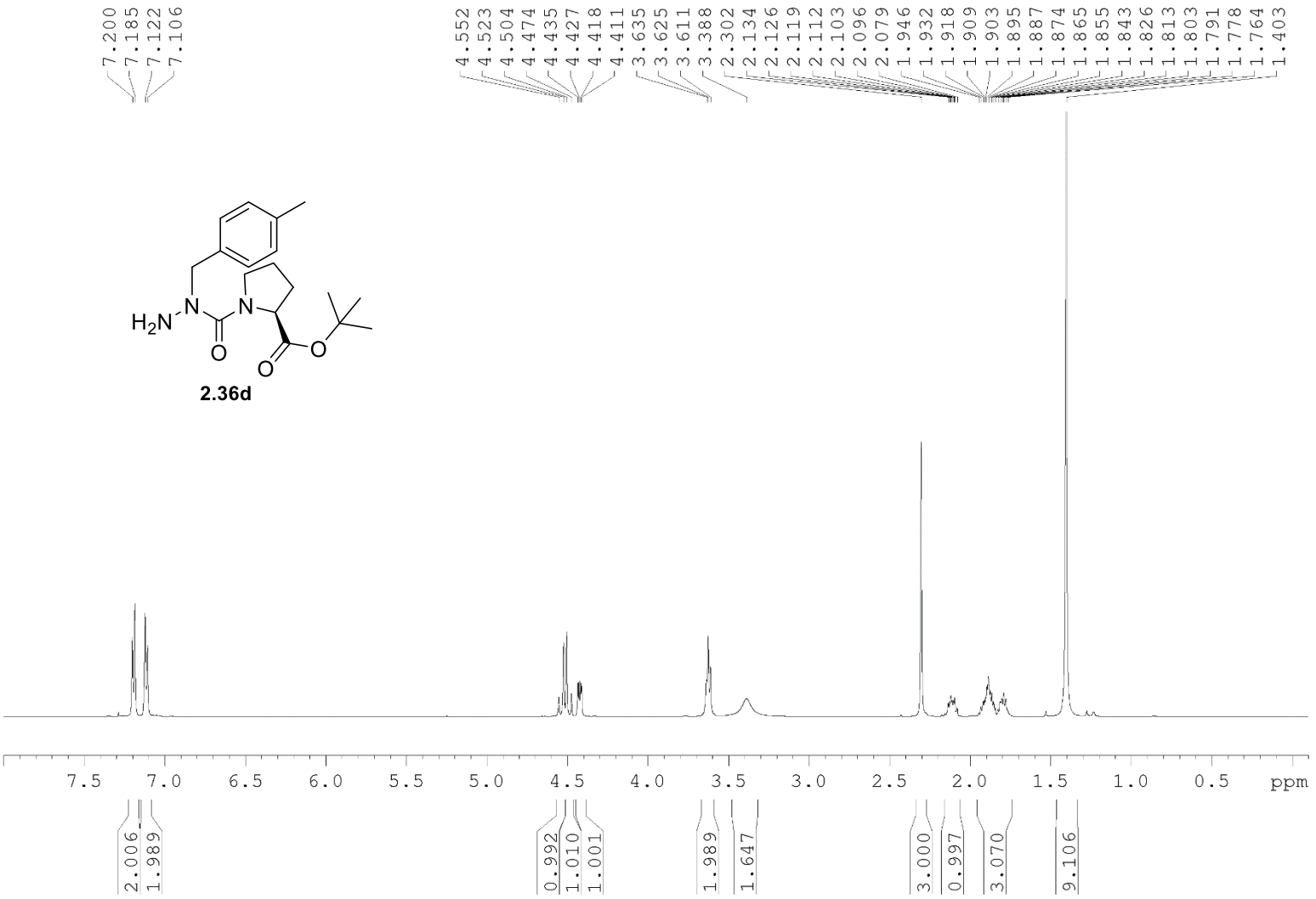

2.36d

^{13}C NMR 125 MHz

Solvent: $CDCl_3$

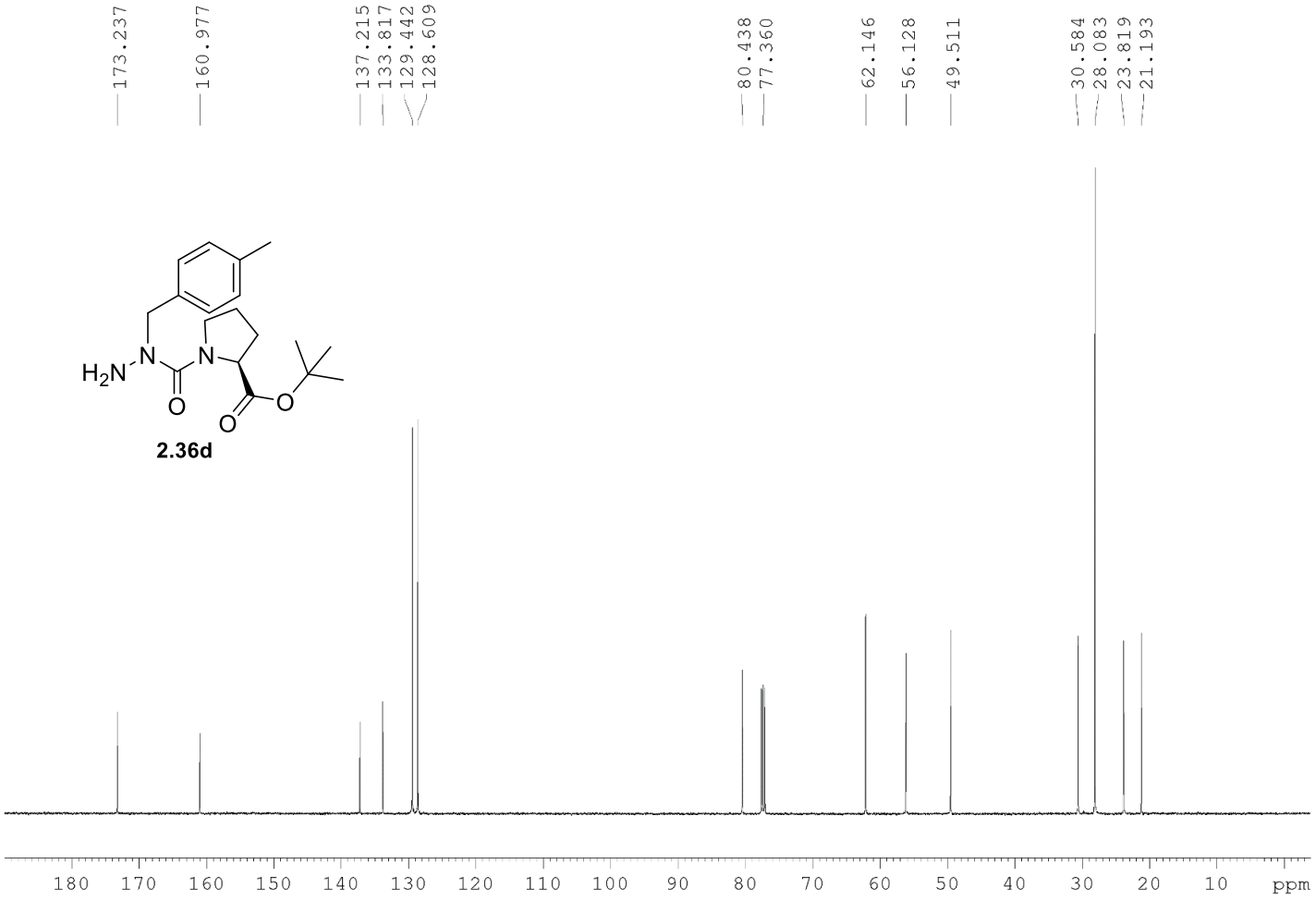

^{1}H NMR 300MHz

Solvent: $CDCl_3$

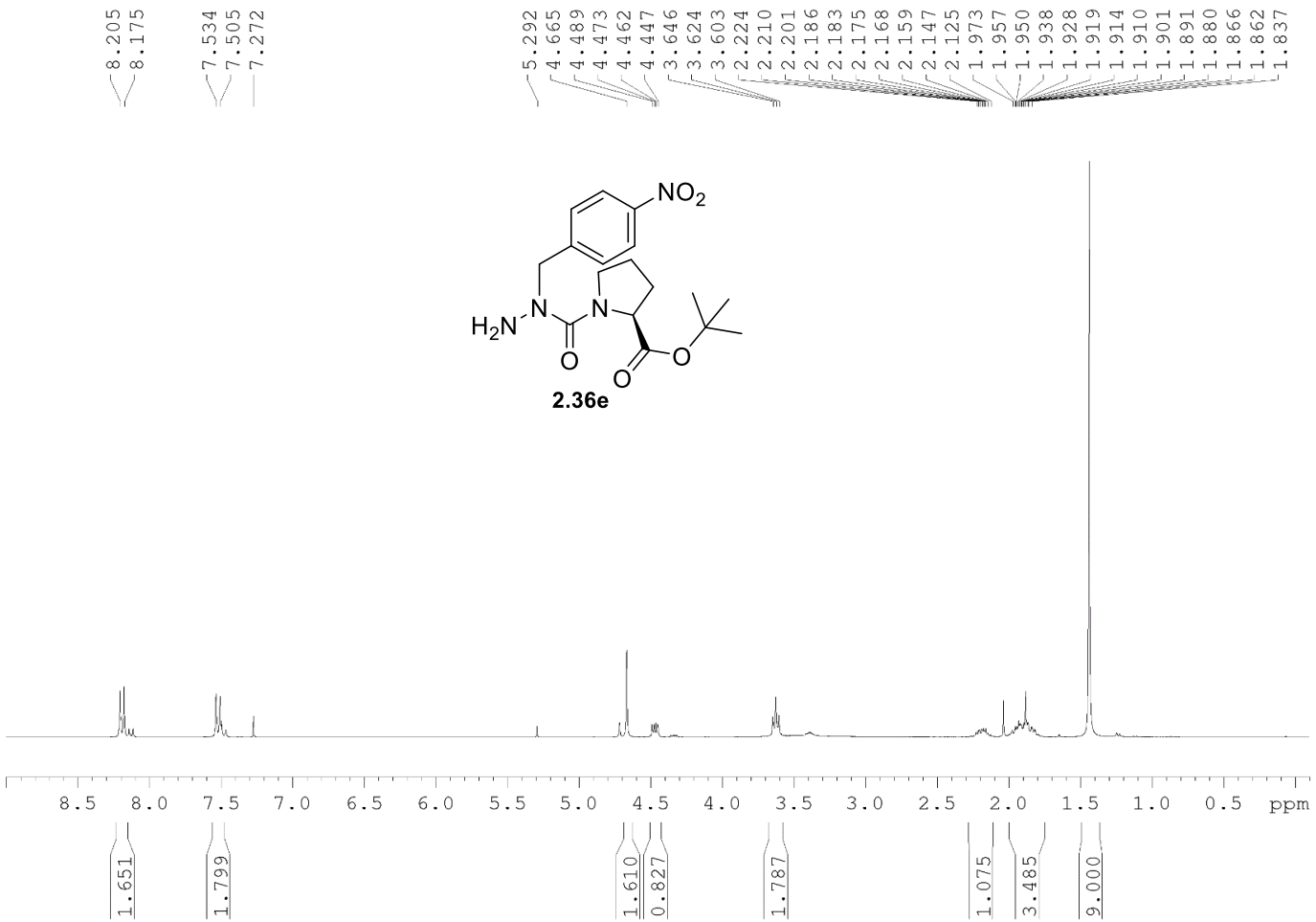

^{13}C NMR 75 MHz

Solvent: $CDCl_3$

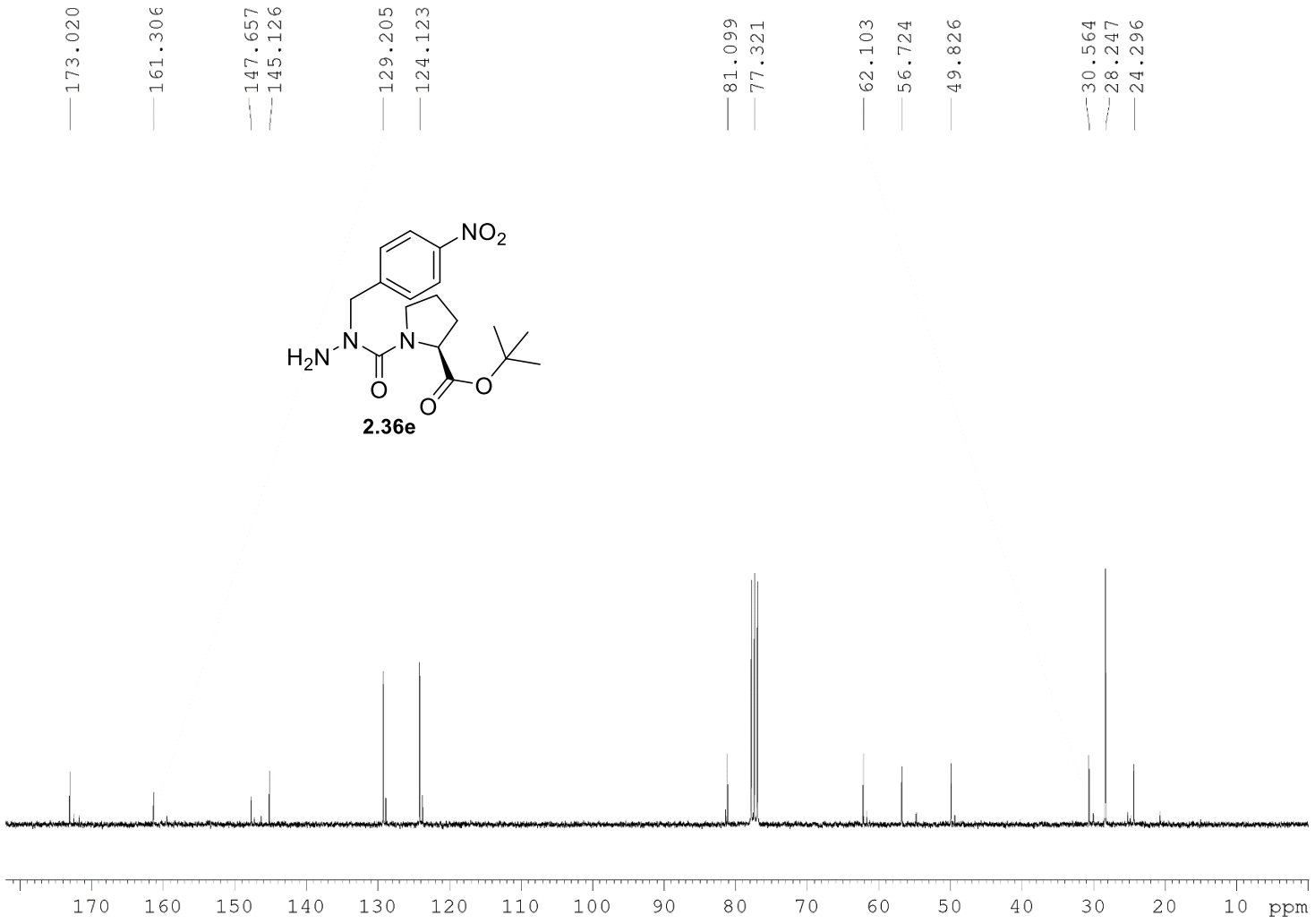

^{1}H NMR 400MHz

Solvent: $CDCl_3$

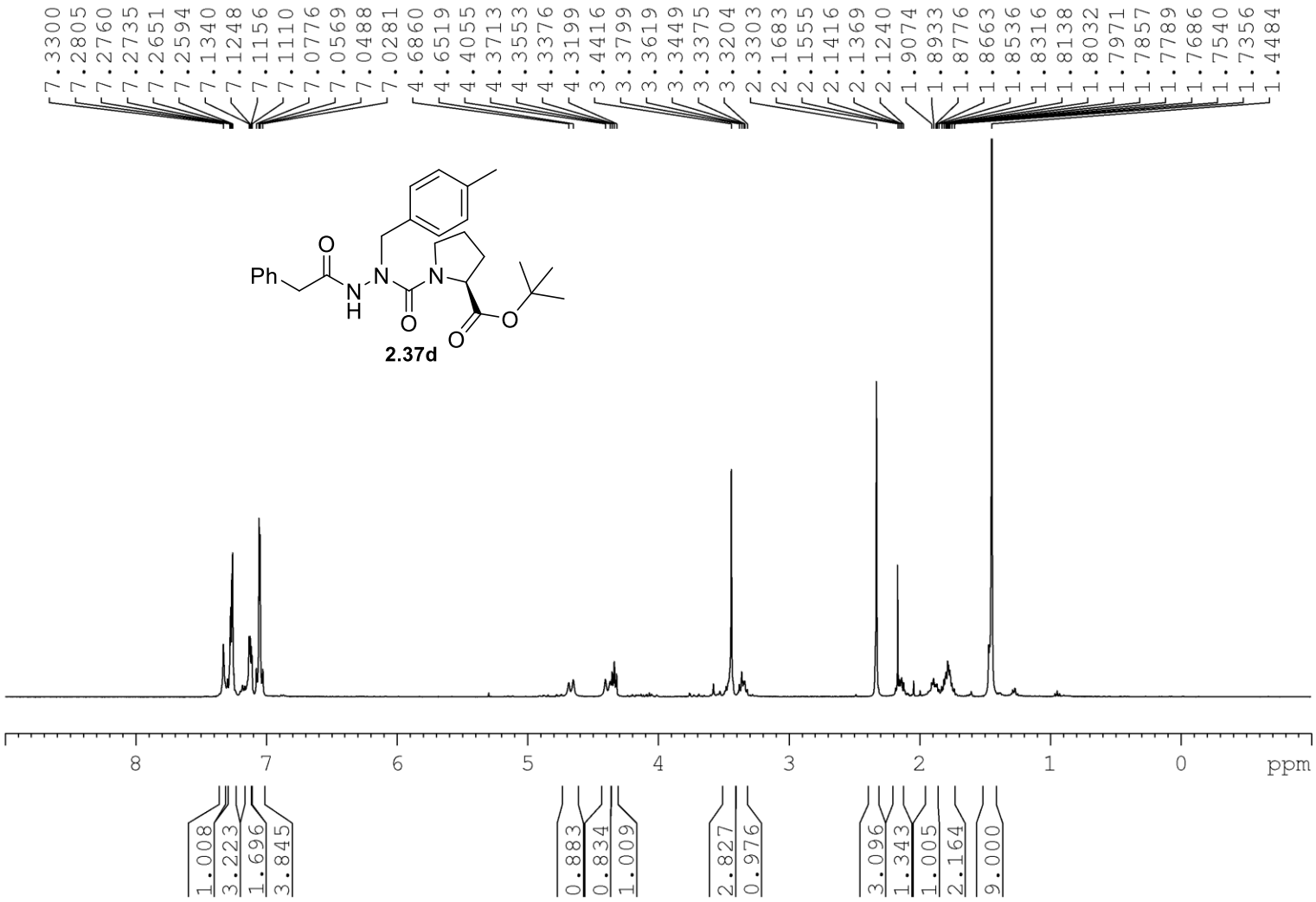

^{13}C NMR 75 MHz

Solvent: $CDCl_3$

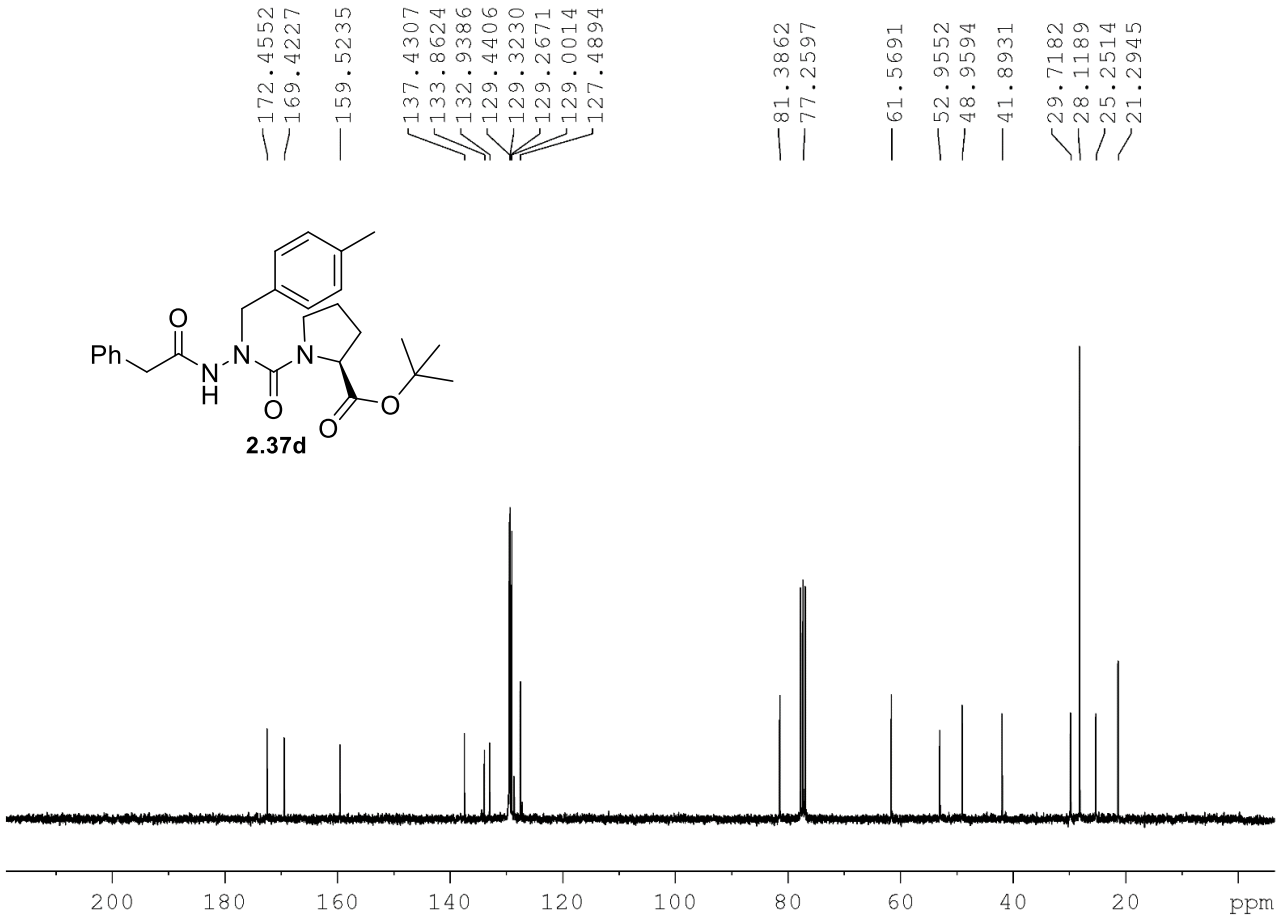

^{1}H NMR 300MHz

Solvent: $CDCl_3$

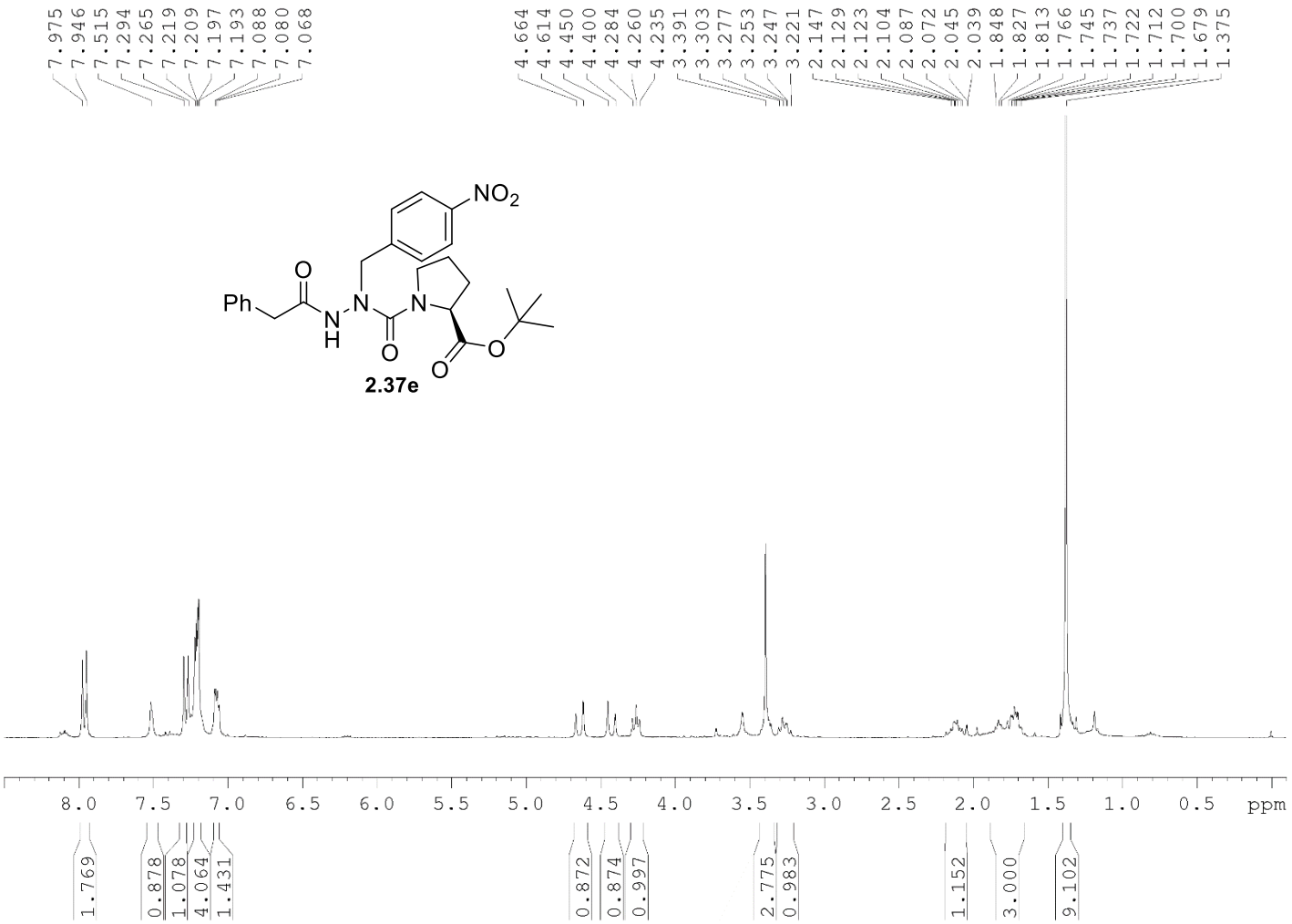

^{13}C NMR 75 MHz

Solvent: $CDCl_3$

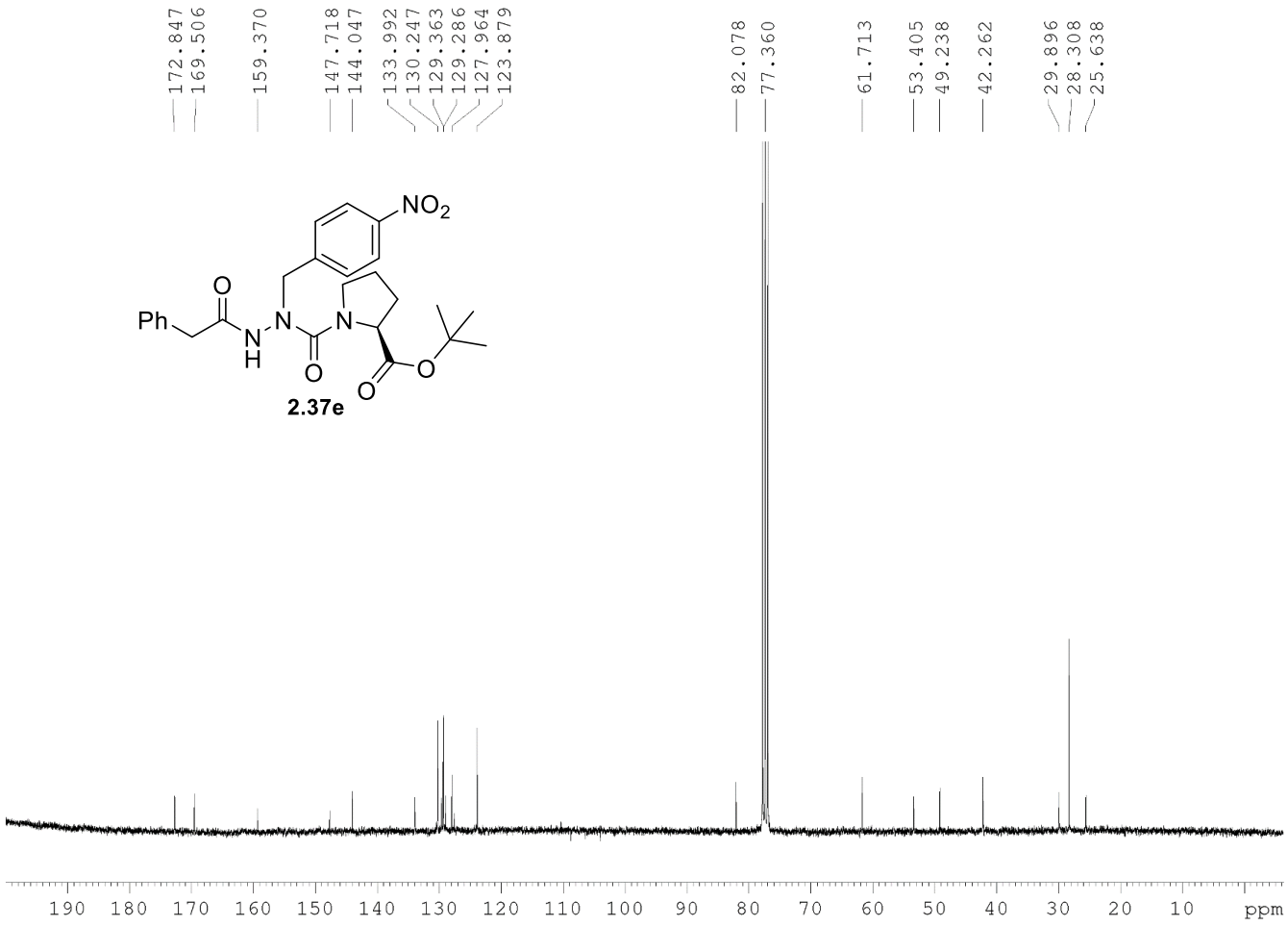

^{1}H NMR 400MHz

Solvent: $CDCl_3$

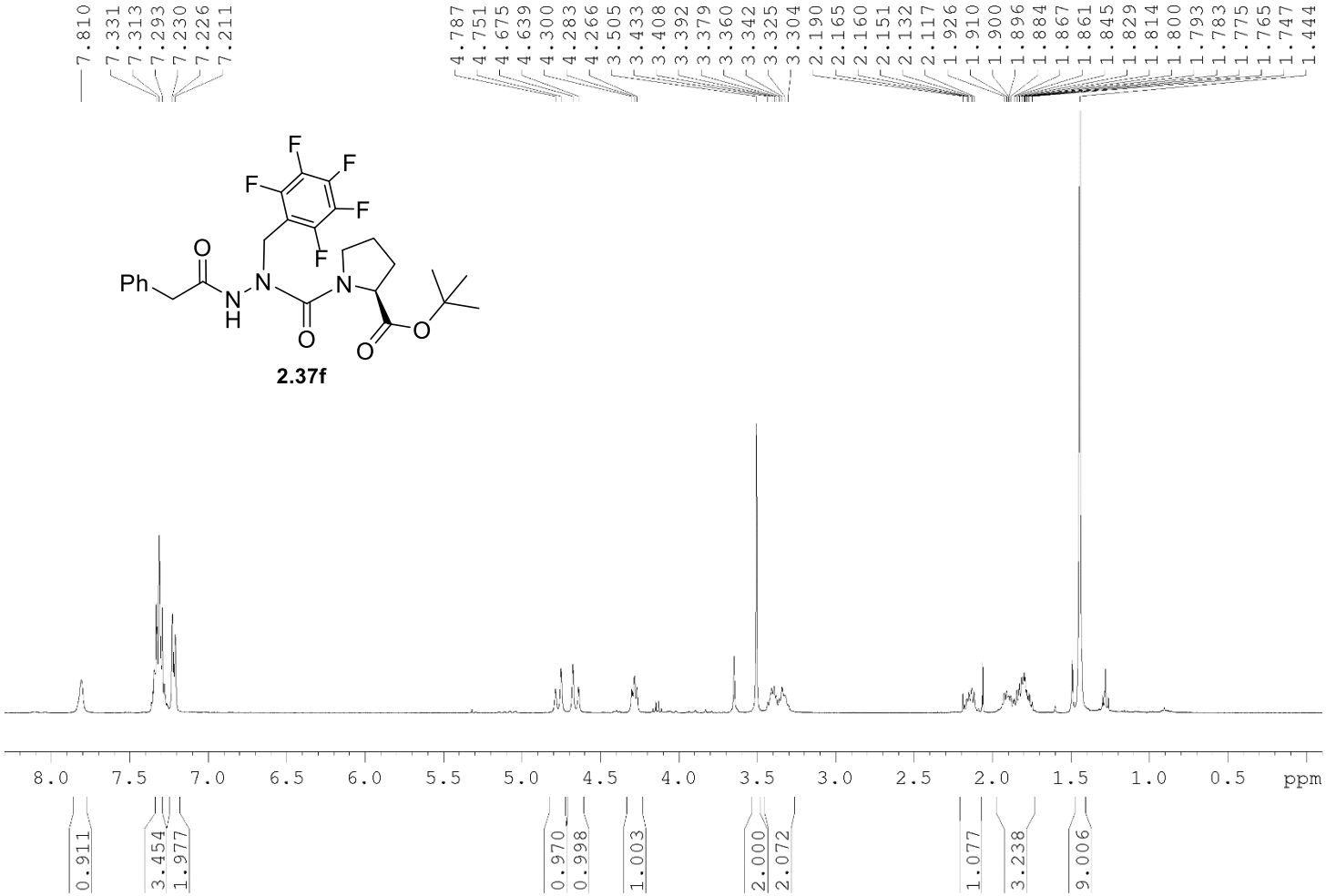

2.37f

^{13}C NMR 75 MHz

Solvent: $CDCl_3$

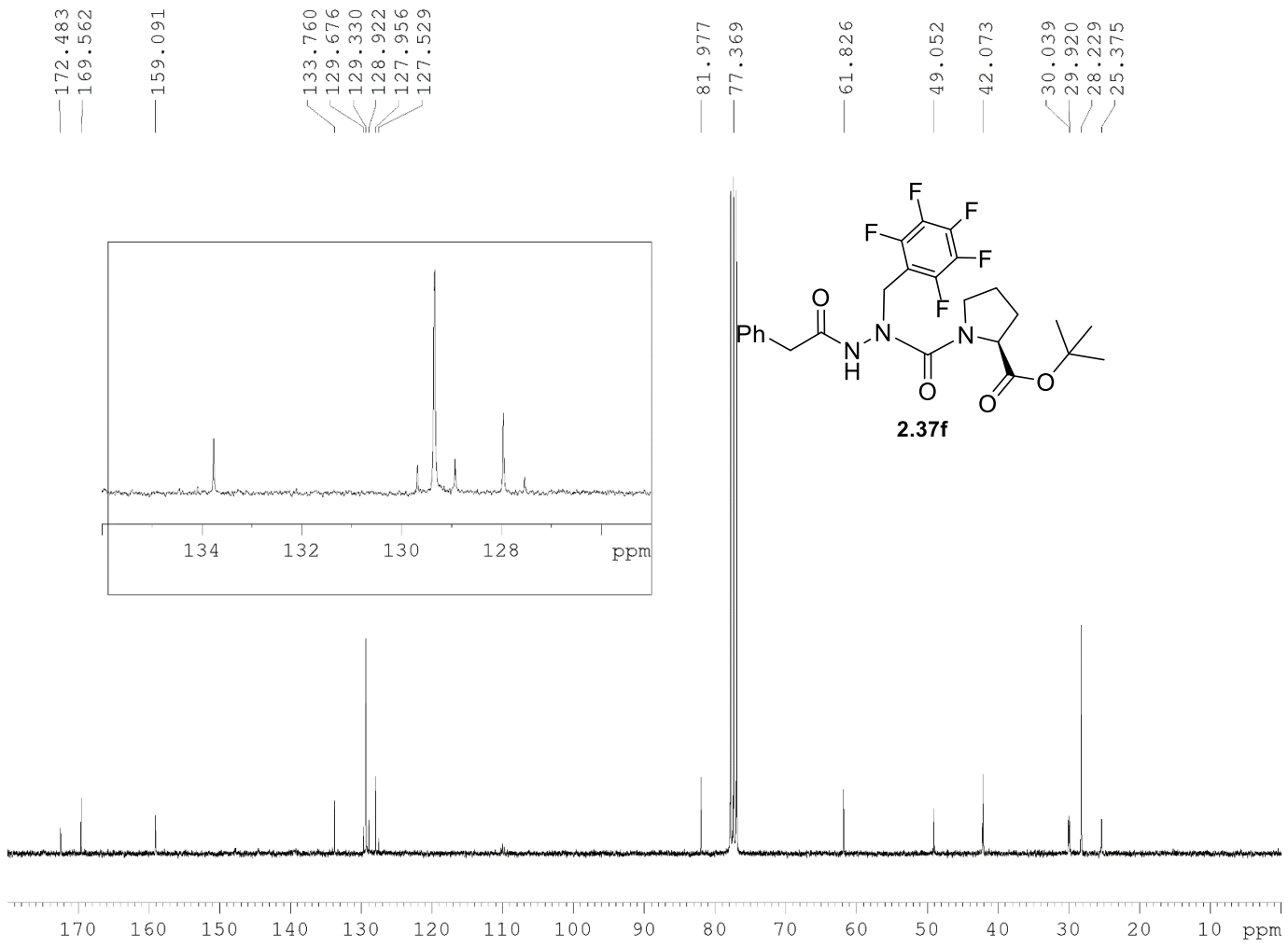

2.37f

^{1}H NMR 400MHz

Solvent: $CDCl_3$

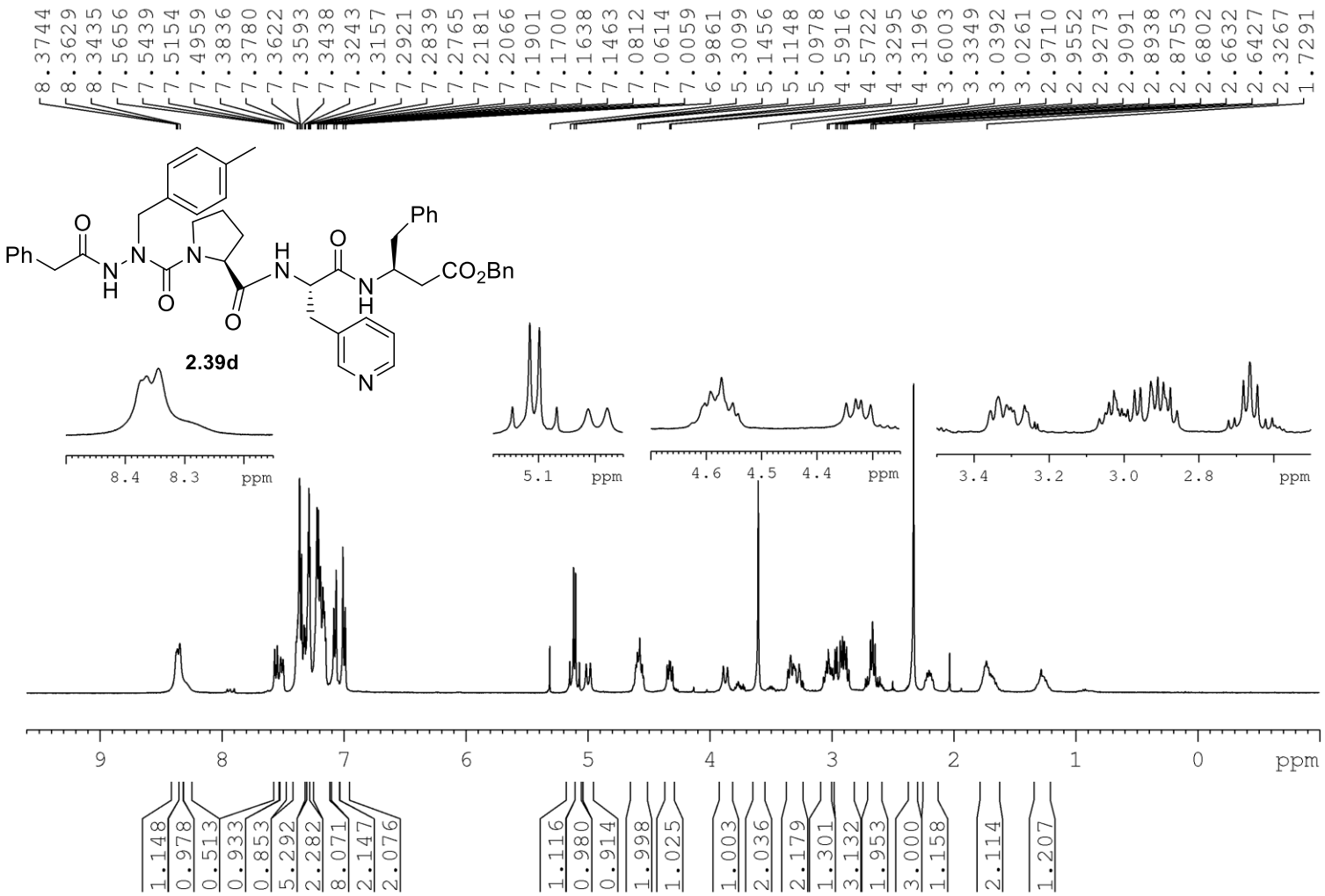

^{13}C NMR 175MHz

Solvent: $CDCl_3$

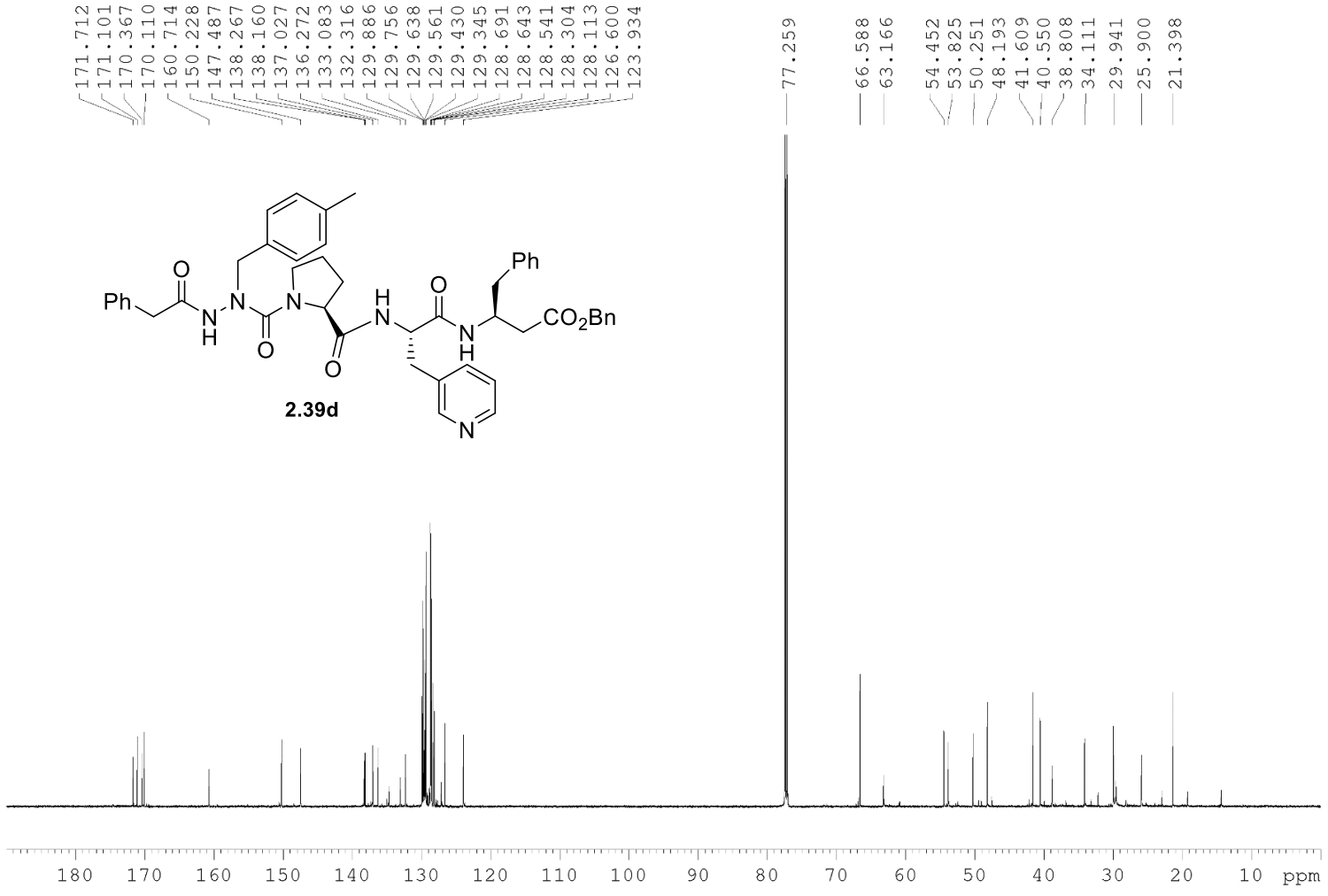

^{1}H NMR 300MHz

Solvent: $CDCl_3$

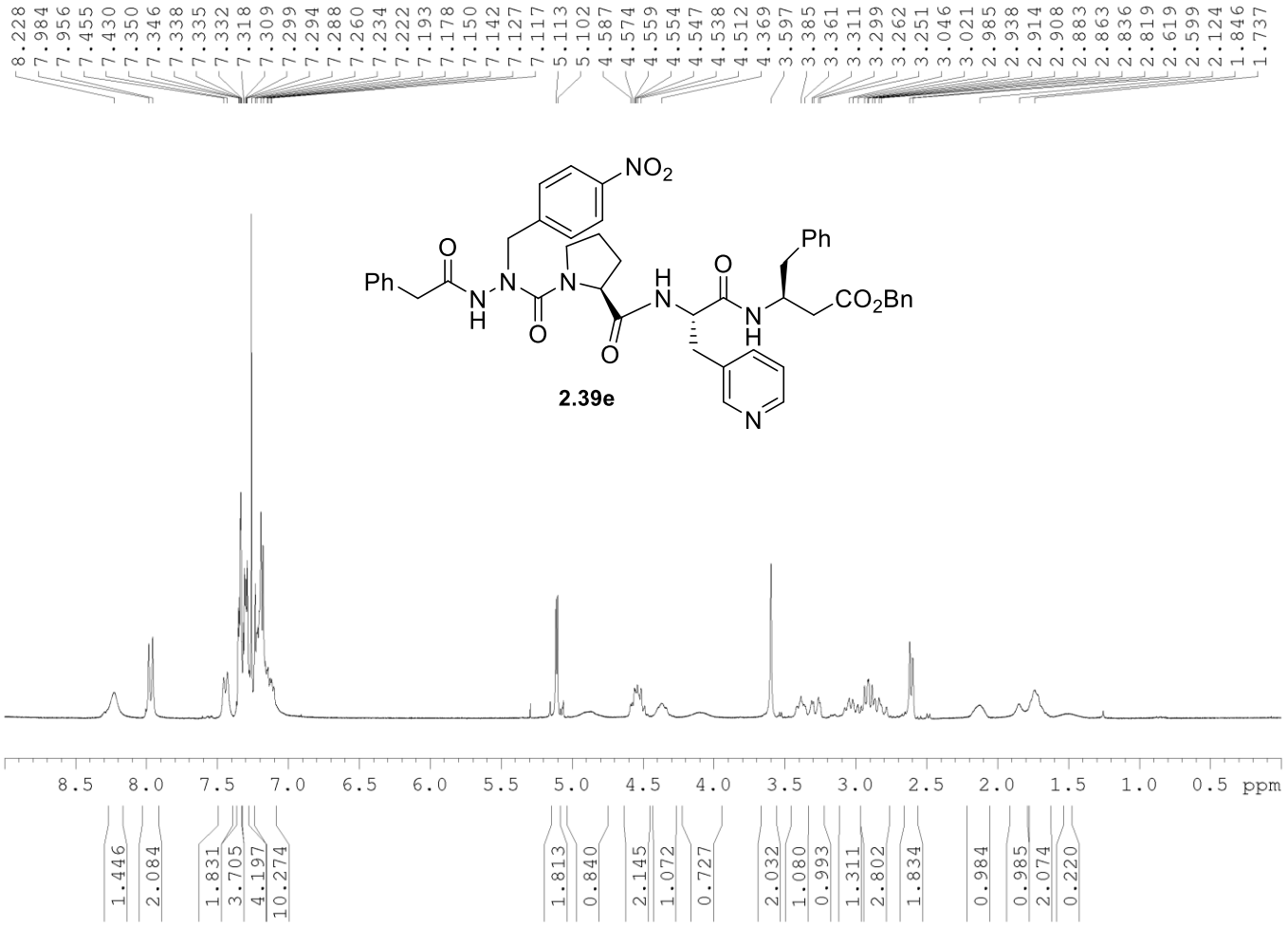

^{13}C NMR 125MHz

Solvent: $CDCl_3$

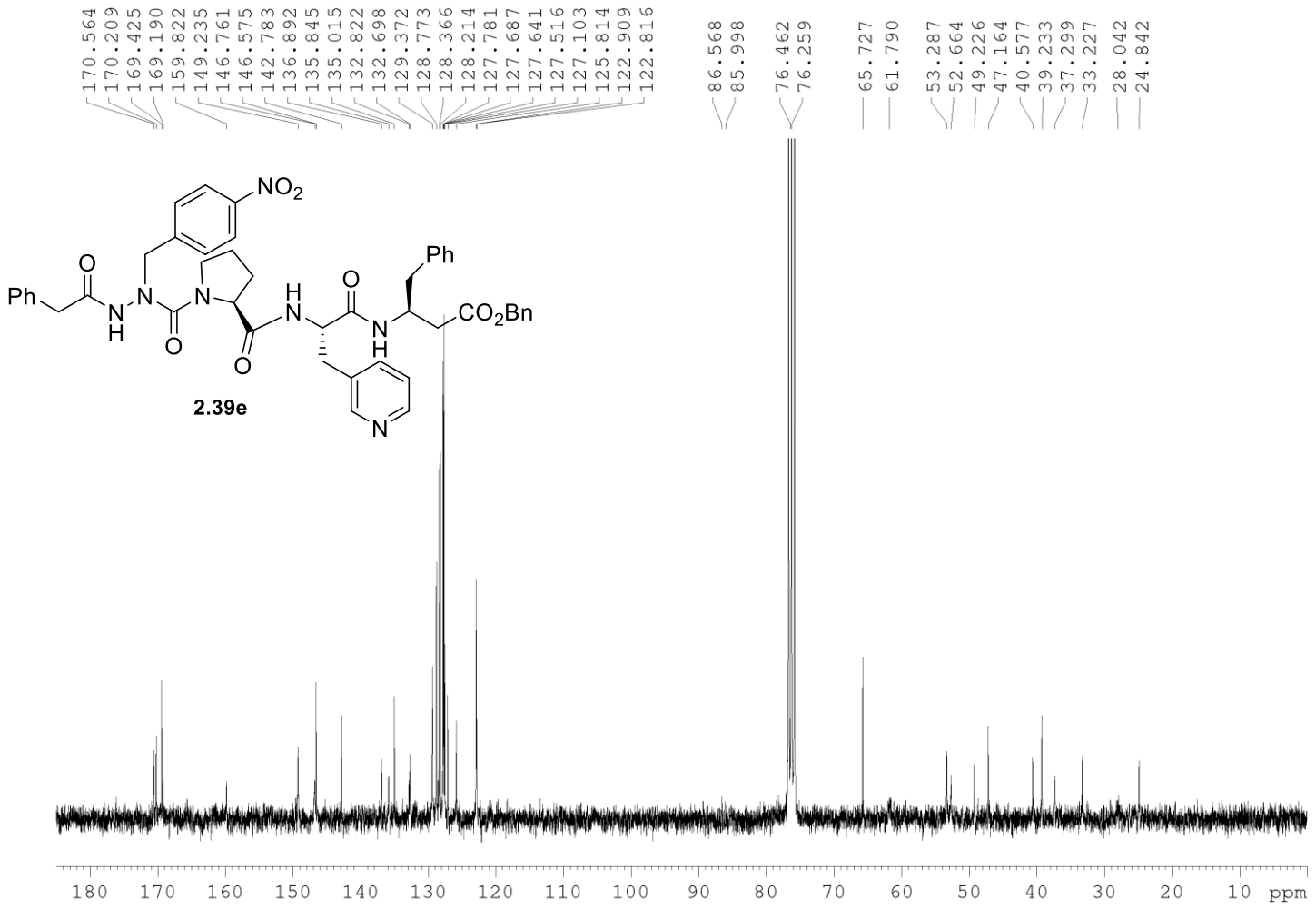

HSQC NMR 300MHz

Solvent: $CDCl_3$

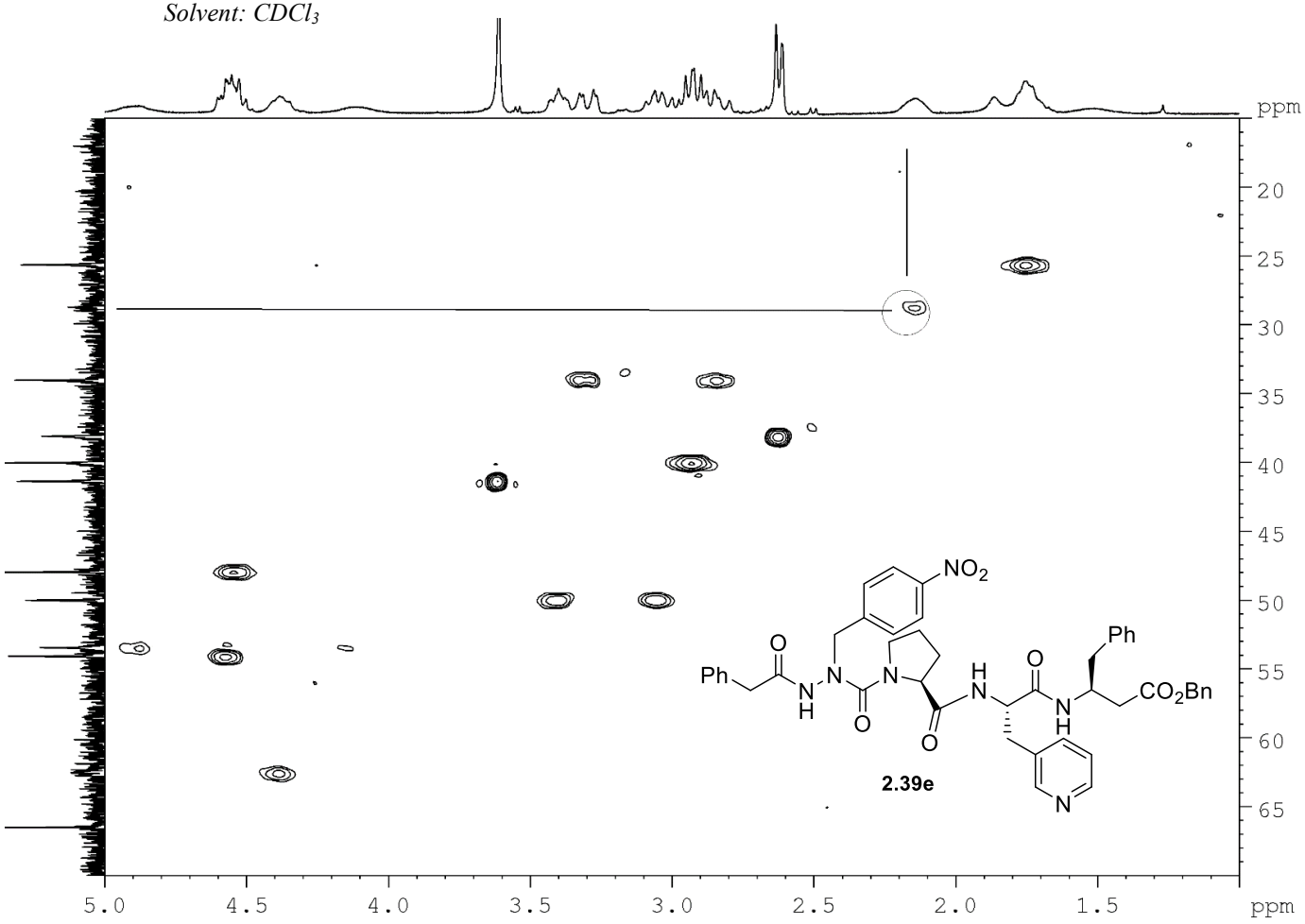

^{1}H NMR 500MHz

Solvent: $CDCl_3$

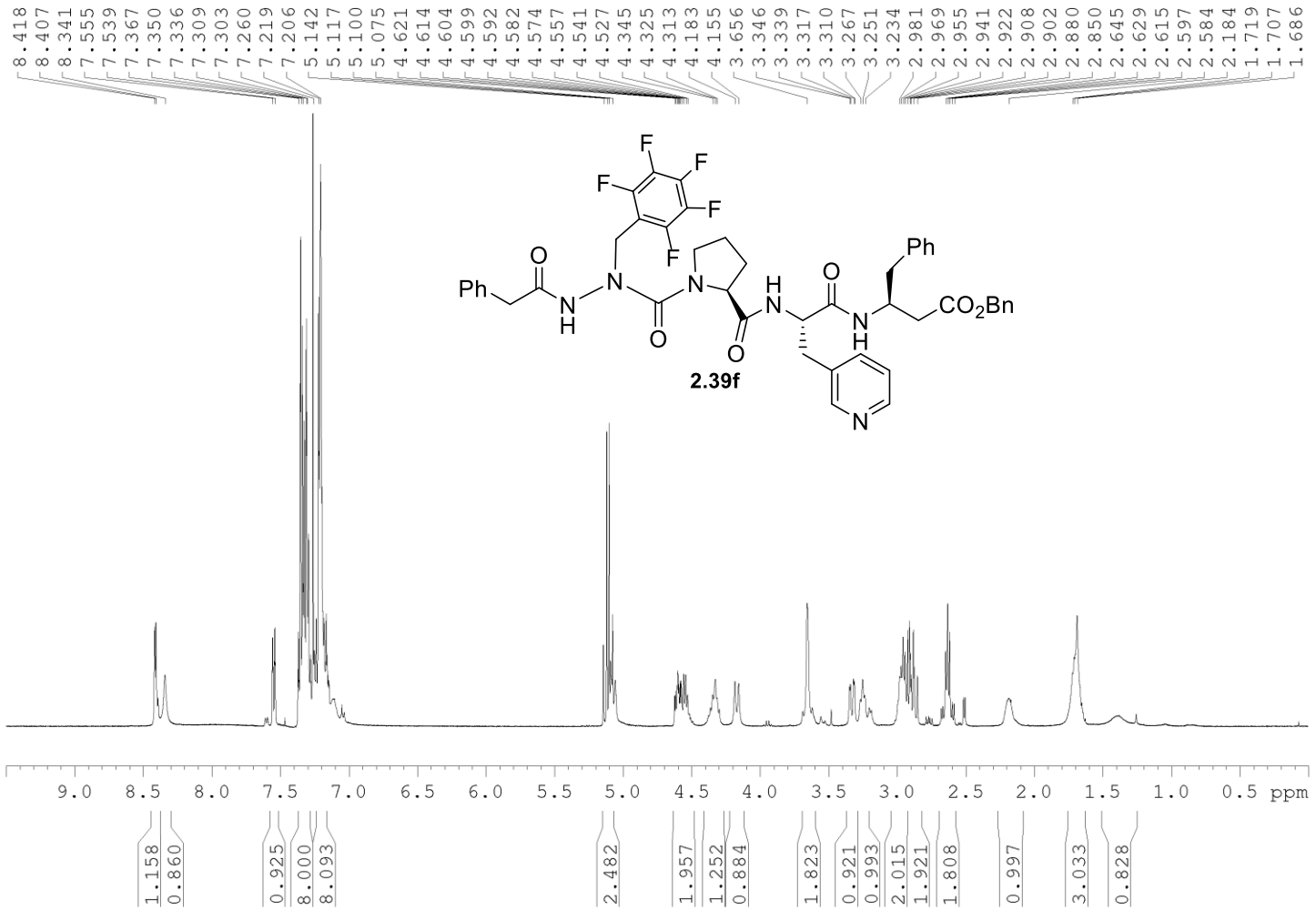

^{13}C NMR 125MHz

Solvent: $CDCl_3$

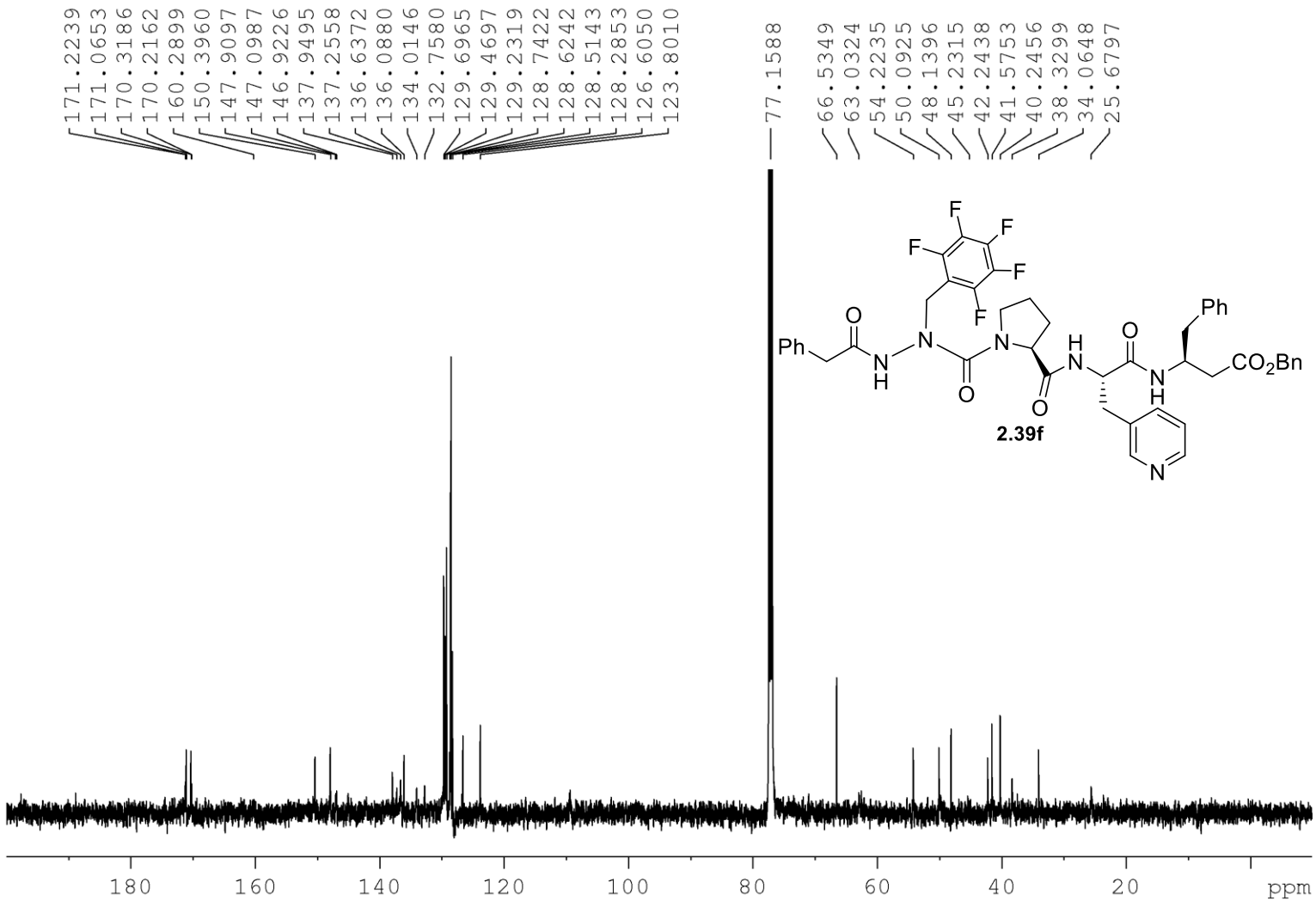

^{1}H NMR 500MHz

Solvent: DMSO-d_6

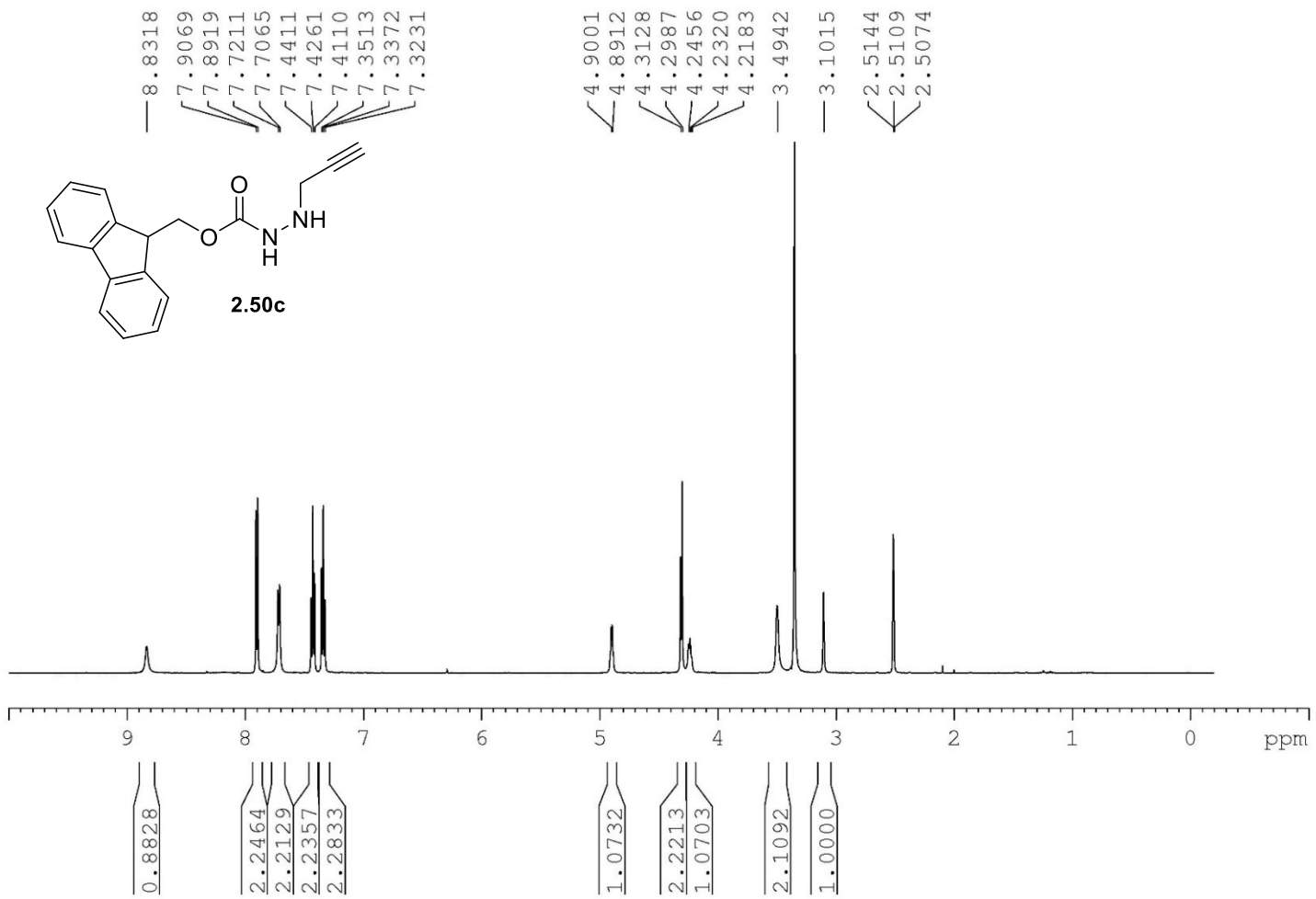

^{13}C NMR 125MHz
Solvent: DMSO-d_6

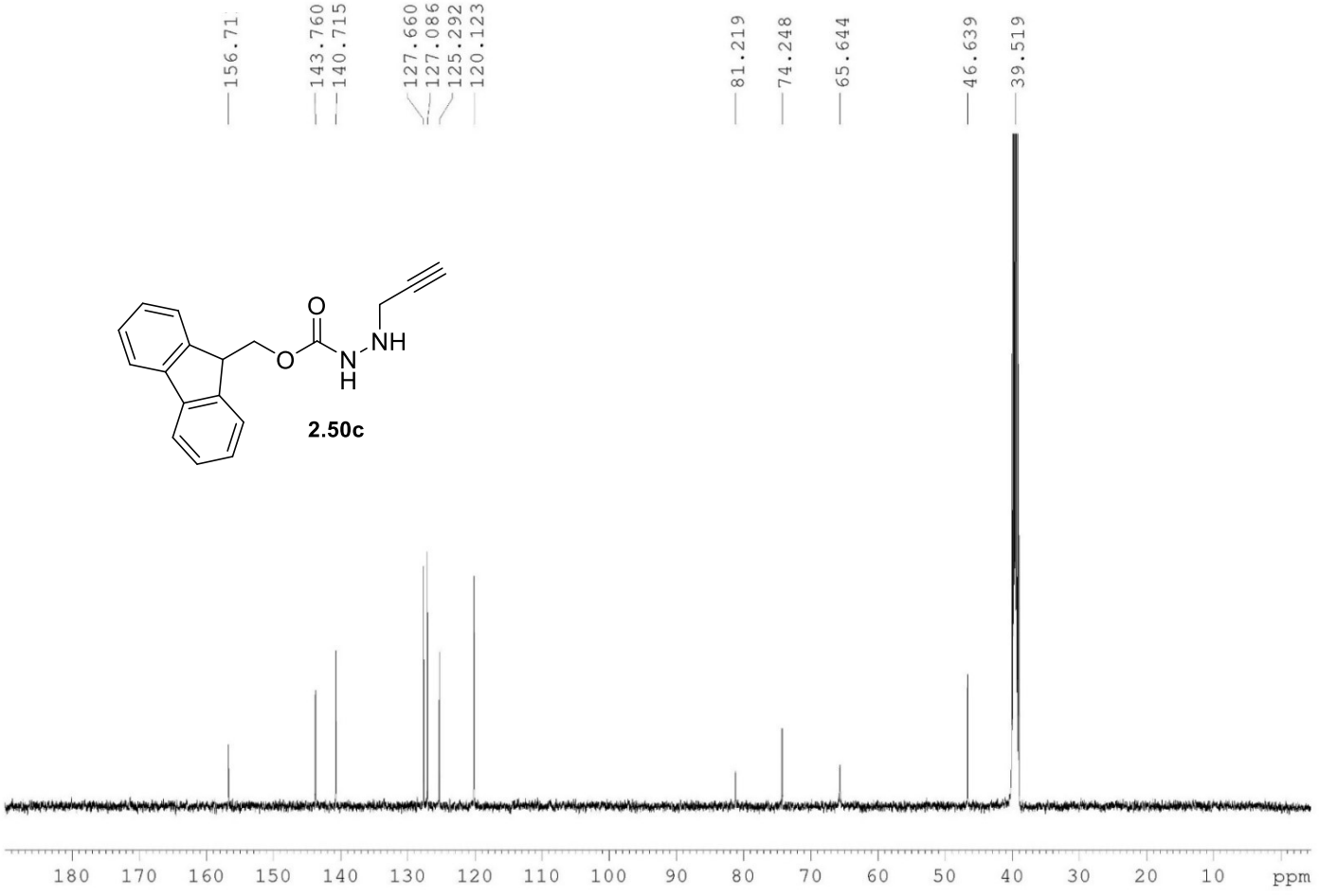

^{1}H NMR 400MHz
Solvent: DMSO-d_6

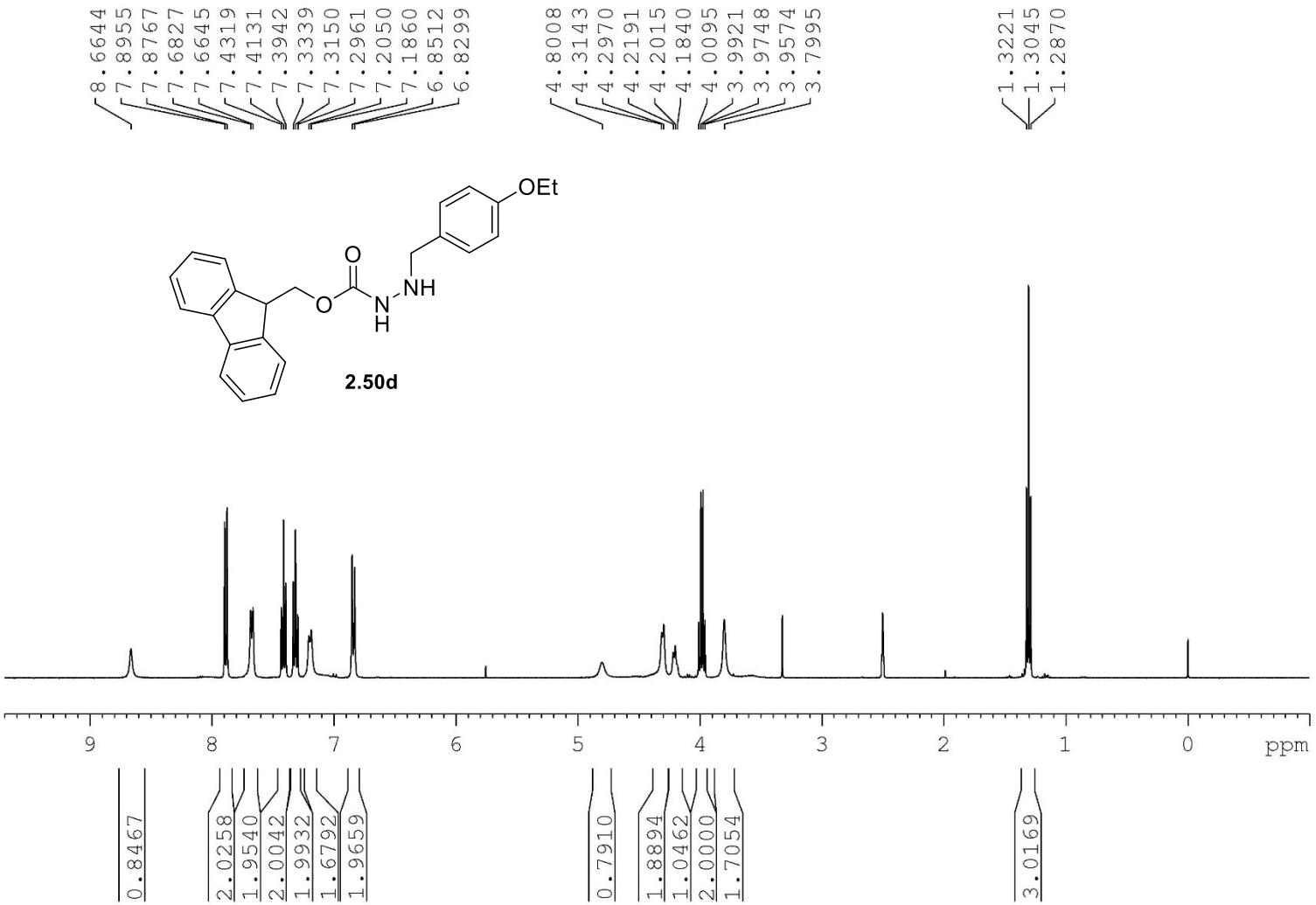

^{13}C NMR 75MHz
Solvent: DMSO d_6

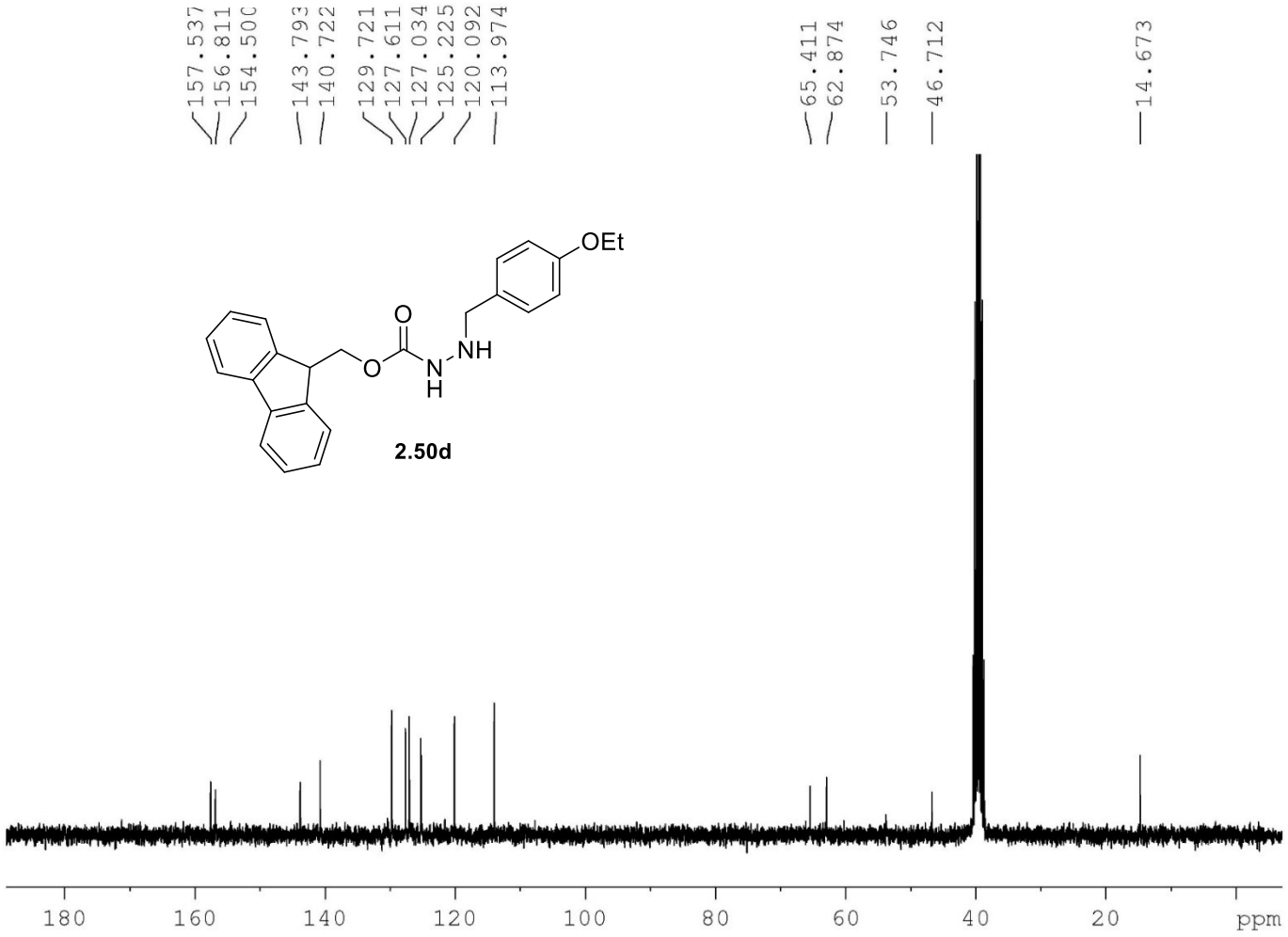

^{1}H NMR 500MHz
Solvent: DMSO-d6 (100 ℃)

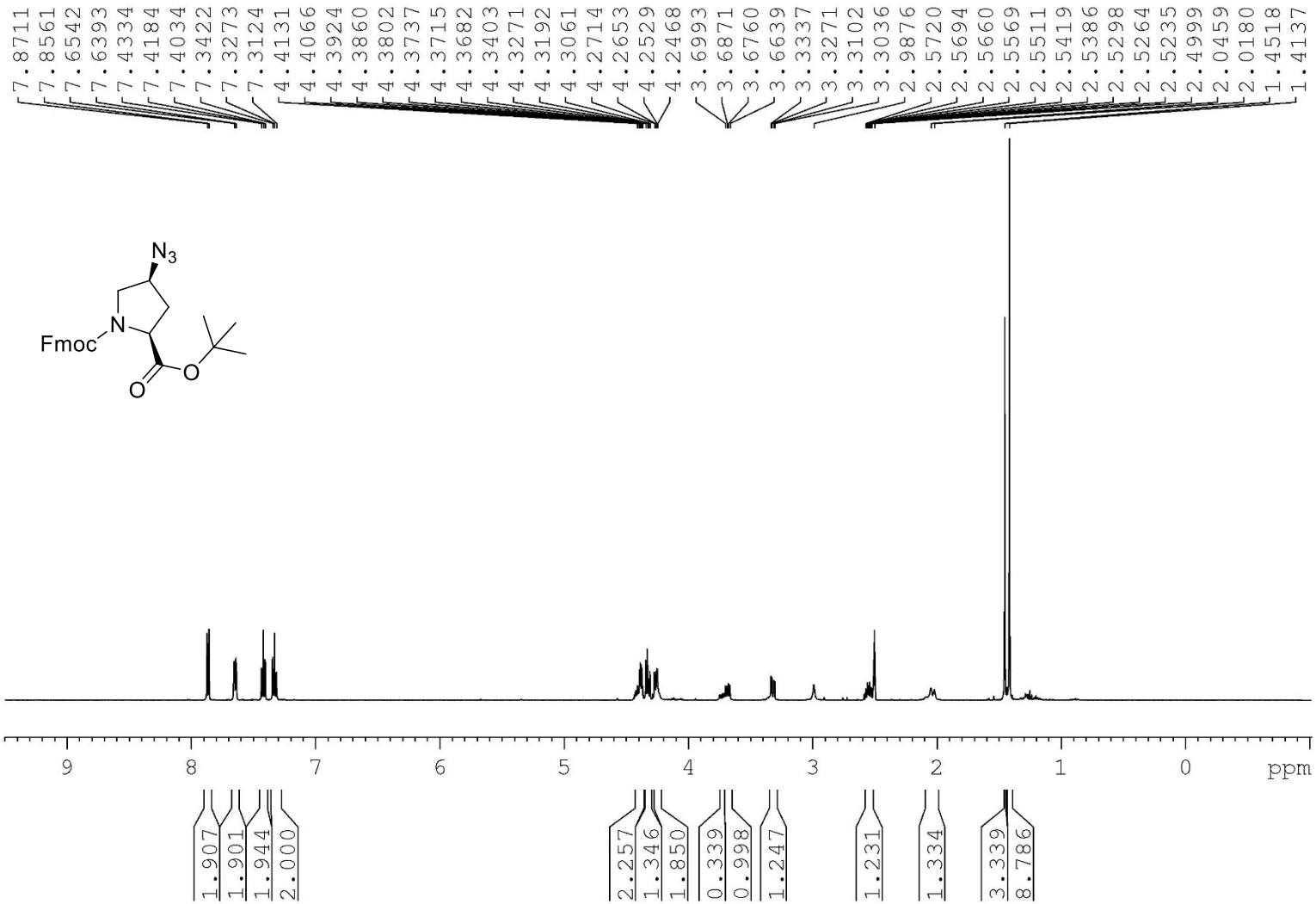

^{13}C NMR 125MHz
Solvent: DMSO-d_6 (100 ℃)

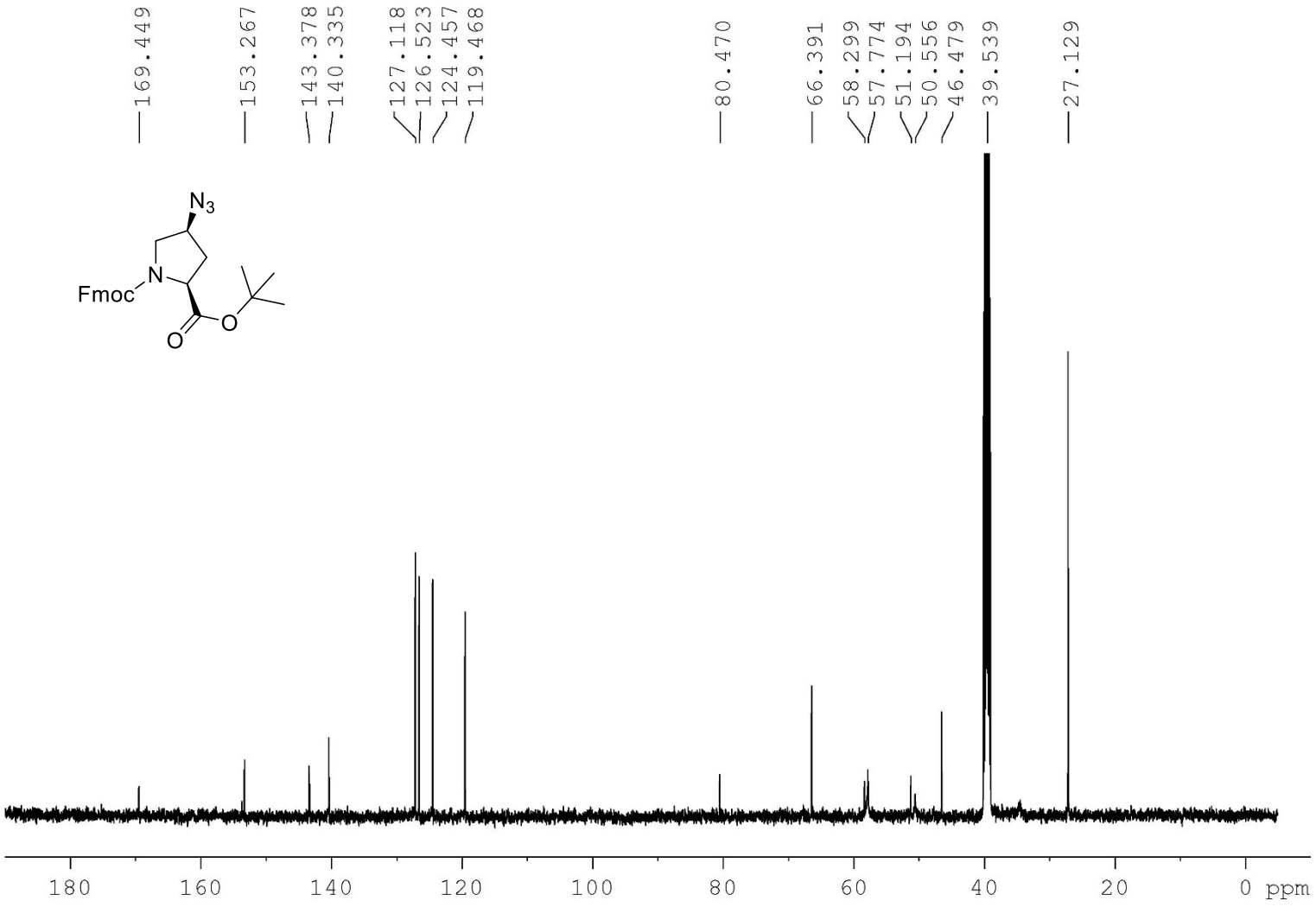

^{1}H NMR 500MHz
Solvent: DMSO-d_6 (100 ℃)

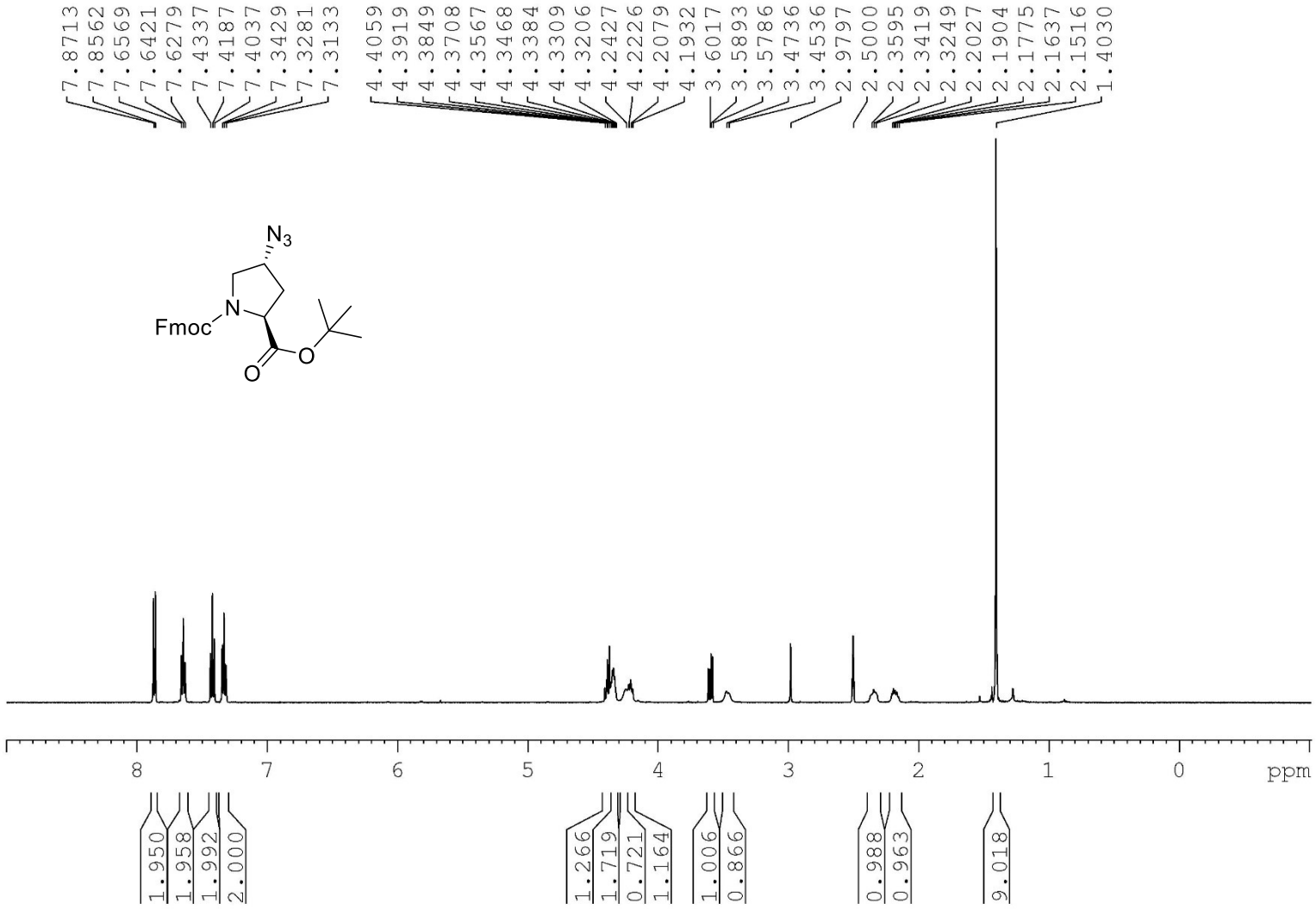

^{13}C NMR 125MHz
Solvent: DMSO d_6 (100 ℃)

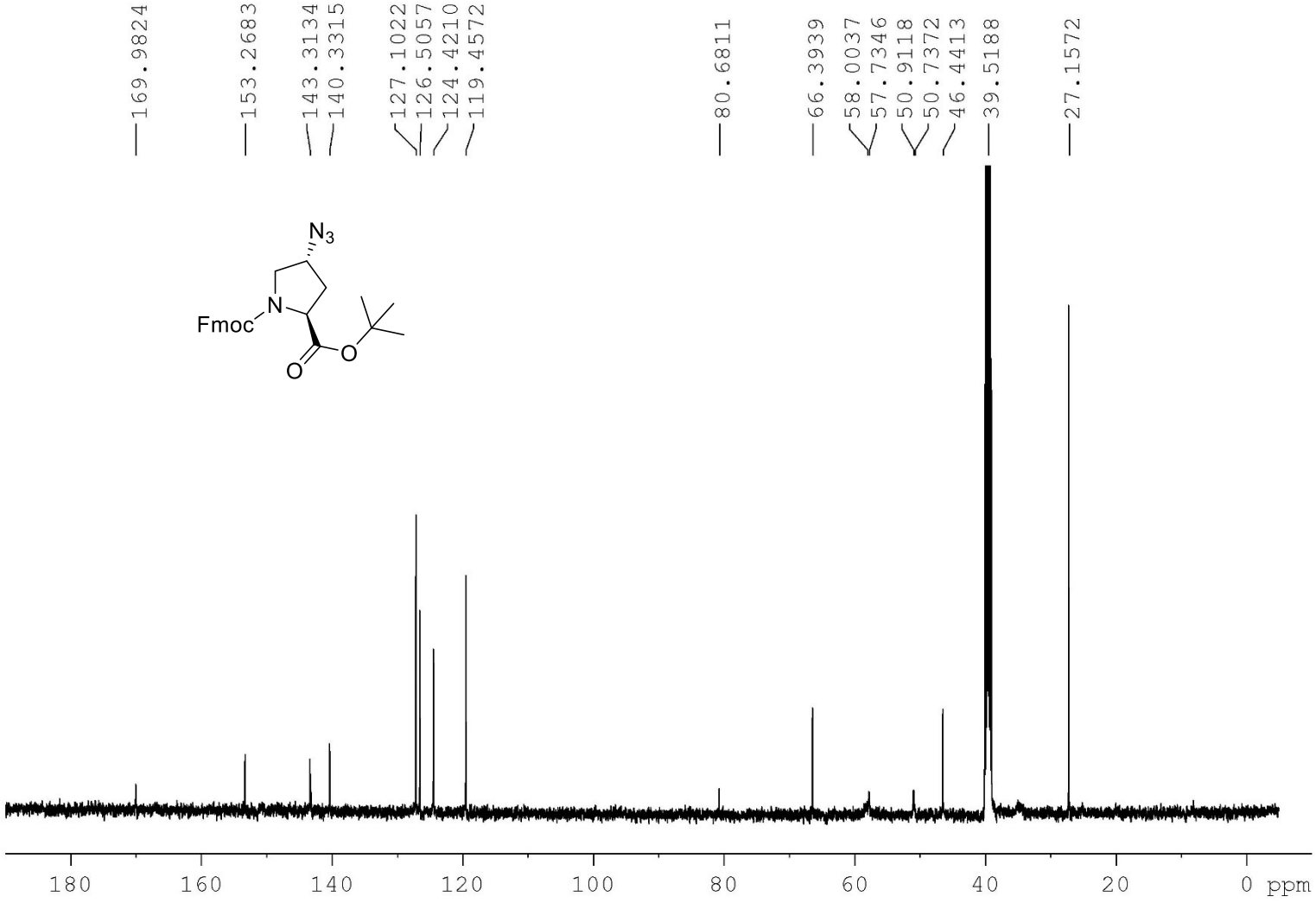

Ascertainment of purity by HPLC

Method A: Analytical HPLC, 70 to 90% MeOH [0.1% formic acid (FA)] in water (0.1% FA) over 20 min, flow rate of 0.5 mL/min on a on a Sunfire C18 analytical column (3.5 µm, 4.6 mm X 100 mm).

Method B: Analytical HPLC, 20 to 80% MeOH or MeCN [0.1% formic acid (FA)] in water (0.1% FA) over 14 min, flow rate of 0.5 mL/min on a on a Sunfire C18 analytical column (3.5 µm, 4.6 mm X 100 mm).

Method C: Analytical HPLC, 30 to 95% MeOH [0.1% formic acid (FA)] in water (0.1% FA) over 14 min, flow rate of 0.5 mL/min on a on a Sunfire C18 analytical column (3.5 µm, 4.6 mm X 100 mm).

Method D: Analytical HPLC, 10 to 90% MeOH or MeCN [0.1% formic acid (FA)] in water (0.1% FA) over 14 min, flow rate of 0.5 mL/min on a on a Sunfire C18 analytical column (3.5 µm, 4.6 mm X 100 mm).

Method E: Analytical HPLC, 40 to 90% MeOH [0.1% formic acid (FA)] in water (0.1% FA) over 12 min, flow rate of 0.5 mL/min on a on a Sunfire C18 analytical column (3.5 µm, 4.6 mm X 100 mm).

Method F: Analytical HPLC, 50 to 90% MeOH [0.1% formic acid (FA)] in water (0.1% FA) over 14 min, flow rate of 0.5 mL/min on a on a Sunfire C18 analytical column (3.5 µm, 4.6 mm X 100 mm).

Method G: Analytical HPLC, 50 to 80% MeOH [0.1% formic acid (FA)] in water (0.1% FA) over 14 min, flow rate of 0.5 mL/min on a on a Sunfire C18 analytical column (3.5 µm, 4.6 mm X 100 mm).

Method H: Analytical HPLC, 30 to 90% MeOH or MeCN[0.1% formic acid (FA)] in water (0.1% FA) over 14 min, flow rate of 0.5 mL/min on a on a Sunfire C18 analytical column (3.5 µm, 4.6 mm X 100 mm).

Method I: Analytical HPLC, 5 to 80% MeCN [0.1% formic acid (FA)] in water (0.1% FA) over 14 min, flow rate of 0.5 mL/min on a on a Sunfire C18 analytical column (3.5 µm, 4.6 mm X 100 mm).

Method J: Analytical HPLC, 30 to 80% MeOH [0.1% formic acid (FA)] in water (0.1% FA) over 12 min, flow rate of 0.5 mL/min on a on a Sunfire C18 analytical column (3.5 µm, 4.6 mm X 100 mm).

Method K: Analytical HPLC, 40 to 70% MeOH [0.1% formic acid (FA)] in water (0.1% FA) over 15 min, flow rate of 0.5 mL/min on a on a Sunfire C18 analytical column (3.5 µm, 4.6 mm X 100 mm).

Method L: Analytical HPLC, 5 to 90% MeCN [0.1% formic acid (FA)] in water (0.1% FA) over 15 min, flow rate of 0.5 mL/min on a on Atlantis dC18 (5 μm, 3.9 mm X 100mm)

Method M: Analytical HPLC, 10 to 90% MeOH [0.1% formic acid (FA)] in water (0.1% FA) over 15 min, flow rate of 0.8 mL/min on a on Atlantis dC18 (5 μm, 3.9 mm X 100mm)

Method G/12 min, **2.6d**, Purity ≥ 98% (MeOH), RT = 7.2

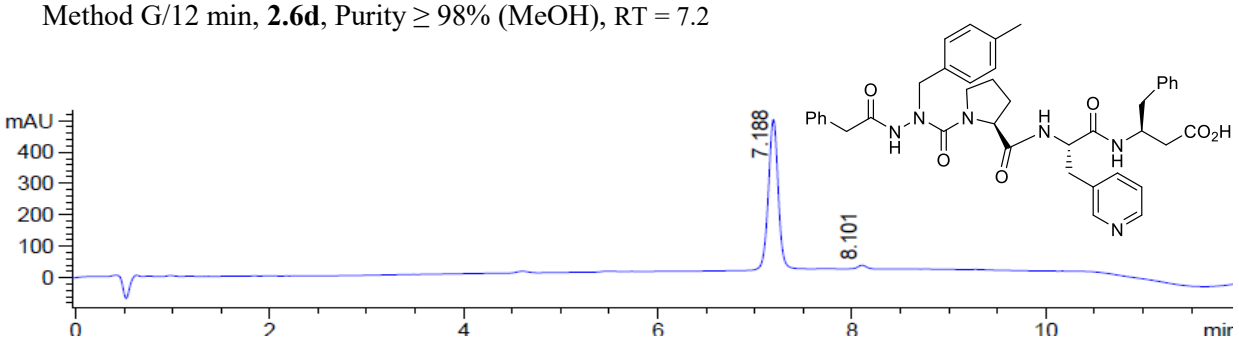

Method B/14 min, **2.6d**, Purity ≥ 96% (MeCN), RT = 5.1

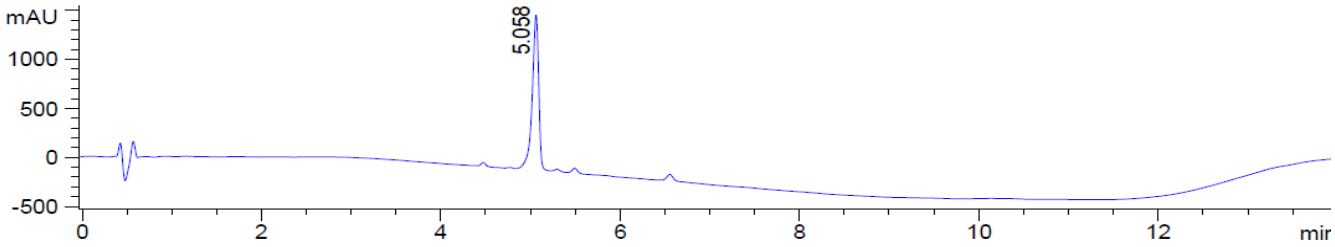

Method C/14 min, **2.6e**, Purity ≥ 99% (MeOH), RT = 7.2

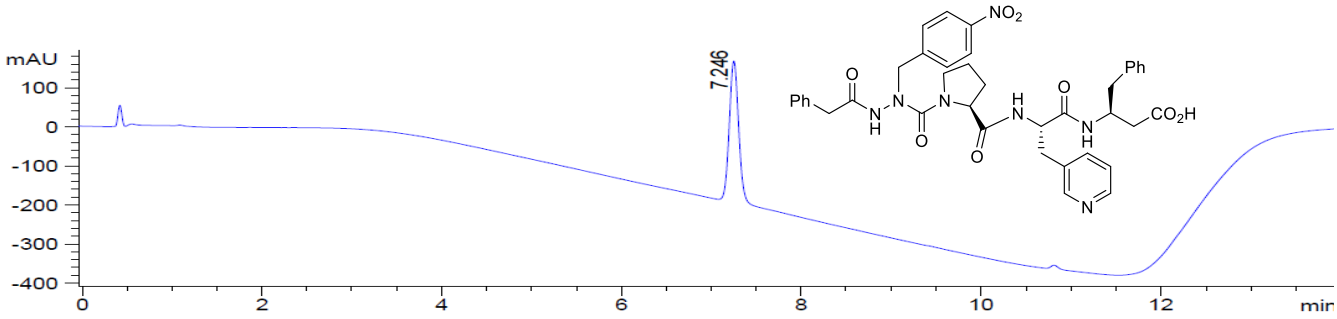

Method D/14 min, **2.6e**, Purity ≥ 99% (MeCN), RT = 6.3

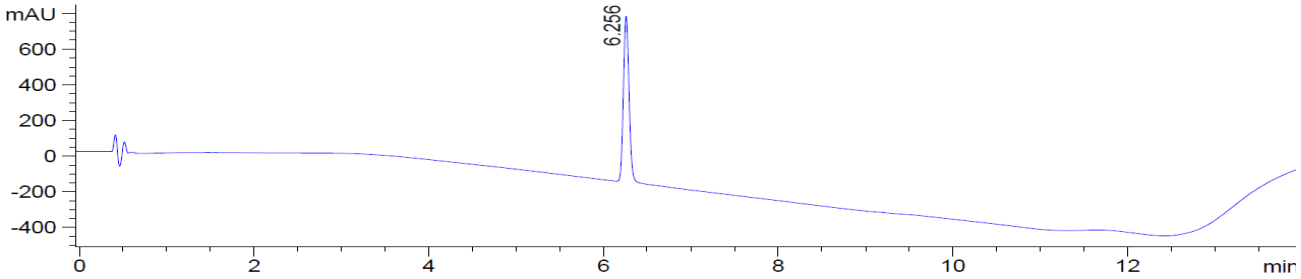

Method A/20 min, **2.6f**, Purity ≥ 99% (MeOH), RT = 10.3

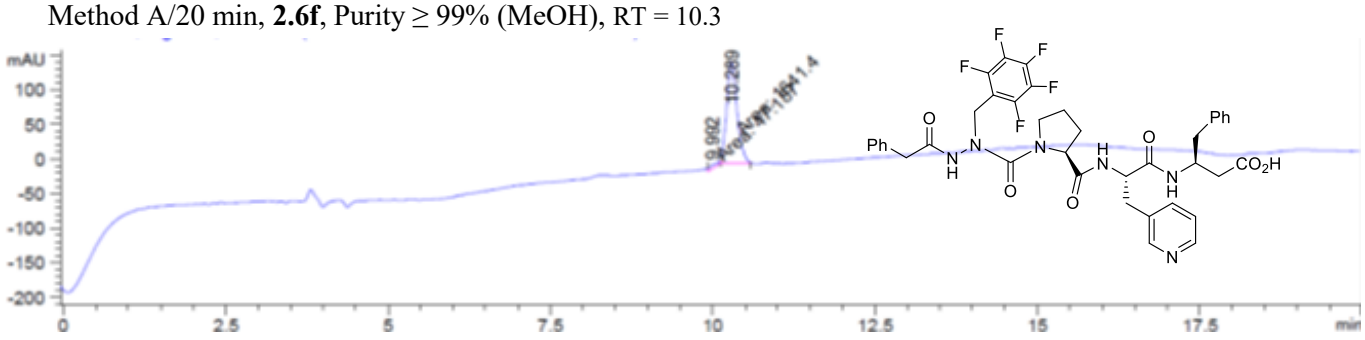

Method B/14 min, **2.6f**, Purity ≥ 99% (MeCN), RT = 5.4

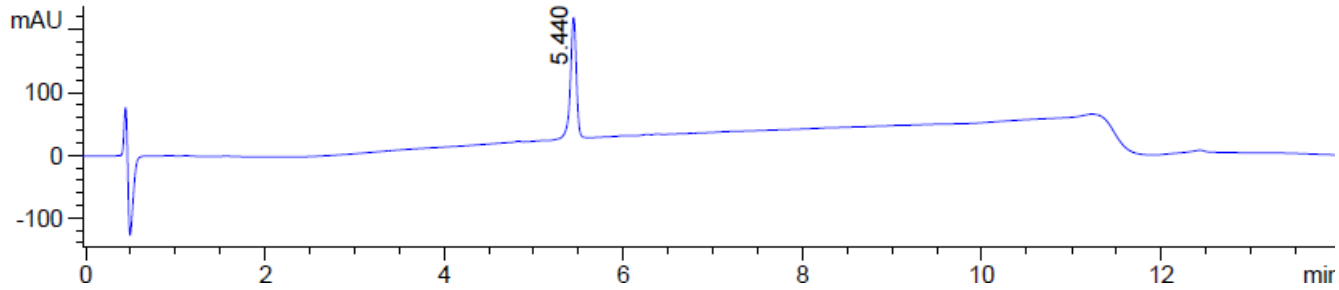

Method E, **2.6g**, Purity ≥ 99% (MeOH), RT = 5.8

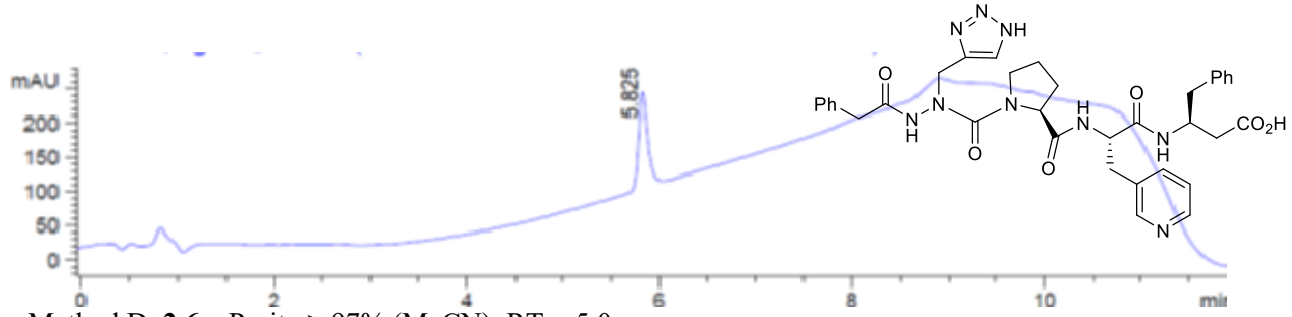

Method D, **2.6g**, Purity ≥ 97% (MeCN), RT = 5.0

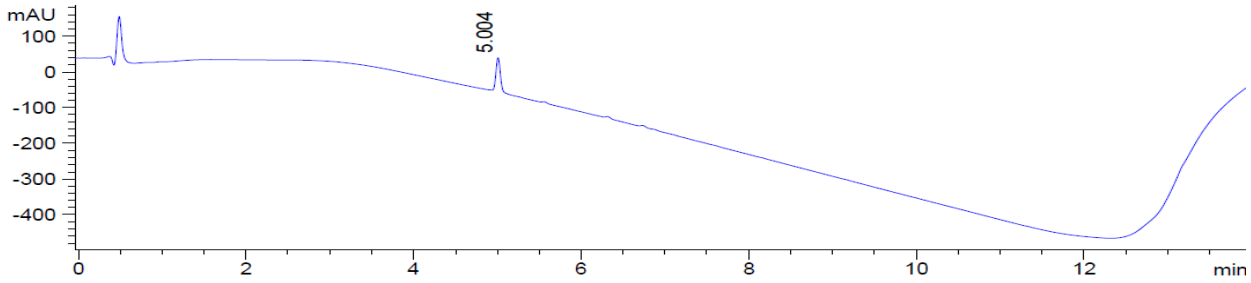

Method F, **2.6h**, Purity ≥ 99% (MeOH), RT = 4.4

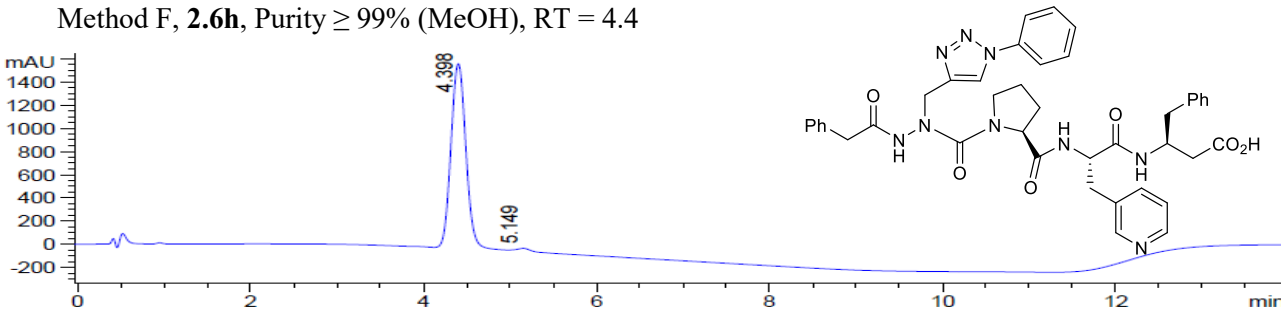

Method D, **2.6h**, Purity ≥ 99% (MeCN), RT = 6.0

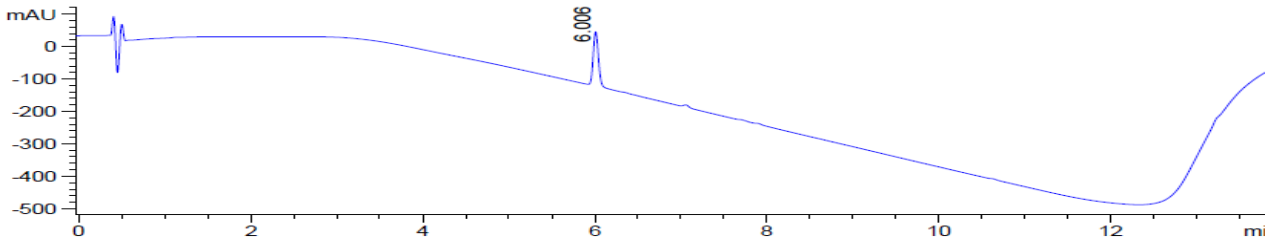

Method G, **2.6i**, Purity ≥ 97% (MeOH), RT = 6.7

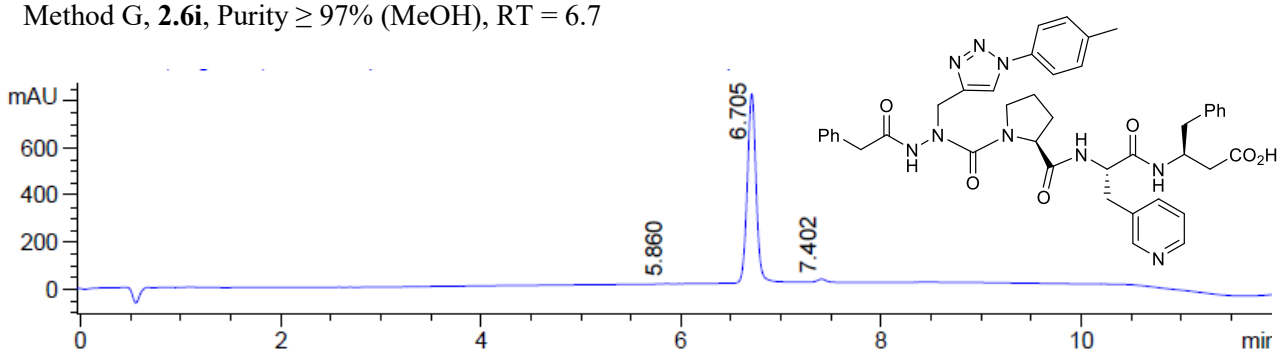

Method D, **2.6i**, Purity ≥ 97% (MeCN), RT = 6.3

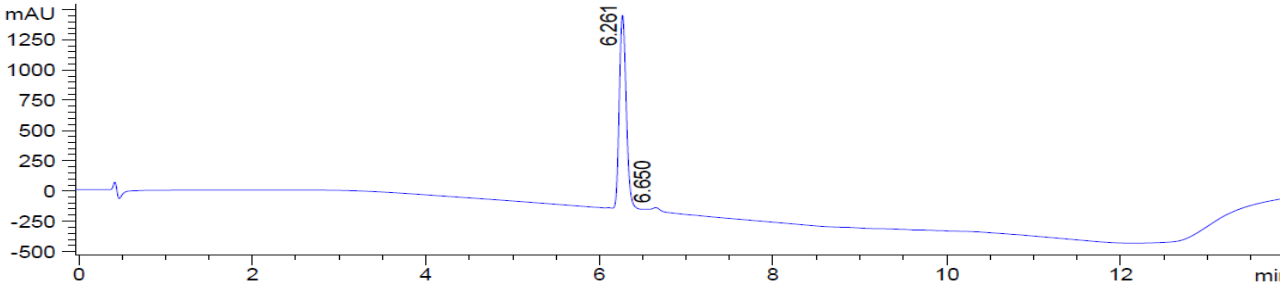

Method B, **2.6j**, Purity ≥ 97% (MeOH), RT = 8.9

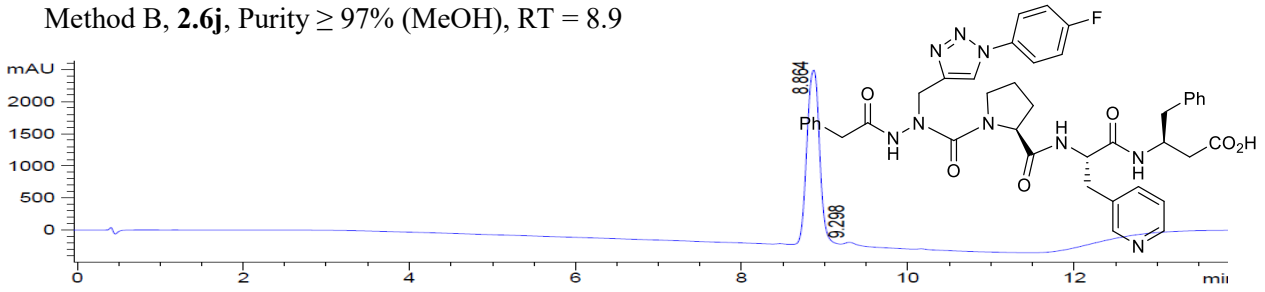

Method D, **2.6j**, Purity ≥ 97% (MeCN), RT = 6.0

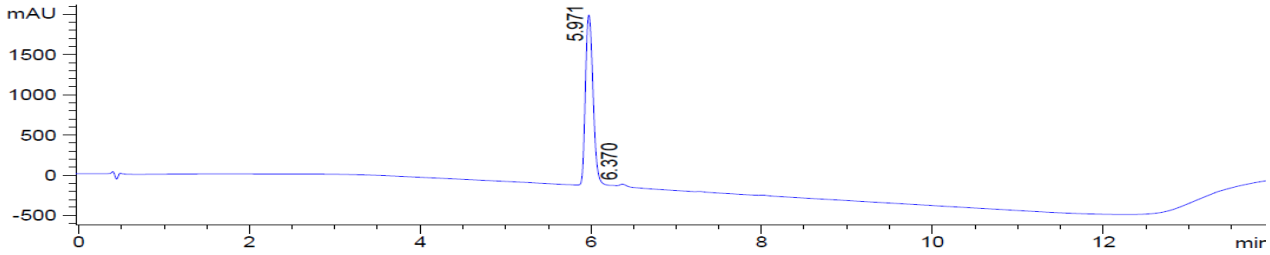

Method G, **2.6k**, Purity ≥ 99% (MeOH), RT = 7.7

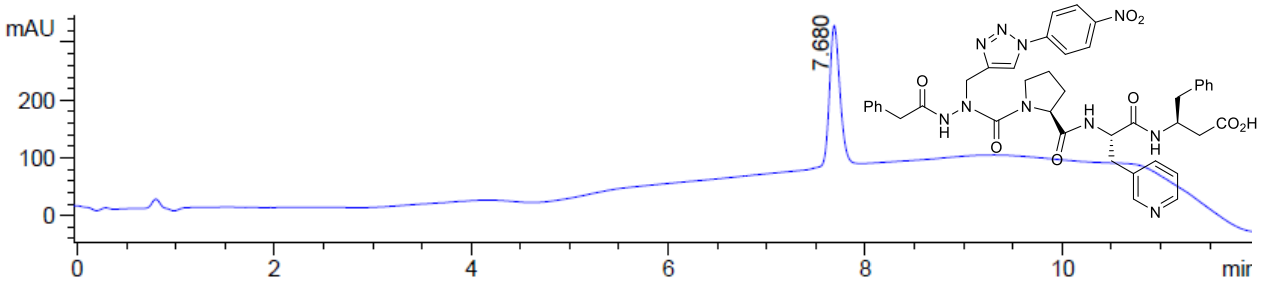

Method D, **2.6k**, Purity ≥ 98% (MeCN), RT = 6.1

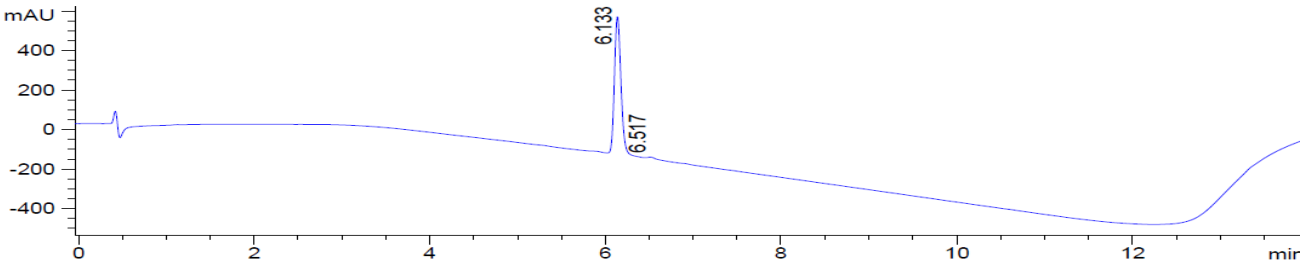

Method H, **2.6l**, Purity ≥ 99% (MeOH), RT = 6.5

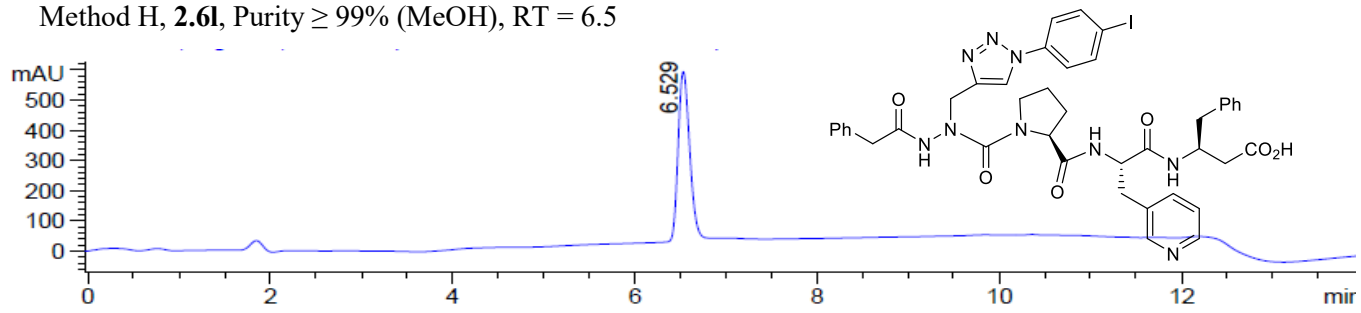

Method H, **2.6l**, Purity ≥ 99% (MeOH), RT = 5.9

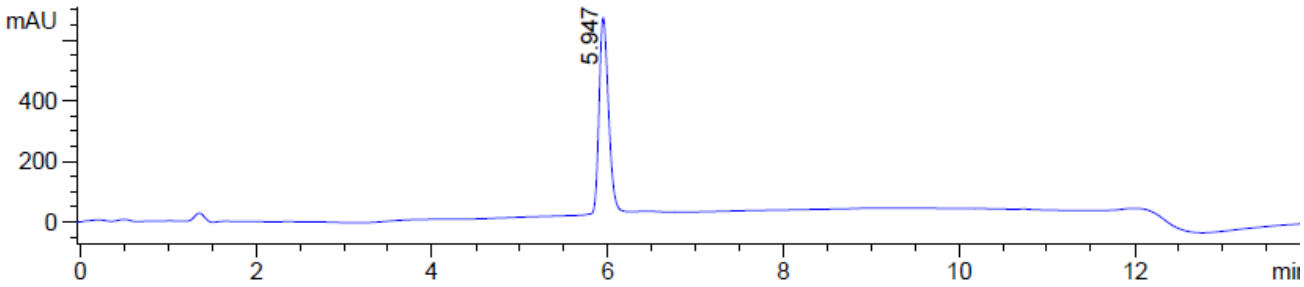

Method B, **2.7**, Purity ≥ 99% (MeOH), RT = 7.6

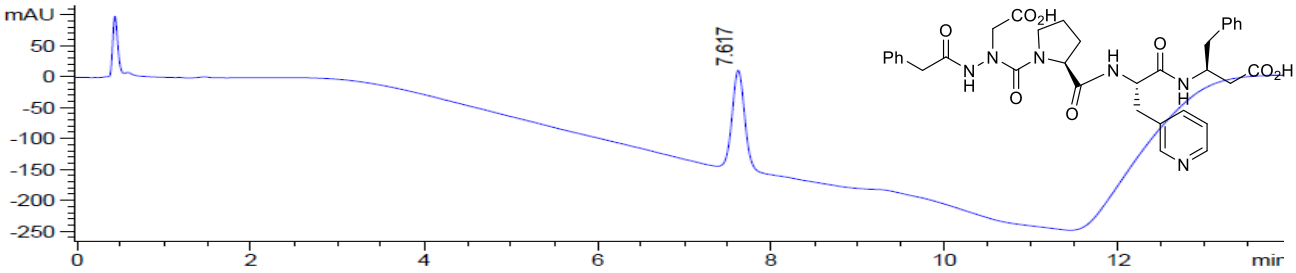

Method D, **2.7**, Purity ≥ 99% (MeCN), RT = 5.0

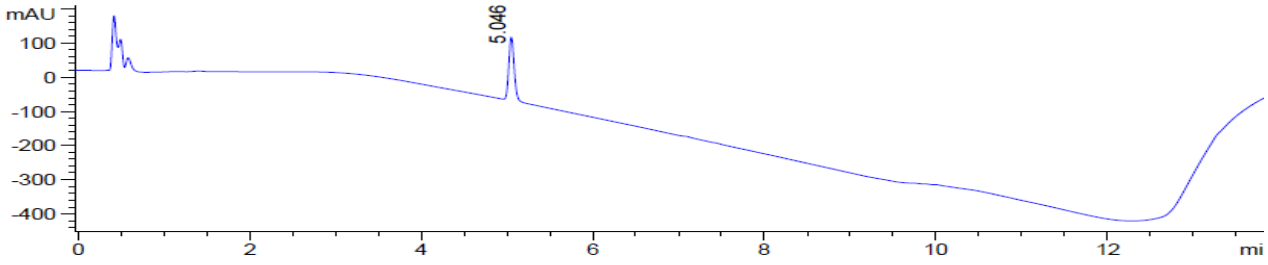

Method B, **2.8m**, Purity ≥ 98% (MeOH), RT = 5.4

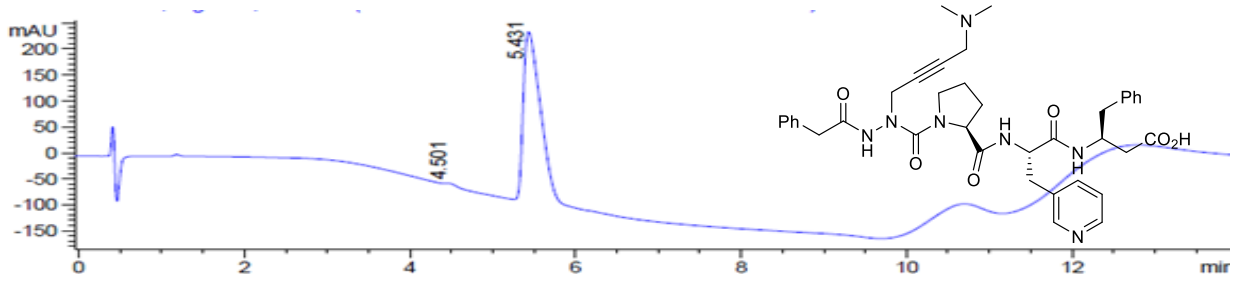

Method D, **2.8m**, Purity ≥ 99% (MeCN), RT = 4.2

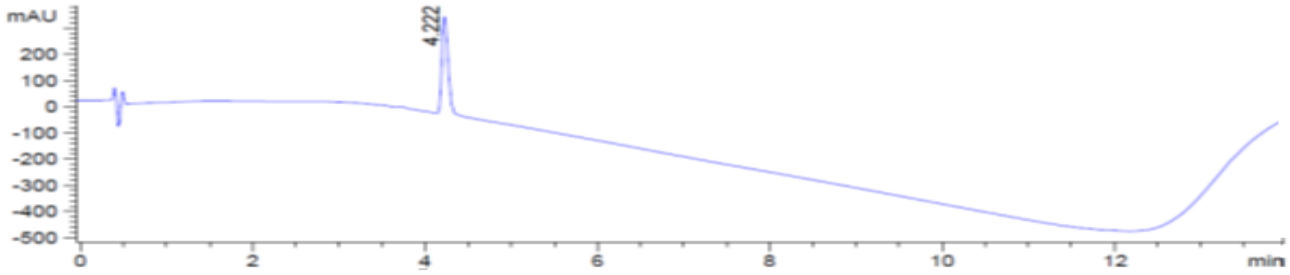

Method D, **2.8n**, Purity ≥ 99% (MeOH), RT = 6.3

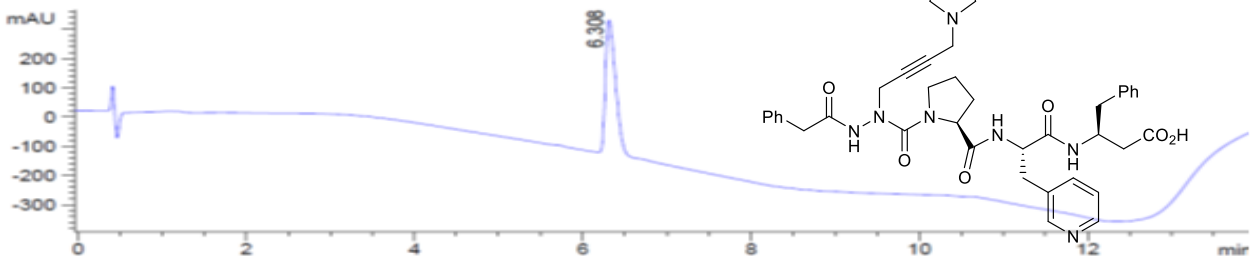

Method D, **2.8n**, Purity ≥ 99% (MeCN), RT = 4.4

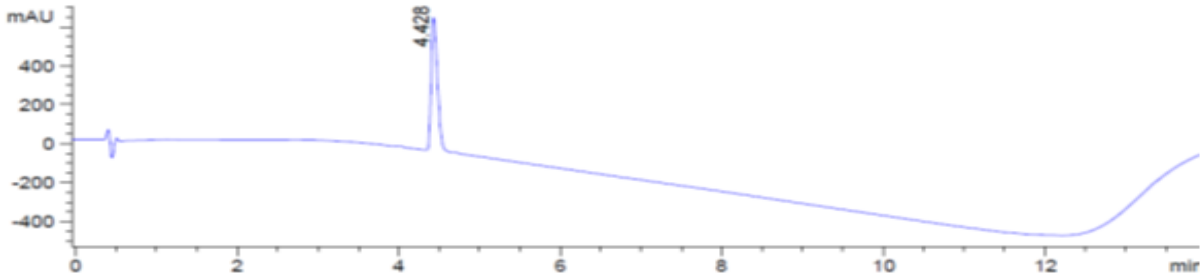

Method B, **2.8o**, Purity ≥ 99% (MeOH), RT = 5.8

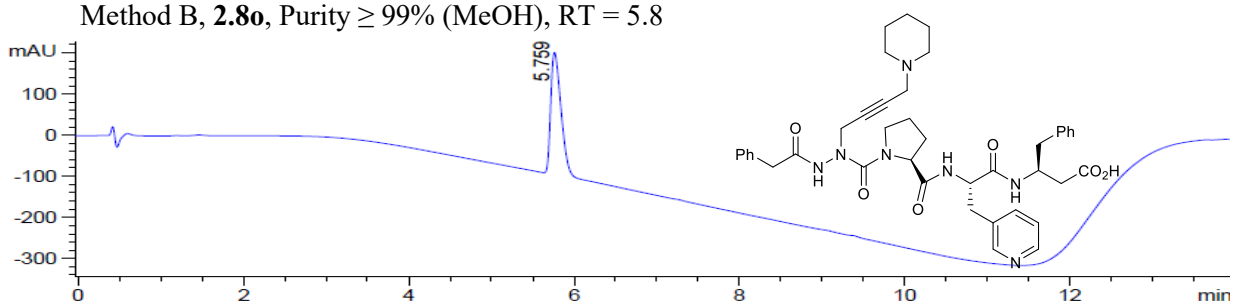

Method I, **2.8o**, Purity ≥ 98% (MeCN), RT = 4.4

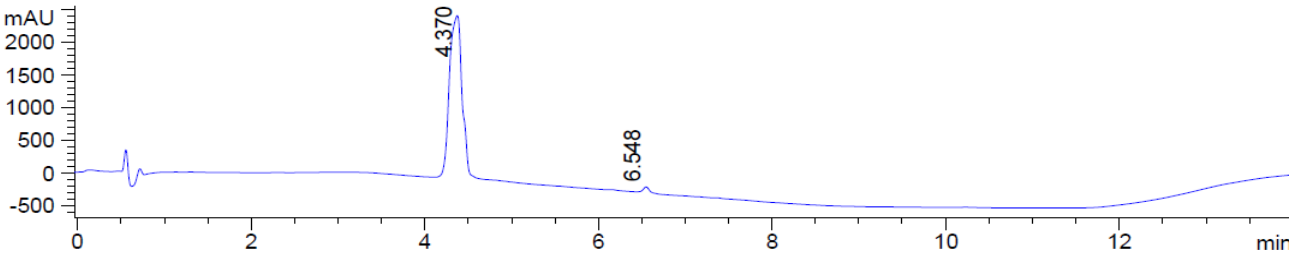

Method J, **2.8p**, Purity ≥ 99% (MeOH), RT = 7.1

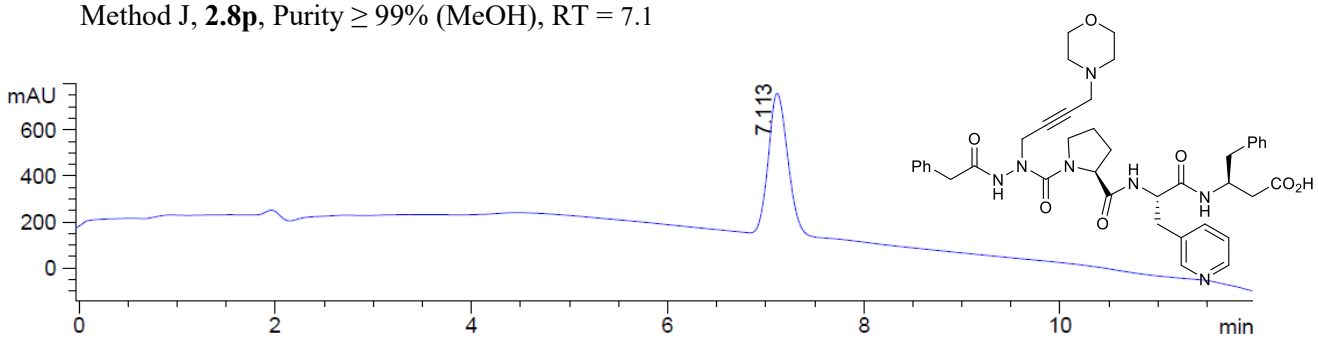

Method I, **2.8p**, Purity ≥ 99% (MeCN), RT = 4.4

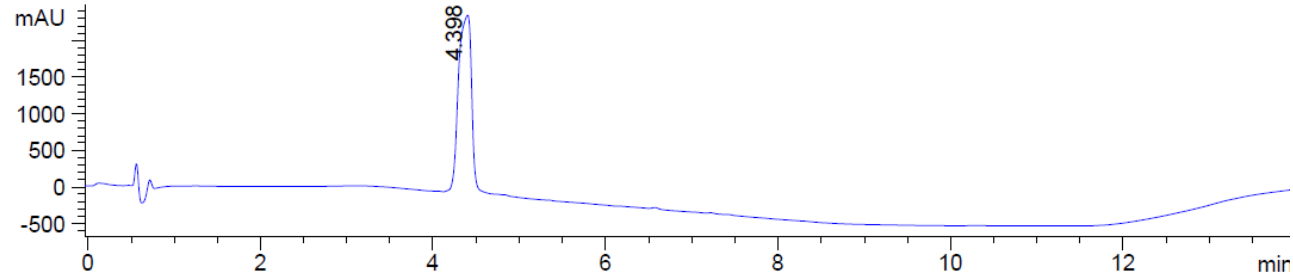

Method E, **2.8q**, Purity ≥ 99% (MeOH), RT = 2.2

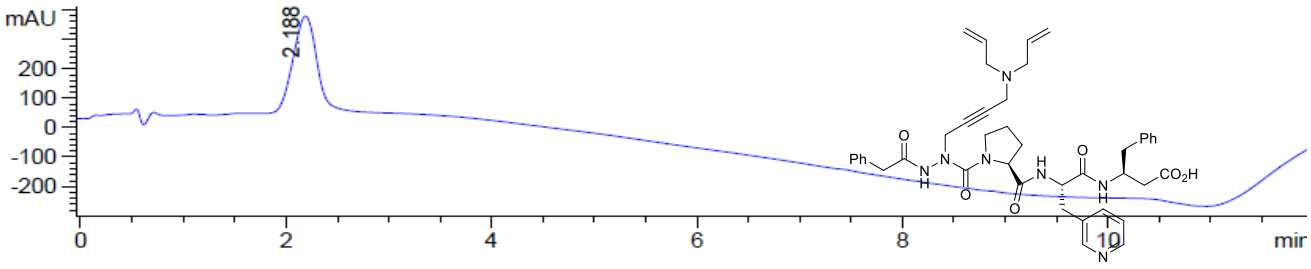

Method I, **2.8q**, Purity ≥ 99% (MeCN), RT = 4.6

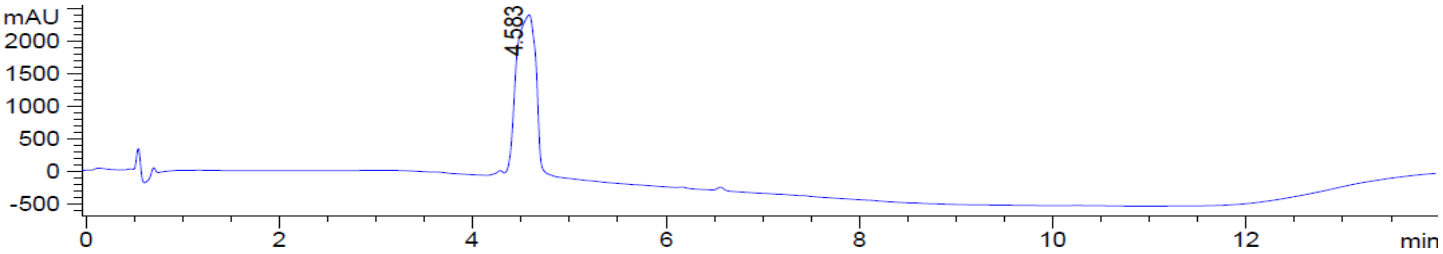

Method B, **2.8r**, Purity ≥ 99% (MeOH), RT = 6.6

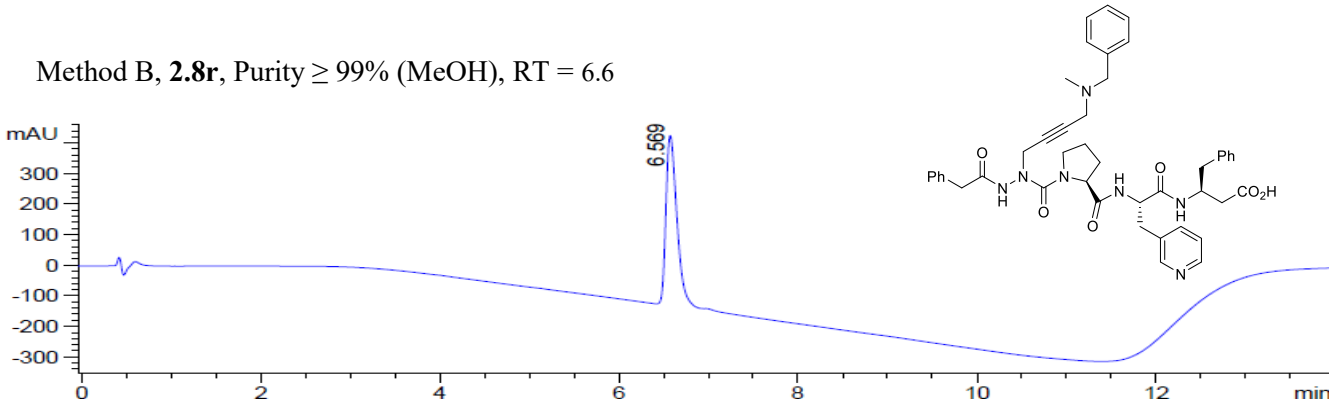

Method D, **2.8r**, Purity ≥ 99% (MeCN), RT = 4.9

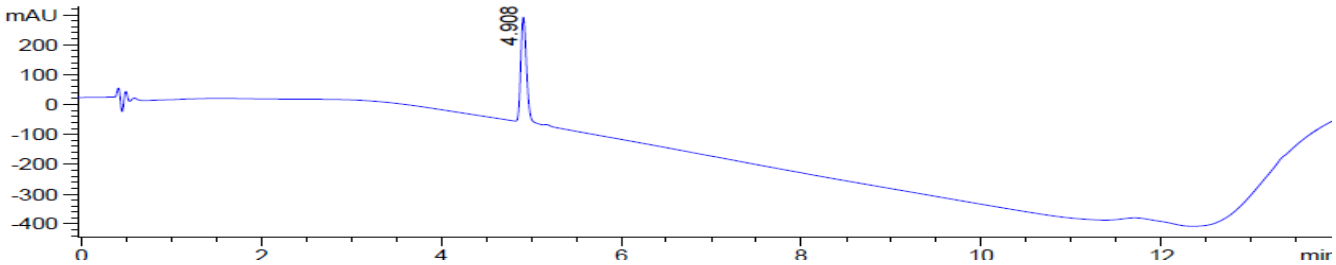

Method B, **2.9m**, Purity ≥ 99% (MeOH), RT = 5.7

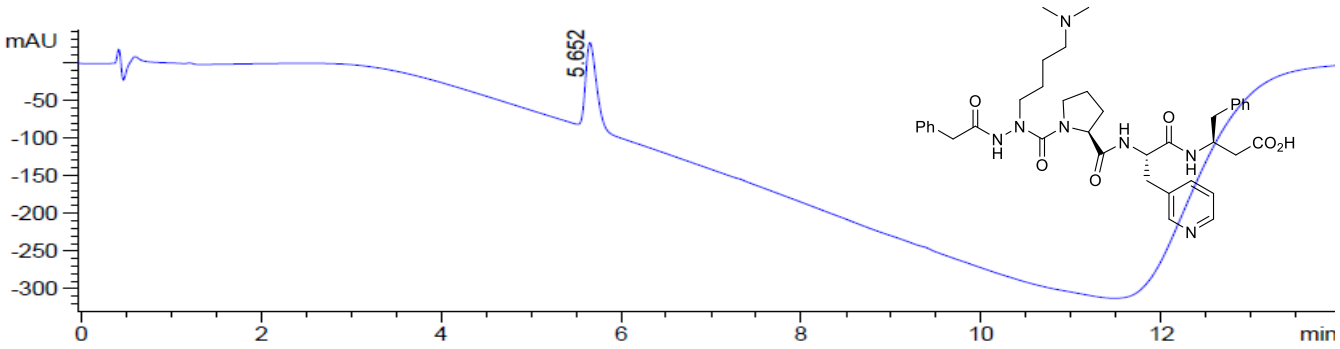

Method D, **2.9m**, Purity ≥ 99% (MeCN), RT = 4.4

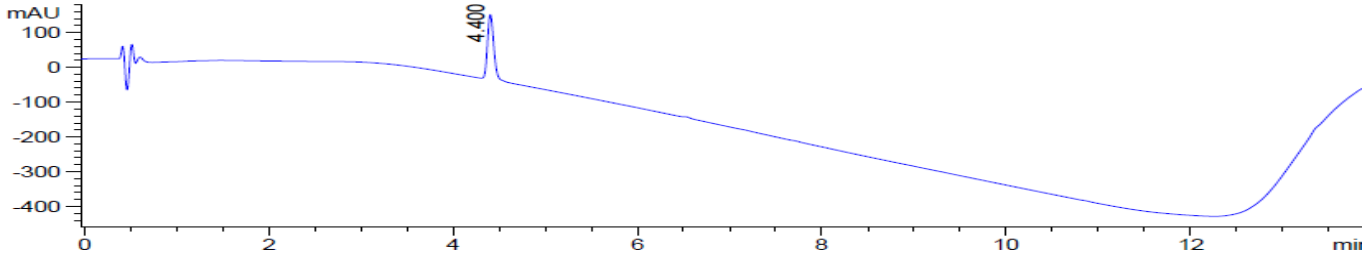

Method B, **2.9n**, Purity ≥ 99% (MeOH), RT = 5.7

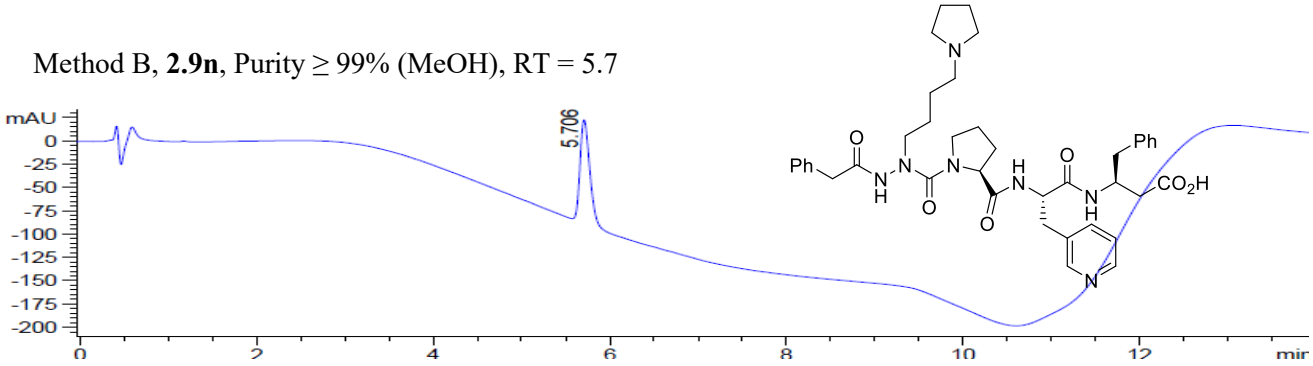

Method D, **2.9n**, Purity ≥ 99% (MeCN), RT = 6.6

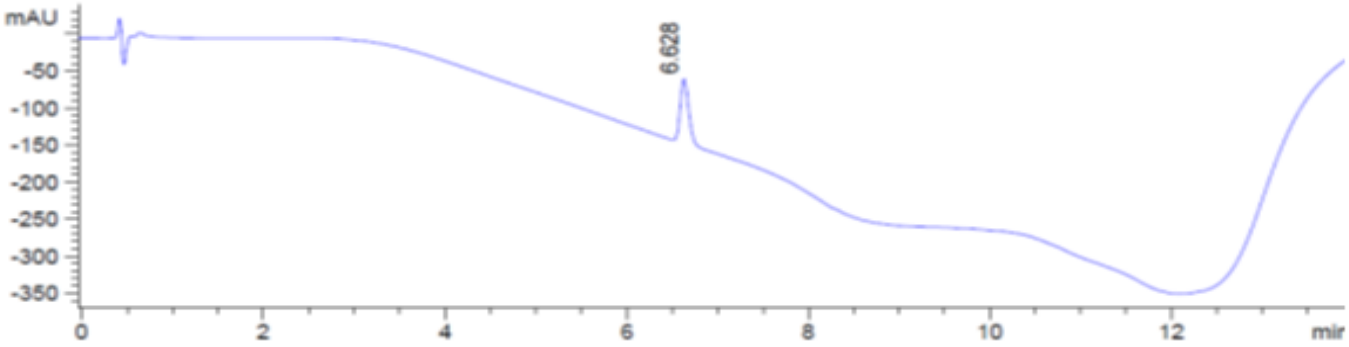

Method D, ***R*-2.11a**, Purity ≥ 99% (MeOH), RT = 6.7

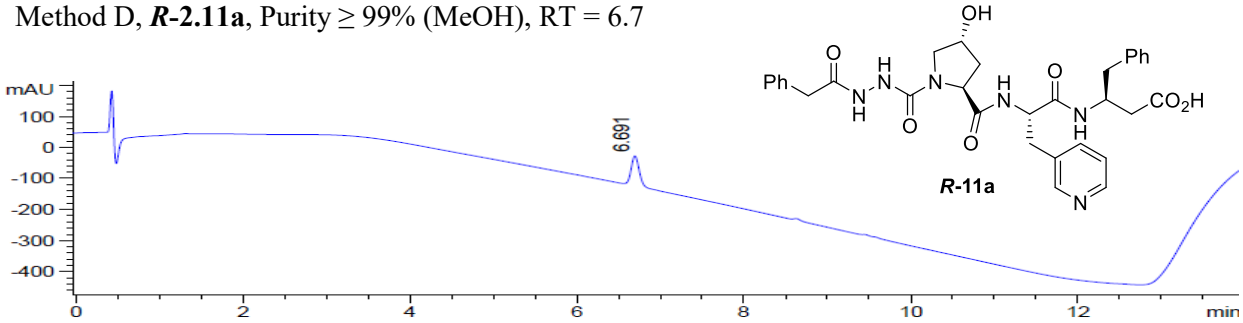

Method D, ***R*-2.11a**, Purity ≥ 99% (MeCN), RT = 4.4

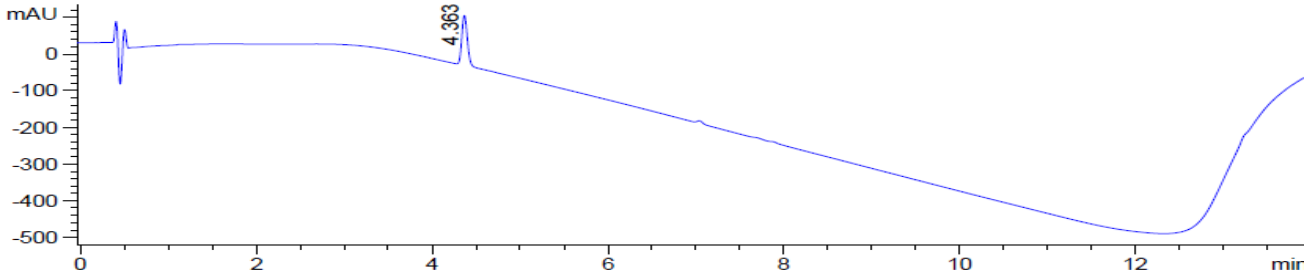

Method E, ***R*-2.11b**, Purity ≥ 99% (MeOH), RT = 6.5

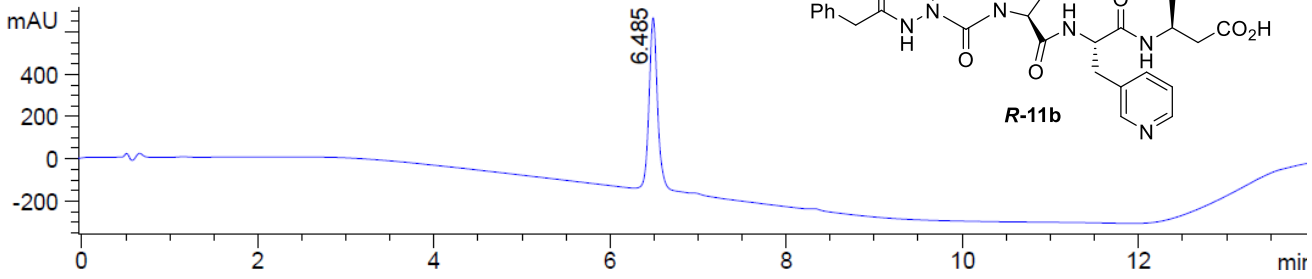

Method D, ***R*-2.11b**, Purity ≥ 96% (MeCN), RT = 5.8

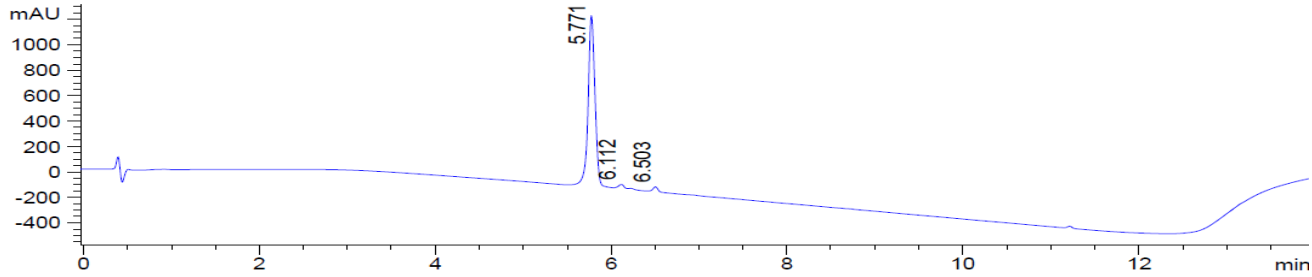

Method K, ***R*-2.11c**, Purity ≥ 99% (MeOH), RT = 5.6

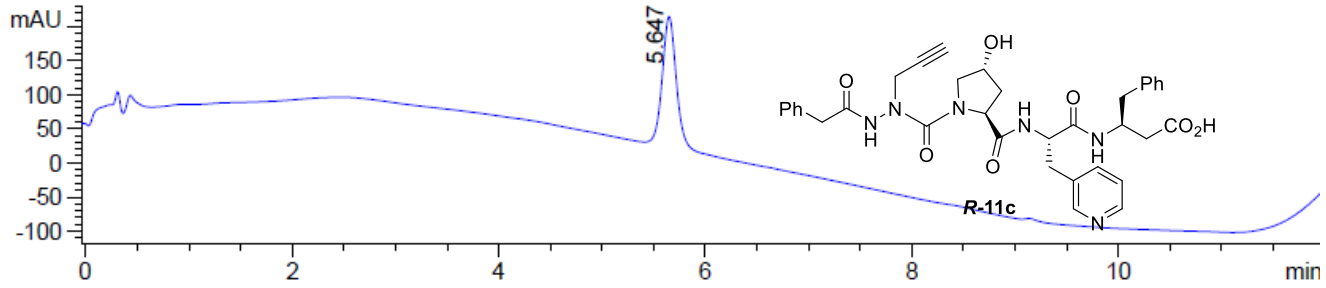

Method D, ***R*-2.11c**, Purity ≥ 99% (MeCN), RT = 5.2

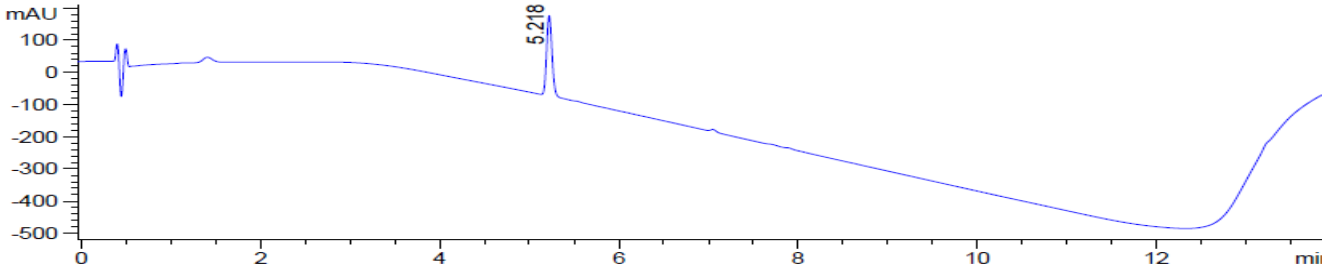

Method D, ***S*-2.11a**, Purity ≥ 99% (MeOH), RT = 6.9

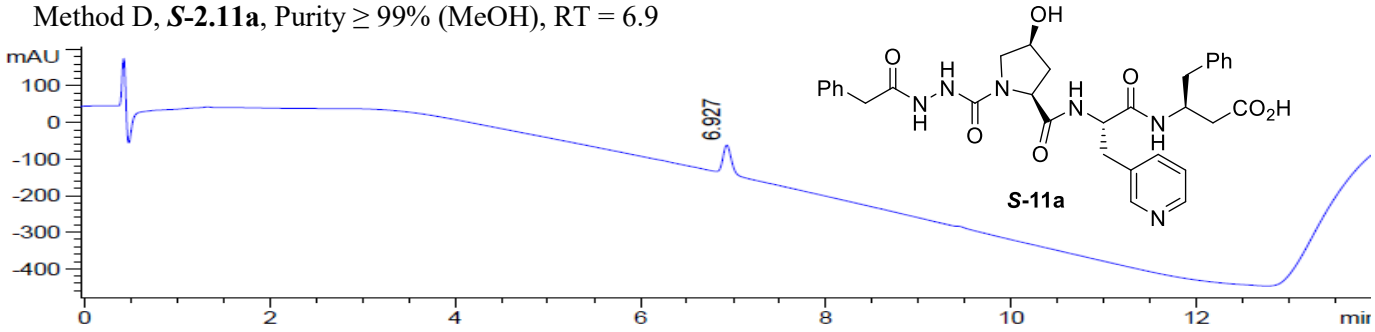

Method D, ***S*-2.11a**, Purity ≥ 99% (MeCN), RT = 4.5

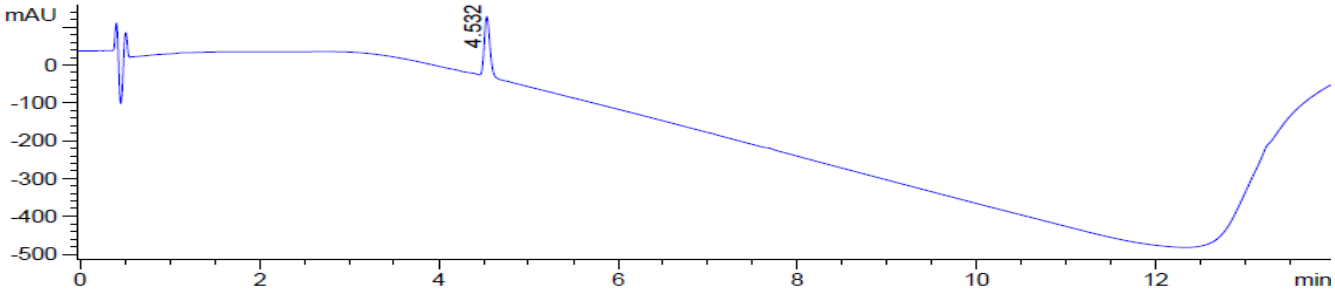

Method C, ***S*-2.11b**, Purity ≥ 99% (MeOH), RT = 6.7

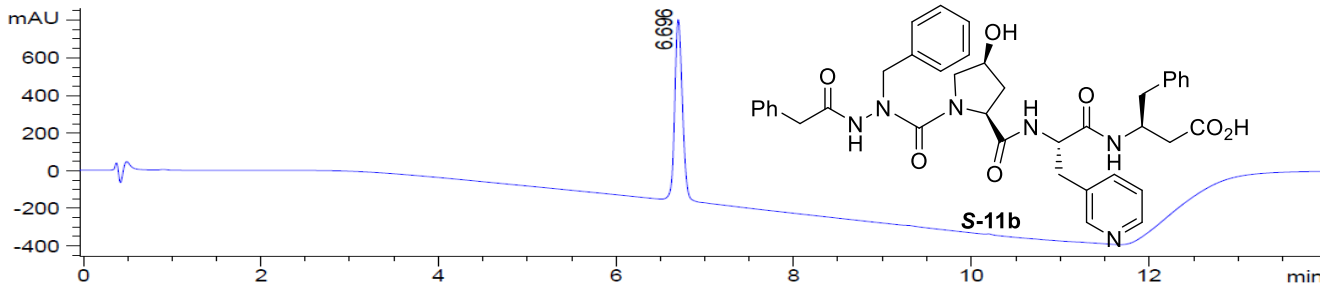

Method D, ***S*-2.11b**, Purity ≥ 99% (MeCN), RT = 5.8

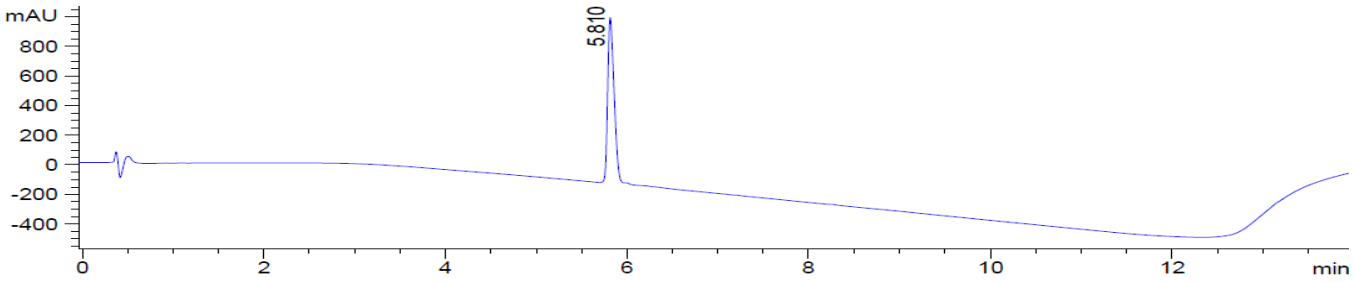

Method D, ***S*-2.11c**, Purity ≥ 99% (MeOH), RT = 8.1

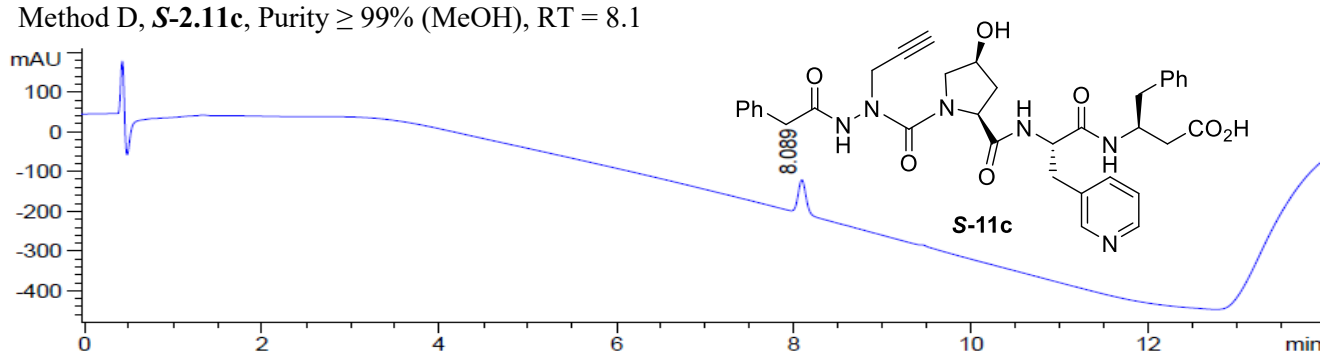

Method D, ***S*-2.11c**, Purity ≥ 99% (MeCN), RT = 5.2

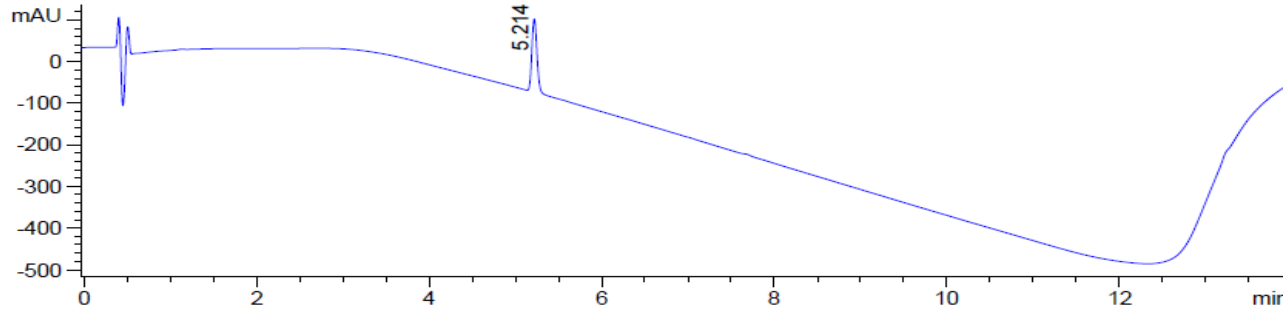

Method D, ***S*-2.12a**, Purity ≥ 91% (MeOH), RT = 7.6

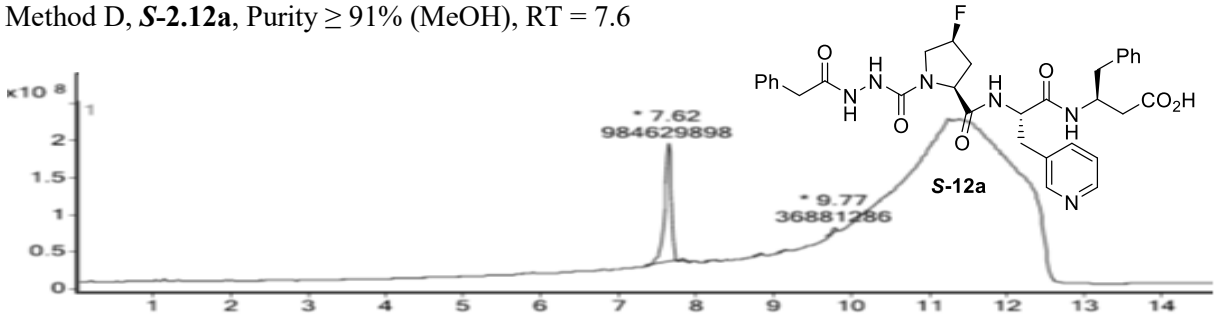

Method D, ***S*-2.12a**, Purity ≥ 82% (MeCN), RT = 6.2

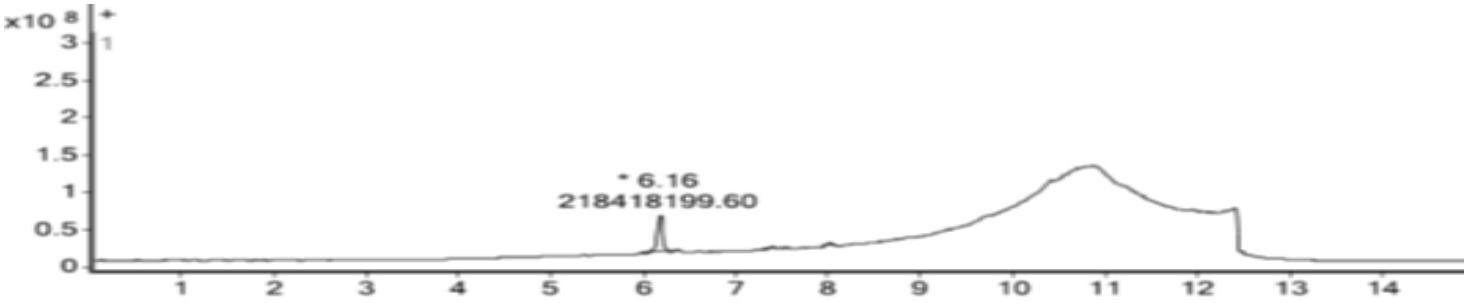

Method D, ***S*-2.12b**, Purity ≥ 99% (MeOH), RT = 7.6

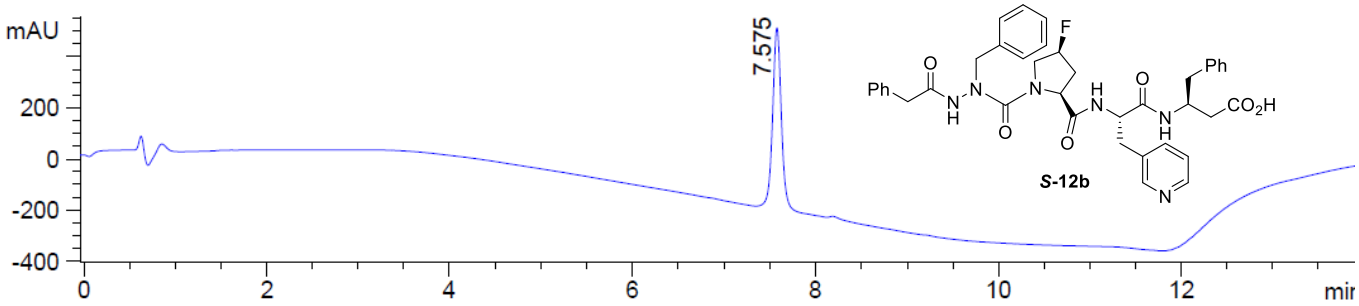

Method D, ***S*-2.12b**, Purity ≥ 99% (MeCN), RT = 6.0

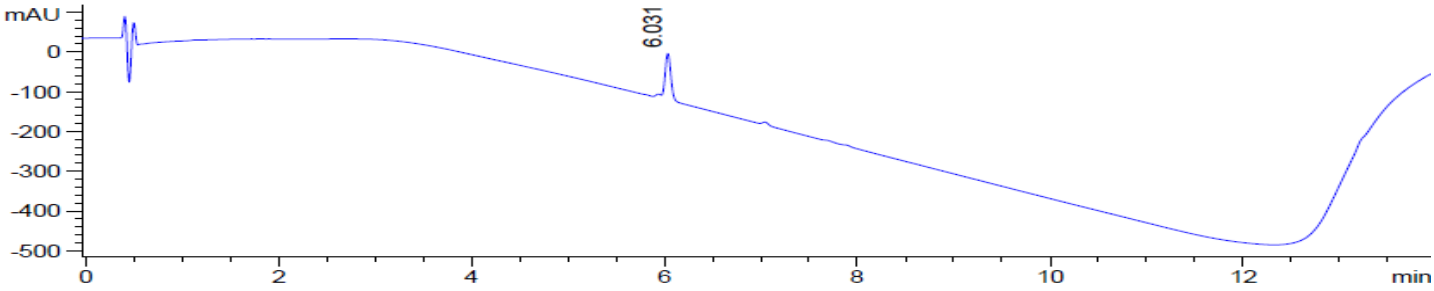

Method D, ***S*-2.12c**, Purity ≥ 99% (MeOH), RT = 5.4

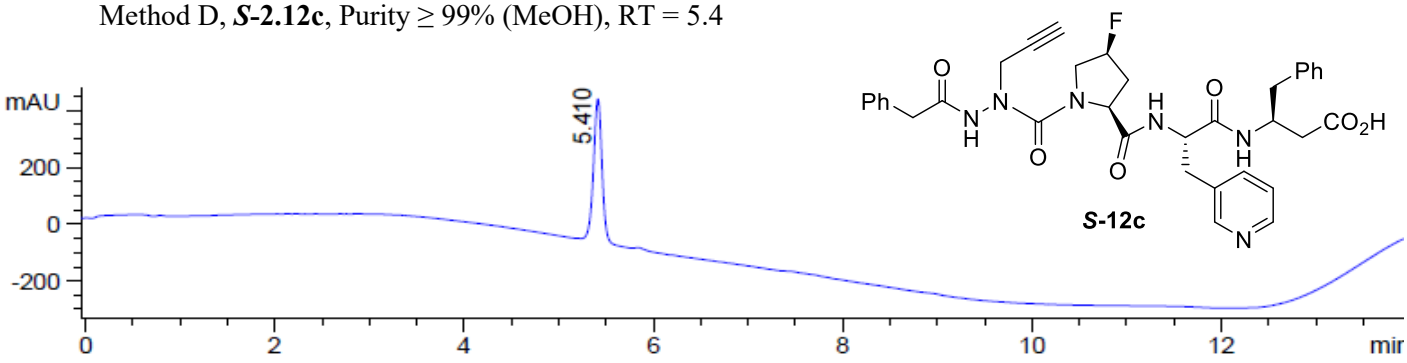

Method D, ***S*-2.12c**, Purity ≥ 99% (MeCN), RT = 5.3

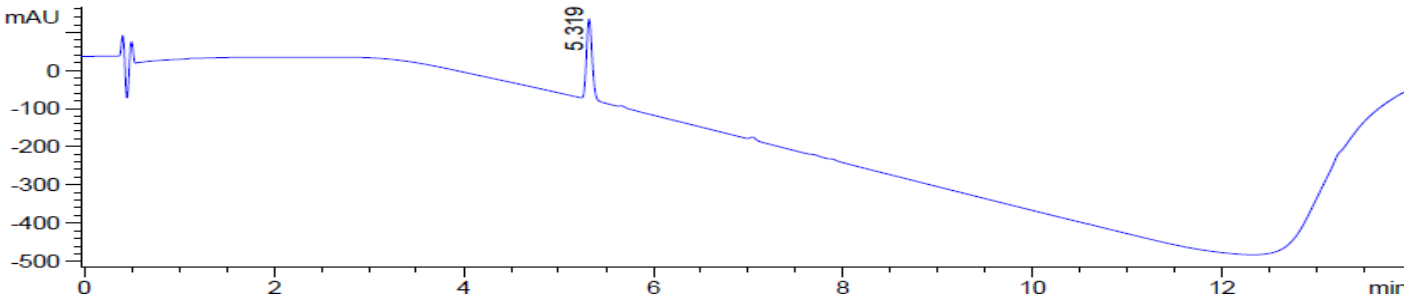

Method D, ***R*-2.12a**, Purity ≥ 95% (MeOH), RT = 6.8

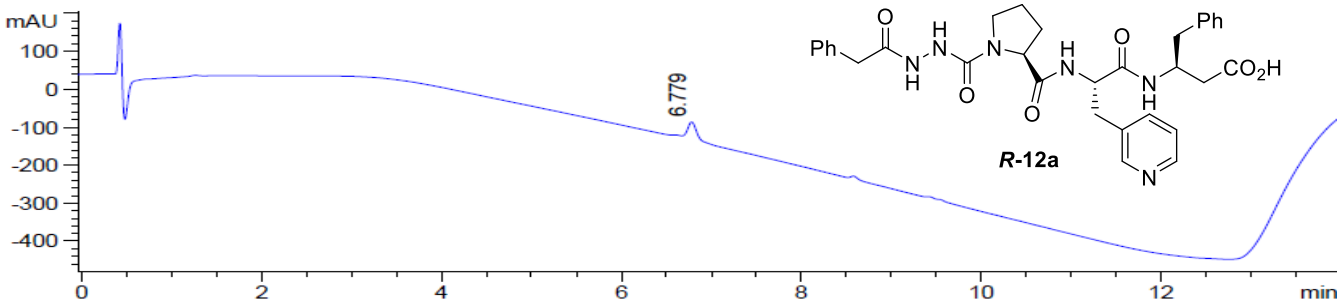

Method D, ***R*-2.12a**, Purity ≥95% (MeCN), RT = 4.6

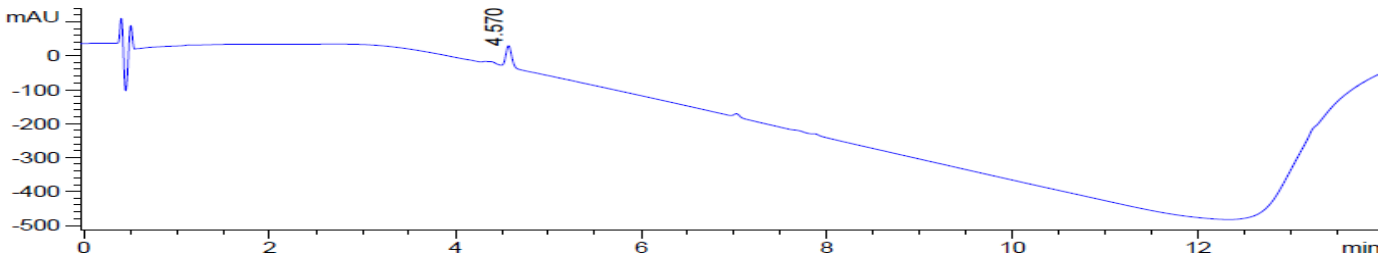

Method D, ***R*-2.12b**, Purity ≥ 97% (MeOH), RT = 9.5

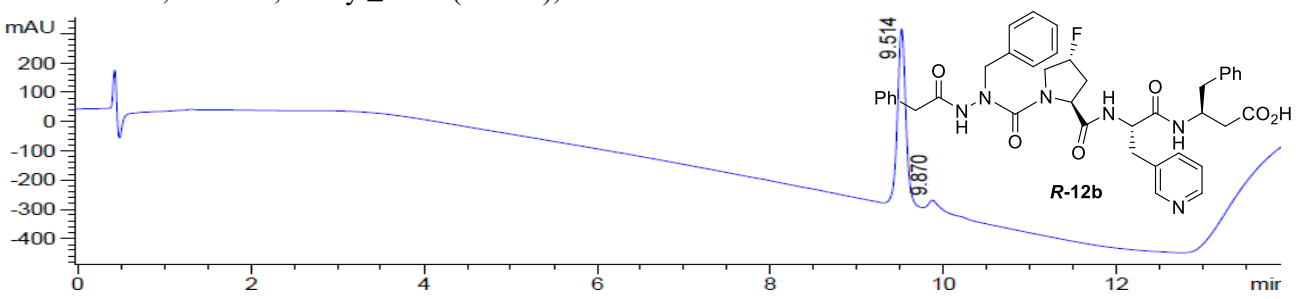

Method D, ***R*-2.12b**, Purity ≥ 97% (MeCN), RT = 6.2

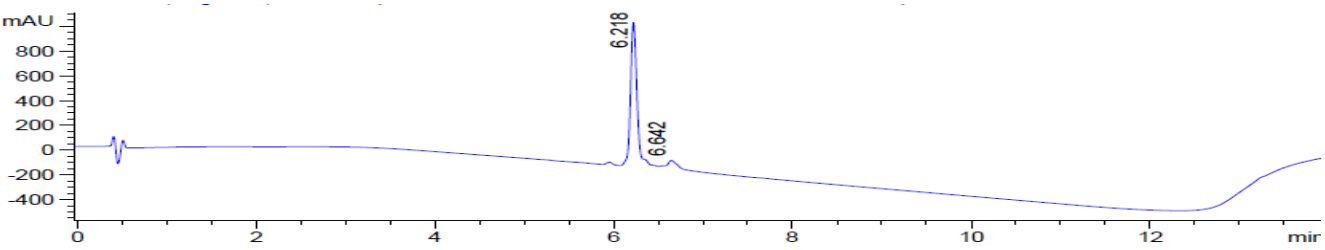

Method D, ***R*-2.12c**, Purity ≥ 95% (MeOH), RT = 8.3

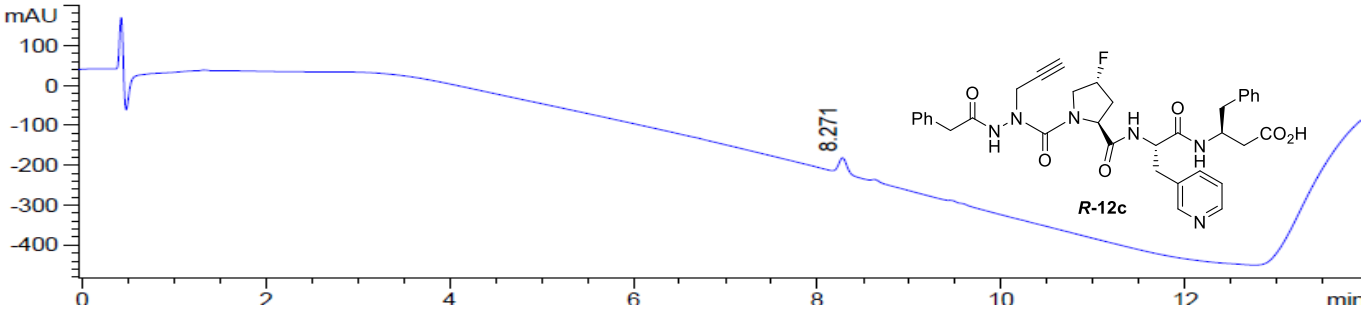

Method D, ***R*-2.12c**, Purity ≥ 95% (MeCN), RT = 5.5

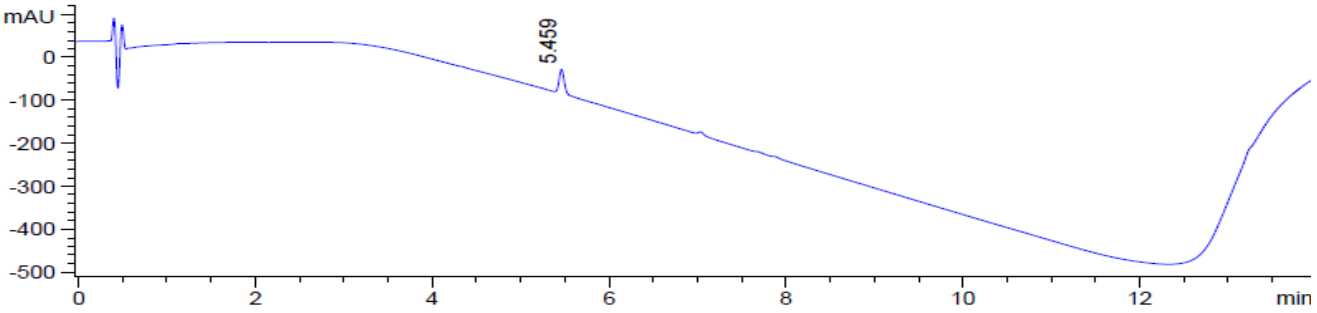

Method D, ***S*-2.13a**, Purity ≥ 99 (MeOH), RT = 5.2

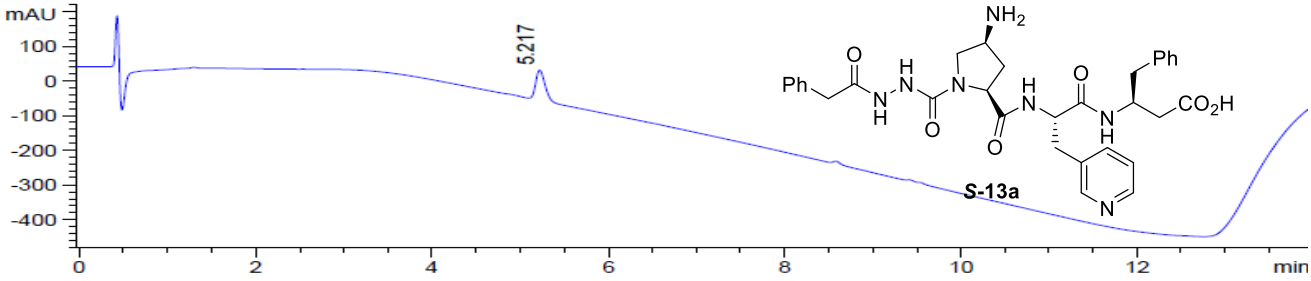

Method D, ***S*-2.13a**, Purity ≥ 99% (MeCN), RT = 4.9

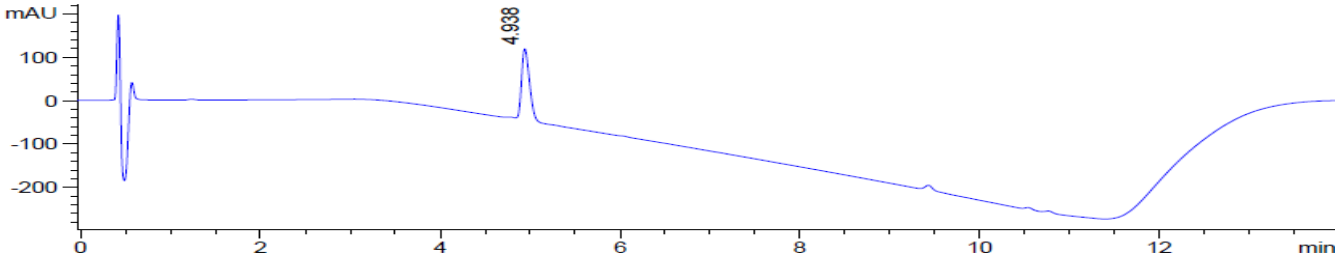

Method D, ***S*-2.13b**, Purity ≥ 95% (MeOH), RT = 8.4

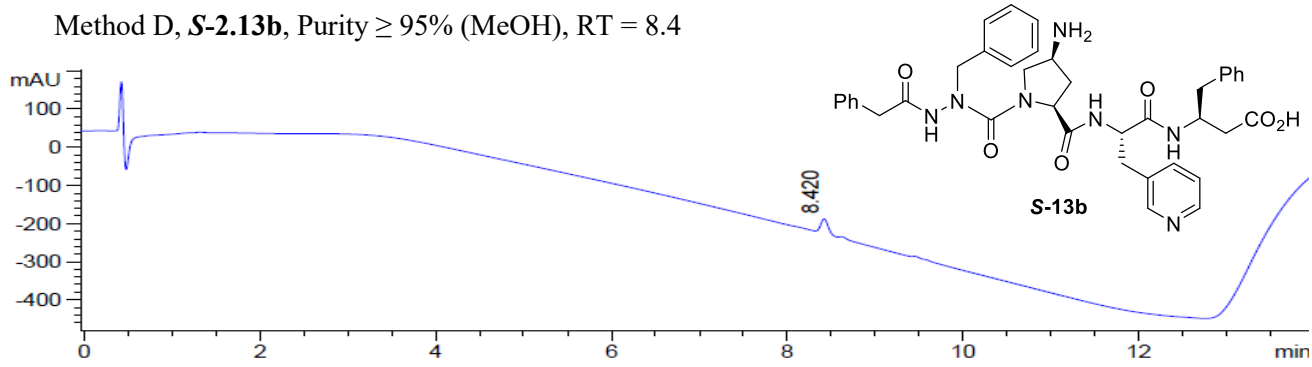

Method D, ***S*-2.13b**, Purity ≥ 95% (MeCN), RT = 5.2

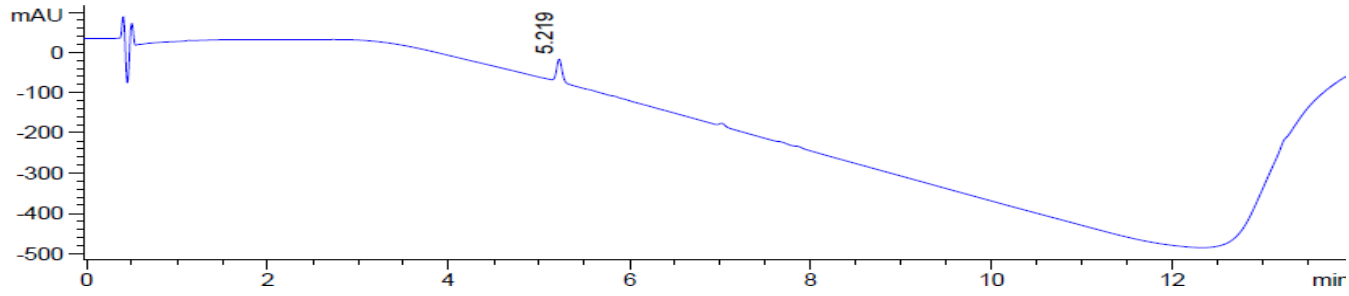

Method D, ***S*-2.13c**, Purity = 93% (MeOH), RT = 7.7

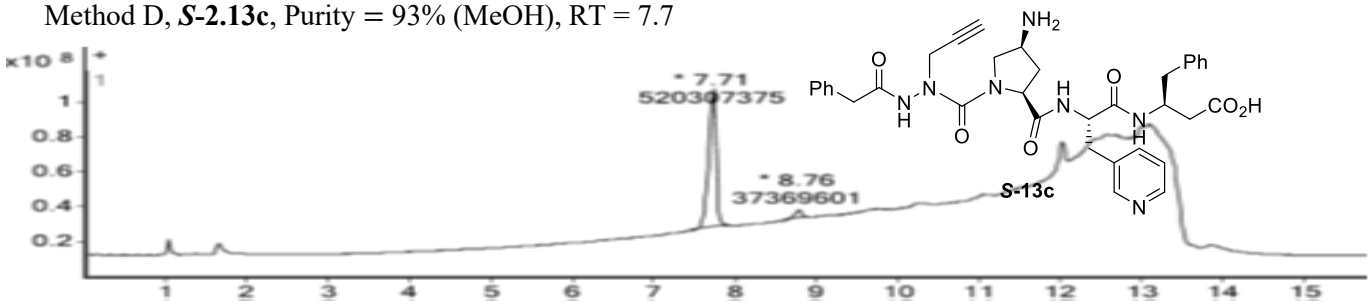

Method L, ***S*-2.13c**, Purity = 91% (MeCN), RT = 6.1

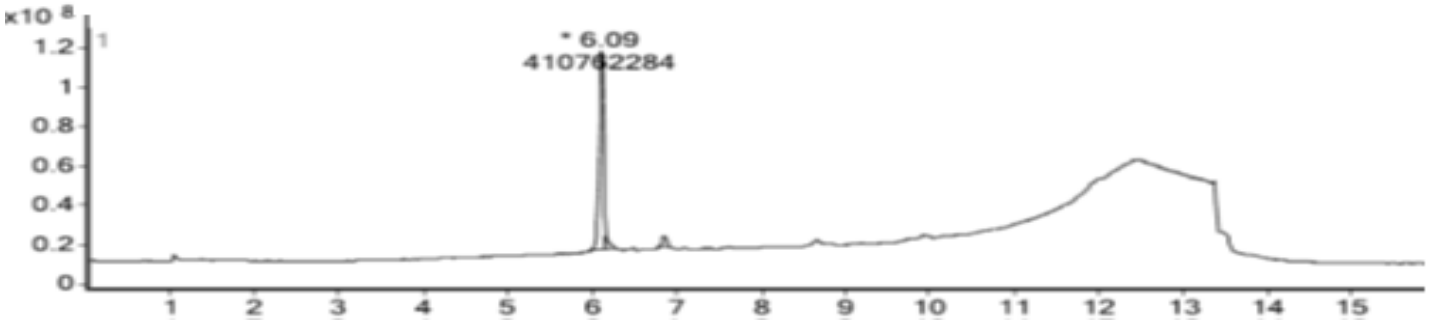

Method D, ***R*-2.13a**, Purity ≥ 99% (MeOH), RT = 5.6

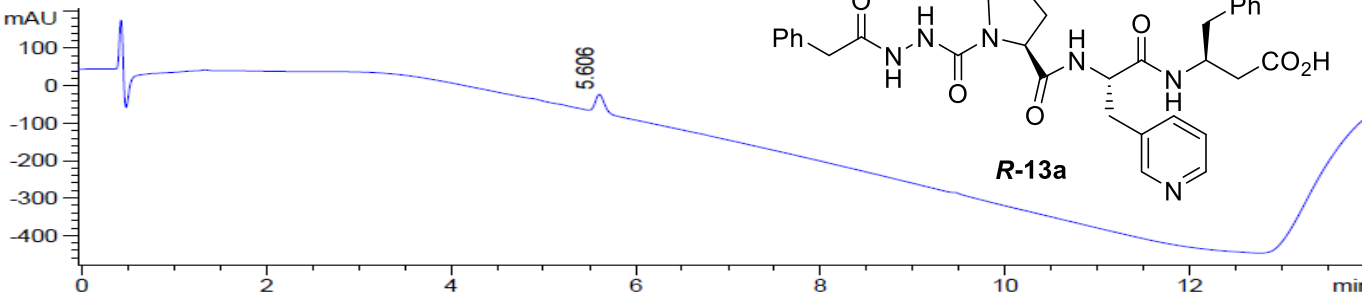

Method D, ***R*-2.13a**, Purity ≥ 95% (MeCN), RT = 5.0

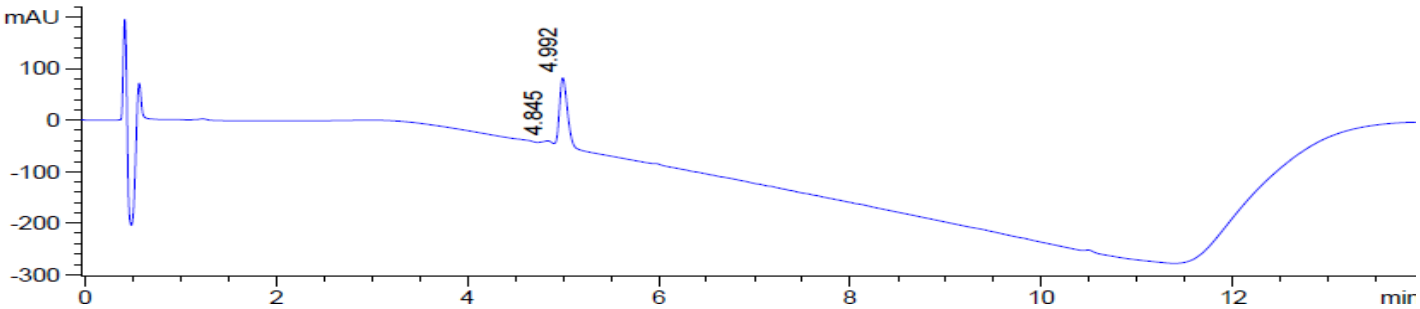

Method D, ***R*-2.13b**, Purity ≥ 99% (MeOH), RT = 8.5

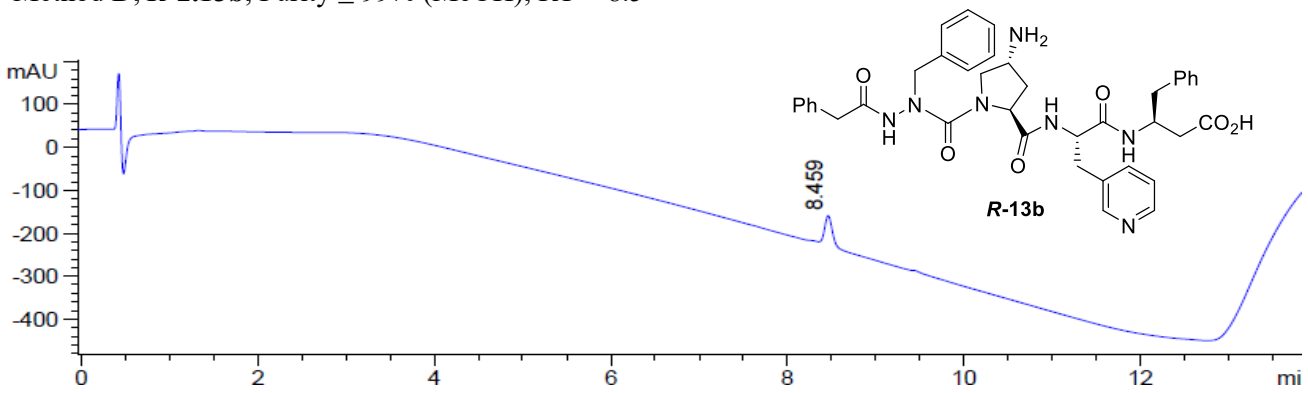

Method D, ***R*-2.13b**, Purity ≥ 99% (MeCN), RT = 5.2

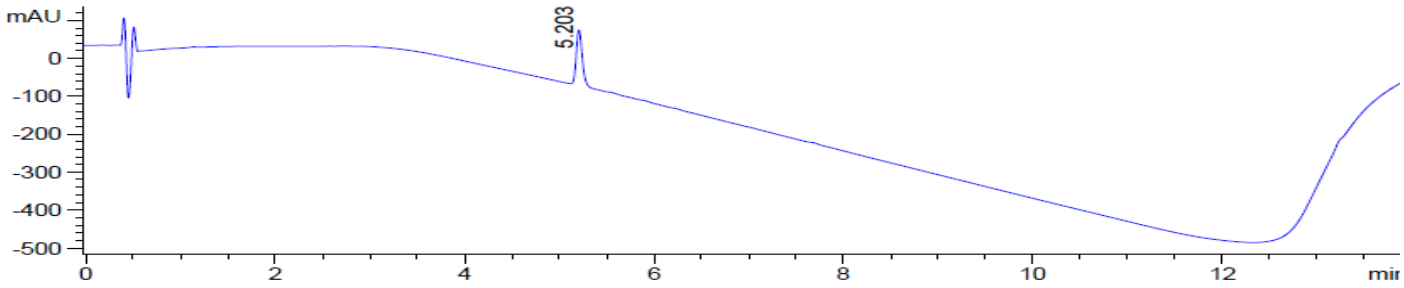

Method D, ***R*-2.13c**, Purity ≥ 96% (MeOH), RT = 7.2

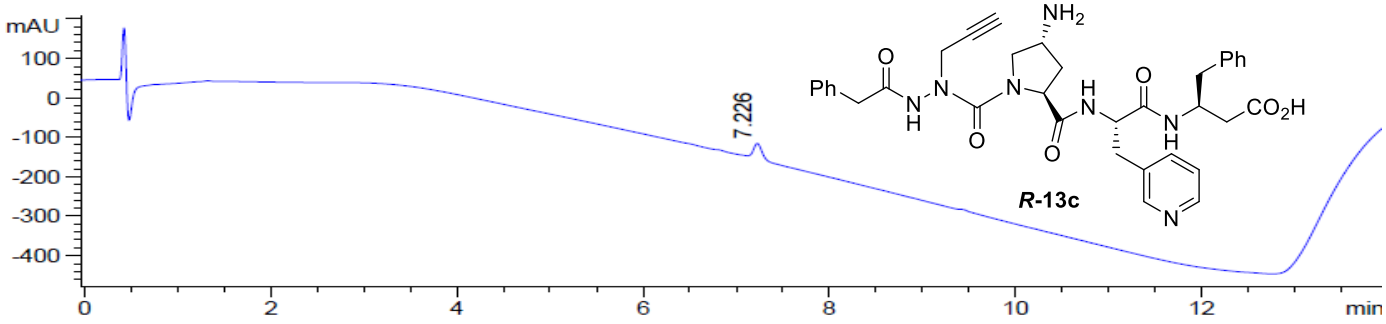

Method D, ***R*-2.13c**, Purity ≥ 96% (MeCN), RT = 4.6

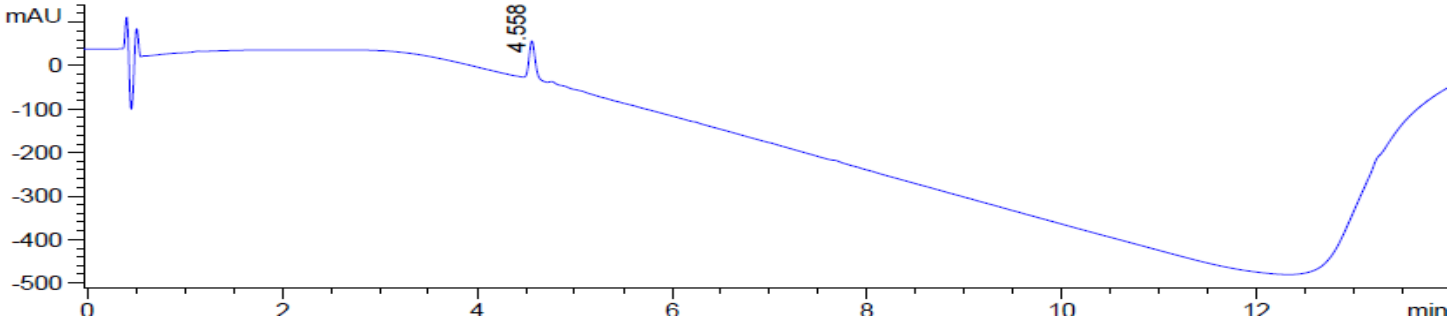

LCMS chromatogram of **2.49** after cleavage of a 1-2 mg of resin using method E, RT = 6.7 on a Sunfire C18 analytical column (100Å, 3.5 µm, 4.6 mm X 100 mm), purity 79% (MeOH)- The silyl group gets deprotected mass in the presence of TFA.

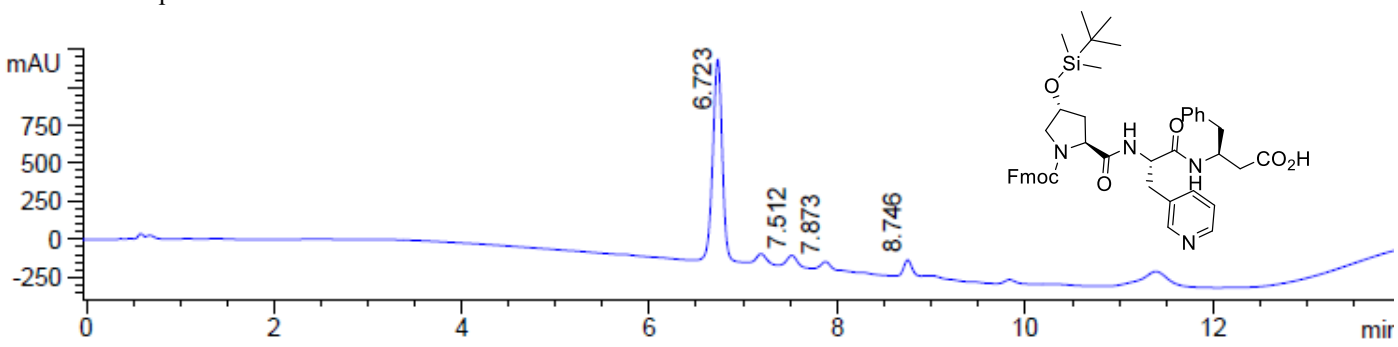

Supporting information Manuscript 2

Fatemeh M. Mir, Marco Crisma, Claudio Toniolo, William D. Lubell. Crystal-State Conformational Analysis of Adm Peptides. Influence of the C-Terminal Substituent

prepared for submission to the journal *Peptide Science* for publication in a special issue devoted to the 8th Peptide Engineering Meeting (PEM 8) held in Berlin, Germany (November 8-10, 2018).

SUPPORTING INFORMATION

Crystal-State Conformational Analysis of Adm Peptides. Influence of the C-Terminal Substituent

Fatemeh M. Mir, Marco Crisma, Claudio Toniolo, William D. Lubell

**Correspondence to:*

Prof. Claudio Toniolo, Department of Chemistry, University of Padova, via Marzolo 1, 35131 Padova, Italy. E-mail: claudio.toniolo@unipd.it

Prof. William D. Lubell, Département de Chimie, Université de Montréal, C. P. 6128, Succursale Centre-Ville, Montréal, Québec, Canada H3C 3J7. E-mail: william.lubell@umontreal.ca

Table S3.1. Crystal data and structure refinement for HCO-Adm-Aib-OMe (**3.2d**).

Identification code	mc291	
Empirical formula	$C_{17}H_{26}N_2O_4$	
Formula weight	322.40	
Temperature	293(2) K	
Wavelength	1.54184 Å	
Crystal system	Monoclinic	
Space group	$P2_1/n$	
Unit cell dimensions	a = 10.3707(2) Å	α= 90°.
	b = 9.75330(14) Å	β= 105.315(2)°.
	c = 17.5483(3) Å	γ = 90°.
Volume	1711.95(5) $Å^3$	
Z	4	
Density (calculated)	1.251 Mg/m^3	
Absorption coefficient	0.726 mm^{-1}	
F(000)	696	
Crystal size	0.400 × 0.400 × 0.200 mm^3	
Theta range for data collection	4.502 to 72.906°.	
Index ranges	$-12 \le h \le 12$, $-12 \le k \le 10$, $-21 \le l \le 21$	
Reflections collected	16966	
Independent reflections	3396 [R(int) = 0.0213]	
Completeness to theta = 67.684°	100.0 %	
Absorption correction	Semi-empirical from equivalents	
Max. and min. transmission	1.00000 and 0.18329	
Refinement method	Full-matrix least-squares on F^2	
Data / restraints / parameters	3396 / 0 / 208	
Goodness-of-fit on F^2	1.047	
Final R indices [I>2sigma(I)]	R_1 = 0.0449, wR_2 = 0.1285	
R indices (all data)	R_1 = 0.0490, wR_2 = 0.1334	
Extinction coefficient	n/a	
Largest diff. peak and hole	0.224 and -0.237 $e.Å^{-3}$	
CCDC deposition No.	1880257	

Table S3.2. Crystal data and structure refinement for HCO-$(Adm)_2$-Gly-OEt (**3.4a**)

Identification code	LUB115
Empirical formula	$C_{27}H_{39}N_3O_5$
Formula weight	485.61
Temperature/K	150
Crystal system	triclinic
Space group	P-1
a/Å	8.2842(3)
b/Å	11.0435(4)
c/Å	13.7725(5)
α/°	98.298(2)
β/°	94.531(2)
γ/°	96.595(2)
Volume/Å^3	1232.69(8)
Z	2
ρ_{calc} g/cm^3	1.308
μ/mm^{-1}	0.468
F(000)	524.0
Crystal size/mm^3	0.07 × 0.07 × 0.03
Radiation	GaKα (λ = 1.34139)
2Θ range for data collection/°	5.668 to 114.056
Index ranges	$-10 \leq h \leq 10$, $-13 \leq k \leq 13$, $0 \leq l \leq 17$
Reflections collected	4981
Independent reflections	4981
Data/restraints/parameters	4981/0/319
Goodness-of-fit on F^2	1.042
Final R indexes [I>=2σ (I)]	R_1 = 0.0684, wR_2 = 0.1647
Final R indexes [all data]	R_1 = 0.1016, wR_2 = 0.1865
Largest diff. peak/hole / e Å^{-3}	0.42/-0.30
CCDC deposition No.	1880258

Table S3.3. Crystal data and structure refinement for HCO-$(Adm)_2$-NH*i*Pr (**3.4b**)

Identification code	LUB119
Empirical formula	$C_{26}H_{39}N_3O_3$
Formula weight	441.60
Temperature/K	150
Crystal system	triclinic
Space group	P-1
a/Å	8.7573(2)
b/Å	10.7821(3)
c/Å	13.2334(4)
α/°	67.550(1)
β/°	88.009(1)
γ/°	83.018(1)
Volume/Å^3	1146.17(5)
Z	2
ρ_{calc} g/cm^3	1.280
μ/mm^{-1}	0.426
F(000)	480.0
Crystal size/mm^3	0.38 × 0.2 × 0.15
Radiation	GaKα (λ = 1.34139)
2Θ range for data collection/°	6.288 to 121.314
Index ranges	$-11 \leq h \leq 11$, $-13 \leq k \leq 14$, $-17 \leq l \leq 17$
Reflections collected	29482
Independent reflections	5258 [R_{int} = 0.0294, R_{sigma} = 0.0193]
Data/restraints/parameters	5258/0/304
Goodness-of-fit on F^2	1.097
Final R indexes [I>=2σ (I)]	R_1 = 0.0464, wR_2 = 0.1172
Final R indexes [all data]	R_1 = 0.0478, wR_2 = 0.1188
Largest diff. peak/hole / e Å^{-3}	0.26/-0.45
CCDC deposition No.	1880259

Table S3.4. Crystal data and structure refinement for HCO-(Adm)$_2$-NH*t*Bu (**3.4c**)

Identification code	LUB1202
Empirical formula	$C_{27}H_{41}N_3O_3$
Formula weight	455.63
Temperature/K	150
Crystal system	trigonal
Space group	$P3_1$
a/Å	11.3115(4)
b/Å	11.3115(4)
c/Å	16.5768(7)
α/°	90
β/°	90
γ/°	120
Volume/Å^3	1836.84(15)
Z	3
ρ_{calc}g/cm^3	1.236
μ/mm^{-1}	0.408
F(000)	744.0
Crystal size/mm^3	0.37 × 0.03 × 0.03
Radiation	GaKα (λ = 1.34139)
2Θ range for data collection/°	4.638 to 109.926
Index ranges	$-13 \leq h \leq 13$, $-13 \leq k \leq 13$, $-19 \leq l \leq 20$
Reflections collected	56160
Independent reflections	4640 [R_{int} = 0.0756, R_{sigma} = 0.0380]
Data/restraints/parameters	4640/1/303
Goodness-of-fit on F^2	1.009
Final R indexes [I>=2σ (I)]	R_1 = 0.0510, wR_2 = 0.1238
Final R indexes [all data]	R_1 = 0.0707, wR_2 = 0.1358
Largest diff. peak/hole / e Å^{-3}	0.17/-0.18
Flack parameter	0.18(14)[a]
CCDC deposition No.	1880260

[a] Racemic twin (95:5)

Table S3.5. Crystal data and structure refinement for HCO-(Adm)$_2$-Aib-OMe (**3.4d**)

Identification code	lub107
Empirical formula	$C_{28}H_{41}N_3O_5$
Formula weight	499.64
Temperature/K	150
Crystal system	orthorhombic
Space group	$P2_12_12_1$
a/Å	10.0593(4)
b/Å	12.4186(5)
c/Å	20.4379(8)
α/°	90
β/°	90
γ/°	90
Volume/Å^3	2553.15(18)
Z	4
ρ_{calc}g/cm^3	1.300
μ/mm^{-1}	0.461
F(000)	1080.0
Crystal size/mm^3	0.18 × 0.16 × 0.04
Radiation	GaKα (λ = 1.34139)
2Θ range for data collection/°	7.246 to 117.342
Index ranges	$-12 \le h \le 11$, $-15 \le k \le 15$, $-25 \le l \le 25$
Reflections collected	37521
Independent reflections	5478 [R_{int} = 0.0471, R_{sigma} = 0.0265]
Data/restraints/parameters	5478/0/342
Goodness-of-fit on F^2	1.110
Final R indexes [I>=2σ (I)]	R_1 = 0.0587, wR_2 = 0.1743
Final R indexes [all data]	R_1 = 0.0608, wR_2 = 0.1758
Largest diff. peak/hole / e Å^{-3}	0.33/-0.28
Flack parameter	0.5(5)[a]
CCDC deposition No.	1880261

[a] Racemic twin (50:50)

NMR

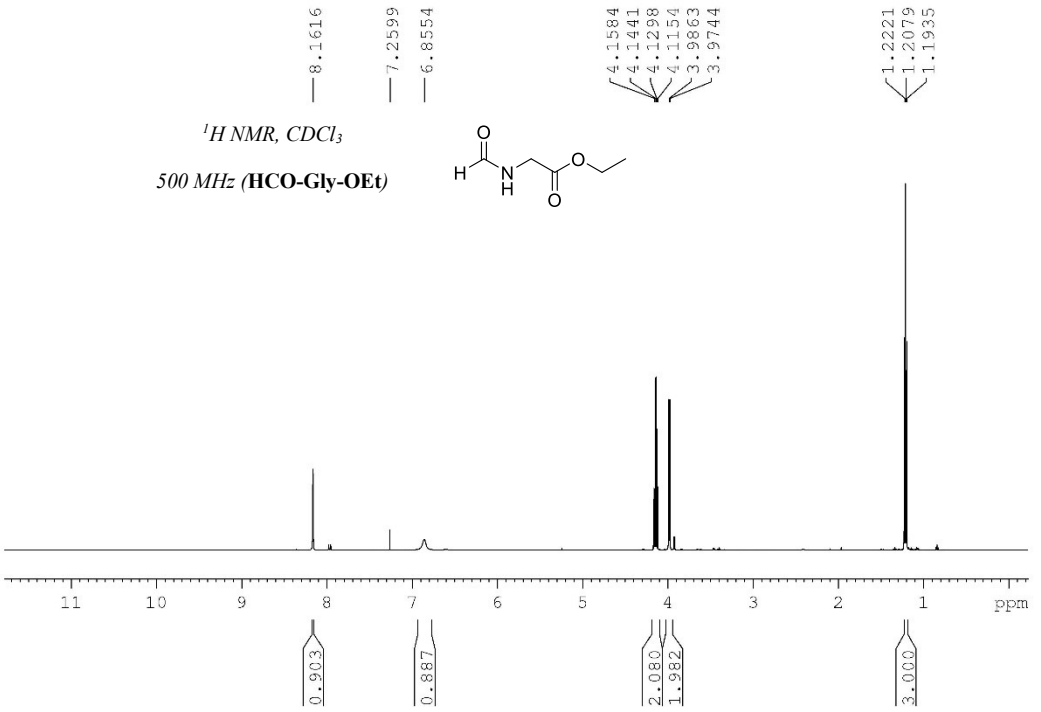

^{1}H NMR, $CDCl_3$

*500 MHz (***HCO-Gly-OEt***)*

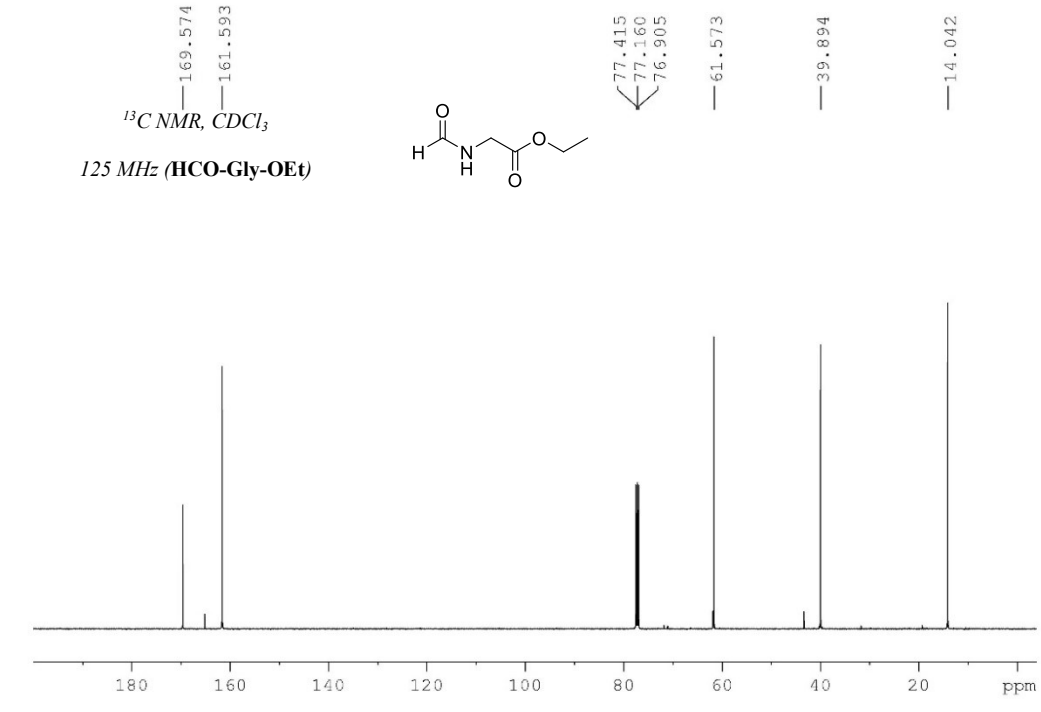

^{13}C NMR, $CDCl_3$

*125 MHz (***HCO-Gly-OEt***)*

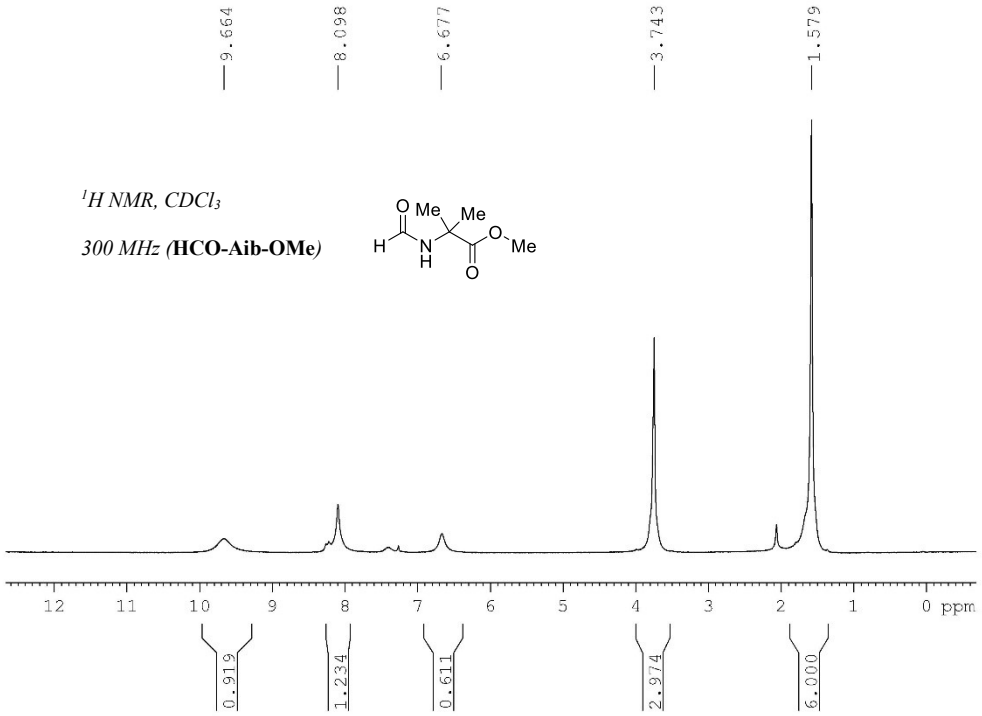
9.664
8.098
6.677
3.743
1.579
^1H NMR, $CDCl_3$
300 MHz (HCO-Aib-OMe)
O
Me
Me
H
N
H
O
O
Me
12
11
10
9
8
7
6
5
4
3
2
1
0 ppm
0.919
1.234
0.611
2.974
6.000

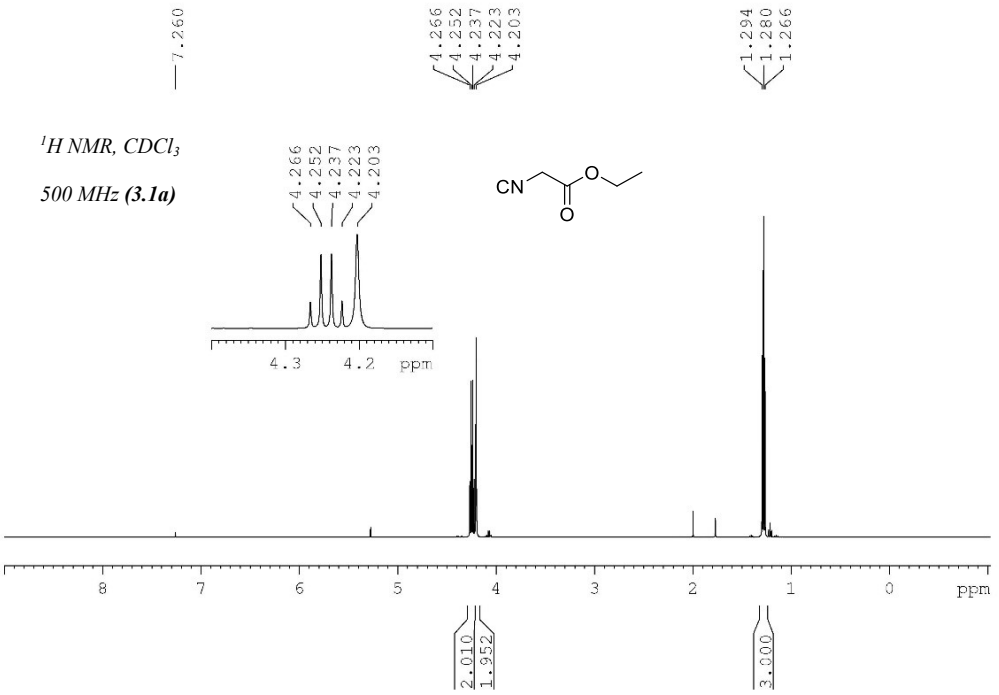
7.260
4.266
4.252
4.237
4.223
4.203
1.294
1.280
1.266
^{1}H NMR, CDCl$_3$
500 MHz (3.1a)
CN
O
O
4.3
4.2
ppm
8
7
6
5
4
3
2
1
0
ppm
2.010
1.952
3.000

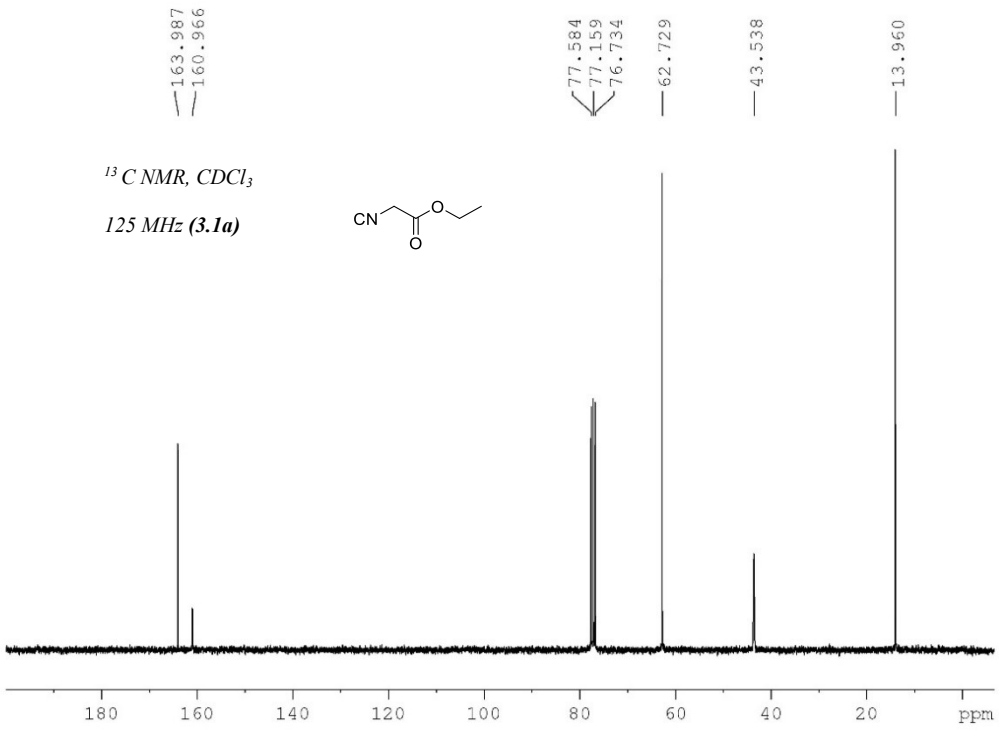
163.987
160.966
77.584
77.159
76.734
62.729
43.538
13.960
^{13}C NMR, CDCl$_3$
125 MHz (3.1a)
CN
O
O
180
160
140
120
100
80
60
40
20
ppm

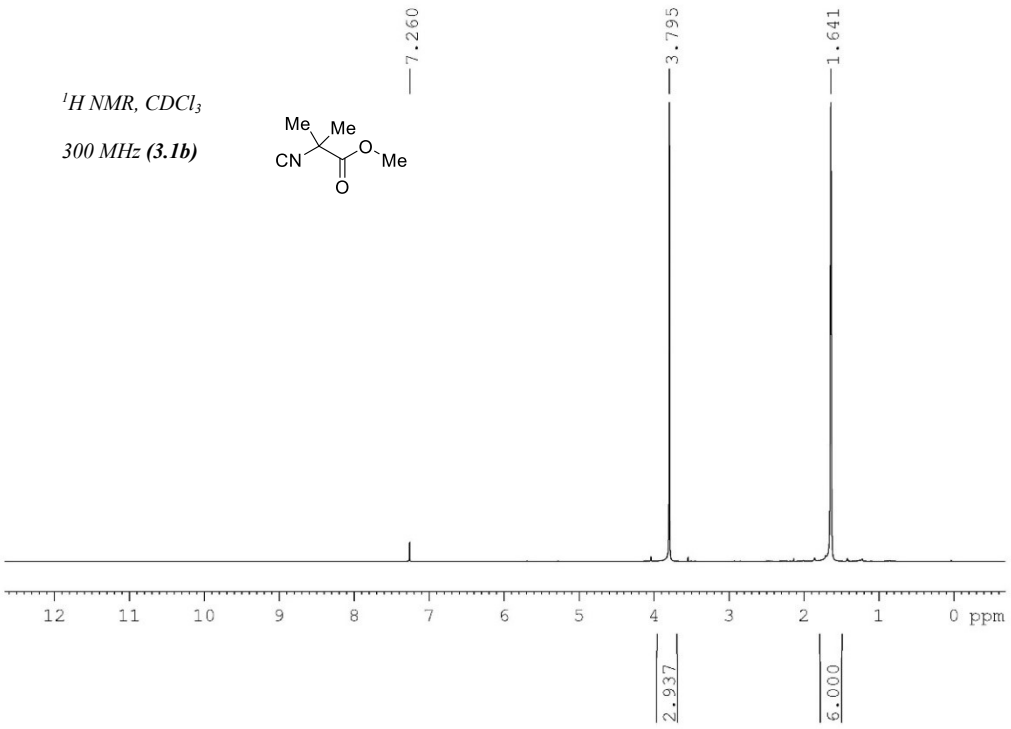
^{1}H NMR, CDCl$_3$
300 MHz (3.1b)
Me
Me
CN
O
Me
O
7.260
3.795
1.641
12
11
10
9
8
7
6
5
4
3
2
1
0 ppm
2.937
6.000

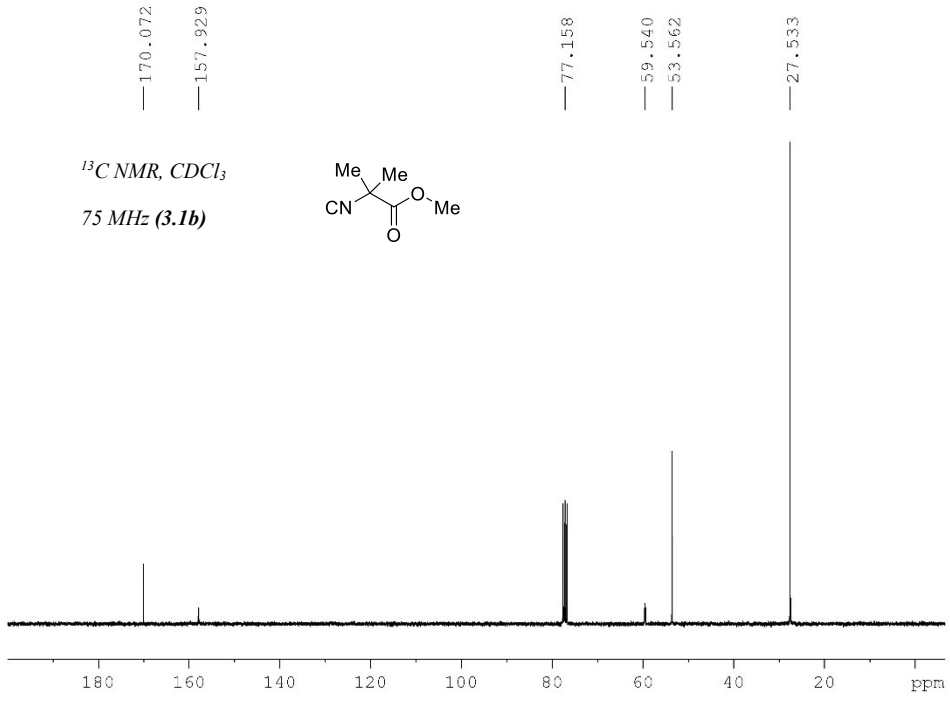
^{13}C NMR, CDCl$_3$
75 MHz (3.1b)
Me
Me
CN
O
Me
O
170.072
157.929
77.158
59.540
53.562
27.533
180
160
140
120
100
80
60
40
20
ppm

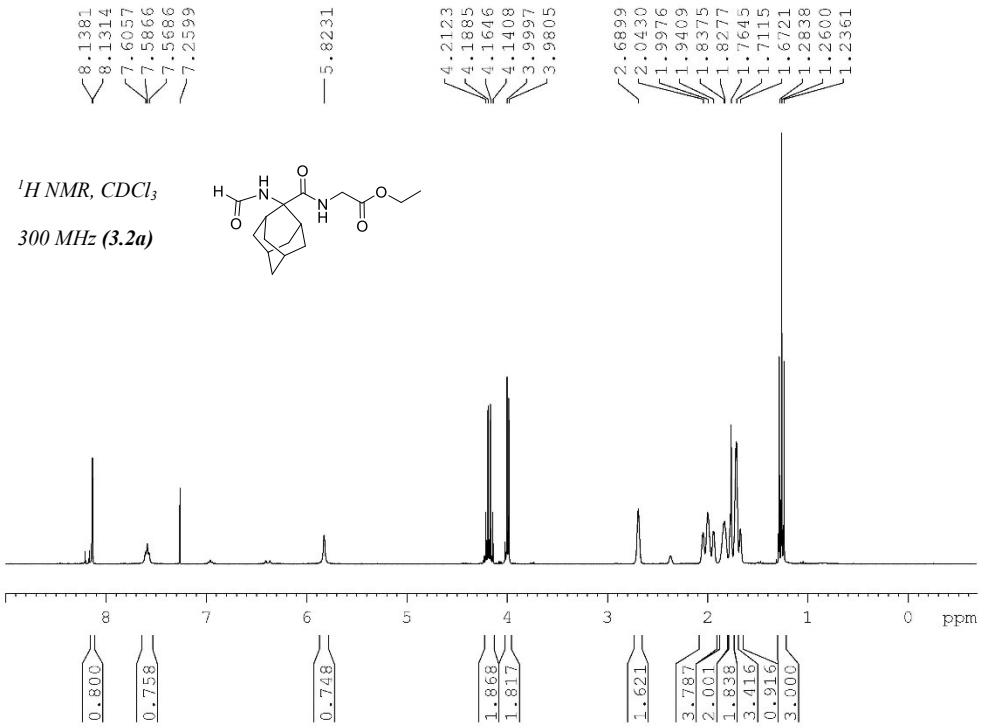

^{1}H NMR, $CDCl_3$

*300 MHz **(3.2a)***

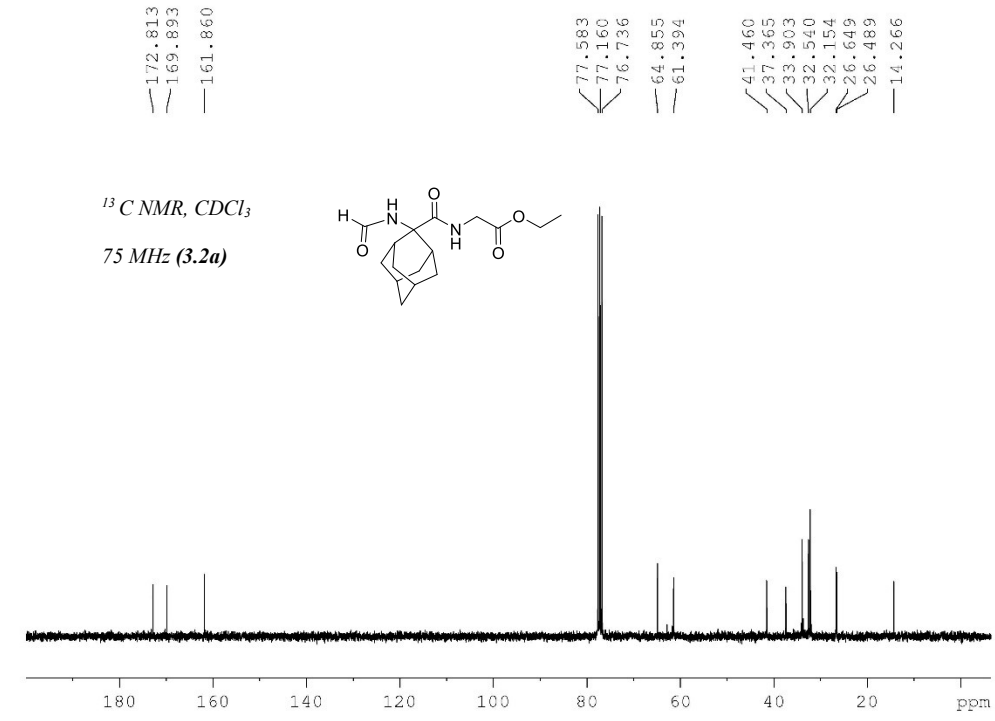

^{13}C NMR, $CDCl_3$

*75 MHz **(3.2a)***

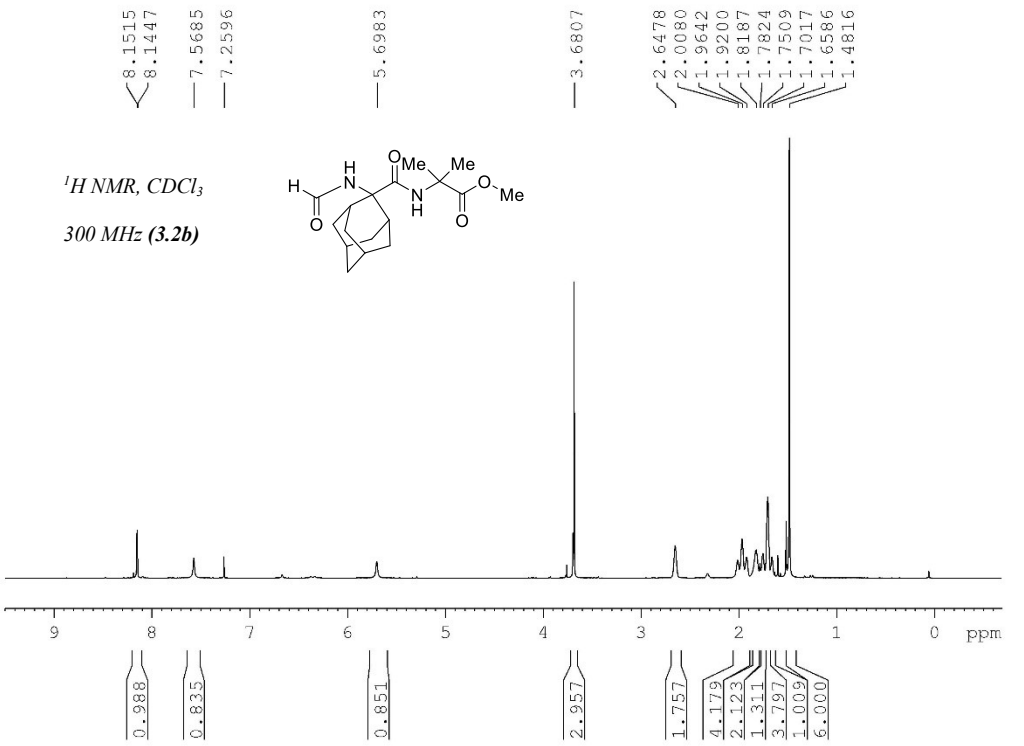

^{1}H NMR, $CDCl_3$

*300 MHz **(3.2b)***

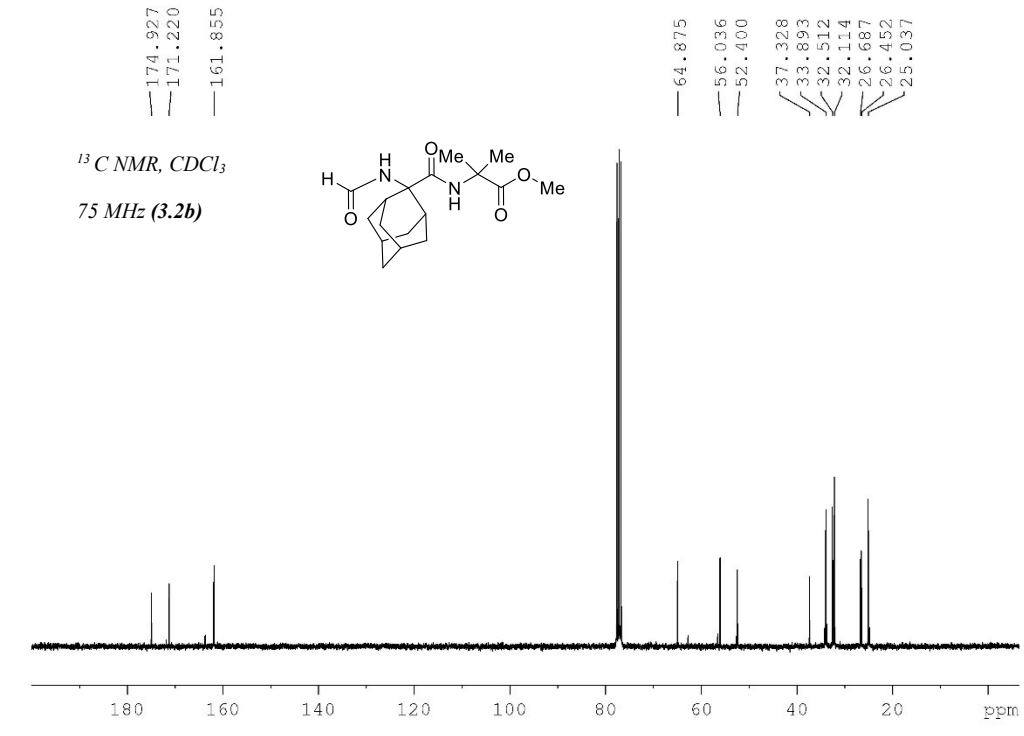

^{13}C NMR, $CDCl_3$

*75 MHz **(3.2b)***

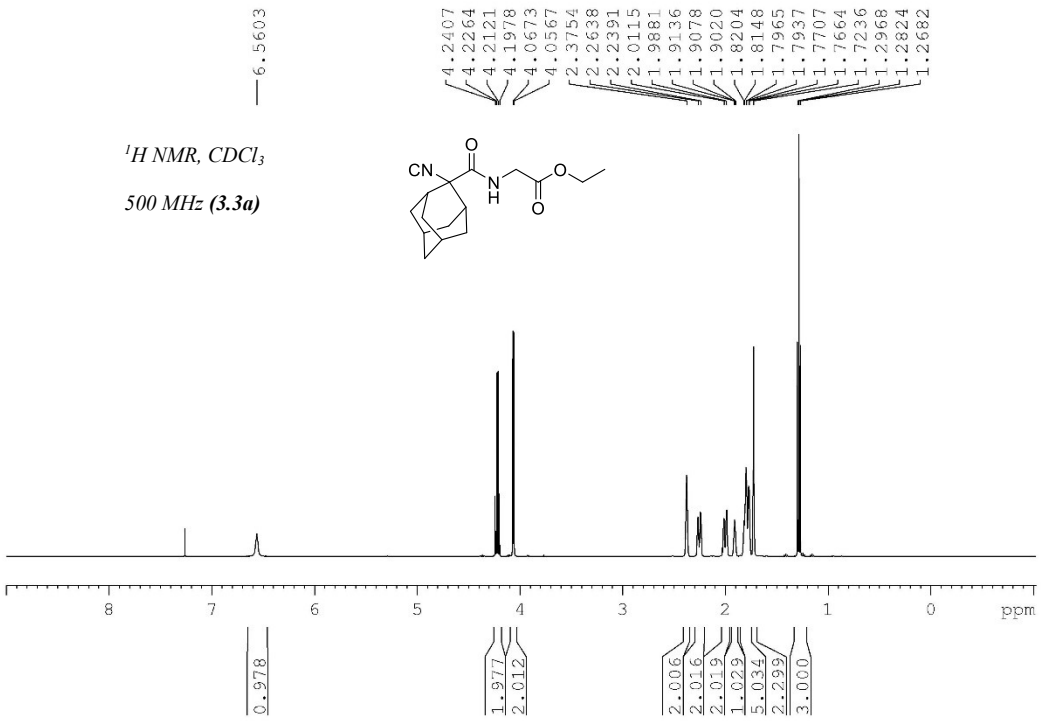
6.5603
4.2407
4.2264
4.2121
4.1978
4.0673
4.0567
2.3754
2.2638
2.2391
2.0115
1.9881
1.9136
1.9078
1.9020
1.8204
1.8148
1.7965
1.7937
1.7707
1.7664
1.7236
1.2968
1.2824
1.2682
^1H NMR, $CDCl_3$
500 MHz (3.3a)
CN
O
N
H
O
O
8
7
6
5
4
3
2
1
0
ppm
0.978
1.977
2.012
2.006
2.016
2.019
1.029
5.034
2.293
3.000

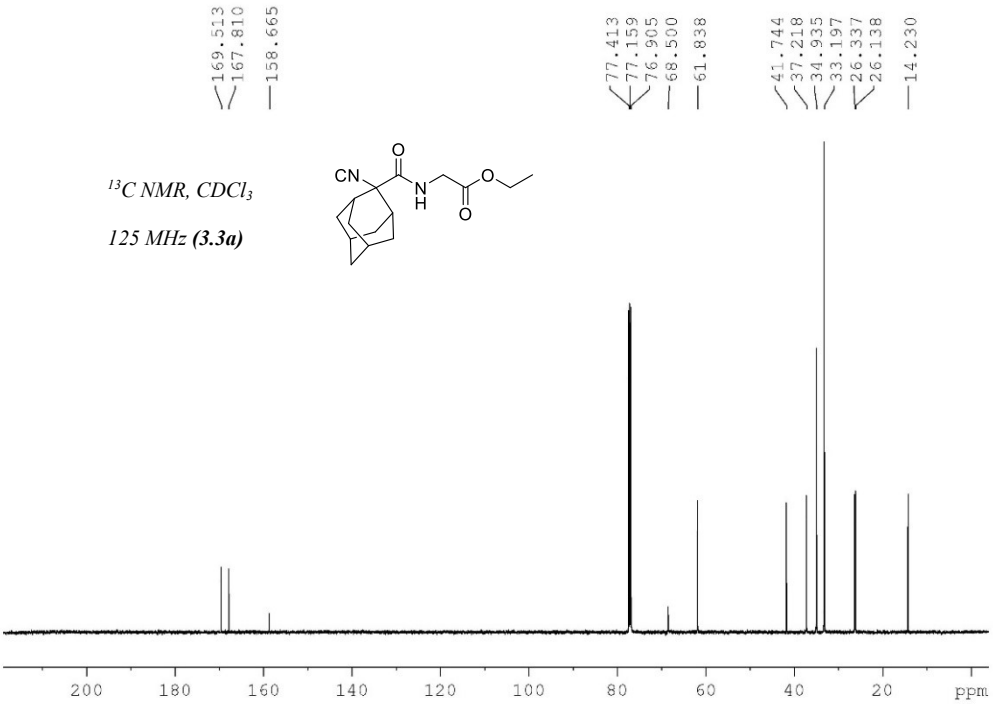
169.513
167.810
158.665
77.413
77.159
76.905
68.500
61.838
41.744
37.218
34.935
33.197
26.337
26.138
14.230
^{13}C NMR, $CDCl_3$
125 MHz (3.3a)
CN
O
N
H
O
O
200
180
160
140
120
100
80
60
40
20
ppm

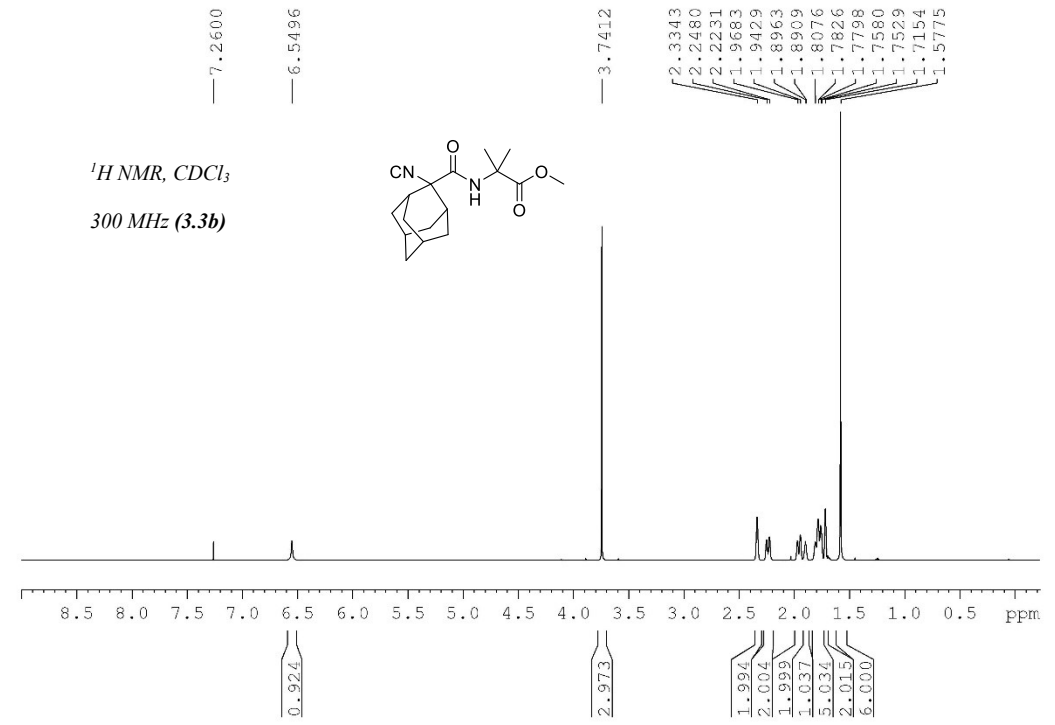

^{1}H NMR, $CDCl_3$

*300 MHz **(3.3b)***

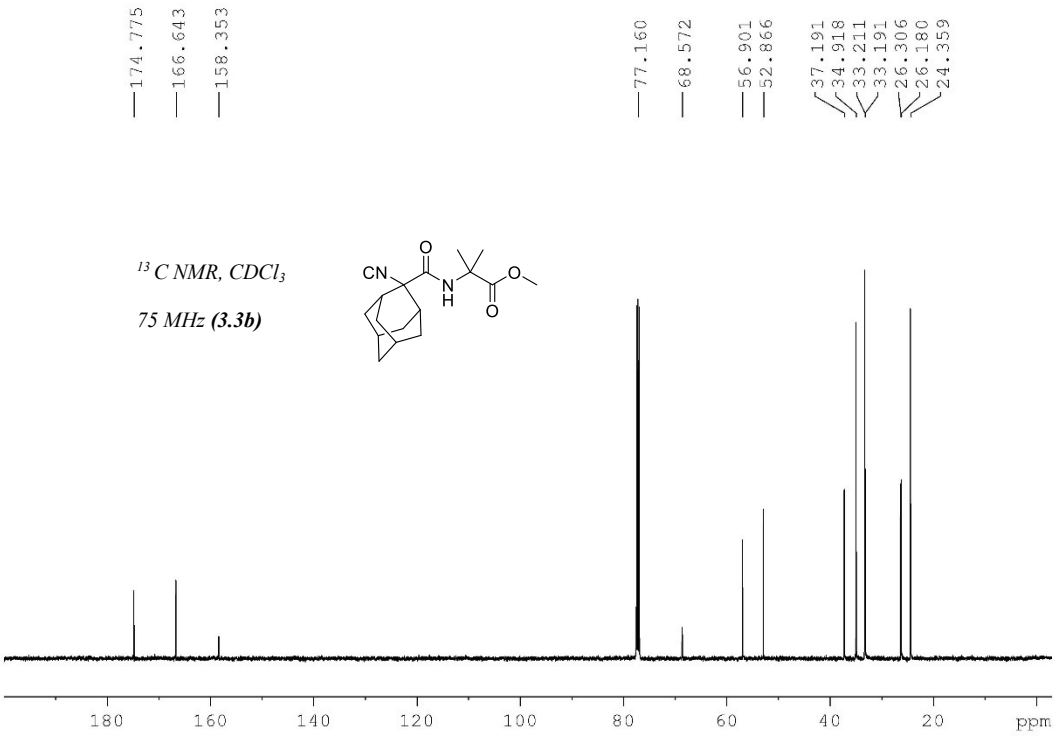

^{13}C NMR, $CDCl_3$

*75 MHz **(3.3b)***

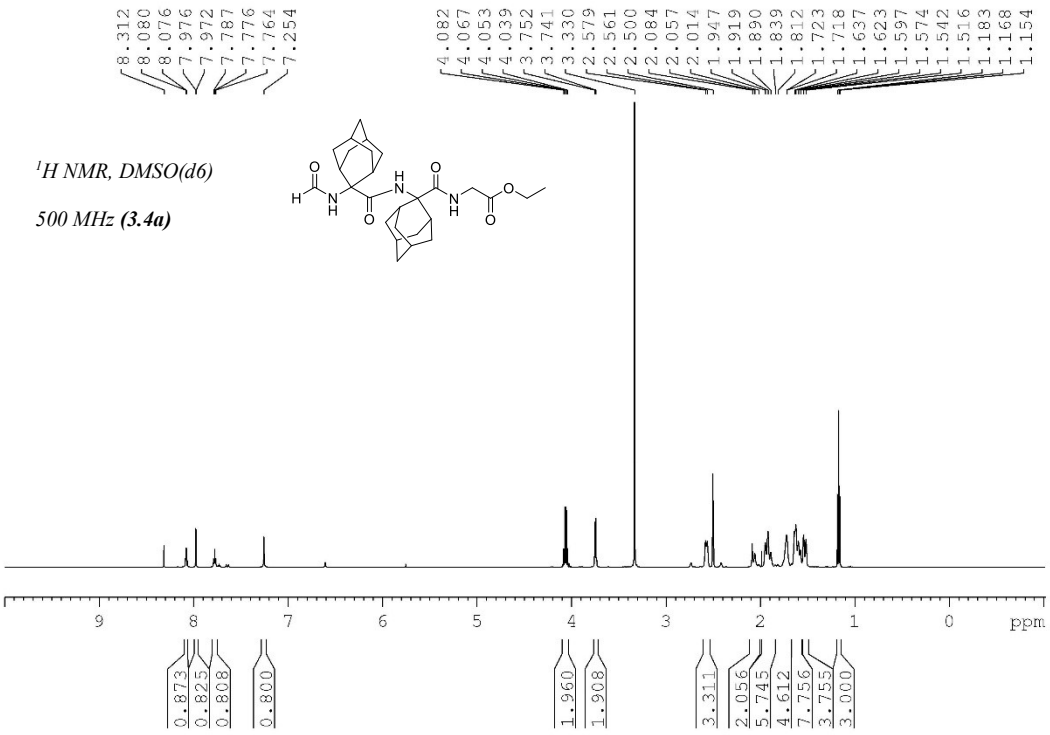

[1]H NMR, DMSO(d6)

*500 MHz **(3.4a)***

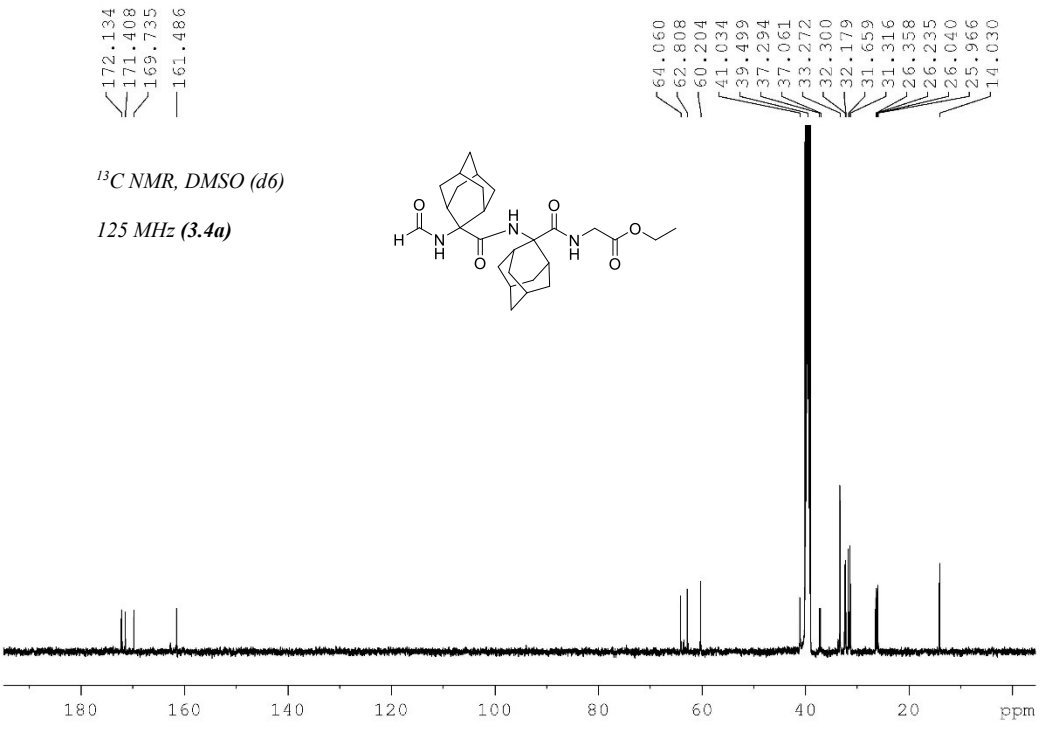

[13]C NMR, DMSO (d6)

*125 MHz **(3.4a)***

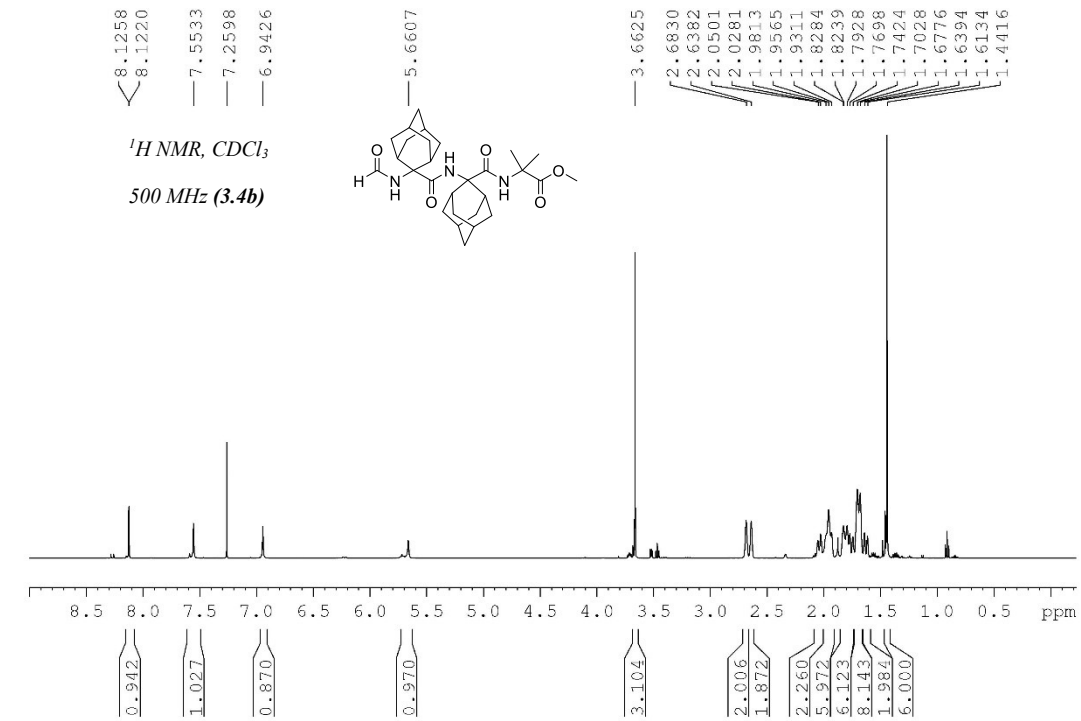
8.1258
8.1220
7.5533
7.2598
6.9426
5.6607
3.6625
2.6830
2.6382
2.0501
2.0281
1.9813
1.9565
1.9311
1.8284
1.8239
1.7928
1.7698
1.7424
1.7028
1.6776
1.6394
1.6134
1.4416
^{1}H NMR, $CDCl_3$
500 MHz (3.4b)
8.5 8.0 7.5 7.0 6.5 6.0 5.5 5.0 4.5 4.0 3.5 3.0 2.5 2.0 1.5 1.0 0.5 ppm
0.942
1.027
0.870
0.970
3.104
2.006
1.872
2.260
5.972
6.123
8.143
1.984
6.000

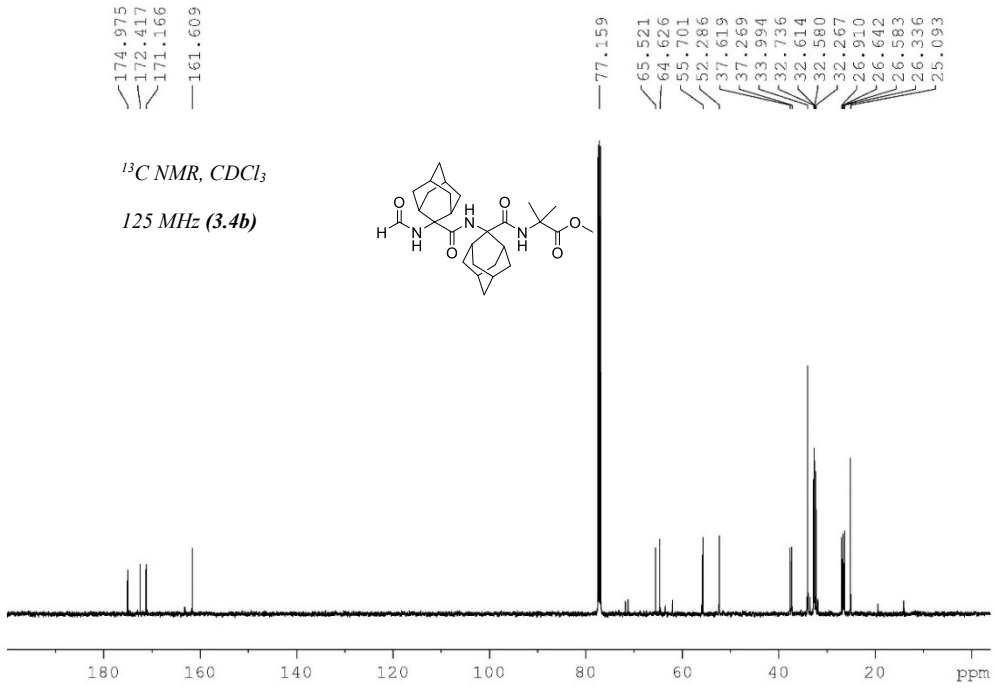
174.975
172.417
171.166
161.609
77.159
65.521
64.626
55.701
52.286
37.619
37.269
33.994
32.736
32.614
32.580
32.267
26.910
26.642
26.583
26.336
25.093
^{13}C NMR, $CDCl_3$
125 MHz (3.4b)
180 160 140 120 100 80 60 40 20 ppm

Supporting information Manuscript 3

Fatemeh M. Mir, Marco Crisma, Claudio Toniolo, William D. Lubell. Isolated α-Turn and Incipient γ-Helix. Under revision for *the Journal of the American Chemical Society.*

SUPPORTING INFORMATION

Isolated α-Turn and Incipient γ-Helix

*Fatemeh M. Mir,[†] Marco Crisma,[‡] Claudio Toniolo,[‡] William D. Lubell[†]**

† Département de Chimie, Université de Montréal, C. P. 6128, Succursale Centre-Ville, Montréal, Québec, Canada H3C 3J7

‡ Department of Chemistry, University of Padova and Institute of Biomolecular Chemistry, Padova Unit, CNR, 35131 Padova, Italy

E-mail : william.lubell@umontreal.ca

Experimental section

General Methods: Unless otherwise specified, all non-aqueous reactions were performed under an inert argon atmosphere. Anhydrous DCM was obtained by passage through a solvent filtration system (Glass Contour, Irvine, CA) and transferred by syringe. Reaction mixture solutions (after aqueous workup) were dried over anhydrous Na_2SO_4, filtered, and rotary-evaporated under reduced pressure. Column chromatography was performed on 230-400 mesh silica gel, and thin-layer chromatography was performed on alumina plates coated with silica gel (Merck 60 F_{254} plates). Visualization of the developed chromatogram was performed by UV absorbance or staining with iodine. Melting points were obtained on a Buchi melting point B-540 apparatus and are uncorrected. Accurate mass measurements were performed on an LC-MSD instrument in electrospray ionization (ESI-TOF) mode at the Université de Montréal Mass Spectrometry facility, and are listed as empirical formula confirmations $[M + H]^+$. Nuclear magnetic resonance (NMR ^1H, ^{13}C, COSY, HMBC) spectra were recorded on Bruker 300, 400, 500 and 700 MHz spectrometers. ^1H and ^{13}C NMR spectra were respectively referenced to $CDCl_3$ (7.26 ppm and 77.16 ppm) or DMSO-d_6 (2.50 ppm, and 39.52 ppm). Coupling constant *J* values were measured in Hertz (Hz) and chemical shift values in parts per million (ppm). Infrared absorption spectra for characterization of compounds were recorded on a Bruker Alpha P FT-IR spectrometer equipped with a single reflection ATR sampling module which allows spectral acquisition from neat solid and liquid samples. Band positions are reported in reciprocal centimeters (cm^{-1}). The FT-IR absorption spectra in $CDCl_3$ (99.8% *d*; Merck) solution were recorded at 293 K using a Perkin-Elmer model 1720X FT-IR spectrophotometer, nitrogen flushed, equipped with a sample-shuttle device, at 2 cm^{-1} nominal resolution, averaging 100 scans. Solvent (baseline) spectra were obtained under the same conditions. For spectral elaboration, the software SpectraCalc (Galactic) was employed. Cells were used with CaF_2 windows and path lengths of 0.1 mm, 1.0 mm, and 10.0 mm.

Reagents: Unless specified otherwise, commercially available reagents were purchased from Aldrich, A & C American Chemicals Ltd., Fluka and Advanced Chemtech™ and used without further purification, including adamantan-2-one, ammonium formate, formic acid, $POCl_3$, and Et_3N.

2-*N*-(Formyl)aminoadamantane-2-*N*'-(*iso*-propyl)carboxamide (4.4a)

A solution of *iso*-propyl isocyanide (**4.3a**, 1 g, 14.5 mmol, 1eq) in MeOH (2M) was treated with adamantan-2-one (2.2 g, 14.5 mmol, 1eq) and ammonium formate (1.1 g, 17.4 mmol, 1.2eq, dissolved in the minimum amount of H_2O). The mixture was stirred for 16h. The volatiles were evaporated. The residue was dissolved in $CHCl_3$, washed with water and brine, and dried over Na_2SO_4. The volatiles were evaporated and the residue was purified by column chromatography using 40% EtOAc in hexanes as eluent. Evaporation of the collected fractions gave Formyl-Adm-NH-*i*-Pr (**4.4a**, 2.4 g, 62%) as white powder: R_f 0.33 (3:97 MeOH:CH_2Cl_2); m.p. 181-185 °C; ^{1}H NMR (500 MHz, $CDCl_3$) δ 1.13 (d, J = 6.5, 6H), 1.65-1.74 (m, 6H), 1.80-1.82 (m, 2H), 1.92-1.96 (m, 4H), 2.64 (br, 2H), 4.01-4.07 (m, 1H), 6.07 (s, 1H), 6.96 (d, J = 7.5, 1H), 8.12 (d, J = 2.5, 1H); ^{13}C NMR (500 MHz, $CDCl_3$): δ 22.6, 26.5, 26.6, 32.1, 32.6, 34.0, 37.4, 41.4, 64.9, 161.7, 171.2; IR (neat) ν = 3320, 3286, 2903, 1652, 1518; HRMS (ESI) *m*/*z* calcd for $C_{15}H_{25}N_2O_2$ 265.1911; found $[M + H]^+$ 265.1916.

2-*N*-(Formyl)aminoadamantane-2-*N*'-(*tert*-butyl)carboxamide (4.4b)

Amide **4.4b** was synthesized from *tert*-butyl isocyanide (**4.3b**, 3 g, 41.6 mmol) according to the procedure described for the synthesis of formamide **4.4a** and purified by column chromatography using 30% EtOAc in hexanes as eluent. Evaporation of the collected fractions gave Formyl-Adm-NH-*t*-Bu (**4.4b**, 8.3g, 72%) as a white powder: R_f 0.2 (7:3 hexanes:EtOAc); m.p. 197-200 °C; ^{1}H NMR (500 MHz, $CDCl_3$): δ 1.32 (s, 9H), 1.3-1.72 (m, 6H), 1.79-1.84 (m, 2H), 1.92-2.00 (m, 4H), 2.60 (br, 2H), 6.16 (s, 1H), 6.95 (s, 1H), 8.11 (d, J = 2.0 Hz, 1H); ^{13}C NMR (500 MHz, $CDCl_3$) δ 26.4, 26.6, 28.6, 32.1, 32.6, 34.1, 37.3, 51.0, 65.4, 161.7, 171.0; IR (neat) ν: 3264, 2906, 1674, 1649, 1540, 1222, 741; HRMS (ESI) *m*/*z* calcd for $C_{16}H_{27}N_2O_2$ 279.2067; found $[M + H]^+$ 279.2066.

2-Isocyanoadamantane-2-*N*'-(*iso*-propyl)carboxamide (4.5a)

Formamide **4.4a** (2 g, 7.6 mmol) in CH_2Cl_2 (8 mL) was treated with Et_3N (6.36 g, 45.6 mmol), cooled to –5 °C, and treated dropwise with $POCl_3$ (1.07 g, 11.4 mmol). After stirring at this temperature for 1-2 h, the reaction mixture was vigorously stirred and treated with a solution of saturated $NaHCO_3$ (8mL). The organic phase was separated, washed with brine, and dried over Na_2SO_4. Evaporation of the volatiles under reduced pressure afforded a yellow powder, which was purified by column chromatography using 30% EtOAc in hexanes as eluent. Evaporation of the collected fractions gave isocyanide **4.5a** (1.70 g, 90%) as white powder: R_f 0.53 (7:3

hexanes:EtOAc); m.p. 130-133 °C; ^{1}H NMR (500 MHz, $CHCl_3$) δ 1.18 (d, *J* = 7.0, 6H), 1.72 (m, 2H), 1.76-1.78 (m, 4H), 1.81 (m, 1H), 1.89-1.91 (m, 1H), 1.96-1.99 (m, 2H), 2.23-2.26 (m, 2H), 2.31 (m, 2H), 4.07-4.14 (m, 1H), 5.74 (br, 1H); ^{13}C NMR (500 MHz, $CDCl_3$) δ 22.4, 26.2, 26.4, 33.3, 35.0 (2C), 37.3, 42.1, 68.6, 158.2, 166.7; IR (neat): ν = 3315, 2915, 2122, 1647, 1533, 653; HRMS (ESI) *m*/*z* calcd for $C_{15}H_{23}N_2O$ 247.1805; found $[M + H]^+$ 247.1810.

2-Isocyanoadamantane-2-*N*'-(*tert*-butyl)carboxamide (4.5b)

Isocyanide **4.5b** was synthesized from formamide **4.4b** (6.75 g, 24.24 mmol) according to the procedure described for the synthesis of isocyanide **4.5a** and purified by column chromatography using 10% EtOAc in hexanes as eluent. Evaporation of the collected fractions gave isocyanide **4.5b** (6 g, 94%) as white powder: R_f 0.36 (9:1 hexanes:EtOAc); m.p. 116-120 °C; ^{1}H NMR (500 MHz, $CHCl_3$) δ 1.37 (s, 9H), 1.71 (m, 2H), 1.75-1.77 (m, 4H), 1.81 (m, 1H), 1.89 (m, 1H), 1.94-1.97 (m, 2H), 2.22-2.24 (m, 2H), 2.28 (m, 2H), 5.69 (s, 1H); ^{13}C NMR (500 MHz, $CDCl_3$) δ 26.2, 26.3, 28.5, 33.3, 35.1, 37.2, 39.4, 51.8, 68.9, 158.0, 166.6; IR (neat) ν: 3363, 2917, 2120, 1660, 1527, 1452, 1214, 583; HRMS (ESI) *m*/*z* calcd for $C_{16}H_{25}N_2O$ 261.19614; found $[M + H]^+$ 261.19712.

Formyl-Adm-Adm-NH-*i*-Pr (4.6a)

Dipeptide **4.6a** was synthesized from isocyanide **4.5a** (1.6 g, 6.47 mmol) according to the procedure described for the synthesis of formamide **4.4a** and purified by column chromatography using 40% hexanes in EtOAc as eluent. Evaporation of the collected fractions gave HCO-Adm-Adm-NH-*i*-Pr (**4.6a**, 2.5 g, 87%) as white powder: R_f 0.25 (4:6 hexanes:EtOAc); m.p. 192-198 °C; ^{1}H NMR (500 MHz, $CHCl_3$) δ 1.10 (d, *J* = 6.6 Hz, 6H), 1.62 (m, 1H), 1.65 (m, 1H), 1.69-1.70 (m, 9H), 1.76 (m, 1H), 1.79-1.83 (m, 4H), 1.93-1.95 (m, 6H), 2.00 (m, 1H), 2.03 (m, 1H), 2.64-2.66 (m, 4H), 3.99-4.07 (m, 1H), 5.74 (s, 1H), 6.81 (d, *J* = 7.9, 1H), 6.92 (s, 1H), 8.13 (d, *J* = 1.9, 1H); ^{13}C NMR (500 MHz, $CDCl_3$) δ 22.8, 26.4, 26.6 (2C), 26.9, 32.2, 32.6, 32.7, 32.8, 34.0, 34.2, 37.3, 37.7, 41.1, 64.7, 65.3, 161.3, 171.2, 172.1; IR (neat) ν: 3360, 2904, 1677, 1511, 751. HRMS (ESI) *m*/*z* calcd for $C_{26}H_{40}N_3O_3$ 442.3060; found $[M + H]^+$ 442.3073.

Formyl-Adm-Adm-NH-*t*-Bu (4.6b)

Dipeptide **4.6b** was synthesized from isocyanide **4.5b** (2 g, 7.65 mmol) according to the procedure described for the synthesis of formamide **4.4a** and purified by column chromatography using 30% EtOAc in hexanes as eluent. Evaporation of the collected fractions gave HCO-Adm-Adm-NH-*t*-Bu (**4.6b**, 2.96 g, 85%) as white powder: R_f 0.21 (7:3 hexanes:EtOAc); m.p. 228-230 °C; ^{1}H NMR

(500 MHz, $CDCl_3$) δ 1.30 (s, 9H), 1.62 (m, 1H), 1.64 (m, 1H), 1.68-1.72 (m, 8H), 1.75 (m, 1H), 1.78-1.82 (m, 5H), 1.94-1.96 (m, 6H), 2.00 (m, 1H), 2.03 (m, 1H), 2.63 (m, 2H), 2.68 (m, 2H), 5.55 (s, 1H), 6.83 (s, 1H), 6.93 (s, 1H), 8.13 (d, J = 1.9 Hz, 1H); ^{13}C NMR (500 MHz, $CDCl_3$): δ 26.3, 26.5, 26.6, 26.9, 28.8, 32.3, 32.6, 32.7, 32.8, 34.1, 34.2, 37.3, 37.6, 50.7, 65.3, 65.4, 161.0, 170.9, 171.9; IR (neat) ν: 3256, 2917, 1684, 1655, 1538, 1499, 1217; HRMS (ESI) *m*/*z* calcd for $C_{27}H_{42}N_3O_3$ 456.3221; found $[M + H]^+$ 456.3242.

'Isocyano'-Adm-Adm-NH-*i*-Pr (4.7a)

Isocyanide **4.7a** was synthesized from dipeptide **4.6a** (2.4 g, 5.4 mmol) according the procedure described for the synthesis of isocyanide **4.5a**, and purified by column chromatography using 20% EtOAc in hexanes as eluent. Evaporation of the collected fractions gave 'CN'-Adm-Adm-NH-*i*-Pr (**4.7a**, 2.23 g, 97%) as white powder: R_f 0.51 (7:3 hexanes:EtOAc); m.p 228-235 °C; ^{1}H NMR (500 MHz, $CHCl_3$) δ 1.12 (d, *J* = 6.5 Hz, 6H), 1.71-1.72 (m, 7H), 1.77 (m, 3H), 1.80 (m, 4H), 1.86-1.92 (m, 6H), 1.97-2.00 (m, 2H), 2.22-2.25 (m, 2H), 2.31 (m, 2H), 2.72 (m, 2H), 4.02-4.09 (m, 1H), 5.73 (s, 1H), 6.84 (d, *J* = 8.0 Hz, 1H); ^{13}C NMR (500 MHz, $CDCl_3$): δ 22.8, 26.1, 26.2, 26.4, 26.7, 32.4, 32.9, 33.2, 33.4, 34.2, 35.0, 37.1, 37.3, 41.3, 64.8, 69.0, 158.8, 167.2, 170.3; IR (neat) ν: 3357, 2856, 2135, 1677, 1632, 1527, 753. HRMS (ESI) *m*/*z* calcd for $C_{26}H_{38}N_3O_2$ 424.2959, found $[M + H]^+$ 424.2967.

'Isocyano'-Adm-Adm-NH-*t*-Bu (4.7b)

Isocyanide **7a** was synthesized from dipeptide **4.6b** (1.16g, 2.54 mmol) according the procedure described for the synthesis of isocyanide **4.5a**, and purified by column chromatography using 30% EtOAc in hexanes as eluent. Evaporation of the collected fractions gave 'CN'-Adm-Adm-NH-*i*-Pr (**4.7b**, 0.62g, 56%) as white powder: R_f 0.67 (7:3 Hex:EtOAc); m.p. 207-210 °C; ^{1}H NMR (500 MHz, $CDCl_3$) δ 1.32 (s, 9H), 1.69-1.72 (m, 7H), 1.77 (m, 3H), 1.79-1.82 (m, 4H), 1.87-1.90 (m, 6H), 1.98-2.00 (m, 2H), 2.22-2.25 (m, 2H), 2.33 (m, 2H), 2.68 (m, 2H), 5.30 (s, 1H), 6.91 (s, 1H); ^{13}C NMR (500 MHz, $CDCl_3$): δ 26.1, 26.2, 26.4, 26.7, 28.8, 32.6, 32.9, 33.2, 33.5, 34.2, 35.0, 37.1, 37.3, 51.0, 65.4, 68.9, 158.6, 167.1, 170.2; IR (neat) ν = 3321, 2919, 2123, 1654, 1537, 1509, 1452; HRMS (ESI) *m*/*z* calcd for $C_{27}H_{40}N_3O_2$ 438.3115; found $[M + H]^+$ 438.3131.

Formyl-Adm-Adm-Adm-NH-*i*-Pr (4.1)

Peptide **4.1** was synthesized from isocyanide **4.7a** (1.18 g, 2.8 mmol) according to the procedure described for the synthesis of formamide **4.4a**. After 24 h, solid ammonium formate (1

eq) was freshly added to the reaction mixture, which was worked up after 48 h, when complete disappearance of **4.7a** was observed by TLC. After evaporation of the volatiles, the residue was purified by column chromatography using 30% EtOAc in hexanes as eluent. Evaporation of the collected fractions gave HCO-Adm-Adm-Adm-NH-*i*-Pr (**4.1**, 1.06 g, 61%) as white powder: R_f 0.24 (7:3 Hex:EtOAc); m.p.> 250 °C; ^{1}H NMR (500 MHz, $CDCl_3$) δ 1.14 (d, *J* = 6.5 Hz, 6H), 1.63-1.72 (m, 16H), 1.76-1.78 (m, 5H), 1.83 (m, 3H), 1.90-1.93 (m, 4H), 1.95-1.97 (m, 6H), 2.08-2.11 (m, 2H), 2.63-2.66 (m, 6H), 3.91-3.98 (m, 1H), 5.57 (s, 1H), 7.00 (s, 1H), 7.01 (s, 1H), 7.17 (s, 1H), 8.10 (d, *J* = 2.0 Hz, 1H); ^{13}C NMR (quantitative analysis, 700 MHz, $CDCl_3$) δ 22.7 (2C), 26.4, 26.7 (3C), 26.9, 27.0, 32.2 (2C), 32.4 (2C), 32.6 (2C), 32.8 (2C), 33.1 (4C), 34.2 (6C), 37.3, 37.5, 37.7, 41.4, 64.3, 65.5, 65.8, 162.3, 170.9, 172.1, 173.3; IR (neat) ν: 3309, 2909, 2860, 1681, 1647, 1525, 1497, 1470; HRMS (ESI) *m*/*z* calcd for $C_{37}H_{55}N_4O_4$ 619.4218; found $[M + H]^+$ 619.4226.

Formyl-Adm-Adm-Adm-NH-*t*-Bu (4.2)

Peptide **4.2** was synthesized from isocyanide **4.7b** (0.6 g, 1.37 mmol) according to the procedure described for the synthesis of formamide **4.4a**. The mixture left to react for 48h. Each day freshly made sat. solution of $NH_4^+HCO_2^-$ (1eq) was added to the mixture. The solvent was removed after completion of the reaction. To the white solid was added H_2O and extracted with CH_2Cl_2. The organic layer was washed with brine and dried over Na_2SO_4. Evaporation of the solvent gave a white solid which was purified by column chromatography using 30% EtOAc in hexanes as eluent. Evaporation of the collected fractions gave HCO-Adm-Adm-Adm-NH-*t*-Bu (**4.2**, 0.52, 61%) as white powder: R_f 0.32 (7:3 hexanes:EtOAc); m.p. > 250 °C; ^{1}H NMR (500 MHz, $CDCl_3$) δ 1.31 (s, 9H), 1.58 (m, 1H), 1.61-1.62 (m, 2H), 1.66-1.69 (m, 12H), 1.73 (m, 2H), 1.77-1.82 (m, 6H), 1.89-1.97 (m, 11H), 2.05-2.08 (m, 2H), 2.63-2.65 (m, 6H), 5.59 (s, 1H), 6.69 (s, 1H), 7.07 (s, 1H), 7.16 (s, 1H), 8.10 (d, *J* = 2.0 Hz, 1H); ^{13}C NMR (700 MHz, $CDCl_3$) δ 26.3, 26.6 (3C), 26.9 (2C), 28.7 (3C), 32.2 (2C), 32.5 (2C), 32.6 (2C), 32.7 (2C), 33.1 (4C), 34.1 (4C), 34.2 (2C), 37.3 , 37.5, 37.7, 50.8, 65.0 (2C), 65.7, 162.1, 170.9, 171.4, 172.9; IR (neat) ν: 2907, 2857, 1673, 1513, 749; HRMS (ESI) *m*/*z* calcd for $C_{38}H_{57}N_4O_4$ 633.4374; found $[M + H]^+$ 633.4394.

Crystallography data and Molecular structure for compounds

General Methods for making crystals: Tripeptide **4.1** was crystallized by dissolving 3-4 mg of peptide **4.1** in 1 mL of acetone and equilibrating hexane vapour into the mother liquor in a closed

container to provide slow formation of crystals. Crystals of **4.1** were similarly obtained from equilibrating hexane vapour into other solvent systems: acetone with drops of $CHCl_3$, large blocks; EtOAc/Acetone/ drops of $CHCl_3$, needles. Crystals of peptide **4.2** was grown respectively from mixture of acetone/EtOAc and DMSO using the liquid-vapour saturation method.

Peptide 4.1 (LUB118)

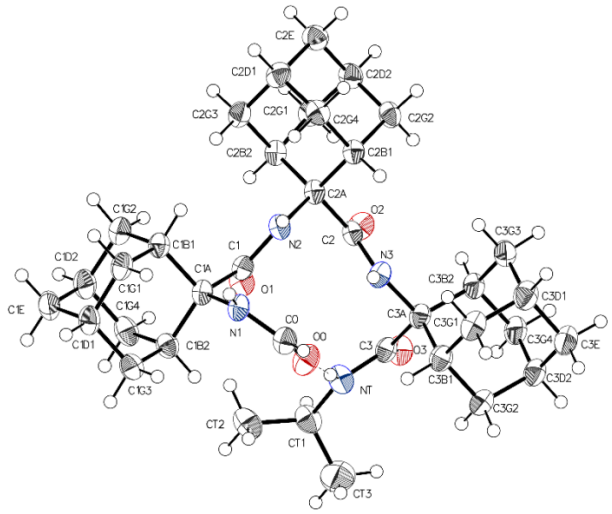

Table 1 Crystal data and structure refinement for lub118.

Identification code	lub118
Empirical formula	$C_{37}H_{54}N_4O_4$
Formula weight	618.84
Temperature/K	150
Crystal system	monoclinic
Space group	$P2_1/c$
a/Å	14.6491(6)

b/Å	14.7140(6)
c/Å	16.1495(7)
α/°	90
β/°	109.618(2)
γ/°	90
Volume/Å^3	3278.9(2)
Z	4
ρ_{calc}g/cm^3	1.254
μ/mm^{-1}	0.413
F(000)	1344.0
Crystal size/mm^3	0.138 × 0.043 × 0.04
Radiation	GaKα (λ = 1.34139)
2Θ range for data collection/°	5.572 to 110.142
Index ranges	-17 ≤ h ≤ 17, -17 ≤ k ≤ 17, -19 ≤ l ≤ 19
Reflections collected	38793
Independent reflections	6204 [R_{int} = 0.0774, R_{sigma} = 0.0613]
Data/restraints/parameters	6204/0/409
Goodness-of-fit on F^2	1.020
Final R indexes [I>=2σ (I)]	R_1 = 0.0577, wR_2 = 0.1226
Final R indexes [all data]	R_1 = 0.1106, wR_2 = 0.1466
Largest diff. peak/hole / e Å^{-3}	0.26/-0.23

Table 2 Fractional Atomic Coordinates ($\times 10^4$) and Equivalent Isotropic Displacement Parameters ($Å^2 \times 10^3$) for lub118. U_{eq} is defined as 1/3 of of the trace of the orthogonalised U_{IJ} tensor.

Atom	*x*	*y*	*z*	U(eq)
C0	2831.5(18)	1375.2(18)	5715.0(16)	34.8(6)
O0	2834.7(13)	1076.6(13)	5001.9(11)	43.4(5)
N1	2179.1(13)	1928.2(14)	5841.8(12)	29.9(5)
C1A	1293.6(16)	2218.8(17)	5136.8(14)	27.4(6)
C1B1	796.9(16)	2987.3(17)	5484.4(15)	29.9(6)
C1B2	575.8(17)	1412.6(17)	4860.8(15)	31.7(6)
C1G1	545.2(17)	2664.1(18)	6285.1(15)	34.2(6)
C1G2	-145.6(17)	3264.8(18)	4754.8(16)	35.2(6)
C1G3	353.2(18)	1085.1(18)	5676.0(16)	36.2(6)
C1G4	-383.8(17)	1693.5(19)	4156.7(16)	39.4(7)
C1D1	-128.4(17)	1843.8(18)	6029.3(16)	37.0(6)
C1D2	-851.4(17)	2458.0(19)	4510.9(16)	39.0(7)
C1E	-1074.0(18)	2128(2)	5318.1(17)	41.2(7)
C1	1620.8(16)	2596.6(17)	4388.7(15)	28.4(6)
O1	1246.9(11)	2397.7(12)	3612.4(10)	34.2(4)
N2	2361.5(13)	3205.0(13)	4660.3(11)	26.8(5)

C2A	2663.4(16)	3747.7(16)	4033.7(14)	26.6(5)
C2B1	3551.8(16)	4332.7(17)	4553.4(14)	28.7(6)
C2B2	1840.5(17)	4409.3(17)	3514.6(14)	28.9(6)
C2G1	3298.6(17)	4967.0(17)	5197.9(15)	32.3(6)
C2G2	3863.7(17)	4911.7(18)	3902.7(16)	33.2(6)
C2G3	1590.0(17)	5027.0(18)	4173.2(16)	34.0(6)
C2G4	2150.5(17)	5028.6(18)	2891.2(15)	33.9(6)
C2D1	2473.6(18)	5603.2(18)	4692.0(16)	35.3(6)
C2D2	3048.2(18)	5568.0(17)	3408.2(16)	34.4(6)
C2E	2807.0(19)	6181.9(18)	4063.7(16)	37.6(6)
C2	2967.2(16)	3081.8(17)	3433.2(15)	27.6(5)
O2	2749.3(12)	3207.0(12)	2639.0(10)	35.8(4)
N3	3553.7(13)	2393.1(13)	3839.6(12)	29.6(5)
C3A	3948.5(16)	1721.6(17)	3366.0(15)	29.3(6)
C3B1	4559.8(17)	1018.7(18)	4052.8(15)	33.5(6)
C3B2	4633.4(17)	2165.3(18)	2934.2(16)	33.4(6)
C3G1	5410.1(18)	1489.7(19)	4744.7(16)	39.2(7)
C3G2	4962.8(18)	301.2(18)	3581.9(16)	36.1(6)
C3G3	5473.7(18)	2637.0(19)	3640.0(18)	41.3(7)
C3G4	5063.6(19)	1443.3(18)	2482.2(17)	38.1(6)
C3D1	6072.9(18)	1937.8(19)	4307.2(17)	42.4(7)
C3D2	5636.4(18)	743.9(19)	3151.7(16)	37.5(6)

C3E	6474.0(18)	1208.1(19)	3851.1(18)	42.8(7)
C3	3076.0(17)	1232.7(17)	2680.2(15)	30.6(6)
O3	2943.9(12)	1236.3(12)	1884.9(10)	37.8(4)
NT	2486.1(14)	793.8(15)	3019.9(13)	36.5(5)
CT1	1697.9(18)	205.5(19)	2492.3(17)	39.6(7)
CT2	917(2)	173(2)	2910.0(18)	48.4(8)
CT3	2081(2)	-721(2)	2392(2)	74.2(11)

Table 3 Anisotropic Displacement Parameters ($Å^2 \times 10^3$) for lub118. The Anisotropic displacement factor exponent takes the form: $-2\pi^2[h^2a^{*2}U_{11}+2hka^*b^*U_{12}+\ldots]$.

Atom	U_{11}	U_{22}	U_{33}	U_{23}	U_{13}	U_{12}
C0	35.7(14)	42.6(16)	28.1(13)	4.8(12)	13.4(11)	3.3(13)
O0	48.9(11)	54.4(12)	31.3(10)	1.4(9)	19.3(8)	11.8(9)
N1	28.5(11)	40.3(13)	22.0(10)	-2.1(9)	9.9(8)	3.4(10)
C1A	24.8(12)	36.4(15)	21.1(11)	-0.4(11)	7.7(10)	1.8(11)
C1B1	27.7(12)	36.0(15)	27.8(13)	-1.3(11)	11.6(10)	0.9(11)
C1B2	31.7(13)	35.4(15)	29.4(13)	-1.5(11)	12.2(11)	-3.4(11)
C1G1	31.4(13)	44.8(16)	29.6(13)	-0.9(12)	14.6(11)	4.5(12)
C1G2	30.2(13)	43.3(16)	32.8(13)	3.7(12)	11.6(11)	5.7(12)
C1G3	35.9(14)	39.2(16)	35.9(14)	2.7(12)	15.2(11)	-3.4(12)
C1G4	32.7(14)	51.6(18)	32.1(14)	-3.9(13)	8.6(11)	-11.1(13)
C1D1	33.9(14)	49.5(17)	33.5(14)	4.6(13)	19.0(11)	2.5(13)

C1D2	24.9(13)	50.6(18)	37.7(14)	3.2(13)	5.4(11)	0.3(12)
C1E	28.8(14)	49.4(18)	48.6(16)	2.2(14)	17.3(12)	-1.0(12)
C1	27.5(12)	33.9(14)	24.1(13)	0.4(11)	8.9(10)	4.1(11)
O1	35.4(9)	45.4(11)	21.6(9)	-2.1(8)	9.0(7)	-5.2(8)
N2	26.6(10)	36.6(12)	17.2(9)	-0.1(9)	7.4(8)	-2.8(9)
C2A	24.7(12)	34.7(14)	20.7(11)	-2.2(10)	8.0(9)	-1.5(11)
C2B1	26.7(13)	34.0(14)	25.6(12)	-2.5(11)	9.0(10)	-1.1(11)
C2B2	25.8(12)	36.9(15)	23.4(12)	0.2(11)	7.3(10)	1.1(11)
C2G1	32.9(13)	37.6(15)	25.7(12)	-4.9(11)	9.0(10)	-5.9(12)
C2G2	31.8(13)	39.8(16)	31.7(13)	-4.3(12)	15.4(11)	-5.4(12)
C2G3	33.1(14)	37.7(15)	34.3(14)	4.4(12)	15.3(11)	6.3(12)
C2G4	36.3(14)	38.7(15)	26.0(13)	3.5(11)	9.5(11)	4.0(12)
C2D1	41.7(15)	37.3(15)	30.8(13)	-2.9(12)	17.4(12)	2.9(12)
C2D2	40.6(15)	36.6(15)	31.0(13)	2.1(12)	18.4(12)	-2.7(12)
C2E	42.8(15)	35.6(16)	36.9(14)	1.3(12)	16.8(12)	-1.5(12)
C2	23.3(12)	35.4(15)	24.4(13)	-2.4(11)	8.4(10)	-4.2(11)
O2	43.1(10)	43.4(11)	21.5(9)	-0.5(8)	11.4(7)	5.4(8)
N3	30.7(11)	38.1(12)	20.4(10)	-3.0(9)	9.2(8)	4.9(10)
C3A	27.9(12)	34.9(14)	26.4(12)	-4.2(11)	10.8(10)	1.7(11)
C3B1	32.3(13)	38.7(16)	29.5(13)	-0.7(12)	10.4(11)	4.3(12)
C3B2	30.7(13)	38.7(15)	34.4(14)	-1.3(12)	15.7(11)	0.4(11)
C3G1	34.8(14)	49.6(17)	30.4(13)	-5.3(12)	7.3(11)	7.4(13)

C3G2	34.4(14)	37.1(15)	37.0(14)	-3.0(12)	12.0(12)	6.9(12)
C3G3	34.2(14)	40.9(16)	54.6(17)	-8.7(14)	22.6(13)	-4.4(13)
C3G4	36.4(14)	46.7(17)	37.2(14)	-2.8(13)	20.3(12)	1.3(13)
C3D1	31.0(14)	50.2(18)	42.1(15)	-12.1(14)	7.1(12)	0.8(13)
C3D2	34.8(14)	43.0(16)	38.8(14)	-5.8(12)	17.9(12)	4.9(12)
C3E	32.3(14)	49.8(18)	47.4(16)	-3.5(14)	14.7(12)	5.7(13)
C3	30.2(13)	36.4(15)	27.2(13)	-2.6(11)	12.3(11)	4.3(11)
O3	38.3(10)	51.2(12)	24.5(9)	-1.9(8)	11.4(7)	0.7(9)
NT	36.7(12)	48.8(14)	24.3(10)	-5.9(10)	10.5(9)	-8.2(11)
CT1	38.5(15)	46.9(17)	31.5(14)	-8.3(13)	9.3(12)	-10.5(13)
CT2	47.2(17)	56(2)	41.9(16)	-5.9(14)	15.3(13)	-16.7(15)
CT3	60(2)	61(2)	94(3)	-34(2)	15.5(19)	-10.3(18)

Table 4 Bond Lengths for lub118.

Atom	Atom	Length/Å	Atom	Atom	Length/Å
C0	O0	1.234(3)	C2G2	C2D2	1.535(3)
C0	N1	1.322(3)	C2G3	C2D1	1.539(3)
N1	C1A	1.473(3)	C2G4	C2D2	1.523(3)
C1A	C1B1	1.548(3)	C2D1	C2E	1.525(3)
C1A	C1B2	1.548(3)	C2D2	C2E	1.521(3)
C1A	C1	1.545(3)	C2	O2	1.227(3)
C1B1	C1G1	1.534(3)	C2	N3	1.348(3)

C1B1	C1G2	1.539(3)	N3	C3A	1.481(3)
C1B2	C1G3	1.536(3)	C3A	C3B1	1.560(3)
C1B2	C1G4	1.538(3)	C3A	C3B2	1.546(3)
C1G1	C1D1	1.526(4)	C3A	C3	1.558(3)
C1G2	C1D2	1.536(4)	C3B1	C3G1	1.532(3)
C1G3	C1D1	1.530(4)	C3B1	C3G2	1.531(3)
C1G4	C1D2	1.525(4)	C3B2	C3G3	1.534(3)
C1D1	C1E	1.531(3)	C3B2	C3G4	1.539(3)
C1D2	C1E	1.525(4)	C3G1	C3D1	1.529(4)
C1	O1	1.223(3)	C3G2	C3D2	1.530(4)
C1	N2	1.361(3)	C3G3	C3D1	1.535(4)
N2	C2A	1.469(3)	C3G4	C3D2	1.524(4)
C2A	C2B1	1.551(3)	C3D1	C3E	1.527(4)
C2A	C2B2	1.557(3)	C3D2	C3E	1.522(4)
C2A	C2	1.545(3)	C3	O3	1.233(3)
C2B1	C2G1	1.533(3)	C3	NT	1.335(3)
C2B1	C2G2	1.537(3)	NT	CT1	1.466(3)
C2B2	C2G3	1.534(3)	CT1	CT2	1.511(4)
C2B2	C2G4	1.535(3)	CT1	CT3	1.504(4)
C2G1	C2D1	1.530(3)			

Table 5 Bond Angles for lub118.

Atom	Atom	Atom	Angle/°	Atom	Atom	Atom	Angle/°
O0	C0	N1	126.4(2)	C2B2	C2G3	C2D1	110.52(19)
C0	N1	C1A	123.6(2)	C2D2	C2G4	C2B2	109.94(19)
N1	C1A	C1B1	109.32(18)	C2G1	C2D1	C2G3	108.8(2)
N1	C1A	C1B2	109.69(19)	C2E	C2D1	C2G1	109.0(2)
N1	C1A	C1	106.55(17)	C2E	C2D1	C2G3	110.1(2)
C1B2	C1A	C1B1	107.91(19)	C2G4	C2D2	C2G2	109.6(2)
C1	C1A	C1B1	109.12(19)	C2E	C2D2	C2G2	109.5(2)
C1	C1A	C1B2	114.18(18)	C2E	C2D2	C2G4	109.4(2)
C1G1	C1B1	C1A	110.8(2)	C2D2	C2E	C2D1	109.4(2)
C1G1	C1B1	C1G2	108.65(19)	O2	C2	C2A	122.1(2)
C1G2	C1B1	C1A	109.03(19)	O2	C2	N3	121.4(2)
C1G3	C1B2	C1A	108.22(19)	N3	C2	C2A	116.23(19)
C1G3	C1B2	C1G4	108.27(19)	C2	N3	C3A	123.08(18)
C1G4	C1B2	C1A	111.8(2)	N3	C3A	C3B1	107.80(18)
C1D1	C1G1	C1B1	109.5(2)	N3	C3A	C3B2	112.1(2)
C1D2	C1G2	C1B1	110.2(2)	N3	C3A	C3	107.80(18)
C1D1	C1G3	C1B2	110.4(2)	C3B2	C3A	C3B1	107.23(19)
C1D2	C1G4	C1B2	109.6(2)	C3B2	C3A	C3	112.10(19)
C1G1	C1D1	C1G3	109.9(2)	C3	C3A	C3B1	109.7(2)
C1G1	C1D1	C1E	109.1(2)	C3G1	C3B1	C3A	110.5(2)
C1G3	C1D1	C1E	109.5(2)	C3G2	C3B1	C3A	109.21(19)

C1G4	C1D2	C1G2	108.5(2)	C3G2	C3B1	C3G1	108.6(2)
C1G4	C1D2	C1E	109.7(2)	C3G3	C3B2	C3A	109.6(2)
C1E	C1D2	C1G2	110.2(2)	C3G3	C3B2	C3G4	108.1(2)
C1D2	C1E	C1D1	109.2(2)	C3G4	C3B2	C3A	110.7(2)
O1	C1	C1A	124.4(2)	C3D1	C3G1	C3B1	110.2(2)
O1	C1	N2	121.5(2)	C3D2	C3G2	C3B1	110.3(2)
N2	C1	C1A	114.07(19)	C3B2	C3G3	C3D1	110.2(2)
C1	N2	C2A	121.85(18)	C3D2	C3G4	C3B2	110.2(2)
N2	C2A	C2B1	108.72(17)	C3G1	C3D1	C3G3	108.1(2)
N2	C2A	C2B2	110.67(18)	C3E	C3D1	C3G1	109.1(2)
N2	C2A	C2	107.72(19)	C3E	C3D1	C3G3	110.8(2)
C2B1	C2A	C2B2	107.56(19)	C3G4	C3D2	C3G2	108.9(2)
C2	C2A	C2B1	108.99(18)	C3E	C3D2	C3G2	109.6(2)
C2	C2A	C2B2	113.11(18)	C3E	C3D2	C3G4	109.8(2)
C2G1	C2B1	C2A	110.78(18)	C3D2	C3E	C3D1	109.2(2)
C2G1	C2B1	C2G2	108.8(2)	O3	C3	C3A	122.9(2)
C2G2	C2B1	C2A	109.01(18)	O3	C3	NT	122.2(2)
C2G3	C2B2	C2A	108.61(18)	NT	C3	C3A	114.9(2)
C2G3	C2B2	C2G4	107.2(2)	C3	NT	CT1	122.6(2)
C2G4	C2B2	C2A	112.21(19)	NT	CT1	CT2	109.0(2)
C2D1	C2G1	C2B1	109.73(19)	NT	CT1	CT3	110.4(2)
C2D2	C2G2	C2B1	110.27(19)	CT3	CT1	CT2	112.7(3)

Table 6 Hydrogen Bonds for lub118.

D	H	A	d(D-H)/Å	d(H-A)/Å	d(D-A)/Å	D-H-A/°
N1	H1	O2[1]	0.88	1.98	2.745(2)	143.8
N1	H1	O3[1]	0.88	2.61	3.181(3)	123.1
N3	H3	O0	0.88	2.61	3.117(3)	117.4
NT	HT	O0	0.88	2.22	3.095(3)	177.6

[1]+X,1/2-Y,1/2+Z

Table 7 Torsion Angles for lub118.

A	B	C	D	Angle/°	A	B	C	D	Angle/°
C0	N1	C1A	C1B1	-170.2(2)	C2B2	C2A	C2B1	C2G1	60.3(2)
C0	N1	C1A	C1B2	71.7(3)	C2B2	C2A	C2B1	C2G2	-59.4(2)
C0	N1	C1A	C1	-52.4(3)	C2B2	C2A	C2	O2	16.2(3)
O0	C0	N1	C1A	5.2(4)	C2B2	C2A	C2	N3	-169.11(19)
N1	C1A	C1B1	C1G1	-58.6(2)	C2B2	C2G3	C2D1	C2G1	-60.6(2)
N1	C1A	C1B1	C1G2	-178.08(19)	C2B2	C2G3	C2D1	C2E	58.8(3)
N1	C1A	C1B2	C1G3	58.0(2)	C2B2	C2G4	C2D2	C2G2	57.3(3)
N1	C1A	C1B2	C1G4	177.16(19)	C2B2	C2G4	C2D2	C2E	-62.8(3)
N1	C1A	C1	O1	132.8(2)	C2G1	C2B1	C2G2	C2D2	-58.5(2)

N1	C1A	C1	N2	-49.0(3)	C2G1	C2D1	C2E	C2D2	61.5(3)
C1A	C1B1	C1G1	C1D1	-59.0(2)	C2G2	C2B1	C2G1	C2D1	59.7(2)
C1A	C1B1	C1G2	C1D2	62.3(3)	C2G2	C2D2	C2E	C2D1	-60.3(3)
C1A	C1B2	C1G3	C1D1	61.7(2)	C2G3	C2B2	C2G4	C2D2	61.7(2)
C1A	C1B2	C1G4	C1D2	-59.0(3)	C2G3	C2D1	C2E	C2D2	-57.8(3)
C1A	C1	N2	C2A	-169.76(19)	C2G4	C2B2	C2G3	C2D1	-59.6(2)
C1B1	C1A	C1B2	C1G3	-61.0(2)	C2G4	C2D2	C2E	C2D1	59.8(3)
C1B1	C1A	C1B2	C1G4	58.2(2)	C2	C2A	C2B1	C2G1	-176.76(19)
C1B1	C1A	C1	O1	-109.3(3)	C2	C2A	C2B1	C2G2	63.6(2)
C1B1	C1A	C1	N2	68.9(2)	C2	C2A	C2B2	C2G3	179.30(19)
C1B1	C1G1	C1D1	C1G3	57.7(3)	C2	C2A	C2B2	C2G4	-62.4(2)
C1B1	C1G1	C1D1	C1E	-62.4(3)	C2	N3	C3A	C3B1	-178.1(2)
C1B1	C1G2	C1D2	C1G4	-61.9(3)	C2	N3	C3A	C3B2	64.2(3)
C1B1	C1G2	C1D2	C1E	58.3(3)	C2	N3	C3A	C3	-59.7(3)
C1B2	C1A	C1B1	C1G1	60.7(2)	O2	C2	N3	C3A	-2.3(3)
C1B2	C1A	C1B1	C1G2	-58.8(2)	N3	C3A	C3B1	C3G1	-61.7(2)
C1B2	C1A	C1	O1	11.5(3)	N3	C3A	C3B1	C3G2	178.84(19)
C1B2	C1A	C1	N2	-170.23(19)	N3	C3A	C3B2	C3G3	58.4(3)
C1B2	C1G3	C1D1	C1G1	-60.1(3)	N3	C3A	C3B2	C3G4	177.59(18)

C1B2	C1G3	C1D1	C1E	59.7(3)	N3	C3A	C3	O3	121.5(2)
C1B2	C1G4	C1D2	C1G2	59.2(3)	N3	C3A	C3	NT	-59.6(3)
C1B2	C1G4	C1D2	C1E	-61.3(3)	C3A	C3B1	C3G1	C3D1	-60.5(3)
C1G1	C1B1	C1G2	C1D2	-58.5(3)	C3A	C3B1	C3G2	C3D2	62.0(3)
C1G1	C1D1	C1E	C1D2	61.0(3)	C3A	C3B2	C3G3	C3D1	62.3(3)
C1G2	C1B1	C1G1	C1D1	60.7(3)	C3A	C3B2	C3G4	C3D2	-59.8(3)
C1G2	C1D2	C1E	C1D1	-59.0(3)	C3A	C3	NT	CT1	-172.4(2)
C1G3	C1B2	C1G4	C1D2	60.1(3)	C3B1	C3A	C3B2	C3G3	-59.7(2)
C1G3	C1D1	C1E	C1D2	-59.3(3)	C3B1	C3A	C3B2	C3G4	59.5(2)
C1G4	C1B2	C1G3	C1D1	-59.6(3)	C3B1	C3A	C3	O3	-121.4(2)
C1G4	C1D2	C1E	C1D1	60.4(3)	C3B1	C3A	C3	NT	57.5(3)
C1	C1A	C1B1	C1G1	-174.75(18)	C3B1	C3G1	C3D1	C3G3	59.7(3)
C1	C1A	C1B1	C1G2	65.7(2)	C3B1	C3G1	C3D1	C3E	-60.8(3)
C1	C1A	C1B2	C1G3	177.53(19)	C3B1	C3G2	C3D2	C3G4	-60.4(3)
C1	C1A	C1B2	C1G4	-63.3(3)	C3B1	C3G2	C3D2	C3E	59.7(3)
C1	N2	C2A	C2B1	-177.24(19)	C3B2	C3A	C3B1	C3G1	59.2(2)
C1	N2	C2A	C2B2	64.8(3)	C3B2	C3A	C3B1	C3G2	-60.3(2)
C1	N2	C2A	C2	-59.3(3)	C3B2	C3A	C3	O3	-2.4(3)
O1	C1	N2	C2A	8.6(3)	C3B2	C3A	C3	NT	176.5(2)
N2	C2A	C2B1	C2G1	-59.6(2)	C3B2	C3G3	C3D1	C3G1	-60.8(3)

N2	C2A	C2B1	C2G2	-179.28(18)	C3B2	C3G3	C3D1	C3E	58.6(3)
N2	C2A	C2B2	C2G3	58.3(2)	C3B2	C3G4	C3D2	C3G2	58.6(3)
N2	C2A	C2B2	C2G4	176.62(18)	C3B2	C3G4	C3D2	C3E	-61.5(3)
N2	C2A	C2	O2	138.8(2)	C3G1	C3B1	C3G2	C3D2	-58.6(3)
N2	C2A	C2	N3	-46.5(2)	C3G1	C3D1	C3E	C3D2	60.7(3)
C2A	C2B1	C2G1	C2D1	-60.2(3)	C3G2	C3B1	C3G1	C3D1	59.4(3)
C2A	C2B1	C2G2	C2D2	62.4(2)	C3G2	C3D2	C3E	C3D1	-60.2(3)
C2A	C2B2	C2G3	C2D1	61.9(2)	C3G3	C3B2	C3G4	C3D2	60.3(3)
C2A	C2B2	C2G4	C2D2	-57.5(3)	C3G3	C3D1	C3E	C3D2	-58.2(3)
C2A	C2	N3	C3A	-177.04(19)	C3G4	C3B2	C3G3	C3D1	-58.5(3)
C2B1	C2A	C2B2	C2G3	-60.3(2)	C3G4	C3D2	C3E	C3D1	59.4(3)
C2B1	C2A	C2B2	C2G4	58.0(2)	C3	C3A	C3B1	C3G1	-178.82(19)
C2B1	C2A	C2	O2	-103.4(2)	C3	C3A	C3B1	C3G2	61.7(2)
C2B1	C2A	C2	N3	71.3(2)	C3	C3A	C3B2	C3G3	179.8(2)
C2B1	C2G1	C2D1	C2G3	58.7(3)	C3	C3A	C3B2	C3G4	-61.0(3)
C2B1	C2G1	C2D1	C2E	-61.4(3)	C3	NT	CT1	CT2	-153.7(2)
C2B1	C2G2	C2D2	C2G4	-60.8(2)	C3	NT	CT1	CT3	82.0(3)
C2B1	C2G2	C2D2	C2E	59.1(3)	O3	C3	NT	CT1	6.6(4)

Table 8 Hydrogen Atom Coordinates (Å×10^4) and Isotropic Displacement Parameters (Å^2×10^3) for lub118.

Atom	*x*	*y*	*z*	U(eq)
H0	3348.1	1189.62	6222.5	42
H1	2279.51	2134.03	6376.73	36
H1B1	1240.61	3523.39	5653.04	36
H1B2	878.51	906.87	4630.18	38
H1GA	1145.39	2496.19	6766.84	41
H1GB	223.92	3160.87	6496.44	41
H1GC	-450.28	3778.79	4959.86	42
H1GD	3.96	3466.88	4229.72	42
H1GE	-82.71	551.27	5519.95	43
H1GF	961.95	897.18	6136.91	43
H1GG	-259.46	1900.83	3621.17	47
H1GH	-827.4	1165.34	3997.81	47
H1D1	-272.46	1619.61	6556.81	44
H1D2	-1466.44	2650.33	4046.93	47
H1EA	-1524.64	1605.34	5158.11	49
H1EB	-1387.68	2620.72	5542.89	49
H2	2668.26	3275.32	5227.11	32
H2B1	4097.83	3925.03	4886.23	34
H2B2	1254.81	4052.42	3170.98	35

H2GA	3099.15	4603.07	5623.79	39
H2GB	3875.28	5328.81	5529.48	39
H2GC	4453.1	5261.69	4225.34	40
H2GD	4020.41	4510.25	3477.07	40
H2GE	1381.85	4650.6	4585.77	41
H2GF	1045.84	5432.14	3854.48	41
H2GG	2292.47	4655.71	2438.79	41
H2GH	1616.5	5451.19	2589.49	41
H2D1	2298.15	6005.85	5114.34	42
H2D2	3264.16	5947.24	2994.4	41
H2EA	2287.79	6612.49	3747.21	45
H2EB	3386.59	6538.01	4399.36	45
H3	3709.36	2340.16	4413.17	35
H3B1	4138.85	717.76	4347.56	40
H3B2	4265.31	2623.29	2489.9	40
H3GA	5160.82	1955.88	5056.1	47
H3GB	5782.86	1038.16	5182.42	47
H3GC	5324.44	-163.77	4009.63	43
H3GD	4421.14	-4.8	3127.28	43
H3GE	5214.02	3100.1	3946.43	50
H3GF	5892.86	2948.91	3359.34	50
H3GG	4534.83	1136.41	2015.42	46

H3GH	5494.79	1739.78	2204.67	46
H3D1	6620.17	2251.05	4762.6	51
H3D2	5895.6	268.16	2847.93	45
H3EA	6915.91	1488.3	3575.76	51
H3EB	6845.79	754.78	4287.22	51
HT	2574.22	860.31	3583.01	44
HT1	1414.37	481.01	1894.29	48
HT2A	1184.56	-85.42	3501.86	73
HT2B	379.47	-205.78	2551.86	73
HT2C	681.69	790.06	2947.34	73
HT3A	2571.96	-664.74	2106.46	111
HT3B	1547.9	-1103.85	2031.86	111
HT3C	2372.38	-998.55	2973.25	111

Experimental

Single Crystals of $C_{37}H_{54}N_4O_4$, lub118, were crystallized from Acetone. A suitable crystal of $C_{37}H_{54}N_4O_4$ lub118 was selected and mounted on a Mylar cryoloop on a Bruker Venture Metaljet diffractometer. The crystal was kept at 150 K during data collection. Using Olex2 [1], the structure was solved with the ShelXT [2] structure solution program using Intrinsic Phasing and refined with the XL [3] refinement package using Least Squares minimisation.

Crystal structure determination of lub118

Crystal Data for $C_{37}H_{54}N_4O_4$ (M =618.84 g/mol): monoclinic, space group $P2_1/c$ (no. 14), a = 14.6491(6) Å, b = 14.7140(6) Å, c = 16.1495(7) Å, β = 109.618(2)°, V = 3278.9(2) Å^3, Z = 4, T = 150 K, μ(GaKα) = 0.413 mm^{-1}, *Dcalc* = 1.254 g/cm^3, 38793 reflections measured (5.572° ≤ 2Θ ≤ 110.142°), 6204 unique (R_{int} = 0.0774, R_{sigma} = 0.0613) which were used in all calculations. The final R_1 was 0.0577 (I > 2σ(I)) and wR_2 was 0.1466 (all data).

Refinement model description

Number of restraints - 0, number of constraints - unknown.

Details:

```
1. Fixed Uiso
 At 1.2 times of:
  All C(H) groups, All C(H,H) groups, All N(H) groups
 At 1.5 times of:
  All C(H,H,H) groups
2.a Ternary CH refined with riding coordinates:
 C1B1(H1B1), C1B2(H1B2), C1D1(H1D1), C1D2(H1D2), C2B1(H2B1), C2B2(H2B2),
 C2D1(H2D1), C2D2(H2D2), C3B1(H3B1), C3B2(H3B2), C3D1(H3D1), C3D2(H3D2),
 CT1(HT1)
2.b Secondary CH2 refined with riding coordinates:
 C1G1(H1GA,H1GB), C1G2(H1GC,H1GD), C1G3(H1GE,H1GF), C1G4(H1GG,H1GH), C1E(H1EA,
 H1EB), C2G1(H2GA,H2GB), C2G2(H2GC,H2GD), C2G3(H2GE,H2GF), C2G4(H2GG,H2GH),
 C2E(H2EA,H2EB), C3G1(H3GA,H3GB), C3G2(H3GC,H3GD), C3G3(H3GE,H3GF), C3G4(H3GG,
 H3GH), C3E(H3EA,H3EB)
2.c Aromatic/amide H refined with riding coordinates:
 C0(H0), N1(H1), N2(H2), N3(H3), NT(HT)
2.d Idealised Me refined as rotating group:
 CT2(HT2A,HT2B,HT2C), CT3(HT3A,HT3B,HT3C)
```

This report has been created with Olex2, compiled on 2018.05.29 svn.r3508 for OlexSys. Please let us know if there are any errors or if you would like to have additional features.

Piptide 4.2 (lub132)

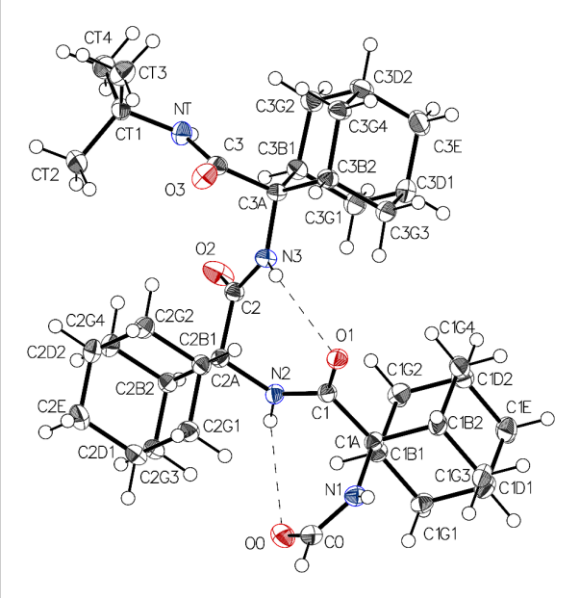

Table 1 Crystal data and structure refinement for lub132.

Identification code	lub132
Empirical formula	$C_{38}H_{56}N_4O_4$
Formula weight	632.86
Temperature/K	150
Crystal system	triclinic
Space group	P-1
a/Å	7.7427(3)
b/Å	10.1000(3)
c/Å	20.7549(7)
α/°	90.0300(10)
β/°	95.7130(10)
γ/°	90.8690(10)
Volume/Å^3	1614.81(10)
Z	2
ρ_{calc}g/cm^3	1.302
μ/mm^{-1}	0.427
F(000)	688.0
Crystal size/mm^3	0.15 × 0.12 × 0.08
Radiation	GaKα (λ = 1.34139)
2Θ range for data collection/°	3.722 to 121.502
Index ranges	-10 ≤ h ≤ 10, -13 ≤ k ≤ 13, -27 ≤ l ≤ 26
Reflections collected	42140
Independent reflections	7412 [R_{int} = 0.0354, R_{sigma} = 0.0242]
Data/restraints/parameters	7412/0/435

Goodness-of-fit on F^2	1.071
Final R indexes [I>=2σ (I)]	$R_1 = 0.0495$, $wR_2 = 0.1279$
Final R indexes [all data]	$R_1 = 0.0543$, $wR_2 = 0.1319$
Largest diff. peak/hole / e $Å^{-3}$	0.42/-0.41

Table 2 Fractional Atomic Coordinates (×10^4) and Equivalent Isotropic Displacement Parameters (Å^2×10^3) for lub132. U_{eq} is defined as 1/3 of of the trace of the orthogonalised U_{IJ} tensor.

Atom	*x*	*y*	*z*	U(eq)
C0	-193.0(18)	9282.8(13)	7545.7(7)	25.0(3)
O0	1080.2(14)	9998.9(10)	7528.8(5)	31.4(2)
N1	-560.3(14)	8160.7(11)	7202.6(5)	22.4(2)
C1A	598.3(16)	7487.4(12)	6780.6(6)	18.9(2)
C1B1	1563.3(16)	8451.9(12)	6356.7(6)	19.9(3)
C1B2	-570.3(17)	6564.6(13)	6323.0(6)	22.6(3)
C1G1	247.8(18)	9268.5(13)	5928.4(6)	23.5(3)
C1G2	2674.6(18)	7659.8(14)	5922.6(7)	25.6(3)
C1G3	-1890.0(18)	7389.9(14)	5896.2(7)	26.3(3)
C1G4	535(2)	5789.7(13)	5885.5(7)	27.8(3)
C1D1	-923.7(19)	8356.3(14)	5482.2(7)	26.6(3)
C1D2	1506(2)	6749.3(15)	5468.8(7)	28.9(3)
C1E	195(2)	7587.8(15)	5047.0(7)	30.2(3)
C1	1813.4(16)	6664.8(12)	7264.0(6)	18.5(2)
O1	1451.3(12)	5507.1(9)	7389.8(5)	22.5(2)
N2	3199.8(14)	7339.6(11)	7553.3(5)	19.2(2)
C2A	4432.7(16)	6850.1(12)	8088.5(6)	17.8(2)
C2B1	3477.9(17)	6296.8(12)	8656.7(6)	19.9(3)
C2B2	5587.7(17)	8035.9(12)	8353.6(6)	20.9(3)
C2G1	2375.2(18)	7385.8(13)	8923.8(7)	24.3(3)
C2G2	4813.7(19)	5824.4(14)	9199.7(6)	25.9(3)
C2G3	4484.4(18)	9118.2(13)	8630.4(7)	24.9(3)
C2G4	6926.5(18)	7559.3(14)	8901.2(7)	27.2(3)
C2D1	3542.4(19)	8547.9(14)	9185.9(7)	27.2(3)
C2D2	5980(2)	6985.7(15)	9456.9(7)	28.9(3)
C2E	4872(2)	8058.4(16)	9728.4(7)	32.1(3)
C2	5604.2(16)	5823.1(12)	7778.7(6)	19.6(2)
O2	7025.1(14)	6161.2(10)	7613.1(6)	36.0(3)
N3	4944.3(14)	4594.3(10)	7692.3(5)	19.8(2)
C3A	5847.9(16)	3378.4(12)	7519.6(6)	18.2(2)
C3B1	6963.0(17)	3586.7(13)	6945.6(6)	20.5(3)
C3B2	4432.7(16)	2320.7(12)	7313.9(6)	20.9(3)

C3G1	5781.7(19)	4076.6(14)	6355.6(7)	26.2(3)
C3G2	7784.1(18)	2277.6(14)	6755.1(7)	24.3(3)
C3G3	3261.9(17)	2785.0(14)	6721.0(7)	25.2(3)
C3G4	5313.2(18)	1027.3(13)	7146.7(7)	24.8(3)
C3D1	4356.5(19)	3038.5(15)	6153.6(7)	28.5(3)
C3D2	6361.9(18)	1237.9(14)	6565.1(7)	27.0(3)
C3E	5187(2)	1729.9(15)	5979.1(7)	31.4(3)
C3	6805.3(17)	2936.1(12)	8181.4(6)	20.8(3)
O3	5928.1(13)	2585.6(11)	8613.2(5)	29.0(2)
NT	8546.1(15)	2991.5(12)	8250.9(6)	23.6(2)
CT1	9668.1(17)	2728.5(14)	8860.3(6)	24.0(3)
CT2	9478(2)	3865.1(16)	9334.7(8)	33.8(3)
CT3	9206(2)	1397.9(16)	9155.2(8)	32.6(3)
CT4	11511.7(18)	2670.7(16)	8667.1(8)	30.5(3)

Table 3 Anisotropic Displacement Parameters ($Å^2×10^3$) for lub132. The Anisotropic displacement factor exponent takes the form: $-2\pi^2[h^2a^{*2}U_{11}+2hka^*b^*U_{12}+\ldots]$.

Atom	U_{11}	U_{22}	U_{33}	U_{23}	U_{13}	U_{12}
C0	25.4(6)	23.8(6)	25.7(6)	-1.1(5)	1.9(5)	5.0(5)
O0	33.1(6)	24.3(5)	36.2(6)	-5.4(4)	1.1(4)	-2.3(4)
N1	20.6(5)	22.5(5)	24.5(5)	0.1(4)	3.8(4)	1.0(4)
C1A	18.7(6)	18.3(6)	19.6(6)	1.6(4)	1.0(5)	0.5(4)
C1B1	20.1(6)	18.8(6)	20.7(6)	2.3(5)	1.0(5)	0.0(4)
C1B2	24.6(6)	19.7(6)	22.4(6)	1.6(5)	-2.7(5)	-2.7(5)
C1G1	26.4(6)	20.3(6)	23.9(6)	5.8(5)	2.3(5)	3.2(5)
C1G2	24.4(6)	31.0(7)	22.2(6)	4.0(5)	4.6(5)	6.1(5)
C1G3	23.5(6)	28.5(7)	25.3(7)	2.2(5)	-4.6(5)	-1.2(5)
C1G4	38.0(8)	20.9(6)	23.2(6)	-1.8(5)	-3.7(6)	2.3(5)
C1D1	27.4(7)	28.1(7)	23.2(6)	6.2(5)	-3.2(5)	2.7(5)
C1D2	36.2(8)	30.3(7)	20.5(6)	-1.4(5)	3.0(6)	9.2(6)
C1E	38.7(8)	32.1(7)	19.2(6)	2.1(5)	-1.3(6)	3.4(6)
C1	19.5(6)	18.9(6)	17.1(5)	0.4(4)	2.3(4)	1.6(4)
O1	24.3(5)	17.4(4)	25.1(5)	1.7(3)	-0.6(4)	0.1(3)
N2	22.3(5)	16.3(5)	18.4(5)	2.5(4)	-1.3(4)	-0.7(4)
C2A	18.9(6)	16.0(5)	17.9(6)	0.8(4)	-0.7(4)	0.4(4)
C2B1	23.2(6)	18.8(6)	17.6(6)	0.9(4)	1.6(5)	0.2(5)
C2B2	21.7(6)	16.9(6)	23.4(6)	-0.9(5)	-1.0(5)	-1.1(5)
C2G1	26.3(7)	25.4(6)	21.7(6)	-0.7(5)	4.4(5)	3.5(5)
C2G2	33.4(7)	24.1(6)	19.7(6)	3.2(5)	-1.0(5)	4.3(5)
C2G3	28.2(7)	18.0(6)	27.6(7)	-4.1(5)	-1.8(5)	1.5(5)

C2G4	23.2(6)	27.8(7)	28.7(7)	-3.0(5)	-6.3(5)	1.0(5)
C2D1	32.7(7)	23.8(6)	25.0(7)	-7.0(5)	1.8(5)	4.7(5)
C2D2	32.9(7)	31.0(7)	21.1(6)	-1.0(5)	-6.9(5)	4.5(6)
C2E	40.4(8)	33.0(7)	21.8(7)	-7.0(6)	-2.3(6)	2.0(6)
C2	21.2(6)	18.4(6)	19.3(6)	0.0(4)	1.9(5)	0.7(5)
O2	31.1(5)	26.8(5)	53.2(7)	-11.5(5)	20.2(5)	-8.0(4)
N3	18.9(5)	16.8(5)	24.2(5)	-0.7(4)	4.7(4)	0.8(4)
C3A	19.0(6)	15.7(5)	20.2(6)	0.2(4)	2.7(5)	1.3(4)
C3B1	21.0(6)	20.5(6)	20.5(6)	-0.3(5)	4.4(5)	-0.6(5)
C3B2	19.6(6)	17.8(6)	25.5(6)	-1.0(5)	3.4(5)	-0.3(5)
C3G1	31.1(7)	25.6(6)	21.9(6)	3.0(5)	3.2(5)	1.7(5)
C3G2	22.5(6)	26.2(7)	25.0(6)	-3.8(5)	5.8(5)	2.3(5)
C3G3	20.4(6)	24.9(6)	29.6(7)	-4.3(5)	-1.7(5)	1.5(5)
C3G4	24.3(6)	16.9(6)	33.4(7)	-2.5(5)	3.1(5)	0.5(5)
C3D1	29.4(7)	31.6(7)	23.2(6)	-1.8(5)	-3.4(5)	3.2(6)
C3D2	26.7(7)	22.7(6)	32.2(7)	-7.4(5)	5.3(6)	3.1(5)
C3E	31.6(7)	34.5(8)	27.7(7)	-10.6(6)	1.4(6)	-1.5(6)
C3	23.0(6)	17.3(6)	22.2(6)	-0.1(4)	2.7(5)	1.1(5)
O3	24.8(5)	37.2(6)	26.0(5)	8.2(4)	6.2(4)	1.6(4)
NT	22.0(6)	28.2(6)	20.6(5)	0.6(4)	2.1(4)	-2.3(4)
CT1	20.9(6)	28.6(7)	22.0(6)	-5.0(5)	-0.9(5)	0.9(5)
CT2	31.1(8)	38.6(8)	30.8(7)	-14.1(6)	-2.4(6)	5.5(6)
CT3	31.1(7)	35.0(8)	31.7(7)	5.7(6)	2.3(6)	4.0(6)
CT4	21.6(7)	35.1(8)	34.8(8)	-7.5(6)	2.3(6)	0.4(5)

Table 4 Bond Lengths for lub132.

Atom	Atom	Length/Å	Atom	Atom	Length/Å
C0	O0	1.2171(18)	C2G2	C2D2	1.532(2)
C0	N1	1.3496(18)	C2G3	C2D1	1.532(2)
N1	C1A	1.4861(16)	C2G4	C2D2	1.536(2)
C1A	C1B1	1.5463(17)	C2D1	C2E	1.535(2)
C1A	C1B2	1.5466(17)	C2D2	C2E	1.534(2)
C1A	C1	1.5551(17)	C2	O2	1.2284(16)
C1B1	C1G1	1.5343(17)	C2	N3	1.3401(16)
C1B1	C1G2	1.5384(18)	N3	C3A	1.4837(15)
C1B2	C1G3	1.5394(18)	C3A	C3B1	1.5519(17)
C1B2	C1G4	1.5309(19)	C3A	C3B2	1.5475(17)
C1G1	C1D1	1.528(2)	C3A	C3	1.5633(17)
C1G2	C1D2	1.535(2)	C3B1	C3G1	1.5403(18)
C1G3	C1D1	1.5354(19)	C3B1	C3G2	1.5440(18)

C1G4	C1D2	1.537(2)	C3B2	C3G3	1.5322(18)
C1D1	C1E	1.531(2)	C3B2	C3G4	1.5380(17)
C1D2	C1E	1.538(2)	C3G1	C3D1	1.538(2)
C1	O1	1.2325(15)	C3G2	C3D2	1.5326(19)
C1	N2	1.3513(17)	C3G3	C3D1	1.537(2)
N2	C2A	1.4811(15)	C3G4	C3D2	1.534(2)
C2A	C2B1	1.5528(17)	C3D1	C3E	1.537(2)
C2A	C2B2	1.5511(17)	C3D2	C3E	1.532(2)
C2A	C2	1.5672(17)	C3	O3	1.2264(16)
C2B1	C2G1	1.5389(17)	C3	NT	1.3415(17)
C2B1	C2G2	1.5333(18)	NT	CT1	1.4879(17)
C2B2	C2G3	1.5427(18)	CT1	CT2	1.5302(19)
C2B2	C2G4	1.5423(18)	CT1	CT3	1.529(2)
C2G1	C2D1	1.536(2)	CT1	CT4	1.5226(19)

Table 5 Bond Angles for lub132.

Atom	Atom	Atom	Angle/°	Atom	Atom	Atom	Angle/°
O0	C0	N1	126.89(13)	C2G3	C2D1	C2G1	108.63(11)
C0	N1	C1A	126.38(11)	C2G3	C2D1	C2E	109.88(12)
N1	C1A	C1B1	113.51(10)	C2E	C2D1	C2G1	109.66(12)
N1	C1A	C1B2	106.75(10)	C2G2	C2D2	C2G4	109.10(11)
N1	C1A	C1	103.61(10)	C2G2	C2D2	C2E	109.68(12)
C1B1	C1A	C1B2	107.84(10)	C2E	C2D2	C2G4	109.72(12)
C1B1	C1A	C1	114.23(10)	C2D2	C2E	C2D1	109.09(11)
C1B2	C1A	C1	110.66(10)	O2	C2	C2A	120.56(11)
C1G1	C1B1	C1A	109.92(10)	O2	C2	N3	123.09(12)
C1G1	C1B1	C1G2	109.13(11)	N3	C2	C2A	116.32(11)
C1G2	C1B1	C1A	109.53(10)	C2	N3	C3A	128.16(11)
C1G3	C1B2	C1A	109.88(11)	N3	C3A	C3B1	112.99(10)
C1G4	C1B2	C1A	110.19(11)	N3	C3A	C3B2	107.21(10)
C1G4	C1B2	C1G3	108.87(11)	N3	C3A	C3	103.08(9)
C1D1	C1G1	C1B1	110.21(11)	C3B1	C3A	C3	117.42(10)
C1D2	C1G2	C1B1	109.95(11)	C3B2	C3A	C3B1	107.91(10)
C1D1	C1G3	C1B2	109.66(11)	C3B2	C3A	C3	107.68(10)
C1B2	C1G4	C1D2	110.10(11)	C3G1	C3B1	C3A	108.71(10)
C1G1	C1D1	C1G3	109.07(11)	C3G1	C3B1	C3G2	107.97(11)
C1G1	C1D1	C1E	109.08(12)	C3G2	C3B1	C3A	111.18(10)
C1E	C1D1	C1G3	110.00(12)	C3G3	C3B2	C3A	110.68(10)
C1G2	C1D2	C1G4	108.30(11)	C3G3	C3B2	C3G4	109.20(11)
C1G2	C1D2	C1E	109.50(12)	C3G4	C3B2	C3A	109.04(10)

C1G4	C1D2	C1E	109.75(12)	C3D1	C3G1	C3B1	110.36(11)
C1D1	C1E	C1D2	109.47(11)	C3D2	C3G2	C3B1	110.11(11)
O1	C1	C1A	120.99(11)	C3B2	C3G3	C3D1	109.77(11)
O1	C1	N2	123.95(12)	C3D2	C3G4	C3B2	110.29(11)
N2	C1	C1A	114.94(10)	C3G3	C3D1	C3G1	109.44(11)
C1	N2	C2A	126.02(10)	C3E	C3D1	C3G1	109.86(12)
N2	C2A	C2B1	111.78(10)	C3E	C3D1	C3G3	108.57(12)
N2	C2A	C2B2	108.01(10)	C3G2	C3D2	C3G4	107.99(11)
N2	C2A	C2	106.19(9)	C3E	C3D2	C3G2	109.50(12)
C2B1	C2A	C2	114.44(10)	C3E	C3D2	C3G4	110.45(12)
C2B2	C2A	C2B1	107.54(10)	C3D2	C3E	C3D1	109.33(11)
C2B2	C2A	C2	108.69(10)	O3	C3	C3A	118.41(11)
C2G1	C2B1	C2A	109.96(10)	O3	C3	NT	123.53(12)
C2G2	C2B1	C2A	109.55(10)	NT	C3	C3A	118.04(11)
C2G2	C2B1	C2G1	109.00(10)	C3	NT	CT1	125.57(11)
C2G3	C2B2	C2A	110.99(10)	NT	CT1	CT2	108.69(11)
C2G4	C2B2	C2A	109.66(10)	NT	CT1	CT3	111.39(11)
C2G4	C2B2	C2G3	108.26(11)	NT	CT1	CT4	105.62(11)
C2D1	C2G1	C2B1	110.21(11)	CT3	CT1	CT2	111.03(12)
C2D2	C2G2	C2B1	110.10(11)	CT4	CT1	CT2	111.20(12)
C2D1	C2G3	C2B2	109.77(11)	CT4	CT1	CT3	108.80(12)
C2D2	C2G4	C2B2	109.69(11)				

Table 6 Hydrogen Bonds for lub132.

D	H	A	d(D-H)/Å	d(H-A)/Å	d(D-A)/Å	D-H-A/°
N1	H1	O2[1]	0.95(2)	1.99(2)	2.9161(15)	164.6(17)
C1B1	H1B1	O0	1.00	2.37	2.9486(16)	116.2
C1B2	H1B2	O2[1]	1.00	2.66	3.4311(18)	134.4
N2	H2	O0	0.833(19)	2.572(18)	3.1665(15)	129.4(15)
C2B1	H2B1	O1	1.00	2.41	3.0250(15)	119.2
N3	H3	O1	0.86(2)	2.31(2)	2.8804(14)	124.5(16)

[1]-1+X,+Y,+Z

Table 7 Torsion Angles for lub132.

A	B	C	D	Angle/°	A	B	C	D	Angle/°
C0	N1	C1A	C1B1	-42.33(17)	C2B2	C2A	C2B1	C2G2	-60.77(13)
C0	N1	C1A	C1B2	161.01(12)	C2B2	C2A	C2	O2	-20.05(16)

C0	N1	C1A	C1	82.12(15)	C2B2	C2A	C2	N3	161.76(11)
O0	C0	N1	C1A	6.7(2)	C2B2	C2G3	C2D1	C2G1	-59.47(14)
N1	C1A	C1B1	C1G1	-58.16(14)	C2B2	C2G3	C2D1	C2E	60.49(14)
N1	C1A	C1B1	C1G2	-178.06(10)	C2B2	C2G4	C2D2	C2G2	59.44(14)
N1	C1A	C1B2	C1G3	62.11(13)	C2B2	C2G4	C2D2	C2E	-60.74(14)
N1	C1A	C1B2	C1G4	-177.93(10)	C2G1	C2B1	C2G2	C2D2	-59.14(14)
N1	C1A	C1	O1	92.17(13)	C2G1	C2D1	C2E	C2D2	59.71(16)
N1	C1A	C1	N2	-84.06(12)	C2G2	C2B1	C2G1	C2D1	58.78(14)
C1A	C1B1	C1G1	C1D1	-60.55(14)	C2G2	C2D2	C2E	C2D1	-60.15(15)
C1A	C1B1	C1G2	C1D2	61.63(14)	C2G3	C2B2	C2G4	C2D2	60.30(14)
C1A	C1B2	C1G3	C1D1	60.84(14)	C2G3	C2D1	C2E	C2D2	-59.62(15)
C1A	C1B2	C1G4	C1D2	-60.64(14)	C2G4	C2B2	C2G3	C2D1	-60.20(14)
C1A	C1	N2	C2A	171.96(10)	C2G4	C2D2	C2E	C2D1	59.67(16)
C1B1	C1A	C1B2	C1G3	-60.20(13)	C2	C2A	C2B1	C2G1	179.85(10)
C1B1	C1A	C1B2	C1G4	59.76(13)	C2	C2A	C2B1	C2G2	60.07(13)
C1B1	C1A	C1	O1	-143.84(12)	C2	C2A	C2B2	C2G3	176.77(10)
C1B1	C1A	C1	N2	39.93(15)	C2	C2A	C2B2	C2G4	-63.67(13)
C1B1	C1G1	C1D1	C1G3	59.56(14)	C2	N3	C3A	C3B1	-47.42(17)
C1B1	C1G1	C1D1	C1E	-60.61(14)	C2	N3	C3A	C3B2	-166.18(12)
C1B1	C1G2	C1D2	C1G4	-60.39(14)	C2	N3	C3A	C3	80.34(15)
C1B1	C1G2	C1D2	C1E	59.26(14)	O2	C2	N3	C3A	13.3(2)
C1B2	C1A	C1B1	C1G1	59.89(13)	N3	C3A	C3B1	C3G1	-57.68(13)
C1B2	C1A	C1B1	C1G2	-60.01(13)	N3	C3A	C3B1	C3G2	-176.40(10)
C1B2	C1A	C1	O1	-21.92(16)	N3	C3A	C3B2	C3G3	61.30(13)
C1B2	C1A	C1	N2	161.85(11)	N3	C3A	C3B2	C3G4	-178.56(10)
C1B2	C1G3	C1D1	C1G1	-59.56(15)	N3	C3A	C3	O3	65.25(14)
C1B2	C1G3	C1D1	C1E	60.04(14)	N3	C3A	C3	NT	-113.17(12)
C1B2	C1G4	C1D2	C1G2	59.82(14)	C3A	C3B1	C3G1	C3D1	-61.27(14)
C1B2	C1G4	C1D2	C1E	-59.67(15)	C3A	C3B1	C3G2	C3D2	58.85(14)
C1G1	C1B1	C1G2	C1D2	-58.74(14)	C3A	C3B2	C3G3	C3D1	59.64(14)
C1G1	C1D1	C1E	C1D2	60.46(15)	C3A	C3B2	C3G4	C3D2	-63.13(14)
C1G2	C1B1	C1G1	C1D1	59.58(14)	C3A	C3	NT	CT1	174.19(11)
C1G2	C1D2	C1E	C1D1	-60.03(15)	C3B1	C3A	C3B2	C3G3	-60.70(13)
C1G3	C1B2	C1G4	C1D2	59.93(14)	C3B1	C3A	C3B2	C3G4	59.44(13)
C1G3	C1D1	C1E	C1D2	-59.14(15)	C3B1	C3A	C3	O3	-169.83(12)
C1G4	C1B2	C1G3	C1D1	-59.93(14)	C3B1	C3A	C3	NT	11.74(16)

C1G4	C1D2	C1E	C1D1	58.72(15)	C3B1	C3G1	C3D1	C3G3	59.53(14)
C1	C1A	C1B1	C1G1	−176.66(10)	C3B1	C3G1	C3D1	C3E	−59.59(15)
C1	C1A	C1B1	C1G2	63.45(13)	C3B1	C3G2	C3D2	C3G4	−59.11(14)
C1	C1A	C1B2	C1G3	174.20(10)	C3B1	C3G2	C3D2	C3E	61.21(14)
C1	C1A	C1B2	C1G4	−65.84(13)	C3B2	C3A	C3B1	C3G1	60.68(13)
C1	N2	C2A	C2B1	−51.10(16)	C3B2	C3A	C3B1	C3G2	−58.05(13)
C1	N2	C2A	C2B2	−169.21(11)	C3B2	C3A	C3	O3	−47.88(15)
C1	N2	C2A	C2	74.34(14)	C3B2	C3A	C3	NT	133.69(12)
O1	C1	N2	C2A	−4.1(2)	C3B2	C3G3	C3D1	C3G1	−57.95(14)
N2	C2A	C2B1	C2G1	−59.39(13)	C3B2	C3G3	C3D1	C3E	61.96(14)
N2	C2A	C2B1	C2G2	−179.17(10)	C3B2	C3G4	C3D2	C3G2	61.99(14)
N2	C2A	C2B2	C2G3	61.96(13)	C3B2	C3G4	C3D2	C3E	−57.73(15)
N2	C2A	C2B2	C2G4	−178.48(10)	C3G1	C3B1	C3G2	C3D2	−60.33(14)
N2	C2A	C2	O2	95.94(14)	C3G1	C3D1	C3E	C3D2	58.92(15)
N2	C2A	C2	N3	−82.25(13)	C3G2	C3B1	C3G1	C3D1	59.45(14)
C2A	C2B1	C2G1	C2D1	−61.33(14)	C3G2	C3D2	C3E	C3D1	−59.72(15)
C2A	C2B1	C2G2	C2D2	61.22(14)	C3G3	C3B2	C3G4	C3D2	57.92(14)
C2A	C2B2	C2G3	C2D1	60.20(14)	C3G3	C3D1	C3E	C3D2	−60.73(15)
C2A	C2B2	C2G4	C2D2	−60.92(14)	C3G4	C3B2	C3G3	C3D1	−60.41(14)
C2A	C2	N3	C3A	−168.55(11)	C3G4	C3D2	C3E	C3D1	59.09(15)
C2B1	C2A	C2B2	C2G3	−58.84(13)	C3	C3A	C3B1	C3G1	−177.49(10)
C2B1	C2A	C2B2	C2G4	60.73(13)	C3	C3A	C3B1	C3G2	63.78(14)
C2B1	C2A	C2	O2	−140.25(13)	C3	C3A	C3B2	C3G3	171.63(10)
C2B1	C2A	C2	N3	41.56(15)	C3	C3A	C3B2	C3G4	−68.23(13)
C2B1	C2G1	C2D1	C2G3	60.56(14)	C3	NT	CT1	CT2	−70.49(17)
C2B1	C2G1	C2D1	C2E	−59.54(14)	C3	NT	CT1	CT3	52.15(17)
C2B1	C2G2	C2D2	C2G4	−59.80(15)	C3	NT	CT1	CT4	170.11(13)
C2B1	C2G2	C2D2	C2E	60.40(14)	O3	C3	NT	CT1	−4.1(2)
C2B2	C2A	C2B1	C2G1	59.01(13)					

Table 8 Hydrogen Atom Coordinates (Å×10^4) and Isotropic Displacement Parameters (Å^2×10^3) for lub132.

Atom	*x*	*y*	*z*	U(eq)
H0	−1015.2	9541.07	7830.45	30
H1	−1490(30)	7638(19)	7336(9)	35(5)

H1B1	2330.85	9060.38	6641.98	24
H1B2	-1207.12	5928.98	6586.98	27
H1GA	-468.51	9785.24	6204.48	28
H1GB	871.8	9898.46	5665.23	28
H1GC	3330.89	8276.57	5663.71	31
H1GD	3519.53	7122.32	6195.18	31
H1GE	-2656.07	6795.53	5611.65	32
H1GF	-2621.95	7890.24	6173.12	32
H1GG	-219.84	5186.4	5601.7	33
H1GH	1380.95	5246.58	6154.52	33
H1D1	-1782.57	8897.38	5208.34	32
H1D2	2231.93	6238.24	5186.27	35
H1EA	820.41	8214.07	4782.46	36
H1EB	-553.75	7005.19	4750.05	36
H2	3300(20)	8142(19)	7469(8)	26(4)
H2B1	2707.94	5536.02	8499	24
H2B2	6211.79	8418.75	7995.98	25
H2GA	1514.69	7703.06	8575.41	29
H2GB	1736.22	7019.01	9275.06	29
H2GC	4206.16	5443.26	9555.97	31
H2GD	5532.58	5124.68	9032.41	31
H2GE	5242.35	9870.64	8790.89	30
H2GF	3625.12	9449.42	8285.17	30
H2GG	7664.1	6873.1	8732.83	33
H2GH	7685.17	8310.58	9062.62	33
H2D1	2813.98	9247.9	9359.47	33
H2D2	6851.83	6665.54	9807.94	35
H2EA	5623.48	8805.82	9899.47	39
H2EB	4262.67	7691.62	10087.52	39
H3	3930(30)	4455(19)	7815(10)	37(5)
H3B1	7898	4261.09	7066.94	25
H3B2	3711.68	2156.92	7680.59	25
H3GA	5241.28	4919.11	6464.92	31
H3GB	6484.66	4244.85	5990.11	31
H3GC	8479.86	2434.59	6386.51	29
H3GD	8568.71	1948.69	7124.24	29
H3GE	2672.9	3608.8	6827.09	30
H3GF	2361.16	2100.57	6596.78	30
H3GG	6093.41	733.19	7524.78	30
H3GH	4419.93	326.88	7043.7	30
H3D1	3596.29	3368.1	5771.35	34
H3D2	6904.83	386.21	6453.84	32

H3EA	4268.51	1059.56	5853.18	38
H3EB	5876.93	1868.24	5607.44	38
HT	9000(20)	3380(19)	7949(10)	33(5)
HT2A	9796.42	4703.77	9137.25	51
HT2B	10243.95	3719.59	9732.53	51
HT2C	8271.76	3899.76	9438.09	51
HT3A	8026.56	1428.46	9286.83	49
HT3B	10027.68	1218.47	9534.28	49
HT3C	9268.48	694.14	8833.48	49
HT4A	11604.2	1921.76	8372.71	46
HT4B	12325.93	2557.37	9055.14	46
HT4C	11791.55	3495.6	8449.05	46

Experimental

Single crystals of $C_{38}H_{56}N_4O_4$ **[lub132]** were **[crystallized from Acetone/EtOAc]**. A suitable crystal was selected and **[mounted on a cryoloop]** on a **Bruker Venture Metaljet** diffractometer. The crystal was kept at 150 K during data collection. Using Olex2 [1], the structure was solved with the XT [2] structure solution program using Intrinsic Phasing and refined with the XL [3] refinement package using Least Squares minimisation.

Crystal structure determination of [lub132]

Crystal Data for $C_{38}H_{56}N_4O_4$ (M =632.86 g/mol): triclinic, space group P-1 (no. 2), a = 7.7427(3) Å, b = 10.1000(3) Å, c = 20.7549(7) Å, α = 90.0300(10)°, β = 95.7130(10)°, γ = 90.8690(10)°, V = 1614.81(10) Å^3, Z = 2, T = 150 K, μ(GaKα) = 0.427 mm^{-1}, *Dcalc* = 1.302 g/cm^3, 42140 reflections measured (3.722° ≤ 2Θ ≤ 121.502°), 7412 unique (R_{int} = 0.0354, R_{sigma} = 0.0242) which were used in all calculations. The final R_1 was 0.0495 (I > 2σ(I)) and wR_2 was 0.1319 (all data).

Refinement model description

Number of restraints - 0, number of constraints - unknown.

Details:

```
1. Fixed Uiso
 At 1.2 times of:
  All C(H) groups, All C(H,H) groups
 At 1.5 times of:
  All C(H,H,H) groups
2.a Ternary CH refined with riding coordinates:
 C1B1(H1B1), C1B2(H1B2), C1D1(H1D1), C1D2(H1D2), C2B1(H2B1), C2B2(H2B2),
 C2D1(H2D1), C2D2(H2D2), C3B1(H3B1), C3B2(H3B2), C3D1(H3D1), C3D2(H3D2)
2.b Secondary CH2 refined with riding coordinates:
 C1G1(H1GA,H1GB), C1G2(H1GC,H1GD), C1G3(H1GE,H1GF), C1G4(H1GG,H1GH), C1E(H1EA,
 H1EB), C2G1(H2GA,H2GB), C2G2(H2GC,H2GD), C2G3(H2GE,H2GF), C2G4(H2GG,H2GH),
 C2E(H2EA,H2EB), C3G1(H3GA,H3GB), C3G2(H3GC,H3GD), C3G3(H3GE,H3GF), C3G4(H3GG,
 H3GH), C3E(H3EA,H3EB)
2.c Aromatic/amide H refined with riding coordinates:
 C0(H0)
2.d Idealised Me refined as rotating group:
 CT2(HT2A,HT2B,HT2C), CT3(HT3A,HT3B,HT3C), CT4(HT4A,HT4B,HT4C)
```

This report has been created with Olex2, compiled on 2018.05.29 svn.r3508 for OlexSys. Please let us know if there are any errors or if you would like to have additional features.

Peptide 4.2 *bis*-DMSO solvate (LUB125)

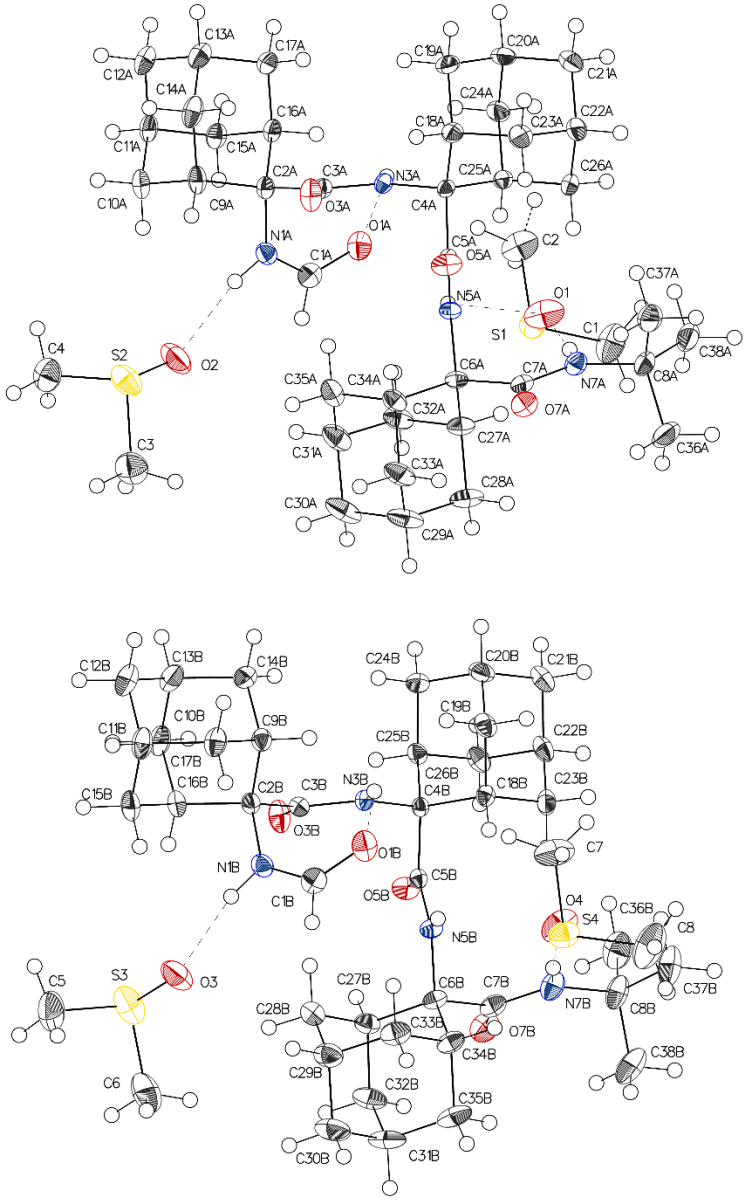

Table 1 Crystal data and structure refinement for LUB125.

Identification code	LUB125
Empirical formula	$C_{42}H_{68}N_4O_6S_2$
Formula weight	789.12
Temperature/K	150
Crystal system	orthorhombic

Space group	Pbcn
a/Å	9.8603(3)
b/Å	43.0350(14)
c/Å	38.9591(12)
α/°	90
β/°	90
γ/°	90
Volume/$Å^3$	16531.8(9)
Z	16
$\rho_{calc}g/cm^3$	1.268
μ/mm^{-1}	1.022
F(000)	6848.0
Crystal size/mm^3	0.38 × 0.13 × 0.06
Radiation	GaKα (λ = 1.34139)
2Θ range for data collection/°	3.572 to 121.596
Index ranges	$-12 \leq h \leq 12$, $-55 \leq k \leq 55$, $-50 \leq l \leq 50$
Reflections collected	305415
Independent reflections	19053 [R_{int} = 0.0575, R_{sigma} = 0.0229]
Data/restraints/parameters	19053/0/993
Goodness-of-fit on F^2	1.110
Final R indexes [I>=2σ (I)]	R_1 = 0.0625, wR_2 = 0.1585
Final R indexes [all data]	R_1 = 0.0715, wR_2 = 0.1645
Largest diff. peak/hole / e $Å^{-3}$	0.81/-0.79

Table 2 Fractional Atomic Coordinates (×10^4) and Equivalent Isotropic Displacement Parameters (Å^2×10^3) for LUB125. U_{eq} is defined as 1/3 of of the trace of the orthogonalised U_{IJ} tensor.

Atom	*x*	*y*	*z*	U(eq)
O1B	5207.6(15)	4791.9(4)	5924.4(4)	30.3(3)
O3B	689.4(14)	4704.6(4)	5992.5(4)	27.4(3)
O5B	517.6(14)	5352.7(3)	6382.7(4)	22.9(3)
O7B	718.3(15)	6104.3(4)	6333.5(4)	30.5(3)
N1B	3512.5(17)	4678.6(4)	5539.4(4)	21.4(3)
N3B	2706.2(16)	4763.7(3)	6261.5(4)	15.1(3)
N5B	2655.0(16)	5454.7(3)	6207.9(4)	16.9(3)
N7B	2735.5(18)	6016.4(4)	6596.0(5)	26.7(4)
C1B	4651(2)	4815.6(5)	5639.1(5)	25.9(4)
C2B	2668.6(19)	4455.0(4)	5734.1(5)	17.3(4)
C3B	1905.2(19)	4651.6(4)	6010.2(5)	17.0(3)
C4B	2258.5(18)	4975.8(4)	6537.7(4)	14.0(3)
C5B	1712.8(18)	5280.0(4)	6370.2(4)	15.0(3)
C6B	2342.0(19)	5758.2(4)	6049.0(5)	18.7(4)
C7B	1830(2)	5978.3(4)	6341.1(5)	23.2(4)
C8B	2585(2)	6233.3(5)	6888.1(6)	32.8(5)
C9B	3529(2)	4189.0(4)	5892.5(5)	19.6(4)
C10B	4317(2)	4019.7(5)	5608.2(5)	25.6(4)
C11B	3331(2)	3874.6(5)	5349.5(6)	29.2(5)
C12B	2413(3)	3640.2(5)	5534.6(6)	33.7(5)
C13B	1603(2)	3808.4(5)	5815.5(6)	29.2(5)

C14B	2587(2)	3955.9(5)	6073.7(5)	24.8(4)
C15B	2463(2)	4134.7(5)	5190.9(5)	27.8(4)
C16B	1668(2)	4306.4(5)	5475.4(5)	21.4(4)
C17B	743(2)	4068.5(5)	5654.5(6)	27.1(4)
C18B	3517.8(18)	5042.5(4)	6765.0(5)	16.5(3)
C19B	4052(2)	4737.1(5)	6919.1(5)	22.8(4)
C20B	2963(2)	4585.7(5)	7144.1(5)	25.2(4)
C21B	2588(2)	4807.9(5)	7436.0(5)	28.1(4)
C22B	2046(2)	5112.9(5)	7285.4(5)	23.9(4)
C23B	3123(2)	5264.5(5)	7058.3(5)	22.6(4)
C24B	1708(2)	4521.2(5)	6923.7(5)	23.6(4)
C25B	1156.2(19)	4826.3(4)	6767.3(5)	17.6(4)
C26B	787(2)	5045.6(5)	7065.1(5)	22.9(4)
C27B	1297(2)	5721.1(5)	5757.3(5)	23.3(4)
C28B	1855(2)	5493.2(5)	5487.7(5)	28.0(4)
C29B	3178(2)	5621.1(5)	5331.7(6)	30.7(5)
C30B	2911(3)	5937.7(6)	5161.5(6)	40.0(6)
C31B	2346(3)	6163.8(5)	5430.7(6)	37.6(6)
C32B	1030(2)	6033.1(5)	5577.5(6)	33.6(5)
C33B	4224(2)	5664.8(5)	5616.0(6)	27.9(4)
C34B	3675(2)	5888.6(5)	5889.8(6)	24.8(4)
C35B	3370(3)	6204.6(5)	5721.3(7)	35.3(5)
C36B	1370(3)	6143.4(7)	7109.1(7)	43.0(6)
C37B	3897(3)	6203.6(7)	7094.6(7)	44.4(6)

C38B	2435(3)	6566.8(6)	6753.8(8)	44.8(6)
O1A	4837.4(15)	3133.2(4)	6557.0(4)	27.3(3)
O3A	9292.6(14)	3251.8(4)	6425.7(4)	27.5(3)
O5A	9452.8(14)	2567.4(3)	6096.6(4)	24.7(3)
O7A	9264.6(14)	1826.9(3)	6244.5(4)	25.0(3)
N1A	6570.4(17)	3310.5(4)	6898.0(4)	20.3(3)
N3A	7269.7(15)	3166.3(3)	6165.2(4)	15.0(3)
N5A	7349.5(15)	2491.5(3)	6308.6(4)	14.9(3)
N7A	7255.1(17)	1910.3(4)	5974.7(4)	21.3(3)
C1A	5442(2)	3150.6(5)	6834.2(5)	23.3(4)
C2A	7305.6(18)	3517.3(4)	6659.0(5)	16.8(3)
C3A	8071.0(19)	3300.6(4)	6402.7(5)	16.7(3)
C4A	7709.3(18)	2931.6(4)	5911.5(4)	13.9(3)
C5A	8264.4(18)	2644.6(4)	6112.2(4)	14.9(3)
C6A	7692.5(18)	2204.1(4)	6498.1(5)	16.7(3)
C7A	8175.9(19)	1960.1(4)	6227.0(5)	18.7(4)
C8A	7423(2)	1687.9(5)	5689.2(5)	26.1(4)
C9A	8331(2)	3709.0(5)	6873.7(5)	22.1(4)
C10A	7570(2)	3905.5(5)	7144.2(5)	25.0(4)
C11A	6594(2)	4132.4(5)	6965.2(5)	23.8(4)
C12A	7393(2)	4351.8(5)	6729.1(6)	27.9(4)
C13A	8167(2)	4160.0(5)	6461.9(6)	26.4(4)
C14A	9124(2)	3931.5(5)	6640.5(6)	27.3(4)
C15A	5578(2)	3942.8(4)	6752.1(5)	21.4(4)

C16A	6333.7(19)	3751.4(4)	6478.2(5)	17.9(4)
C17A	7158(2)	3971.6(4)	6246.9(5)	22.2(4)
C18A	8800(2)	3061.6(4)	5661.7(5)	19.9(4)
C19A	8238(2)	3351.8(5)	5478.0(5)	26.0(4)
C20A	6970(2)	3269.1(5)	5270.3(5)	26.9(4)
C21A	7315(3)	3022.1(5)	4999.5(5)	30.6(5)
C22A	7873(2)	2731.6(5)	5179.4(5)	26.7(4)
C23A	9148(2)	2818.2(5)	5384.2(5)	25.7(4)
C24A	5887(2)	3137.9(5)	5512.4(5)	22.7(4)
C25A	6433.1(19)	2848.0(4)	5696.2(5)	16.6(3)
C26A	6810(2)	2602.7(4)	5427.4(5)	22.5(4)
C27A	6385(2)	2085.9(5)	6679.8(5)	22.4(4)
C28A	6712(2)	1787.8(5)	6880.7(6)	32.2(5)
C29A	7761(3)	1855.5(6)	7159.6(6)	36.4(6)
C30A	7216(3)	2104.5(6)	7405.3(6)	39.4(6)
C31A	6933(2)	2404.0(6)	7203.0(5)	31.7(5)
C32A	5855(2)	2332.7(5)	6929.4(5)	26.3(4)
C33A	9061(2)	1971.0(6)	6989.9(6)	31.3(5)
C34A	8773(2)	2267.6(5)	6779.0(5)	21.7(4)
C35A	8225(2)	2517.5(5)	7026.7(5)	28.3(4)
C36A	7572(3)	1355.9(5)	5829.9(7)	36.2(5)
C37A	8666(3)	1777.1(5)	5472.2(6)	32.8(5)
C38A	6129(3)	1712.8(5)	5472.6(6)	35.9(5)
S1	3172.7(6)	2384.0(2)	6178.1(2)	25.73(19)

S1B	3134(9)	2310(2)	5883(2)	61(3)
O1	4581.5(16)	2320.7(4)	6038.6(5)	41.9(4)
C1	2099(3)	2126.6(7)	5952.1(8)	44.2(6)
C2	2643(2)	2737.7(6)	5984.5(8)	41.3(6)
S2	8389.5(6)	3198.3(2)	7818.7(2)	37.02(15)
O2	7155(2)	3182.5(5)	7590.1(4)	44.7(5)
C3	8296(3)	2865.6(7)	8090.2(7)	44.6(6)
C4	8016(2)	3481.9(6)	8136.2(7)	37.9(5)
S3	1691.5(6)	4949.7(2)	4682.3(2)	45.45(18)
O3	2994.0(19)	4891.6(5)	4876.7(4)	42.1(4)
C5	1876(3)	4740.3(8)	4291.2(8)	52.2(7)
C6	1825(3)	5327.8(7)	4500.8(7)	48.2(7)
S4	6822.8(6)	5607.2(2)	6455.3(2)	32.59(14)
O4	5395.9(17)	5645.1(4)	6578.1(5)	42.8(4)
C7	7345(2)	5230.1(6)	6599.9(8)	41.7(6)
C8	7880(3)	5830.5(8)	6726.9(10)	61.6(9)

Table 3 Anisotropic Displacement Parameters ($Å^2×10^3$) for LUB125. The Anisotropic displacement factor exponent takes the form: $-2\pi^2[h^2a^{*2}U_{11}+2hka^*b^*U_{12}+\ldots]$.

Atom	U_{11}	U_{22}	U_{33}	U_{23}	U_{13}	U_{12}
O1B	21.4(7)	42.1(9)	27.5(8)	-4.0(7)	3.6(6)	-7.3(6)
O3B	17.8(7)	38.6(8)	25.8(7)	-11.1(6)	-3.9(6)	6.4(6)
O5B	15.1(6)	25.1(7)	28.3(7)	5.4(6)	1.6(5)	3.5(5)
O7B	22.8(7)	27.0(7)	41.8(9)	-4.6(7)	3.5(6)	7.4(6)
N1B	22.5(8)	25.4(8)	16.4(7)	0.3(6)	2.5(6)	-1.3(7)

N3B	14.9(7)	15.3(7)	15.0(7)	-2.6(5)	1.4(6)	1.7(6)
N5B	13.9(7)	15.5(7)	21.2(7)	2.7(6)	1.4(6)	1.7(6)
N7B	22.9(9)	22.8(8)	34.3(9)	-9.5(7)	1.9(7)	3.5(7)
C1B	24.1(10)	28.2(10)	25.2(10)	-2.1(8)	7.9(8)	-2.9(8)
C2B	18.1(9)	18.6(8)	15.0(8)	-1.9(7)	-0.1(7)	-0.7(7)
C3B	18.0(9)	17.7(8)	15.4(8)	0.8(6)	-0.1(7)	-0.1(7)
C4B	14.3(8)	15.1(8)	12.5(7)	-1.5(6)	0.6(6)	-0.4(6)
C5B	15.9(8)	15.8(8)	13.3(8)	-1.9(6)	-0.3(6)	0.5(6)
C6B	17.3(9)	14.0(8)	24.7(9)	2.3(7)	2.6(7)	0.7(7)
C7B	22.6(10)	16.7(9)	30.4(10)	-0.4(8)	5.9(8)	0.9(7)
C8B	29.5(11)	29.6(11)	39.2(12)	-17.5(10)	2.3(10)	1.0(9)
C9B	20.1(9)	18.9(9)	19.8(9)	-3.0(7)	-2.1(7)	2.4(7)
C10B	21.6(10)	26.4(10)	28.9(10)	-9.7(8)	0.3(8)	4.1(8)
C11B	30.2(11)	30.2(11)	27.0(10)	-14.8(9)	2.8(9)	2.1(9)
C12B	35.9(12)	26.0(10)	39.2(12)	-12.9(9)	-1.4(10)	-2.8(9)
C13B	31.8(11)	23.3(10)	32.4(11)	-5.7(8)	3.3(9)	-7.4(9)
C14B	32.9(11)	18.3(9)	23.4(9)	-0.7(7)	0.0(8)	0.0(8)
C15B	30.0(11)	34.5(11)	18.7(9)	-10.3(8)	-0.5(8)	-2.1(9)
C16B	19.3(9)	26.8(10)	18.0(9)	-5.7(7)	-3.2(7)	0.6(8)
C17B	19.5(9)	31.0(11)	30.9(11)	-9.2(9)	-0.7(8)	-4.5(8)
C18B	12.6(8)	18.3(8)	18.6(8)	-1.0(7)	-2.4(7)	-0.4(7)
C19B	20.5(9)	26.1(10)	21.7(9)	0.1(8)	-5.7(8)	6.1(8)
C20B	32.3(11)	22.5(9)	20.9(9)	6.3(8)	-2.6(8)	4.5(8)
C21B	32.2(11)	36.4(11)	15.7(9)	1.5(8)	-3.6(8)	2.8(9)

C22B	27.4(10)	29.9(10)	14.3(8)	-3.8(7)	-1.2(8)	4.7(8)
C23B	24.0(10)	22.9(9)	20.9(9)	-5.4(7)	-5.8(8)	0.1(8)
C24B	30.4(11)	20.7(9)	19.5(9)	3.6(7)	1.7(8)	-4.7(8)
C25B	16.2(8)	23.1(9)	13.5(8)	0.8(7)	1.2(7)	-3.9(7)
C26B	20.2(9)	32.2(10)	16.3(8)	-0.7(8)	3.3(7)	2.4(8)
C27B	22.2(10)	23.1(9)	24.6(10)	6.5(8)	-1.8(8)	1.7(8)
C28B	34.4(12)	27.4(10)	22.2(10)	2.6(8)	-2.9(9)	-1.7(9)
C29B	38.0(12)	28.5(11)	25.5(10)	3.5(8)	8.0(9)	3.3(9)
C30B	50.6(15)	37.4(13)	31.8(12)	15.4(10)	10.5(11)	2.1(11)
C31B	45.9(14)	25.6(11)	41.3(13)	18.2(10)	11.0(11)	6.8(10)
C32B	34.2(12)	32.3(11)	34.4(12)	14.2(9)	0.8(10)	11.1(9)
C33B	25.4(10)	25.5(10)	32.6(11)	3.7(8)	10.8(9)	0.2(8)
C34B	22.0(10)	19.5(9)	33.1(11)	2.5(8)	6.6(8)	-3.8(8)
C35B	38.9(13)	19.6(10)	47.4(14)	7.7(9)	14.0(11)	-4.6(9)
C36B	40.1(14)	46.0(14)	43.0(14)	-16.4(12)	11.0(12)	-0.4(12)
C37B	39.4(14)	45.8(15)	47.8(15)	-26.1(12)	-5.7(12)	1.3(11)
C38B	42.9(14)	26.1(11)	65.3(17)	-16.7(12)	2.5(13)	-0.6(10)
O1A	19.7(7)	32.2(8)	30.0(8)	-5.5(6)	2.9(6)	-4.1(6)
O3A	16.7(7)	34.2(8)	31.7(8)	-12.7(6)	-4.4(6)	6.3(6)
O5A	15.1(6)	25.0(7)	33.8(8)	8.7(6)	5.1(6)	4.3(5)
O7A	20.5(7)	23.2(7)	31.4(7)	0.1(6)	0.4(6)	6.8(6)
N1A	22.5(8)	21.6(8)	17.0(7)	-1.0(6)	0.2(6)	2.6(6)
N3A	14.6(7)	13.7(7)	16.6(7)	-2.0(5)	0.9(6)	1.2(5)
N5A	12.0(7)	15.1(7)	17.6(7)	3.6(6)	0.6(6)	2.7(5)

N7A	20.5(8)	17.7(7)	25.8(8)	-1.7(6)	-1.0(7)	2.3(6)
C1A	20.4(9)	23.5(9)	25.9(10)	-2.3(8)	7.6(8)	1.0(7)
C2A	15.4(8)	17.6(8)	17.5(8)	-3.9(7)	-1.2(7)	1.7(7)
C3A	16.6(8)	15.3(8)	18.2(8)	-0.6(7)	-0.1(7)	2.0(7)
C4A	15.2(8)	11.8(7)	14.6(8)	-0.8(6)	2.3(6)	0.2(6)
C5A	16.5(8)	13.3(8)	15.0(8)	-1.4(6)	0.1(7)	0.5(6)
C6A	15.3(8)	15.7(8)	19.2(8)	5.1(7)	0.4(7)	2.4(7)
C7A	20.0(9)	14.3(8)	21.8(9)	3.1(7)	2.4(7)	0.4(7)
C8A	33.9(11)	16.2(9)	28.2(10)	-4.4(8)	-3.2(9)	0.3(8)
C9A	17.1(9)	26.4(10)	22.7(9)	-9.0(8)	-5.4(7)	2.5(7)
C10A	25.0(10)	28.6(10)	21.5(9)	-11.0(8)	-3.5(8)	1.3(8)
C11A	26.6(10)	21.3(9)	23.5(9)	-10.1(8)	1.2(8)	3.7(8)
C12A	29.5(11)	20.0(9)	34.3(11)	-10.3(8)	2.4(9)	-1.4(8)
C13A	27.4(10)	20.4(9)	31.3(11)	-5.7(8)	6.3(9)	-2.9(8)
C14A	17.1(9)	28.3(10)	36.6(11)	-13.0(9)	0.4(8)	-3.8(8)
C15A	19.3(9)	20.0(9)	24.9(9)	-5.4(7)	-0.3(7)	4.2(7)
C16A	17.1(8)	16.2(8)	20.3(9)	-4.7(7)	-2.7(7)	2.0(7)
C17A	28.2(10)	16.8(8)	21.6(9)	-2.1(7)	1.1(8)	2.2(8)
C18A	22.1(9)	18.7(9)	18.8(9)	0.4(7)	6.4(7)	-2.9(7)
C19A	39.1(12)	16.5(9)	22.3(9)	3.0(7)	8.2(9)	-4.4(8)
C20A	42.4(12)	18.6(9)	19.7(9)	6.5(7)	1.5(9)	3.1(9)
C21A	47.5(14)	28.1(10)	16.2(9)	3.1(8)	1.4(9)	1.6(10)
C22A	41.9(12)	21.4(9)	16.7(9)	-3.1(7)	3.1(8)	2.2(9)
C23A	30.5(11)	25.0(10)	21.5(9)	-1.5(8)	10.7(8)	1.1(8)

C24A	26.6(10)	21.4(9)	19.9(9)	2.4(7)	-4.0(8)	4.1(8)
C25A	17.7(8)	15.3(8)	16.9(8)	1.5(6)	-1.5(7)	-0.8(7)
C26A	33.4(11)	14.8(8)	19.2(9)	-3.1(7)	-3.6(8)	-1.6(8)
C27A	19.8(9)	21.5(9)	25.9(10)	8.7(8)	5.3(8)	0.6(7)
C28A	34.1(12)	23.8(10)	38.5(12)	15.4(9)	9.3(10)	2.2(9)
C29A	39.5(13)	38.8(13)	30.8(11)	20.5(10)	5.9(10)	13.6(10)
C30A	40.4(13)	56.0(15)	21.9(10)	14.3(10)	8.1(10)	13.7(12)
C31A	34.3(12)	40.8(12)	20.1(10)	2.4(9)	5.3(9)	12.0(10)
C32A	22.1(10)	32.1(11)	24.6(10)	8.7(8)	7.5(8)	6.6(8)
C33A	30.0(11)	39.2(12)	24.6(10)	9.9(9)	-2.1(9)	14.6(9)
C34A	19.2(9)	27.3(10)	18.6(9)	2.5(7)	-2.0(7)	4.5(8)
C35A	30.4(11)	33.5(11)	21.0(9)	-3.4(8)	-3.5(8)	5.0(9)
C36A	45.9(14)	16.9(10)	45.9(13)	1.1(9)	-5.6(11)	-1.7(9)
C37A	43.6(13)	24.2(10)	30.7(11)	-5.3(9)	7.0(10)	4.5(10)
C38A	45.7(14)	23.3(10)	38.7(13)	-5.2(9)	-14.2(11)	-4.8(10)
S1	19.6(3)	31.7(3)	25.9(3)	2.9(2)	-2.4(2)	-5.5(2)
O1	16.2(7)	41.5(9)	68.0(12)	18.3(9)	-3.4(8)	-0.9(7)
C1	23.9(11)	45.6(14)	63.0(17)	-16.7(13)	5.5(11)	-9.1(10)
C2	22.9(11)	37.6(13)	63.4(17)	8.3(12)	-1.4(11)	0.4(10)
S2	27.7(3)	57.3(4)	26.1(3)	2.5(2)	4.9(2)	-2.0(3)
O2	49.4(11)	61.2(12)	23.5(8)	5.9(8)	-9.0(8)	-6.7(9)
C3	44.1(15)	44.9(15)	44.8(14)	1.5(12)	-8.4(12)	12.0(12)
C4	26.4(11)	42.1(13)	45.4(14)	-4.9(11)	-9.1(10)	-3.6(10)
S3	25.1(3)	81.5(5)	29.8(3)	1.5(3)	2.9(2)	-11.4(3)

O3	38.0(9)	60.6(12)	27.7(8)	13.2(8)	-4.4(7)	-9.3(8)
C5	45.7(16)	65.5(19)	45.5(15)	-11.6(14)	-11.5(13)	-12.8(14)
C6	36.4(14)	68.6(19)	39.6(14)	-6.6(13)	-14.6(11)	16.3(13)
S4	24.2(3)	30.9(3)	42.7(3)	5.4(2)	0.9(2)	-2.9(2)
O4	20.5(8)	33.0(9)	75.0(13)	-0.3(9)	-0.3(8)	1.4(7)
C7	22.5(11)	35.2(12)	67.3(17)	16.5(12)	4.5(11)	4.2(9)
C8	34.7(15)	64(2)	86(2)	-21.0(18)	-0.8(15)	-20.1(14)

Table 4 Bond Lengths for LUB125.

Atom	Atom	Length/Å	Atom	Atom	Length/Å
O1B	C1B	1.244(3)	N5A	C5A	1.354(2)
O3B	C3B	1.222(2)	N5A	C6A	1.479(2)
O5B	C5B	1.220(2)	N7A	C7A	1.355(3)
O7B	C7B	1.224(3)	N7A	C8A	1.477(3)
N1B	C1B	1.326(3)	C2A	C3A	1.561(2)
N1B	C2B	1.481(2)	C2A	C9A	1.550(3)
N3B	C3B	1.347(2)	C2A	C16A	1.559(2)
N3B	C4B	1.478(2)	C4A	C5A	1.561(2)
N5B	C5B	1.352(2)	C4A	C18A	1.555(2)
N5B	C6B	1.478(2)	C4A	C25A	1.555(2)
N7B	C7B	1.345(3)	C6A	C7A	1.564(3)
N7B	C8B	1.479(3)	C6A	C27A	1.556(3)
C2B	C3B	1.562(2)	C6A	C34A	1.552(3)
C2B	C9B	1.553(3)	C8A	C36A	1.538(3)

C2B	C16B	1.549(3)	C8A	C37A	1.537(3)
C4B	C5B	1.558(2)	C8A	C38A	1.533(3)
C4B	C18B	1.552(2)	C9A	C10A	1.546(3)
C4B	C25B	1.548(2)	C9A	C14A	1.534(3)
C6B	C7B	1.564(3)	C10A	C11A	1.538(3)
C6B	C27B	1.542(3)	C11A	C12A	1.536(3)
C6B	C34B	1.558(3)	C11A	C15A	1.536(3)
C8B	C36B	1.525(4)	C12A	C13A	1.532(3)
C8B	C37B	1.529(4)	C13A	C14A	1.531(3)
C8B	C38B	1.535(4)	C13A	C17A	1.533(3)
C9B	C10B	1.536(3)	C15A	C16A	1.540(3)
C9B	C14B	1.539(3)	C16A	C17A	1.540(3)
C10B	C11B	1.534(3)	C18A	C19A	1.543(3)
C11B	C12B	1.535(3)	C18A	C23A	1.544(3)
C11B	C15B	1.538(3)	C19A	C20A	1.531(3)
C12B	C13B	1.536(3)	C20A	C21A	1.536(3)
C13B	C14B	1.534(3)	C20A	C24A	1.532(3)
C13B	C17B	1.538(3)	C21A	C22A	1.535(3)
C15B	C16B	1.545(3)	C22A	C23A	1.535(3)
C16B	C17B	1.538(3)	C22A	C26A	1.530(3)
C18B	C19B	1.538(3)	C24A	C25A	1.536(2)
C18B	C23B	1.539(3)	C25A	C26A	1.533(3)
C19B	C20B	1.532(3)	C27A	C28A	1.537(3)
C20B	C21B	1.531(3)	C27A	C32A	1.532(3)

C20B	C24B	1.532(3)	C28A	C29A	1.529(4)
C21B	C22B	1.534(3)	C29A	C30A	1.534(4)
C22B	C23B	1.529(3)	C29A	C33A	1.526(3)
C22B	C26B	1.537(3)	C30A	C31A	1.536(3)
C24B	C25B	1.546(3)	C31A	C32A	1.536(3)
C25B	C26B	1.540(3)	C31A	C35A	1.528(3)
C27B	C28B	1.539(3)	C33A	C34A	1.544(3)
C27B	C32B	1.538(3)	C34A	C35A	1.543(3)
C28B	C29B	1.541(3)	S1	O1	1.5163(18)
C29B	C30B	1.538(3)	S1	C1	1.767(3)
C29B	C33B	1.525(3)	S1	C2	1.777(3)
C30B	C31B	1.535(4)	S1B	O1	1.551(9)
C31B	C32B	1.526(3)	S1B	C1	1.319(9)
C31B	C35B	1.527(4)	S1B	C2	1.943(9)
C33B	C34B	1.536(3)	S2	O2	1.5094(19)
C34B	C35B	1.540(3)	S2	C3	1.783(3)
O1A	C1A	1.235(3)	S2	C4	1.776(3)
O3A	C3A	1.226(2)	S3	O3	1.5119(19)
O5A	C5A	1.220(2)	S3	C5	1.779(3)
O7A	C7A	1.219(2)	S3	C6	1.779(3)
N1A	C1A	1.332(3)	S4	O4	1.4950(18)
N1A	C2A	1.478(2)	S4	C7	1.793(2)
N3A	C3A	1.347(2)	S4	C8	1.769(3)
N3A	C4A	1.478(2)			

Table 5 Bond Angles for LUB125.

Atom	Atom	Atom	Angle/°	Atom	Atom	Atom	Angle/°
C1B	N1B	C2B	127.91(17)	C9A	C2A	C3A	110.33(15)
C3B	N3B	C4B	125.10(15)	C9A	C2A	C16A	107.53(15)
C5B	N5B	C6B	122.95(15)	C16A	C2A	C3A	113.21(14)
C7B	N7B	C8B	125.33(18)	O3A	C3A	N3A	123.58(17)
O1B	C1B	N1B	126.78(19)	O3A	C3A	C2A	122.05(17)
N1B	C2B	C3B	105.75(14)	N3A	C3A	C2A	114.33(15)
N1B	C2B	C9B	112.07(15)	N3A	C4A	C5A	107.98(13)
N1B	C2B	C16B	107.03(15)	N3A	C4A	C18A	112.06(14)
C9B	C2B	C3B	112.89(14)	N3A	C4A	C25A	106.35(14)
C16B	C2B	C3B	111.41(15)	C18A	C4A	C5A	110.83(14)
C16B	C2B	C9B	107.59(15)	C18A	C4A	C25A	107.78(14)
O3B	C3B	N3B	123.30(17)	C25A	C4A	C5A	111.78(14)
O3B	C3B	C2B	122.34(17)	O5A	C5A	N5A	122.38(16)
N3B	C3B	C2B	114.33(16)	O5A	C5A	C4A	121.86(16)
N3B	C4B	C5B	108.48(13)	N5A	C5A	C4A	115.75(15)
N3B	C4B	C18B	106.89(14)	N5A	C6A	C7A	107.11(14)
N3B	C4B	C25B	111.93(14)	N5A	C6A	C27A	108.12(14)
C18B	C4B	C5B	111.10(14)	N5A	C6A	C34A	111.20(15)
C25B	C4B	C5B	110.41(14)	C27A	C6A	C7A	109.89(15)
C25B	C4B	C18B	108.00(14)	C34A	C6A	C7A	112.66(15)

O5B	C5B	N5B	122.64(17)	C34A	C6A	C27A	107.78(15)
O5B	C5B	C4B	122.16(16)	O7A	C7A	N7A	123.79(18)
N5B	C5B	C4B	115.19(15)	O7A	C7A	C6A	123.14(17)
N5B	C6B	C7B	107.32(15)	N7A	C7A	C6A	113.07(16)
N5B	C6B	C27B	110.89(15)	N7A	C8A	C36A	110.15(18)
N5B	C6B	C34B	107.99(15)	N7A	C8A	C37A	109.99(17)
C27B	C6B	C7B	112.55(16)	N7A	C8A	C38A	106.02(17)
C27B	C6B	C34B	107.91(16)	C37A	C8A	C36A	110.61(19)
C34B	C6B	C7B	110.10(15)	C38A	C8A	C36A	109.89(18)
O7B	C7B	N7B	123.94(19)	C38A	C8A	C37A	110.07(19)
O7B	C7B	C6B	122.67(19)	C10A	C9A	C2A	109.99(16)
N7B	C7B	C6B	113.39(17)	C14A	C9A	C2A	110.19(16)
N7B	C8B	C36B	110.67(19)	C14A	C9A	C10A	108.05(17)
N7B	C8B	C37B	105.51(18)	C11A	C10A	C9A	110.02(16)
N7B	C8B	C38B	109.7(2)	C12A	C11A	C10A	109.94(18)
C36B	C8B	C37B	110.3(2)	C12A	C11A	C15A	109.71(17)
C36B	C8B	C38B	110.7(2)	C15A	C11A	C10A	108.39(16)
C37B	C8B	C38B	109.8(2)	C13A	C12A	C11A	109.35(16)
C10B	C9B	C2B	109.84(16)	C12A	C13A	C17A	109.45(17)
C10B	C9B	C14B	109.09(16)	C14A	C13A	C12A	110.17(18)
C14B	C9B	C2B	109.46(16)	C14A	C13A	C17A	107.99(16)
C11B	C10B	C9B	110.24(17)	C13A	C14A	C9A	110.84(17)
C10B	C11B	C12B	109.44(18)	C11A	C15A	C16A	110.07(16)
C10B	C11B	C15B	108.69(17)	C15A	C16A	C2A	109.26(15)

C12B C11B C15B	109.82(19)	C17AC16A C2A	109.74(15)
C11B C12B C13B	109.36(17)	C17AC16AC15A	109.36(15)
C12B C13B C17B	109.80(19)	C13AC17AC16A	110.39(16)
C14B C13B C12B	109.48(19)	C19AC18A C4A	109.46(16)
C14B C13B C17B	108.35(17)	C19AC18AC23A	107.71(16)
C13B C14B C9B	110.52(17)	C23AC18A C4A	110.38(15)
C11B C15B C16B	109.98(17)	C20AC19AC18A	110.51(16)
C15B C16B C2B	109.95(16)	C19AC20AC21A	110.07(19)
C17B C16B C2B	110.92(16)	C19AC20AC24A	109.22(16)
C17B C16B C15B	107.92(17)	C24AC20AC21A	108.79(17)
C13B C17B C16B	110.04(17)	C20AC21AC22A	109.25(16)
C19B C18B C4B	109.83(15)	C23AC22AC21A	109.46(18)
C19B C18B C23B	109.09(15)	C26AC22AC21A	109.73(18)
C23B C18B C4B	109.64(15)	C26AC22AC23A	108.71(16)
C20B C19B C18B	110.27(16)	C22AC23AC18A	110.29(17)
C19B C20B C24B	108.84(16)	C20AC24AC25A	110.00(16)
C21B C20B C19B	109.21(18)	C24AC25A C4A	110.32(15)
C21B C20B C24B	109.52(18)	C26AC25A C4A	109.37(15)
C20B C21B C22B	109.56(16)	C26AC25AC24A	109.01(15)
C21B C22B C26B	109.49(18)	C22AC26AC25A	110.38(15)
C23B C22B C21B	110.15(17)	C28AC27A C6A	109.34(16)
C23B C22B C26B	108.56(16)	C32AC27A C6A	110.16(16)
C22B C23B C18B	109.91(16)	C32AC27AC28A	109.09(17)
C20B C24B C25B	110.56(16)	C29AC28AC27A	110.17(19)

C24B C25B C4B	109.50(15)	C28AC29AC30A	109.8(2)
C26B C25B C4B	110.27(15)	C33AC29AC28A	108.83(18)
C26B C25B C24B	107.87(15)	C33AC29AC30A	109.7(2)
C22B C26B C25B	110.23(16)	C29AC30AC31A	109.26(17)
C28B C27B C6B	109.29(16)	C32AC31AC30A	108.3(2)
C32B C27B C6B	111.10(17)	C35AC31AC30A	110.30(19)
C32B C27B C28B	107.87(17)	C35AC31AC32A	109.19(17)
C27B C28B C29B	110.14(18)	C27AC32AC31A	110.08(17)
C30B C29B C28B	109.9(2)	C29AC33AC34A	110.19(17)
C33B C29B C28B	109.26(17)	C33AC34A C6A	110.87(17)
C33B C29B C30B	108.6(2)	C35AC34A C6A	108.89(16)
C31B C30B C29B	109.24(18)	C35AC34AC33A	107.93(17)
C32B C31B C30B	109.3(2)	C31AC35AC34A	110.50(18)
C32B C31B C35B	109.08(19)	O1 S1 C1	104.94(12)
C35B C31B C30B	109.8(2)	O1 S1 C2	105.71(11)
C31B C32B C27B	110.29(18)	C1 S1 C2	98.59(14)
C29B C33B C34B	110.11(18)	O1 S1B C2	97.0(4)
C33B C34B C6B	110.36(16)	C1 S1B O1	130.5(6)
C33B C34B C35B	109.07(18)	C1 S1B C2	109.4(5)
C35B C34B C6B	108.83(17)	O2 S2 C3	105.79(13)
C31B C35B C34B	110.12(19)	O2 S2 C4	105.94(12)
C1A N1A C2A	127.12(17)	C4 S2 C3	97.34(13)
C3A N3A C4A	125.48(15)	O3 S3 C5	104.97(13)
C5A N5A C6A	122.45(15)	O3 S3 C6	106.73(12)

C7A	N7A	C8A	125.02(17)	C6	S3	C5	96.64(15)	
O1A	C1A	N1A	126.68(19)	O4	S4	C7	105.57(11)	
N1A	C2A	C3A	106.28(14)	O4	S4	C8	107.70(14)	
N1A	C2A	C9A	107.50(15)	C8	S4	C7	97.72(16)	
N1A	C2A	C16A	111.86(15)					

Table 6 Hydrogen Bonds for LUB125.

D	H	A	d(D-H)/Å	d(H-A)/Å	d(D-A)/Å	D-H-A/°
N1B	H1B	O3	0.88	1.93	2.787(2)	165.8
N3B	H3B	O1B	0.88	2.12	2.797(2)	133.4
N5B	H5B	O4	0.88	2.64	3.171(2)	119.5
N7B	H7B	O4	0.88	2.19	3.072(2)	176.6
N1A	H1A	O2	0.88	1.96	2.812(2)	162.4
N3A	H3A	O1A	0.88	2.22	2.846(2)	127.5
N5A	H5A	O1	0.88	2.45	3.016(2)	122.5
N7A	H7A	O1	0.88	2.30	3.183(2)	175.5

Table 7 Torsion Angles for LUB125.

A	B	C	D	Angle/°	A	B	C	D	Angle/°
N1B	C2B	C3B	O3B	108.3(2)	N1A	C2A	C3A	O3A	-103.1(2)
N1B	C2B	C3B	N3B	-69.87(19)	N1A	C2A	C3A	N3A	74.81(18)
N1B	C2B	C9B	C10B	-57.2(2)	N1A	C2A	C9A	C10A	-60.5(2)

N1B	C2B	C9B	C14B	-176.91(15)	N1A	C2A	C9A	C14A	-179.54(15)
N1B	C2B	C16B	C15B	60.6(2)	N1A	C2A	C16A	C15A	57.22(19)
N1B	C2B	C16B	C17B	179.88(16)	N1A	C2A	C16A	C17A	177.12(14)
N3B	C4B	C5B	O5B	112.48(19)	N3A	C4A	C5A	O5A	-114.77(19)
N3B	C4B	C5B	N5B	-66.89(19)	N3A	C4A	C5A	N5A	64.06(19)
N3B	C4B	C18B	C19B	-60.43(18)	N3A	C4A	C18A	C19A	-57.2(2)
N3B	C4B	C18B	C23B	179.72(14)	N3A	C4A	C18A	C23A	-175.57(15)
N3B	C4B	C25B	C24B	57.72(19)	N3A	C4A	C25A	C24A	60.45(18)
N3B	C4B	C25B	C26B	176.25(14)	N3A	C4A	C25A	C26A	-179.66(14)
N5B	C6B	C7B	O7B	-122.2(2)	N5A	C6A	C7A	O7A	125.23(19)
N5B	C6B	C7B	N7B	58.5(2)	N5A	C6A	C7A	N7A	-55.5(2)
N5B	C6B	C27B	C28B	-57.8(2)	N5A	C6A	C27A	C28A	-179.72(17)
N5B	C6B	C27B	C32B	-176.74(16)	N5A	C6A	C27A	C32A	-59.8(2)
N5B	C6B	C34B	C33B	60.1(2)	N5A	C6A	C34A	C33A	176.57(15)
N5B	C6B	C34B	C35B	179.77(17)	N5A	C6A	C34A	C35A	58.0(2)
C1B	N1B	C2B	C3B	74.6(2)	C1A	N1A	C2A	C3A	-75.4(2)
C1B	N1B	C2B	C9B	-48.8(3)	C1A	N1A	C2A	C9A	166.47(18)
C1B	N1B	C2B	C16B	-166.51(19)	C1A	N1A	C2A	C16A	48.6(2)
C2B	N1B	C1B	O1B	-3.1(3)	C2A	N1A	C1A	O1A	4.0(3)
C2B	C9B	C10B	C11B	-61.2(2)	C2A	C9A	C10A	C11A	-60.7(2)
C2B	C9B	C14B	C13B	61.8(2)	C2A	C9A	C14A	C13A	60.7(2)
C2B	C16B	C17B	C13B	-60.0(2)	C2A	C16A	C17A	C13A	-61.43(19)
C3B	N3B	C4B	C5B	-60.0(2)	C3A	N3A	C4A	C5A	59.8(2)
C3B	N3B	C4B	C18B	-179.87(16)	C3A	N3A	C4A	C18A	-62.5(2)

C3B	N3B	C4B	C25B	62.1(2)	C3A	N3A	C4A	C25A	179.93(16)
C3B	C2B	C9B	C10B	-176.44(15)	C3A	C2A	C9A	C10A	-176.02(16)
C3B	C2B	C9B	C14B	63.80(19)	C3A	C2A	C9A	C14A	65.0(2)
C3B	C2B	C16B	C15B	175.74(16)	C3A	C2A	C16A	C15A	177.27(15)
C3B	C2B	C16B	C17B	-65.0(2)	C3A	C2A	C16A	C17A	-62.83(19)
C4B	N3B	C3B	O3B	-3.2(3)	C4A	N3A	C3A	O3A	3.3(3)
C4B	N3B	C3B	C2B	175.00(15)	C4A	N3A	C3A	C2A	-174.54(15)
C4B	C18B	C19B	C20B	-60.8(2)	C4A	C18A	C19A	C20A	-60.5(2)
C4B	C18B	C23B	C22B	61.76(19)	C4A	C18A	C23A	C22A	59.3(2)
C4B	C25B	C26B	C22B	-59.8(2)	C4A	C25A	C26A	C22A	-62.1(2)
C5B	N5B	C6B	C7B	61.1(2)	C5A	N5A	C6A	C7A	-59.0(2)
C5B	N5B	C6B	C27B	-62.2(2)	C5A	N5A	C6A	C27A	-177.35(16)
C5B	N5B	C6B	C34B	179.80(16)	C5A	N5A	C6A	C34A	64.5(2)
C5B	C4B	C18B	C19B	-178.61(14)	C5A	C4A	C18A	C19A	-177.89(15)
C5B	C4B	C18B	C23B	61.54(19)	C5A	C4A	C18A	C23A	63.7(2)
C5B	C4B	C25B	C24B	178.67(14)	C5A	C4A	C25A	C24A	178.07(15)
C5B	C4B	C25B	C26B	-62.80(18)	C5A	C4A	C25A	C26A	-62.04(18)
C6B	N5B	C5B	O5B	3.8(3)	C6A	N5A	C5A	O5A	-5.0(3)
C6B	N5B	C5B	C4B	-176.88(15)	C6A	N5A	C5A	C4A	176.22(15)
C6B	C27B	C28B	C29B	-61.3(2)	C6A	C27A	C28A	C29A	62.2(2)
C6B	C27B	C32B	C31B	58.7(2)	C6A	C27A	C32A	C31A	-60.0(2)
C6B	C34B	C35B	C31B	-62.2(2)	C6A	C34A	C35A	C31A	61.3(2)
C7B	N7B	C8B	C36B	63.6(3)	C7A	N7A	C8A	C36A	61.0(3)
C7B	N7B	C8B	C37B	-177.1(2)	C7A	N7A	C8A	C37A	-61.2(2)

C7B	N7B	C8B	C38B	-58.9(3)	C7A	N7A	C8A	C38A	179.81(18)
C7B	C6B	C27B	C28B	-178.05(16)	C7A	C6A	C27A	C28A	63.7(2)
C7B	C6B	C27B	C32B	63.0(2)	C7A	C6A	C27A	C32A	-176.44(15)
C7B	C6B	C34B	C33B	176.99(17)	C7A	C6A	C34A	C33A	-63.2(2)
C7B	C6B	C34B	C35B	-63.4(2)	C7A	C6A	C34A	C35A	178.22(16)
C8B	N7B	C7B	O7B	-5.4(3)	C8A	N7A	C7A	O7A	0.7(3)
C8B	N7B	C7B	C6B	173.91(19)	C8A	N7A	C7A	C6A	-178.57(17)
C9B	C2B	C3B	O3B	-128.8(2)	C9A	C2A	C3A	O3A	13.2(3)
C9B	C2B	C3B	N3B	53.0(2)	C9A	C2A	C3A	N3A	-168.94(16)
C9B	C2B	C16B	C15B	-60.0(2)	C9A	C2A	C16A	C15A	-60.59(19)
C9B	C2B	C16B	C17B	59.3(2)	C9A	C2A	C16A	C17A	59.32(18)
C9B	C10B	C11B	C12B	-60.2(2)	C9A	C10A	C11A	C12A	-60.3(2)
C9B	C10B	C11B	C15B	59.8(2)	C9A	C10A	C11A	C15A	59.7(2)
C10B	C9B	C14B	C13B	-58.4(2)	C10A	C9A	C14A	C13A	-59.4(2)
C10B	C11B	C12B	C13B	60.3(2)	C10A	C11A	C12A	C13A	58.8(2)
C10B	C11B	C15B	C16B	-59.3(2)	C10A	C11A	C15A	C16A	-60.7(2)
C11B	C12B	C13B	C14B	-59.8(2)	C11A	C12A	C13A	C14A	-58.3(2)
C11B	C12B	C13B	C17B	59.0(2)	C11A	C12A	C13A	C17A	60.3(2)
C11B	C15B	C16B	C2B	60.7(2)	C11A	C15A	C16A	C2A	62.1(2)
C11B	C15B	C16B	C17B	-60.4(2)	C11A	C15A	C16A	C17A	-58.1(2)
C12B	C11B	C15B	C16B	60.4(2)	C12A	C11A	C15A	C16A	59.4(2)
C12B	C13B	C14B	C9B	59.3(2)	C12A	C13A	C14A	C9A	59.7(2)
C12B	C13B	C17B	C16B	-60.6(2)	C12A	C13A	C17A	C16A	-59.8(2)
C14B	C9B	C10B	C11B	58.7(2)	C14A	C9A	C10A	C11A	59.6(2)

C14B	C13B	C17B	C16B	58.9(2)	C14A	C13A	C17A	C16A	60.2(2)
C15B	C11B	C12B	C13B	-58.9(2)	C15A	C11A	C12A	C13A	-60.3(2)
C15B	C16B	C17B	C13B	60.5(2)	C15A	C16A	C17A	C13A	58.4(2)
C16B	C2B	C3B	O3B	-7.6(3)	C16A	C2A	C3A	O3A	133.76(19)
C16B	C2B	C3B	N3B	174.19(16)	C16A	C2A	C3A	N3A	-48.4(2)
C16B	C2B	C9B	C10B	60.2(2)	C16A	C2A	C9A	C10A	60.1(2)
C16B	C2B	C9B	C14B	-59.52(19)	C16A	C2A	C9A	C14A	-58.94(19)
C17B	C13B	C14B	C9B	-60.4(2)	C17A	C13A	C14A	C9A	-59.8(2)
C18B	C4B	C5B	O5B	-130.31(18)	C18A	C4A	C5A	O5A	8.3(2)
C18B	C4B	C5B	N5B	50.3(2)	C18A	C4A	C5A	N5A	-172.85(15)
C18B	C4B	C25B	C24B	-59.68(18)	C18A	C4A	C25A	C24A	-59.90(18)
C18B	C4B	C25B	C26B	58.86(19)	C18A	C4A	C25A	C26A	59.99(18)
C18B	C19B	C20B	C21B	-60.2(2)	C18A	C19A	C20A	C21A	-59.9(2)
C18B	C19B	C20B	C24B	59.3(2)	C18A	C19A	C20A	C24A	59.5(2)
C19B	C18B	C23B	C22B	-58.5(2)	C19A	C18A	C23A	C22A	-60.2(2)
C19B	C20B	C21B	C22B	59.7(2)	C19A	C20A	C21A	C22A	58.9(2)
C19B	C20B	C24B	C25B	-59.2(2)	C19A	C20A	C24A	C25A	-59.1(2)
C20B	C21B	C22B	C23B	-59.7(2)	C20A	C21A	C22A	C23A	-59.3(2)
C20B	C21B	C22B	C26B	59.7(2)	C20A	C21A	C22A	C26A	59.9(2)
C20B	C24B	C25B	C4B	60.4(2)	C20A	C24A	C25A	C4A	60.4(2)
C20B	C24B	C25B	C26B	-59.6(2)	C20A	C24A	C25A	C26A	-59.8(2)
C21B	C20B	C24B	C25B	60.1(2)	C21A	C20A	C24A	C25A	61.1(2)
C21B	C22B	C23B	C18B	59.2(2)	C21A	C22A	C23A	C18A	61.0(2)
C21B	C22B	C26B	C25B	-60.6(2)	C21A	C22A	C26A	C25A	-59.1(2)

C23B	C18B	C19B	C20B	59.4(2)	C23A	C18A	C19A	C20A	59.5(2)
C23B	C22B	C26B	C25B	59.7(2)	C23A	C22A	C26A	C25A	60.6(2)
C24B	C20B	C21B	C22B	-59.4(2)	C24A	C20A	C21A	C22A	-60.7(2)
C24B	C25B	C26B	C22B	59.7(2)	C24A	C25A	C26A	C22A	58.6(2)
C25B	C4B	C5B	O5B	-10.5(2)	C25A	C4A	C5A	O5A	128.59(18)
C25B	C4B	C5B	N5B	170.13(15)	C25A	C4A	C5A	N5A	-52.6(2)
C25B	C4B	C18B	C19B	60.16(18)	C25A	C4A	C18A	C19A	59.50(18)
C25B	C4B	C18B	C23B	-59.69(19)	C25A	C4A	C18A	C23A	-58.88(19)
C26B	C22B	C23B	C18B	-60.7(2)	C26A	C22A	C23A	C18A	-58.8(2)
C27B	C6B	C7B	O7B	0.1(3)	C27A	C6A	C7A	O7A	-117.5(2)
C27B	C6B	C7B	N7B	-179.27(17)	C27A	C6A	C7A	N7A	61.7(2)
C27B	C6B	C34B	C33B	-59.8(2)	C27A	C6A	C34A	C33A	58.2(2)
C27B	C6B	C34B	C35B	59.8(2)	C27A	C6A	C34A	C35A	-60.4(2)
C27B	C28B	C29B	C30B	-59.4(2)	C27A	C28A	C29A	C30A	58.9(2)
C27B	C28B	C29B	C33B	59.7(2)	C27A	C28A	C29A	C33A	-61.2(2)
C28B	C27B	C32B	C31B	-61.1(2)	C28A	C27A	C32A	C31A	60.0(2)
C28B	C29B	C30B	C31B	58.6(3)	C28A	C29A	C30A	C31A	-60.3(3)
C28B	C29B	C33B	C34B	-58.6(2)	C28A	C29A	C33A	C34A	59.0(2)
C29B	C30B	C31B	C32B	-59.6(3)	C29A	C30A	C31A	C32A	61.0(3)
C29B	C30B	C31B	C35B	60.1(3)	C29A	C30A	C31A	C35A	-58.4(3)
C29B	C33B	C34B	C6B	59.6(2)	C29A	C33A	C34A	C6A	-59.0(2)
C29B	C33B	C34B	C35B	-59.9(2)	C29A	C33A	C34A	C35A	60.2(2)
C30B	C29B	C33B	C34B	61.3(2)	C30A	C29A	C33A	C34A	-61.2(2)
C30B	C31B	C32B	C27B	61.7(3)	C30A	C31A	C32A	C27A	-61.5(2)

C30B	C31B	C35B	C34B	-58.9(2)	C30A	C31A	C35A	C34A	59.2(2)
C32B	C27B	C28B	C29B	59.6(2)	C32A	C27A	C28A	C29A	-58.4(2)
C32B	C31B	C35B	C34B	60.9(2)	C32A	C31A	C35A	C34A	-59.7(2)
C33B	C29B	C30B	C31B	-60.9(3)	C33A	C29A	C30A	C31A	59.3(3)
C33B	C34B	C35B	C31B	58.3(2)	C33A	C34A	C35A	C31A	-59.1(2)
C34B	C6B	C7B	O7B	120.5(2)	C34A	C6A	C7A	O7A	2.6(3)
C34B	C6B	C7B	N7B	-58.8(2)	C34A	C6A	C7A	N7A	-178.08(16)
C34B	C6B	C27B	C28B	60.3(2)	C34A	C6A	C27A	C28A	-59.4(2)
C34B	C6B	C27B	C32B	-58.7(2)	C34A	C6A	C27A	C32A	60.45(19)
C35B	C31B	C32B	C27B	-58.4(3)	C35A	C31A	C32A	C27A	58.7(2)

Table 8 Hydrogen Atom Coordinates (Å×10^4) and Isotropic Displacement Parameters (Å^2×10^3) for LUB125.

Atom	*x*	*y*	*z*	U(eq)
H1B	3223.24	4726.34	5332.31	26
H3B	3562.65	4706.24	6261.25	18
H5B	3492.16	5384.57	6196.46	20
H7B	3477.71	5903.07	6588.38	32
H1BA	5086.71	4945.46	5475.6	31
H9B	4181.61	4277.74	6062.66	24
H10A	4919.7	4168.6	5488.81	31
H10B	4888.59	3855.12	5711.01	31
H11B	3852.92	3766.46	5164.76	35
H12A	2972.28	3473.92	5638.49	40
H12B	1782.9	3543.4	5368.14	40

H13B	999.17	3657.06	5936.22	35
H14A	3136.57	3791.32	6183.89	30
H14B	2065.66	4064	6255.14	30
H15A	1819.92	4044.54	5022.98	33
H15B	3055.18	4283.45	5068.05	33
H16B	1098.17	4472.86	5369.28	26
H17A	206.49	4173.39	5835.22	33
H17B	105.12	3978.28	5485.52	33
H18B	4243.42	5140.43	6621.98	20
H19A	4310.59	4593.07	6732.05	27
H19B	4870.32	4779.7	7058.8	27
H20B	3315.81	4386.48	7241.48	30
H21A	3396.66	4850.3	7579	34
H21B	1887.06	4711.41	7583.55	34
H22B	1797.46	5257.72	7476.11	29
H23A	3934.9	5314.25	7197.48	27
H23B	2765.77	5460.75	6961.49	27
H24A	996.67	4423.08	7066.62	28
H24B	1947.14	4374.87	6737.15	28
H25B	329.48	4781.27	6627.13	21
H26A	423.24	5242.84	6972.14	27
H26B	75.71	4948.72	7208.91	27
H27B	428.6	5638.33	5853.18	28
H28A	1174.54	5462.72	5303.92	34

H28B	2032.13	5289.26	5596.4	34
H29B	3534.68	5471.69	5156.94	37
H30A	3764.81	6021.09	5064.75	48
H30B	2251.17	5913.05	4971.9	48
H31B	2163.51	6369.68	5320.82	45
H32A	364.35	6002.99	5390.05	40
H32B	640.58	6182.53	5743.76	40
H33A	5072.88	5749.33	5517.77	33
H33B	4432.13	5461.47	5722.63	33
H34B	4368.82	5916.54	6074.46	30
H35A	2999.77	6349.34	5895.18	42
H35B	4218.42	6295.01	5629.39	42
H36A	540.47	6154.65	6971.1	65
H36B	1298.63	6286.72	7303.71	65
H36C	1490.07	5930.93	7194.48	65
H37A	3984.51	5990.76	7181.16	67
H37B	3875.41	6348.89	7288.29	67
H37C	4672.87	6252.29	6946.81	67
H38A	3222.44	6619.79	6611.9	67
H38B	2378.89	6710.84	6948.11	67
H38C	1607.54	6582.81	6615.51	67
H1A	6916.25	3290.82	7105.05	24
H3A	6412.45	3223.1	6160.74	18
H5A	6520.18	2565.72	6324.16	18

H7A	6499.2	2018.86	5981.46	26
H1AA	5062.08	3038.41	7020.91	28
H9A	8977.11	3565.13	6991.74	26
H10C	7052.35	3766.88	7299.06	30
H10D	8230.8	4023.3	7284.31	30
H11A	6095.72	4256.69	7141.7	29
H12C	6761.85	4496.13	6612.24	34
H12D	8038.82	4476.39	6866.53	34
H13A	8699.09	4301.44	6309.25	32
H14C	9793.94	4048.18	6779.12	33
H14D	9625.34	3810.35	6465.53	33
H15C	4925.81	4084.69	6639.17	26
H15D	5062.63	3801.71	6904.65	26
H16A	5662.17	3634.56	6335.51	21
H17C	7655.51	3849.02	6072.62	27
H17D	6534.93	4114.62	6125.44	27
H18A	9636.86	3117.68	5792.75	24
H19C	8009.12	3512.82	5649.97	31
H19D	8939.02	3437.71	5322.87	31
H20A	6613.4	3459.59	5154.32	32
H21C	7999.14	3104.88	4837.7	37
H21D	6490.64	2967.66	4867.39	37
H22A	8105.31	2570.22	5004.24	32
H23C	9842.99	2903.64	5226.91	31

H23D	9526.67	2629.95	5494.34	31
H24C	5065.44	3082.99	5379.54	27
H24D	5633.49	3297.36	5683.96	27
H25A	5715.53	2762.73	5851.28	20
H26C	7173.93	2415.82	5543.54	27
H26D	5989.85	2540.96	5297.8	27
H27A	5674.57	2040.3	6503.76	27
H28C	5873.12	1705.74	6987	39
H28D	7069.21	1628.05	6721.76	39
H29A	7955.56	1660.77	7290.8	44
H30C	7890.5	2146.01	7587.83	47
H30D	6370.68	2030.2	7515.07	47
H31A	6587.59	2568.21	7362.23	38
H32C	5017.83	2256.77	7041.67	32
H32D	5631.44	2524.82	6801.68	32
H33C	9428.79	1807.44	6837.3	38
H33D	9748.89	2016.57	7168.1	38
H34A	9630.39	2342.56	6669.76	26
H35C	8921.18	2565.52	7202.01	34
H35D	8030.2	2710.46	6897.41	34
H36D	8385	1343.29	5973.74	54
H36E	7652.59	1209.56	5638.26	54
H36F	6771.65	1303.19	5967.38	54
H37D	8548.45	1988.13	5382.55	49

H37E	8757.82	1631.14	5280.47	49
H37F	9482.4	1768.7	5615.15	49
H38D	5338.89	1666.46	5616.29	54
H38E	6173.11	1563.86	5282.66	54
H38F	6048.98	1923.89	5380.55	54
H1C	2231.23	2154.48	5704.73	66
H1D	1151.61	2170.66	6010.92	66
H1E	2317.52	1912	6015.39	66
H2AA	3183.71	2909.91	6076.14	62
H2AB	1682.5	2773.57	6035.01	62
H2AC	2772.39	2724.77	5735.44	62
H2BD	3297.01	2825.64	6147.2	62
H2BE	1733.19	2743.44	6085.25	62
H2BF	2652.63	2859.75	5772.08	62
H3C	7412.48	2861.31	8205.57	67
H3D	9018.66	2875.54	8262.44	67
H3E	8403.78	2676.98	7951.94	67
H4A	7937.81	3686.55	8027.72	57
H4B	8745.67	3486.21	8306.92	57
H4C	7158.03	3429.35	8249.23	57
H5C	2723.89	4801.7	4178.79	78
H5D	1109.57	4786.83	4139.66	78
H5E	1897	4516.89	4339.93	78
H6A	1783.43	5483.6	4684	72

H6B	1074.43	5361.42	4340.02	72
H6C	2689.04	5346.73	4378.48	72
H7C	7192.84	5213.14	6847.8	62
H7D	8310.75	5200.86	6550.32	62
H7E	6816.09	5070.34	6480.7	62
H8A	7674.62	6051.6	6696.62	92
H8B	8832.14	5792.22	6668.11	92
H8C	7719.99	5771.37	6966.39	92

Table 9 Atomic Occupancy for LUB125.

Atom	*Occupancy*	Atom	*Occupancy*	Atom	*Occupancy*
S1	0.894(2)	S1B	0.106(2)	H2AA	0.894(2)
H2AB	0.894(2)	H2AC	0.894(2)	H2BD	0.106(2)
H2BE	0.106(2)	H2BF	0.106(2)		

Experimental

Single crystals of $C_{42}H_{68}N_4O_6S_2$ LUB125 were crystallized in DMSO. A suitable crystal was selected and mounted on a Mylar Cryoloop on a Bruker Venture Metaljet diffractometer. The crystal was kept at 150 K during data collection. Using Olex2 [1], the structure was solved with the XT [2] structure solution program using Intrinsic Phasing and refined with the XL [3] refinement package using Least Squares minimisation.

Crystal structure determination of LUB125

Crystal Data for $C_{42}H_{68}N_4O_6S_2$ (M =789.12 g/mol): orthorhombic, space group Pbcn (no. 60), a = 9.8603(3) Å, b = 43.0350(14) Å, c = 38.9591(12) Å, V = 16531.8(9) Å^3, Z = 16, T = 150 K, μ(GaKα) = 1.022 mm^{-1}, *Dcalc* = 1.268 g/cm^3, 305415 reflections measured (3.572° ≤ 2Θ ≤ 121.596°), 19053 unique (R_{int} = 0.0575, R_{sigma} = 0.0229) which were used in all calculations. The final R_1 was 0.0625 (I > 2σ(I)) and wR_2 was 0.1645 (all data).

Refinement model description

Number of restraints - 0, number of constraints - unknown.

Details:

```
1. Fixed Uiso
 At 1.2 times of:
  All C(H) groups, All C(H,H) groups, All N(H) groups
 At 1.5 times of:
  All C(H,H,H) groups, All C(H,H,H,H,H,H) groups
2. Others
 Sof(S1B)=Sof(H2BD)=Sof(H2BE)=Sof(H2BF)=1-FVAR(1)
 Sof(S1)=Sof(H2AA)=Sof(H2AB)=Sof(H2AC)=FVAR(1)
3.a Ternary CH refined with riding coordinates:
 C9B(H9B), C11B(H11B), C13B(H13B), C16B(H16B), C18B(H18B), C20B(H20B),
 C22B(H22B), C25B(H25B), C27B(H27B), C29B(H29B), C31B(H31B), C34B(H34B),
 C9A(H9A), C11A(H11A), C13A(H13A), C16A(H16A), C18A(H18A), C20A(H20A),
 C22A(H22A), C25A(H25A), C27A(H27A), C29A(H29A), C31A(H31A), C34A(H34A)
3.b Secondary CH2 refined with riding coordinates:
 C10B(H10A,H10B), C12B(H12A,H12B), C14B(H14A,H14B), C15B(H15A,H15B), C17B(H17A,
 H17B), C19B(H19A,H19B), C21B(H21A,H21B), C23B(H23A,H23B), C24B(H24A,H24B),
 C26B(H26A,H26B), C28B(H28A,H28B), C30B(H30A,H30B), C32B(H32A,H32B), C33B(H33A,
 H33B), C35B(H35A,H35B), C10A(H10C,H10D), C12A(H12C,H12D), C14A(H14C,H14D),
 C15A(H15C,H15D), C17A(H17C,H17D), C19A(H19C,H19D), C21A(H21C,H21D), C23A(H23C,
 H23D), C24A(H24C,H24D), C26A(H26C,H26D), C28A(H28C,H28D), C30A(H30C,H30D),
 C32A(H32C,H32D), C33A(H33C,H33D), C35A(H35C,H35D)
3.c Aromatic/amide H refined with riding coordinates:
 N1B(H1B), N3B(H3B), N5B(H5B), N7B(H7B), C1B(H1BA), N1A(H1A), N3A(H3A),
 N5A(H5A), N7A(H7A), C1A(H1AA)
3.d Idealised Me refined as rotating group:
 C36B(H36A,H36B,H36C), C37B(H37A,H37B,H37C), C38B(H38A,H38B,H38C), C36A(H36D,
 H36E,H36F), C37A(H37D,H37E,H37F), C38A(H38D,H38E,H38F), C1(H1C,H1D,H1E),
```

```
C2(H2AA,H2AB,H2AC), C2(H2BD,H2BE,H2BF), C3(H3C,H3D,H3E), C4(H4A,H4B,H4C),
C5(H5C,H5D,H5E), C6(H6A,H6B,H6C), C7(H7C,H7D,H7E), C8(H8A,H8B,H8C)
```

This report has been created with Olex2, compiled on 2018.05.29 svn.r3508 for OlexSys. Please let us know if there are any errors or if you would like to have additional features.

NMR Spectra

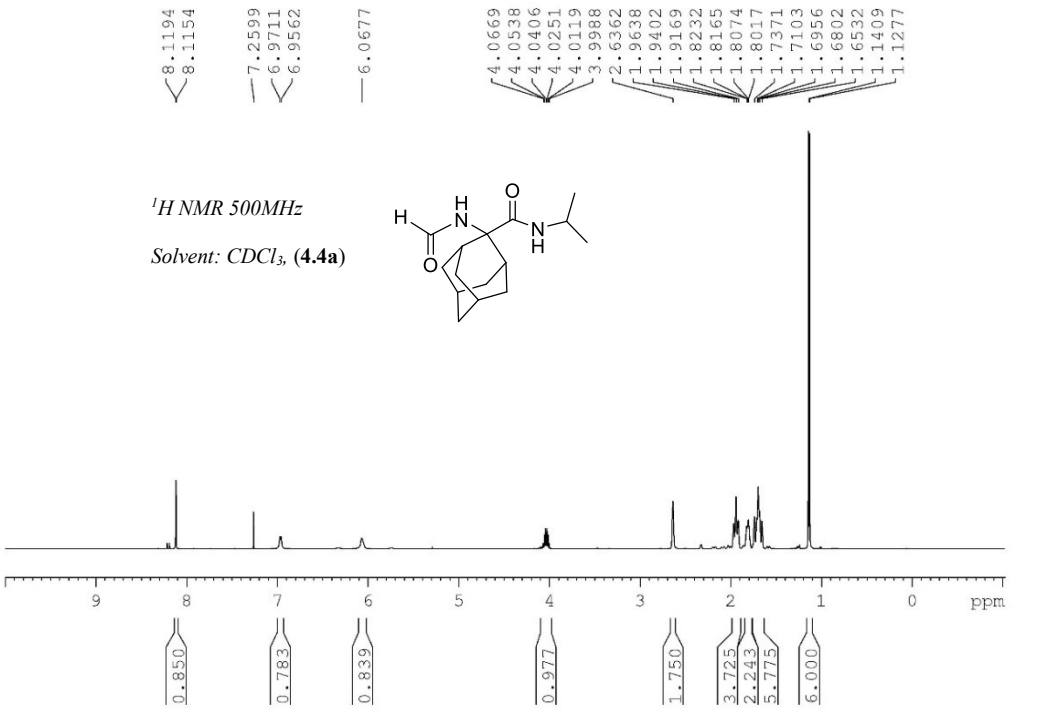

[1]H NMR 500MHz

Solvent: $CDCl_3$, (**4.4a**)

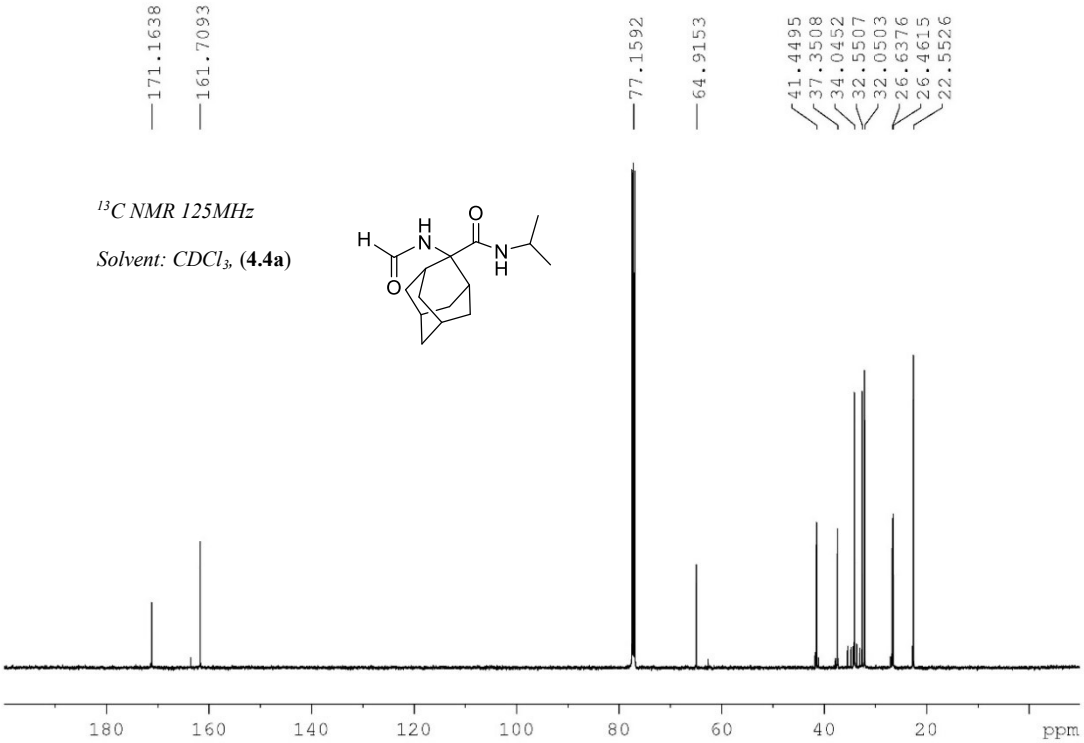

[13]C NMR 125MHz

Solvent: $CDCl_3$, (**4.4a**)

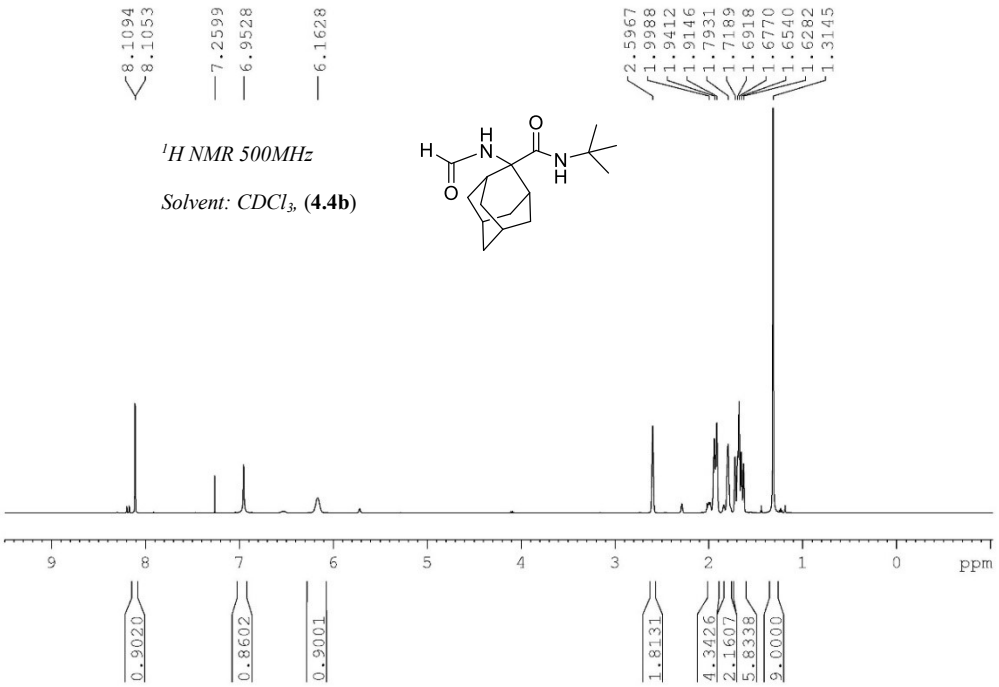

^{1}H NMR 500MHz

Solvent: $CDCl_3$, (**4.4b**)

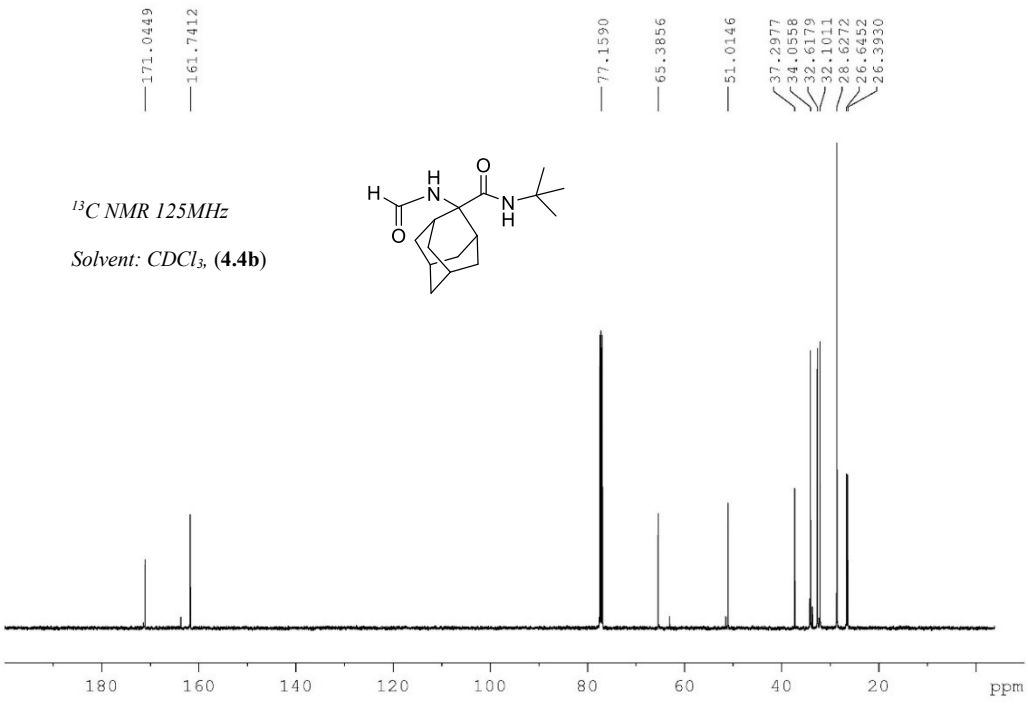

^{13}C NMR 125MHz

Solvent: $CDCl_3$, (**4.4b**)

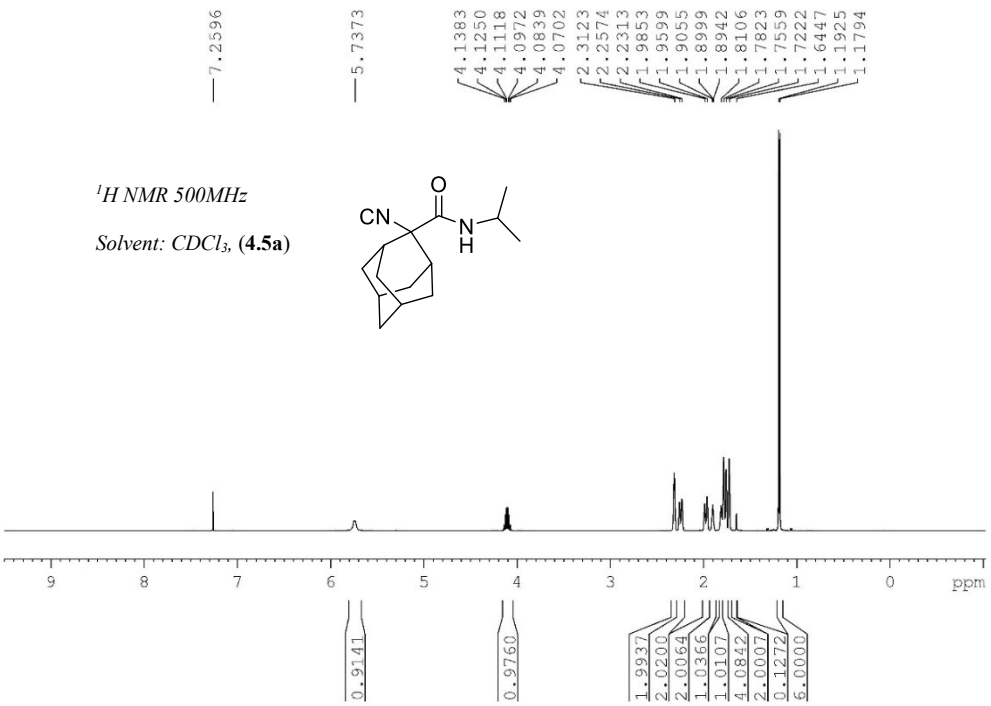

[1]H NMR 500MHz

Solvent: $CDCl_3$, (**4.5a**)

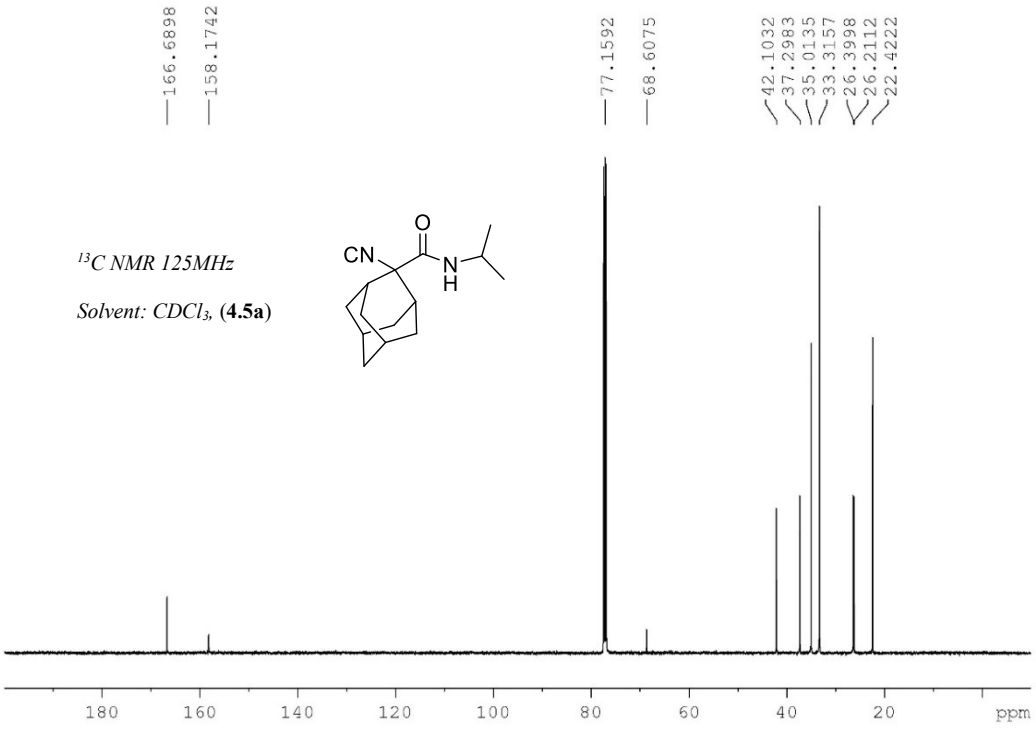

[13]C NMR 125MHz

Solvent: $CDCl_3$, (**4.5a**)

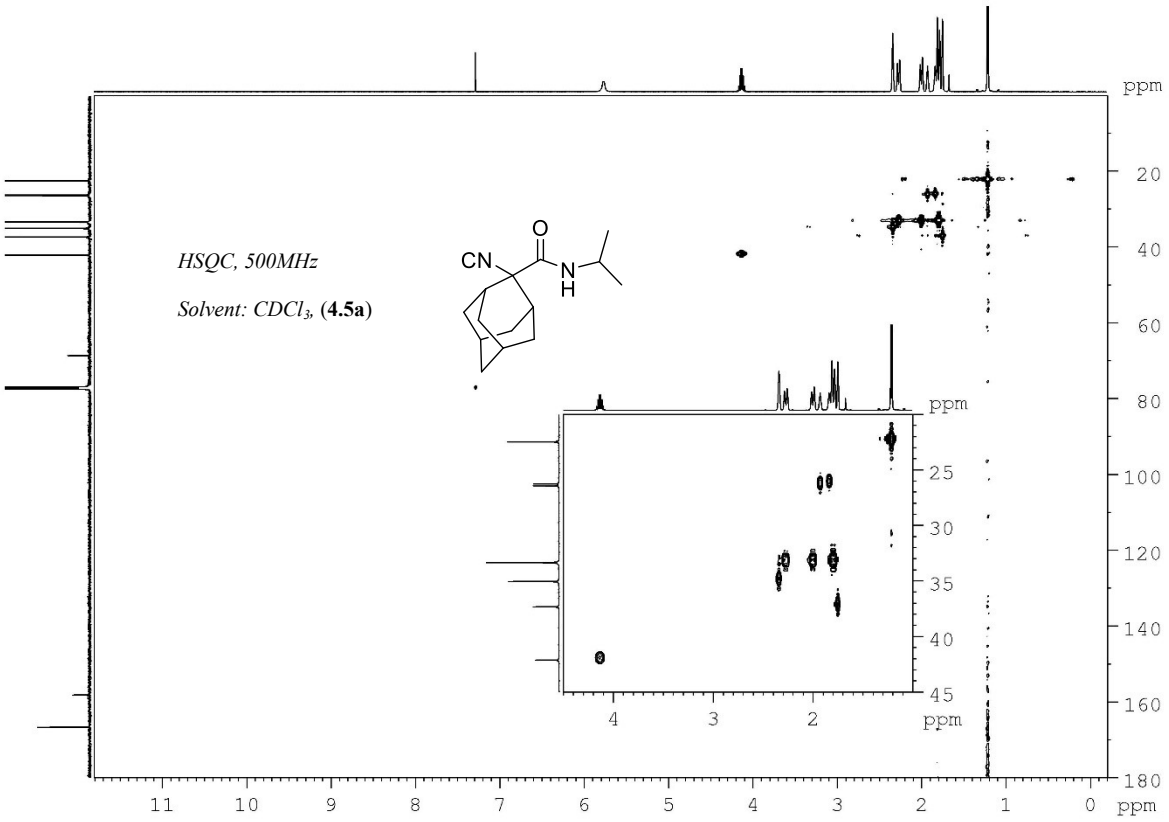
HSQC, 500MHz
Solvent: CDCl3, (4.5a)
CN
O
N
H
ppm
11 10 9 8 7 6 5 4 3 2 1 0 ppm
20 40 60 80 100 120 140 160 180
4 3 2 ppm
25 30 35 40 45

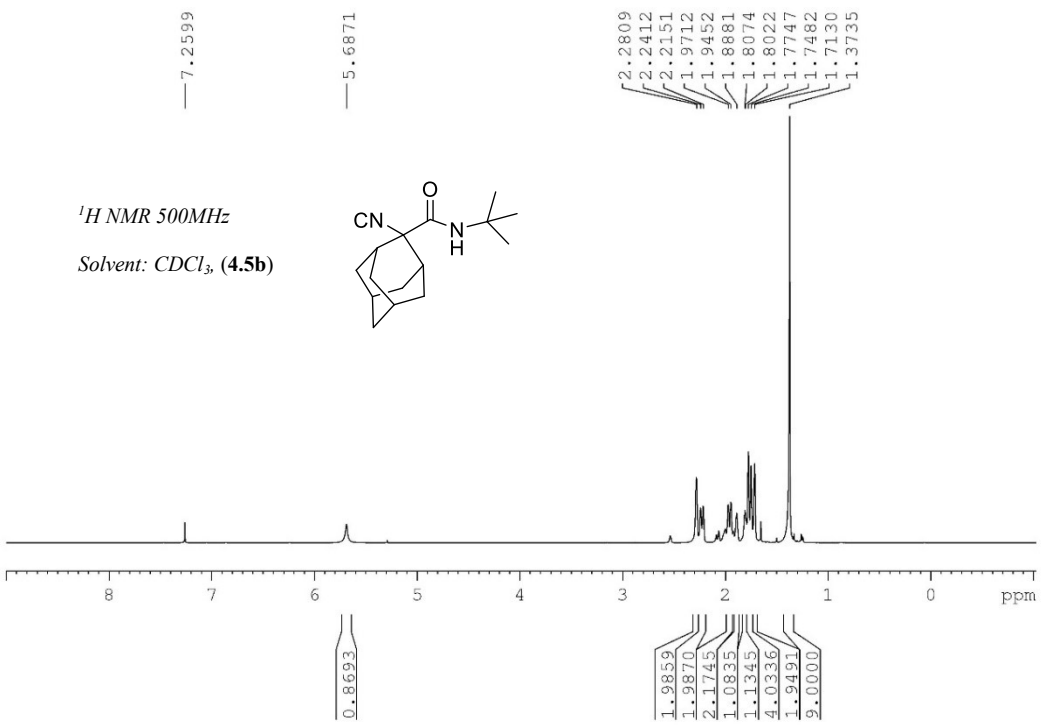

^{1}H NMR 500MHz

Solvent: $CDCl_3$, (**4.5b**)

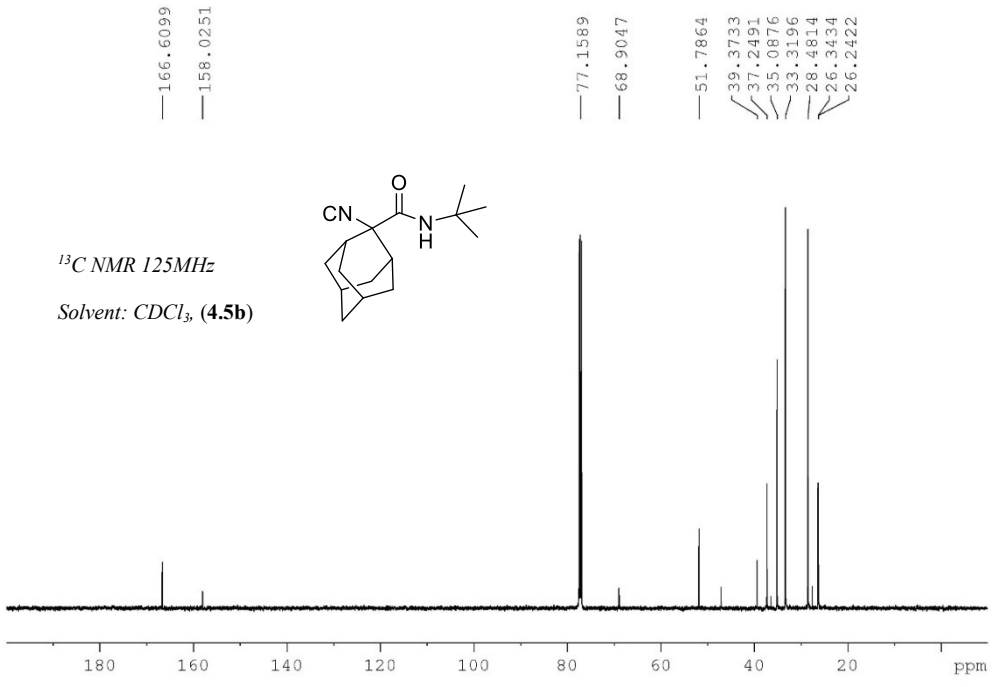

^{13}C NMR 125MHz

Solvent: $CDCl_3$, (**4.5b**)

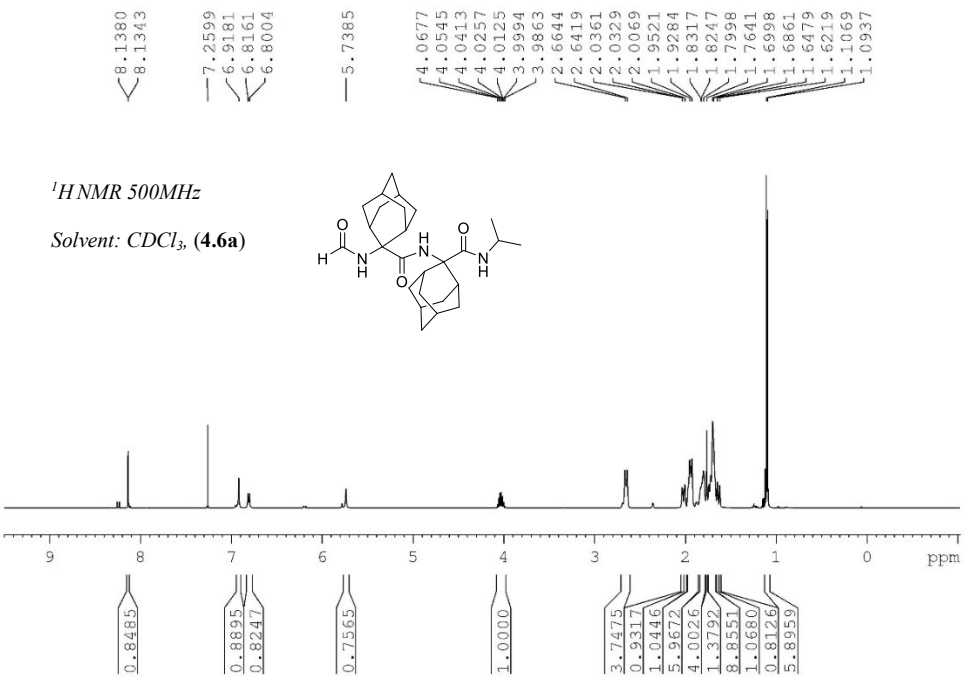

[1]H NMR 500MHz

Solvent: $CDCl_3$, (**4.6a**)

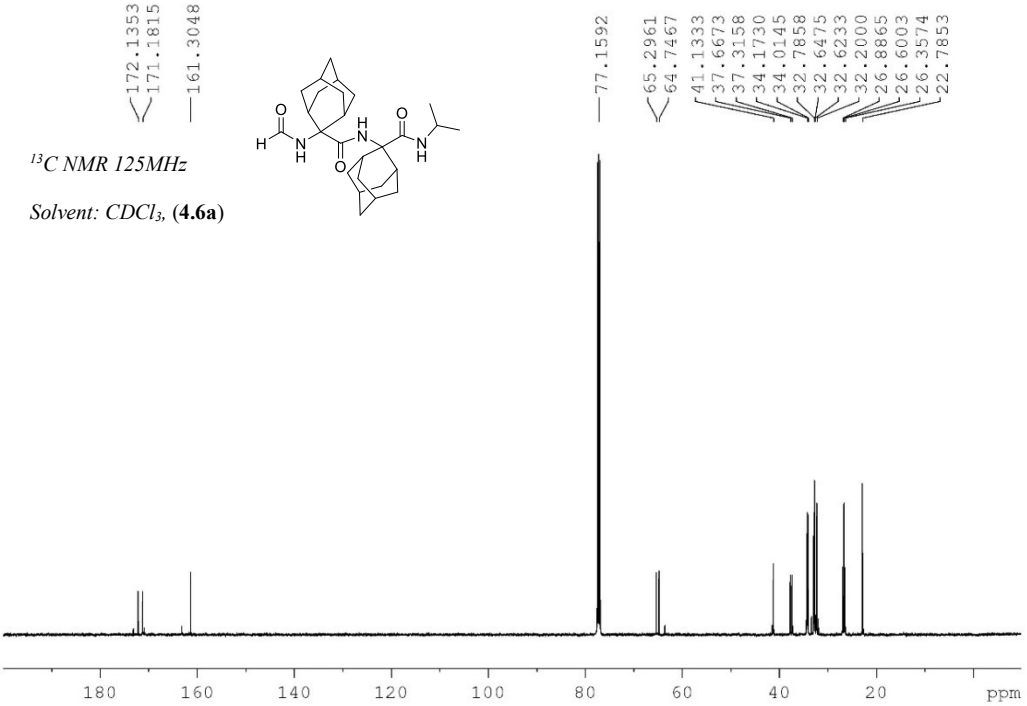

[13]C NMR 125MHz

Solvent: $CDCl_3$, (**4.6a**)

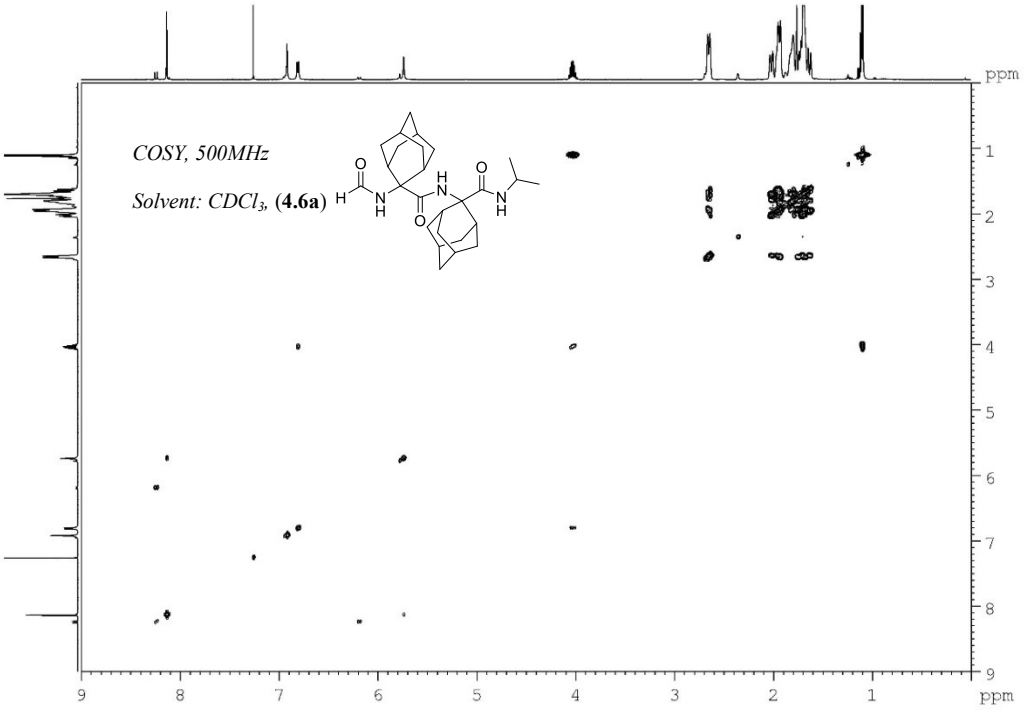
COSY, 500MHz
Solvent: CDCl3, (4.6a)
ppm
ppm

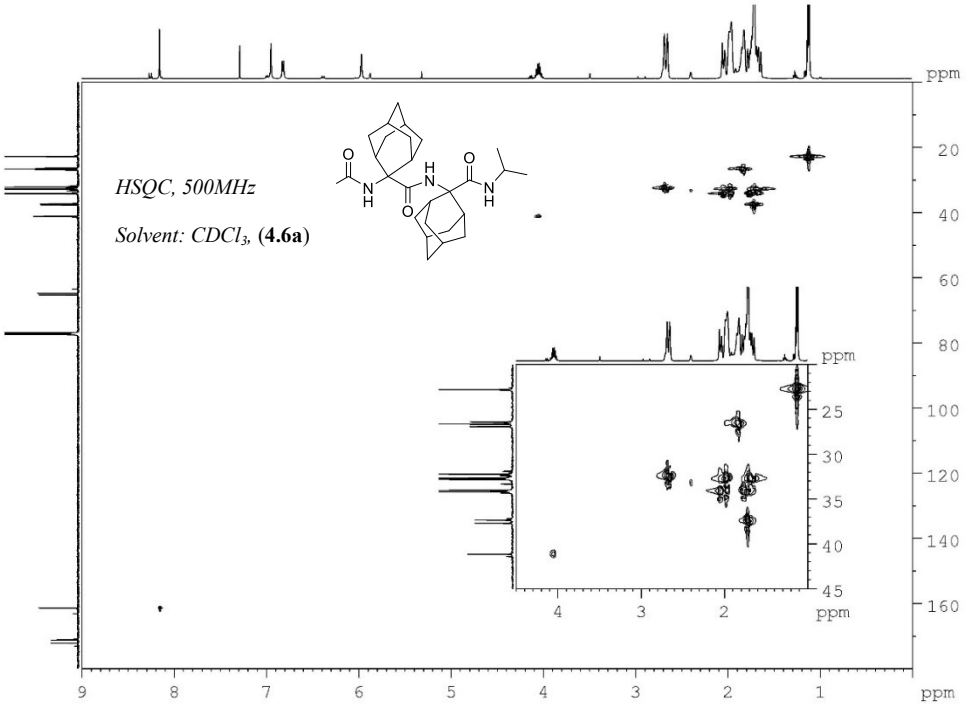
HSQC, 500MHz
Solvent: CDCl3, (4.6a)
ppm
ppm
ppm
ppm

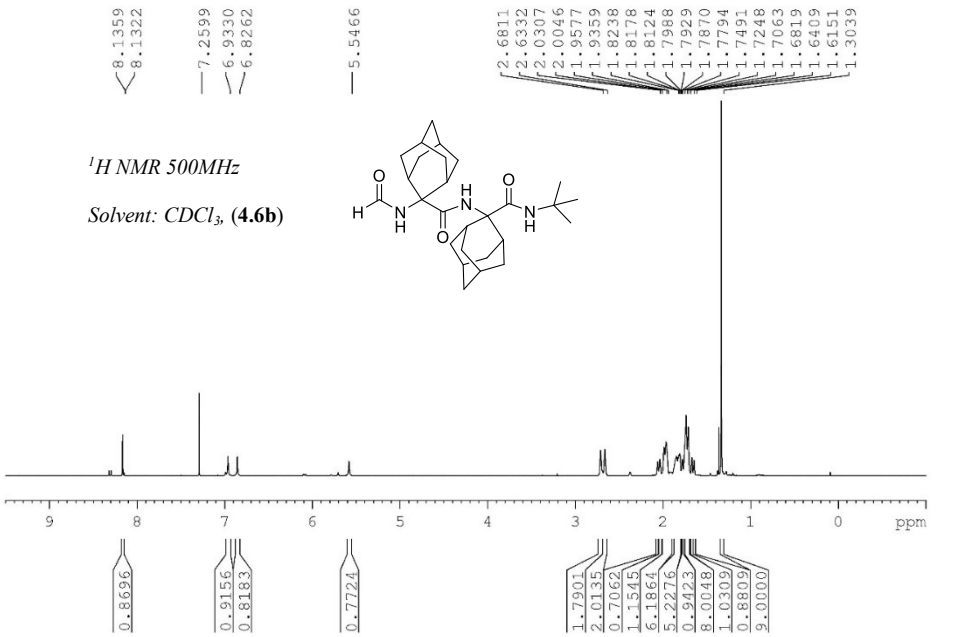

[1]H NMR 500MHz

Solvent: $CDCl_3$, (**4.6b**)

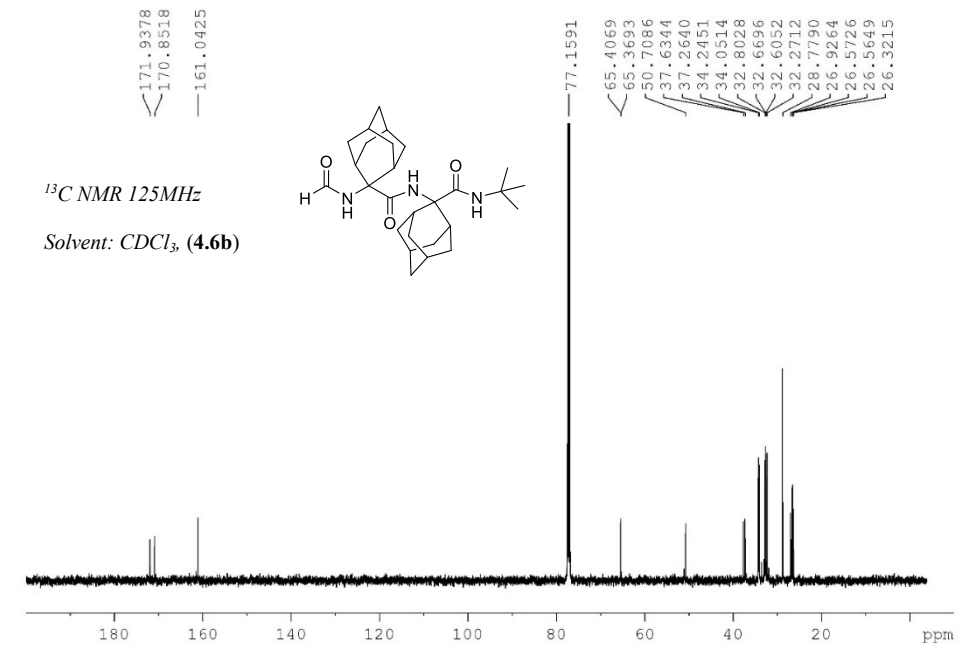

[13]C NMR 125MHz

Solvent: $CDCl_3$, (**4.6b**)

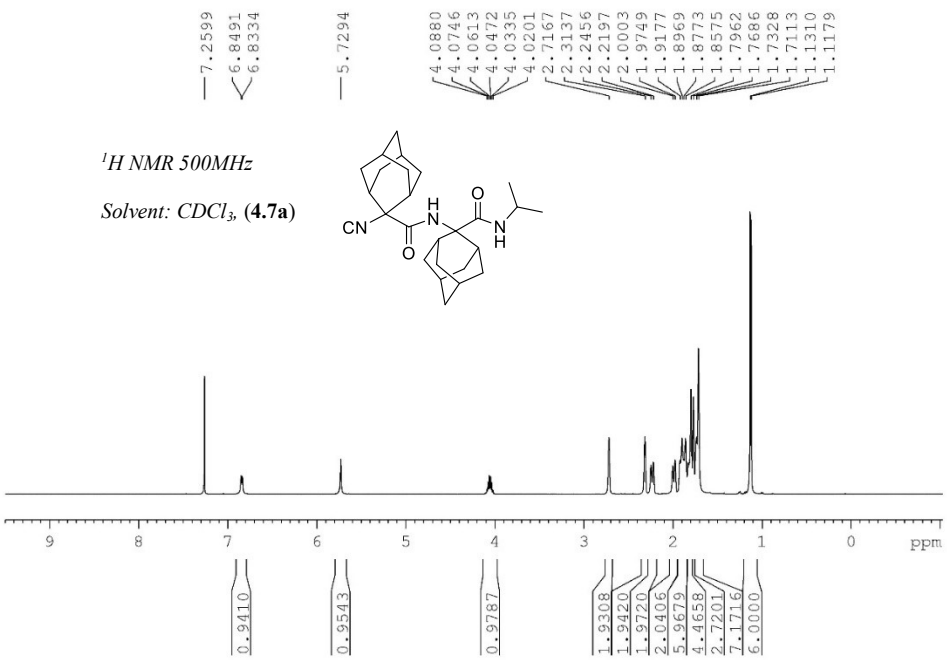

^{1}H NMR 500MHz

Solvent: $CDCl_3$, (**4.7a**)

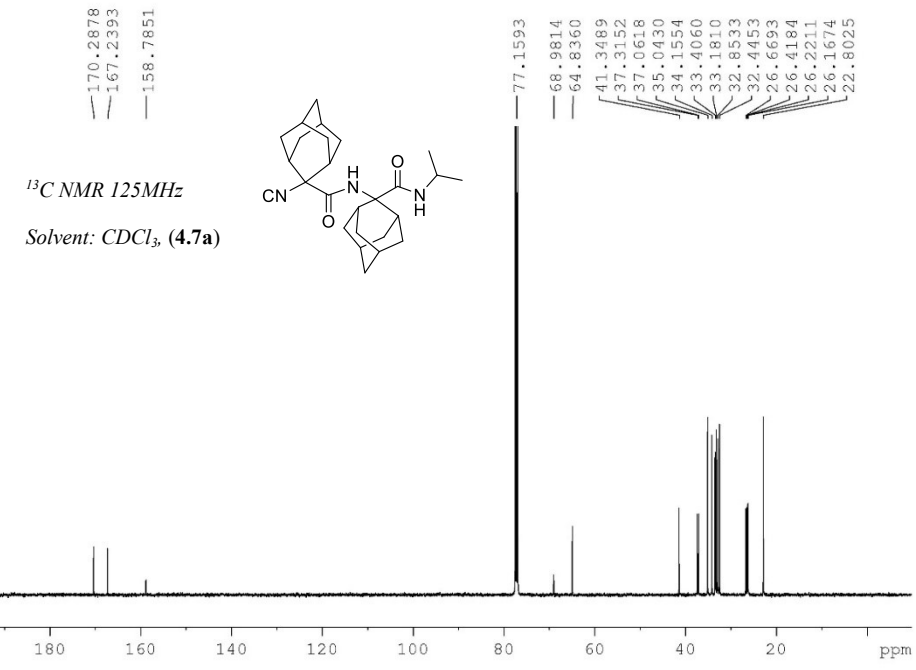

^{13}C NMR 125MHz

Solvent: $CDCl_3$, (**4.7a**)

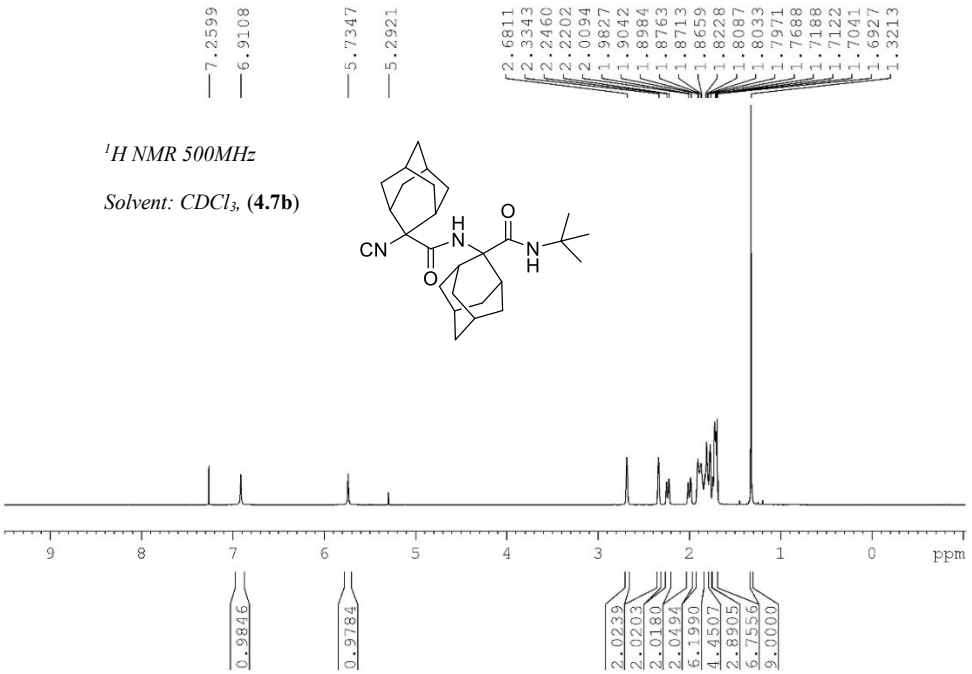

[1]H NMR 500MHz

Solvent: $CDCl_3$, (**4.7b**)

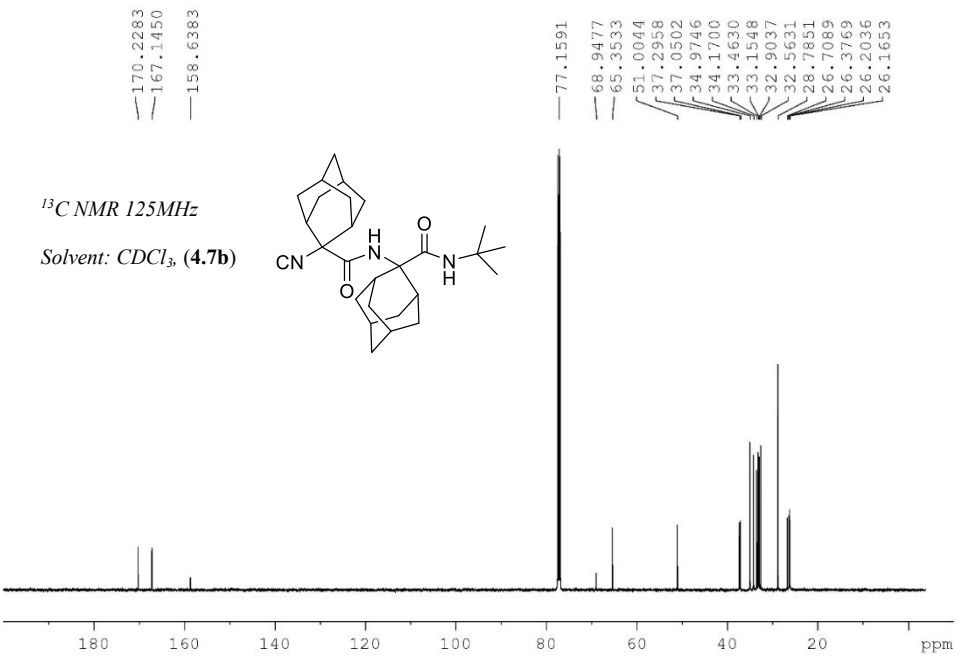

[13]C NMR 125MHz

Solvent: $CDCl_3$, (**4.7b**)

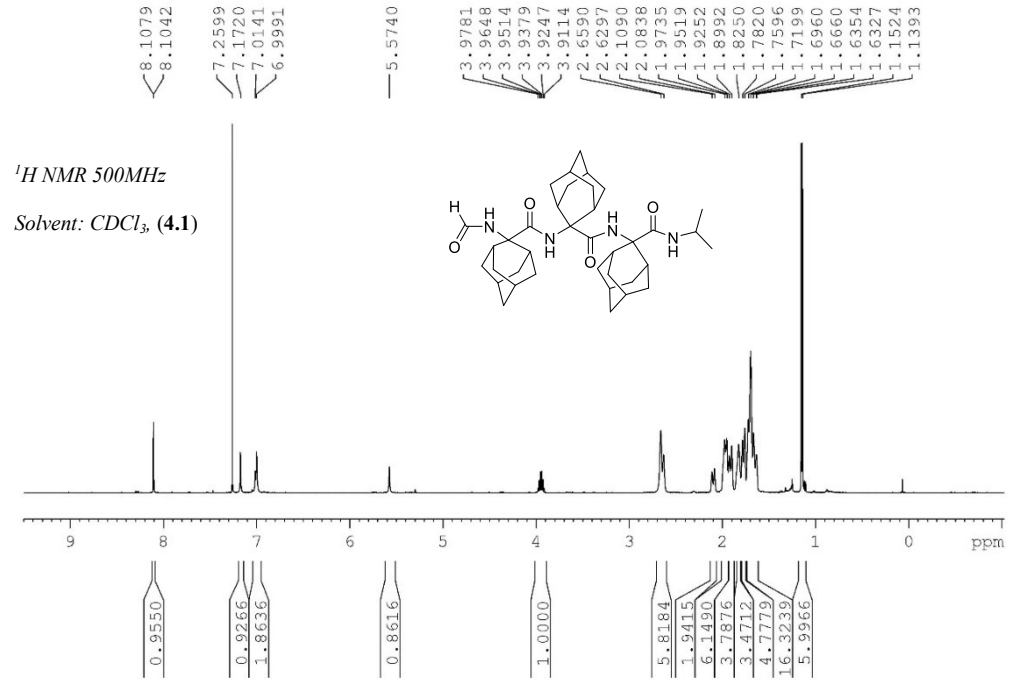

^{1}H NMR 500MHz

Solvent: $CDCl_3$, (**4.1**)

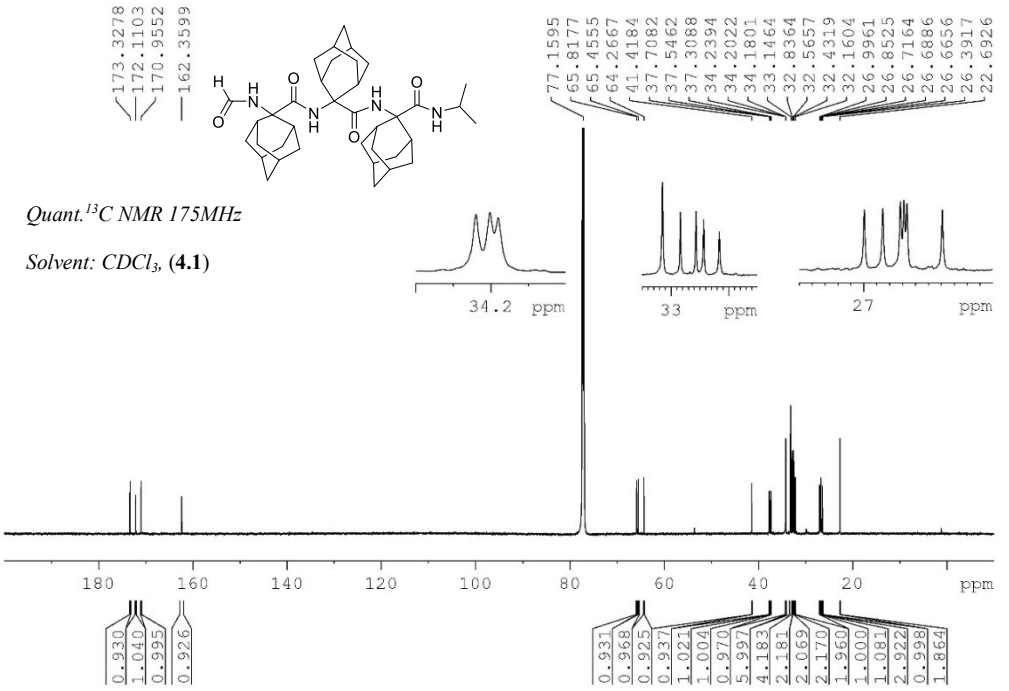

Quant.^{13}C NMR 175MHz

Solvent: $CDCl_3$, (**4.1**)

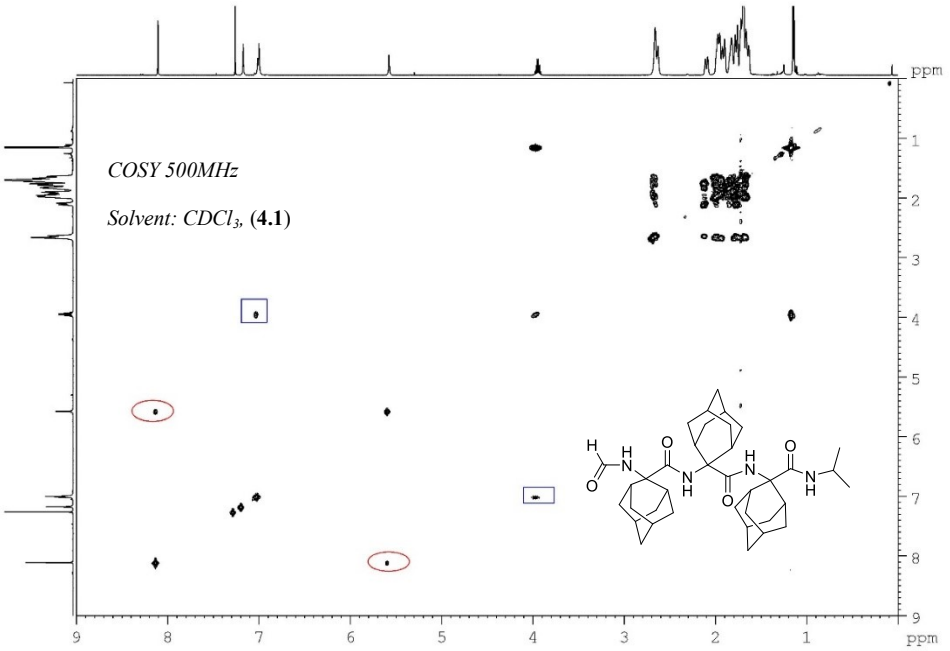
COSY 500MHz
Solvent: CDCl3, (4.1)
ppm
ppm

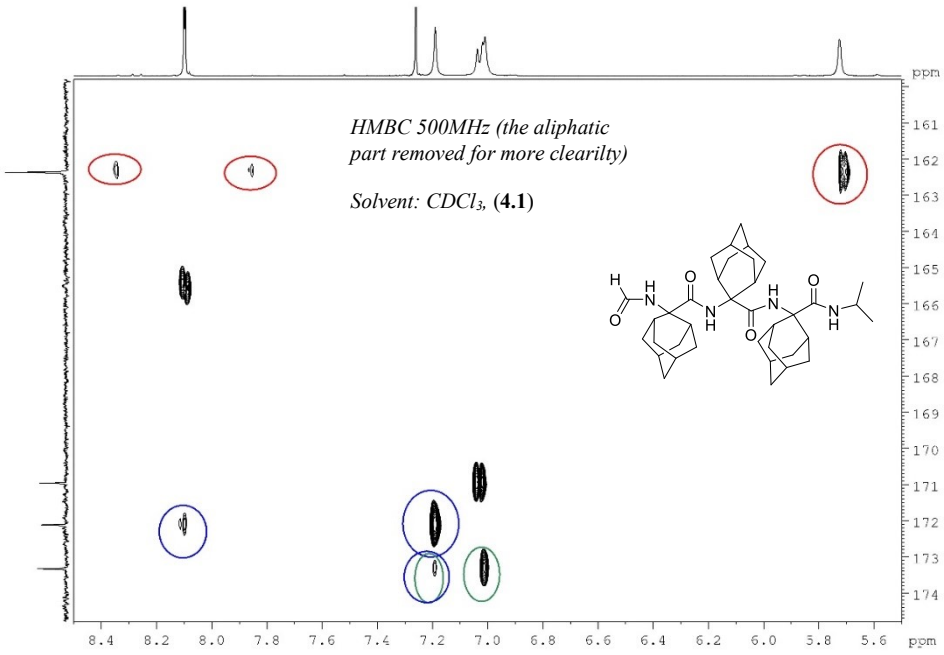
HMBC 500MHz (the aliphatic part removed for more clearilty)
Solvent: CDCl3, (4.1)
ppm
ppm

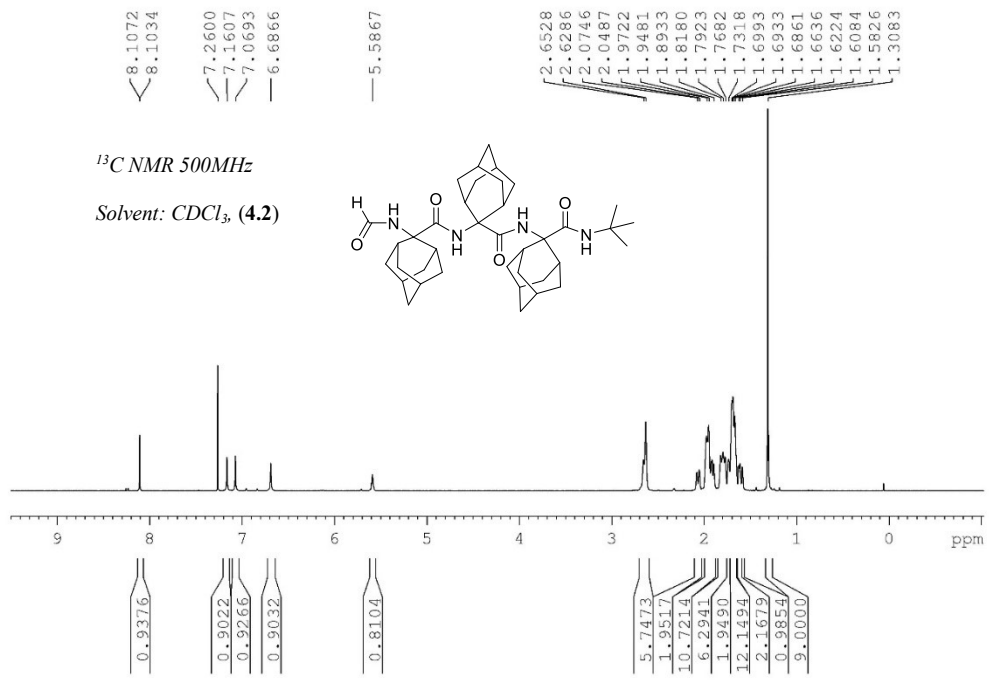

^{13}C NMR 500MHz

Solvent: $CDCl_3$, (**4.2**)

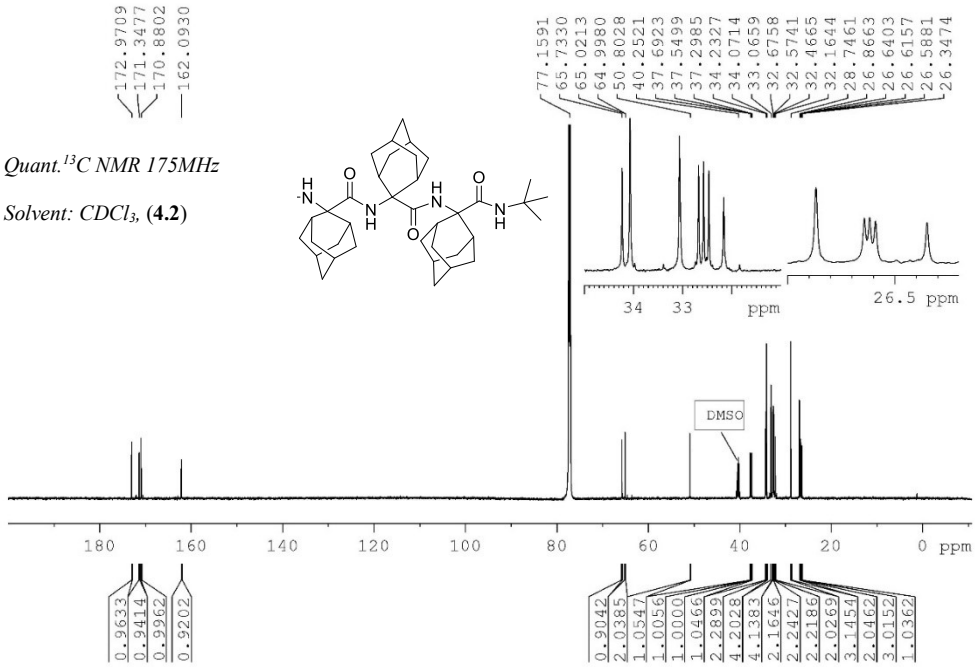

Quant.^{13}C NMR 175MHz

Solvent: $CDCl_3$, (**4.2**)

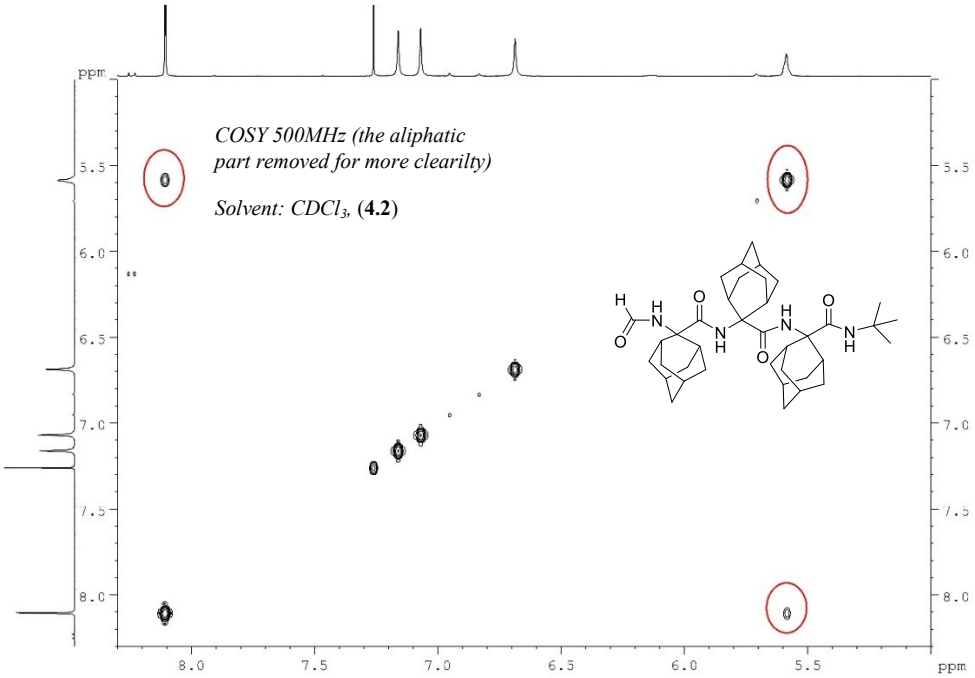
COSY 500MHz (the aliphatic
part removed for more clearilty)
Solvent: CDCl3, (4.2)
ppm
8.0
7.5
7.0
6.5
6.0
5.5

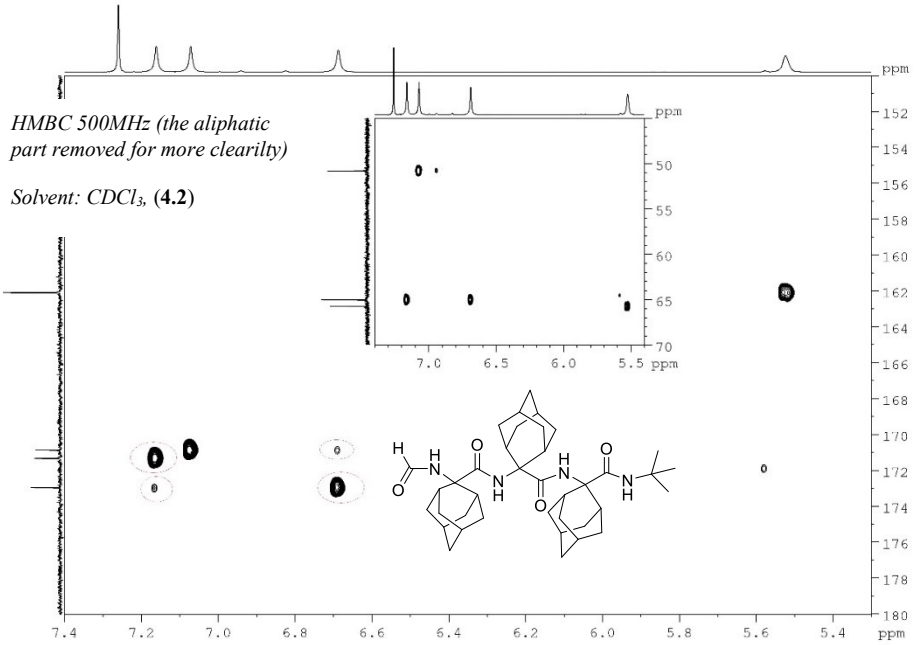
HMBC 500MHz (the aliphatic
part removed for more clearilty)
Solvent: CDCl3, (4.2)
ppm
7.4
7.2
7.0
6.8
6.6
6.4
6.2
6.0
5.8
5.6
5.4

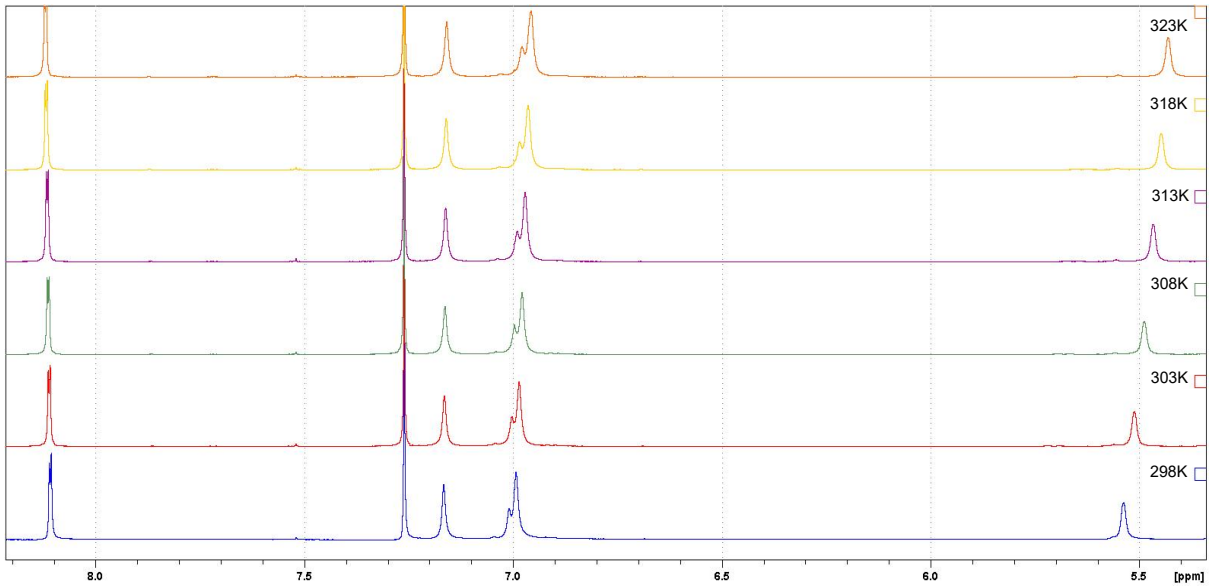

Effect of temperature changes on N-H signal chemical shifts (400 MHz) of **4.1** in $CDCl_3$.

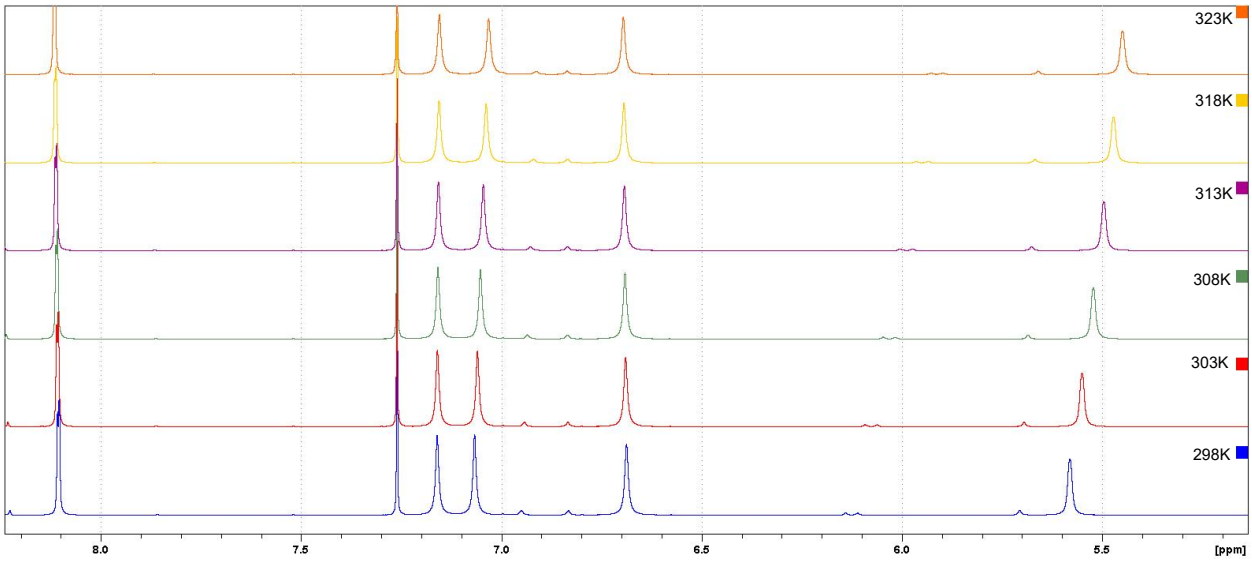

Effect of temperature changes on N-H signal chemical shifts (400 MHz) of **4.2** in $CDCl_3$.

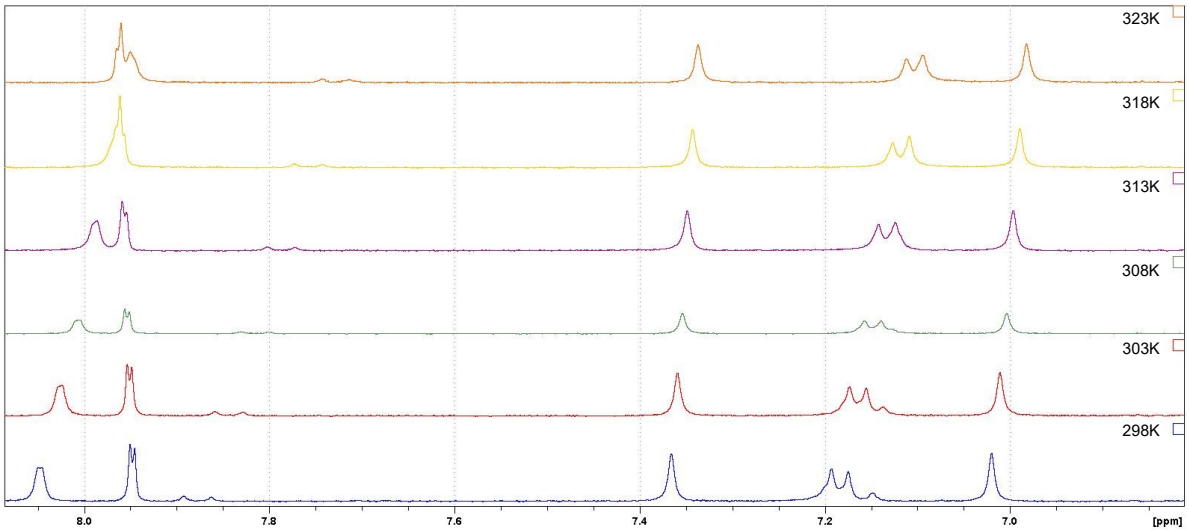

Effect of temperature changes on N-H signal chemical shifts (400 MHz) of **4.1** in DMSO-d_6.

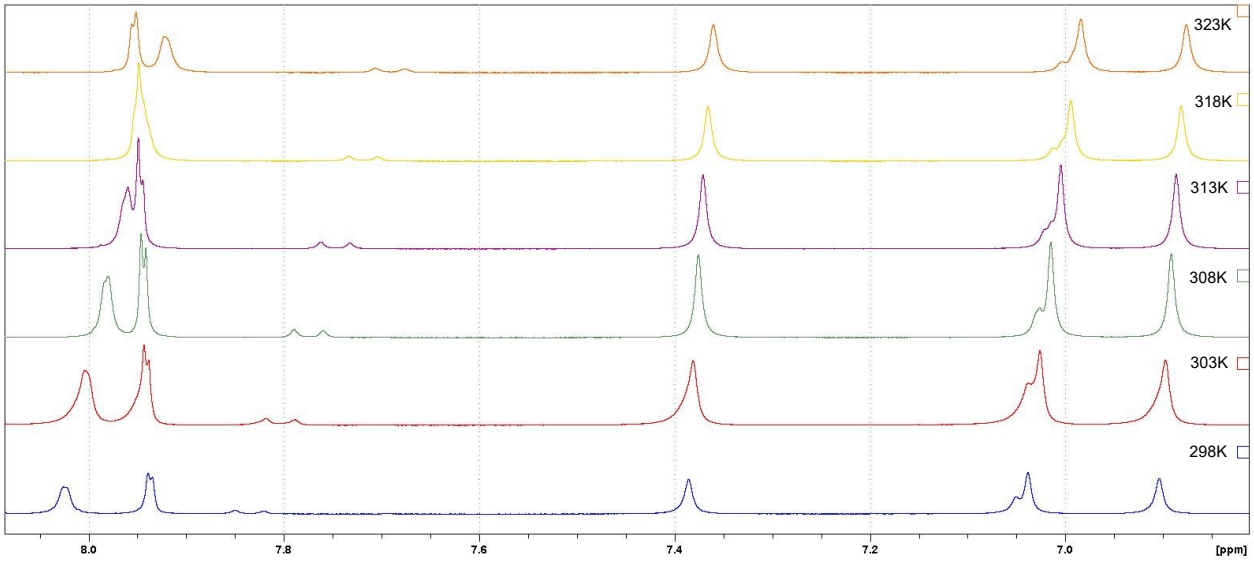

Effect of temperature changes on N-H signal chemical shifts (400 MHz) of **4.2** in DMSO-d_6.

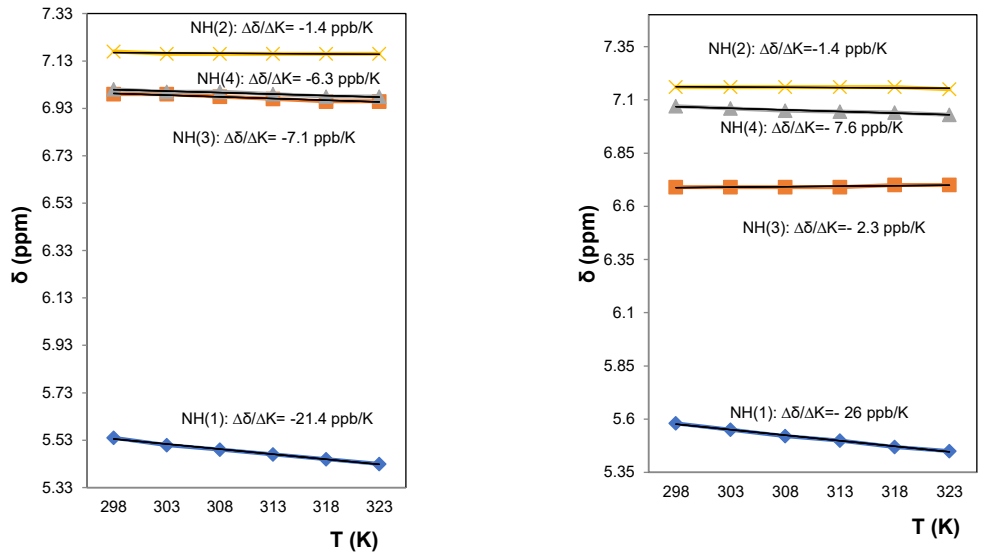

Figure S(4.1). Plot of changes of NH signal chemical shifts in the NMR spectra of peptides **4.1** (left) and **4.2** (right) as a function of temperature in $CDCl_3$.

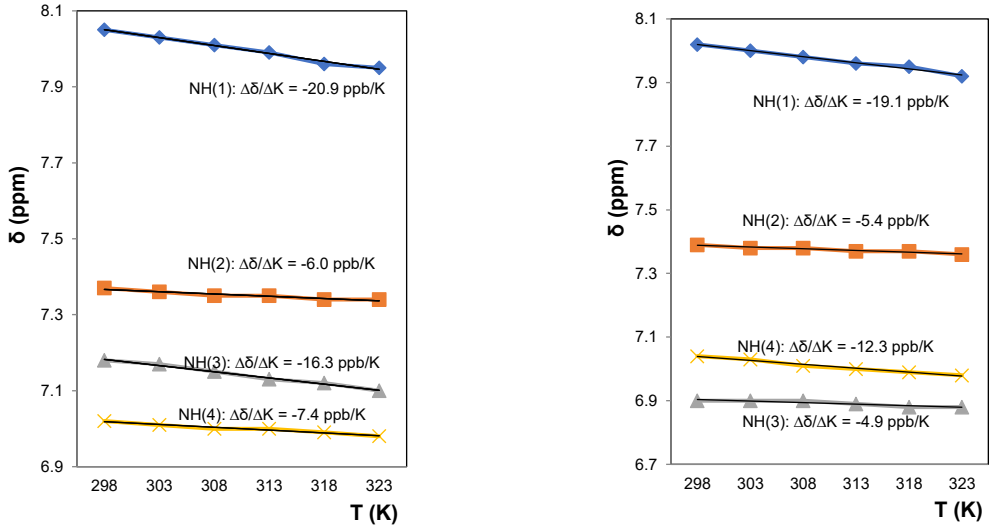

Figure S(4.2). Plot of changes of NH signal chemical shifts in the NMR spectra of peptides **4.1** (left) and **4.2** (left) as a function of temperature in DMSO-d_6.

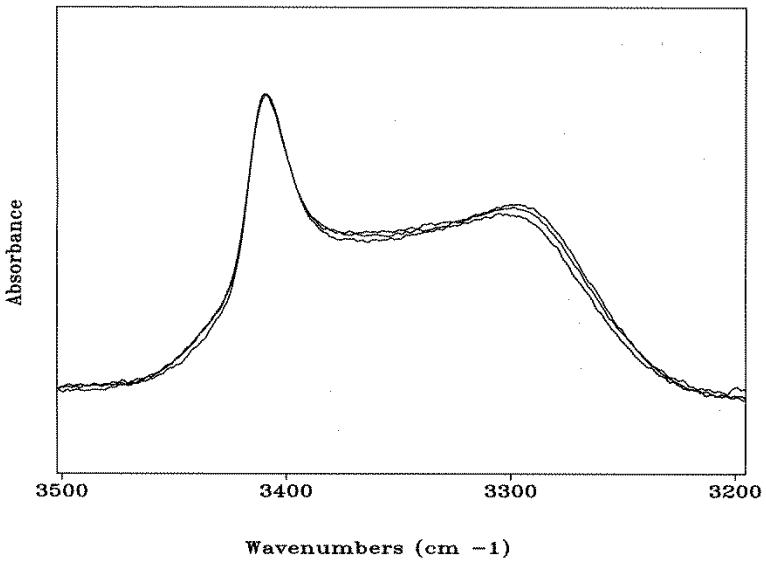

Figure S(4.3). Overlay of the FT-IR absorption spectra (N-H stretching region) of peptide **4.1** in $CDCl_3$ solution at the concentrations 10.0 mM, 1.0 mM, and 0.1 mM.

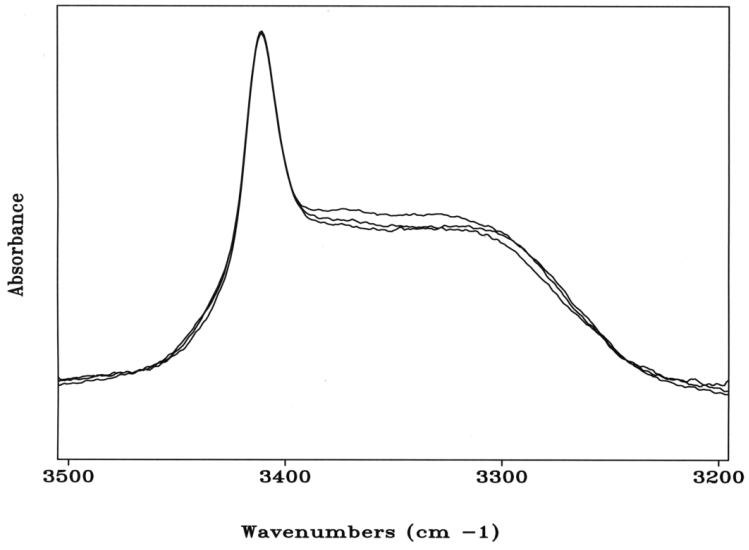

Figure S(4.4). Overlay of the FT-IR absorption spectra (N-H stretching region) of peptide **4.2** in $CDCl_3$ solution at the concentrations 10.0 mM, 1.0 mM, and 0.1 mM.

References:

1. Dolomanov, O.V., Bourhis, L.J., Gildea, R.J, Howard, J.A.K. & Puschmann, H. (2009), J. Appl. Cryst. 42, 339-341.
2. Sheldrick, G.M. (2015). Acta Cryst. A71, 3-8.
3. Sheldrick, G.M. (2015). Acta Cryst. C71, 3-8.

Supporting information of

Chapter 5

NMR

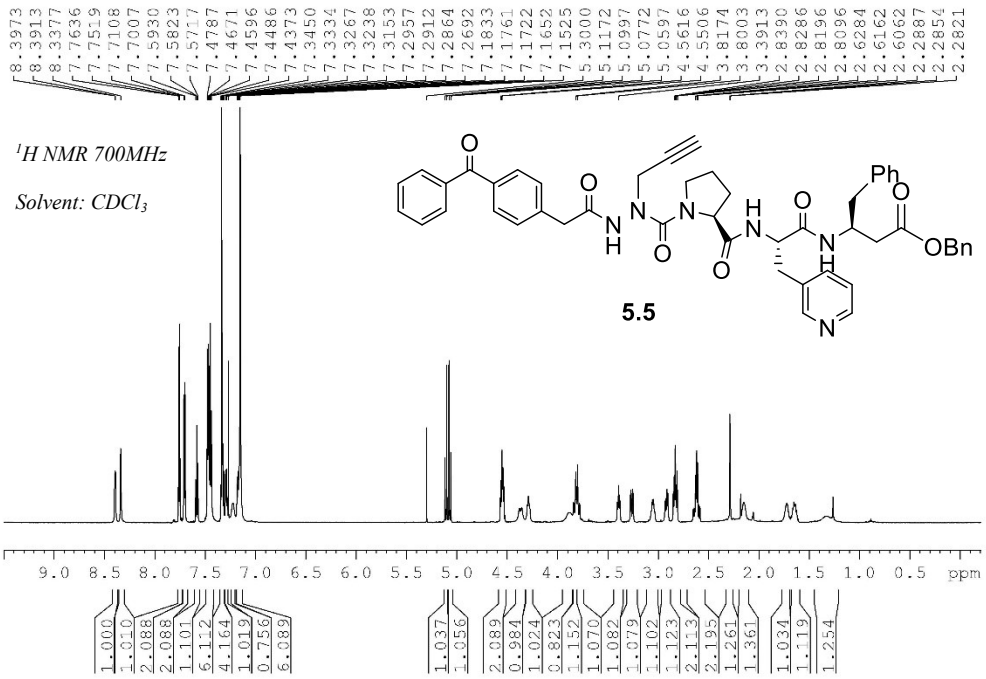
^{1}H NMR 700MHz
Solvent: CDCl$_3$
5.5

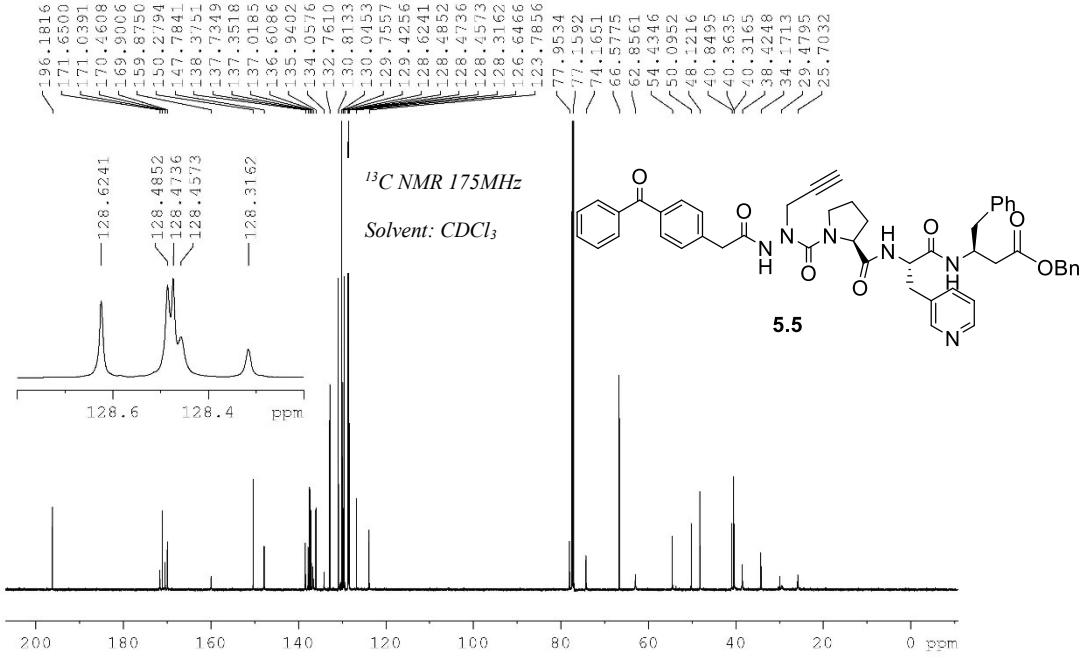
^{13}C NMR 175MHz
Solvent: CDCl$_3$
5.5

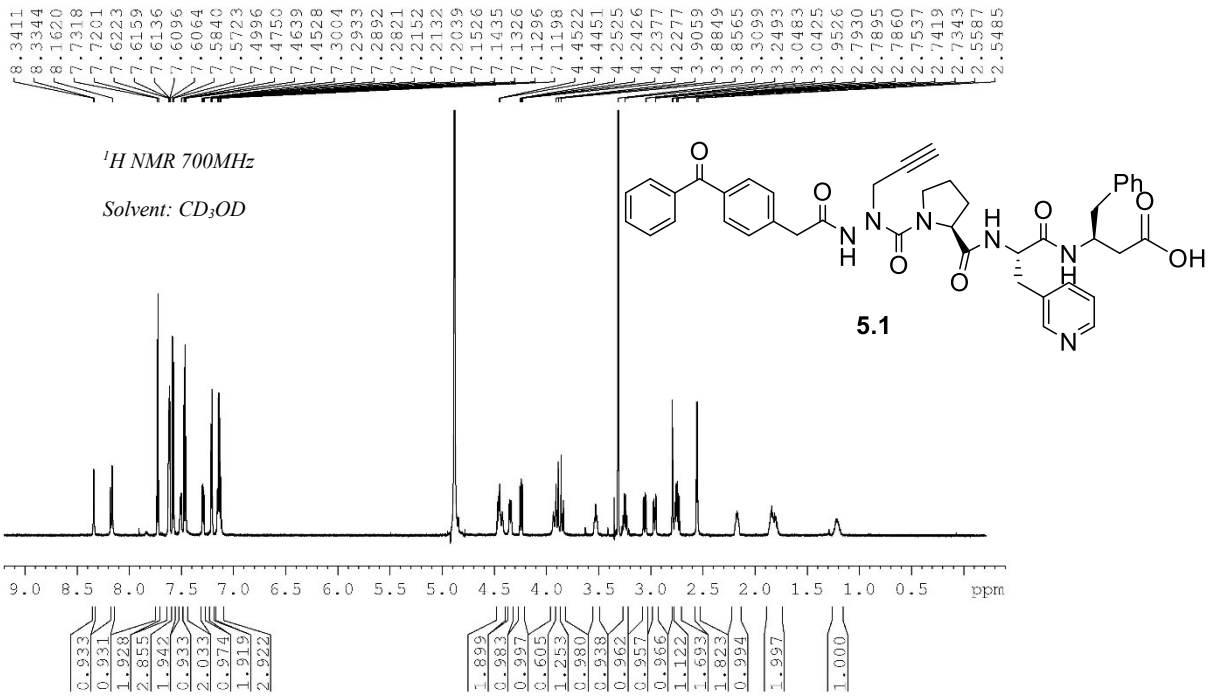
^{1}H NMR 700MHz
Solvent: CD_3OD
5.1

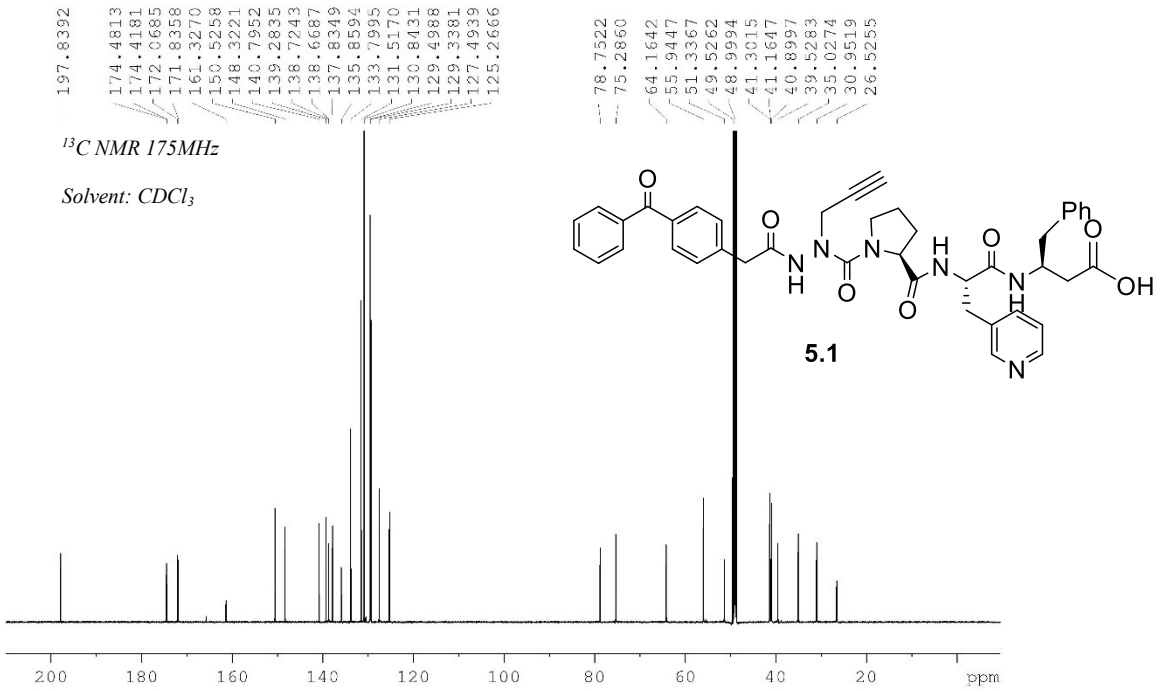
^{13}C NMR 175MHz
Solvent: $CDCl_3$
5.1

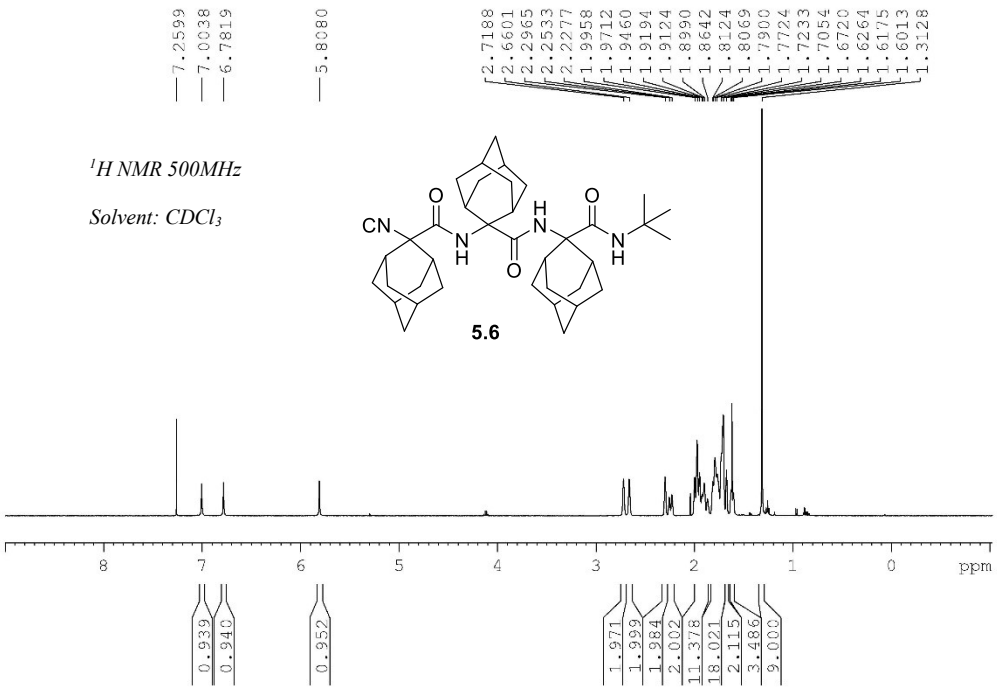

^{1}H NMR 500MHz

Solvent: $CDCl_3$

5.6

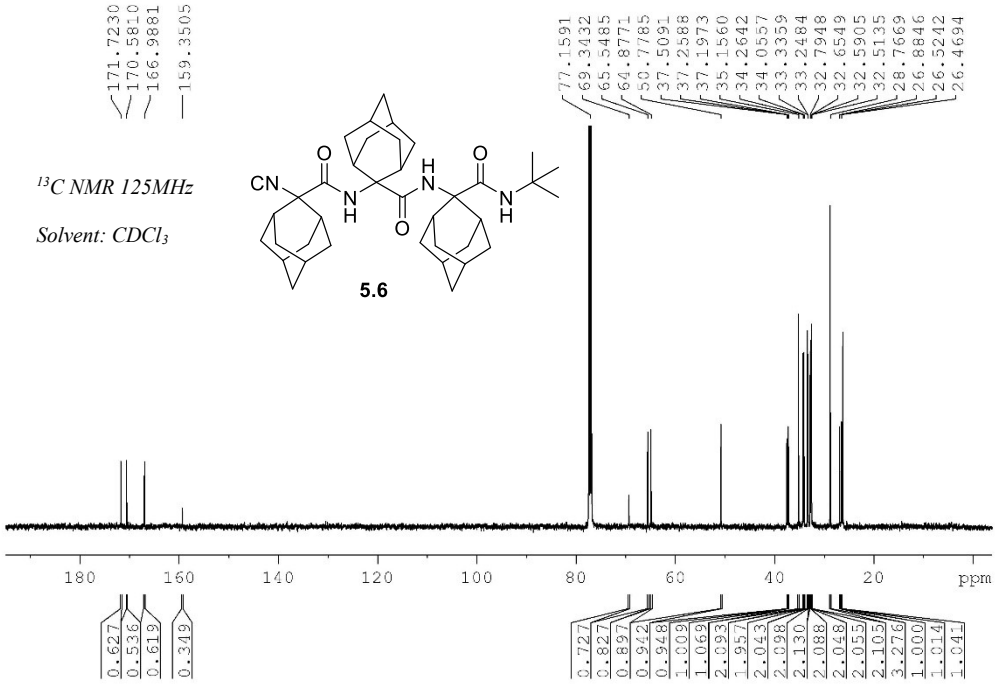

^{13}C NMR 125MHz

Solvent: $CDCl_3$

5.6

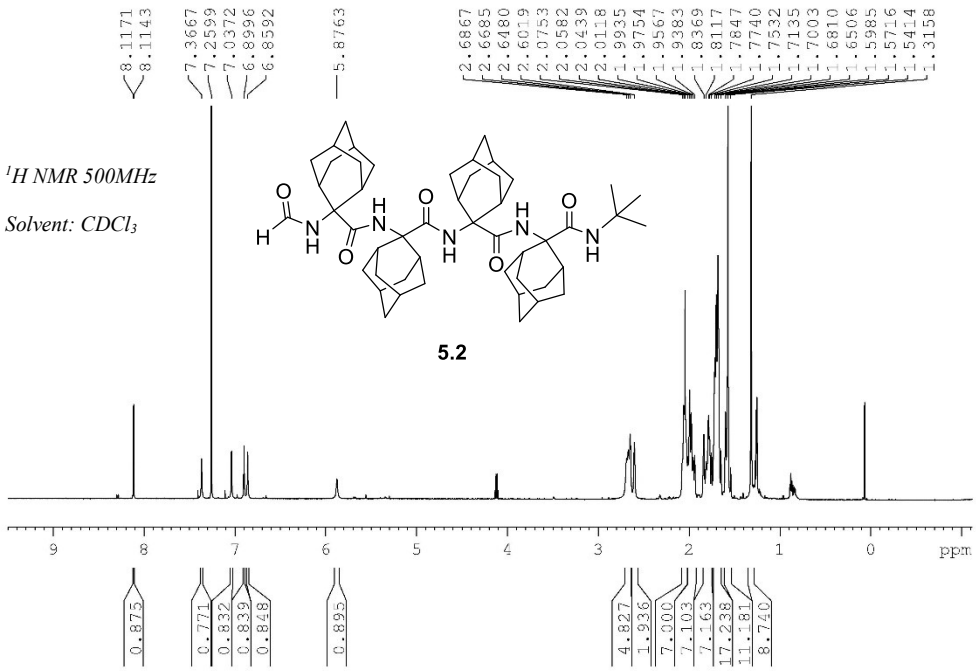

^{1}H NMR 500MHz

Solvent: $CDCl_3$

5.2

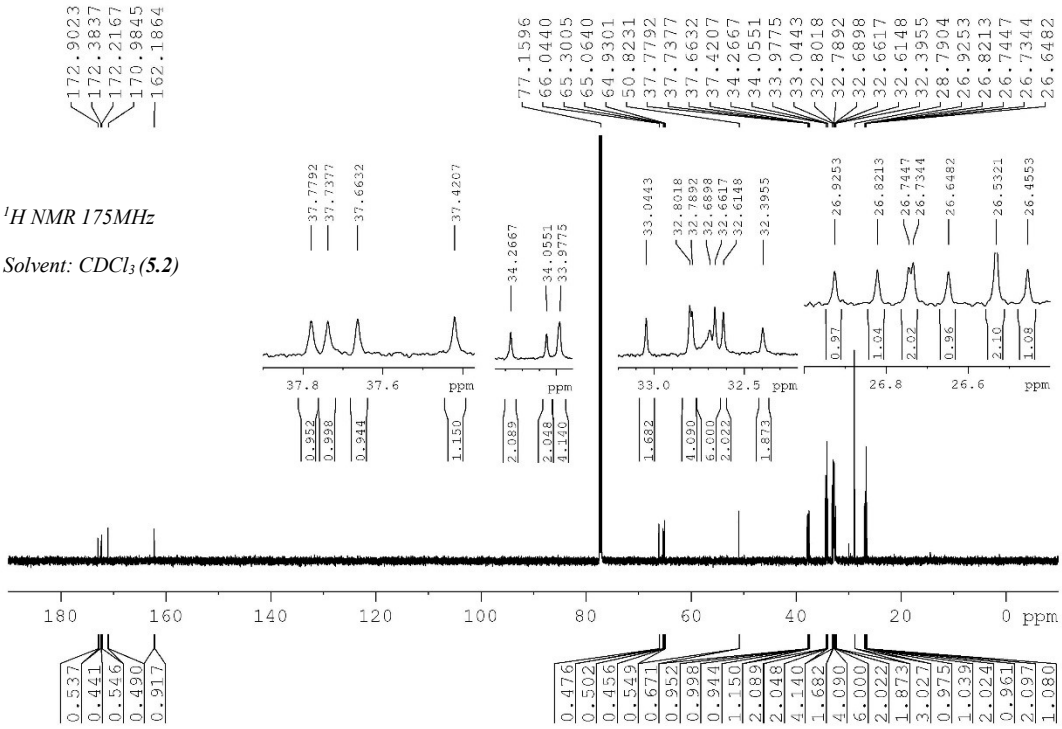

^{1}H NMR 175MHz

*Solvent: $CDCl_3$ **(5.2)***